THE UNIVERSITY OF HULL

Nanocarrier-formulated antimicrobials and microfluidics-based screening assays

being a Thesis submitted for the Degree of

Doctor of Philosophy

in the University of Hull

by

Saba Sahib Mohsen Al-Obaidy

BSc (University of Babylon, Iraq, 1998)
MSc (University of Baghdad, Iraq, 2006)

April 2018

Acknowledgements

Immeasurable appreciation and deepest gratitude go to my supervisors Prof. Gillian M Greenway and Prof. Vesslin N Paunov for their help, support, advice, valuable comments and suggestions that benefited in the progress and completion this study, and special thanks to Prof. Paunov for his research proposal.

I would like to express my sincere gratitude to my colleagues in the lab, Mohammad Al-Awady, Osama Alswafy, Dr Anupam Das, Ben Thompson, Jevan Medlock and Ahmed Al-Mamoori for sharing their knowledge and materials with me, really it was a great time I spent with them, and special thanks to all my Iraqi friends.

I also would like to thank Mr Sinclair and Mrs Lowry for all the assistance with the sample preparation for the transmittance and scanning electron microscope work and Dr Iles for his work to manufacture the master mould of the microfluidic device.

I would also like to express my big thanks to my parents, my brothers and my sister for their unceasing encouragement and prayers, and great special thanks to my husband for all his generous support in every aspect of my life, as I dedicate this work to them as well as my boys Ali and Hasan.

Last, but not least, I am grateful to the University of Hull for giving me the opportunity to study, especially the Chemistry Department.

Finally, I would like to express my deep gratitude to the Iraqi Government- Ministry of Higher Education and Scientific Research (MOHESR), the Iraqi cultural Attaché in London, and The University of Babylon - Iraq, for supporting me all financially.

Saba

Presentations

- Poster presentation in chemistry colloquia, July 2015, University of Hull, the poster entitled ***'Nanocarrier Formulated Antibiotics'.***

- Poster presentation in the 6th PhD Experience Conference, (7-8th) April 2015, University of Hull, the poster entitled ***'Nanocarrier Formulated Antibiotics'.***

- Oral presentation in chemistry colloquia 21st July 2016 which was held in the Department of Chemistry at the University of Hull. The talk entitled ***'Nanocarrier Formulated Antimicrobials'.***

- Poster presentation in Bioinspired Materials conference September 2016, Manchester Metropolitan University, the poster entitled ***'simple microfluidic platform to evaluate biological inspired nano-particles for focussed delivery of anti-bacterials***'.

- Poster presentation in Analytical Research Forum 2017 (ARF17), July 7th 2017, Royal Society of Chemistry, (London), the poster entitled, ***'simple microfluidic platform to evaluate biological inspired nano-particles for focussed delivery of anti-bacterials***'. The poster was awarded a prize as the best poster.

Abbreviations

BRB	Berberine chloride
BRB-NPs	Encapsulated berberine
CHX	Chlorhexidine di-gluconate
CHX-NPs	Encapsulated chlorhexidine
CTAB	Cetyl trimethyl ammonium bromide
CUR	Curcumin
CUR-NPs	Encapsulated curcumin
PDAC	Poly(diallyldimethylammonium chloride)
E.E	Encapsulation efficiency
FT-IR	Fourier Transform Infrared
M.B.	Magnetic beads
NPs	Nanoparticles
ODTAB	Octadecyltrimethyl ammonium bromide
PDMS	Polydimethylsiloxane
P407	Poloxamer 407
SEM	Scanning electron microscopy
Shellac NPs	Shellac nanoparticles
SDS	Sodium dodycel sulphate
SLNs	Solid lipid nanoparticles
TEM	Transmission electron microscopy
UV	Ultraviolet
UV-Vis	Ultraviolet and visible
VCM	Vancomycin hydrochloride
VCM-NPs	Encapsulated vancomycin

Abstract

Antibiotics and other antimicrobial agents have allowed the successful treatment of a range of infectious diseases. However, due to their extensive use a range of bacteria have developed multiple resistances to many antibiotics at therapeutically acceptable doses. In this thesis, one possible solution to overcome antimicrobial resistance was presented. This approach is based on the development of nanocarrier-formulated antimicrobial agents which have been encapsulated into biodegradable nanoparticles (NPs). A novel type of very efficient nanocarrier based on shellac; natural polymeric material of insect origin was designed. This nanocarrier was used to encapsulate and deliver antibiotics or antimicrobial agents such as berberine chloride (BRB), chlorhexidine di-gluconate (CHX), curcumin (CUR), and vancomycin hydrochloride (VCM). The nanocarrier was formulated and loaded with antimicrobial agent in two steps: (i) The first step involved controlled precipitation of aqueous ammonium shellac salts by a simultaneous pH change and adsorption of surface active polymer (Poloxamer 407) in the presence of the active antimicrobial component. In this step, simultaneously drug-loaded shellac nanoparticles was formed and coated them with a sterically stabilizing polymer, which can be allowed to maintain their stability and ensure long shelf-life. Stable shellac nanoparticles were produced at pH 5 with a particle hydrodynamic diameter of 66±5 nm with zeta potential –18±8 mV. (ii) The second step involved charge-reversing the produced shellac nanoparticles by doping with insoluble cationic surfactant (ODTAB), which gave them a positive surface charge in order to promote the nanocarrier adhesion to the negatively charged cell membranes of typical bacterial cells. Physical and chemical parameters such as the effect of different concentrations of the surface active polymer as well as the berberine, chlorhexidine, curcumin and vancomycin concentrations were studied on the size distribution of the produced nanoparticles and their zeta potential.

Optimal nanocarrier stability was obtained at a fixed ratio of (0.25:0.2) wt.% of shellac : Poloxamer 407 concentrations. Using 0.01 wt.%-0.07 wt.% concentration range of BRB, CHX, CUR and VCM with 0.25 wt.% shellac at pH 5 to be encapsulated within shellac NPs. The maximum encapsulation efficiencies of 60%, 92%, 100% and 87.5% for BRB, CHX, CUR, and VCM, respectively, were achieved. The release profiles of BRB, CHX, CUR and VCM loaded the developed shellac nanocarriers at pH 5.5 and pH 7.4 were studied, and sustained release from the formulations was confirmed upon dilution over a period. TEM images revealed that the NPs and the formulated antimicrobial nanoparticles

have a spherical shape and agree with the DLS (zetasizer) measurements. The interaction between the NPs and the antimicrobials was characterized using FTIR and UV-visible techniques.

The importance of the nanocarrier architecture on the antimicrobial activity of the loaded agent was studied. The antimicrobial activity of BRB-, CHX-, CUR-, and VCM-loaded shellac nanocarriers was studied upon incubation with microalgae, yeast, and *E.coli* at different incubation times. Although the free BRB, CHX, CUR and VCM in aqueous solution showed significant antimicrobial effect on these microorganisms, they showed weaker antimicrobial action when they were encapsulated within shellac NPs without doping with ODTAB. This reduction in activity was due to the repulsion between the negatively charged shellac NPs and the negative cell membrane which did not allow the encapsulated antimicrobials to be released near the cell wall vicinity. In addition to this, the attraction between the cationic antimicrobial agent and the shellac NPs led to slower the drug release. However, upon functionalization of the loaded-shellac NPs with a cationic surfactant ODTAB, their surface charge changed from negative to positive. Optimum conditions were found where the nanocarriers become cationic and still maintained their stability due to steric interactions. Consequently, the antimicrobial activity of these ODTAB-coated shellac NPs loaded with antimicrobial agents showed a significantly higher antimicrobial effect than the equivalent overall concentration of the free antimicrobials in solution. This effect was due to the strong electrostatic adhesion with the cell membrane which allowed the antimicrobial agents to be released directly into the microbial cell. Hence the cationically functionalized nanocarrier provides a boost of the antimicrobial action of the loaded agent.

A microfluidic device for cell trapping was also designed which is suitable for microscreening cell based assay. The microfluidic composed of two layers; a top layer of PDMS which contains connecting tubing, and the bottom layer was a microscope glass with two inlet channels, microchamber, and one outlet channels. Microbial cells trapped inside the microchamber with the antimicrobial agents was tested by using magnetic beads as a chamber “gate keeper” to trap the cells inside the microchamber and allow the fluids and the tested formulation to pass through the outlet channel. This is expected to lead further development of high throughput systems for testing antimicrobial agents on a range of microbial cells.

Table of Contents

List of Figures

List of tables

Chapter 1 : Introduction

1.1 Nanotechnology and Nanocarriers

Nanotechnology is the science that commonly deals with materials sized from few nanometers (nm) to several hundred nm, depending on their proposed use.[1] This science has brought to the fore nanosized inorganic and organic particles which possess unique physicochemical, optical, and biological properties which can be manipulated for desired applications such as synthetic textiles, food packaging products and the medicinal and therapeutic field.[2, 3] In medicine, the primary advantage of nanoparticles as carrier is their size which is similar to the dimensions and structure of most biological molecules like membrane receptors, antibodies, protein and nucleic acids,[4] and this allow them to overcome cellular barriers to improve the delivery of different drugs and drugs candidates.[5] Another interesting path for their exploration in medicine is their use as antimicrobials to target highly pathogenic and drug-resistant microbes, besides their ability to overcome problems with the physicochemical characteristics of the drug such as drug instability in biological fluids, poor solubility, and poor bioavailability.[6] But, for the application of nanoparticles in biology, biocompatibility is a highly desired characteristic, which means, the materials have the ability to perform without the exertion of undesired local or systemic effect.[7] The main aims for enquiry of nano-bio-technologies in drug delivery involve of i) a high amount of drug delivered with particular targeting, ii) a decrease in toxicity while keeping therapeutic effects, and iii) biocompatibility and high safety.[8] Figure 1.1 shows that there are different functions of nanocarriers in medicine.

Nanoparticles size can express a strong adhesion due to the increased contact area for van der Waals attraction. For instance, Lamprecht et al.[9] observed that the uptake or the adhesion of polystyrene particle to inflamed colonic mucosa was different, and the deposition was 5.2%, 9.1%, and 14.5% for 10 mm, 1000 nm, and 100 nm particles, respectively.

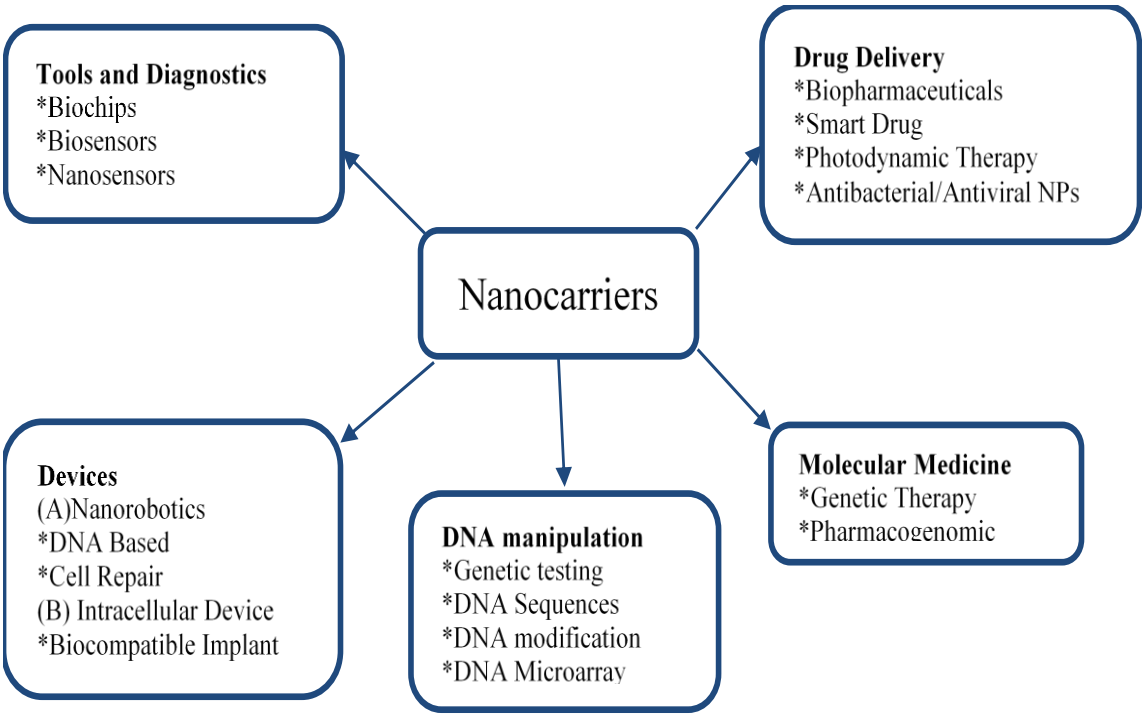

Figure 1.1: Different functions of nanocarriers[10]

1.2 Types of Nanocarriers

Many different types of nanocarriers have been prepared from different biodegradable materials as described below.[10] Figure 1.2

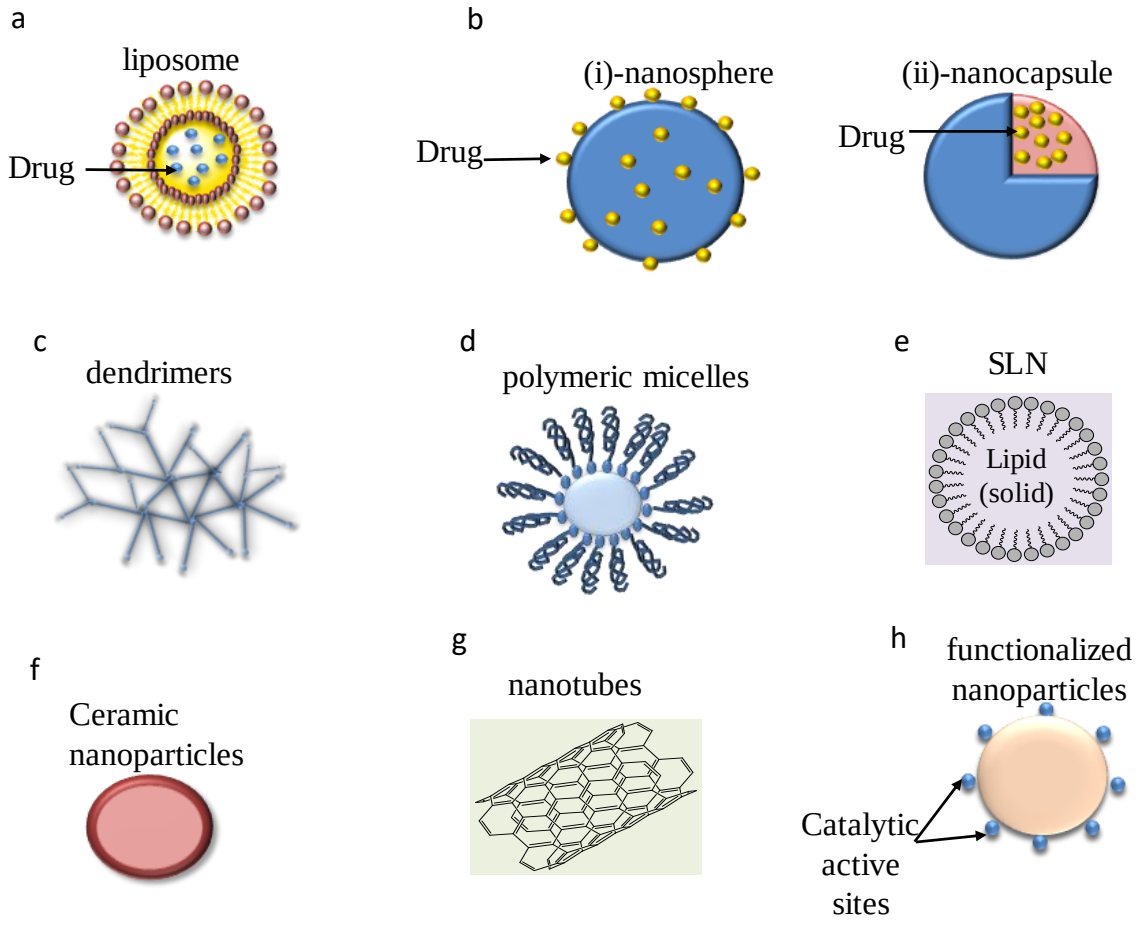

Figure 1.2: some types of nanoparticles (a) Liposomes: formed by phospholipids bilayers surrounding an aqueous core. (b) Polymeric nanoparticles (i) nanosphere in which the drug is dispersed throughout the polymeric matrix. (ii) Nanocapsule in which the drug is encapsulated within a polymeric membrane. (c) Dendrimers are highly branched polymers of macromolecular compounds. (d) Polymeric micelles: are amphiphilic block copolymers with self-association structure in aqueous solution. (e) Solid lipid nanoparticles (SLN): colloidal nanoparticles made from solid lipid. (f) Ceramic nanoparticles: made up of inorganic compounds. (g) Nanotubes: lipid formed in a self-assembling structure. (h) Functionalized nanoparticles: carriers with the catalytically active site is used as bioimaging or cell marker.[10]

- **Nanocrystals and Nanosuspensions:** Nanocrystals are formed by the aggregation of hundreds or thousands of molecules that combine in a crystalline form, the pure drug is composed with only a thin coating included of surfactant or combination of surfactants. The technique to produce nanocrystals is known as 'nanonisation'.[11]
- **Nanotubes and Nanowires:** Atoms are arranged to form a self-assembling sheet of tubes and thread-like structures of nanoscale range like carbon nanotube which offers some advantages by increasing the internal volume and ease of functional modification of inner and outer surfaces.[12]
- **Ceramic Nanoparticles:** These nanoparticles are made up of inorganic (ceramic) compounds such as titania, silica and alumina. They exist in sizes less than 50 nm. The entrapped molecules such as proteins, enzymes and drugs are totally protected by these nanoparticles against the denaturizing effects of external pH and temperature as the material shows no swelling and porosity changes with change in pH.[13]
- **Liposomes:** These are nanoparticles are spherical shaped self-assembling closed colloidal particles containing bilayered natural or synthetic phospholipids.[14] They have many advantages being amphiphilic in character, and biocompatible. It is also easy to modify their surfaces. Liposomes have been used successfully in the field of biology, biochemistry and medicine.[15]
- **Solid Lipid Nanoparticles (SLN):** These formulated nanoparticles employ the use of solid lipids. SLN particles prepared from solid lipids are submicron colloidal carriers (50-1000 nm) dispersed either in water or an aqueous surfactant solution. They have a solid hydrophobic core and a monolayer of phospholipid coating. The drug is located into the solid core of SLN which is dispersed or dissolved in the solid high melting fat medium.[16]
- **Hydrogel Nanoparticles:** These nanoparticles are prepared by the self-assembly and self-aggregation of natural amphiphilic polymers such as hydrophobized polysaccharides like agarose, cholesteroyl pullulan, and cholesteroyl dextran where the cholesterol groups offer cross-linking points in a non-covalent manner.[17, 18]
- **Copolymerized Peptide Nanoparticles (CPP):** Another modification of a polymer-based system is copolymerized peptide nanoparticles. It is a novel approach utilized for delivery of therapeutic peptides as drug–polymer conjugates in which the drug moiety is covalently bound to the carrier instead of being physically entrapped. [19]

- **Polymeric Micelles:** These systems contain amphiphilic block copolymers such as Pluronics (polyoxyethylene polyoxypropylene) block copolymers that form micelles in aqueous solution by self-association. This type of nanoparticle is characterized by their size and surface properties. Polymeric micelles offer a number of advantages like slow dissolution *in vivo* due to their thermodynamic stability in physiological solution, and they act as suitable carrier for water insoluble drugs owing to their core–shell structure.[20, 21]
- **Dendrimers:** are macromolecular compounds that comprise of a series of branches around an inner core whose size and shape can be altered as desired. They represent a unique class of polymers that are fabricated from monomers using either convergent or divergent step growth polymerization.[22]
- **Functionalized Nanocarriers** These nanocarriers combine the functionalities of biomolecules and non-biologically derived molecular species used for special functions such as markers for research in cell, biosensing, molecular biology, bioimaging and marking of immunogenic moieties to targeted drug delivery. These nanocarriers are monodisperse-sized particles which has well-defined surface structure and uniform shape. [23,24]
- **Polymeric Nanoparticles:** These colloidal carriers can be designed using biodegradable and biocompatible polyesters or poly(alkylacyanoacrylate), or natural polymers such as chitosan, albumin and heparin.[25] Polymeric nanoparticles can be found in two shapes depending on the method of preparation, nanospheres, or nanocapsules and the drug is either dissolved, entrapped, encapsulated or attached to the nanoparticle matrix. Polymeric materials show several required properties including biocompatibility, biodegradability, surface modification, and simplicity of functionalization of polymers.[26] These features make it them good for effective entrapment or encapsulation of drugs that are usually sensitive to the changes in the environments.[27]

1.3 Synthesis of Polymeric Nanoparticles for Drug Delivery System

As been mentioned previously, there are different types of nanoparticles, so they can be prepared from different natural materials, for example proteins, polysaccharides and synthetic polymers. The choice of matrix materials is dependent on various factors including: (a) the final required size of the nanoparticles; (b) the characteristic properties of the drug, like aqueous solubility and stability; (c) surface characteristics like charge and permeability; (d) degree of biodegradability, biocompatibility and toxicity; (e) the desired drug release profile; and (f) antigenicity of the final product. [28]

The most three frequency methods used to prepare polymer nanoparticles are:

1. Dispersion of preformed polymers; which is the most common method used to produce biodegradable nanoparticles from different materials such as poly (D, L glycolide), poly (lactic acid) (PLA) and poly (cyanoacrylates) (PCA). This technique consists of two methods; the solvent evaporation method and the solvent diffusion or spontaneous emulsification method.[29]
2. Polymerization of monomers; where the nanoparticles are prepared from monomers by a polymerization method in an aqueous solution in which the drug is perhaps dissolved.[30]
3. Ionic gelation or coacervation of hydrophilic polymers; the ionic gelation method is based on the transition of the material from liquid to gel owing to ionic interaction at room temperature. While the coacervative method depends on two aqueous phases mixed together, one is positively charged and the other is negatively charged, so they interact electrostatically.[31, 32]

More specialized techniques such as supercritical fluid technology[33] and particle replication in non-wetting templates (PRINT)[34] have also been used for the production of nanoparticles. The last one was claimed to have entire control of particle size, shape and composition, which could be good for mass production of nanoparticles in industry. This technique is a soft lithography technique based on the use of highly fluorinated perfluoropolyether (PFPE) moulds that are capable of moulding most hydrophilic and hydrophobic liquids to create useful materials in the patterned arrays formula of features, isolated particles and arrays of particles.[35]

Also, there are other ways have been used to prepare nanoparticles which can be classified as[36]:

- Chemical reaction and polymerisation technique.
- Bottom-up technique.
- Top-down technique.
- Combination technique.

The chemical reaction produces nanoparticles that consist of pure active pharmaceutical ingredient (API). These techniques are commercially important and have been used to manufacture materials used for pharmaceutical coating in dispersed latex form. In bottom-up method; also referred as solvent/antisolvent method, the starter material is a drug molecule and it based on classical precipitation of poorly soluble active pharmaceutical ingredient (API) which are dissolved in a water miscible organic solvent. While the top-down technique is in contrast to a bottom-up technique which starts with bulky API particles then breaks them down to nanoparticles of drugs, so this type of method also regarded as top-down technology, and it is very important and successful commercially. It based on two technologies; one is wet ball milling (WBM), and the second is high pressure homogenization (HPH). The combination technique combines the bottom-up and top-down techniques.[37]

1.4 Advantages and Disadvantages of Nanocarriers

The most important properties that make nanoparticles have unique characteristics is their size, the small size and the high surface area to volume ratio, large surface area of the nanoparticles improves their interaction with the microbes to carry out abroad range of probable antimicrobial activities.[38] Nanocarrier offers numbers of advantages making them ideal drug delivery vehicles such as

- The particle size and surface characteristics of nanoparticles can be manipulated to improve both active and passive targeting of drugs through parenteral or oral administration.[39]
- There is a complementary relationship between nanotechnology and biotechnology that works to link the gaps between ‘the structure’ and ‘the function’ of biomolecules as well as acting to relate between ‘human physiology’ and ‘pathophysiology’.[40]

- Nanoparticles have been engineered to have a comparable scale to natural molecules such as proteins, DNA and viruses, which are of the size of 10's of nanometres. Because of their nanosize, nanocarriers have the ability to overcome the resistance of physiological barriers in the body by delivering directly efficient drug to various parts of the body. So they can be designed to eliminate the problems of drug delivery and can be used in various important applications in specific areas as gene therapy, drug delivery imaging, biomarkers, biosensors and novel drug discovery techniques.[41-43]
- Nanocarriers help to improve aqueous solubility of poorly soluble drugs and that enhance the drug delivery efficiency, timed release of drug molecules, and precise drug targeting.[44-47]
- The surface properties of nanocarriers can be modified with small molecules like proteins, peptides, and nucleic acids to target drug delivery[44, 48, 49] which will be not recognised by immune system and efficiently targeted to particular tissue types.[50]

Drug toxicity can be reduced by using targeted nano drug carriers system, and this system provides more efficient drug distribution. The drug availability can increase at the infected, and this may allow a decline in dosage to avoid general toxicity.[51]

On the other hand, nanocarriers have some potential hazards as they exhibit difficulty in handling, storage, besides, due to their small size, nanocarriers could cause unintended environments and harmful consequences, *e.g.* they could cross the nuclear envelope of a cell and cause unintended genetic damage and mutations.[52] With current concern about plastics in the environment there is a need to consider using environmentally biodegradable NPs from renewable natural materials such as lignin, cellulose and shellac.

They can also enter the human body through accidental or involuntary contact by several routes such as the olfactory pathway to the lungs, or could enter vital organs through the blood stream and could be potentially harmless for human as well as the environment. Therefore in this project, we used shellac; the natural insect residue to prepare stable nanocarriers loaded with different antibiotic agents as drug delivery system.

1.5 Shellac

Owing to their relative abundance, low cost, bio-degradable and eco-friendly profiles, natural polymeric materials have attracted attention as potential pharmaceutical excipients.[53] Shellac or lac (regularly used synonymously)[54] is the refined product of the natural material Lac secreted by the small parasitic insect *Kerria lacca* on different host trees in South Eastern Asia. Shellac has a complex mixture of polar and non-polar components consisting of polyhydroxy polycarboxylic esters, lactones and anhydrides with the main acid components being aleuritic and terpenic acids (Figure 1.3), [55, 56] it is water resistance and biocompatible, with a pKa of 6.9 to 7.5 and is acid resistant.[57] Shellac, like other polymers with carboxylic groups, is practically insoluble in acidic to neutral aqueous medium (pH < 7),[58] and insoluble in hydrocarbon solvents, water, glycerol, and ester, while it dissolves in aqueous alkali solutions, alcohol, ketones and organic acids. This is due to the fact that shellac consists of carboxyl, hydroxyl and carbonyl groups.[55] Palit[59, 60] discovered that the solubility of shellac in non-solvent liquids like acetone can be enhanced by adding 5 -10 percent of water to it, that way the shellac polar part will absorb the polar solvent of the mixture (water), and the big hydrocarbon group goes into fat solvent component of the mixture (acetone).

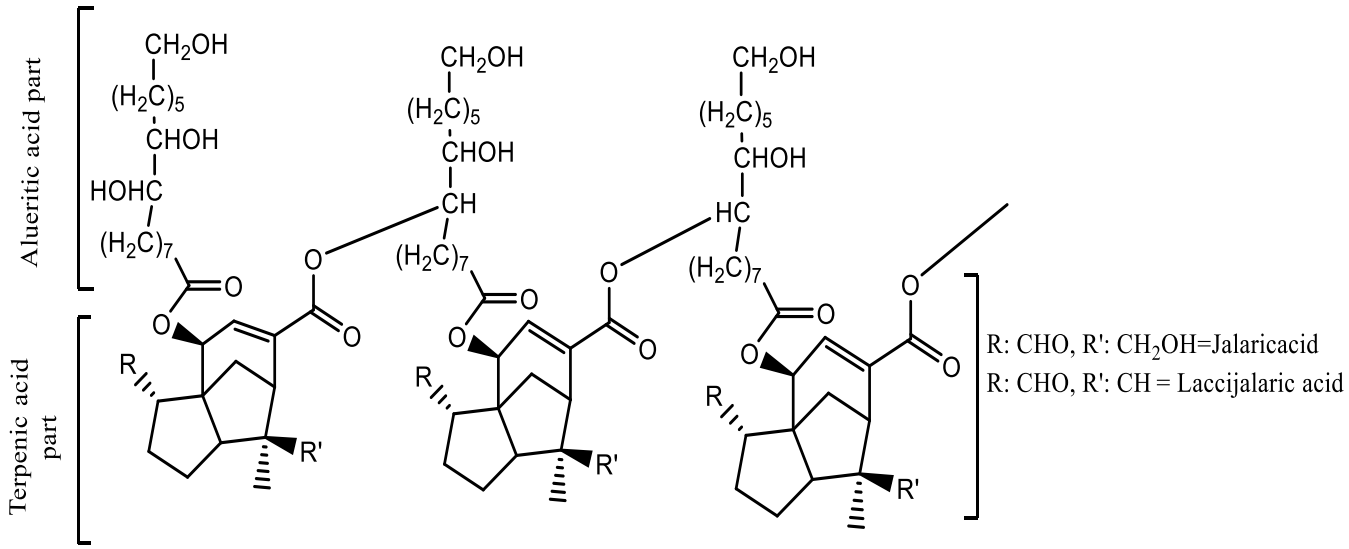

Figure 1.3: Chemical structure of shellac[61]

1.5.1 Shellac Composition

Elemental analysis showed that shellac contains carbon, oxygen, hydrogen, and a negligible amount of ash. Orange shellac comprises approximately 68 % carbon, 23 % oxygen and 9 % hydrogen. The orange shellac has a molecular weight of 1006 $gm.mol^{-1}$, while for bleached shellac it is 949 $gm.mol^{-1}$. The average shellac molecule has an empirical formula which is $C_{60}H_{90}O_{15}$.[62] In 1899, Tschirch *et al*. was the first one who performed the systematic analysis of shellac composition after fractionation of the material in different solvents.[63] The type of shellac depends on its component and constituent acids are liberated on hydrolysis to mainly acid type, hydroxyl aliphatic acids which are insoluble in water and terpenic acids that are water soluble and these two types are found almost in an equal amount.[64] Aleuritic form the main basic acid among aliphatic acids at about 35%, while jalaric acids with 25% is considered the main acid among terpenic acids. Other isolated acids are laccijalaric and shellolic/epishellolic (~8%), and butolic (~8%),[54, 65] However, even with all this attention, shellac composition is still not completely understood, because its composition is highly variable depending on its source and the type of purification.[66] As well as, shellac collected from branches of the trees consists of (70-80%) resin, (6-7%) wax, (4-8%) colouring matter, and (15-25%) other materials like moisture and debris.[67]

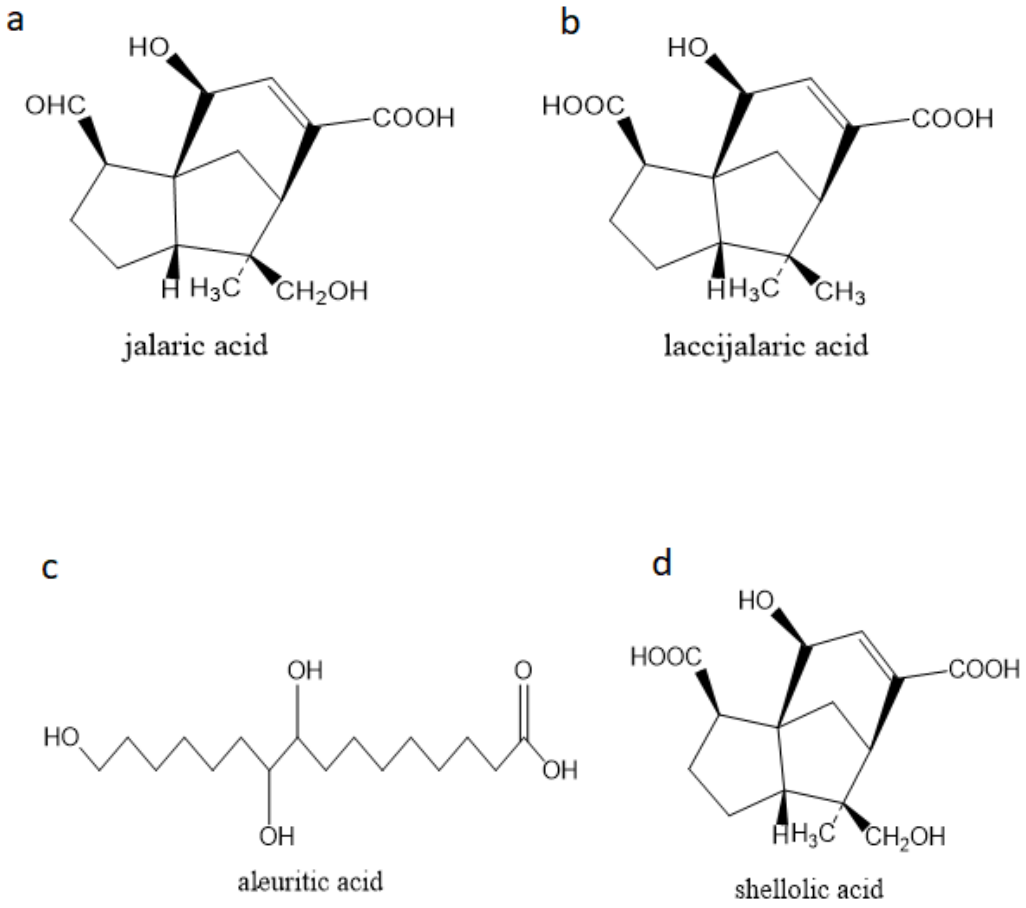

Figure 1.4: Shows the main components of shellac[68] , (a) jalaric acid; (b) laccijalaric acid; (c) aleuritic acid; (d) shellolic acid.

1.5.2 Properties of Shellac

Due to the fact that high gloss shellac or shellac modified resins are nontoxic, biologically degradable, hypoallergenic, are hard, have excellent adhesion and electrical properties they have a grown in importance.[69] It is a tough, brittle and resinous solid, and odorless in the cold but has a characteristic smell when it is heated and melted. This smell relates partially to aleuritic acid, which is considered as a starting material for the manufacture of flavors.[70, 71] The color of shellac is dependent on the process of refining and the type of seedlac; which is the least processed shellac and all other shellac products are made from this raw seedlac resin, and can range from light yellow to deep red.[72] As

well as at pH< 7, shellac is soluble in ethanol, methanol and partly soluble in ether, ethyl acetate and chloroform.[73] It suffers from aging for the reason that acids contain more than one hydroxyl group and several carboxyl groups which allows of self-esterification of the material.[74] This esterification is accompanied by a loss of solubility, a decline in the acidity and an increase in the glass transition temperature.[73, 75] This aging is observed as so-called blocking of the material when the individual shellac flakes stick together. Shellac therefore should be stored at temperatures below 27 °C and protected from light,[76] the addition of antioxidants will prolong the stability.[77] Otherwise shellac stability can greatly be improved by salt formation with ammonia,[78] or organic alkali shellac as 2-amino-2-methyl-1-propanol.[57, 79] This salt formation is presumed to create a steric hindrance and thus decrease self-esterification.

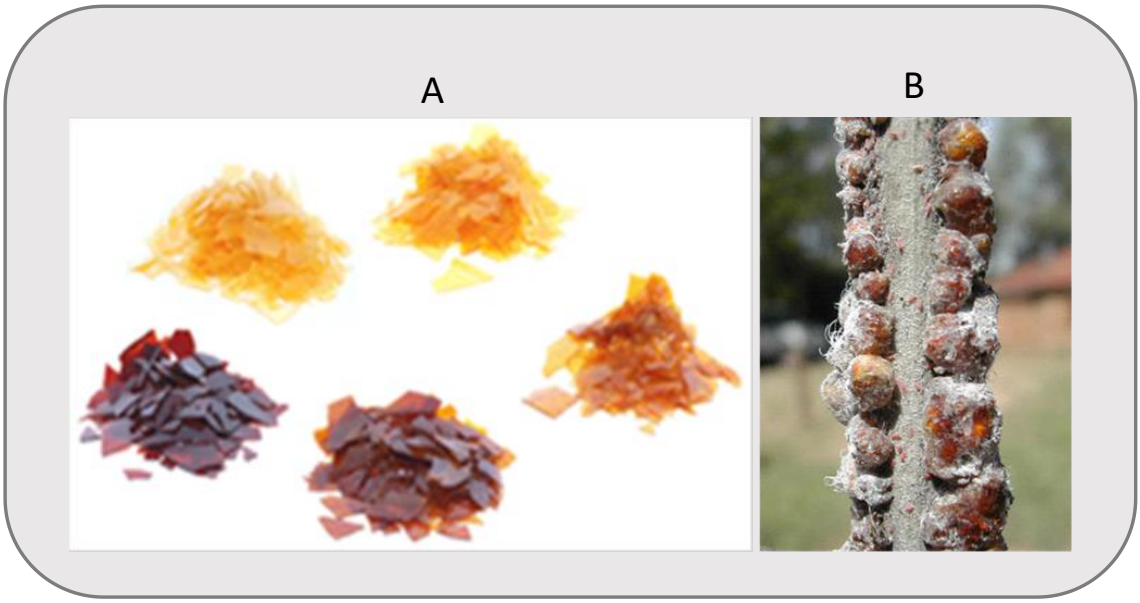

Figure 1.5: A) Different grades of purified shellac, B) Shellac resin on a tree branch by *Kerria lacca* [80]

1.5.3 Applications of Shellac

For many years shellac has been used as an ingredient in colours and lacquers,[81] as well as a protective layer for artistic objects[82, 83] and music instruments. It is also used in dentistry as a material for dental baseplates,[84, 85] and has been used as a varnish to decrease dental hypersensitivity as an epoxy resins modified with fluoride.[86, 87] Besides, these uses, shellac has been used as a coating material on confectionary and as a matrix material in so-called biocomposites for industrial applications.[81, 88-90] It is also used commercially as

a wood coating, a binder, food supplements, food additives (E904) and in cosmetic products as well as an encapsulate for pharmaceuticals.[91, 92] More recently it has been used as a barrier coating for fruits and vegetables against gases and moisture.[93] Traditional Chinese medicine used shellac for the treatment of measles, macula, scabies and antidote for poisons due to its claimed biological activities as clearing heat, cooling blood and removing toxins.[94] Shellac has been widely used as a moisture barrier coating for pellets and tablets in the form of aqueous or alcoholic solutions because of its low water vapour and oxygen absorbance. But due to its low stability and solubility at intestine pH which is between 3.8 and 6.9, shellac has had limited use in pharmaceutical industry. Therefore, Limmatvapirat *et.al*, prepared an aqueous ammoniacal solutions of shellac by dissolving it with 2-amino-2-methyl-1-propanol (AMP) and ammonium hydroxide (AMN) at various ratios to be used to coat films in salt forms to enhance its stability and solubility. The aqueous solutions are easy to handle and have a low viscosity even at high shellac concentrations.[57] Another important application of shellac is microencapsulation,[95, 96] for example as an extra coating on gelatine microspheres,[97] when modified by esterification with glycerol to improve encapsulation properties.[98-100] Xue and Zhang produced and characterised calcium–shellac microspheres loaded with carbamide peroxide (CP) as a tooth whitening age.[101] As drug delivery system, shellac has seldom been used as colloidal nanoparticle, Patel *et.al*.[102] prepared shellac NPs with average particle sizes from 150 nm to 300 nm using a xanthan gum polymer as stabilizer, these NPs were loaded with silibinin (as an acid unsteady bioactive compound) for oral administering to be released in the gastro-intestinal pHs. Also, shellac with polyvinylpyrrolidone (PVP) has been successfully used to fabricate core-shell nanoparticles which were loaded with ferulic acid (FA) using a coaxial electrospraying process. These NPs had a particle diameter of 530± 80 nm with a clear core-shell structure.[103] Kraisit *et al*.[61] used chitosan as a stabiliser to prepare shellac nanoparticles with a size range between 100 to 300nm. The ionic cross-linking method was followed to prepare the nanoparticles which were then encapsulated with bovine serum albumin. Moreover, Krause and Muller prepared an aqueous shellac dispersion using techniques like high pressure homogenisation; the obtained particle size was rather large (~5µm).[104]

1.6 Surfactants

Surfactants are organic materials, which play a role in decreasing the surface tension of water at low concentrations. They are absorbed mainly on the surface of the solution creating a thin monolayer and are known as surface active substances. Surfactants have an important role in industrial processes and products, such as the production and processing of foods, agrochemicals, pharmaceuticals, cosmetics, laundry products, paints, petroleum, mineral ores, coatings and adhesives, photographic films, and in fuel additives and lubricants. Surfactants have also found wide application in biological and medical systems, soil remediation techniques, as well as another environment, health, and safety applications. The dissolved surfactants at a certain value of concentration will begin to assemble and organise themselves into more complex units, called micelles. This characteristic concentration, where the assembling process begins, is known as the critical micelle concentration CMC, and this occurs due to the existence of both hydrophobic and hydrophilic groups in each surfactant molecule, and this micelles formation gives surfactants excellent detergency and solubilization properties.[105]

Surfactants can be classified according to the charge present in the hydrophilic part of the molecule (after dissociation in aqueous solution). Figure 1.6 shows various types of surfactants.[106]

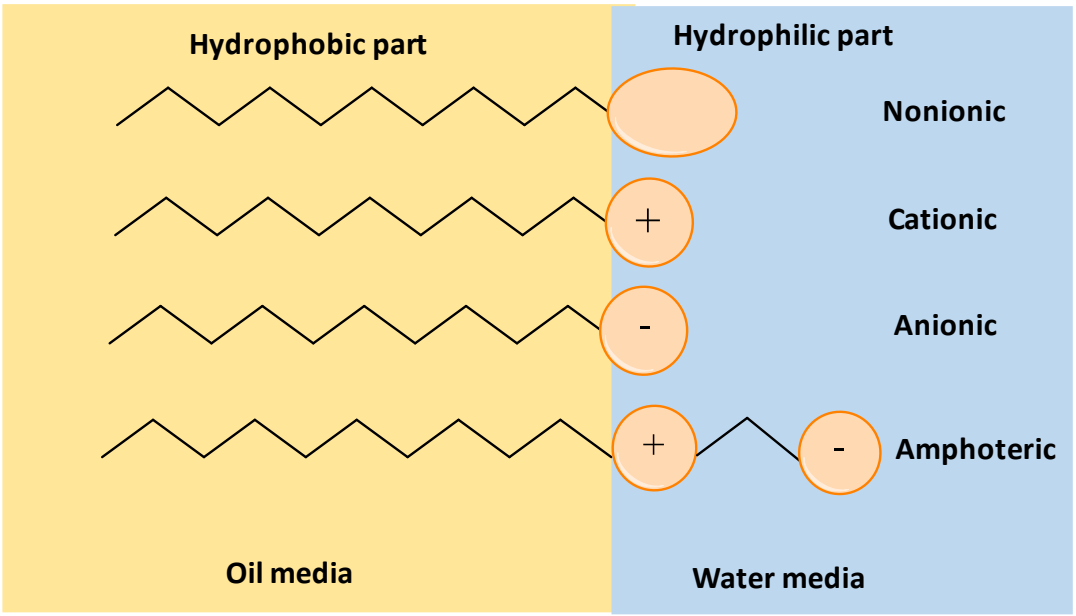

Figure 1.6: A schematic shows different types of surfactants.

Anionic Surfactants these surfactants have an amphiphilic anion, and a cation parts, which are dissociated in water providing an alkaline metal (Na^+, K^+) or quaternary ammonium. They are the most commonly used surfactants, and account for about 50 % of the world production such as alkylbenzene sulfonates (detergents), (fatty acid) soaps, lauryl sulfate (foaming agent), di-alkyl sulfosuccinate (wetting agent), lignosulfonates (dispersants) etc.

Cationic Surfactants are dissociated in water into an amphiphilic cation and an anion part, most frequently a halide. An enormous amount of this class relates to nitrogen compounds such as fatty amine salts and quaternary ammoniums, these surfactants have one or more long chain of the alkyl type, often coming from natural fatty acids. These surfactants have commercial importance such as in corrosion inhibition. If the surfactant molecule exhibits both anionic and cationic dissociations, it is called amphoteric or zwitterionic. Betaines and sulfobetaines are examples of synthetic products while aminoacids and phospholipids are a case of natural substances.

Nonionic Surfactants These are non-ionized in aqueous solution since their hydrophilic group is of a non-dissociable type, such as alcohol, phenol, ether, ester, or amide. Many of these nonionic surfactants have hydrophilic polyethylene glycol chain. Polyethylene oxide is prepared using the polycondensation method, and the surfactant is known as polyethoxylated nonionics. Block copolymers, which are one of the nonionic surfactants and usually involved in a various class, e.g. polymeric surfactants. The non-ionic water-soluble polymers and surfactants are getting increased attention as they are milder and environmentally friendlier. In this project Poloxamer 407, a nonionic copolymer was used as a stabilizer for shellac particles depending on steric repulsion among the shellac particles surrounded by Poloxamer 407 micelles in water.

1.6.1 Poloxamer 407

Poloxamer 407 (P407) is an amphiphilic non-ionic block copolymer surfactant, with a molecular weight of about 12,600 (9,840-14,600) g/mol, available by the registered trademark of Pluronic F127\ (BASF Laboratories, Wyandoote, USA) and Synperonic PE/ F127 (Croda International Plc, USA).[107, 108] These copolymers consist of ethylene oxide (EO) and propylene oxide (PO) blocks organized in a triblock structure poly (ethylene oxide)$_a$ – poly (propyleneoxide)$_b$ – poly(ethyleneoxide)$_a$ $(PEO)_a$–$(PPO)_b$–$(PEO)_a$ with

chemical formula of $HO[CH_2\text{-}CH_2O]_a\ [CH(CH_3)\text{-}CH_2O]_b\ [CH_2\text{-}CH_2O]_aOH$, (a=101, b=56), containing approximately 70% PEO and 30% PPO, Figure 1.7. P407 is more soluble in cold water than hot because at low temperature the solvation and hydrogen bonding increase.[109] At 20 to 30% w/w concentrations of P407 in aqueous solution reverse thermal gelation is seen.[110] It is liquid at low temperatures (4-5° C), but it becomes a gel when warming to room temperature (20°C).[111] Poloxamer 407 can be prepared by sequential polymerisation of PO and EO monomers in the presence of sodium or potassium hydroxide then purified using chromatographic fractionation.[107]

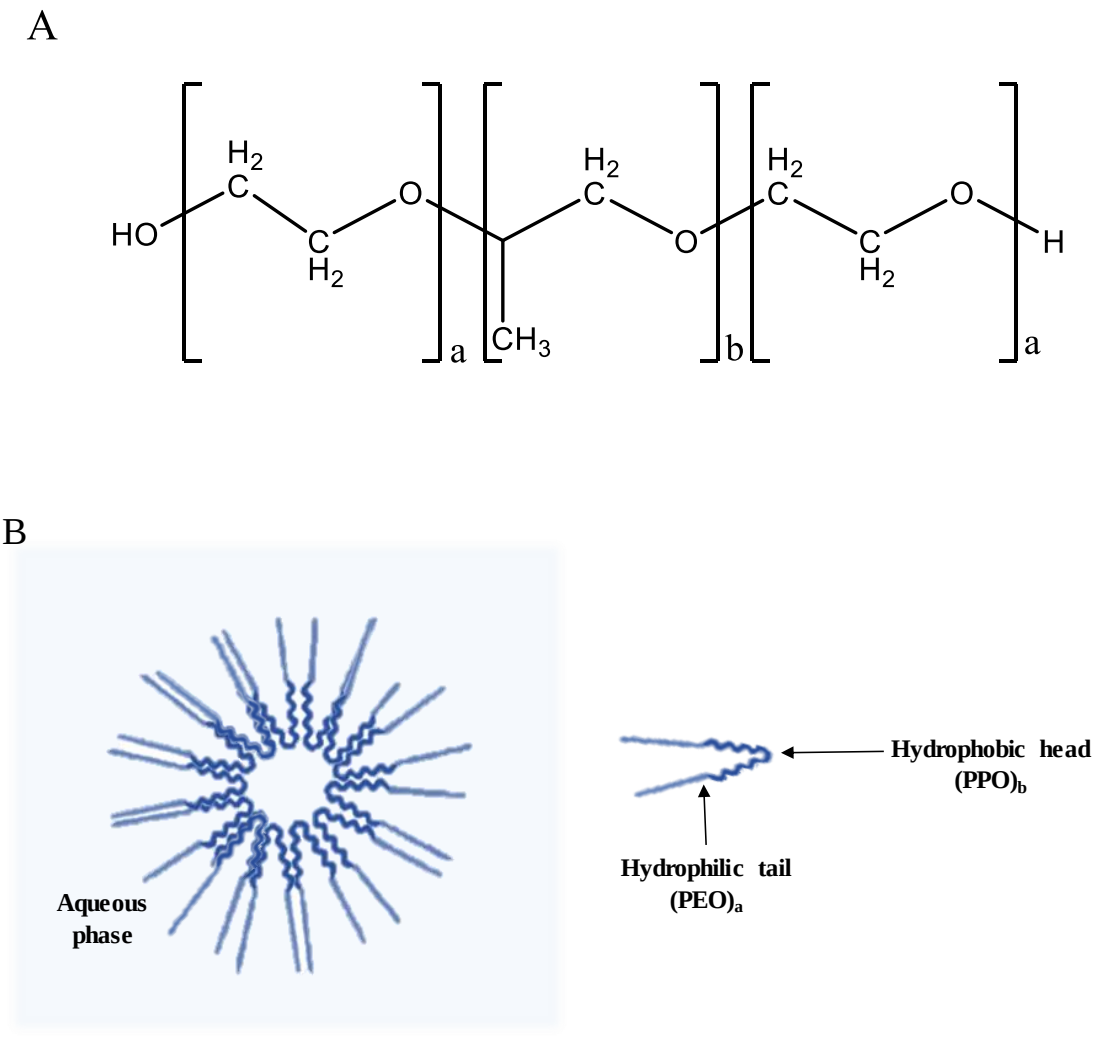

Figure 1.7: A); Chemical structure of the Poloxamer 407 surfactant block copolymer B); Proposed scheme for micelles of P407 in aqueous media shows the hydrophilic tail and hydrophobic head.

Poloxamer 407 has been used since the 1950s in industrial and pharmaceutical preparations and has been widely used in the formulation of medications due to its low toxicity. As the FDA guide has presented Poloxamer 407 as an inactive ingredient for different kinds of preparations for inhalation, as an oral solution, suspensions and ophthalmic or topical formulations.[112] Poloxamer 407 gel have been suggested as potential topical drug delivery systems owing to its advantages over traditional bases regarding ease of application, and drug release characteristics. Many studies have been carried out on the development of topical/dermal formulations comprising analgesic or anti-inflammatory drugs due to the possibility of delivering these drugs through the skin for local pain and inflammation at low doses.[113-118]. In this study, P407 was used in this project as a stabilizer for preparing shellac nanoparticle as drug delivery nanocarrier for wound dressing, due to its ability to surround shellac particles and disperse them in aqueous solution owing to the steric repulsion property. In the literature, Shellac was prepared as a tablet with Poloxamer 407 in its matrix comprising hydrophobic or hydrophilic drugs using the molten technique. Differential scanning calorimetry (DSC), powder X-ray diffractometry (PXRD) and thermogravimetric analysis (TGA) techniques were used to characterize the tablet, while drug release was studied in distilled water at 50 rpm and 37°C.[119]

1.7 Antibacterial and Antibiotics

An antimicrobial is the general name that called on an agent that kills microorganisms or ends their growth. While Antibiotics or antibacterial agents are a kind of antimicrobial that used to treat and prevent the bacterial infection. [120, 121] Also, disinfectants and antiseptics agents are kinds of antimicrobial agents. Antiseptics agents are used to reduce infection during surgery against living tissue, while disinfectants are used to kill many kinds of microbes on non-living surfaces or to inhibit the spread of illness. [122]

According to the microorganisms that antimicrobial agents act principally against, antimicrobial medicines can be grouped. For instance, antibiotics are used to kill bacteria while to kill fungi, antifungals are used. Also, they can be classified according to their function. Microbicidal are agents that kill microbes, while those that only prevent their growth are called biostatic. Antimicrobial chemotherapy is a term usually used for antimicrobial medicines that treat infection, whereas if these medicines used to prevent infection is called antimicrobial prophylaxis.[123]

In this project different kinds of antimicrobial agents included; berberine as antibacterial agent, chlorhexidine; as antiseptic agent, curcumin the natural antimicrobial agent, and vancomycin the antibiotic agent which have been used in dermal formulations. Basically, antibiotics can save lives and are effective in treating diseases caused by bacterial infections. However, like all drugs, they have the potential to cause undesirable side effects. Many of these side effects are not dangerous, although they can make life miserable while the drug is being taken. In general, antibiotics rarely cause serious side effects. The most common side effects from antibiotics are vomiting, diarrhea, and nausea. Fungal infections of the mouth, digestive tract and vagina can also occur with antibiotics because they destroy the protective 'good' bacteria in the body.[124] Table 1.1 shows some natural and synthetic antimicrobial agents which are frequently used in topical or dermal formulations with their physicochemical properties, bactericidal action and some disease treatment.

Table 1.1: Some topical antimicrobial agents with their physicochemical properties and their antimicrobial effect and treatments.

Antimicrobial agent	**Physicochemical properties**	**Bactericidal actions**	**Disease treatment**	**Ref**
Berberine chloride	Natural antibiotic, moderately soluble in methanol, slightly soluble in ethanol, and very slightly soluble in water	Antifungal, such as *Candida albicans*, *Candida tropicalis, and Mycobacterium smegmatis.* Antibacterial against gram-negative bacteria like *Staphylococcus aureus*, *Entamoeba histolytica*, and *Leishmania donovani.*	Diabetes, skin treatment, arrhythmia, hypertension, and gastrointestinal diseases. Its potential chemotherapeutic ability against cancers, reduce the metastasis of human gastric cancer, bone cancer, prostate cancer, and breast cancer.	125-128
Chlorohexidine di-gluconate	Synthetic antiseptic, colourless, odourless with bitter taste, strong base, and soluble in water.	Against Gram-negative and Gram-positive bacteria, yeasts, fungi, some viruses including Human Immunodeficiency Virus.	Oral antiseptic inhibit plaque growth and prevent the gingivitis, skin cleanser, in disinfection of operation fields and treatment of burns.	129-131
Hydrogen peroxide	Disinfectant and antiseptic agent, colourless liquid solubile in water.	Against viruses, gram-positive more than gram-negative bacteria, yeasts, and bacterial spores.	Control external bacteria and parasites in wounds, bacterial gill disease in rainbow trout *(Oncorhynchus mykiss).*	122, 132
Curcumin	Natural yellow coloured powder, insoluble in water, quite soluble in organic solvents	Gram-positive bacteria and the Gram-negative bacteria like; *Salmonella typhimurium* and *Escherichia coli.*	Block tumour initiation, transformation, invasion, tumour promotion, metastasis and angiogenesis, skin ailments, like psoriasis, skin carcinogenesis, dermatitis and scleroderma.	133-136
Silver	White and brilliant metal, ductile and malleable, high electrical and thermal conductivity and low contact resistance	Against a broad spectrum of bacteria, viruses, and fungi, Gram-positive pathogens such as *Staphylococcus aureus,* a low prevalence of Ag^{+} resistance in Gram-negative pathogens	Controlling bacterial growth in dental work, catheters, and burn wounds.	137-139
Honey	Natural antibacterial agent, sweet viscous liquid,	Against wide range of bacteria, fungi, and viruses.	Heals wounds arising from trauma and surgery, burns, and cough	140, 141

1.7.1 Berberine Chloride

Berberine chloride (molecular formula $C_{20}H_{19}NO_5$.HCl and a molecular weight of 371.81 g.mol^{-1}) (Figure 1.8) is an isoquinoline alkaloid antimicrobial existing in the roots, rhizome, and stem bark of number of commonly therapeutic plant species such as *Berberis vulgaris* (barberry), *Hydrastis Canadensis* (goldenseal) (Ranunculaceae), *Coptis Chinensis* (Coptis or goldenthread) (Ranunculaceae), *Arcangelisia flava* (Menispermaceae), *B. aquifolium* (Oregon grape), and *B. aristata* (tree turmeric). It is bright yellow under ultraviolet light, and has a weak characteristic odour, with a bitter taste. Berberine is moderately soluble in methanol, slightly soluble in ethanol, and very slightly soluble in water. Berberine belongs to the structural class of protoberberines.[142, 143] *Coptis Chinensis* (*Rhizoma coptidis*) and Baical Skullcap Root (*Radix Scutellaria*), which comprise of a large amount of berberine and other protoberberines, have been widely recommended by traditional Chinese physicians as heat-clearing and detoxicating medicine for thousands of years. Berberine activity was widely studied in the 20th Century and it was found to possess a significant pharmacological and biological activity having antimicrobial, antihelmintic, anti-inflammatory, and anti-oxidative effects.[126-128] Moreover, due to the beneficial properties of berberine, it has been suggested that this may also affect other diseases such as diabetes, arrhythmia, hypertension, and gastrointestinal diseases.[125] A modern study has shown its potential chemotherapeutic ability against cancers.[144] It has been reported that berberine has an ability to reduce the metastasis of human gastric cancer, bone cancer, prostate cancer, and breast cancer.[145-148]. Fukudaa *et al.* found that berberine can inhibit the enzyme cyclooxygenase-2 (COX-2) which is expressed in colon cancer cells abundantly and acting an important role in colon tumorigenesis. The genera *Coptis* and *Berberis* efficiently inhibit COX-2 transcriptional enzyme activity in colon cancer cells at concentrations more than 0.3 μM.[149]

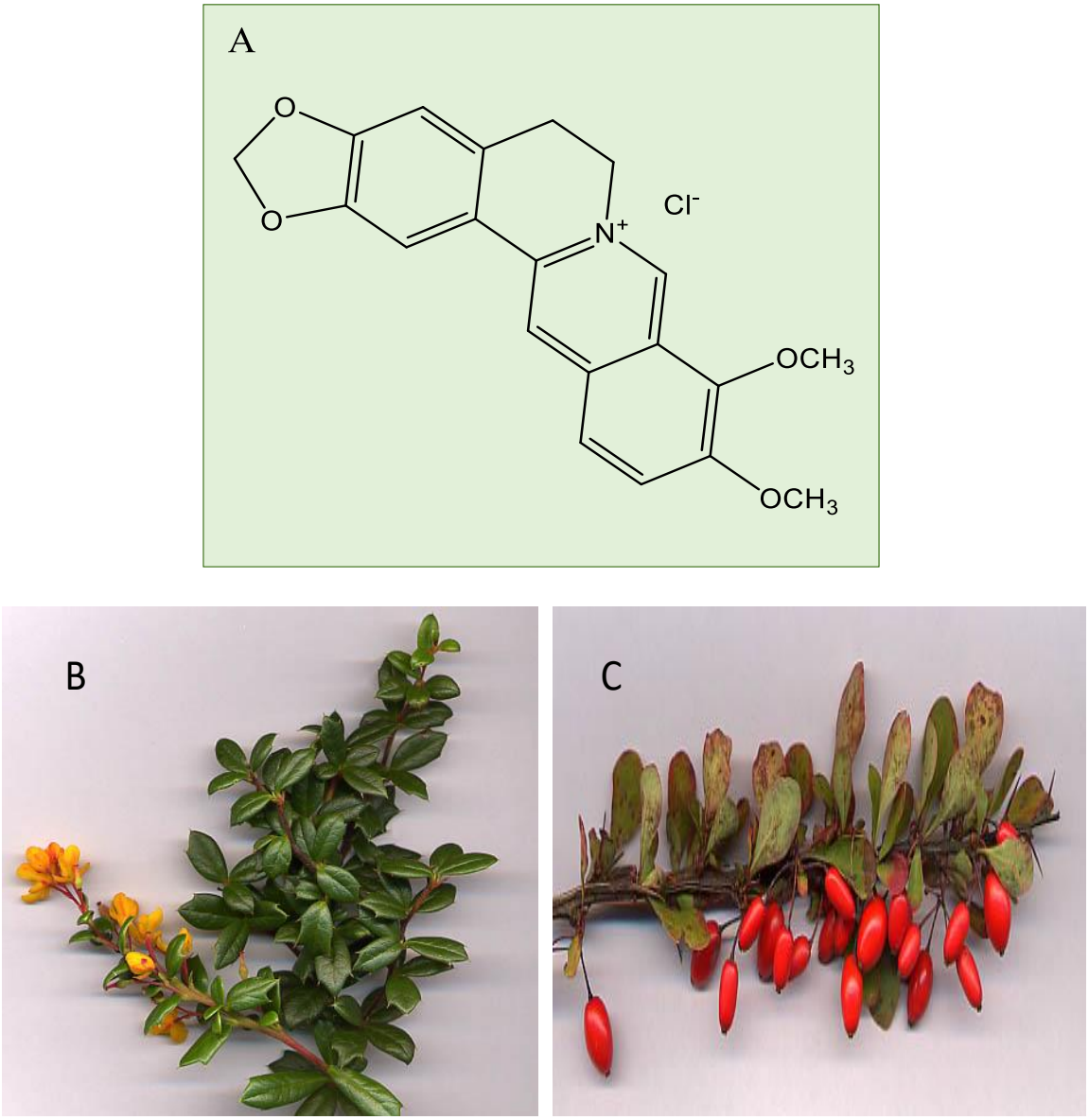

Figure 1.8: A) the chemical structure of berberine chloride, B) Berberis darwinii shoot with flowers, C) Berberis thunbergii shoot with fruit.[150]

1.7.2 Nanoencapsulation of Berberine

After observing all these properties of berberine, researchers decided to encapsulate it in NPs for drug delivery facilitation, to overcome its poor solubility in aqueous medium, low absorption in the gastrointestinal tract, and quick body metabolism and to enhance bioavailability and to sustained drug release.[151] Berberine has been reported to be incorporated in drug delivery systems based on liposomes, solid lipid nanoparticles and nanoemulsion.[152] Several approaches have been used to prepare berberine hydrochloride liposomes, such as the active loading method, the thin film evaporation method and a combination of the active loading and thin film evaporation methods.[152] By using thin film evaporation and an active loading method berberine hydrochloride was encapsulated within liposomes with average size of 2.2–3.5 μm, and encapsulation efficiency 78.51% ± 2.45%, with a loading drug ratio of 30.21.[153] Solid lipid nanoparticles (SLNs) can be prepared from biodegradable solid lipids using mixture of lipid materials: glycerol tripalmitate: soybean phospholipid (1:6:6). These nanoparticles had good stability with a mean diameter of 76.8 nm and zeta potential of 7.87 mV, the drug loading percent was 4.2%, with encapsulation ratio of 58%. BBR-SLNs at high dose (100 mg/kg) showed more potent effects when compared to an equivalent dose of BBR.[154] Using also a high-pressure homogenization method, [155] berberine hydrochloride (BH) was loaded within solid lipid nanoparticle (SLN) using glyceryl monostearate, a stable BH-loaded SLNs system was developed with an average particle size of 81.42±8.48 nm and ζ- potential of -28.67±0.71 mV. The significant slower release of BH from SLNs than free BH was achieved with appropriate drug entrapment efficiency of 70.33±1.53 and loading drug ratio of 2.85±0.04. *In vitro* study was applied on breast cancer MCF-7 cells, HepG 2, and A549 cancer cells. BH-loaded SLNs showed significant inhibition of these cells.[156] Khemani *et al.* loaded berberine onto polylactide glycolic acid nanoparticles using biodegradable poly (D, L-lactide-co-glycolide) with ratio of 75 : 25 by single emulsion as well as multiple emulsion solvent evaporation techniques with size range 180–310nm. The NPs were dispersed with mean particle size of 267.9 nm. The encapsulation was 65% out of which 56.8% drug was released within 6 hours in 0.9% NaCl. [157] Moreover, berberine chloride has been entrapped with O-hexadecyl-dextran nanoparticles (BC-HDD NPs), and these were evaluated for their cytoprotective efficacy in high glucose stressed primary hepatocytes, the obtained results compared with large berberine chloride (BBR) treatment. This study showed that BC-HDD NPs were as effective more than as BBR in inhibiting high glucose induced oxidative stress, mitochondrial depolarization and downstream events of apoptotic cell

death.[158] Table 1.2 shows some characteristics of berberine loaded with different nanocarriers.

Table 1.2: Characteristics of the formulation of BRB within nanocarriers.

Nanocarrier used to load BRB	**Particle size (nm)**	**Zeta potential (mV)**	**E.E %**	**loading drug %**	**Ref.**
Liposomes	2200-3500	-	78.51	30.21	153
SLNs using lipid materials: glycerol tripalmitate: soybean phospholipid	76.8	7.87	58	4.2	154
SLNs using glyceryl monostearate	81.42	-28.67	70.33	2.85	156
Polylactide glycolic acid	267.9	-	65	-	157
O-hexadecyl-dextran	238	-	24.28	-	158
PEG–lipid–PLGA NPs/BBR–SPC	149.6 ± 5.1	-26.8 ± 0.9	89	-	159

As can be seen in table 1.2, berberine was loaded within natural nanocarriers but not all of thier *in vitro* characteristics were achieved, and most of these nanocarriers have negative surface charge which decrease the attraction between them and the cell membrane. In this project the aim was to construct a nanocarrier consists of different components and systematically studied by characterising the size, zeta potential, encapsulation efficiency, drug release, and drug content as well as the cytotoxicity of each component on different microorganisms. Shellac NPs which contain carboxylic groups as well as hydrophobic part were used to be loaded with berberine. These NPs were stabilised by Poloxamer 407 micelles by conducting steric repulsion between the particles, which can also play a synergistic effect as antibacterial, as it has been used as topical/ dermal formulation.[112] Besides, these nanocarriers can be coated with cationic electrolyte to inverse the surface charge from negative to positive and this can promote the adhesion with the cell membrane with balancing the stability at the same time. The positive charge of the nanocarrier allow

it to deliver and boost antibacterial agents at any type of microorganisms and at low amount near or inside the cell vicinity. All these characteristics allow the nanocarrier to amplify the efficiency of encapsulated berberine more than 10 times than the free berberine.

1.7.3 Chlorhexidine Di-gluconate

Chlorhexidine di-gluconate (1E)-2-[6-[[amino-[(Z)-[amino-(4-chloroanilino) methylidene]amino]methylidene]amino]hexyl]-1-[amino-(4-chloroanilino) methylidene] guanidine (figure 1.9) has a molecular formula of $C_{22}H_{30}Cl_2N_{10}$. 2 $C_6H_{12}O_7$ with a 897.8 $g.mol^{-1}$ molecular weight. It is a synthetic colourless topical antiseptic and disinfectant has been made industrially since 1954. Chlorhexidine is a chlorophenyl-bis-biguanide symmetrical molecule having two chloroguanide chains joined by a hexamethylene chain. It is a strong base, and at physiological pH is dicationic. It is usually insoluble in water, so it formulated with either acetic acid or gluconic acid to form water-soluble diacetate or di-gluconate salts. Its solutions have neither colour nor odour but have a very bitter taste.[160] Chlorhexidine can be found in three formulas; the di-gluconate, acetate and hydrochloride salts. Many studies and most oral formulations and products have used the di-gluconate salts, which is made as 20% v/v concentrate.[161] Chlorhexidine di-gluconate is a safe, well-known as antiplaque and antigingivitis agent and is commonly used as chemotherapeutic in the treatment of periodontitis, presenting an action against Gram-negative and Gram-positive bacteria, yeasts, fungi, some viruses including Human Immunodeficiency Virus and Hepatitis B virus. It also has an action against Streptococcus mutants by making its nature as an anticariogenic. Studies have also revealed that chlorhexidine is able to neutralize pathogenic agents such a Porphyromans gingivalis, *Streptococcus aureus* and *Prevotella intermedia*.[162-164] One of the most important properties of chlorhexidine is its oral retentiveness which depends on different factors like temperature, pH, concentration and the solution contact time with oral structure.[165] To inhibit plaque growth and prevent the gingivitis, a 0.2% solution of chlorhexidine gluconate can be used for mouth rinsing twice a day for 1 min.[166] Chlorhexidine has a few side effect including brown discolouration of the teeth, tongue dorsum, and bitter taste, as well an oral mucosal erosion and an idiosyncratic reaction may occur, and this depends on the dose. Chlorhexidine shows poor absorption in the gut with very low toxicity without any teratogenic alterations. There is no sign of carcinogenic substances formation.[167, 168]

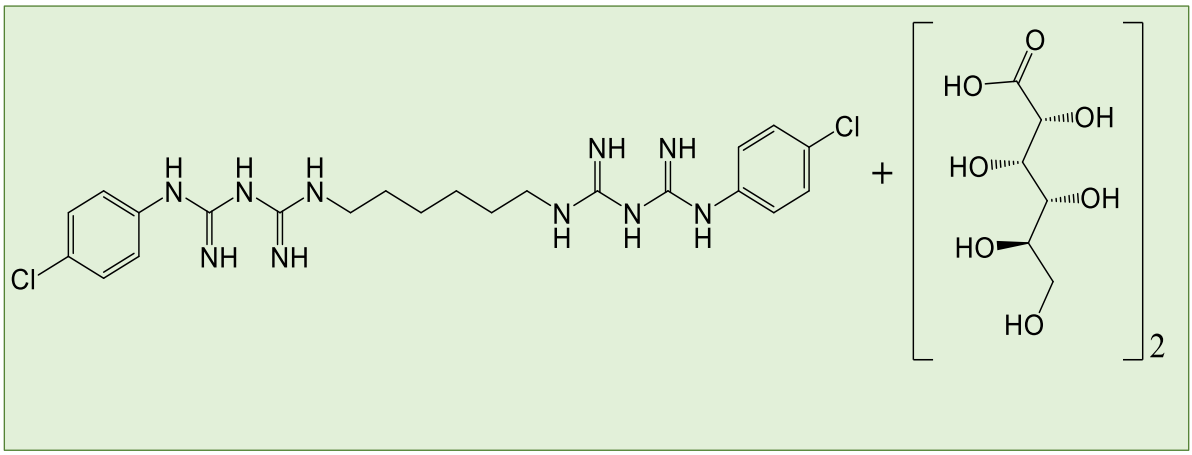

Figure 1.9: The chemical structure of chlorhexidine di-gluconate.

1.7.4 Nanoencapsulation of Chlorhexidine

To minimize problems resulting from using large dosage of chlorhexidine and instead of looking for another antiseptic, researcher decided to use chlorhexidine as nano and at low dosage with long sustain release. The sustained bactericidal activity of chlorhexidine base loaded poly(ϵ-caprolactone), PCL, nanocapsules against *Staphylococcus epidermidis* vaccinated onto porcine ear skin has been investigated. Interfacial polymer deposition following solvent displacement was used to prepare chlorhexidine loaded nanocapsules. After that the nanocapsules were characterized by photon correlation spectroscopy, electrophoretic measurements, transmission and scanning electron microscopy. The results displayed that chlorhexidine nanocapsules in aqueous suspension had a 200–300 nm size and a positive charge. These showed similar minimum inhibitory concentrations against several bacteria with chlorhexidine di-gluconate aqueous solution.[169] A single emulsion, solvent evaporation technique was used to prepare microparticles with poly (dl-lactic-co-glycolic acid), chlorhexidine di-gluconate and a linking complex of either methylated-*β*-cyclodextrin or hydroxypropyl-*β*-cyclodextrin. The encapsulation efficiency and release of the chlorhexidine derivatives from the microparticles was found to be a function of the lipophilicity of the cyclodextrin. Complexation of the poorly water soluble chlorhexidine free base with the more hydrophilic hydroxypropyl-*β*-cyclodextrin showed a 62% higher encapsulation efficiency and longer period of sustained release over a 2-week duration than complexation with the more lipophilic methylated-*β*-cyclodextrin.[170] Seneviratne *et al.* reported a novel procedure

for preparation of mesoporous silica nanoparticle encapsulated with pure (non-salt form) chlorhexidine, namely nano- chlorhexidine; and showed their morphological profile and mechanical properties. Its antimicrobial properties have been expansively characterized by using planktonic bacteria, mono-species and mixed-species models of oral biofilms.[171] Chlorhexidine hexametaphosphate nanoparticles (CHX HMP NPs) was produced with a total equivalent concentration of CHX to 5.0 mM to be used to coat the dental implants. The CHX HMP NPs had average diameter of 49 nm with composition showing the presence of both phosphorus and chlorine. CHX HMP NP was coated with titanium by depositing then immersing the NPs in pure grade II titanium substrates for 30 s. CHX HMP NP-coated titanium surfaces displayed antimicrobial action against oral primary colonising bacterium *Streptococcus gordonii* within 8 hours. The antimicrobial efficacy was greater in the presence of an acquired pellicle which is postulated to be due to retention of soluble CHX by the pellicle.[172] Table 1.3 shows some of the characteristics of chlorhexidine loaded with different nanocarriers. These nanocarrier either provide high encapsulation efficiency with big particle size or small particle size with low encapsulation efficiency and drug loading content, as well as not all of them were systematically addressed. In the present study, CHX is aiming to be loaded within a nanocarrier at high efficiency and drug loading content and systematically studying by addressing the size, zeta potential, drug release, E.E%, and the drug loading contents as well as the cytotoxicity of each component included in the nanocarrier construction. Also the components of these nanocarriers which consist of shellac, the natural material which contains carboxylic groups that electrostatically attract with CHX molecules and allow to sustain the CHX release for long period. Moreover the presence of P407 as stabilizer agent as well as its role in topical formulations.[112] Furthermore, these nanocarriers loaded with CHX can be functionalized by changing the surface charge from negative to positive using cationic electrolyte which stimulated them to be attracted fast to different kind of cells. These stable nanocarriers allow the CHX to be released directly into the cell membrane and boost the cytotoxic action more than the free CHX by 10 times.

Table 1.3: Characteristics of the formulation of CHX with different nanocarriers.

Nanocarrier used to load CHX	**Particle size (nm)**	**Zeta potential (mV)**	**E.E %**	**loading drug %**	**Ref.**
Poly(ε-caprolactone) nanocapsules (nano-PCL)	273 ± 2.6	24.1 ± 3.3	89.57 ± 2.8	13.17 ± 2.9	173
Calcium phosphate carboxymethyl cellulose NPs	150-200	-37±6	13.1	-	174
Poly(ε -caprolactone) NPs	89.5±1.2	38.86±0.9	60±0.1	-	169
Poly(ε-caprolactone) F1 NPs	198.8	-	45.0 ± 0.5	5.6	175
Hexametaphosphate (0.5 $mmol.L^{-1}$)	81	-45	-	-	176

1.7.5 Curcumin

Curcumin (CUR), is (diferuloylmethane; 1,7-bis[4-hydroxy-3-methoxyphenyl]-1,6-heptadiene -3,5-dione), with a chemical formula $C_{21}H_{20}O_6$, and molecular weight of 368.38 $g.mol^{-1}$. It is natural products found in (*Curcuma longa* L.) turmeric plant and widely used botanical in South Asian culinary and natural medicinal practice. Curcumin is not the only curcuminoid found in turmeric; it is typically accompanied by two minor curcumin analogues, demethoxycurcumin and bisdemethoxycurcumin. [177, 178] It is a food additive and has an E number (E100). Curcumin displays keto-enol tautomerism, in acidic and neutral solutions it has a major keto form, while in the alkaline medium a stable enol form, (figure 1.10).[179] Many littteratures have shown that curcumin exhibits anti-inflammatory, antioxidant, and anticarcinogenic activities.[180-188] Thousands of citations prove that curcumin shows an ability to suppress inflammations. Curcumin was found to be at least ten times more active than even vitamin E as an antioxidant, it inhibits lipid peroxidation and prevents the haemoglobin oxidation.[189] Recent reviews showed that curcumin has anticancer properties in several different systems, it showed an ability to block tumour initiation, transformation, invasion, tumour promotion, metastasis and angiogenesis. It also

suppresses carcinogenesis of the skin, colon, forestomach, and liver in mice as well as mammary carcinogenesis. Moreover, curcumin can inhibit the proliferation of many tumour cells, such as colon carcinoma, T-cell and B-cell leukaemia, breast carcinoma and epidermoid carcinoma.[190] Curcumin is effective against myocardial infarction and atherosclerosis.[133] Regarding skin disease, curcumin has been shown to be active against various skin ailments, like psoriasis, skin carcinogenesis, dermatitis and scleroderma.[134, 135] Furthermore, curcumin has been shown that it reduced blood sugar, glycosylated haemoglobin and haemoglobin levels in an alloxan-induced diabetic type II rat model.[133] Curcumin shows effectiveness against Rheumatoid Arthritis,[133] multiple Sclerosis,[133] Alzheimer's disease,[191] inflammatory bowel disease,[192] cystic fibrosis[193] and many others.[133] (figure 1.11)[194]

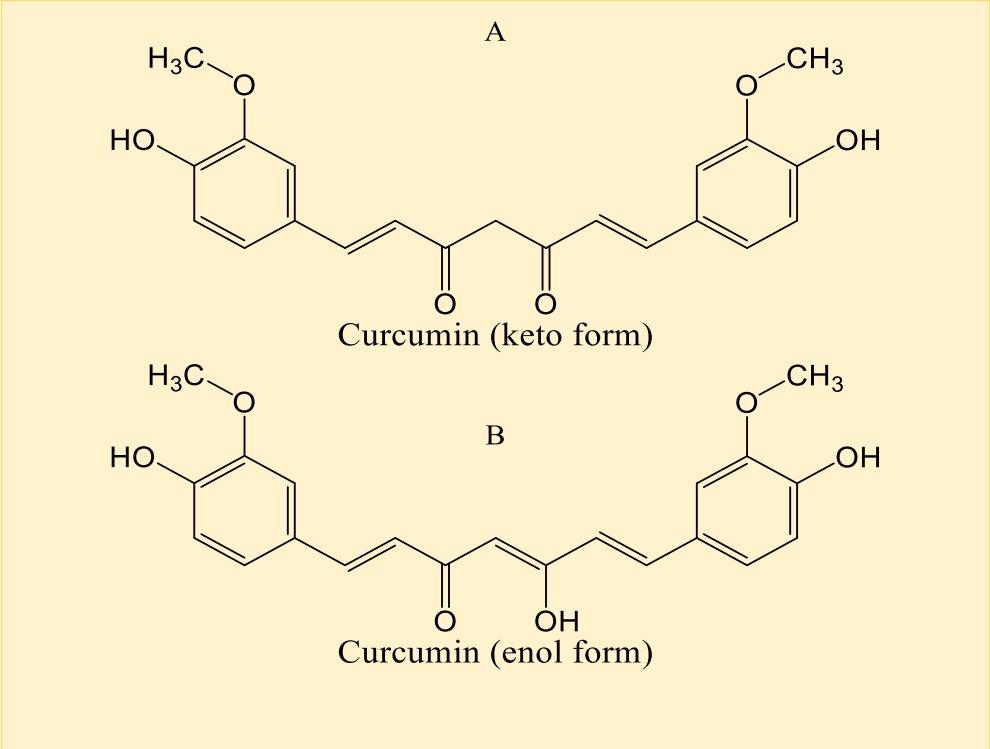

Figure 1.10: The chemical structure of curcumin. A) in acidic and natural medium, B) in alkaline medium.

Figure 1.11: Some diseases that potentially treated by curcumin[194]

1.7.6 Nanoencapsulation of Curcumin

Clinically, curcumin is safe even at a high dose up to (12 g/day),[195] and due to the hydrophobic nature curcumin is insoluble in water. Therefore it shows poor bioavailability, rapid metabolism, poor absorption and rapid systemic elimination.[179] To enhance the curcumin bioavailability many attempts have been developed to encapsulate curcumin within the delivery systems such as biodegradable microspheres, liposomes, polymeric and lipo-NPs, hydrogels and cyclodextrin.[196-203] Curcumin was nanoformalted within three biocompatible polymers, chitosan, pluronic and alginate using ionotropic pre-gelation then by polycationic cross-linking to be delivered to cancer cells. The particles showed spherical shape with an average size of 100 ± 20 nm using scanning electron microscopy and atomic force microscopy. Curcumin encapsulation efficiency (%) in composite NPs increased considerably over ALG-CS NPs without pluronic. At 500 μg mL^{-1} of curcumin

composite NPs, cytotoxicity assay showed they were nontoxic to HeLa cells.[204] Liposomes are considered a good transformer for many hydrophilic and/ or hydrophobic drugs or compounds as they consist of a phospholipid bilayer with an aqueous core. In recent years curcumin has been formulated with many liposomes, using the film evaporation technique, curcumin was loaded within liposomes consisting of dihexyl phosphate (DHP), cholesterol and egg yolk phosphatidyl choline (EYPC). Curcumin was solubilised in the lipophilic bilayer due to its lipophilicity, this was proved by using fluorescent probes, and the curcumin was positioned at the hydrophobic acyl side chain and located adjacent to the glycerol groups. Cationic lipid/polymer conjugate N-dodecyl chitosan-N-[(2-hydroxy-3-trimethylamine) propyl] (HPTMA) chloride has been used to coat liposomes with a size of 73 nm. Due to their cationic surface charge, these nanoparticles had the ability to attach to and penetrate the cells and release the sustained content in about 10 hours. The formulated NPs however only showed a slight improvement in cell killing action than free curcumin.[205] Curcumin also was encapsulated within various polymers, mostly biodegradable ones.[206] Due to its biodegradability and biocompatibility, Poly (D, L-lactic-co-glycolic)(PLGA) is commonly used for drug delivery purposes.[207-210] Curcumin was loaded on PLGA nanospheres using the emulsion-evaporation technique. The particles size obtained using PVA as a surfactant was 264 nm and 77% encapsulation efficiency was found with 15% loading curcumin capacity. The sustained release of curcumin loaded PLGA nanospheres was characterised with the rapid early release of about 24 % after 24 hours, after that a sustained release of 20% of the loaded curcumin was obtained through the followed 20 days. The *in vivo* results on rats showed that curcumin loaded nanospheres enhanced the curcumin oral bioavailability by 9 fold over the curcumin that was administered with piperine as the absorption improved.[211] Song *et al.* used solid dispersion technique to load curcumin into methoxy poly(ethylene glycol)-b-poly(Ɛ-caprolactone-co-p-dioxanone) as amphiphilic micelles. The Curcumin micelles had a small size of 30 nm with an entrapment efficiency of more than 95%, where the drug loading was 12%. These micelles showed slowly release of about 80% of curcumin content during 300 hours.[212] another way was used to increase the curcumin solubility by conjugating it to small amino acid molecules, as well as to both synthetic and natural hydrophilic polymers. Tang *et al*. succeeded in conjugating curcumin to two short oligo(ethylene glycol) chains through β-thioester bonds that are labile with the existence of esterases (Curc-OEG) and intracellular glutathione. The Curc-OEG conjugates particles contained 25 wt.% curcumin, the formed curcumin micelles have a size of 37 nm with release amount of conjugated curcumin less than 12% using hydrolysis during 24 hours at pH 5.0 and 7.4 which demonstrating good

stability of this nanomicelles in PBS.[213] Table 1.4 displays some of the *in vitro* characteristics of curcumin loaded with different nanocarriers, and as can be seen that curcumin was loaded with negatively charged nanocarrier which may repel with the cell membrane. In spite of the encapsulation efficiency of curcumin was good within these nanocarriers but in the present project curcumin can be encapsulated within shellac NPs at 100% and can be systematically studied. Although shellac nanocarrier consists of carboxylic groups it also has hydrophobic part, which provide a good environment for hydrophobic drugs. Moreover the presence of Poloxamer 407 which plays an essential role in stabilizing the NPs also has hydrophobic part which increase the encapsulation of curcumin and sustain its release for many days, which is considered a great factor when uses in wound bandages for long period. Furthermore, the surface of these nanocarriers can be functionalized by using cationic electrolyte to change the charge while maintaining the stability. The cationic nanocarriers will be able to attract to any kind of cells. These positively surface charged nanocarriers loaded with curcumin amplified the cytotoxic effect of curcumin higher than the free curcumin by more than 5 times.

Table 1.4: Characteristics of the formulation of CUR with different nanocarriers.

Nanocarrier used to load CUR	**Particle size (nm)**	**Zeta potential (mV)**	**E.E %**	**loading drug%**	**Ref.**
PLGA/Poloxamer	160 ± 31	-18.7 ± 1.3	90.0 ± 2.1	-	214
Poly (D, L-lactic-co-glycolic)	264	−4.27 ± 0.3	77	15	211
MPEG-P(CL-*co*-TMC) copolymer	27.6± 0.7	0.11±0.34	96.08±3.23	14.07±0.94	215
Alginate (ALG), chitosan (CS), and pluronic F127	100 ± 20	-	14.34	-	204
SLNs consists of stearic acid, Poloxamer, Dioctyl sodium sulfosuccinate, ethanol and lyophilized with mannitol.	450	-	70	-	216

1.7.7 Vancomycin Hydrochloride

Vancomycin (VCM) is a glycopeptide antibiotic produced from *Streptomyces orientalis* bacteria was first isolated in 1952, has the formula of ($C_{66}H_{75}Cl_2N_9O_{24}$) with a molar mass of (1449.25 g.mol^{-1}), (figure 1.12). [217, 218] It is an antibiotic agent against gram-positive bacteria acts by inhibiting the synthesis of the second stage of the cell wall, by binding to peptides that contain D-alanyl-D-alanine very tightly at the end of free carboxyl,[219] Furthermore, studies have revealed that VCM also changes the cell membrane permeability.[220] It is usually prescribed to treat the infections caused by methicillin-resistant Staphylococcus aureus MRSA or given to patients allergic to penicillin or cephalosporin.[221] Vancomycin is soluble in water but absorbed poorly after oral administration.[222] Consequently, it is used largely in intensive care units (ICU) to treat sepsis and hospital infections, as well as for empyema, endocarditis, pneumonia cases, soft tissue abscesses, osteomyelitis and others.[223-225] Owing to its side effects such as phlebitis, hypotension, nephrotoxicity, tachycardia, ototoxicity, chills, hypersensibility reactions, fever and exanthema, and the major concern of the complications of peripheral IV make this drug is the last resort.[223, 225-227] A study was conducted by Caroom et al.[228] using vancomycin powder to reduce the infections obtained after posterior cervical fusion surgery. The current study included 112 patients, control (n=72) and intervention (n=40) groups and they were similar with regard to body mass index, age, estimated blood loss, comorbidities and operative time. The results showed that the risk of surgical site infection SSI was reduced when vancomycin used in multilevel fussed posterior cervical-instrumented for cervical spondylotic myelopathy CSM. The study supported the other studies which confirm that placing vancomycin powder in the wound can decrease the occurrence of postsurgical wound infections.[229-231]

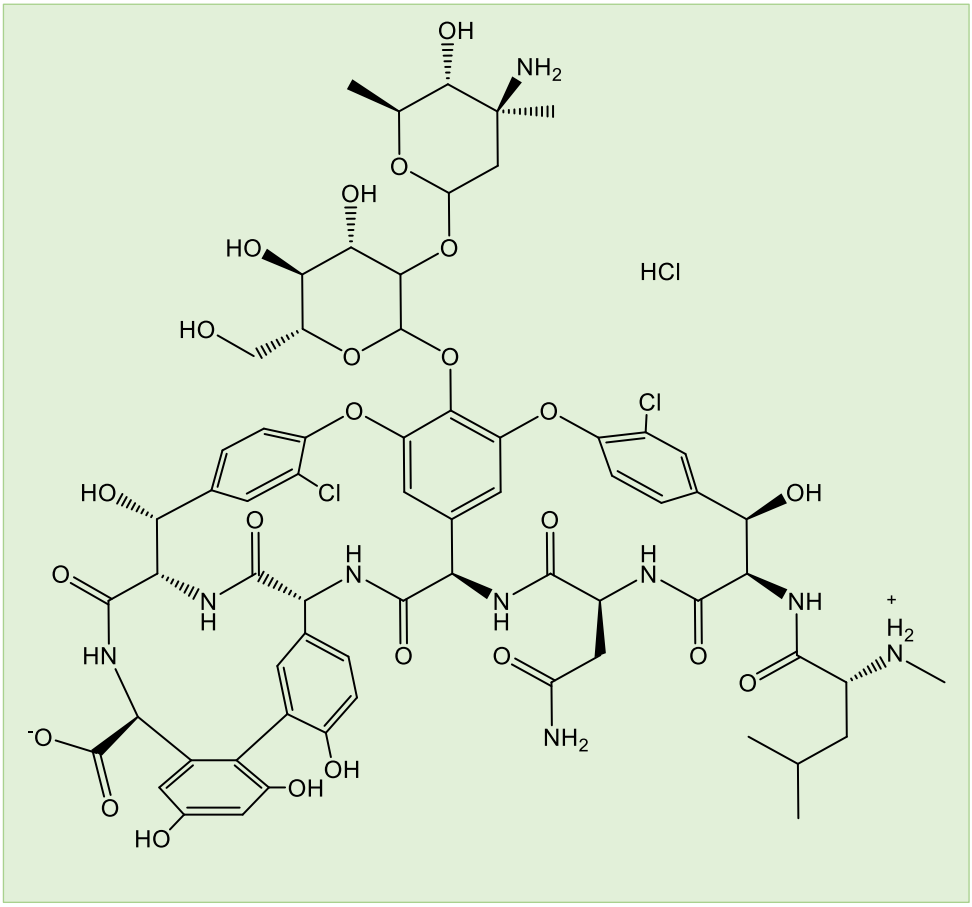

Figure 1.12: Vancomycin hydrochloride chemical structure.

1.7.8 Nanoencapsulation of Vancomycin

High doses of vancomycin may cause side effects like hypotension, tachycardia, ototoxicity, chills, hypersensibility reactions, fever and nephrotoxicity. Instead of trying to find new antibiotics, researchers have turned toward new technique which is using nanocarrier delivery systems such as nanoparticles and liposomes; this system offers great intracellular penetration and the possibility for effective intracellular antibacterial action over extended time periods.[232] VCM was loaded within N-trimethyl chitosan (TMC) for drug delivery application. The prepared nanoparticles had spherical shape with an average particle size of 220 nm. The loading efficiency was 73.65%± 1.83%, and during a 24 hour period, 6.51% ±0.58% of the drug was released within the optimized nanoparticles. Cytological *in vitro* studies revealed that, after exposure to TMC nanoparticles, osteoblasts (OBs) showed higher alkaline phosphatase action. The OB proliferative activity was

improved when using both VCM/TMC and nanoparticles mixtures. Furthermore, the water-soluble carboxy-CdSe/ZnS quantum dots (QDs) uptake by OBs increased by TMC nanoparticles. All data proved that VCM/TMC nanoparticles had a significant antibacterial action against the Gram-positive bacterium *S. aureus* with sustained delivery of VCM to bone infections.[233] Zakeri-Milani *et al.* enhanced the VCM intestinal permeation by loading VCM into (PLGA) poly(lactide-co-glycolide) nanoparticles.[234] Moreover, VCM solid lipid nanoparticles adjuvanted with linoleic acid, showed better antibacterial activity than free VCM towards both resistant and susceptible bacteria.[235] Vancomycin also was successfully encapsulated into amino-polysiloxane matrixes through a one-step room temperature sol-gel method, subsequent, a hybrid materials of biodoped monolithic was manufactured. The vancomycin-containing matrixes were characterised using Fourier transform infrared (FTIR) and ^{29}Si magic angle spinning nuclear magnetic resonance (^{29}Si MAS NMR) solid-state spectroscopies, indicating that the drug was encapsulated. The delivery tests and *in vitro* swelling activities were carried out at 37 °C and pH 7.4, during the first hours the release of vancomycin to the medium did not show any initial burst effect as well as a lag time or zero-release period. Afterward, vancomycin exhibited a sustained release over an extended period of days. This lag time is a requirement to implant bioceramics that would let the surgeon carry out the surgical process with zero drug release.[236] Esmaeili *et al*. [237] prepared superparamagnetic nanoparticles consist of $MnFe_2O_4$ as core to be loaded with vancomycin using a precipitation method. Chitosan was used as cross linker through glutaraldehyde as a shell, and the stability of the particles was modified with PEG against the reticuloendothelial system (RES), the ferrite nanoparticles properties, as well as antibacterial activity, were improved by coating them with chitosan. The surface modification was confirmed using FT-IR; SEM and XRD were used to measure the particle size of about 25 nm and to characterise the crystal structure of these NPs. Vibrating sample magnetometry VSM was used to evaluate the nanoparticles magnetic properties, also, UV–vis spectroscopic technique was used to study the drug loading and release. A liquid broth dilution process was employed to study the antibacterial action of nanoparticles on microorganisms. Table 1.5 represents some of the *in vitro* characteristics of vancomycin loaded with different nanocarriers and as can be seen VCM was loaded at big particle size and some of these nanocarriers have negative surface charge with big size which can repel with the cell membrane, also most literatures showed that VCM cytotoxicity was studied against gram-positive bacteria much more than gram-negative bacteria. In the current study the aim is loading VCM within stable nanocarrier at high efficiency, with size less than 100 nm, well characterised and studying its cytotoxicity

against gram-negative bacteria as well as yeast and algae cells. Shellac can be used to be loaded with VCM, and can be stabilised by using Poloxamer 407 copolymer by conducting steric repulsion between the shellac particles, which is also can play a synergistic effect with the antibacterial agent as it has been used in topical/ dermal formulation.[112] Besides, these nanocarriers can be coated with cationic electrolyte to inverse the surface charge from negative to positive leading to increase the adhesion of the loaded nanocarriers with the cell membrane. The positive charge of the nanocarrier allow it to deliver and boost the antibacterial agent at any type of cells and at low amount near or inside the cell vicinity. In addition, the loaded VCM within shellac NPs allows the antibiotic to be released slowly which mean it can be used as wound bandage for long time and no need to change it each hour.

Table 1.5: Characteristics of the formulation of VCM within different nanocarriers.

Nanocarrier used to load VCM	**Particle size (nm)**	**Zeta potential (mV)**	**E.E %**	**Drug content %**	**Ref.**
N-trimethyl chitosan (TMC)	220	14.6± 0.8	73.65± 1.83	5.8±0.17	233
Poly vinyl alcohol (PVA)	430±31.94	25.7±9.72	89.37±2.36	29.79 ±1.12	238
Liposome formulation F2	78.3	-	78.66	98.62	239
Poly vinyl alcohol (PVA) F2	461 ± 33.45	−7.07 ± 5.96	67.1 ± 2.46	33.58 ± 1.48	240
Polyacrylic acid sodium (PAA)	229.7 ± 47.7	− 30.4 ± 5.3	75.22 ± 1.02	58.40 ± 1.03	241

1.8 Characterization of Nanoparticles

Nanoparticles are characterised by their size, morphology and surface charge; these characters affect the in vivo distribution and physical stability of the nanoparticles. Also the redispersibility of polymers dispersion and in vivo performance affected by the surface charge of the nanoparticles Techniques used to characterise them include transmission electron microscopy (TEM), scanning electron microscopy (SEM), Dynamic light scattering (DLS) and atomic force microscopy (AFM). SEM and TEM can be useful techniques for determining the toxicity of polymeric nanoparticles by ascertaining their overall shape.[36]

1.8.1 Particle Size

The most important characteristic parameter of the nanoparticles is their particle size distribution and the shape which can be detected by SEM. As it is known that drug release and drug targeting are the main application of nanoparticles, it has been noticed that the drug release depends on the particle size. Smaller particles have a greater surface area. Due to the small size, most of the drug will be loaded on the particle surface leading to release the drug fast. While with large particle the drug will diffuse inside them leading to slow release. On the other hand, smaller particles have a tendency to aggregate during transportation and storage.[242] Also the particle size can effect on the polymer degradation, by increasing the particle size of poly(lactic-co-glycolic acid) the degradation rate increased *in vitro*.[243]

There are some tools used to detect the size of the nanoparticles such as:

1.8.1.1 Dynamic Light Scattering

Dynamic light scattering (DLS) or photon-correlation spectroscopy (PSC) is a popular method for determining the particle size in colloidal suspensions at ranges of nanometres. This method is based on Brownian motion. A Doppler shift occurs when monochromatic light (laser) hits the moving particles leading to a change in wavelength of the incoming light, and this change is related to the particle size. The size of the particle can be calculated using Stokes-Einstein equation, (equation 1.1).[244]

$$D_h = \frac{kT}{3\pi\eta Dt} \qquad 1.1$$

Where:

D_h = the hydrodynamic diameter

k = Boltzmann's constant

D_t = the translational diffusion coefficient

T = thermodynamic temperature

η = dynamic viscosity

For accurate particle size and size distribution estimation, photon correlation spectroscopy perform the most common technique which based on DLS,[245] Figure *1.13*.

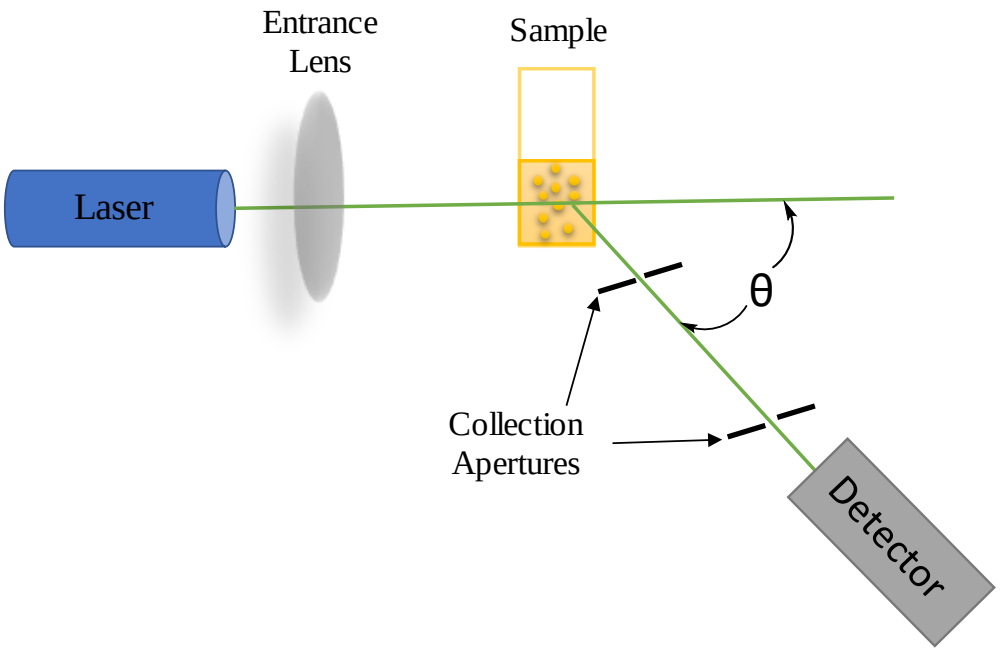

Figure 1.13: Schematic diagram of Dynamic Light Scattering instrument (DLS).[246]

1.8.1.2 Transmission Electron Microscopy (TEM)

TEM provides morphological analysis by direct imagining. To prepare the sample for TEM imaging is time consuming and complex due to the requirement of a very thin sample for the transmittance of electrons, a film or support grid is used to deposit the nanoparticles dispersion. The nanoparticles are fixed using either plastic embedding or negative staining material like uranyl acetate or phosphotungstic acid or derivatives to withstand the high vacuum of the instrument and ease handling. Another methods is exposing the sample to liquid nitrogen after inserting in vitreous ice. The sample surface features are obtained once a beam of electrons transmits through the thin sample and interacts with the nanoparticles as it permits through the solenoids; which are tubes surrounded by coil, consequently, the beam of electrons converts to electromagnetic radiation to form an image. This image can be enhanced by adjusting the voltage to control the velocity of electrons and changing the wavelength of electromagnetic radiation.[247, 248]

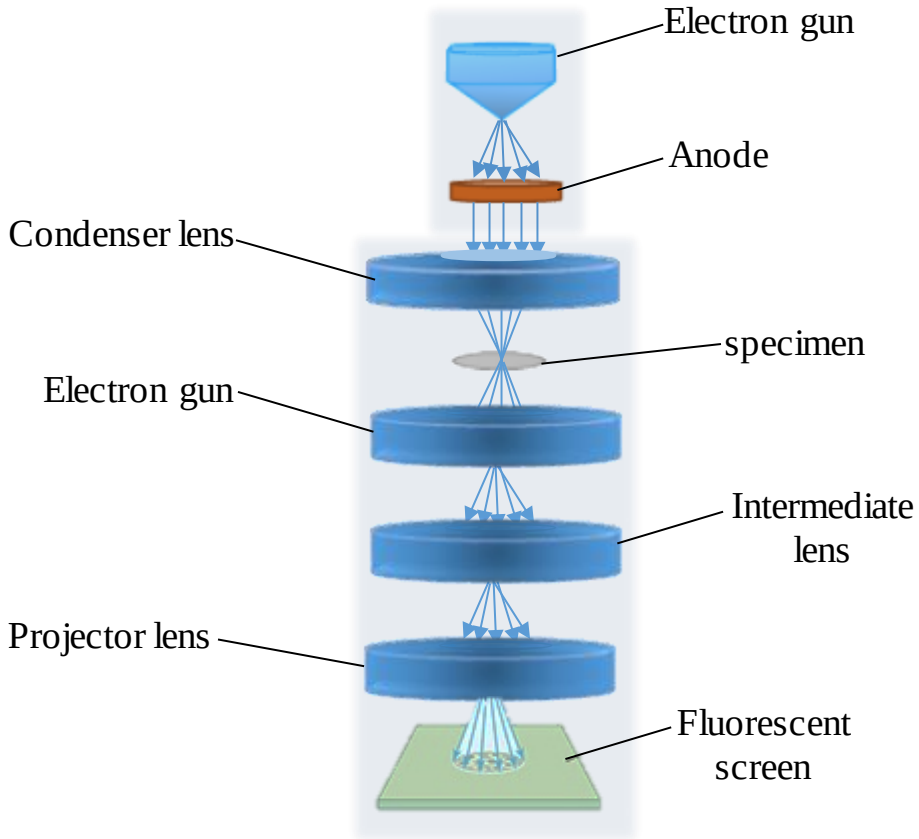

Figure 1.14: Schematic diagram of the components of transmission electron microscopy (TEM).

1.8.1.3 Scanning Electron Microscopy (SEM)

SEM operates on a different principle than TEM. However it frequently gives the same type of data, and the technique offers some advantages in sizing and morphological analysis, but about exact population average and size distribution, it provides limited information. To characterise the sample using SEM instrument, the nanoparticles sample should be dried as a powder, then coated with a conductive metal like gold or carbon by means of a sputter coater after fixing on a sample holder. The sample is scanned by exposing to an intensive fine electron beam.[249, 250] The emitted secondary electrons from the sample surface provide the surface characteristic.

The major difference in the data output between TEM and SEM techniques is the means by which the nanoparticle images are determined. SEM produces perfect 3D images of the dispersed particles while TEM produces 2D images which need further explanation. However, although the images extracted are two dimensional, TEM systems are able to deliver much larger resolution. An SEM instrument manufactured by Jeol Ltd, for example, secures resolution down to 1.2 nm, while a TEM device from the same provider has to resolve images down to 0.17 nm. TEM can provide details of internal composition, a particle's crystallinity and lattice structure. Similarly, SEM delivers this information but is suited well for looking at samples' surface characteristics. Moreover, preparation of sample in TEM takes longer time than with SEM, as the particles are required to be thinly sliced.[251]

1.8.2 Surface Charge

It is very important to characterise the nanoparticles surface charge in terms of intensity and nature as it provides information about their interaction with biological samples besides their interaction with bioactive materials electrostatically. The zeta potential (ζ) is the average electrical potential (ψ) in the interfacial double layer at the shear location, in other words, it is the difference of potentials between the dispersed particles and liquid phase as shown in Figure 1.15. It considered to be an indirect measurement of the surface charge, and this can be used to determine the storage stability of the nanoparticles. To avoid aggregation and ensure stable particles, high values of zeta potential, either negative or positive, should be obtained. Additionally, the zeta potential results predict the surface hydrophobicity and also can provide data about the nature of the material for examples the

successful coating of the surface.[252] The Zeta potential can be measured using Henry's equation by determining the electrophoretic mobility of a particle (velocity) using equation 1.2 below:

$$UE = \frac{2\varepsilon z f(ka)}{3\eta} \qquad (1.2)$$

Where:

UE: the velocity of the particle

ε: the dielectric constant

z: the zeta potential

$f(ka)$: Henry's function which depends on the Debye thickness or double layer.

κ^{-1} : represents the electrostatic interactions around the suspend particle.[253]

η : the viscosity of the medium.

In general, Henry's function has either 1.5 (in polar media) or 1.0 (in non-polar media) value.[254]

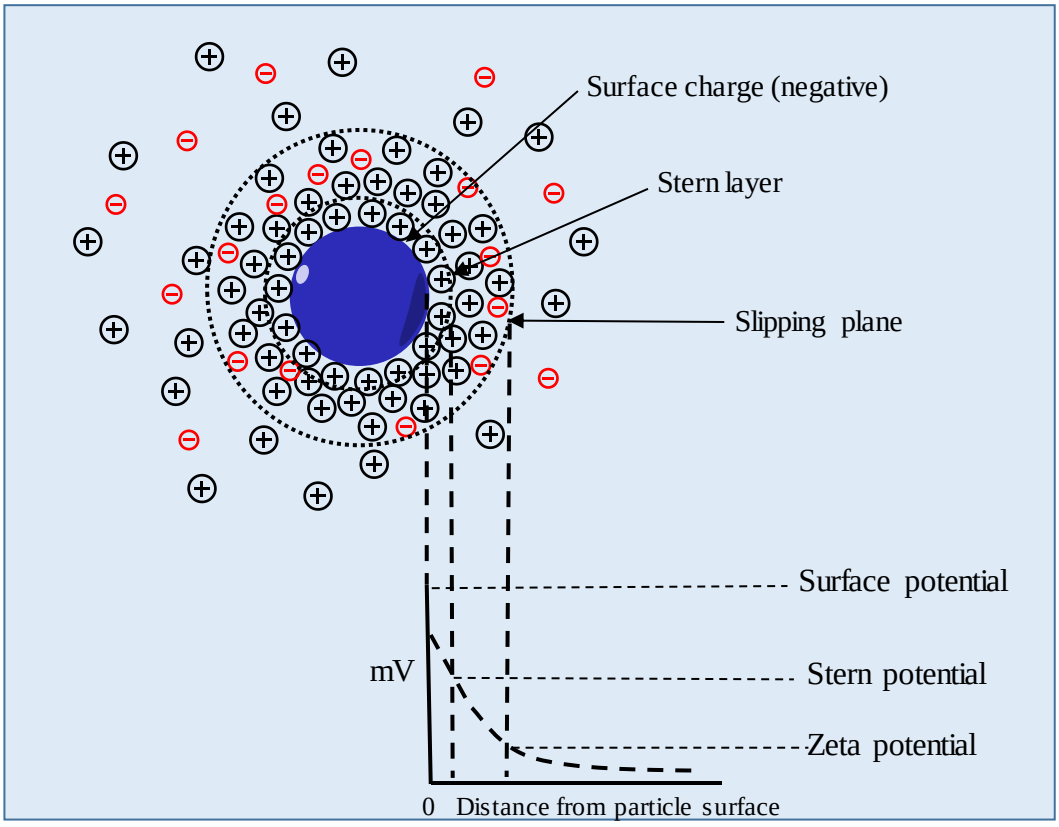

Figure 1.15: Schematic diagram explain measuring the zeta potential of charged particles.

1.8.3 Hydrophobicity of the Nanoparticle Surface

Several techniques can be used to determine the hydrophobicity of the nanoparticle surface such as biphasic partitioning, hydrophobicity interaction chromatography, contact angle measurement and adsorption of probes. Some sophisticated analytical technique has been reported recently for determining the nanoparticle surface, like X-Ray photon correlation spectroscopy, which provides information of the chemical groups on the nanoparticles surface.[255]

1.8.4 Drug Loading

Ideally, an effective nanoparticulate drug delivery system should have a high drug loading capacity in order to reduce the amount of the matrix materials required for the intended site. The composition of the designed nanoparticulate drug delivery system determines the drug entrapment efficiency and the drug loading in the system as well as the solubility of the drug in the matrix material or polymer (solid dispersion or dissolution) and for polymeric materials this is related to the composition of the polymer, its molecular weight and its terminal function groups like carboxyl or ester. For example, polyethylene glycol (PEG) moieties have little or no effect on the drug loading, while the macromolecule or protein shows the greatest drug loading efficiencies near its isoelectric point with minimum solubility and maximum adsorption capacity.[255, 256] There are two ways to load drug within the nanoparticles:

- Incorporation method: the drug is incorporating at the time of nanoparticle preparation.
- Absorption/adsorption technique: the drug is absorbing after the nanoparticle formation by incubating the nanocarrier with a solution of the concentrated drug.

In this research, incorporation method was followed, and the drug was combined with shellac at the time of preparing shellac nanoparticles. Methods such as high-performance liquid chromatography (HPLC) or UV spectrometry are used to measure the drug loading as percentage relative to the polymer after ultrafiltration, centrifugal ultrafiltration, ultracentrifugation or gel filtration.[257]

1.8.5 Drug Release

Basically, the main aim of loading a drug within nanocarrier delivery system is to sustain and release the drug at the targeted site in predetermined controlled rate in order to preserve a constant concentration of drug for a specific period with lowest side effects,[258] as well as being capable to interact and overcome the biological barriers.[259] Many therapeutic agents show success in cell culture but fail to achieve the same results in the human body because of the limitation in targeting the designated area, and this leads to giving patients high drug concentrations resulting in more intense side effects.[10] There are many factors that have been found to affect the drug release rate such as drug solubility; desorption of the surface bound/adsorption of the drug; the diffusion of the drug through the nanoparticulate matrix; and the degradation rate or erosion profile of the polymer matrix.[256, 260] Also the release profile may depend on the size of the nanoparticles; larger particles have a smaller initial burst release, and longer sustained release than smaller particles. In addition, the greater the drug loading, the faster the release rate. For example, PLA nanoparticles drug entrapment 16.7% savoxepine released 90% of their drug load in 24 h, as contrasting to particles containing about 7.1% savoxepine, releasing their content over three weeks.[261] The initial burst release has been thought to be caused by drug adsorbed onto the outside of the particles or poorly entrapped drug. In case of using polymers, like PLGA with a free COOH group and proteins, the burst release is lower and in some cases absent, and drug release is prolonged due to the interaction of the drug with the polymer moieties.[262, 263] Multivesicular liposomes (MVLs) was used to encapsulate cisplatin to form cisplatin-MVLs for sustained release. The *in-vitro* release studies showed that the drug sustained released for 7 days, and the *in-vivo* studies revealed the higher drug accumulation was in spleen, liver, and tumour areas than the cisplatin solution, also higher in plasma concentrations and longer circulation time. The therapeutic efficiency of the cisplatin-MVL against S180 tumour-bearing mice is considerably higher than that of cisplatin as solution.[264] There are several methods which can be used to study the *in vitro* of drug release from the nanoparticles, such as:

- Dialysis bag diffusion technique.
- Reverse dialyses bag technique.
- Side-by-side diffusion cells with biological or artificial membranes.
- Centrifugal ultra-filtration or Ultra-filtration techniques.
- Agitation followed by centrifugation/ultracentrifugation.

1.9 High Throughput Cell Based Screening

High-throughput screening (HTS) is a promising approach widely adopted both in pharmaceutical industry and academia to address the intractable methods of screening drugs. Typically, classic drug screening methods are costly and time-consuming. However, more than 90% of screened drug candidates after entering clinical tests are failing. [265] At the most basic level, high-throughput screening (HTS) involves an automated workstation that handles drugs, solutions and microplates, allowing multiple drugs and their activity on reporter cells to be simultaneously confirmed. In spite of HTS improves the throughput screening appears to be a standard platform for drug discovery, it leaves some unresolved requirements, with monetary cost being the first. The modern method of HTS cell based screening uses either 96, 384, 1536, or 3456 wells microplate for cell growth studies with different concentrations of toxin. The usual working volume for these microplates is in the range of about 2.5 - 10 μL overall volume, a 5 μL per well considers standard volume. [266] Cell-based assays have acquired an established situation in drug screening in the pharmaceutical industry. These assays assist the evaluation of potential drug purposes by characterising their influence in cells and by assessing efficacy and specificity of drug leads functionally. Moreover, these assays provide information about the nature of the pharmacological action of a compound at a specific receptor, intracellular target or ion channel. Cell-based screening processes give information on the potency of the chemical compounds to permeate the cell membrane, as well as a severe cytotoxicity profile. [267]

The 96-well microplate screening process permits for a quite rapid cytotoxicity screening of the toxins with a convenient number of wells for statistical significance. The 96-well screening method protocol is based on cultivating cells in each of the 96 wells. Then, various concentrations of toxin which prepared in culture media are distributed individually into the 96 wells in order to make gradient toxin concentrations alongside the 96-well plate length as shown in Figure 1.16. These measurements of varied concentrations of toxin can be repeated for eight times which allow for screening by microplate well. The 96-well plate including cells and toxin-added culturing media is placed in an incubator, and the cells are cultured continuously for different incubation times, exposed to the toxin. Cell viability assay can be used to screen the cells viability wherein the 96 plates after a particular incubation time. Either a fluorescence or an absorbance or a luminescence measurement can be used to measure the relative intensity of stained cells in each well.

The cytotoxic effect of the toxin can be determined by comparing the relative intensities of viable cells with respect to different concentrations of the toxin as a function of time. [268, 269]

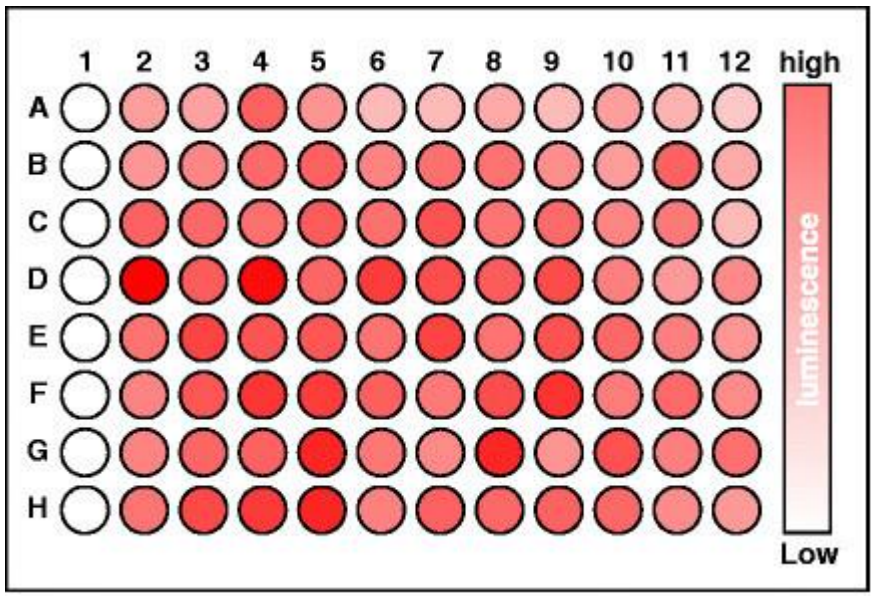

Figure 1.16: A schematic pattern of the 96-well microplate cytotoxicity screening for luminescence method. [270]

1.10 Microfluidic Devices

An alternative approach for toxicology screening is to use microfluidic devices. Microfluidic devices or lab on a chip (LOC) or Micro Total Analysis System (μTAS) are miniaturised systems consisting of micro channels to manipulate small fluid volumes (μL, nL, pL), (Figure 1.17). This technology has been used in a wide range of processes such as extraction,[271, 272] nanoparticle crystallization,[273, 274] enzyme assay,[275, 276] organic synthesis,[277, 278] polymerization,[279, 280] protein folding,[281] analytical assay,[282-284] biological screening,[285, 286] cell analysis,[287, 288] drug delivery studies,[289] bioprocess optimization,[290, 291] and clinical diagnostics.[292, 293] Microfluidic device offers several advantages such as the small size of the device make it an ideal portable platform, the small size of fluids, easy to use, cheap fabrication and operation, very small sample requirements and they are easily disposed. [294] Microfluidic devices are still being developed, they have the possibility to become broadly adopted because they are reproducible, economical, amenability to modifications and easily integrate with other technologies.[295] Current years, many microfluidic systems have been developed to be qualified for rapid mixing without using external actuators, like electric field or stirrer.[296] The most commonly used is including droplet mixers,[297] flow-focusing mixers[298] and those with channels have micromixing structures implanted inside them.[299] Flow focusing presses the solvent stream amid two anti-solvent streams, causing fast solvent exchange by diffusion. Three-dimensional and droplets microchannel geometries produce a complex folding of fluid flows, which can mix two or other streams completely in milliseconds. The achievement of mixing these techniques to form organic nanoparticles by continuous flow has produced lipid nanoparticles and polymeric with narrower average size distribution, greater drug loadings and larger batch-to-batch reproducibility comparative to those prepared with conventional bulk techniques.[300] Likewise, inorganic nanoparticles including transition metals such as iron, cadmium and gold, among others, suffer self-assembly where metal solutes nucleate, growing and agglomerating into nanoclusters.[301]

To produce narrow particle-size distribution, this requires fast nucleation then keeping nanoparticles to grow up to the preferred size without further nucleation, which can be achieved by controlling the time for mixing reagents, the temperature and time of the reaction.[302] In bulk, it is difficult to control these parameters, which may lead to irregular mixing, fluctuations in local temperature and uncontrolled reaction times. In contrast, the mixing time can be controlled when using microfluidic devices by varying the flow rates of the solvent or channel geometry. Furthermore, it is better for heat transfer

due to big surface areas enables to control the temperature, prevents the formation of large temperature gradients. Finally, the channel length is directly related to the time that the reactants need to flow through it in continuous flow synthesis; this time can be controlled by setting the channel length or using reagents at specific downstream locations during the process of the particle formation to quench the reaction.[303]

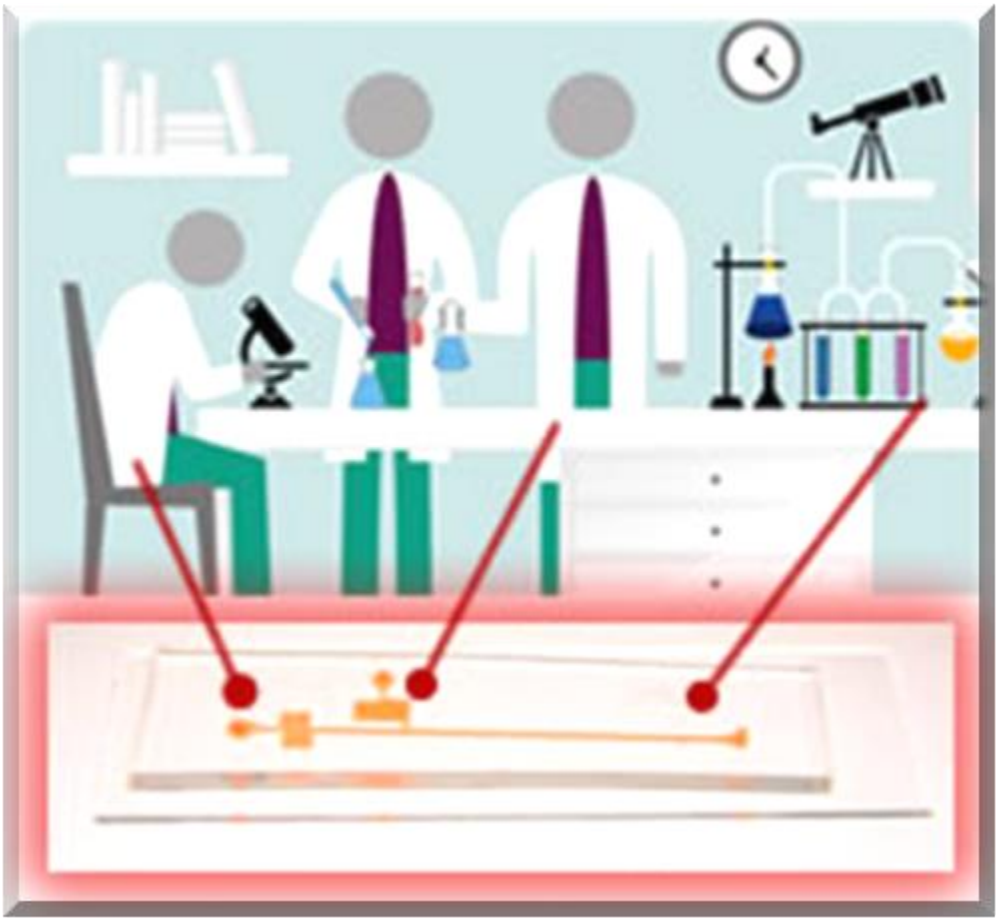

Figure 1.17: Integration and miniaturisation the laboratory processes onto a microfluidic device. This picture was adopted with author permission (Elbuken research group, Dr Calgar Elbuken).[304]

1.11 Materials Used for Microfluidic Devices Manufacturing

To produce a microfluidic device with high quality, three aspects need to be considered : (i) the properties of the material and the expectation of its properties on device performance, (ii) the methodologies of processing and tooling, and (iii) process control measurements.[305] The properties of the material are the primary consideration in construction of microfluidic devices, basically because the selected material should be suitable for the device performance, for example, bio-compatible for biological tests, for

chemical experiment it should be resistant to alkali or acid, etc. Another reasons is that the product quality is significantly affected by the interaction between the tooling or processing methodologies and the materials, which means the quality of the product may be different when using different material even when using same tooling or processing method. Also, the cost of the material is additional consideration for high-volume, large-scale manufacturing. Therefore, it is necessary to investigate the material properties impact on the performance of the device and product quality.[305] Many materials have been cited to manufacture microfluidic devices, such as glass and quartz, silicon, polydimethylsiloxane (PDMS), cyclic-olefin-copolymer (COC), polycarbonate (PC),[306] poly(methyl methacrylate) (PMMA),[307] SU-8,[308] polytetrafluoroethylene (PTFE),[309] polyacrylate,[310] polystyrene,[311] cellulose acetate,[312] and even ceramics.[313]

1.11.1 Soft Polymer

Soft polymers or elastomers have many desirable chemical and physical properties rather than silicon when used for microfluidic device fabrication. They are cheaper than silicon and glass and comprise simpler and inexpensive manufacturing processes like mould replication, mould injection, casting and embossing. They are more rugged mechanically than silicon and glass, and for some applications, polymers can be used more than more brittle materials would typically fail. There are many examples of polymers used to manufacture microfluidic systems such as polyethylene,[314] polyvinylchloride,[314] polyethyleneterephthalate glycol (PETG),[315] polystyrene,[316] polymethyl methacrylate (PMMA),[307] polycarbonate,[306] and polyurethane.[317]

Poly (dimethylsiloxane) (PDMS) has many attractive properties that make it a favourite to be used in microfluidic devices fabrication. It is a soft polymer with desired chemical and physical properties like optical transparency, elasticity, flexible surface chemistry, low water permeability, air permeability and small electrical conductivity. Mixing PDMS with different amounts of cross-linker (5.7, 10.0, 14.3, 21.4, and 42.9 wt.%), a various designated PDMS1, PDMS2, PDMS3, PDMS4, and PDMS5 can be prepared respectively.[318]

A significant advantage of PDMS is its ease and cheap microfabrication. Liquid PDMS pre-polymer can be cured thermally at moderate temperatures (40-70 °C), and it can be cast from photoresist templates to achieve nanoscale resolution devices, which are

cheaper and easier to make than glass templates,[319] PDMS chip can be conformably and reversibly bonded to another section of PDMS, glass, or any other substrates by easily making contact.[320] Oxidation of PDMS surface by oxygen plasma is suitable to bond PDMS to glass, PDMS, or silicon irreversibly or using a thin layer of PDMS as glue.[320] By accumulating several layers of PDMS, multilayer channel structures were fabricated by making holes to connect these layers.[321] PDMS shows other advantage represented by its high elasticity. Integrated valves have been developed by Quake et al.[321] depends on double layers of microchannels, these valves (1 x 106 valves/cm^2) allow high-density integration with picolitre to femtolitre of dead volumes and realised comparable and complicated on-chip manipulation.[322] In contrast to silicon, glass, and other tough materials like polycarbonate and poly(methyl methacrylate) (PMMA), PDMS is gas penetrable as it is critical for long-standing cell culture in closed microchannels; also it has a compatible surface for cell culture. PDMS chip devices are commonly used in bio-related researches, mainly, biochemical assays, cell screening, and cell culture.[323-325] Owing to PDMS ability to handle very small volumes reaching to picoliter to femtoliter makes it excellent in the single-cell study.[326, 327]

1.12 Construction of Microfluidic Devices by Soft Lithography

Soft lithography is representing a non-photolithographic protocol which based on self-assembly and reproduction moulding for performing micro- and nanofabrication. It offers an effective, convenient, and low-cost process for the manufacturing and formation of micro- and nanostructures.[319] The method comprises of replication of a pattern on a master in a soft elastomer (PDMS). The process can be achieved in ambient lab conditions; therefore, it does not need expensive cleanroom facilities for fabrication structures in size range of 20 to 100 μm (this range of size is microfluidics based bioanalysis).[320, 328] A master or mould is produced first using soft lithography technique for PDMS replication. The PDMS is provided in two components, the base and the curing agent. The curing agent has silicon hydride groups which react with the vinyl groups exist in the base forming cross-linked, elastomeric solid as shown in Figure 1.18. To prepare a replica PDMS, two portions (usually at 10:1 (v/v) base: curing agent) are mixed, cast the liquid pre-polymer over the mould, and then cured for 1 h at 70°C. The pre-polymer liquid PDMS adapts and replicates the structure of the master mould up to 10's of nm. Owing to its elasticity and

low surface free energy, PDMS can be peeled off from the mould without destruction the mould or itself. The mould is the limiting factor in producing PDMS replicas.

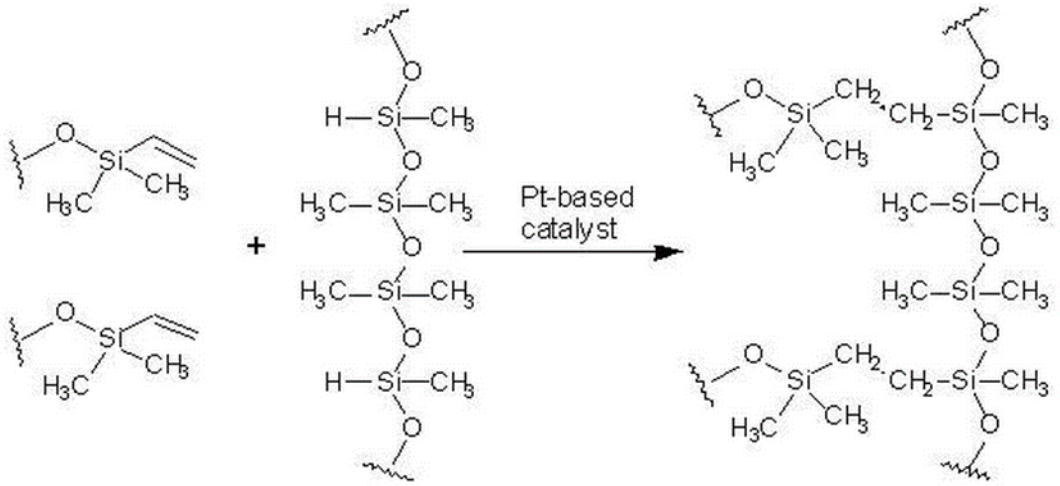

Figure 1.18: Organometallic crosslinking reaction between methylhydrosiloxane oligomer base and curing agent to yield PDMS using H_2PtCl_6-catalysed hydrosilylation.[329]

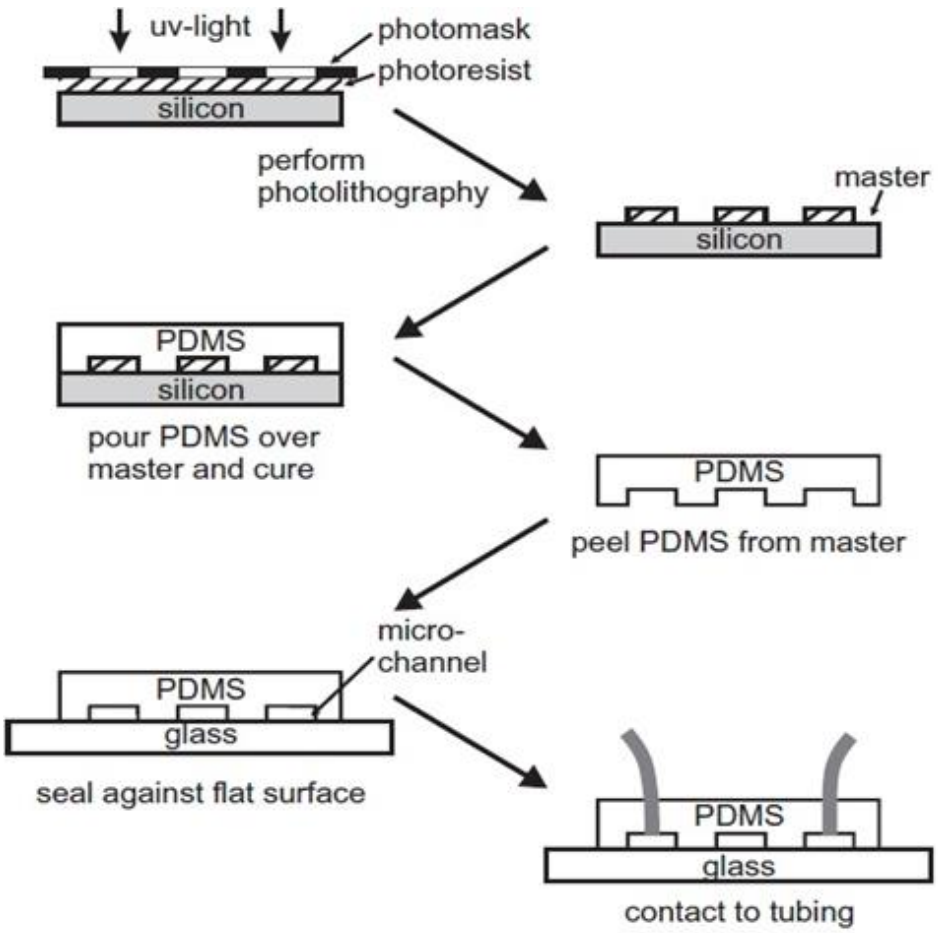

Figure 1.19: Schematic diagram of ideal device fabrication using soft lithography for shaping PDMS as a device material.[330]

Micromoulding technique can be used as well for PDMS replica fabrication by duplicating microstructures on polymer substrates. A mould template is produced by either negative photoresist for patterning, such as SU-8, on a silicon wafer for fixed microstructures less than 50 μm or direct micromachining a PMMA mould for microstructures larger than 50 μm. Then a PDMS mixture is poured over the moulding template, cured, and then peeled off from the template as presented in Figure 1.19. The ideal microstructures offering high feature ratios can be achieved in the PDMS substrate.[331]

1.13 Sealing of PDMS Microfluidic Chips

One of the most significant advantages of PDMS is that it can be sealed to other surfaces or itself, reversibly or irreversibly and without any distortion of the channels.[320, 328, 332] Sealing the PDMS channels is considerably simpler than sealing of glass, thermoplastics or silicon channels.[333, 334] PDMS that has been moulded using a smooth surface can conformably bond to other smooth surfaces, even when they are nonplanar, because PDMS is elastomeric. A reversible seal achieved by simple van der Waals contact it is watertight but cannot resist pressures more than ~5 psi.[320] Adhesive tapes like silicone or cellophane also can be used to seal the PDMS channels reversibly.[335] Cellophane tape offers only a temporary seal while silicone tape provides a much stronger seal, and it is waterproof and supplies a fourth wall composed of PDMS. To make an irreversible seal, PDMS exposes to air plasma for 60 s.[320, 336] Some researchers consider that by oxidising methyl groups of the PDMS silanol groups (Si−OH) will generate on the surface.[337, 338] The oxidised PDMS surface can seal to glass, polystyrene, silicon, silicon nitride, polyethylene, or itself unless these surfaces have also been exposed to an air plasma. Even the sealing process is simple and reproducible, but it requires technical agility. The two surfaces must be brought into contact after oxidation quickly (less than 60 s) because the oxidised PDMS surface will reconstruct in the air.[339] To maintain the hydrophilic nature of the PDMS surface indefinitely, it should contact with water or polar organic solvents.[328, 339] Experimental data show that oxidative sealing works well when the chamber and samples are clean, samples are dry, smooth surfaces on the micron scale and the oxidised surfaces are not mechanically stressed. Sometimes, heating a weak seal in an oven at 70 °C can improve the strength of the seal.

1.14 Microfluidic Devices Cell Based Assays

Developing the robust and quantitative *in vitro* cytotoxicity assays is necessary for assessing the pharmaceutical safety, decreasing animal testing, and for environmental hazards assessment.[340] Applying lab-on-a-chip microfluidic devices for cytotoxicity tests can have advantages in terms of speed, cost and controllability.[341, 342] The use of microfluidics for cell biology applications have many advantages, particularly, microfluidic devices exhibit as small footprints, low reagent consumption, physical properties predictably, controlled real-time of fluid flow, multiplexing capabilities, little fluorescence background, and the potential for efficient and integrated downstream studies. These features of microfluidic, which are difficult to succeed in many traditional multiwall culture plates, can potentially offer significant benefits for high throughput investigation such as screening the dose-response and cytotoxicity tests.[343] PDMS, poly(dimethylsiloxane) has many advantageous properties such as flexibility, easy to fabricate, low fluorescence contribution to the background, and low index of refraction, all these advantages made it the favourite polymer in preparing microfluidic chips. However, the great surface-to-volume ratios that present in a microchannel may produce adverse conditions for cells because of the presence of the porosity, leachables and surface chemistry of PDMS may entrap materials, or the PDMS gas permeability may consequently alter the medium of osmolarity or gas content.[344-346] Microfluidic devices were used as an alternate method to encapsulate cells in picoliters monodisperse aqueous drops in an inactive carrier fluid.[347-349] Microfluidic drop generation and optical trapping were used to encapsulate mammalian cells,[349, 350] as well as *E. coli* cells.[351] Sarah Köster *et al*., succeeded to incubate, encapsulate and manipulate individual cells in pL aqueous drops at a rate of up to several hundred Hz in a carrier fluid using microfluidic devices. The small drops volumes enabled secreted molecules concentrations to attain detectable levels rapidly. 33 pL drops of single hybridoma cells secreted antibodies at detectable concentrations in only 6 hours and remained fully viable.[352]

1.15 Microfluidic Devices based Cytotoxicity Micro Screening

Cell toxicity studies play a vital role in screening the early-stage drug. They could present wide extensive practical information than biochemical assays with lower cost and shorter time than animal examinations.[353] Applications of microfluidics in this field have

included cellular differentiation,[354] mammalian cell patterning,[355-358] dynamic gene expression,[359, 360] and monitoring cellular responses to chemical gradients.[361, 362] Khademhosseini *et al*. developed a multiplexed soft lithographic process to fabricate multi-phenotype cell arrays for drug screening, using reversible sealing of polydimethylsiloxane (PDMS) moulds on surfaces.[363] However, separate microfluidic devices were utilised for cell seeding and drug exposure. While Koh and Pishko have designed a microfluidic system that contains mammalian cells encapsulated with a hydrogel which can be used for cytotoxicity test of toxins.[364] Also, drug metabolites and an induced cytotoxicity assay were characterised simultaneously by using the developed integrated quartz-composed microfluidic device, studying the cytotoxicity of UDP-glucuronosyltransferase (UGT) metabolism of acetaminophen (AP) on hepG2 cells, this confirmed the feasibility of drug metabolism test upon using the microfluidic chip,[365] Figure 1.20.

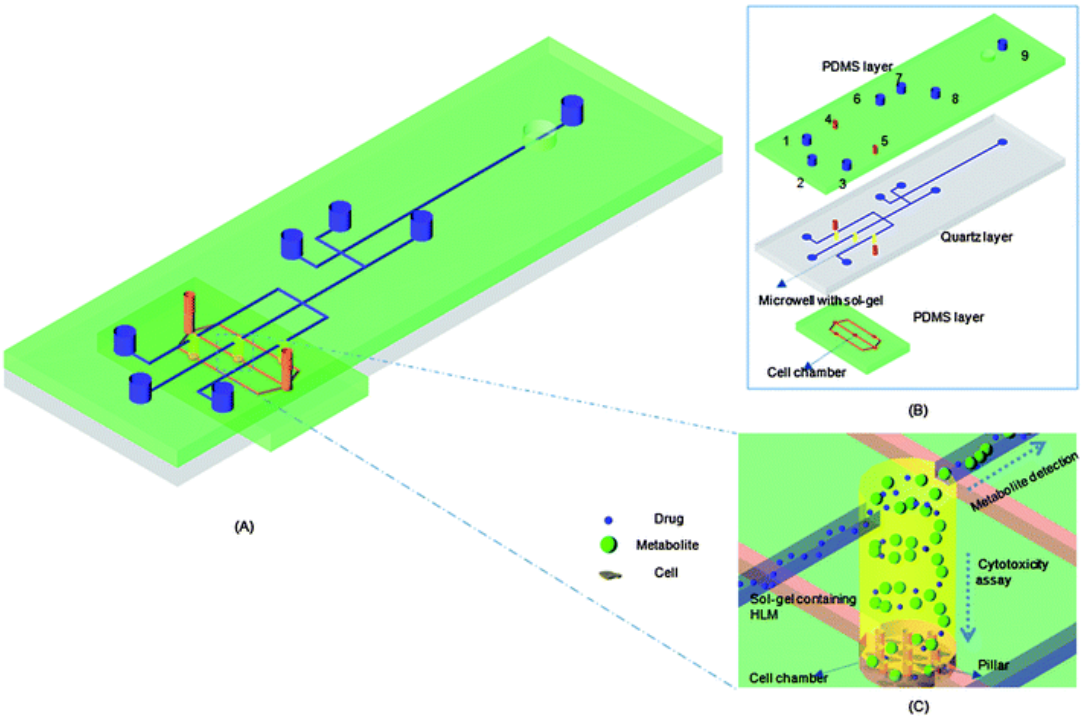

Figure 1.20: (A) Schematic diagram of a three layer microfluidic device for characterization of drug metabolites and cytotoxicity assay at the same time. (B) The device was included three layers, a quartz substrate fixed with separation microchannels and a three-microwell array filled with human liver microsome (HLM) in sol-gel sandwiched between two PDMS substrates. (C) A magnified schematic of one sol-gel bioreactor on the microfluidic device.[365]

A hybrid (PDMS/glass) microfluidic cell culture device was constructed and integrated with a concentration gradient generator for successful cells' seeding. PDMS has an excellent air permeability allowed cells' respiration in the fabricated microdevices. Carcinoma cells (A549) human lung were cultured for several days in the microdevice. This novel method was developed and successfully verified for cells' passaging in the designed microdevice after achieving the confluence of cells in the microchambers. This system was reproducible for several uses and various cell culture and cytotoxic tests. 1,4-dioxane was used as a model of a toxic agent, while iodide propidine (PI) and fluorescein dibutyrate (FDB) were used as viable and dead cells' stains, respectively. The device can be used in high-throughput cell-based evaluates providing significant information on substances' bioactivity, potential drug targets, setting the lowest level of toxicity for tested substances.[366] Figure 1.21.

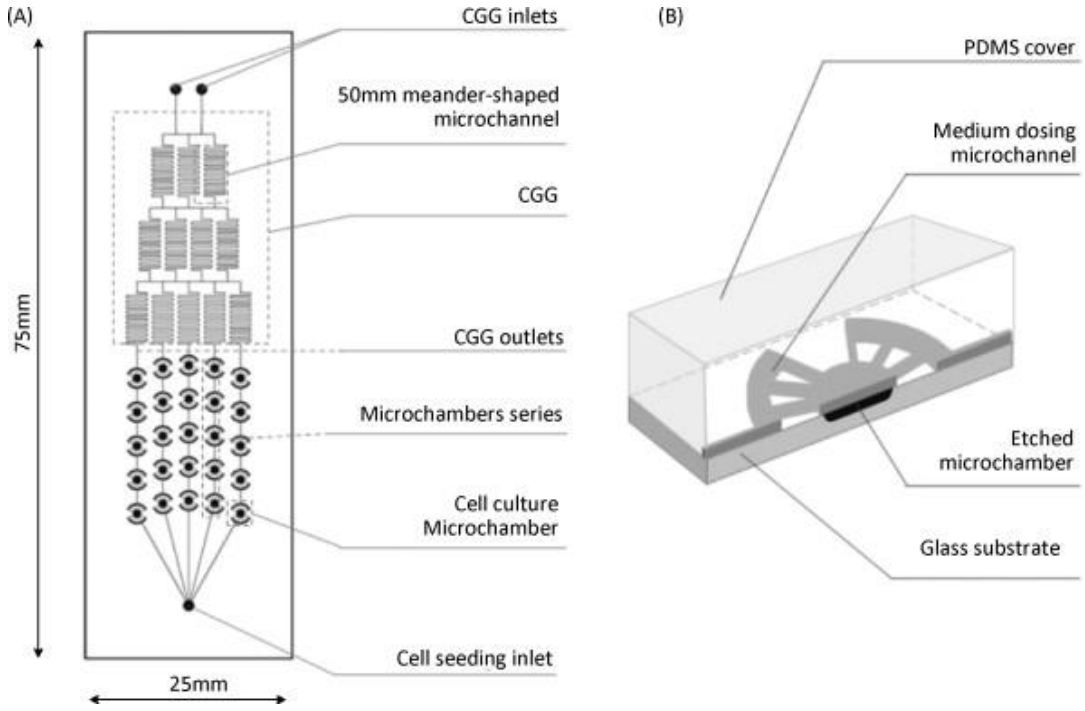

Figure 1.21: (A) microchannels geometry and (B) a microchamber cross-section for cell culture.[366]

O'Neill *et al*. presented a new microfluidic device with two input fluid streams for linear serial dilution. This pattern shows higher feasible productivity as a part of a high throughput cytotoxicity analysis approach. The platform was validated to produce an extremely linear progression of dilutions with 0.9993 R2 value. The averages standard deviation of dilution was 0.76% over six flow rates spanning 0.5 - 16 µL min^{-1}.[367]

1.16 The Aim of the Project

With the increase and emergence of microbial organisms resistant to multiple antibiotics, and the continuing emphasis on health-care costs, many researchers have tried to develop new, and effective antimicrobial agents free of resistance and cost. One possible solution to overcome these problems is using nanocarriers as drug delivery system. Shellac the natural polymeric material was chosen to be used as a nanocarrier, owing to its biodegradable, biocompatible, safe and non toxic material as well as its nature which consists of carboxylic groups and hydrophobic part which can be loaded with cationic and hydrophobic antibiotic agents. The aim of this project is to design a stable and universal nanocarrier able to be loaded with different antibacterial agents , well characterised, can be systematically studied in simple way. Different components can be used to construct a stable and efficient nanocarrier. Poloxamer 407 can be used as stabilizer agent. Its micelles play an essential role in stabilising the shellac particles by creating steric repulsion among shellac particles as well as it has usefullness role in pharmeceutical products. Besides, the surface of the nanocarriers can be functionalised by coating it with cationic electrolyte like ODTAB to inverse the surface charge from negative to positive while maintaing the stability balanced. This positive surface charge of the nanocarrier allow it to be attracted to different kind of microorganism cells and release the drug efficiently near or inside the cell membrane vicinity. In this project shellac NPs aim to be prepared and loaded with BRB, CHX, CUR, and VCM and for wound dressing. Although these antimicrobial were loaded within different nanocarriers as been nentioned in sections 1.7.2, 1.7.4, 1.7.6, and 1.7.8, but not all of their characteristics were achieved, and most of these nanocarriers have negative surface charge which can repel with the cell membrane and hence decrease the cytotoxicity of these antimicrobial agents. While in this project, these antimicrobial agents are planning to be loaded within positively surface charged shellac NPs to promote the adhesion with the cell membrane, as well as full characterised studies. Literatures in section 1.7.2 showed that even when BRB was loaded within a nanocarrier, but not all of their characteristics were accomplished or when their characteristics achieved the encapsulation effeciency or the drug loading content were lesser as well as their surface charge is negative. So none of these nanocarriers contain all desired qualities. In this project BRB is planning to be loaded within a stable nanocarrier even at diluted solution with full characterised, as well as the cationic nanocarriers can amplify the BRB toxicity action 10 times more than the free BRB due to the fast attraction between these nanocarriers and the cell membrane. As well as can be used agianst different kind of cells.

While the aim of encapsulating CHX within shellac NPs is to be encapsulated at high effeciency and at low concentration to decrease its side effects. As can be seen in literature in section 1.7.4 that none of the mentioned nanocarriers achieved more than 90% encapsulation and most of them were not full characterised and their cytotoxicity were studied against one kind of microorganisms. Herein, the cytotoxicity of encapsulated CHX is aiming to be studied against different kind of microorganisms such as algae, yeast, and *E.coli*, and boosting its cytotoxicity 10 times more by loading it within cationic nanocarrier. On the other hand, literatures in section 1.7.6 displayed that encapsulated curcumin showed slight improvement in cell killing action than free curcumin as well as slow release but not more than 10 hours. Moreover, the cytotoxicity of encapsulated curcumin within these nanocarriers were studied on only one kind of cell for each nanocarrier. Herein, curcumin is planning to be loaded with shellac NPs at high efficeincy reaching to 100% to increase its bioavilibilty as it is an insoulible antimicrobial agent, and to sustain its release for very long period. Also it can be used against different kind of cells at very low concentrations less than 5 times than the free curcumin by changing the surface charge of the nanocarrier from negative to positive which can promote the attach of these nanocarriers with the cell membrane. Literatures in section 1.7.8 showed that encapsulated VCM was studied against gram-positive bacteria, with no release for the first hours. In this project VCM is aiming to be encapsulated with shellac NPs and to study its cytotoxicity against gram-negative bacteria as well as different kind of microorganisms such as algae and yeast. Also it is attending to study its release at different pH such as 5.5 and 7.4 as none of the researches showed its cytotoxicity at pH 5.5. Also it is aiming to increase its toxicity by 50 times more than the free VCM by loading it within cationic shellac NPs. Chapter 2 contains the methods and materials for preparation shellac nanocarriers as well as the procedures of loading the antimicrobial agents and surface modification by using cationic electrolyte. Also, it presents the particle characterisation methods and the use of cell viability assays for assessment of antimicrobial action. As well as, the construction and the design of a microfluidic chip with using magnetic beads to be operated as chamber gate keeper for entrapment of cells for testing antimicrobial action. While chapter 3 displays the selection of the materials and the ideas behind the nanocarrier design. Also it shows the *in vitro* characteristics of the loaded antimicrobial agents within shellac NPs such as the particle size, the zeta potential, the encapsulation efficiency, and the drug release at pH 7.4 and 5.5. Furthermore it shows the techniques that use to prove the loaded of these drugs within shellac NPs. It also presents the characteristics of the loaded drugs after coating with cationic electrolyte. Whereas chapter 4 displays the

cytotoxicity of shellac NPs with Poloxamer 407, free BRB and CHX, encapsulated BRB and CHX within shellac NPs, and the coated shellac NPs and encapsulated BRB or CHX, and their cytotoxicity against algae, yeast, and *E.coli.* In Chapter 5, the antimicrobial activity of curcumin (CUR) and vancomycin hydrochloride (VCM) investigates against algae, yeast, and *E.coli*. It shows the cytotoxicity of free CUR and VCM, encapsulated CUR and VCM within shellac NPs as well as the cytotoxicity of encapsulated CUR and VCM coated with ODTAB. While chapter 6 displays the development of a microfluidic device cell- based assay. A fabrication of closed PDMS-glass microfluidic chip is illustrated by bonding PDMS with microscope glass using an oxygen plasma cleaner machine to activate their surfaces. The initial microfluidic device composes of two layers, the top is PDMS which incorporated the channels, and the bottom layer is a microscope slide. The cells are aiming to be trapped inside the micro-chamber by using magnetic beads as gate keeper and allow to be exposed to the studied solution of antimicrobial nanoparticle suspensions. Finally, chapter 7 displays the summary of the entire achievements of this project.

Chapter 2 : Experimental Section

2.1 Materials

2.1.1 General Chemicals Reagents

Shellac was used in a soluble form as ammonium salt at pH > 7, this alkaline solution was a gift from (Stroever Schellack Bremen, Germany) and is commercially available as SSB Aqua Gold (solid content 25%). Poloxamer 407 (purified), berberine chloride, vancomycin hydrochloride (from Streptomyces orientalis) and chlorhexidine di-gluconate (20% in H_2O) were obtained from Sigma-Aldrich. Curcumin was purchased from Fisher Scientific, UK. Purified water was collected from a Milli Q reagent water system (Millipore, UK), and used for all experiments, with a surface tension of 71.9 $mN.m^{-1}$ at 25°C, the resistivity was less than 18 M Ω/cm. Other reagents that were used in this work are tabulated in Table 2.1.

Table 2.1: Chemicals used for the synthesis and characterisation of nanomaterials.

Material	Purity%	Supplier
(3-Aminopropyl)triethoxysilane	99	Sigma-Aldrich, UK
1,1-azobis(cyclohexanecarbonitrile)	98	Sigma-Aldrich, UK
Acetic acid	≥99.7	Fisher, UK
Agarose	High Purity	Sigma-Aldrich, UK
Ammonia	33	BDH, UK
CTAB	>99	Fluka, Germany
Ethanol	Absolute	Fisher, UK
Ferric Chloride	Anhydrous 97	Fisher, UK
Ferrous Chloride	98	Sigma-Aldrich, UK
Glucose	>99	Fisher, UK
Glutaraldehyde solution	25	Sigma-Aldrich, UK
Hitenol BC20	-	Dai-Ichi Kogyo, Japan
Hydrochloric Acid	37	Fisher, UK
Octadecyltrimethyl ammonium bromide (ODTAB)	>97	Fluka, Germany
Oleic Acid	99	Sigma-Aldrich, UK

Peptone	>99	Sigma-Aldrich, UK
Poly (Dimethylsiloxane) SYLGARD® 184 Silicone Elastomer Kit	10:1 (Curing agent: Base)	Dow Corning, USA
Sodium Acetate	>99	Aldrich, UK
Sodium Chloride	99.5	Fisher, UK
Sodium dodecyl sulfate (SDS)	>99	Fluka, Germany
Sodium Hydroxide	99.6	Fisher, UK
Styrene	99.5	Sigma-Aldrich, UK
Tryptone,	>99	Oxido ltd, UK
Tween 20	>99	Fluka, Germany

2.2 Preparation of Shellac NPs

The method followed to prepare shellac NPs depended on adsorbing surfactants on shellac particles with changing the pH from 8 to 5 using diluted HCl. Different types of surfactants were used at different concentrations to obtain stable nanoparticles, such as sodium dodecyl sulfate (SDS) as anionic surfactant, n-Hexadecyltrimethylammonium bromide (CTAB) as cationic surfactant, and Tween 20 and Poloxamer 407 as non-ionic surfactants. At these surfactants only Poloxamer 407 showed good results and was been chosen to be used to prepare stable shellac NPs.

2.2.1 Preparation of Shellac NPs and Loaded with Antimicrobials

Shellac colloidal nanoparticles (Shellac NPs), as in Figure 3.1, were prepared using a simple method by mixing 0.25 w/v% of ammonium shellac solution at pH >7 with different concentrations of Poloxamer 407(P407) then lowering the pH of the solution from 8 to 5 using diluted HCl dropwise and mixing gently, Figure 3.2. Berberine chloride (BRB), chlorhexidine di-gluconate (CHX), curcumin (CUR), and vancomycin hydrochloride (VCM) were loaded on the shellac nanoparticles by mixing shellac, P407 and the antimicrobial together at pH > 7 then lowering the pH to 5 using diluted HCl drop wisely with mixing gently, as in Figure 3.12Figure 3.22, Figure 3.32, and Figure 3.42. Different concentrations of drugs were added to a constant mixture of shellac and Poloxamer 407

with a ratio of 0.25:0.2 w/v%, respectively. The pH of the solution was reduced to 5 by adding 0.01M HCl drop wise and measured using pH –meter Fisher Brand Hydrous 300.

2.2.2 Cationic Functionalisation of Antimicrobial Agents Loaded Shellac Nanoparticles

In order to overcome the cellular barriers of the cells and to improve the delivery of various drug candidates, the surface of the nanocarriers (negatively charged) was coated with octadecyltrimethylammonium bromide (ODTAB) (positively charged electrolyte). Hence, different amounts of ODTAB (0.0025 – 0.1) wt. % were added drop wise to the prepared shellac NPs and shellac NPs loaded drugs at pH 5.5, then the size and the zeta potential were measured using zeta sizer nano ZL.

2.3 Drugs preparation

0.2 g of berberine chloride (molecular formula of $C_{20}H_{18}ClNO_4$, 371.81 g.mol^{-1}) was dissolved in 100 mL Milli Q water as stock solution, 5.0 g of 20 wt.% chlorhexidine di-gluconate (molecular formula of $C_{34}H_{54}Cl_2N_{10}O_{14}$, 897.762 g.mol^{-1}) was dissolved in 100 mL of Milli Q water to prepare 1.0 wt.% stock solution. A 0.5 wt. % stock solution of curcumin was prepared by dissolving 0.5 g of pure curcumin (molecular formula of $C_{21}H_{20}O$, 368.37 g.mol^{-1}) in 100 mL absolute ethanol. Vancomycin hydrochloride ($C_{66}H_{75}Cl_2N_9O_{24}$, with molar mass 1449.3 g.mol^{-1}) stock solution was prepared by dissolving 1.0 g of the drug in 100 mL of PBS buffer (pH 7.4). All drug stock solutions kept in the fridge at 4°C.

2.4 *C.reinhardtii* cc-124 strain Growth Culture Medium

Microalgae (*C. reinhardtii*) were kindly provided by Velev's group from North Carolina State University, USA. This algae culture was grown at 30 °C under fluorescent light. *C. reinhardtii* cultures are known to grow well in tris-acetate phosphate (TAP) growth medium. The TAP medium was prepared according to the classic recipe developed by Gorman & Levine.[368] The TAP medium contains TAP salts, acetic acid, Tris(hydroxymethyl)aminomethane (Tris) and phosphate solution buffers, and Hutner's trace elements. TAP salts were prepared by dissolving ammonium chloride, magnesium sulphate and calcium chloride in deionised water. Phosphate solution was prepared from

potassium phosphate monobasic, potassium phosphate dibasic salts dissolved in deionised water. Hutner's trace elements include traces of iron, manganese, copper, zinc, boron, cobalt and molybdenum. The starting pH of the TAP medium was set to 7.0 by titration with hydrochloric acid and sodium hydroxide. The TAP medium provides all the necessary nutrients for algal growth (carbon, nitrogen, sulphur, phosphorus and trace metals). Table 2.2 shows the amounts of the chemicals that used to prepare the culture media and all were provided by Sigma-Aldrich, UK. [369, 370]

Table 2.2: The amount of the salts that used to prepare *C.reinhardtii* culture media.

Salt	**The amount**
NH_4Cl	15.0 g
$MgSO_4.7H_2O$	4.0 g
$CaCl_2.2H_2O$	2.0 g
K_2HPO_4	28.8 g
KH_2PO_4	14.4 g
EDTA disodium salt	50 g
$ZnSO_4$. 7 H_2O	22 g
H_3BO_3	11.4 g
$MnCl_2$. 4 H_2O	5.06 g
$CoCl_2$. 6 H_2O	1.61 g
$CuSO_4$. 5 H_2O	1.57 g
$(NH_4)_6Mo_7O_{24}$. 4 H_2O	1.10 g
$FeSO_4$. 7 H_2O	4.99 g
Tris	2.42 g
TAP salts	25.0 mL
Phosphate Buffer Solution	0.375 mL
Hutner's Trace Solution	1.0 mL
Glacial Acetic Acid	1.0 mL

Finally, *C.Reinhardtii* was grown in a culture media produced by mixing Tris, TAP salts, phosphate buffer solution, Hutner's trace solution, and glacial acetic acid. The produced solution was diluted using Milli-Q water to 1.0 litre, then autoclaved for an hour at 125°C and 1.5 bar. Cells are then cultivated in this culture media for three days.

2.5 Growth of Baker's yeast (*Saccharomyces Cerevisiae*)

Baker's yeast culture media (YPD medium)[371] was prepared by dissolving 1.0 g of yeast extract, 2.0 g glucose, and 2.0 g peptone in 100 mL Milli-Q water. The YPD media were autoclaved at 1.5 bar and for an hour at 125°C. Then 0.01 g of dried yeast (Sigma Aldrich, UK) was dispersed into the autoclaved culture media and incubated for 24 hours at 30°C with gentle stirring.

2.6 Growth of Escherichia Coli (*E.coli*)

Escherichia coli (E.coli) was kindly provided by Rotchell's group in the School of Environmental Science, University of Hull, UK. The cells were cultured in autoclaved Luria-Bertani medium (LB medium)[372] which was prepared by dissolving 0.5 g yeast extract, 0.5 g sodium chloride, and 1.0 g tryptone, in 100 mL Milli-Q water. After autoclaving the culture media at 1.5 bar at 125°C for one hour, and once it cooled down, a few microliters of the *E.coli* suspension was dispersed in the autoclaved culture media and incubated for 48 hours at 30°C with gentle shaking.

2.7 Fluorescein Diacetate (FDA) Assay

[3', 6'-diacetyle fluorescein (FDA)] (Sigma Aldrich, UK) was used to measure the extent of cell viability.[373] The method was based on the hydrolysis of nonfluorescent fluorescein esters by enzymes like; proteases, lipases and esterases result in the release of a coloured end product fluorescein which was detected by using an automatic cell counter machine. FDA was prepared by dissolving 5.0 mg in 1.0 mL acetone, and the solution was stored at 8°C.[374]

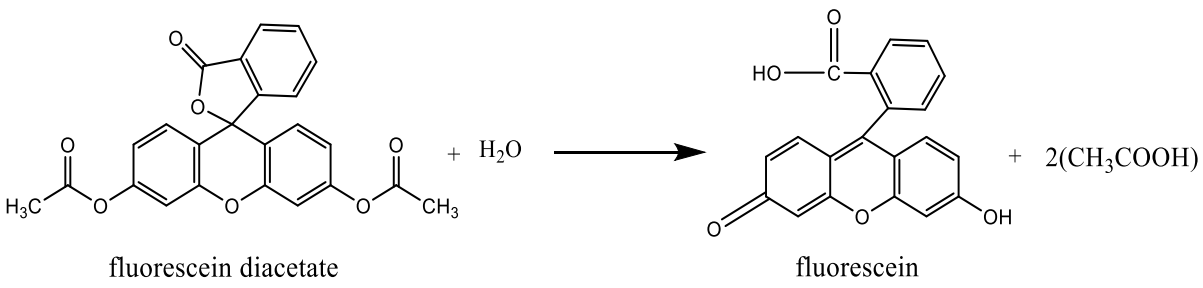

fluorescein diacetate fluorescein

Figure 2.1: Enzymatic conversion of fluorescein diacetate (colourless) to fluorescein (coloured acid yellow) visible at 490 nm. [374]

2.8 BacTiter-Glo Microbial Cell Viability Assay

The BacTiter-Glo microbial cell viability assay (Promega) [375] is a bioluminescence-based test which is directly proportional to the amount of ATP existing in viable cells. The reaction between this reagent and ATP within cells is based on extracting ATP from bacteria. The assay protocol is achieved by adding the BacTiter-Glo reagent directly to the sample and measuring the luminescent signal. The signal measurement depends on the type of bacteria. The luminescence reaction between the reagent and ATP in the presence of molecular oxygen is shown in Figure 2.2.

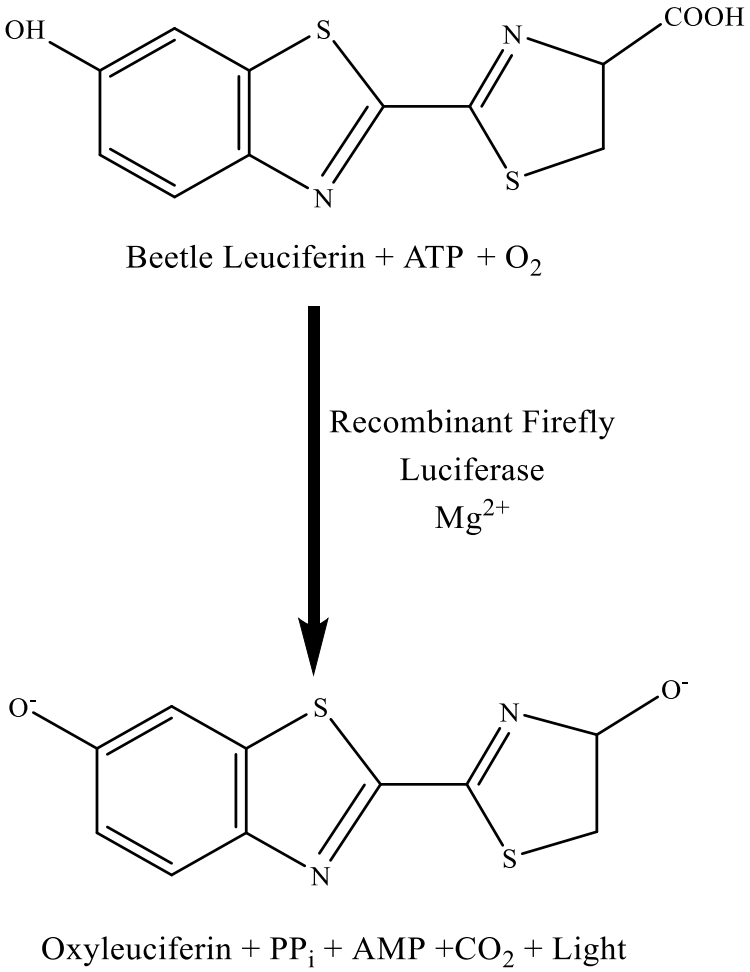

Figure 2.2: The luciferase reaction. Mono-oxygenation of luciferin is catalyzed by luciferase in the presence of Mg^{2+}, ATP and molecular oxygen.

2.9 Instrumentation

A zetasizer nano ZL (Malvern, UK) was used for measuring the average nanosize distribution and zeta potential of shellac nanoparticles. For UV-Visible measurements, a Perkin-Elmer UV-Vis spectrophotometer, USA (model Bio Lambda 10) was used. A Nexcelom Cellometer Auto X4 Fluorescence (fluorescence optics module XB-535-401, Excitation 475 nm /Emission 535 nm) with an assisted automated cell counter (purchased from Bioscience, USA) connected with a computer loaded with Cellometer software was used to measure total live, dead cells, concentration, % viability and cell size. A Mastersizer Model 2000 (Malvern, UK) was used to measure shellac size at microsize. FT-IR spectrometer (Thermo Scientific Nicolet 380 FT-IR, Hemel Hempstead, UK) connected to a computer provided with OMNIC Lite software was used to characterise the formation of shellac NPs and the interaction between the NPs and drugs. Transmission electron microscopy (TEM) (JEM 2011 JEOL, Japan) running at 200 KV and a scanning electron microscope (SEM) (ZEISS EVO 60 EP-SEM, Germany) were used to image the microorganism cells. Olympus microscope (DP70 digital camera, Japan) was used to measure the intensity of the viable cells. Table 2.3 shows some instruments were used during the research.

Table 2.3: shows the general equipment used to obtain the results

Instrument	**Provider and Model**
pH –meter	Fisher Brand Hydrous 300
Mini-Centrifuge	Eppendorff mini spin plus
Homogenizer	IKA Ultra-Turrex, UK
Hotplate with Magnetic Stirrer	IKA C-MAG HS7, UK
Centrifuge	Thermo Biofuge Primo, UK
Mini-Centrifuge	Eppendorff mini spin plus, UK
Shaker	IKA MS 3 Basic, UK
Vortex Mixer	Stuart, UK
Micropipettes	Eppendorff, UK
Syringe pump	Harvard Apparatus, USA

2.10 Characterise Shellac NPs

2.10.1 Average Particle Size and Zeta Potential Characterization

The average particle size and ζ-potential of shellac NPs, drugs loaded shellac NPs, and drugs loaded shellac NPs coated with ODTAB were measured by dynamic light scattering (DLS) technique using a zeta sizer Nano ZL and dip cell. All measurements were carried out in triplicates and using Milli Q water as an essential solvent. Morphological examination of the nanoparticles was performed by transmission electron microscopy (TEM), few drops of the sample were placed on carbon-coated copper grids and negatively stained with 1% uranyl acetate (aq). Once air-dry it was imaged with a Gatan Ultrascan 4000 digital camera attached to the Jeol 2010 TEM running at 200kV.

2.10.2 Fourier Transform Infrared Characterizations

An FT-IR spectroscopy connected to computer was used to characterise the shellac nanoparticles, and drugs loaded shellac nanoparticles formation. Samples were dried in oven for 2 days at 60°C then measured at fingerprint region 4000 – 600 cm^{-1}, this technique has been used to confirm the adsorption of Poloxamer 407 on shellac surface particles and the bonding between the cationic drugs with ionic shellac molecules.

2.10.3 UV-Vis Characterizations

To prove the loading of drugs within shellac nanoparticles a UV-Vis spectrophotometry technique was used. Spectra of samples of drug loaded shellac nanoparticles were dissolved in weak alkaline media (shellac dissolves in pH>7), pure shellac, pure drug, and pure Poloxamer 407 were recorded between 200-700 nm using a spectrophotometer. Microsoft Excel software (Microsoft Win 2010) was used to conduct the modelling charts.

2.10.4 Encapsulation Efficiency and Drug Loading Contents

The encapsulation efficiency and the drug loading content were calculated by measuring the absorptivity of the unencapsulated drugs. The unencapsulated drug (BRB,

CHX, CUR, and VCM) was filtered by using 20 nm syringe filter, and the absorbance of this filtered drug was measured at 422 nm, 255 nm, 426 nm, and 280 nm for each drug, respectively, using UV-Visible spectrophotometer (model Bio Lambda 10, USA). Calibration curves for each drug were made by preparing different concentrations of each drug and measuring the absorbance of each concentration at selected wavelengths. The drug loading contents and encapsulation efficiency were calculated using the equations 2.1 and 2.2 shown below [376]

$$Encapsulation\ Efficiency\ (\%) = \frac{[Total\ Drug - Unencapsulated\ Drug]}{[Total\ Drug]} \times 100 \qquad 2.1$$

$$Drug\ Loading\ Content\ (\%) = \frac{[Total\ Drug - Unencapsulated\ Drug]}{[Total\ Drug - Unencapsulated\ Drug + shellac + Poloxamer\ amount]} \times 100 \qquad (2.2)$$

2.10.5 *In Vitro* Drug Release

The dialysis method was used to determine the drug release profile from shellac nanoparticles. 50 mL of the sample containing antimicrobial agent loaded shellac NPs were dialyzed in dialysis bag of 12-14K MWCO with pore diameter 2.5 nm, this bag was immersed in a 500 mL buffer phosphate solutions (pH 5.5 & 7.4), as can be seen in Figure 2.3. For studying curcumin release, 0.45 wt. % CTAB was dissolved in buffers to keep the curcumin soluble in solution.[377] The bag was stirred gently with an orbital shaker at 37°C and 100 rpm. At specific time intervals, 2 mL of the dialysis solution was taken and analysed by measuring the absorbance in a range of wavelength from 500 nm to 200 nm using UV-Visible spectrophotometer of buffer solution against water sample as a blank, for each drug 1 cm path length cuvette was used. The measurements were taken at series of interval time. All release experiments were carried out in triplicates. The percentage of cumulative drug release was calculated using equation (2.3) which shown below [378]

$$\%\ In\ Vitro\ Drug\ Release = \frac{M_{released}}{M_{total}}\ x\ 100 \qquad (2.3)$$

Where $M_{released}$ is the amount of drug released from the shellac NPs at time *t* and M_{total} is the amount of the total drug loaded within shellac NPs.

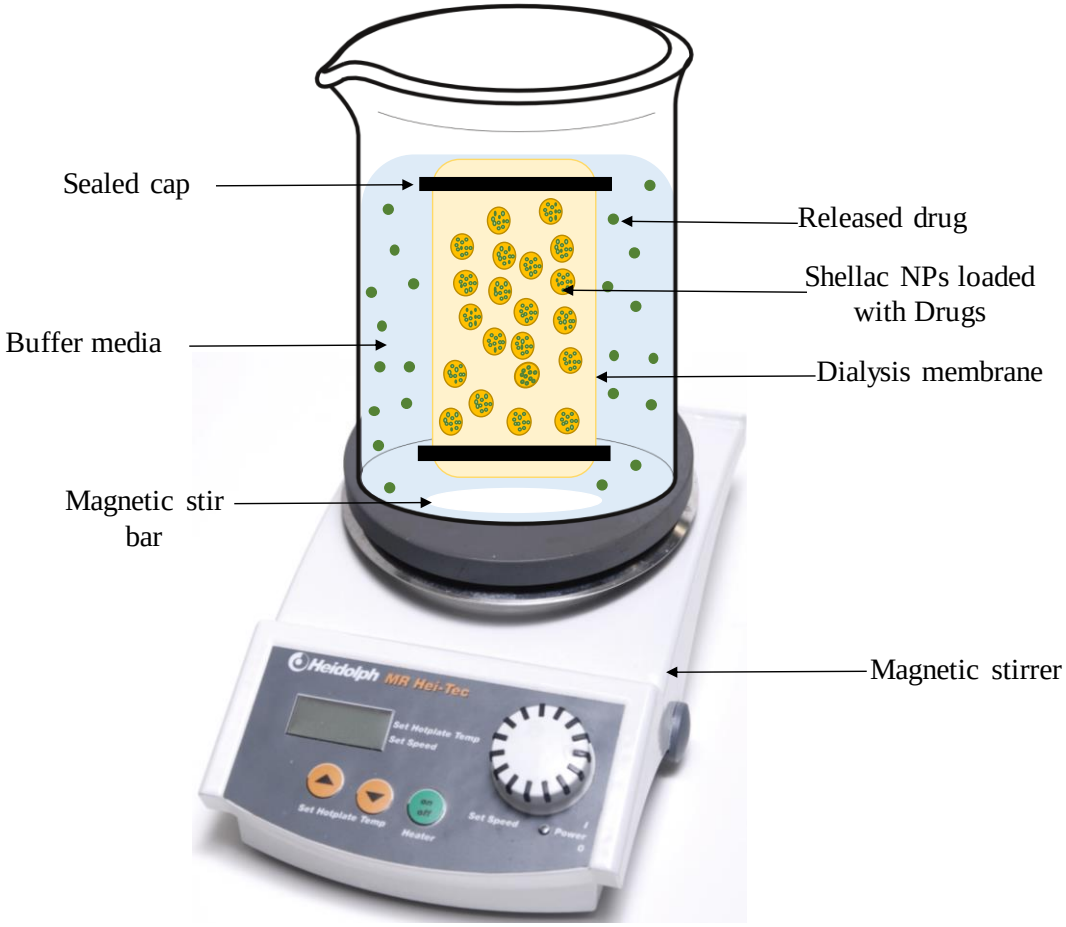

Figure 2.3: Schematic diagram represents the dialysis process using dialysis bag with pore size of 2.5 nm to allow the drug to be released without the nanocarriers.

2.10.6 SEM Characterisations

SEM images were taken for cells and encapsulated shellac NPs coated with ODTAB. The cells were washed with water 3 times to get rid of the culture growth media by centrifugation at 3000-5000 rpm for 3 minutes; then the cells were adhered to washed and dry Aclar sheets or poly lysin coated glass coverslips for an overnight. After that cells were fixed with 2.5 w/v% glutaraldehyde for 2 hours, followed by washing with cacodylate buffer, post fixed for 1 hour in 1% osmium tetroxide, washed again with a cacodylate buffer, then rinsed with a solution of water and ethanol in steps from 50% and up to 100%, and dried using critical point dryer. Finally, they were coated with carbon and imaged using scanning electron microscope SEM.

2.10.7 TEM Characterisations

The shape of shellac NPs and antimicrobial loaded shellac NPs was analysed by using TEM instrument. Few drops of the samples were placed on carbon-coated copper grids and negatively stained with 1% uranyl acetate (aq.) in order to generate contrast in the TEM image, then they were allowed to settle and dried. The images were taken with a Gatan Ultrascan 4000 digital camera attached to a Jeol 2010 TEM running at 200kV. All particle size measurements were made using Gatan Digital Micrograph software.

2.11 Antimicrobial Studies of Drugs Loaded Shellac NPs

To study the effectiveness of loading the drugs within shellac nanoparticles against *C.reinhardtii*, Baker's yeast (*S. cerevisiae*), and *E.coli* cells, different concentrations of drug loaded shellac nanoparticles and ODTAB coated shellac nanoparticles loaded drugs were incubated in the presence of these cells for different incubation time at pH 5.5. Blank shellac nanoparticles without drugs (as a negative control) and pure drug (BRB, CHX, CUR, and VCM) without loading within nanoparticles (as a positive control) were incubated as well with the cells for different time. The cell viability of *C. reinhardtii* and Baker's yeast was measured after incubating 1.0 mL of cells with 15 µL of (5 $mg.mL^{-1}$) of FDA solution in acetone for 10 minutes and washed 3 minutes with Milli Q water by centrifugation at 3000 rpm, using a Nexcelom Cellometer Auto X4 cell counter. The luminescence of *E.coli* cells was measured after incubating the cells with series of concentrations of the nanoparticles loaded the drug at different times, 100 µL of *E.coli* cells were mixed with 100 µL of BacTiter-Glo Microbial cell viability reagent in white opaque 96-well microplate after washing with Milli Q water and shook for 5 minutes, the luminescence was measured using (BMG LABTECH, FLUOstar Omega, Germany) instrument.[379]

2.11.1 Cytotoxic Effect of Shellac NPs on Algae, Yeast and *E.coli*

Different concentrations of shellac NPs (0.0125 – 0.075) wt. % were incubated with microalgae (*C.reinhardtii*), Baker's yeast (*S. cerevisiae*), and (0.005 – 0.075) wt. % were incubated with *E.coli* at pH 5.5. 5.0 mL aliquots of suspension of the washed cells were incubated with a series of 5.0 mL aliquots of aqueous dispersions of shellac NPs solutions. The control sample was treated in the same way (5.0 mL of cell suspension with

5 mL Milli Q water) without exposing them to shellac NPs solution. Then, 1.0 mL aliquots of the suspended cells were taken from each treated sample and washed with Milli Q water by centrifugation at 3000 rpm and for 3 min to remove the excess of shellac NPs suspension. The cells were re-suspended in 1.0 mL of Milli-Q water, incubated with 15 µL of FDA solution in acetone for 10 minutes and then washed three times with Milli Q water by centrifugation at 4000 rpm for 3 minutes. The cell viability was examined by using automatic cell counter concerning algae and yeast while luminescence spectroscopy was utilised to measure the luminescence for *E.coli* using BacTiter-Glo Microbial cell viability reagent.

2.11.2 Cytotoxic Effect of Free Drugs on Algae, Yeast and *E.Coli* Cells

Microalgae (*C.reinhardtii*), Baker's yeast (*S. cerevisiae*), and *E.coli* cells were incubated with different concentrations of free drugs (BRB, CHX, CUR, and VCM) at pH 5.5 and different incubation time. Concentrations of (0.001 – 0.05), (0.001-0.1) and (0.0005-0.05) wt.% of free berberine were incubated with algae, yeast, and *E.coli* respectively. Different concentrations of free CHX at (0.00005-0.01) wt.% were incubated with algae and yeast cells and (0.0001-0.05) wt.% with *E.coli* cells. While concentrations of (0.0001-0.0025) wt.% free curcumin were incubated with algae and yeast cells, respectively, and (0.0001-0.01) wt.% were incubated with *E.coli* cells. Concentrations of (0.001-0.1) wt.%, (0.001-0.25) wt.% and (0.001-0.15) wt.% free VCM were incubated with algae, yeast, and *E.coli* cells respectively.

2.11.3 Cytotoxic Effect of Drugs Loaded Shellac NPs on Algae, Yeast and *E.Coli* Cells

Microalgae (*C.reinhardtii*), Baker's yeast (*S. cerevisiae*), and *E.coli* cells were incubated with different concentrations of drugs (BRB, CHX, CUR, and VCM) loaded shellac NPs at pH 5.5 and different incubation time. Concentrations of (0.001 – 0.01) wt.% BRB-NPs were incubated with algae and yeast cells respectively, and (0.0005-0.01) wt.% of BRB-NPs were incubated with *E.coli* cells. Concentrations of encapsulated CHX at (0.0001-0.01) wt.% were incubated with algae and yeast cells respectively, and (0.0005-0.01) wt.% with *E.coli* cells. While concentrations of (0.0001-0.0025) wt.% of CUR-NPs were incubated with algae and yeast cells, respectively, and (0.0001-0.01) wt.% were

incubated with *E.coli* cells. Also different concentrations of (0.001-0.05) wt.%, (0.001-0.03) wt.% and (0.0005-0.025) wt.% VCM-NPs were incubated with algae, yeast, and *E.coli* cells respectively. Same concentrations of drugs loaded shellac NPs coated with ODTAB were incubated with these microorganisms at same pH (5.5) to investigate the cytotoxicity of drugs as NPs after coating with cationic electrolyte.

2.12 Synthesis of Magnetic Micro Beads

Fe_3O_4 magnetite nanoparticles were prepared by co-precipitation of Fe^{2+} and Fe^{3+} (1:2 molar ratio) with ammonia solution.[380] 0.05 M $FeCl_2.4H_2O$ and 0.1 M of $FeCl_3$ were dissolved in 40.0 mL of Milli-Q water. The solution was heated and stirred for 1 hour at 80 ^{0}C. 1.0 mL oleic acid and 12.0 mL of NH_4OH were added quickly. Then the produced suspension was vigorously stirred for 1 hour at the same temperature, then cooled to room temperature to let the solution to settle. Precipitation was formed, then particles were washed five times with water and ethanol, separated by magnetic decantation and dried in an oven at 80 ^{0}C. The obtained oleic acid coated magnetic nanoparticles OCMNs were easily dispersed in styrene using an ultrasound probe to form oil-based ferrofluids at 30 % amplitude and for 10 minutes. For thermal polymerisation, the thermal initiator 1, 1-Azobis (cyclohexanecarbonitrile) (Vazo) was added. The oil in water emulsion was prepared by mixing 80% of 5% Hitenol BC20 with 20% of oil-based magnetic nanoparticles and homogenised manually. After that, the resulting emulsion was mixed equally with 2% hot agarose, and cooling them under tap water, then heating them up to 72.5 degrees for 3.5 hours. Afterward, the produced particles were heated up to 88 degrees to melt agarose, and the magnetic particles were washed with water at the same temperature many times to get solidified magnetic particles.

2.13 Microfluidic Chip Fabrication

2.13.1 Fabrication of Microfluidic Chip Master Mould

A microfluidic master mould was fabricated to be used later to prepare a closed microfluidic chip which involving bonding PDMS with microscope glass slide. The method which was followed to fabricate the mould was using micromachining of poly (methyl methacrylate PMMA) substrate, and that was carried out by Dr Alex Iles,

department of chemistry, University of Hull. The manufacturing process was milling technique, which is commonly regarded as micromilling. Datron Technology M7 CNC machine was used, and the PMMA moulds were made using standard carbide milling tools aided with AutoCAD software. The mould consists of two inlet channels, one micro chamber, and one outlet channel. The fabricated chip was 75 mm length x 25 mm width with 0.3 mm channel width and the heights of the features increase in 100 µm steps from the 100 µm high shallow outlet channel, to the 200 µm high chamber to the 300 µm high inlet channels as can be seen in Figure 2.4 which is a diagram shows the microfluidic mould dimensions.

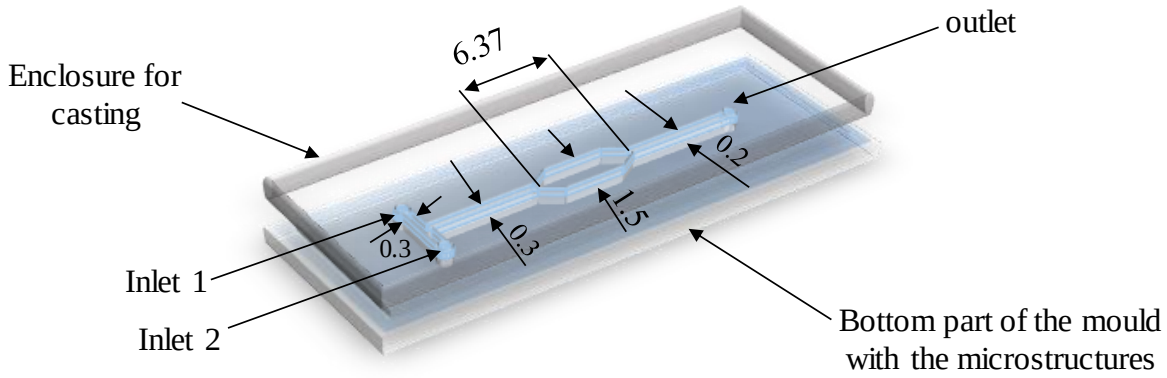

Figure 2.4: Microfluidic mould diagram for cell trapping inside the micro chamber. The two inlets are used for injecting nanoparticles, cells, Milli Q water or buffers, and FDA solution, the micro chamber is for trapping cells with nanoparticles using controlled magnetic beads by using a strong magnet, and the outlet is for flushing out chemicals and cells off-chip.

2.13.2 Fabrication of Closed PDMS-Glass Microfluidic Chip

The PDMS microfluidic top layer (Sylgard 184, Dow Corning, and Midland, MI) was prepared by mixing a 10:1 ratio of the PDMS and the curing agents in a centrifuge tube, then centrifugated for 10 minutes to homogenise the mixture. After that, the mixture was poured into the mould and degassed in a vacuum chamber for an hour before curing in a 70^0C oven for 4 h. The PDMS layer was then detached from the mould by removing the enclosure first then peeling away, and the fluidic connection ports were punched using an 18-gauge flat-tip needle. The PDMS and microscope glass devices were treated by oxygen plasma machine (Plasma Therm Etcher, 50 W, 2 torrs, 60 s) then irreversibly bonded to each other; face up of the glass (bottom plate) and PDMS (top plate), then PDMS/glass microfluidic devices was heated up to 80˚C for an hour to strengthen the bonding between

the glass and PDMS. After that, polytetrafluoroethylene (PTFE) tubes were placed into the holes punched prior to PDMS top plate to be used during pumping of the fluids. The purpose of two inlets channel was one for passing a particular concentration of the nanoparticles, while the second inlet was to inject cells. The two inlets channels could be used to pass the fluorescein diacetate (FDA) solution to determine the cell viability which is already incubated with the nanoparticles at different exposure times inside the micro chamber. The next part of the chip is the micro chamber (1.5 W x 6.37 L) mm. Before passing any materials, magnetic beads were passed using syringe pump and hold using a strong magnet, after that the cells were passed and trapped by the magnetic beads. The final part is the outlet channel which represents the waste, Figure 2.5.

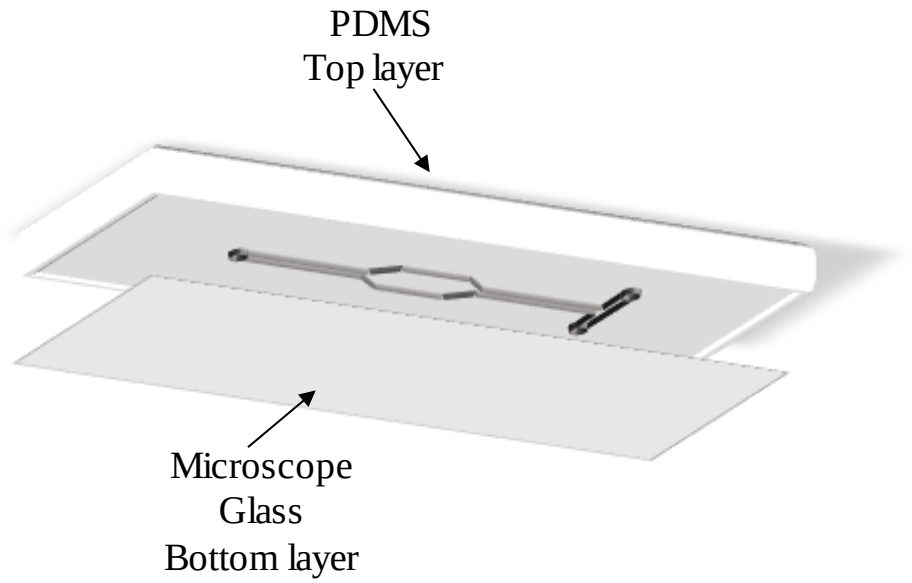

Figure 2.5: Schematic diagram of the PDMS-glass microfluidic chip which fabricated by bonding PDMS after created using mould and microscope glass using plasma machine to activate the surfaces for both of them.

2.13.3 Measuring the Cell Viability

The cell viability after trapped inside the microchamber with nanoparticles and stained with FDA reagents then washed with Milli Q water was measured depending on the fluorescence emission using Olympus microscope. This intensity was compared with the cell intensity incubated once with magnetic beads only which have been used to block the outlet hole of the microchamber and the others when incubated with shellac nanoparticles alone.

Chapter 3 : Characterisation of Shellac NPs Loaded Antimicrobial Agents

Why nanocarriers? Besides having a high surface area to volume ratio, nanocarriers as drug delivery systems have great potential for efficient delivery of various drugs, prolonged drug release, improving drugs solubility, and reducing drug toxicity. Shellac with Poloxamer 407 forms a promising nanocarrier as it consists of hydrophilic, hydrophobic parts as well as hydroxyl and carboxylic groups which can be encapsulated with different kinds of drugs and could be used as a style of amphiphilic polyelectrolyte, Figure 3.1. Further natural polymeric nanoparticles combined with natural products have good biodegradability, biocompatibility, easy to functionalize, with low or none toxicity.[381]

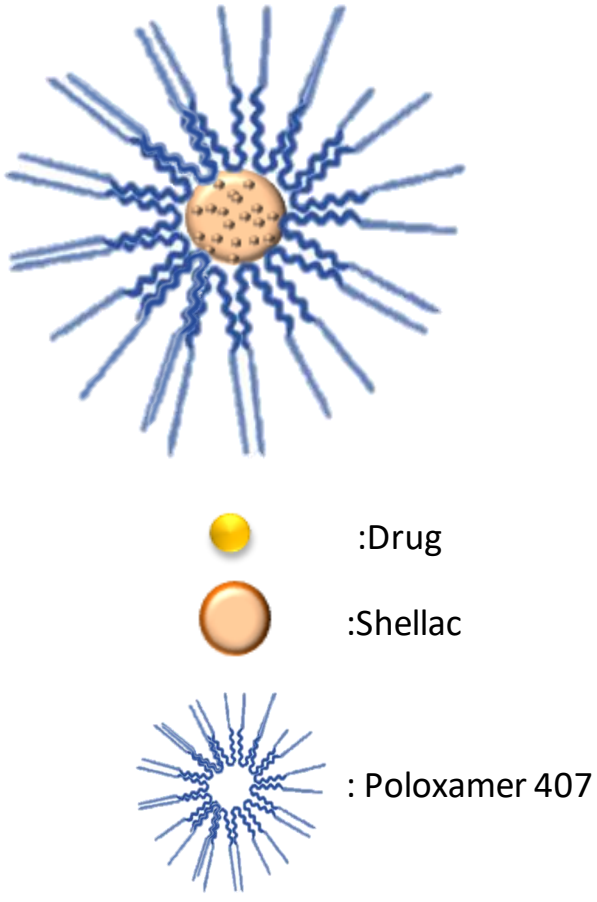

Figure 3.1: Estimated schematic design of shellac nanoparticle loaded with drug molecules and surrounded with Poloxamer 407 micelles at pH 5.

3.1 Preparation of Shellac Nanoparticles

The stability of dispersed particles depends on two principals mechanisms, steric repulsion and electrostatic repulsion. The first one shows a stabilising effect with the assistance of non-ionic surfactants and polymers that are immediately adsorbed at the phase interphase, which creates a strong balance between the attractive and the repulsive forces reliant on the thickness of the adsorbed layer. While the second mechanism of the dispersion system stabilisation is established on an electrostatic repulsion. The surface charge of the disperse phase can be enhanced by adding anionic surfactant which provides the electrostatic protection of the NPs to attract to one another.[382]

To synthesis shellac nanoparticles there were several attempts with different types of surfactants such as sodium dodecyl sulphate (SDS), Cetyltrimethylammonium bromide CTAB, Tween 20 and Poloxamer 407. CTAB and Tween 20 did not give good outcomes, while SDS at different concentrations in 10% ethanol showed nano shellac particle with size around 50 nm, but unfortunately, these nanoparticles were unstable due to the lack of electrostatic repulsive between particles. On the other hand, Poloxamer 407, non-ionic triblock copolymer exhibited a good stabiliser for shellac Particles. Due to its amphiphilic nature, Poloxamer 407 plays a good role in stabilising the nanoparticles as its hydrophobic parts adsorbed on the hydrophobic surface of shellac molecules creating a steric repulsion between each other particles as shown in (Figure 3.2, B).

Consequently, stable shellac nanoparticles were prepared based on the steric repulsion property using Poloxamer 407 surfactant as a stabiliser and accompanied by lowering the pH from 8 to 5. As it is known that Poloxamer 407 is a non-ionic poly (ethylene oxide)(PEO)-poly (propylene oxide) (PPO) poly (ethylene oxide) (PEO) has been widely used in the pharmaceutical formulation as surfactants, solubilising agent, emulsifying agent, and dispersing agent,[383] Figure 3.2, A.

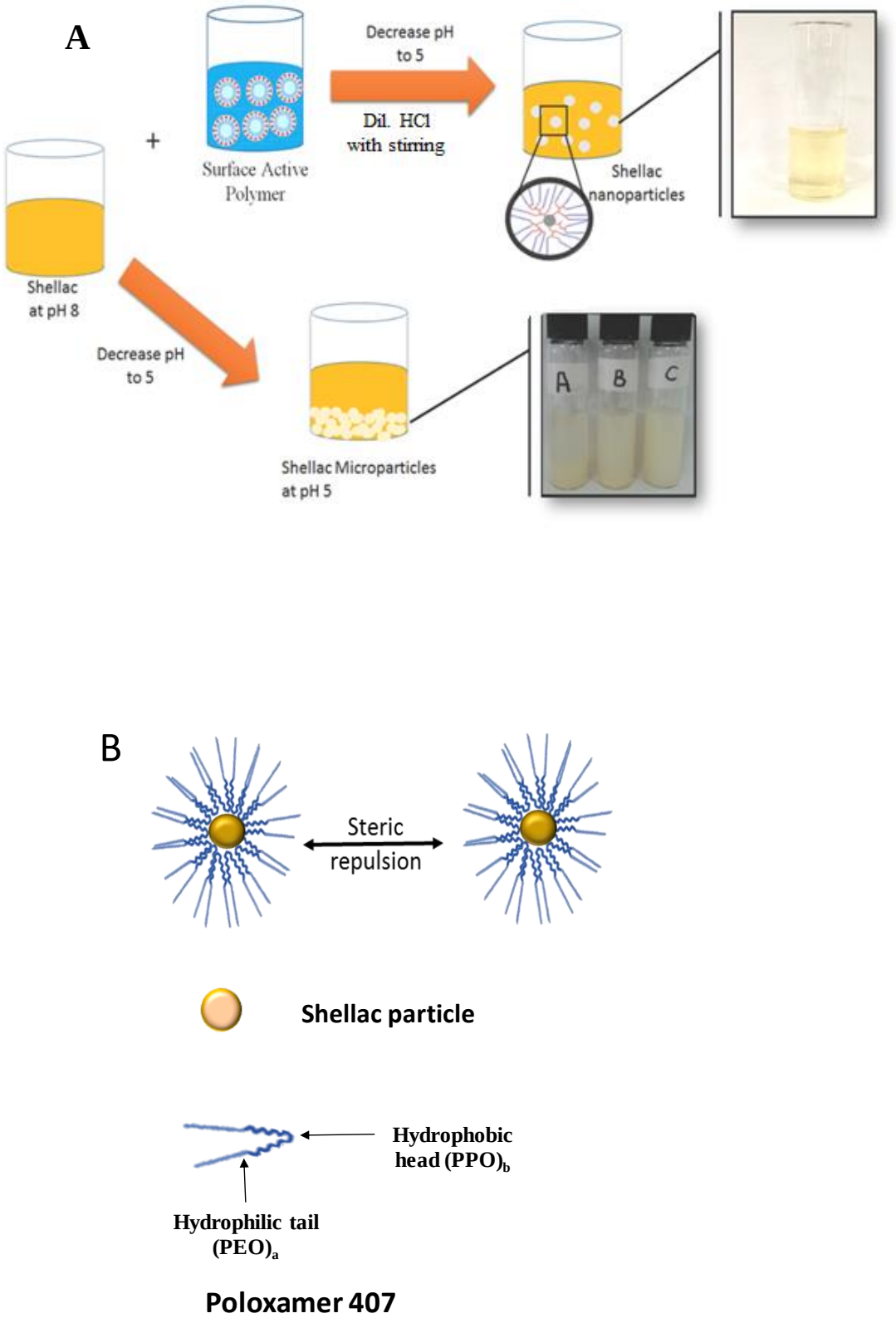

Figure 3.2: Schematic diagram A) preparation of shellac nanoparticles by dropping the pH from 8 to 5 by adding drops of diluted HCl with gentle stir in the presence of P407. B): steric repulsion stability of shellac NPs caused by Poloxamer 407 micelles.

3.2 Characterization of Shellac NPs

3.2.1 Size and Zeta Potential Characterization of Shellac NPs

Shellac nanoparticles were prepared at the size of 66±5 nm, Figure 3.3 and Figure 3.4 show the particle size distribution and the zeta potential of shellac NPs formulated by mixing 0.25 wt.% of shellac with 0.2 wt.% Poloxamer 407 at pH 5 with a zeta potential of –18±8 mV. While Figure 3.5 shows that shellac at pH 5 without adding Poloxamer 407 has particle size about 500 nm with aggregation. Figure 3.6 shows the micelles size of Poloxamer 407 which was around 35 nm and it is with agreement with literature review.[384]

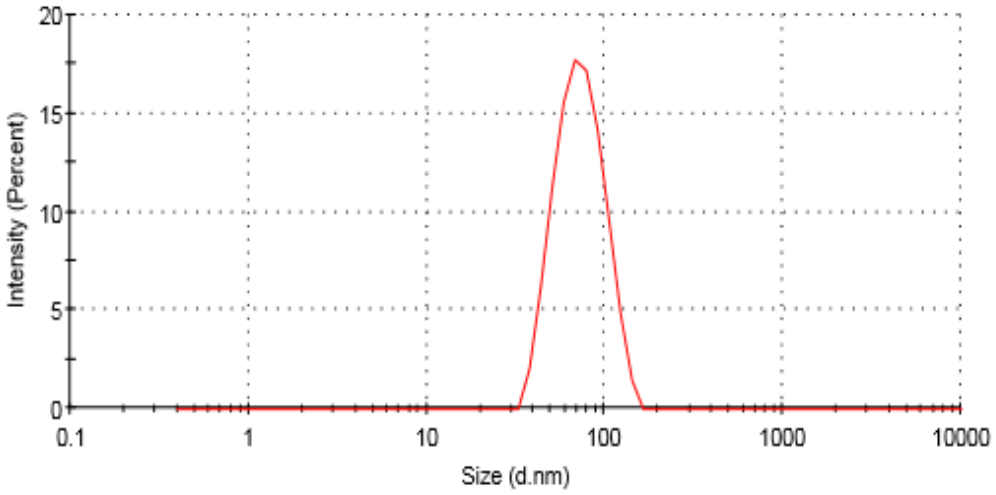

Figure 3.3: The particle size distribution of shellac nanoparticles was obtained by mixing a ratio of 0.25:0.2 w/v% of shellac: Poloxamer 407 which gives a proper nanoparticles size of Shellac NPs in Milli Q water at pH 5.

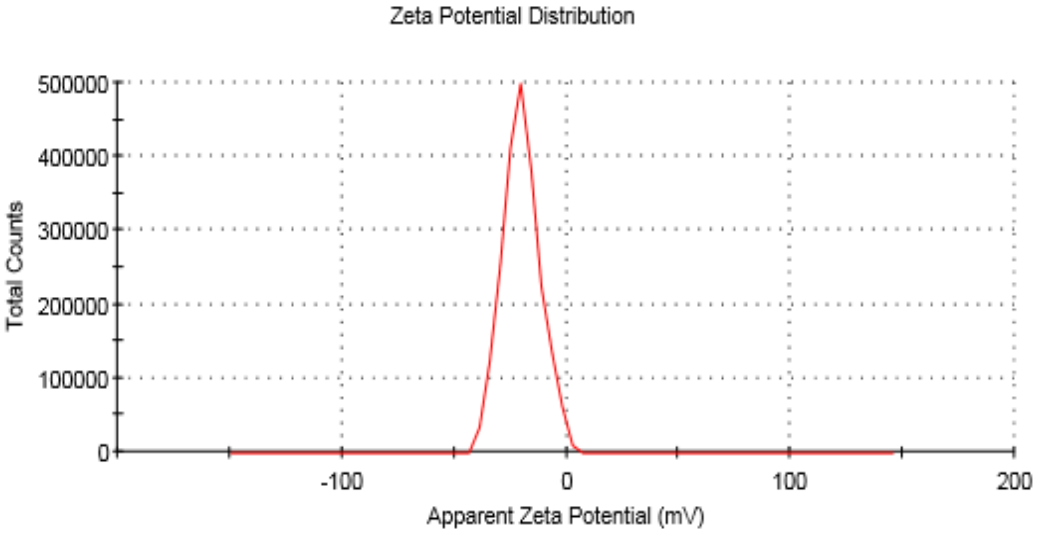

Figure 3.4: The zeta potential of shellac NPs at pH 5 (prepared by mixing 0.25 wt. % ammonium shellac with 0.2 wt. % P407) in Milli Q water.

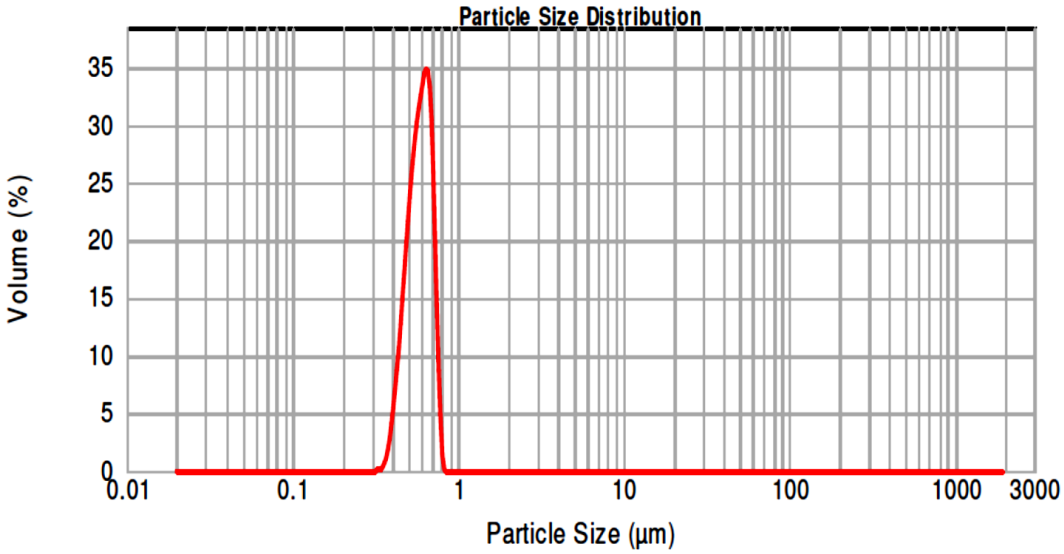

Figure 3.5: The particle size of shellac at pH 5 without using Poloxamer 407 by means of Mastesizer.

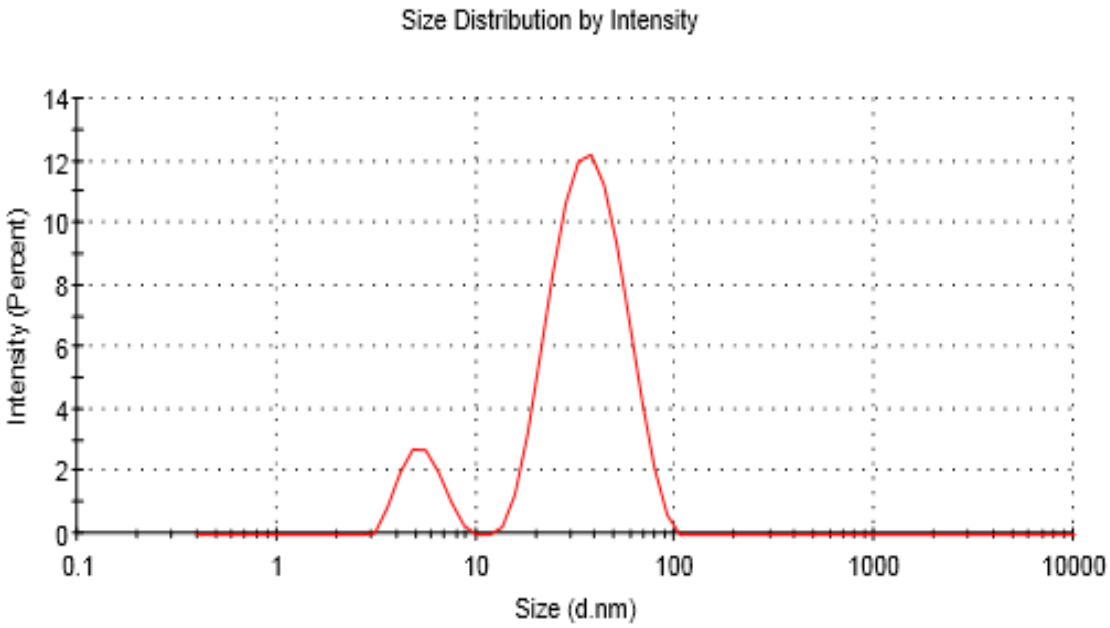

Figure 3.6: The particle size distribution of Poloxamer 407 micelles at pH 5 in Milli Q water by means of zeta sizer instrument.

To achieve a perfect size and surface charge for shellac NPs, different amounts of Poloxamer 407 have been mixed with 0.25 wt.% of shellac solution at pH 8, then measuring the size and the zeta potential after reducing the pH to 5. As it can be seen from Figure 3.7 that when using low amount of Poloxamer 407 the particle size is high and reaches to 122 nm at 0.01 wt.% Poloxamer 407 then the particle size decreases while the

amount of Poloxamer 407 increases, at 0.2 wt.% and higher amount of Poloxamer 407 a plateaued line of nanosized particles can be seen. Therefore 0.25:0.2 wt.% of shellac : Poloxamer 407, respectively, considered the best ratio to obtain stable shellac NPs and been fixed for further experiments. On the other hand, the surface charge of the shellac decreased during the amount of Poloxamer 407 increased.

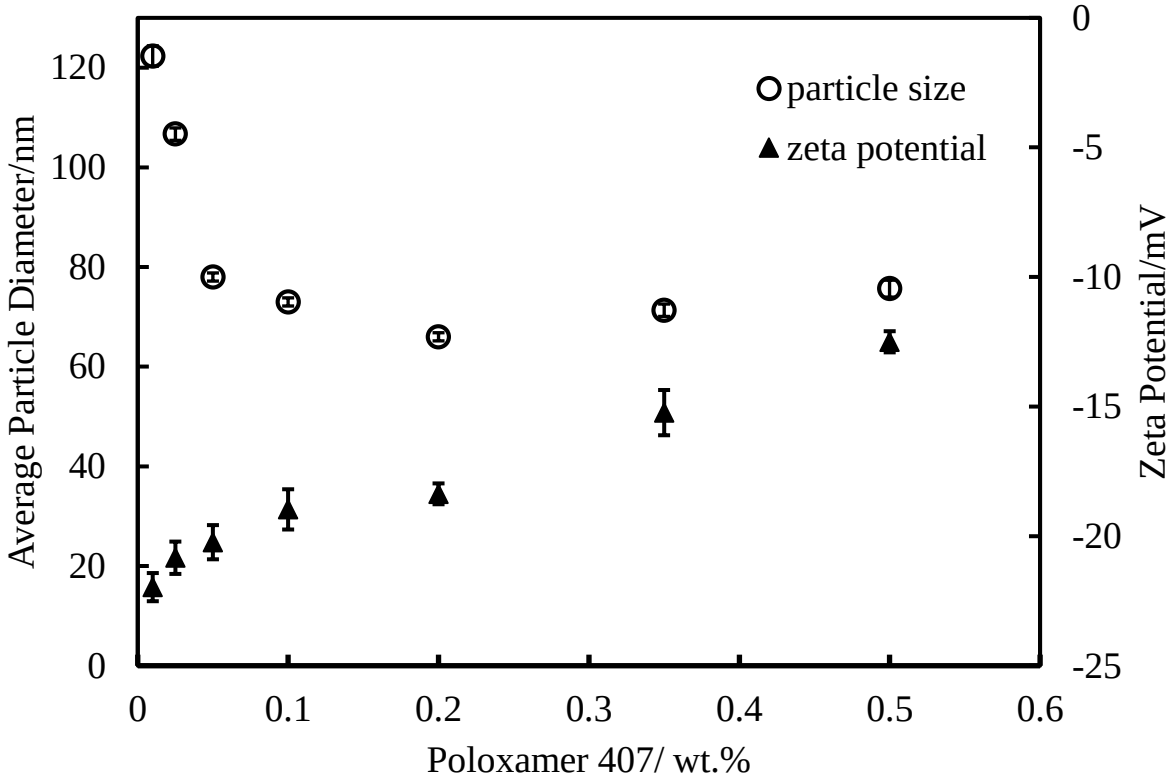

Figure 3.7: The size and zeta potential of shellac NPs using 0.25% of shellac with different concentrations of Poloxamer 407 in Milli Q water at pH 5, (n=3).

Figure 3.8, A shows the TEM image of the shellac NPs suspension after drying up, and it reveals a spherical shape of the NPs with size of 33±10.87 nm as can be seen in figure 3.8, B. This supports the result obtained by using the zeta sizer equipment that shellac NPs has nanosize.

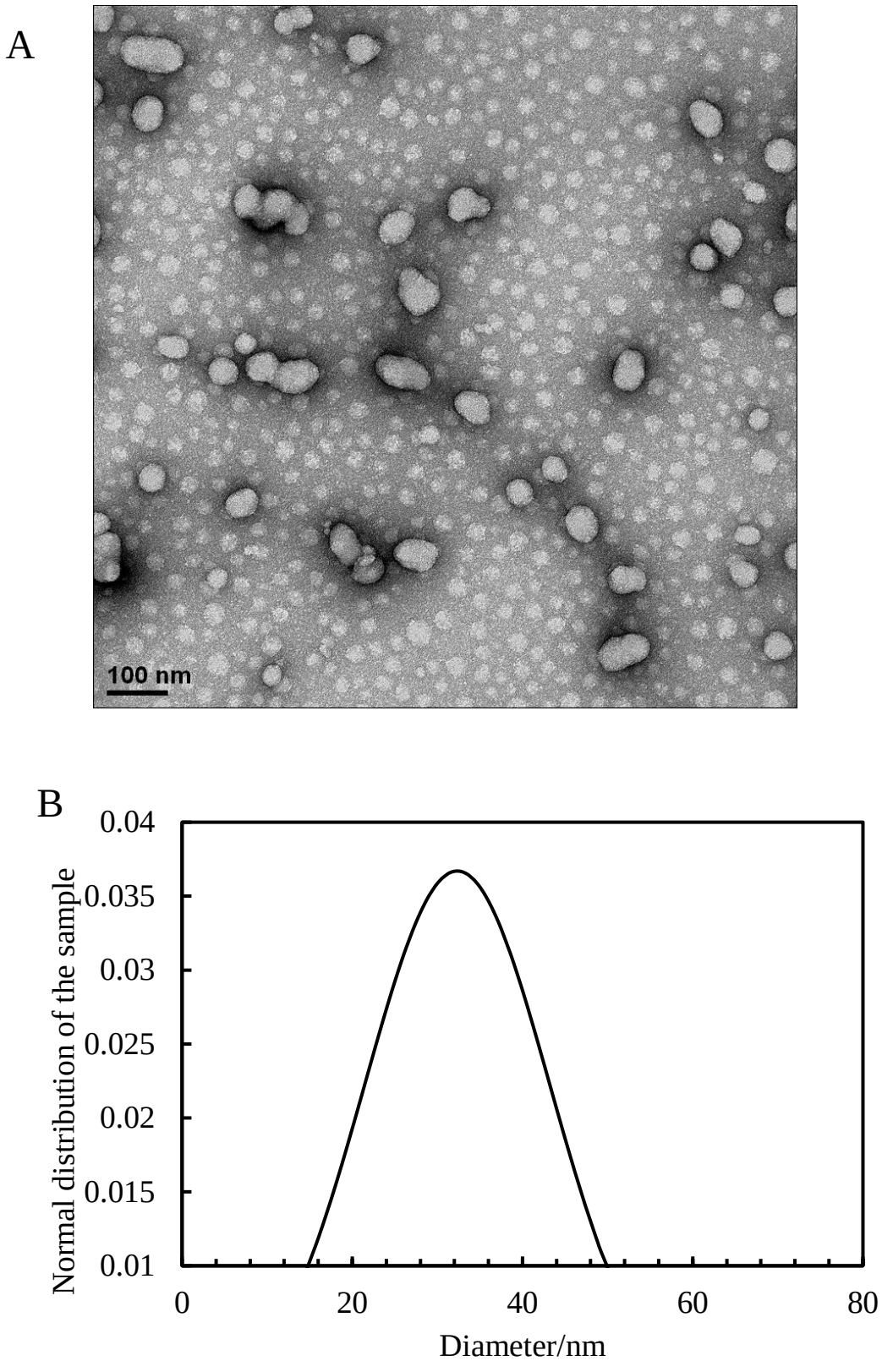

Figure 3.8: (A): The TEM image of shellac NPs, (B) the shellac NPs size distribution for a solution consisting of 0.25 wt. % shellac with 0.2 wt. % P 407 in Milli Q water and negatively stained with 1% uranyl acetate.

3.2.2 Effect of pH on Particle Size and Zeta Potential

To study the effect of different pH on the size and the surface charge of shellac nanoparticles, the size and the zeta potential of the NPs was observed using DLS technique at a range of pH media, the size of the nanoparticles did not change at a range of pH from 4 to7.5 as shown in Figure 3.9, while the charge of the nanoparticles changed from -21mV at pH 7 to -5.3 mV at pH 4 due to the protonation of shellac carboxylic groups, this proves that this nanocarrier can potentially use at different range of pH.

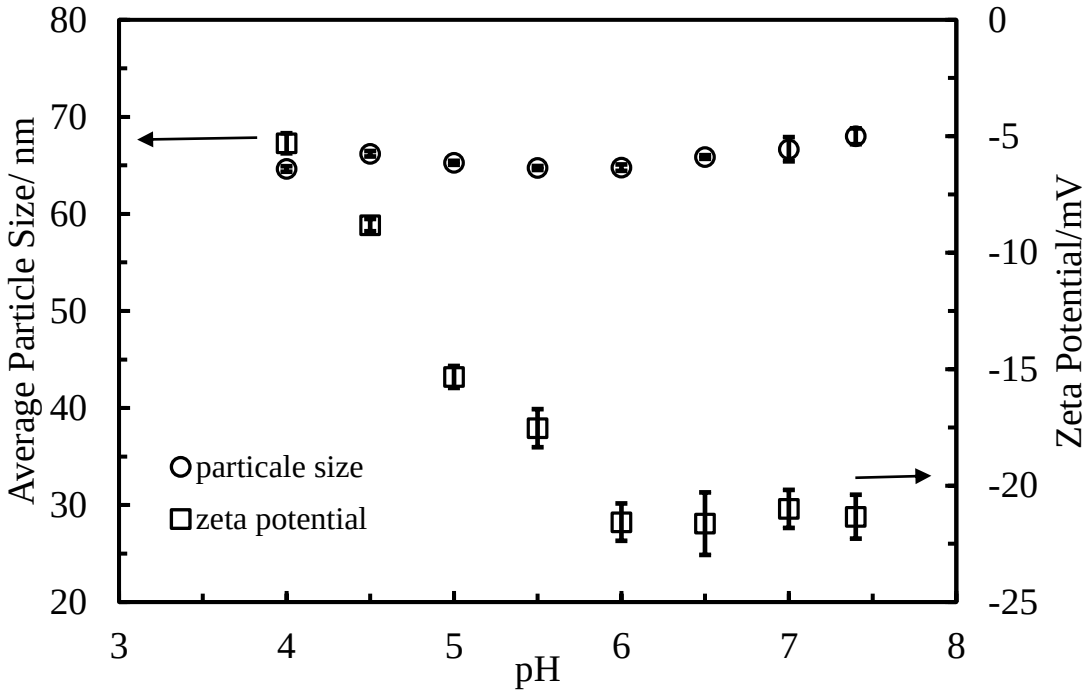

Figure 3.9: The average particle diameter and the surface charge of shellac NPs at different pH using DLS technique, (n=3).

3.2.3 The Effect of the Time on the Size and Zeta Potential of Shellac NPs

In order to investigate shellac NPs storage condition, size distribution and zeta potential of the nanoparticles were observed as a function of time, up to 90 days in Milli Q water. Figure 3.10 shows the size and surface charge of shellac NPs and as it can be seen that shellac NPs are stable within period last more than three months with the size of around

68 nm and surface charge of -18 mV. This can prove that these NPs can be saved for a long time without aggregation and used later to encapsulate with drugs.

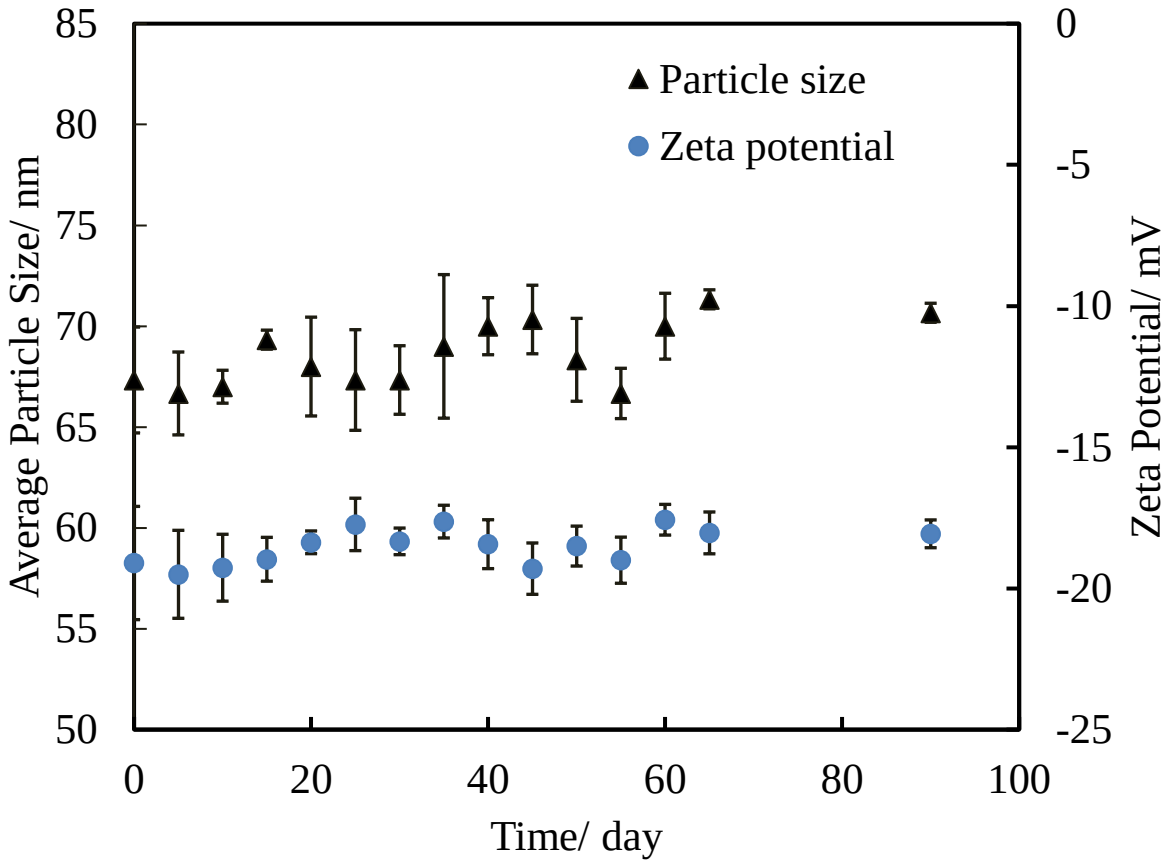

Figure 3.10: The average particle diameter and the surface charge of shellac NPs at different time using DLS technique, (n=3).

3.2.4 FTIR Studies for Shellac, Poloxamer 407, and Shellac NPs

The infrared absorption spectra of shellac, Poloxamer 407, and shellac nanoparticles are represented in Figure 3.11, the spectrum of shellac (blue line) shows the broad main peak at 3319 cm^{-1} which belongs to the absorption of O-H stretching vibration band, and a peak at 1707 cm^{-1} represents carbonyl stretching vibration band (C=O) and C-O stretching band appears at 1247 cm^{-1}.[57, 94] Poloxamer 407 spectrum (black line) shows a principal absorption peaks at 2878 cm^{-1} for C-H aliphatic stretching and at 1342 cm^{-1} for the absorption of (in-plane O-H bend), another principal peak can be observed at 1097 cm^{-1} which belong to the absorption of C-O stretch.[385] The IR spectrum of the nanoparticles (brown line) shows no difference to Poloxamer 407 or shellac spectrum but only a slight shift of some peaks, in comparison to shellac and Poloxamer 407 spectra. Some of Poloxamer 407 peaks were merged with shellac peaks as there is no chemical reaction

between shellac and Poloxamer 407, the attraction is an adsorption of the hydrophobic part of Poloxamer 407 on shellac surface, and O-H stretching band still exist at 3392 cm^{-1}, while carbonyl stretching vibration (C=O) and C-O stretching bands appeared at 1711 cm^{-1} and 1241 cm^{-1}, respectively, as shown in Figure 3.11.

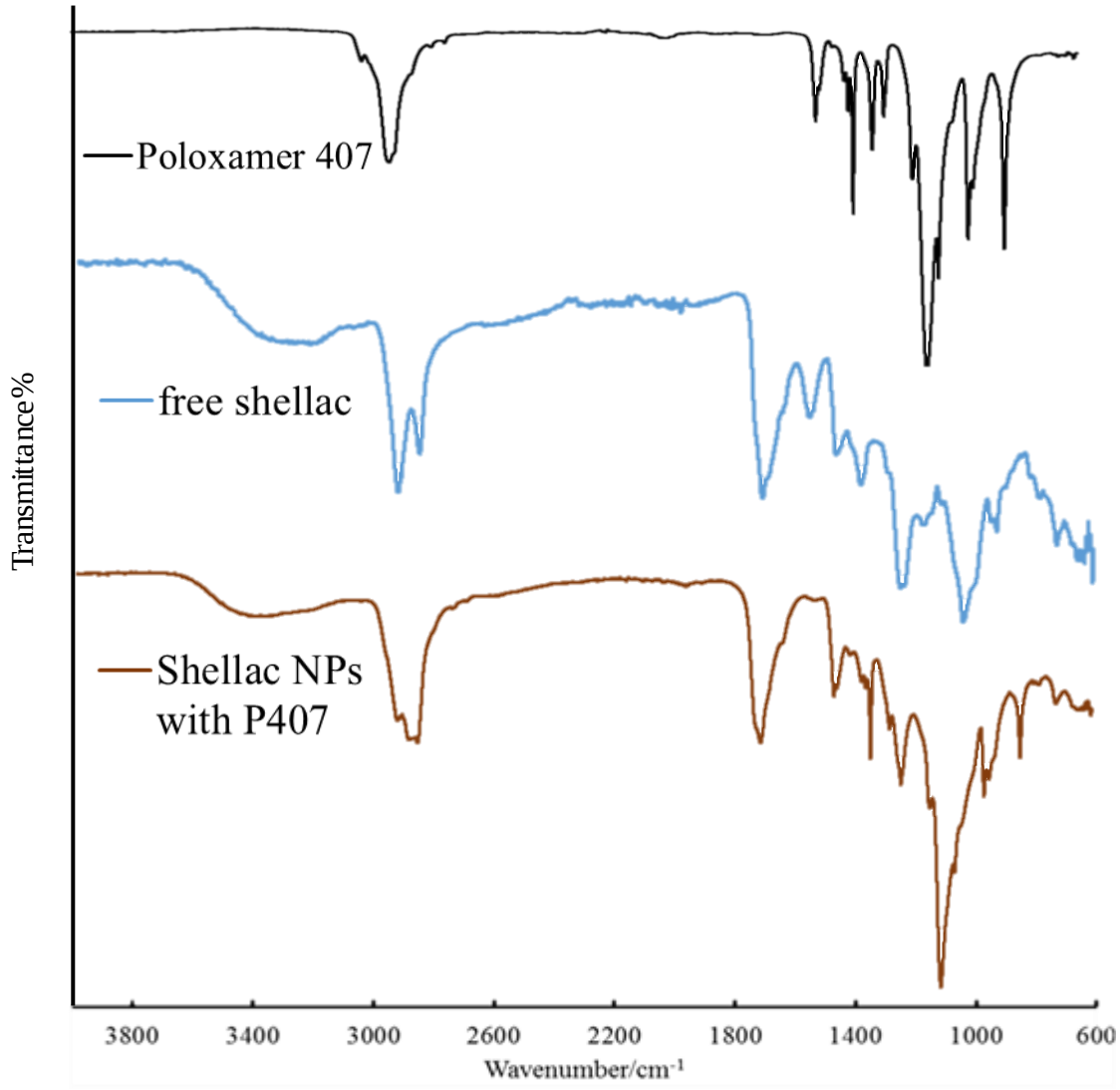

Figure 3.11: FTIR spectra of Poloxamer 407, free shellac, and Shellac NPs with Poloxamer 407.

3.3 Encapsulation and Characterization of Berberine Chloride Loaded within Shellac NPs

Berberine chloride was encapsulated within shellac nanoparticles by mixing the three components shellac, Poloxamer 407 and berberine at pH > 7 then decreasing the pH to 5 to protonate the shellac carboxylic groups and thus decreasing the shellac solubility and dispersing it as a nanoparticle. BRB can interact with shellac particle electrostatically owing to the interaction between the nitrogen atom of BRB with the carboxylic groups in shellac, as can be seen in figure 3.12. figure 3.13 shows that shellac NPs can be loaded with berberine up to 0.07 wt. %, at higher concentrations the NPs are not stable and aggregate, while the zeta potential of the NPs changed from -20 mV at 0.01 wt.% BRB to -14.8 mV at 0.07 wt.% BRB, and this decrease in surface charge attributed to the increasing of berberine amount which possess positive charge. At 0.03 wt.% of berberine loaded shellac NPs shows stable particles with a size of 77 ±34 nm, this can be observed in Figure 3.14 with a zeta potential of -18.6±7 mV (Figure 3.15). TEM image shows the spherical particles of shellac NPs after loading with berberine chloride as can be seen in Figure 3.16.

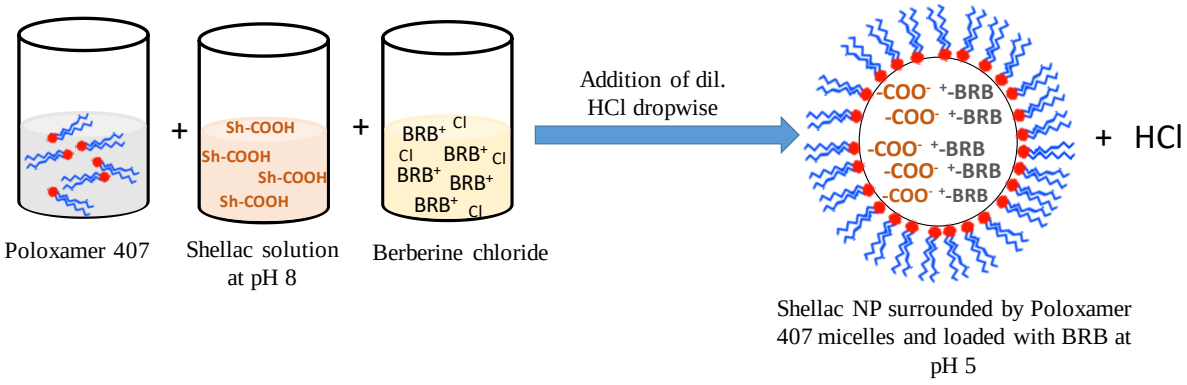

Figure 3.12: Schematic diagram represents the process of preparing shellac NPs loaded with Breberine chloride at pH 5 by mixing shellac, BRB, and P407 at pH 8 then reducing the pH to 5 using dil. HCl.

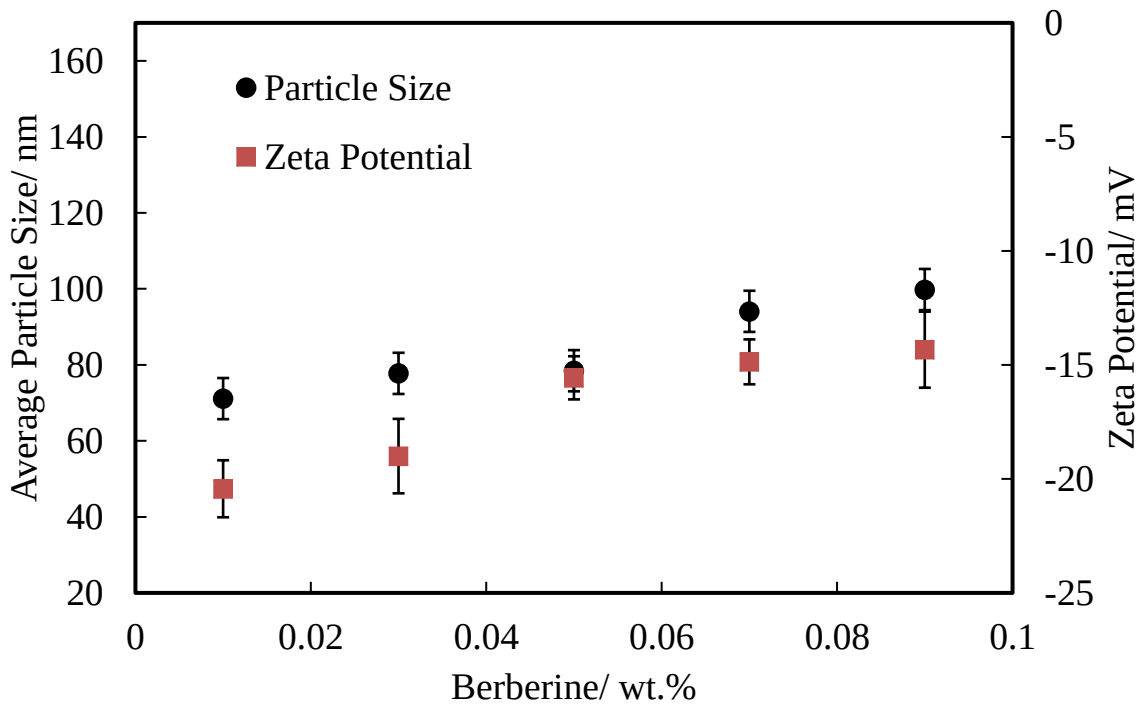

Figure 3.13: The effect of loading different concentrations of berberine chloride on the size of 0.25 wt. % shellac nanoparticles at pH 5, (n=3).

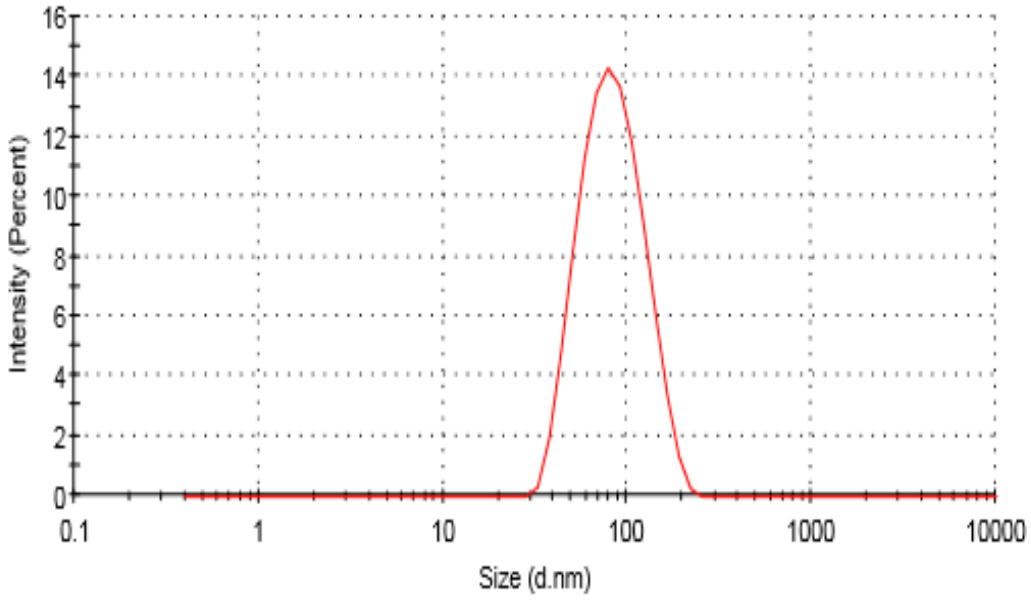

Figure 3.14: The average particle size of 0.03 wt.% berberine loaded shellac nanoparticles at pH 5 in Milli Q water using DLS technique.

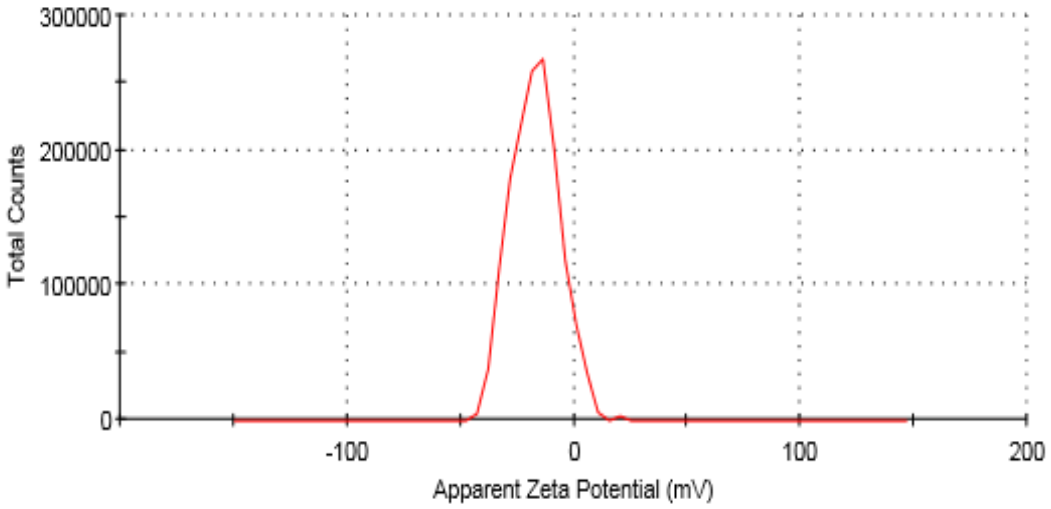

Figure 3.15 : The zeta potential of shellac NPs loaded berberine at pH 5 (prepared by mixing 0.25 wt. % ammonium shellac with 0.2 wt. % P407 and 0.03 wt. % BRB in Milli Q water.

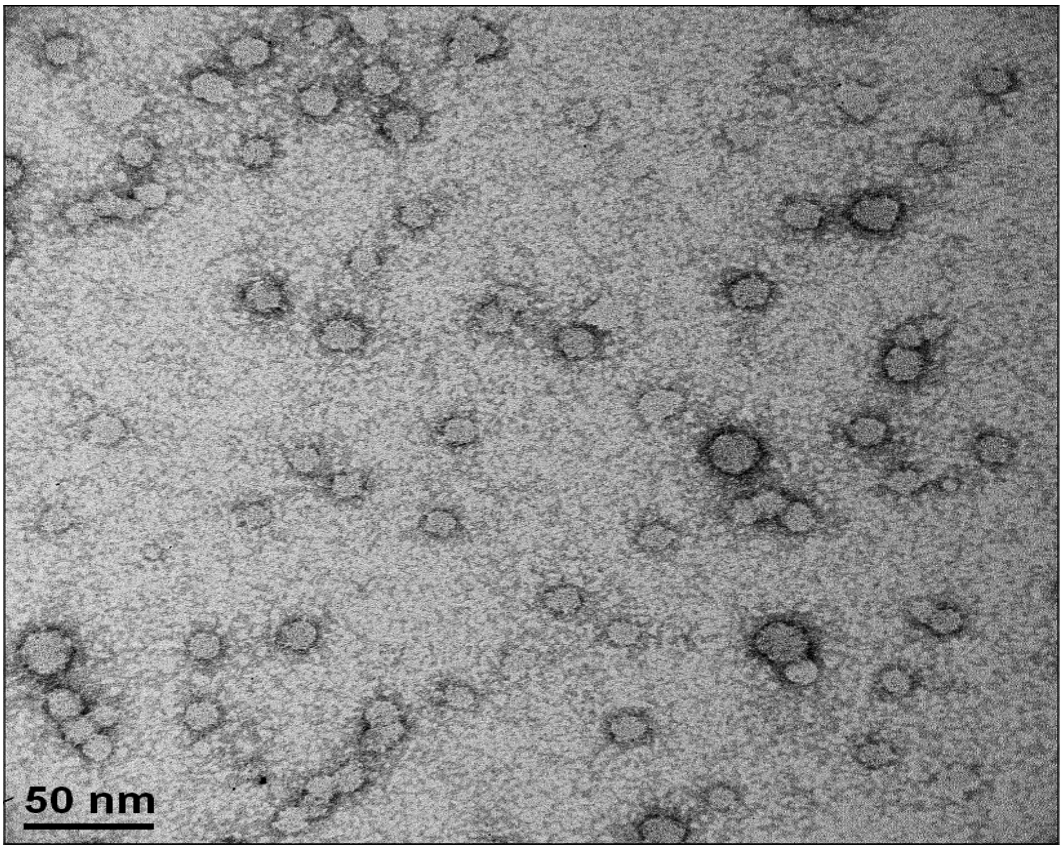

Figure 3.16: TEM image of the encapsulated berberine chloride with shellac NPs for a solution consisting of 0.25 wt. % shellac with 0.2 wt. % P 407 and 0.03 wt. % berberine chloride in Milli Q water, the NPs were negatively stained with 1% uranyl acetate.

3.3.1 FTIR Spectroscopy Studies of Free Berberine, Shellac NPs, and BRB NPs

The infrared spectrum of free berberine chloride characterised by a principal peak which absorbed at 1602 cm^{-1} related to -C=N- quaternary iminium ion, and a peak at 1504 cm^{-1} (C=C stretching vibration of aromatic ring) (Figure 3.17, red line). [157] While shellac NPs shows a broad peak at 3392 cm^{-1} belongs to O-H stretching vibration peak and for carbonyl C=O stretching band at 1711 cm^{-1} (Figure 3.17, brown line). The intensity of these peaks were declined when berberine was loaded into shellac nanoparticles, and most berberine peaks merged within shellac NPs peaks, this proves the reaction between berberine and shellac, while the broad band of O-H stretching which belongs to shellac still exist with slight shifting as can be seen in Figure 3.17, green line.

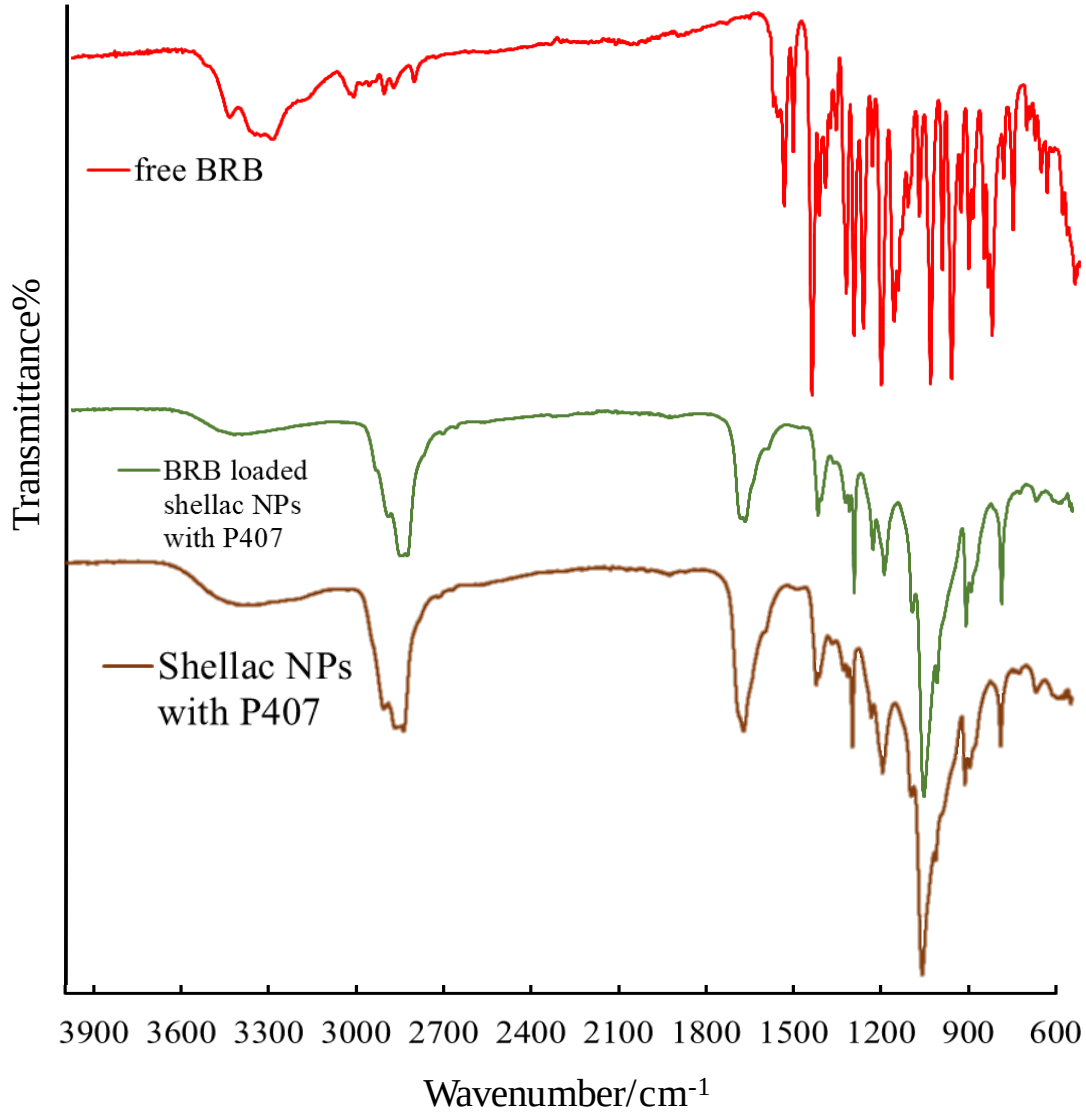

Figure 3.17: FTIR spectra of free BRB, 0.03 wt.% BRB-NPs, and Shellac NPs with P407 at a range of wavenumber 4000-600 cm^{-1}.

3.3.2 UV-Visible Spectrophotometric Studies

The UV-Vis technique was used to identify the encapsulation of berberine within shellac nanoparticles. Figure 3.18 shows the absorption spectrum of shellac, Poloxamer 407, and berberine loaded shellac nanoparticles. The shellac spectra (black line) shows random peaks at 300 nm – 200 nm and that is because it contains different carboxylic acid components with no significant maximum wavelength, while the pure berberine (blue line) has four absorption peaks, one which was in the visible area with a wavelength of 422 nm and three peaks in the UV region with wavelengths at 350 nm, 265 nm and 230 nm respectively. These spectra show there is no spectral interference between the absorbance of shellac, berberine and Poloxamer (the later has no significant peak between 700 -200 nm, red line) in visible and near UV area. The green line shows the absorbance spectrum for the berberine-loaded shellac nanoparticles (BRB-NPs) and as it can be clearly observed two peaks appeared at 422 and 350 nm which belong to berberine and no specific peaks around wavelengths 300 to 200 nm and that belong to shellac absorption, this provides a clear evidence that the cationic berberine is conjugated with the anionic carboxyl groups of shellac.

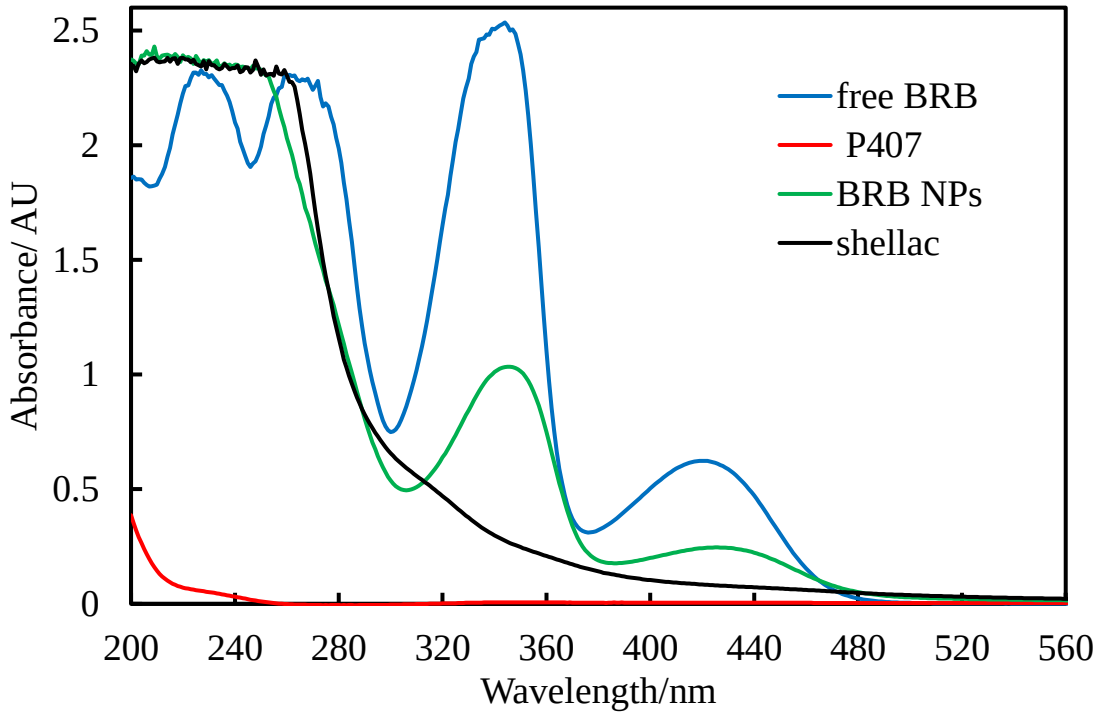

Figure 3.18: Absorption spectrum of Berberine, free shellac, Berberine loaded shellac NPs and Poloxamer 407 using UV-Vis spectrophotometry technique.

3.3.3 Berberine Encapsulation Efficiency and Drug Loading Contents

The berberine encapsulation efficiency within the NPs was measured at pH 5. It was found that the highest encapsulated amount of berberine within shellac nanoparticles was about 60% at 0.03:0.25:0.2 w/v% of berberine: shellac: Poloxamer 407 amount respectively, as apparent from Figure 3.20. While the berberine loading contents can be observed from Table 3.1.

The encapsulation efficiency and drug loading of berberine (BRB) in the NPs were calculated using equations below:

$$\text{Berberine Encapsulation (\%)} = \frac{[w_{BRB} - w_U]}{w_{BRB}} \times 100 \qquad 3.1$$

$$\text{Drug Loading Content (\%)} = \frac{[w_{BRB} - w_U]}{[w_{BRB} - w_U + w_{sh+P407}]} \times 100 \qquad 3.2$$

Where W_{BRB} is the total amount of berberine added to the shellac at pH 8, W_U is the unencapsulated amount of berberine obtained after filtration using 20 nm syringe filter, and $W_{sh+P407}$ is the amount of shellac and Poloxamer used to prepare the whole system.

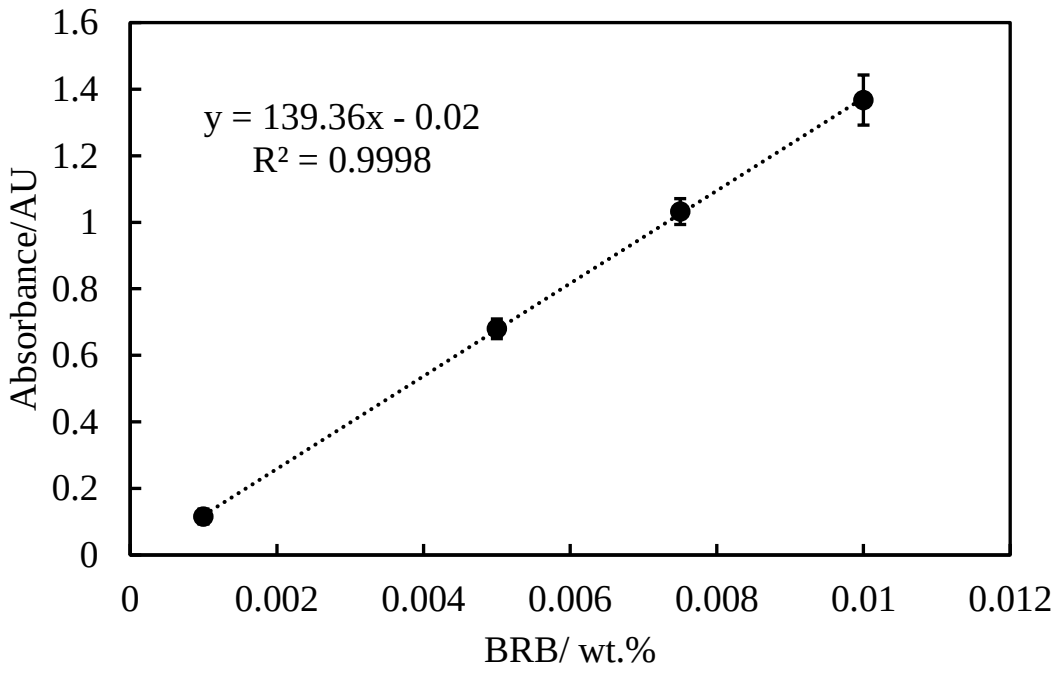

Figure 3.19: The calibration curve of berberine chloride at 422 nm in Milli Q water, (n=3).

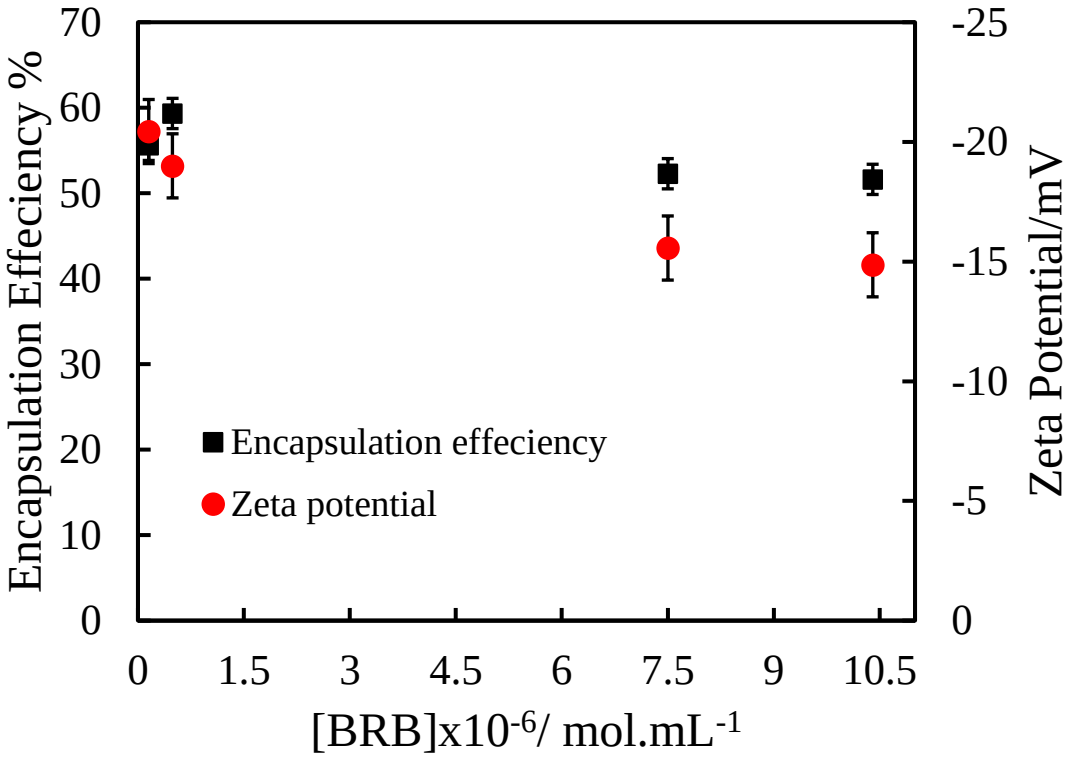

Figure 3.20: The encapsulation efficiency percent of different concentrations of berberine loaded shellac nanoparticle at pH 5, (n=3).

Table 3.1 shows the berberine amount loaded into shellac nanoparticles, and can be seen by increasing the drug amount the loading percent increased.

Table 3.1. The drug loading percent of different concentrations of BRB.

Mol.mL^{-1}BRB loaded 2.5x10^{-6} mol.mL^{-1} shellac NPs and 1.6x10^{-7} mol.mL^{-1} P407	Drug Loading (%)
1.52x10^{-7}	5.4
4.9x10^{-7}	15.6
7.5x10^{-6}	22
10.4x10^{-6}	28

3.3.4 Berberine Release Study

In order to monitor the amount of released berberine from shellac NPs at a specific pH, the berberine loaded shellac NPs suspension was placed into a dialysis bag which allowed the berberine to be released from the nanoparticles then diffused through its pores. The dialysis device was placed into a beaker which had already being filled once with phosphate buffer solution (pH 5.5) and the other with PBS solution pH 7.4. After that, the in vitro drug release was measured using a UV-Visible spectrophotometer. All release experiments were carried out in triplicate. The percentage of cumulative drug release was calculated by using the below equation

$$\%\ In\ Vitro\ Drug\ Release = \frac{M_{released}}{M_{total}} x\ 100 \qquad 3.3$$

Where $M_{released}$ is the amount of drug released from the shellac NPs at time *t* and M_{total} is the amount of drug loaded into shellac NPs. As can be seen from
Figure 3.21 the releasing % of berberine at pH 5.5 is higher than at pH 7.4 and that because of at pH 5.5 the hydrophobicity of shellac nanoparticles is higher and that lead to increasing the releasing drug amount, and it reached to 100% after 8 hours, while at pH 7.4 the releasing % was about 75% after 8 hours.

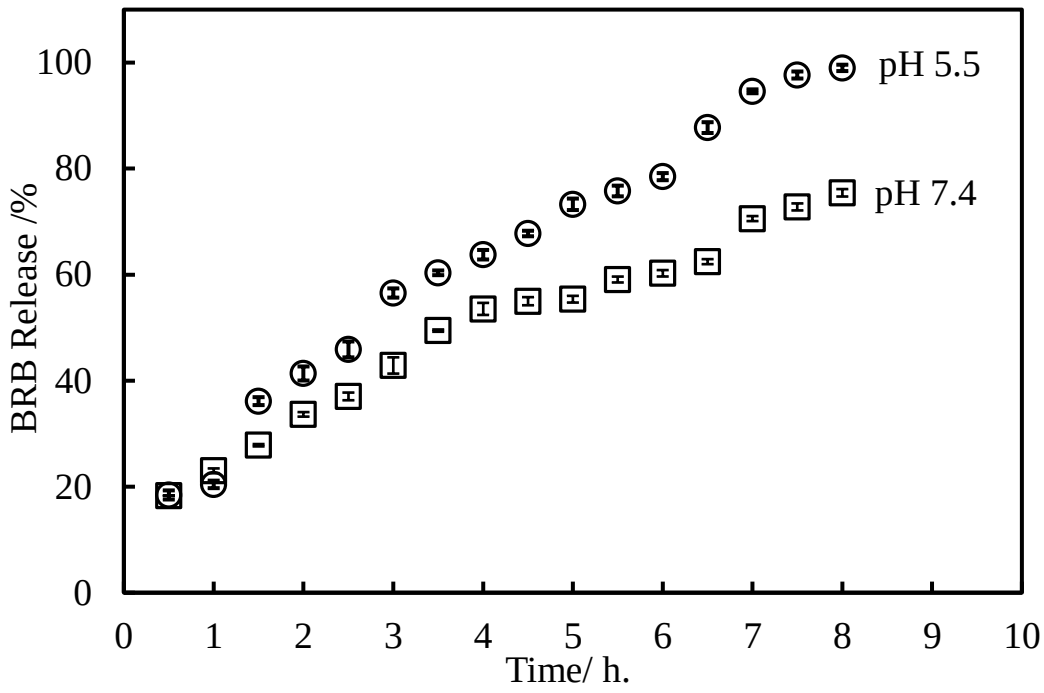

Figure 3.21: The percentage of in vitro berberine release as a function of time at different pH. The measurements were carried out using Perkin Elmer UV-Visible Spectrophotometer at a range of wavelength (220-700) nm, (n=3).

3.4 Encapsulation and Characterisation of Chlorhexidine Di-gluconate Loaded within Shellac NPs

The method that was used to encapsulate chlorhexidine was the same that was used to encapsulate berberine within shellac nanoparticles by mixing the three components shellac, Poloxamer 407, and chlorhexidine at pH >7 then decreasing the pH to 5 to protonate shellac carboxylic groups and thus decreasing the solubility and dispersed as nanoparticles, as can be seen in figure 3.22. Figure 3.23 shows the size of chlorhexidine loaded shellac NPs and it was about 79±30 nm with surface charge of -11±8 mV. The size of shellac NPs has been increased from 66 nm to 79 nm, and this indicated that there is an interaction between shellac NPs and chlorhexidine. While the zeta potential decreased from -18 mV to -11 mV due to the interaction between shellac carboxylic group and chlorhexidine nitrogen atoms, (Figure 3.24).

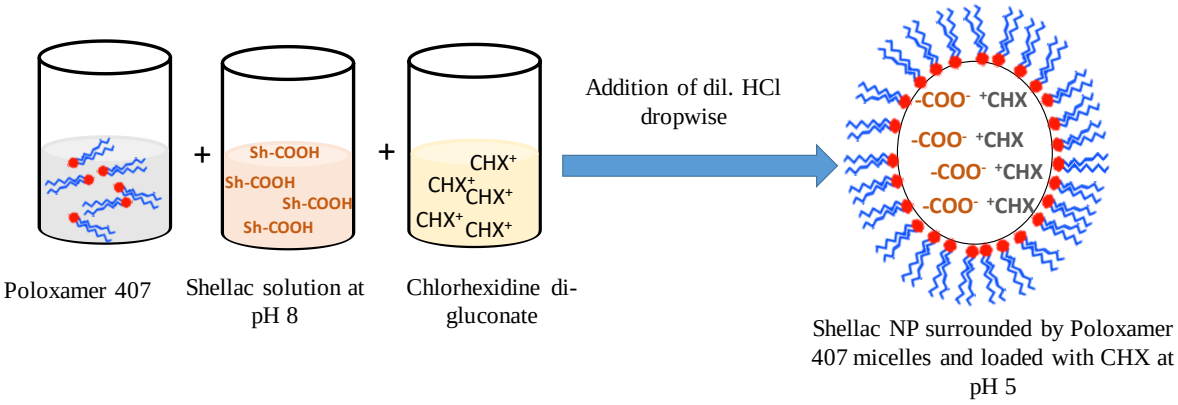

Figure 3.22: Schematic diagram represents the process of preparing shellac NPs loaded with CHX at pH 5 by mixing shellac, CHX, and P407 at pH 8 then reducing the pH to 5 using dil. HCl.

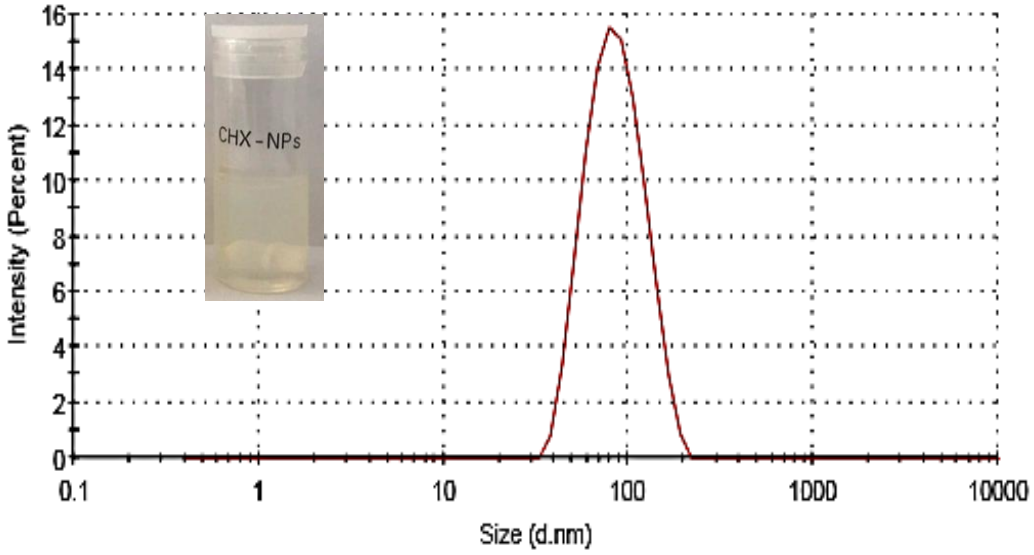

Figure 3.23: The average particle size of chlorhexidine loaded shellac nanoparticles at pH 5 in Milli Q water.

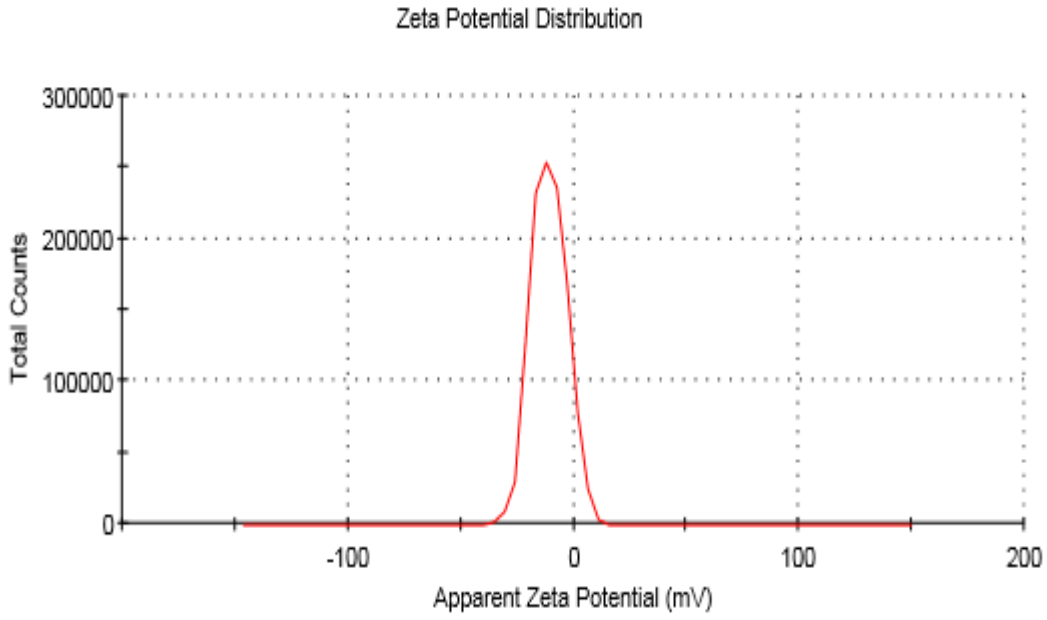

Figure 3.24: The zeta potential of shellac NPs loaded with chlorhexidine at pH 5 (prepared by mixing 0.25 wt. % ammonium shellac with 0.2 wt. % P407 and 0.03 wt. % CHX in Milli Q water.

The size and the zeta potential of shellac nanoparticles loaded chlorhexidine di-gluconate were measured (prepared by mixing 0.25wt.% ammonium shellac with 0.2% Poloxamer 407 and different concentrations of chlorhexidine di-gluconate were added, then lowering the pH to 5 using dil. HCl) using zetasizer Malvern Nano ZS. As can be seen from Figure 3.25 at high concentration of chlorhexidine the size of the nanoparticles started

increasing due to the increase of loaded amounts of chlorhexidine, and it reached to about 150 nm at 0.05 wt. % chlorhexidine, while the surface charge of the nanoparticles decreased from -20 mV to less than -1 mV and this resulted from the increasing amount of the loaded high positively charged chlorhexidine di-gluconate as it contains 10 nitrogen atoms. The decrease in the zeta potential amount can also indicate that the chlorhexidine has interacted with shellac NPs. Transmittance electron microscopy (TEM) of chlorhexidine loaded shellac NPs was examined as shown in Figure 3.26. The picture reveals that CHX loaded shellac NPs has a spherical shape.

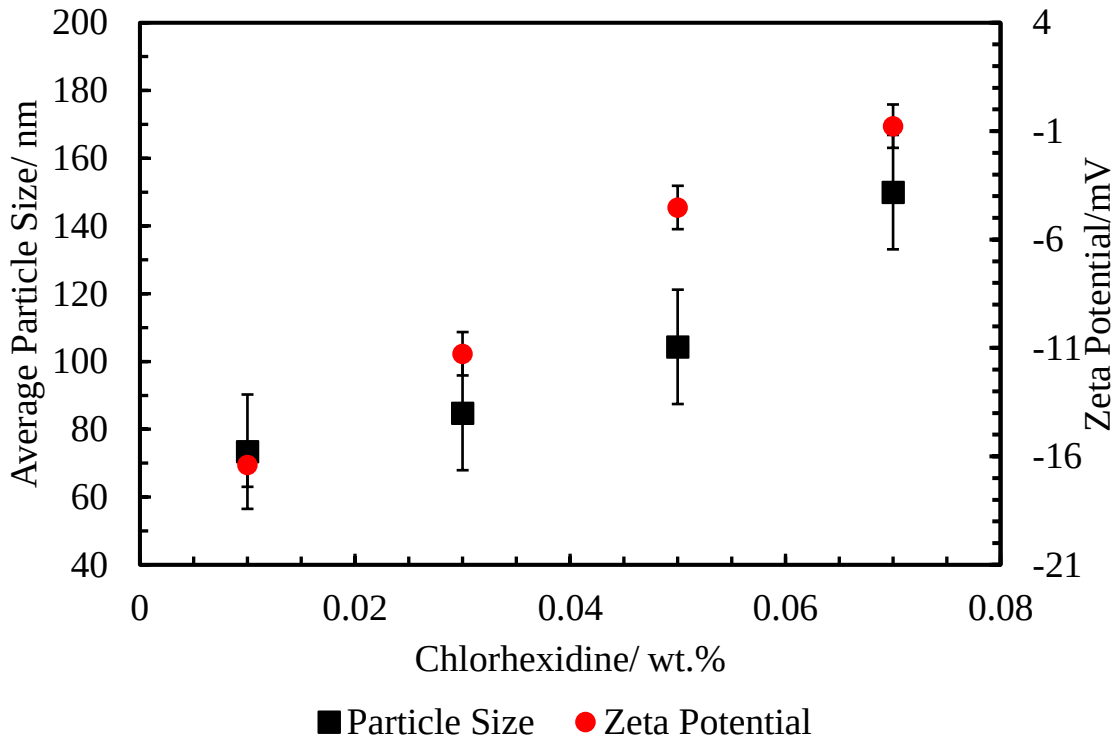

Figure 3.25: The effect of the various concentrations of chlorhexidine on 0.25 wt. % shellac nanoparticles size at pH 5 using Milli Q water, (n=3).

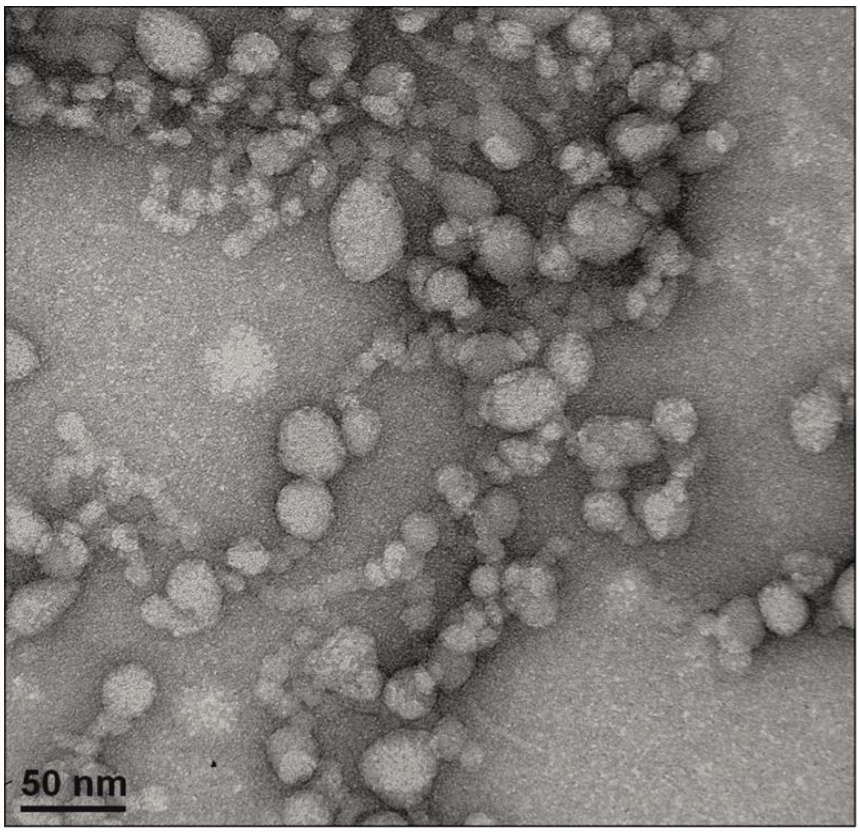

Figure 3.26: The TEM image for the encapsulated chlorohexidine with shellac NPs for a solution consisting of 0.25 wt. % shellac with 0.2 wt. % P 407 and 0.05 wt. % chlorohexidine di-gluconate in Milli Q water.

3.4.1 FTIR Spectroscopy of Shellac NPs, Free CHX, and CHX-NPs

To prove the conjugation between shellac NPs and CHX, FTIR can provide good information for this. Shellac NPs spectrum (Figure 3.27, brown line) was explained in section 3.2.4. Chlorhexidine spectrum (Figure 3.27, blue line) is characterised in principal stretching vibrations from 3300 cm^{-1} to 3500 cm^{-1} for the N-H group, and a stretching bands at 2850 cm^{-1} to 3000 cm^{-1} which belong to the aliphatic C-H group. A characteristic peak relates to the stretching vibration band at 1672 cm^{-1} for the aliphatic C=N group. There are another peaks which are assigned to C=C group in the aromatic ring at wavelengths from 1450 cm^{-1} to 1550 cm^{-1} and at 1251 cm^{-1} which relates to the stretching vibration of aliphatic amine (C-N) group, these results are with agreement with literatures.[174, 386, 387] CHX NPs spectrum (Figure 3.27, green line) shows a broad band which belongs to the overlapping of O-H and N-H bands for both shellac and CHX. Most chlorhexidine bands were merged with shellac NPs bands and with small shifting, these are characterised at 1710, 1342, and 1240 cm^{-1} for C=O, O-H, and C-O stretching, respectively.

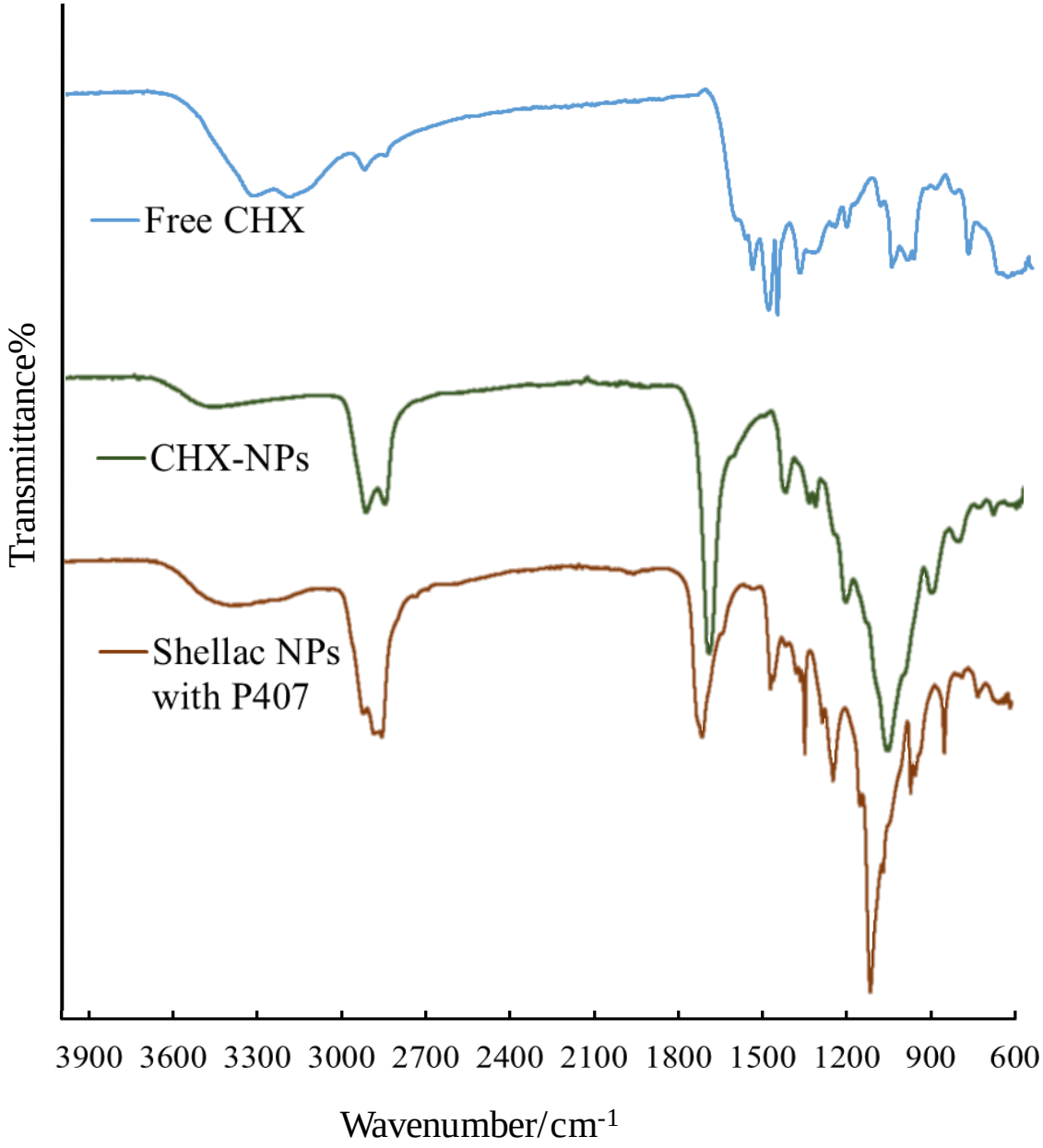

Figure 3.27. The Fourier Transform-IR spectrum of chlorhexidine, 0.03 wt.%. CHX loaded shellac NPs, and shellac NPs.

3.4.2 The UV-Visible Studies

The UV-Vis technique was used to prove the encapsulation of chlorhexidine within shellac NPs, after removing all the chlorhexidine excess by the centrifugation/washing process which was carried out three times. The UV-visible spectra of shellac, chlorhexidine and chlorhexidine loaded shellac NPs are given in Figure 3.28. The shellac spectra (red line) shows a random peaks at 300 to 200 nm because it contains different components with no significant maximum wavelength, while the chlorhexidine (green line) has three absorption peaks, all in UV region at wavelengths 255, 231 and 209 nm, also Poloxamer 407 did not show any peaks above 200 nm. While the black line which represents the absorbance spectrum of chlorhexidine loaded shellac nanoparticles showed two peaks appeared at 260 nm and 227 nm and these belong to the absorbance of chlorhexidine and shellac as well. This can support what has been proven before that there is an interaction between chlorhexidine and shellac NPs.

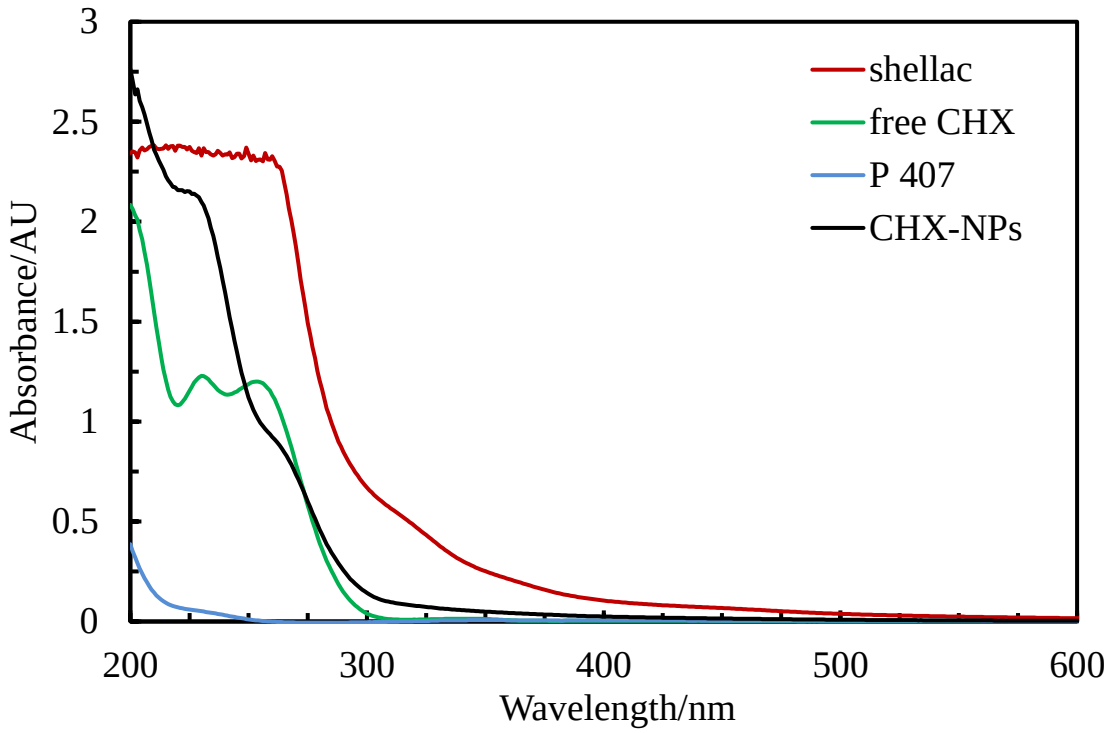

Figure 3.28: The absorption spectrum of chlorhexidine, free shellac, chlorhexidine loaded shellac NPs and Poloxamer 407 using UV-Vis spectrophotometry technique.

3.4.3 Chlorhexidine Encapsulation Efficiency and Loading Content Measurements

The encapsulation efficiency and the percentage of the drug loading content of chlorhexidine (CHX) were determined indirectly by measuring the unencapsulated amount of chlorhexidine using the linear regression equation calculated from the calibration curve of chlorhexidine (figure 3.29). Figure 3.30 shows that the encapsulation efficiency of chlorhexidine into shellac NPs was high reaching about 92% of the total chlorhexidine concentration with drug loading percent of 16% (Table 3.2). The high encapsulation efficiency is owing to the strong interaction between shellac and CHX molecules as chlorhexidine is a cationic molecule with 10 nitrogen atoms that interact with carboxyl groups of shellac. Mathematical equations were used to calculate the encapsulation efficiency and drug loading that mention in chapter two section 2.10.4.

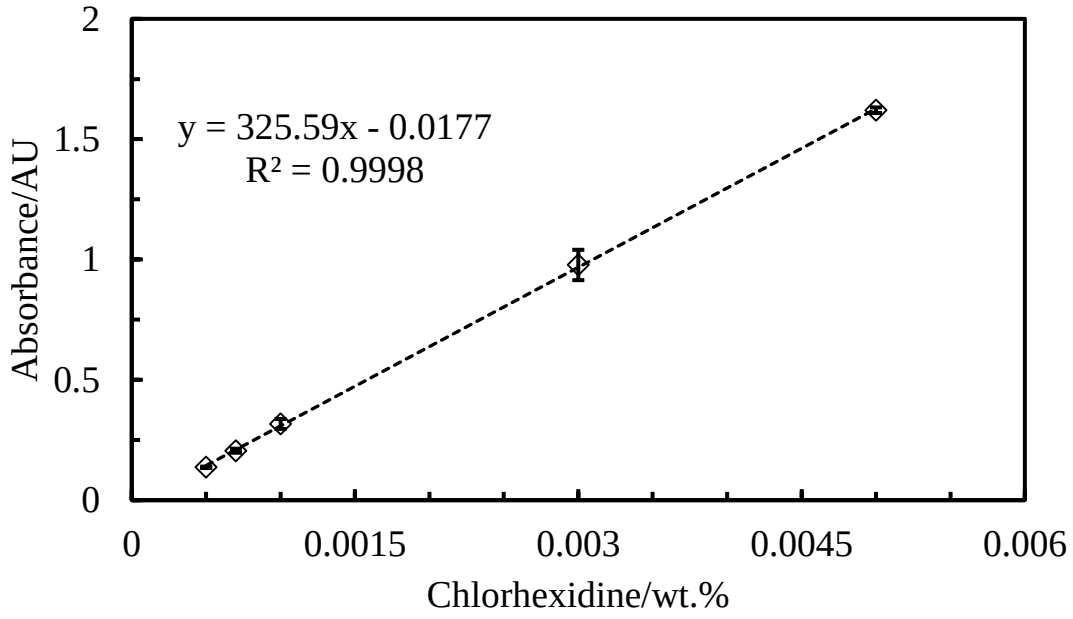

Figure 3.29: The calibration curve of different concentrations of chlorhexidine at 255 nm in Milli Q water, (n=3).

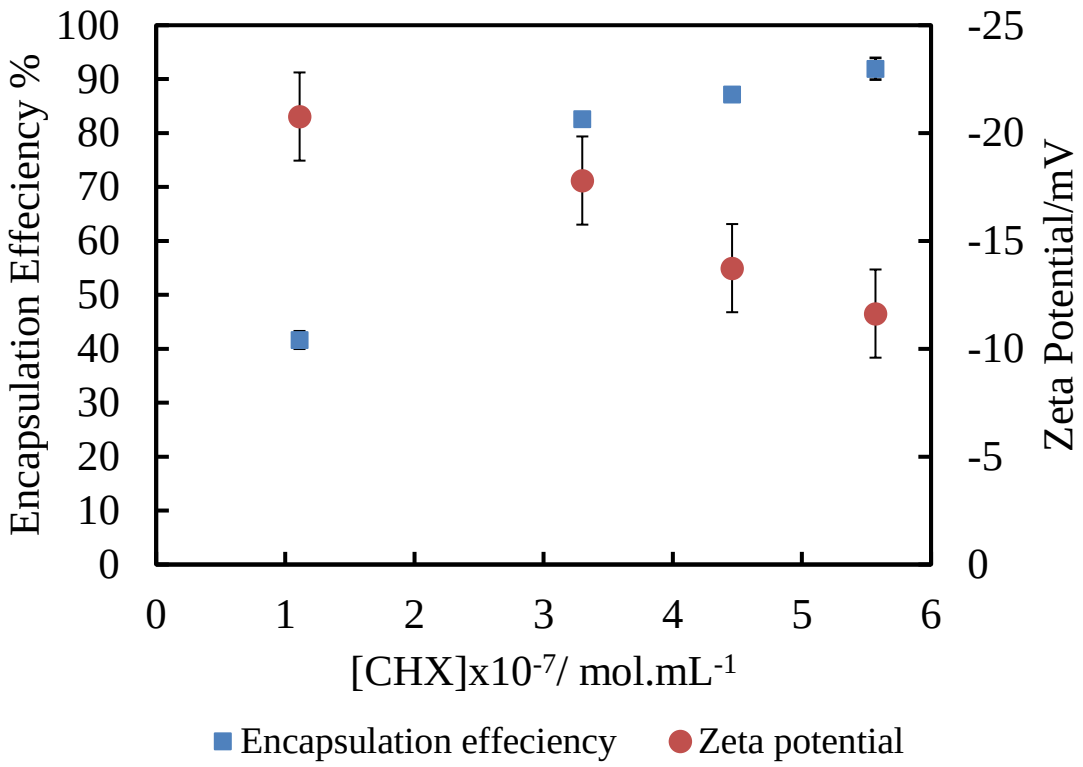

Figure 3.30: The encapsulation efficiency percent of different concentrations of chlorhexidine loaded shellac nanoparticle at pH 5, (n=3).

Table 3.2. The drug loading percent of different concentrations of CHX.

Mol.mL^{-1} CHX loaded 25x10^{-6} mol.mL^{-1} shellac NPs with1.6x10^{-6}mol.mL^{-1} P407	Drug Loading (%)
1.11 x10^{-7}	1.7
3.3 x10^{-7}	9.3
4.46 x10^{-7}	12.8
5.57 x10^{-7}	16

3.4.4 *In Vitro* Chlorhexidine Release Studies

In vitro studies were conducted to monitor the amount of released chlorhexidine from shellac NPs at a specific pH, the chlorhexidine (CHX) loaded shellac NPs suspension was placed into a dialysis bag with a pore size of 2.5 nm which allowed to be released from the nanoparticles and diffused through its pores. The dialysis device was placed into a beaker which had already being filled once with phosphate buffer solution of pH 5.5 and the other with PBS solution pH 7.4. After that, the drug release was measured using a UV-Visible

spectrophotometer. All release experiments were carried out in triplicate. The percentage of collective drug release was calculated by using equation below

$$\%\ In\ Vitro\ Drug\ Release = \frac{M_{released}}{M_{total}} x\ 100$$

Where $M_{released}$ is the amount of chlorhexidine released from the shellac NPs at time *t*, and M_{total} is the whole amount of the chlorhexidine loaded into shellac NPs.

Figure 3.31 shows that the releasing % of chlorhexidine at pH 5.5 is higher than at pH 7.4 and that because of at pH 5.5 carboxylic groups of shellac nanoparticles are protonated which lead to increase the released drug amount and it reached to about 36% after 8 hours, while at pH 7.4 the releasing was very slow and after 8 hours only 12% of drug released.

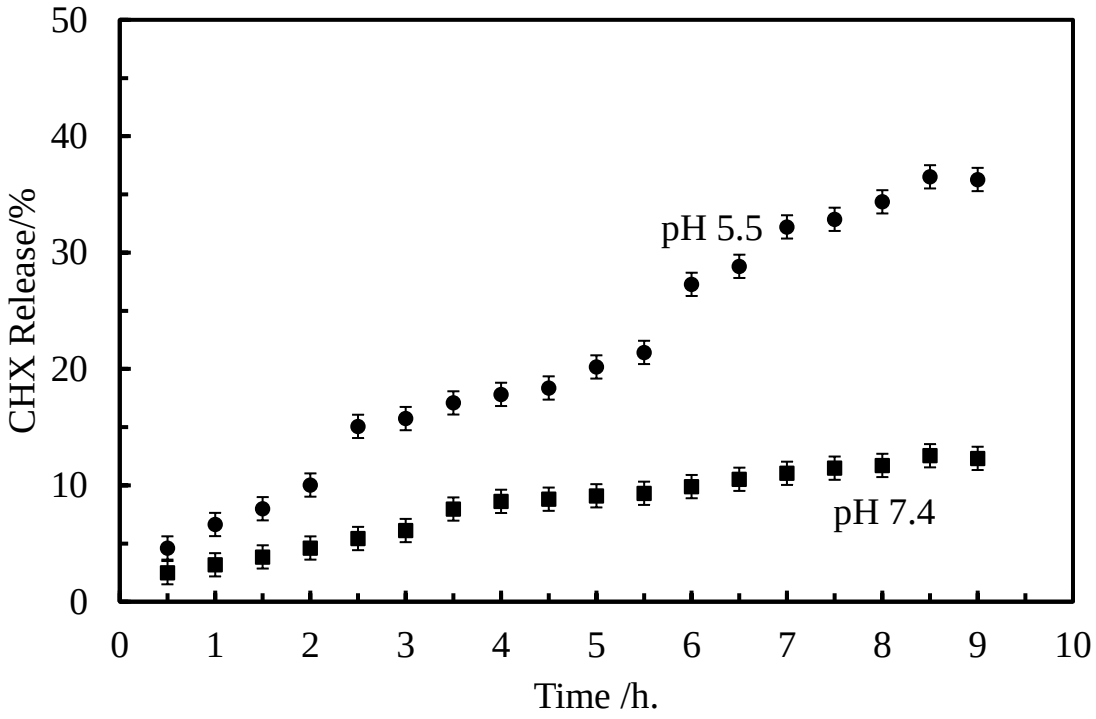

Figure 3.31: The percentage of in vitro chlorhexidine release as a function of time at pH5.5 and 7.4. The measurements were carried out using Perkin Elmer UV-Visible Spectrophotometer at a range of wavelength (200-700) nm, (n=3).

3.5 Encapsulation and Characterization of Curcumin Loaded within Shellac NPs

Curcumin is almost water insoluble and has poor bioavailability for the reasons of its poor intestinal absorption, rapid metabolism, low intrinsic activity, high rate of metabolism, and/or rapid elimination and clearance from the body.[179, 388] In order to improve its water solubility and to reduce bioavailability, curcumin was formulated into biodegradable nanoparticles. Curcumin the hydrophobic polyphenolic compound was encapsulated within shellac NPs by mixing shellac with curcumin and Poloxamer 407 at pH >7 then reducing the pH to 5 by adding drops of diluted HCl. The interaction between shellac and curcumin is hydrophobic-hydrophobic interaction as shellac is a hydrophobic polymer (Figure 3.32).[389] Curcumin is stable at acidic pH but unstable at neutral and basic pH. [390] Curcumin nanoparticles were formulated at the size of 87±26 nm with surface charge of -5±0.6 mV (Figure 3.33Figure 3.34). Figure 3.35 shows that shellac NPs can be loaded with curcumin up to 0.05 wt. % and at higher concentration an aggregation occurs. However, the zeta sizer charge decreased while the loaded amount of curcumin increased. Curcumin nanoparticles sample was further examined by transmittance electron microscopy (TEM). Curcumin exhibits a spherical type morphology as can be seen in Figure 3.36.

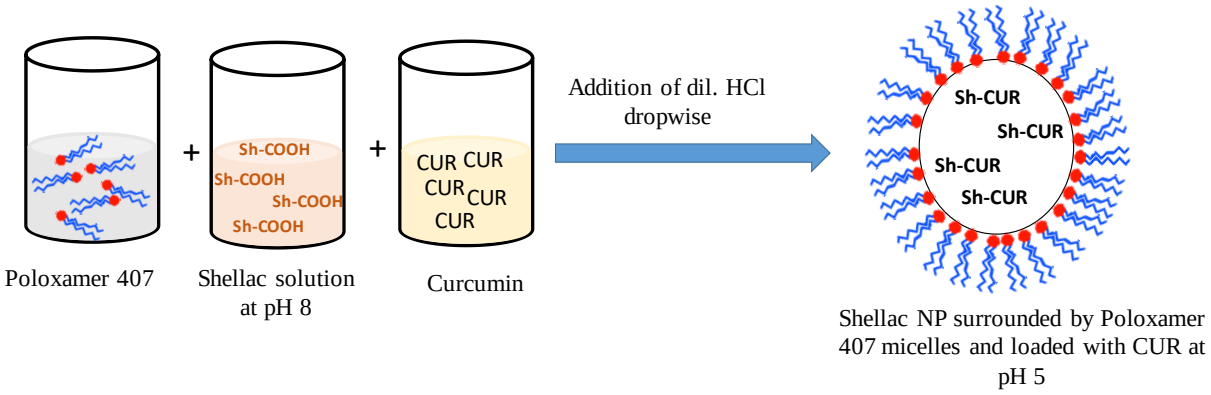

Figure 3.32: Schematic diagram represents the process of preparing shellac NPs loaded with CUR at pH 5 by mixing shellac, CUR, and P407 at pH 8 then reducing the pH to 5 using dil. HCl.

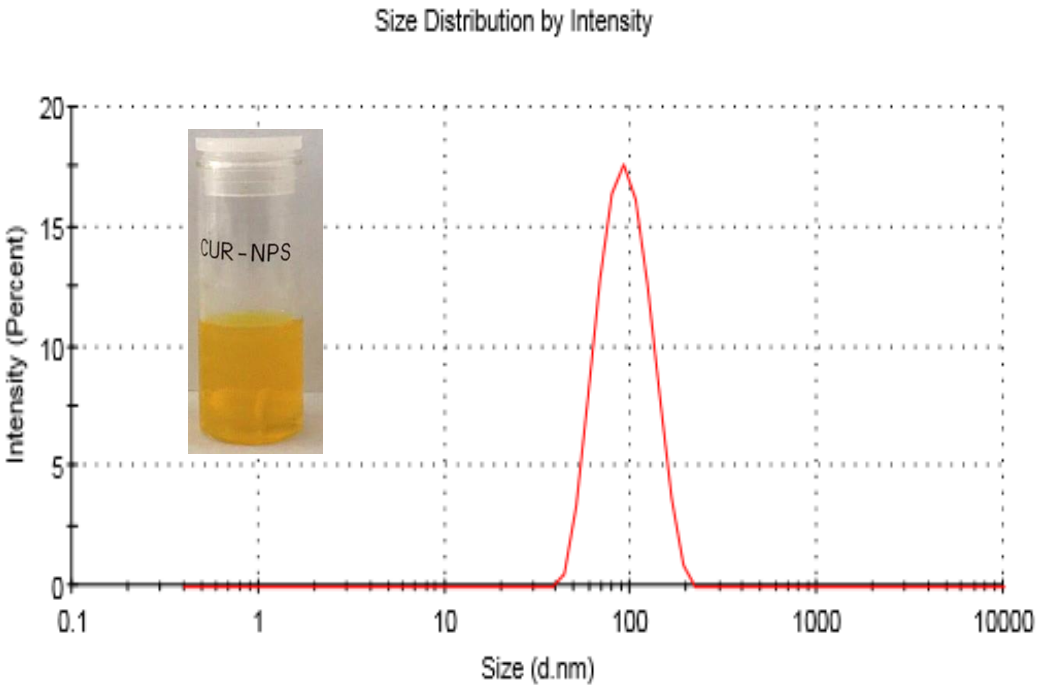

Figure 3.33: Particle size distribution of 0.03 wt. % curcumin loaded shellac nanoparticles in Milli Q water at pH 5.

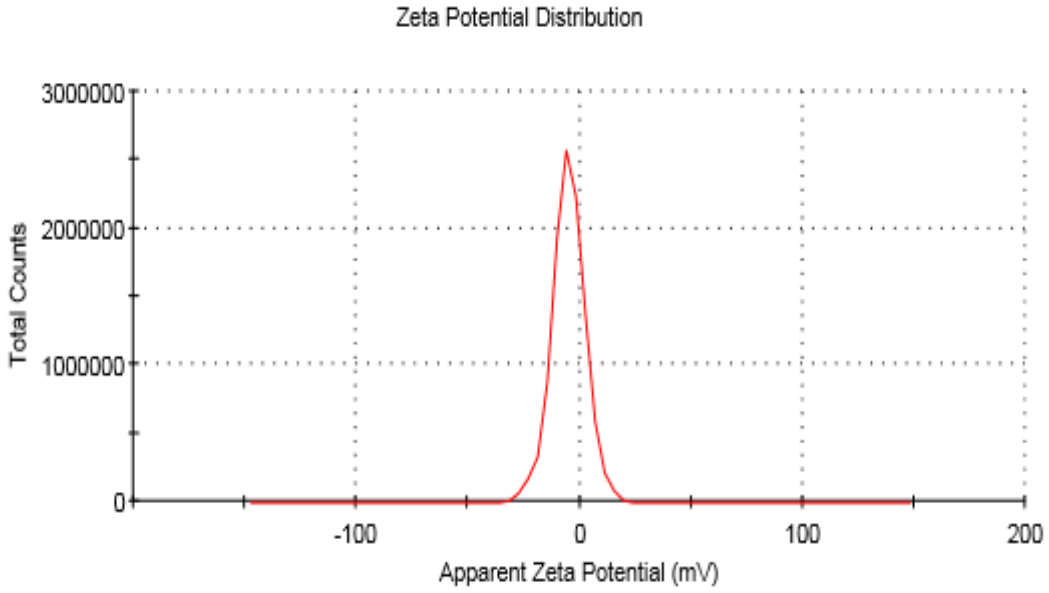

Figure 3.34: The zeta potential of 0.03 wt. % curcumin loaded shellac NPs at pH 5 in Milli Q water.

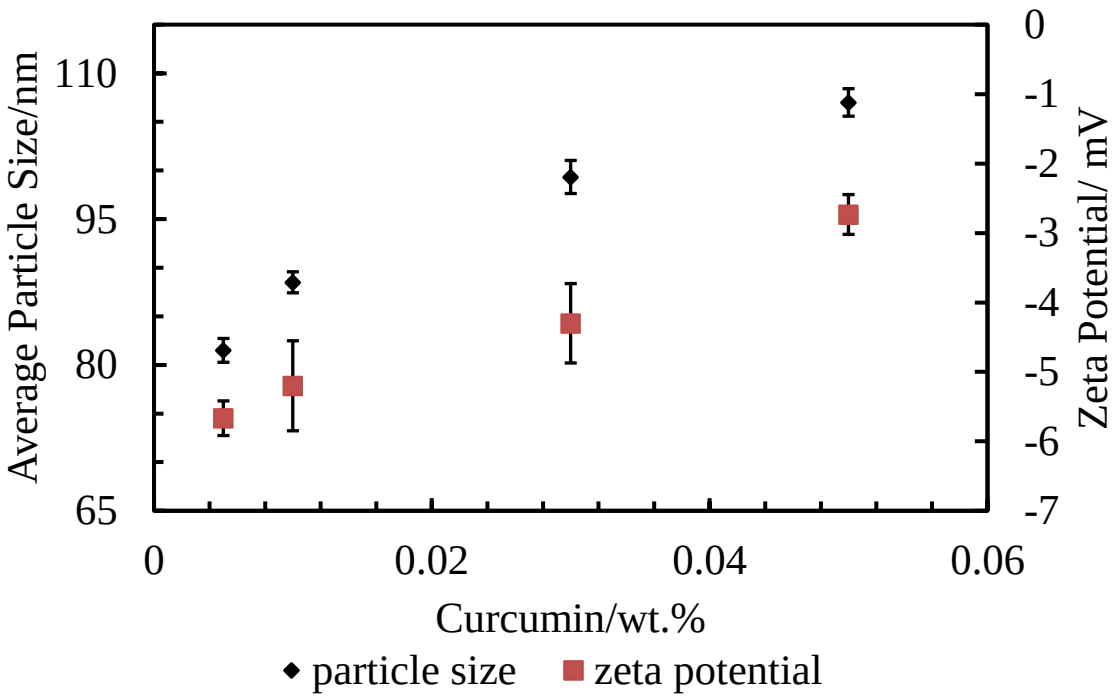

Figure 3.35: The effect of loading different concentrations of curcumin on the size of 0.25 wt. % shellac nanoparticles at pH 5, (n=3).

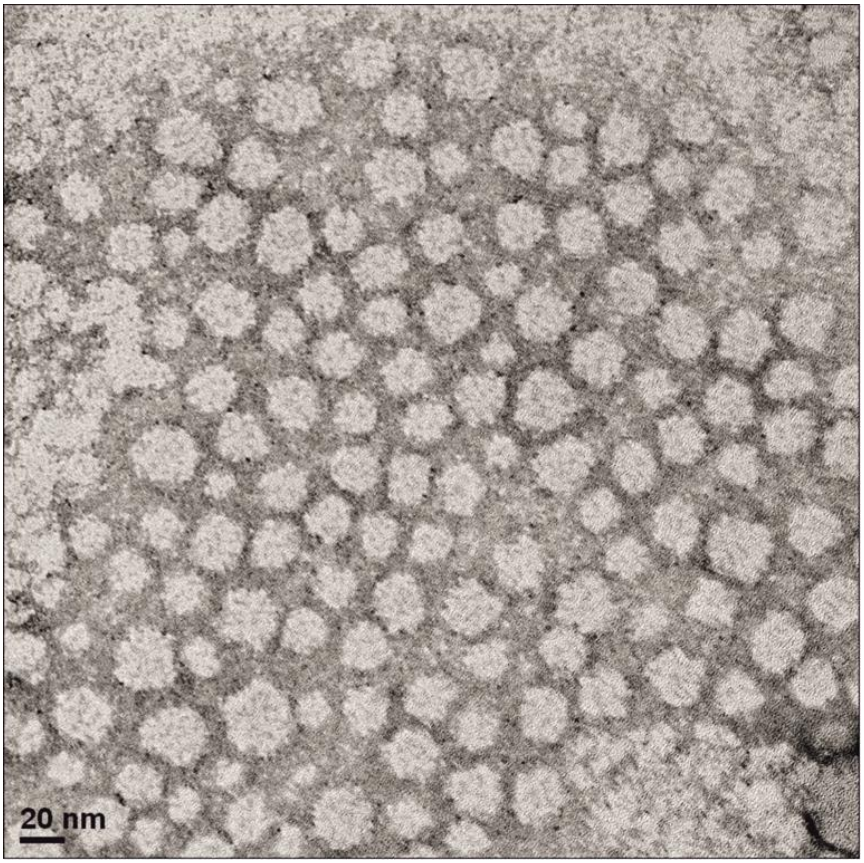

Figure 3.36: The TEM image of 0.03 wt. % curcumin loaded shellac NPs negatively stained with 1% uranyl acetate in Milli Q water.

3.5.1 FTIR Studies of Shellac NPs, Free CUR, and CUR NPs

Free curcumin FTIR spectrum, Figure 3.37 (red spectrum) shows one sharp peak at 3510 cm^{-1} demonstrating the presence of O-H. (C=C) and (C=O) vibration have strong peaks and were predominantly mixed at 1625 cm^{-1}. A symmetric stretching vibrations of the aromatic ring (C=C ring) shows a strong band at 1601 cm^{-1}. The 1504 cm^{-1} peak is distributed to the (C=O), whereas enol C–O peak appeared at 1271 cm^{-1}. The other characteristic peaks are as displays: C–O–C peak at 1024 cm^{-1}, benzoate trans-CH vibration at 961 cm^{-1} and vibration cis-CH of aromatic ring at 712 cm^{-1}. All these results are in line with the literature reports. [391, 392] The shellac NPs spectrum has been explained in section 3.2.4. CUR-NPs spectrum (blue line, Figure 3.37) shows a broad peak around 3350 cm^{-1} which belongs to the absorption of O-H stretching vibration band for shellac and curcumin molecules. Most curcumin principle peaks were fused with shellac NPs bands and shifted slightly. Few of curcumin peaks appeared, like C=O, enol C-O, and benzoate trans -CH peaks are assigned at 1514 cm^{-1}, 1279 cm^{-1}, and 962 cm^{-1} respectively. The presence of these peaks proposed that curcumin was encapsulated within the nanoparticles by hydrophobic-hydrophobic interaction and had not reacted with shellac molecules.

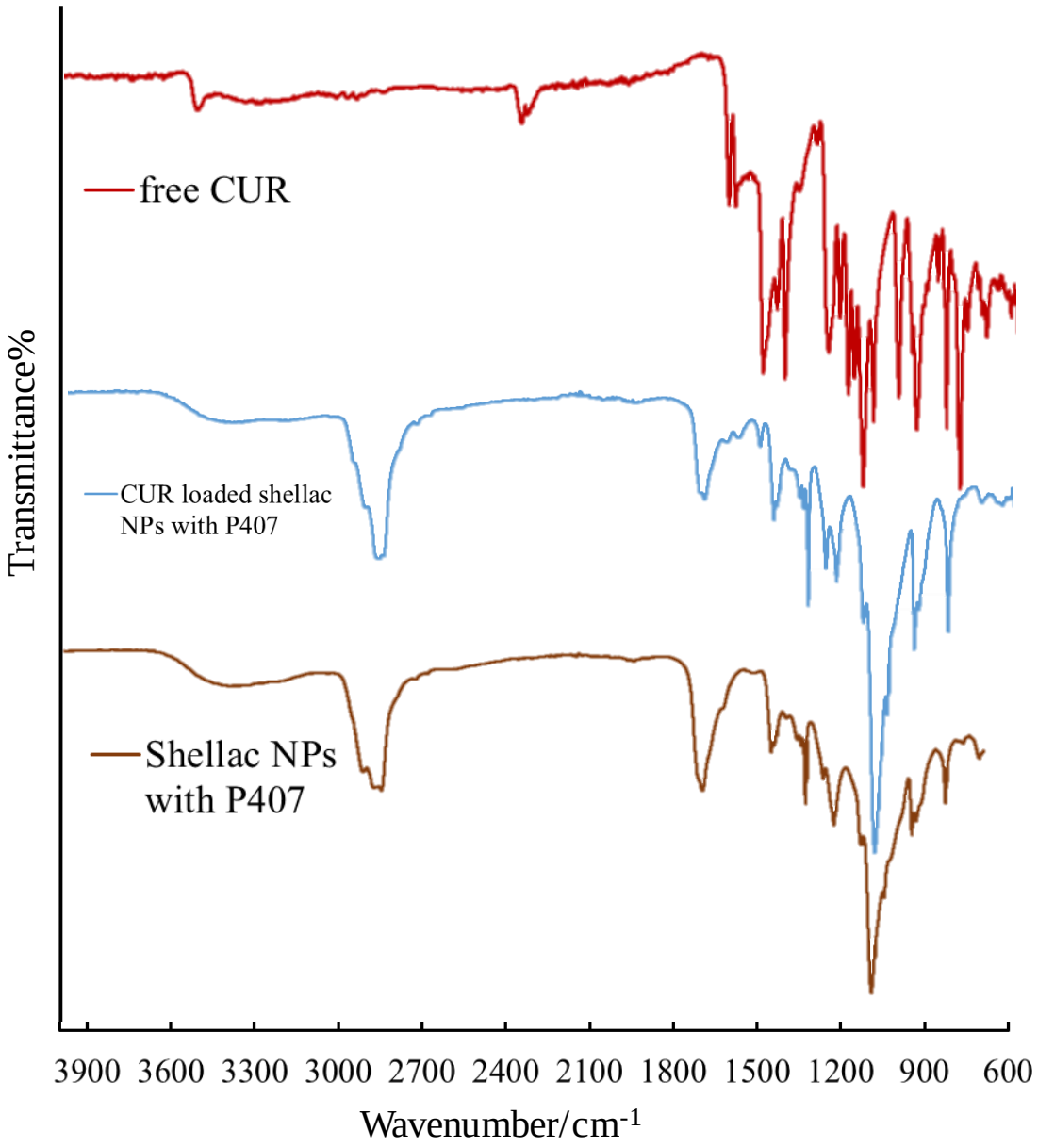

Figure 3.37: The Fourier Transform-IR spectrum of free curcumin, 0.03 wt.% CUR-NPs, and Shellac NPs with P407 at a range of wavenumber 600-4000 cm^{-1}

3.5.2 UV-Vis Spectroscopy of Shellac, Poloxamer 407, Free CUR, and CUR NPs

The optical properties for shellac, curcumin, and curcumin nanoparticle show distinct difference among samples. Curcumin solution (in water) looks turbid, while curcumin NPs appears transparent yellow indicating solubilisation of curcumin. Interestingly though, the Poloxamer shell confirms a hydrophobic surface to the curcumin core into the shellac-Cur complex and the outer hydrophilic portion of the Poloxamer supports in the solubility of the complex in water. UV-Vis spectroscopy study proved the encapsulation of curcumin within shellac NPs. Free curcumin has strong absorption at 426 nm and a weak peak at 270 nm (grey line, Figure 3.38). While shellac has random absorption in UV region with no significant peaks (green line, Figure 3.38). CUR NPs shows the presence of two peaks, one broad peak in the visible region at around 440 nm, and the second appeared in UV region at 240 nm which belong to curcumin NPs (blue line, Figure 3.38). The appearance of these peaks indicated that curcumin has loaded within shellac nanoparticles.

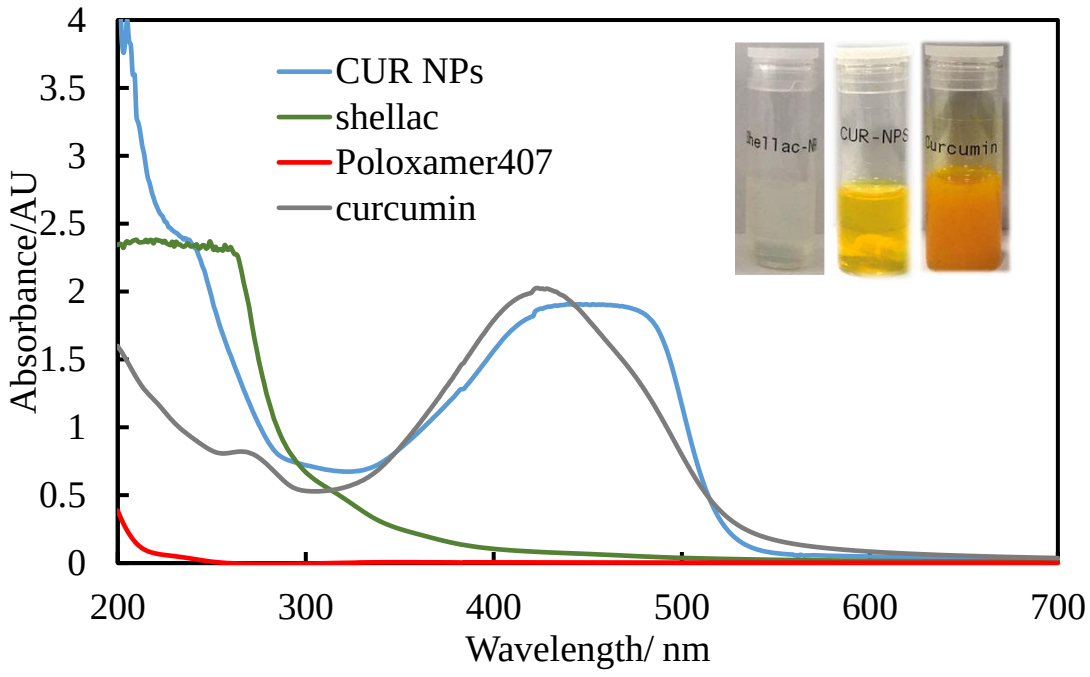

Figure 3.38. The absorption spectrum of curcumin, free shellac, curcumin loaded shellac NPs and Poloxamer 407 using UV-Vis spectrophotometry technique at range (700-200) nm.

3.5.3 Curcumin Encapsulation Efficiency and Drug Loading Content Measurements

The encapsulation efficiency of curcumin within shellac NPs was calculated indirectly by determining the amount of curcumin in the supernatant after filtering samples using syringe filter of 20 nm pore size by UV-Vis spectrophotometer. Figure 3.40 shows that curcumin can be encapsulated within shellac NPs up to 100% at pH 5 with loading amount of 33.8% at 13.6 $x10^{-6}$ $mol.mL^{-1}$, as can be seen in Table 3.3. The high trapping amount of curcumin within shellac particles attributed to the high affinity between curcumin and shellac and Poloxamer molecules as they all contain hydrophobic parts.

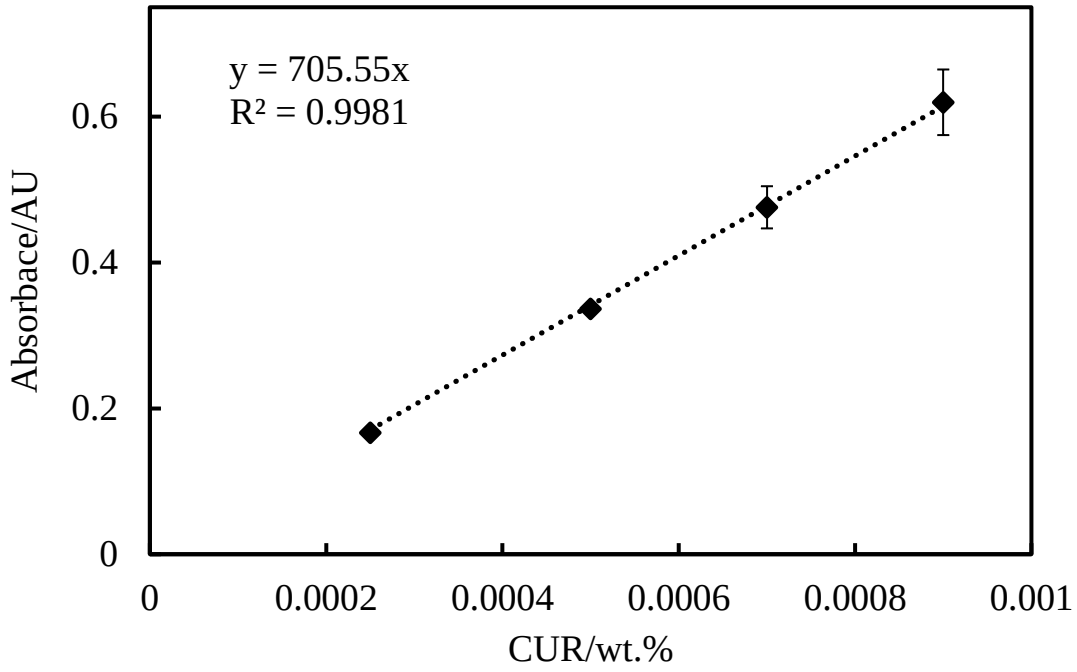

Figure 3.39. The calibration curve of varies concentrations of curcumin at 426 nm in Milli Q water using UV-Vis spectrophotometer, (n=3).

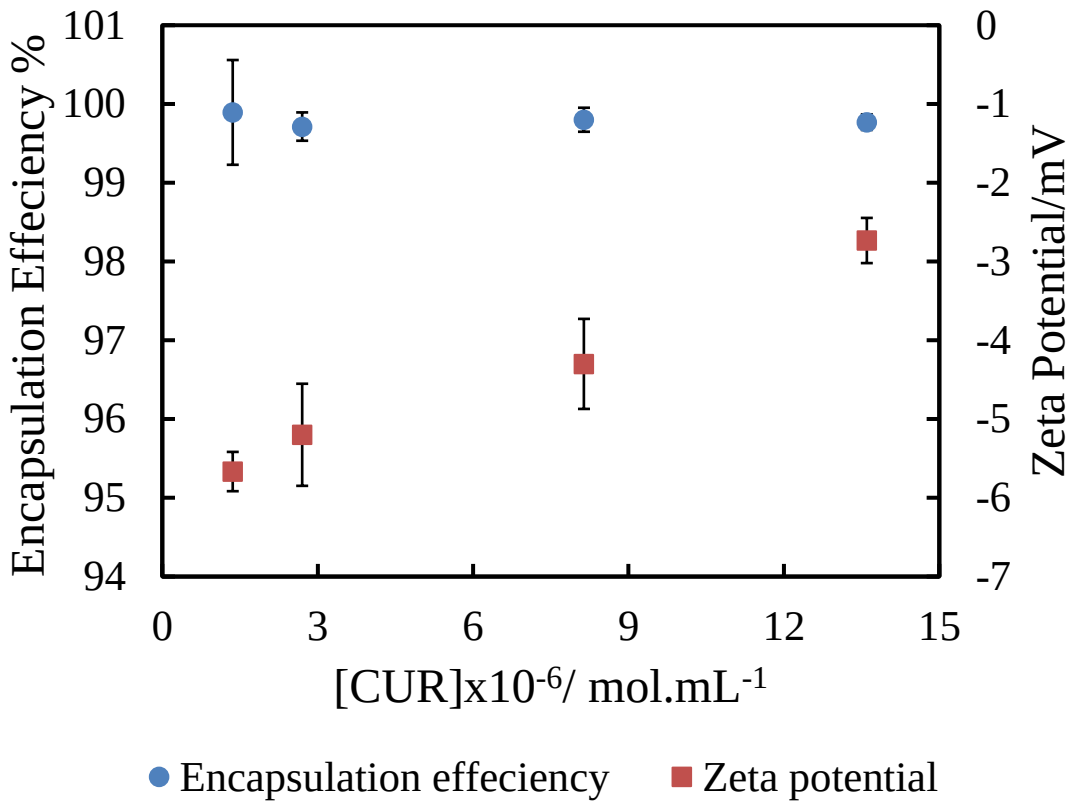

Figure 3.40: The encapsulation efficiency percent of different concentrations of curcumin loaded shellac nanoparticle at pH 5, (n=3).

Table 3.3: The drug loading percent of different concentrations of curcumin within shellac NPs at pH 5.

Mol.mL^{-1} CUR loaded 25x10^{-6} mol.mL^{-1} shellac NPs with1.6x10^{-6}mol.mL^{-1} P407	Drug Loading (%)
1.36 x10^{-6}	5
2.7 x10^{-6}	9.2
8.14 x10^{-6}	23
13.6 x10^{-6}	33.8

3.5.4 *In Vitro* Curcumin Release Studies

In vitro curcumin release studies were investigated to observe the amount of released curcumin at a specific pH. 0.45 wt. % Cetyltrimethylammonium bromide (CTAB) was added to buffer solution to maintain the solubility of curcumin after releasing throughout the dialysis bag.[377] Figure 3.41 shows that curcumin releasing was very slow at pH 5.5 and was slower at 7.4, only about 3.5% was released after 2 days at pH 5.5 and a half this amount at pH 7.4. The slow release could be attributed to the high affinity between curcumin and shellac nanoparticles as they express hydrophobic-hydrophobic interaction, this confirms that shellac can be loaded with curcumin for sustain drug release for long drug activity as it could be used for many days as well as reducing the side effect of high drug usage.

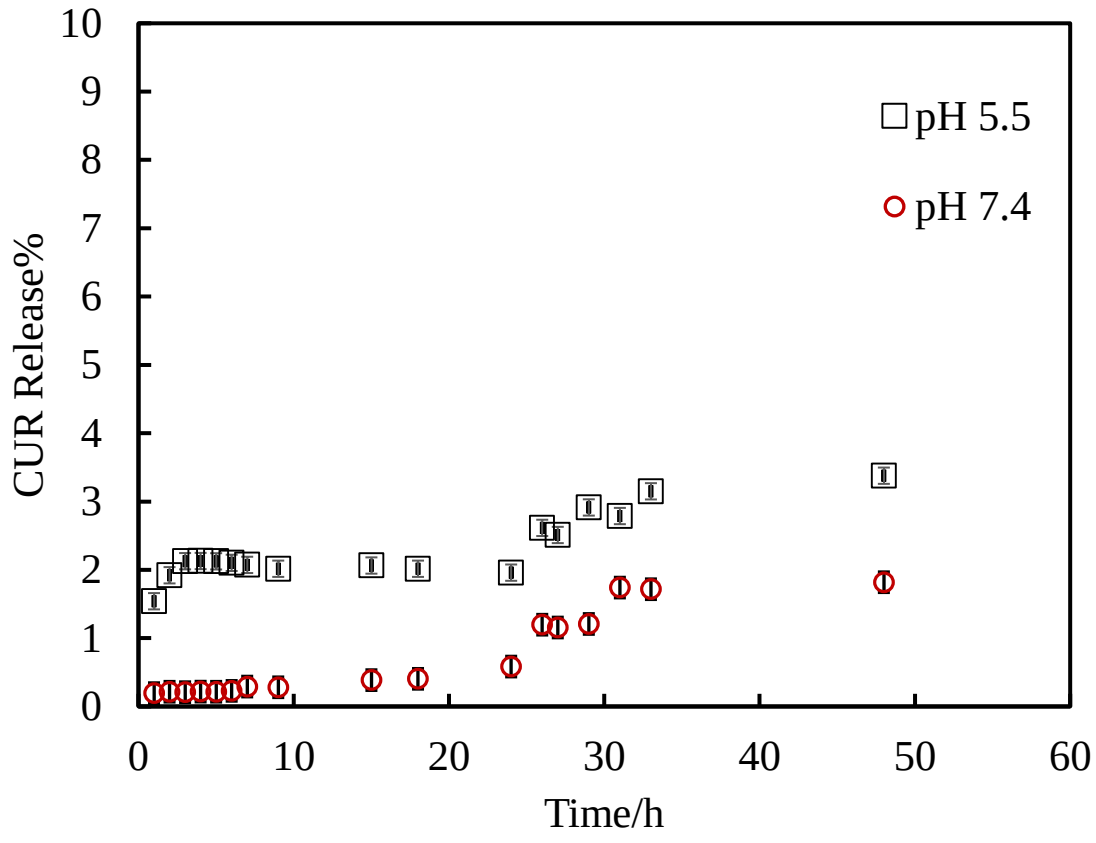

Figure 3.41: The percentage of in vitro curcumin release as a function of time at pH5.5 and 7.4. The measurements were carried out using Perkin Elmer UV-Visible Spectrophotometer at a range of wavelength (200-700) nm, (n=3).

3.6 Encapsulation and Characterisation of Vancomycin Hydrochloride Loaded within Shellac NPs

The method that been used to encapsulate vancomycin hydrochloride within shellac NPs was the same that used to encapsulate the other drugs (BRB, CHX, and CUR) but the pH reduces to 6 instead of 5 by adding drops of diluted HCl to increase the entrapment efficiency of the drug, (Figure 3.42). Figure 3.43 shows the vancomycin NPs size distribution which is 80±24 nm at 0.05 wt. % VCM loaded shellac NPs with zeta potential of -7 mV as shown in Figure 3.44. TEM micrograph verified that vancomycin NPs is spherical in shape as clear in Figure 3.45

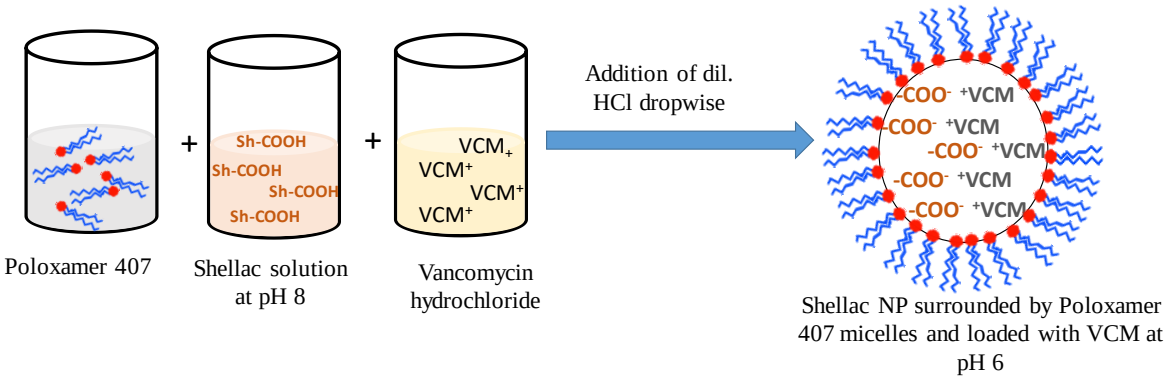

Figure 3.42: Schematic diagram represents the process of preparing shellac NPs loaded with VCM at pH 5 by mixing shellac, VCM, and P407 at pH 8 then reducing the pH to 5 using dil. HCl.

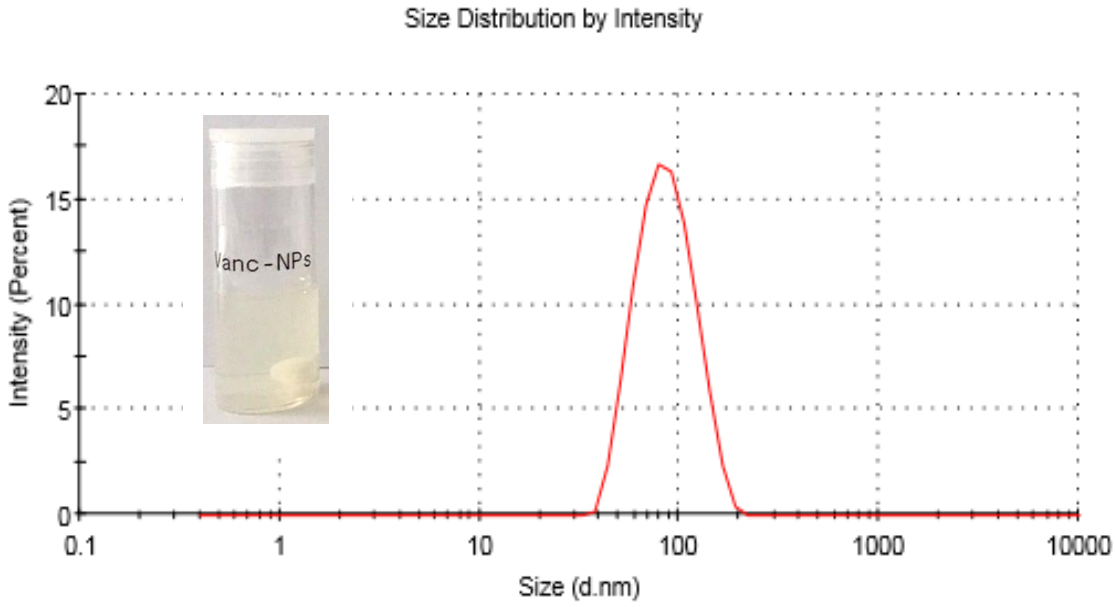

Figure 3.43: The average particle size of vancomycin loaded shellac NPs at pH 6 in Milli Q water. The encapsulated VCM prepared by mixing shellac, P407 and VCM at pH 8 then reduce the pH to 5 using dil. HCl.

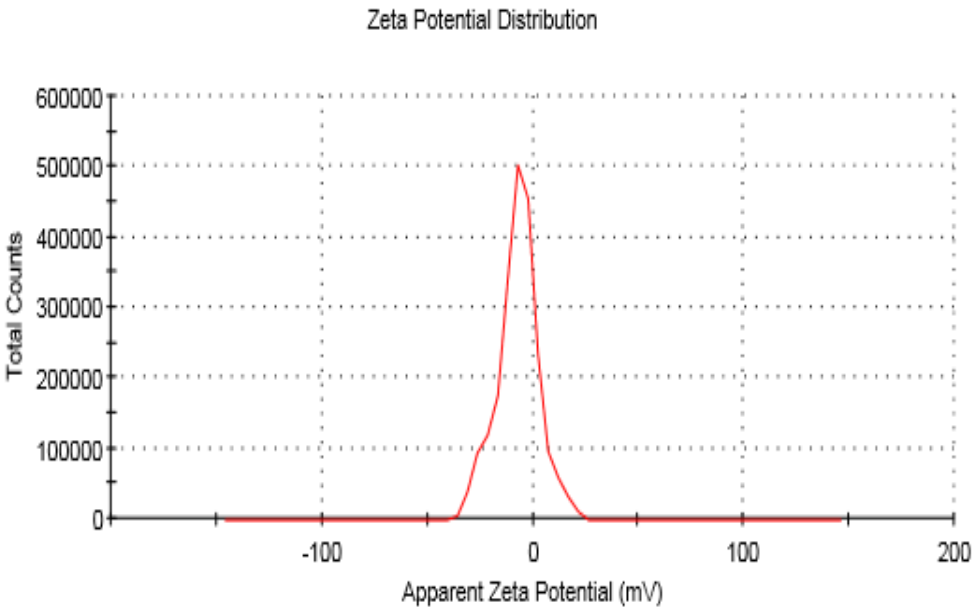

Figure 3.44: The zeta potential of 0.05 wt. % vancomycin loaded shellac NPs at pH 6 in Milli Q water.

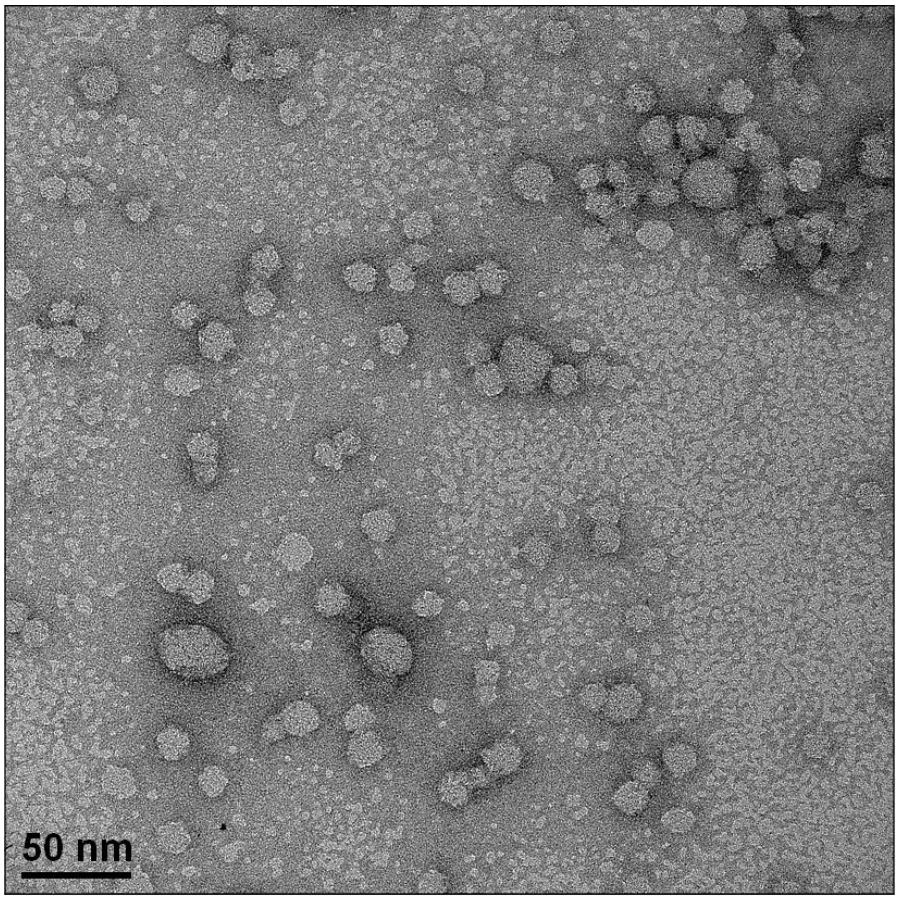

Figure 3.45: TEM image for 0.03 wt.% vancomycin NPs at pH 6 stained with 1% uranyl acetate.

Figure 3.46 illustrates that shellac NPs can be loaded with vancomycin up to 0.07 wt. % and any increase in vancomycin concentrations resulting in a continuous increase in particle size from 80 nm at 0.01% to 96 nm at 0.07wt. %, higher than this amount an aggregation occurs. Although the surface charge of vancomycin NPs was dropped from -9 mV to -4 mV when the loaded amount of VCM increased due to the interaction between shellac NPs carboxylic group with vancomycin amine groups as can be seen in Figure 3.46.

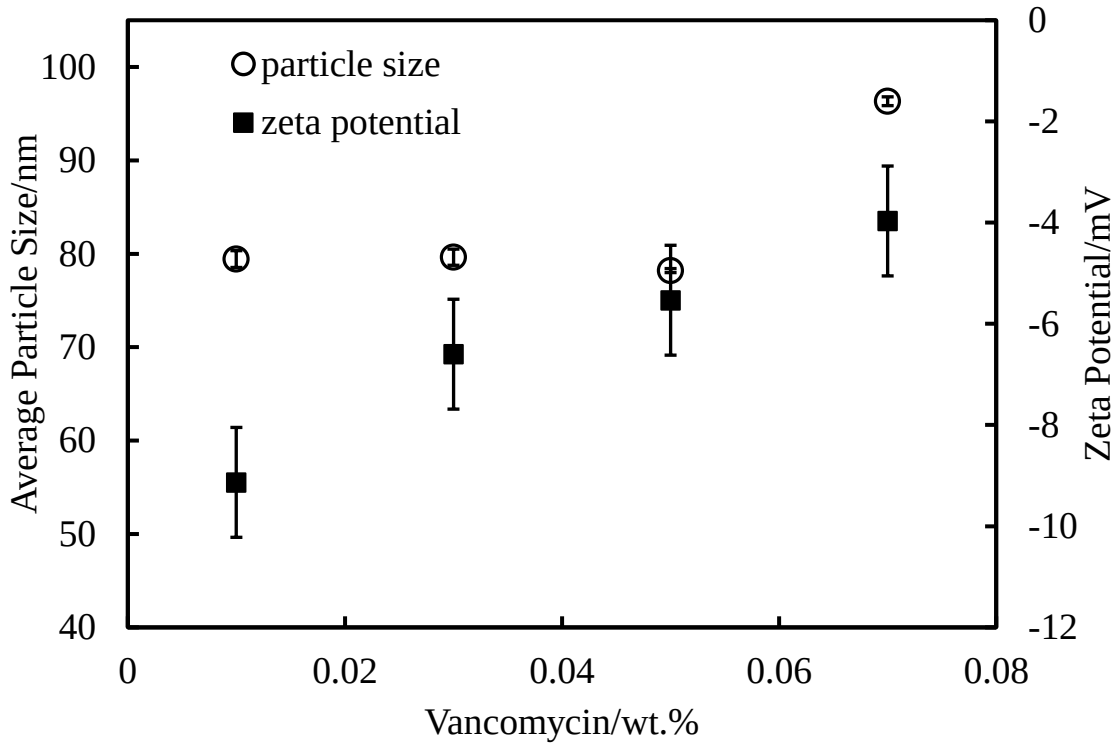

Figure 3.46: The particles size and zeta potential of different concentrations of vancomycin loaded shellac NPs at pH 6, (n=3).

3.6.1 FTIR Measurements of Shellac NPs, Free VCM, and VCM NP

The FTIR spectra of Vancomycin, shellac NPs, and vancomycin loaded shellac NPs, are represented in Figure 3.47. The FTIR of free vancomycin (purple line) revealed a phenolic OH stretching band at 3261 cm^{-1}, stretching aromatic C=C associated with amide I at 1644 cm−1, C=O stretching association with secondary amide shows peak at 1488 cm^{-1}, C-O phenolic, C-N-H amide II, and Ar-O-Ar showed peaks at wavenumbers at 1395 cm^{-1},1585 cm^{-1}, and 1059 cm^{-1} respectively.[236, 239] The shellac NPs spectrum has been clarified in section 3.2.4 and it shows identical spectrum with VCM NPs IR spectrum (blue line) hence most vancomycin functional group are the same of shellac functional

groups (O-H, C=C, and C-H), only small shoulders appear at 1648 cm^{-1} and 1060 cm^{-1} for aromatic C=O amide I and Ar-O-Ar stretching respectively which belong to vancomycin, and this proves the encapsulation of vancomycin with shellac NPs.

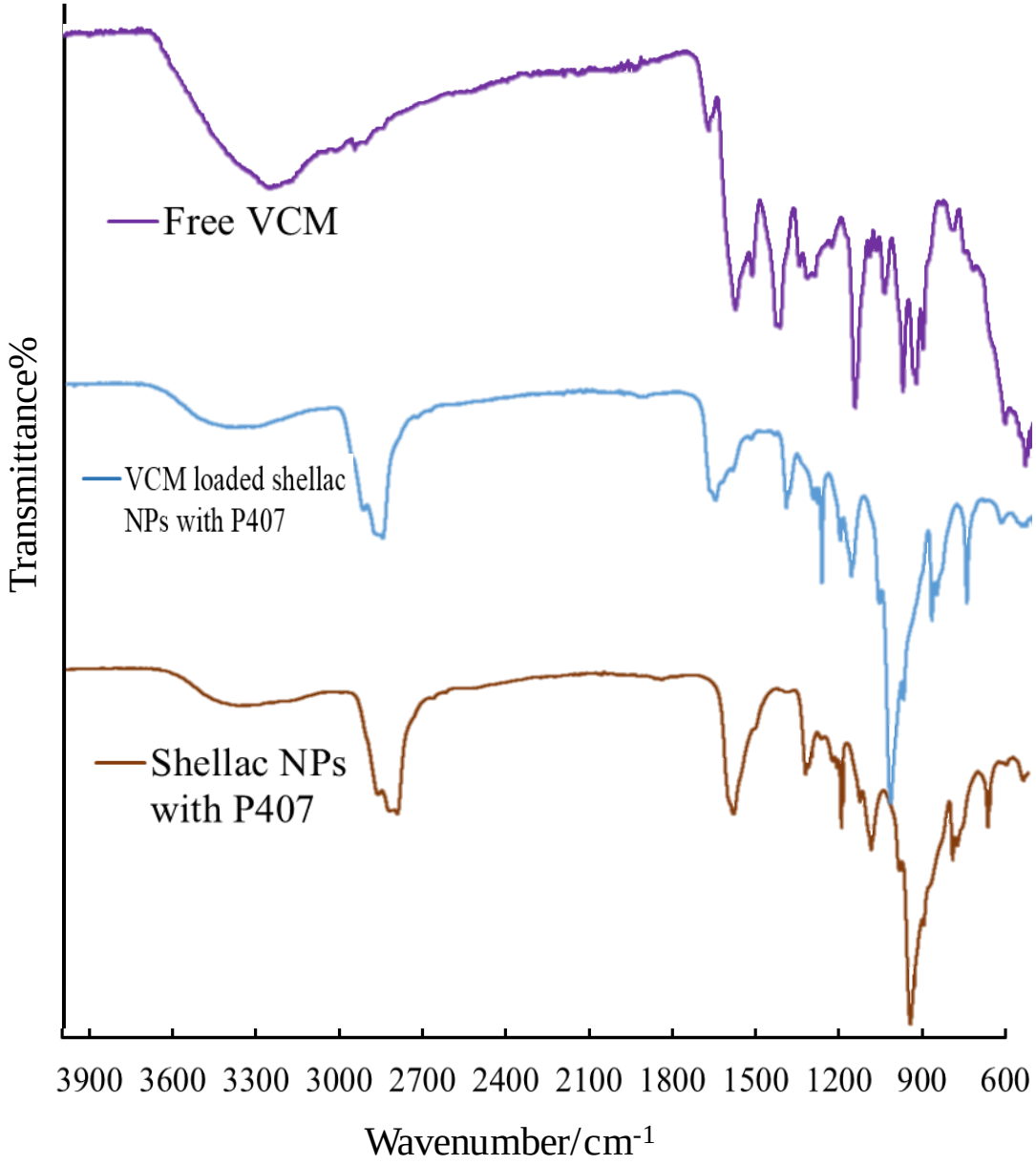

Figure 3.47: FTIR spectrum of shellac NPs, 0.03 wt.% VCM NPs, and free VCM at wavenumber range of 4000-600cm^{-1}.

3.6.2 The UV-Visible Measurements of Free VCM, Shellac NPs, P407, and VCM loaded Shellac NPs

The UV-Spectrophotometric method was developed for quantification of encapsulation of vancomycin within shellac NPs. A sample of vancomycin loaded shellac NPs was dissolved in weak basic medium then measured spectrophotometrically at a range of wavelength 200 nm -500 nm, as well as for free shellac, free vancomycin and Poloxamer 407. Figure 3.48 shows the spectra of all components and as it can be seen that free VCM spectrum (blue line) showed a characteristic peak at 280 nm with random peaks start from 236 nm to 200 nm, while shellac spectrum also displayed random peaks started from 264 nm to 200 nm, whereas Poloxamer 407 does not show a specific peak at UV-Vis area. The purple line which represents VCM NPs reveal a peak at 304 nm, and this belongs to vancomycin but shifted due to the interaction with shellac and random peaks start from 247 nm to 200 nm which belong for both shellac and VCM NPs. This confirms besides other technique that VCM has been encapsulated within shellac NPs.

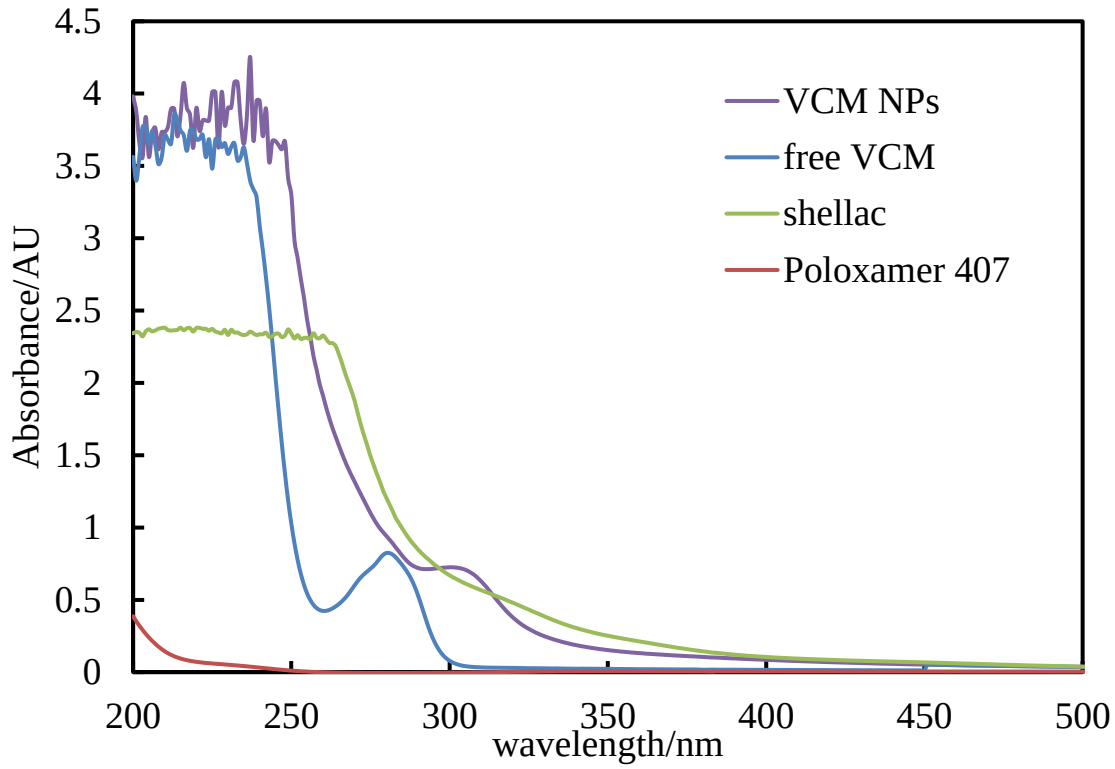

Figure 3.48: Absorption spectrum of free vancomycin, free shellac, and vancomycin loaded shellac NPs, and Poloxamer 407 using UV-Vis spectrophotometry technique at range (700-200) nm.

3.6.3 Vancomycin Encapsulation Efficiency and Drug Loading Content Measurements

The effect of vancomycin concentration on the encapsulation efficiency was examined indirectly by measuring the amount of unencapsulated vancomycin and reliant on the liner equation obtained from VCM calibration curve, (Figure 3.49). Vancomycin was encapsulated with shellac NPs by following the procedure mentioned in section 2.2.1. As can be seen from Figure 3.50 that the encapsulation efficiency of VCM at pH 5 was low. Therefore to enhance it many attempts have been tried either by changing the pH or by doubling the amounts of shellac and Poloxamer 407. At pH 6 the encapsulation efficiency at 0.03 wt.% VCM increased from 19% at pH 5 to be 87.5% at pH 6, and it is slightly higher when using double amount of shellac and Poloxamer (0.5:0.4) wt.%, respectively, while the drug loading contents within shellac NPs were dropped from 13.6% to 7.6% at $48.3x10^{-7}$ $mol.mL^{-1}$ of VCM when using doubled amount of shellac and Poloxamer, (Table 3.4). Hence VCM was encapsulated at pH 6 by using the same amount of shellac and Poloxamer 407 (0.25:0.2) wt.%, and this was used in the all next experiments.

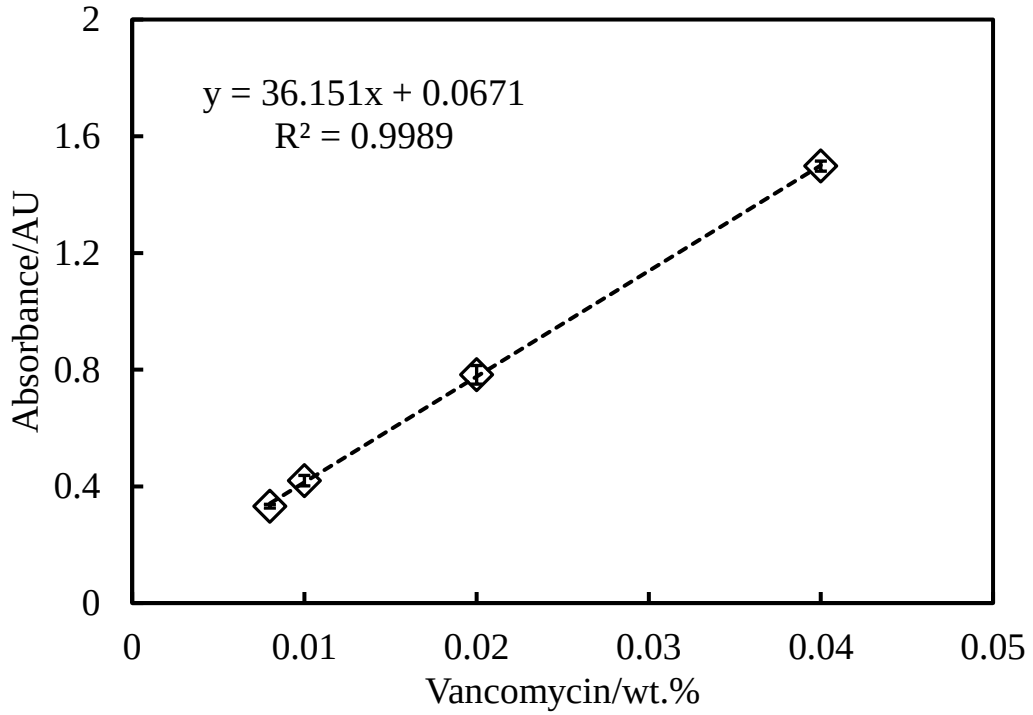

Figure 3.49: The standard curve of different concentrations of vancomycin hydrochloride at wavelength 280 nm, (n=3).

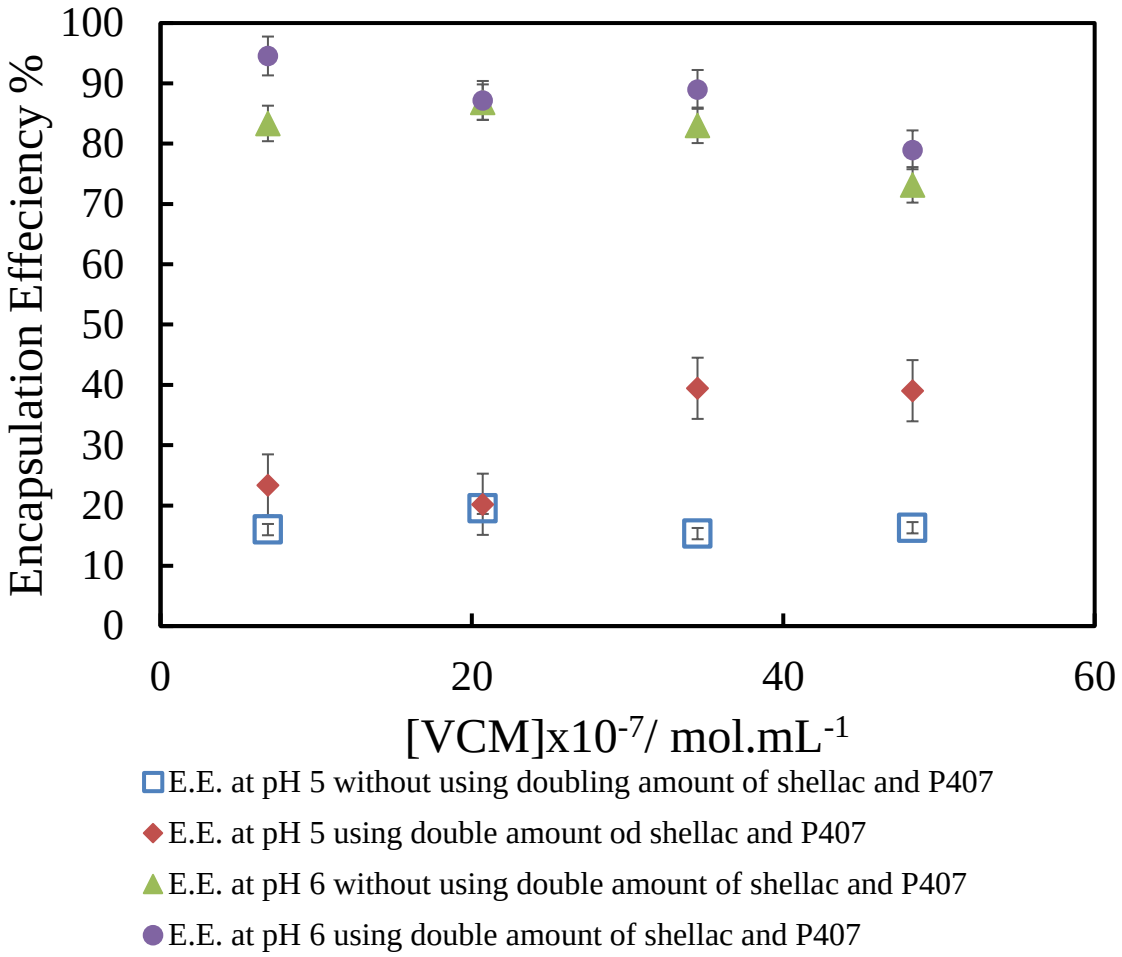

Figure 3.50: The encapsulation efficiency percent of different concentrations of vancomycin loaded shellac nanoparticle at pH 5 and pH 6 once with using double amounts of shellac and Poloxamer 407 and other without doubling their amounts, (n=3).

Table 3.4: Vancomycin loading content at pH 6 once encapsulated with (2.5 shellac + 0.16 P 407) $x10^{-5}$ $mol.mL^{-1}$ and second encapsulated within (5.0 shellac+ 0.32 P407) $x10^{-5}$ $mol.mL^{-1}$.

$Mol.mL^{-1}$ VCM loaded shellac NPs	Drug loading (%) without using double amounts of shellac and Poloxamer 407	Drug loading (%) using double amount of shellac and Poloxamer 407
$6.9x10^{-7}$	2.33	0.9
$20.7\ x10^{-7}$	6.8	3.5
$34.5\ x10^{-7}$	10.6	5.8
$48.3\ x10^{-7}$	13.6	7.6

3.6.4 *In Vitro* Vancomycin Release Study

Figure 3.51 shows VCM release profile from shellac NPs at pH 5.5 and 7.4 for 30 hours. As can be seen that the releasing % of VCM loaded shellac NPs at pH 5.5 is higher than at pH 7.4. At the first hours the releasing of VCM was slow and close at both pHs, but after 24 hours the releasing increased at pH 5.5 and reached to 48.5% of total VCM amount while at pH 7.4 it was 24% only. The high release amount of VCM at pH 5.5 attributed to the protonation of shellac carboxylic groups at acidic media which lead to release more VCM molecules. In comparising this releasing with literatur, with shellac NPs VCM shows sustain release at a period of time. [236]

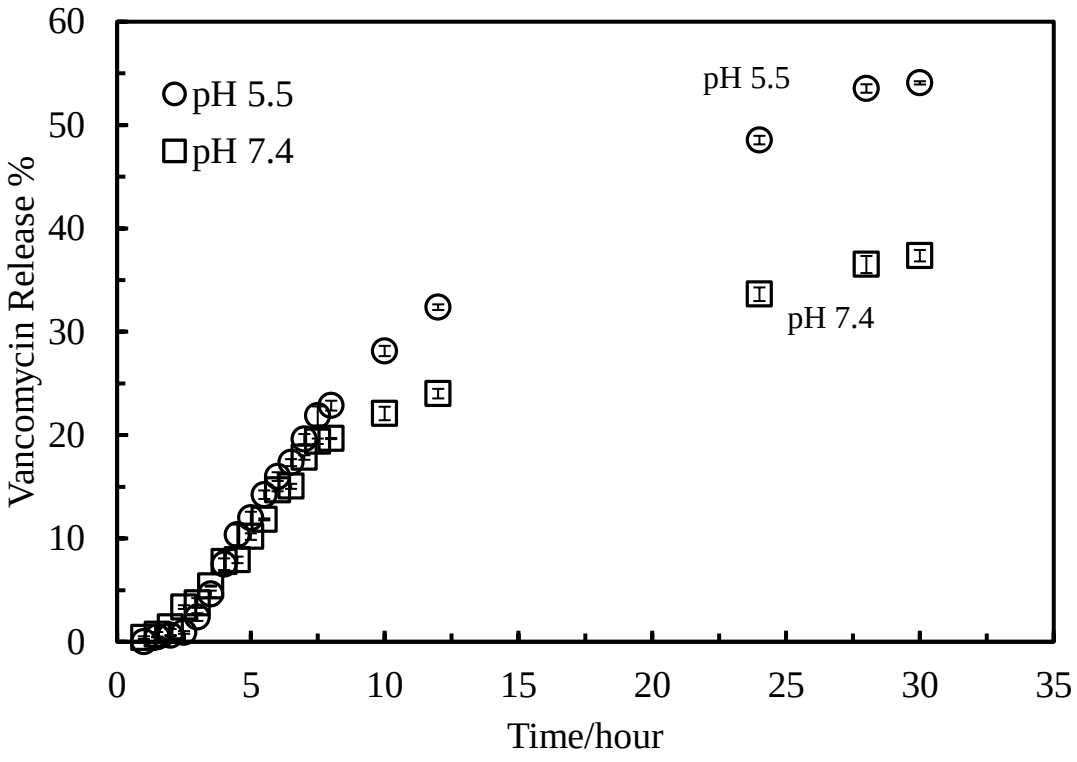

Figure 3.51: *in vitro* vancomycin release profile as a function of time at acetate buffer solution 5.5 and phosphate buffer saline 7.5 measured in a range of wavelength (200 -700 nm) using Perkin Elmer UV-Visible Spectrophotometer, (n=3).

3.7 Functionalization of Shellac NPs

Drug nanocarriers are having a positively charged surface commonly exhibit better association and internalisation rates.[5] To ensure delivery of the largest amount of drugs to microorganisms, the attraction between the NPs and cell membrane should be modified. ODTAB (octadecyltrimethyl ammonium bromide), the cationic electrolyte was used to coat shellac NPs as well as drugs loaded shellac NPs through the adsorption of ODTAB particles on shellac NPs (Figure 3.52). However, to coat shellac at the nanoscale range, different concentrations ODTAB was added after shellac NPs prepared. Figure 3.54 shows that the surface charge of shellac NPs converted to positive at 0.05 wt. % of ODTAB to be 8.5 mV with the size of 108 nm. According to SEM image, shellac NPs maintain their spherical shape after coating, (Figure 3.55).

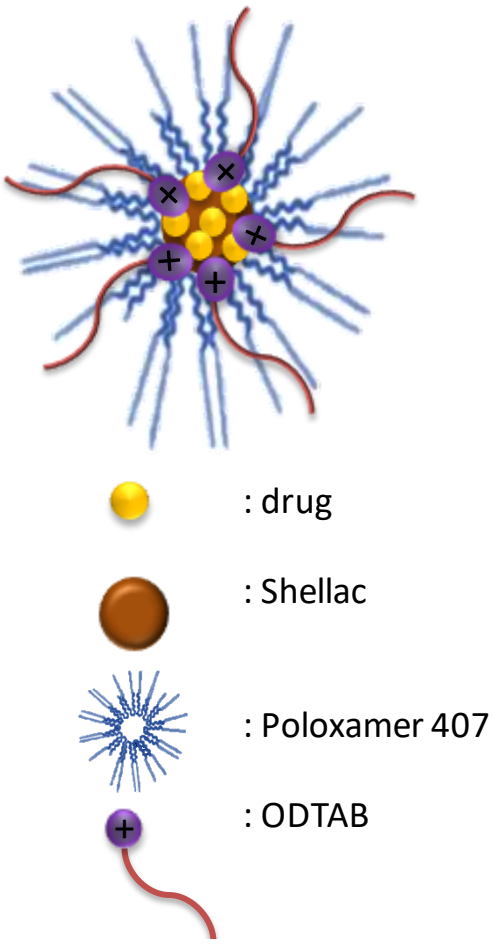

Figure 3.52: Schematic design shows shellac NPs loaded with drugs and coated with ODTAB. The formulated nanocarrier prepared by adding drop wise ODTAB at pH 5 with stirring gently.

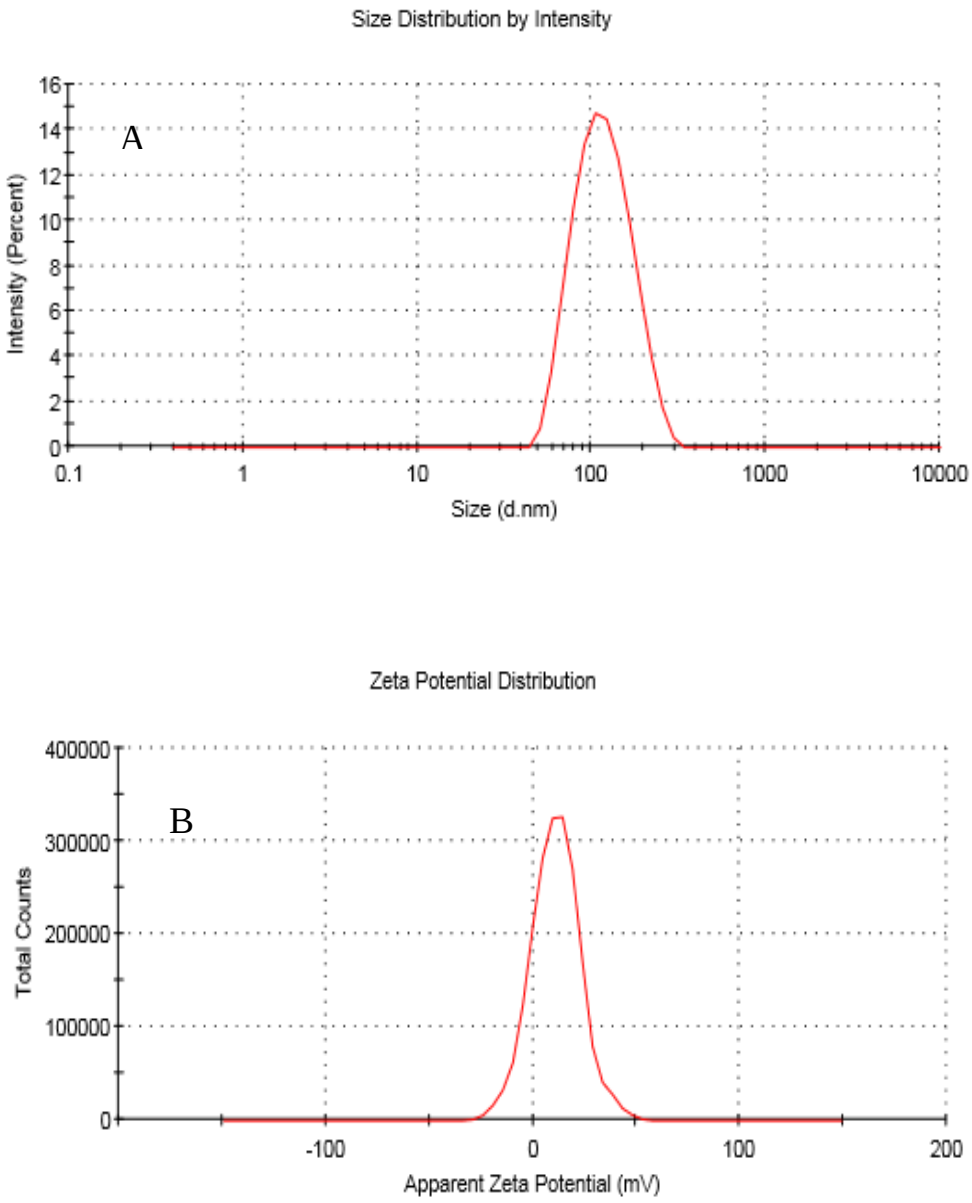

Figure 3.53: Average Particle size (A) and zeta potential (B) of 0.25 wt. % shellac NPs coated with 0.05 wt. % ODTAB.

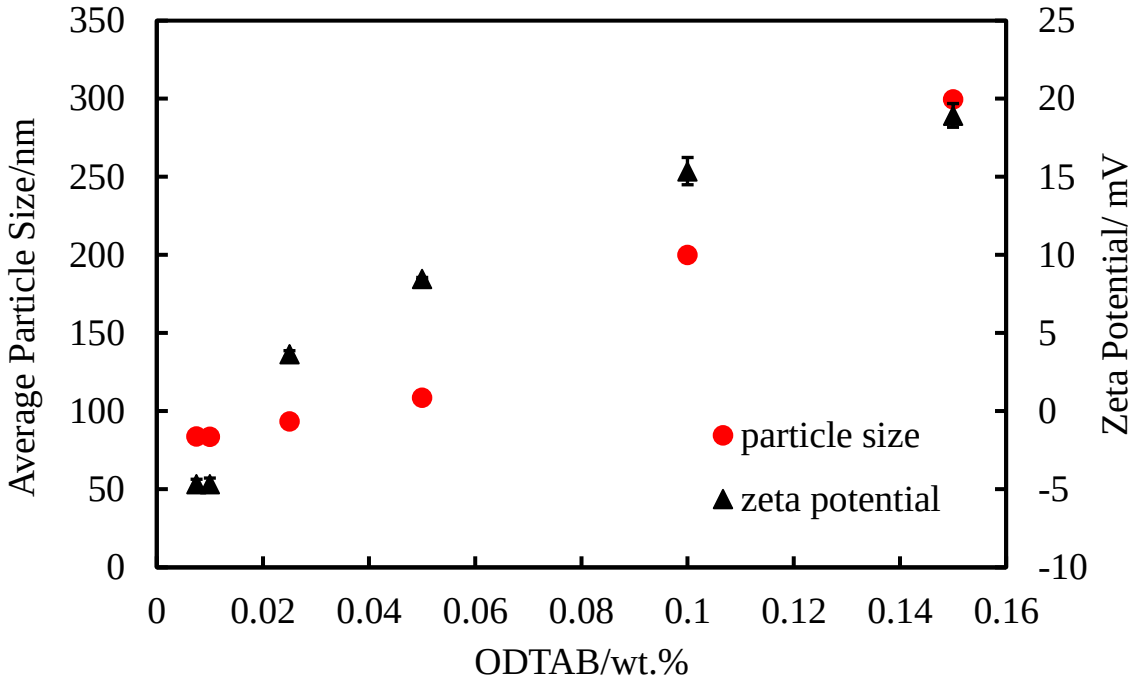

Figure 3.54: the effect of coating Shellac NPs with different concentrations of ODTAB on the size and zeta potential at pH 5, (n=3).

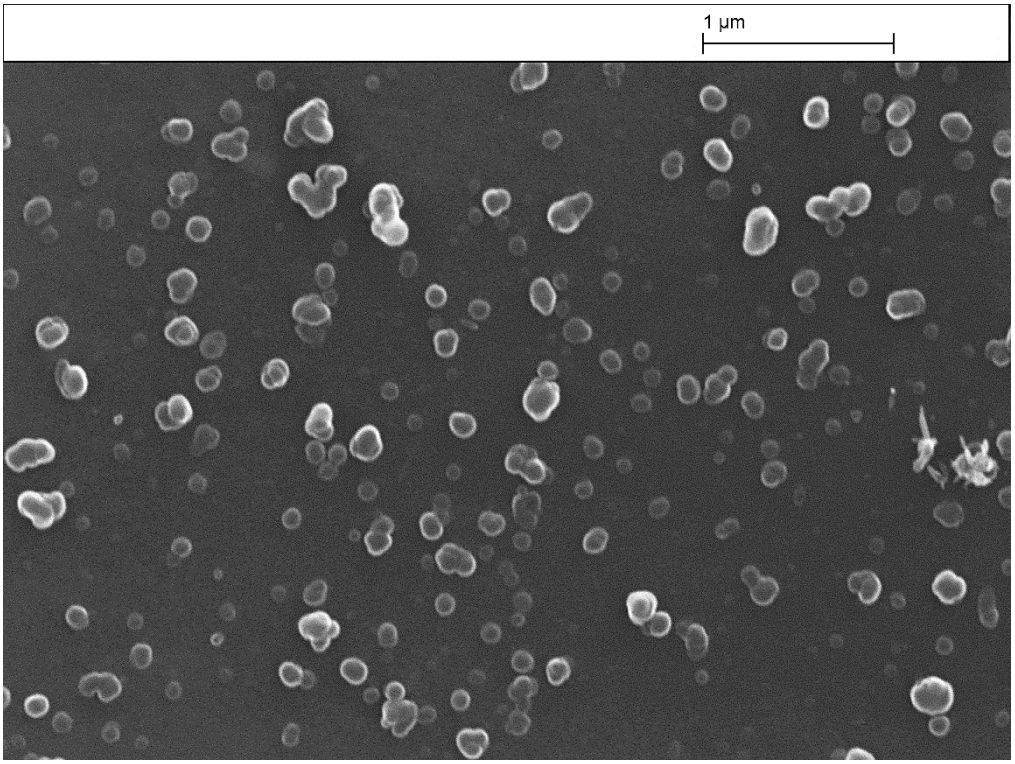

Figure 3.55: Scanning electron microscopy picture of shellac NPs coated with 0.05 wt.% ODTAB. The NPs was coated with carbon

3.7.1 Functionalization of Berberine NPs

Berberine NPs was coated with cationic electrolyte ODTAB to change the surface charge from negative to positive to become more efficient, (Figure 3.56, A) shows the size of berberine after coating which became larger and it was 141 nm with surface charge of of 13 mV (Figure 3.56, B) at 0.03 wt. % of berberine loaded shellac NPs after coated with 0.05 wt.% ODTAB. As it can be seen from Figure 3.57 that the size of BRB-NPs increased directly when the amount of ODTAB increased, while the surface charged converted from negative to positive. Choosing 0.05 wt. % of ODTAB to be used in the further experiment as best results in terms of the surface charge and the particle size. SEM image (Figure 3.58) shows a spherical shape of berberine NPs after coating with ODTAB.

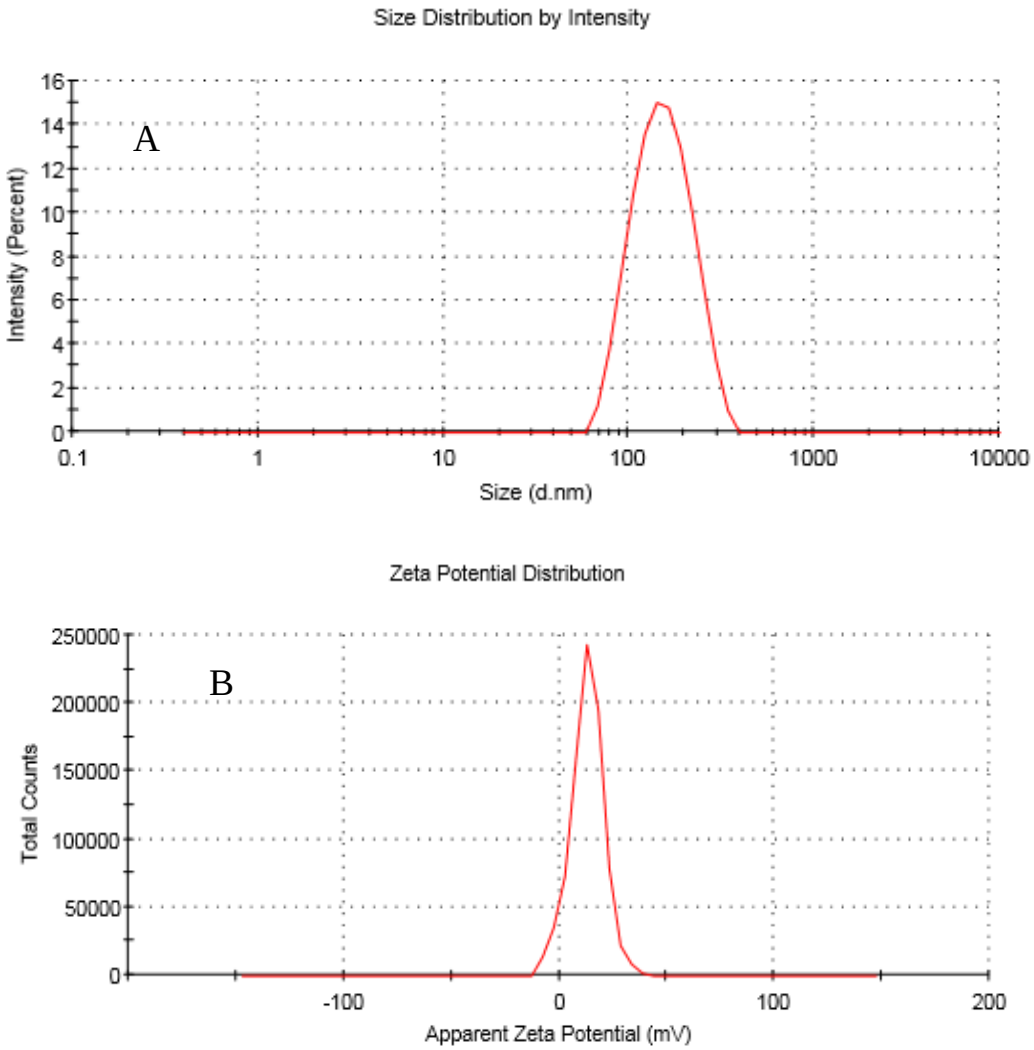

Figure 3.56: 0.03 wt. % BRB loaded Shellac NPs average size (A) and zeta potential (B) after coating with 0.05 wt. % of ODTAB at pH 5.

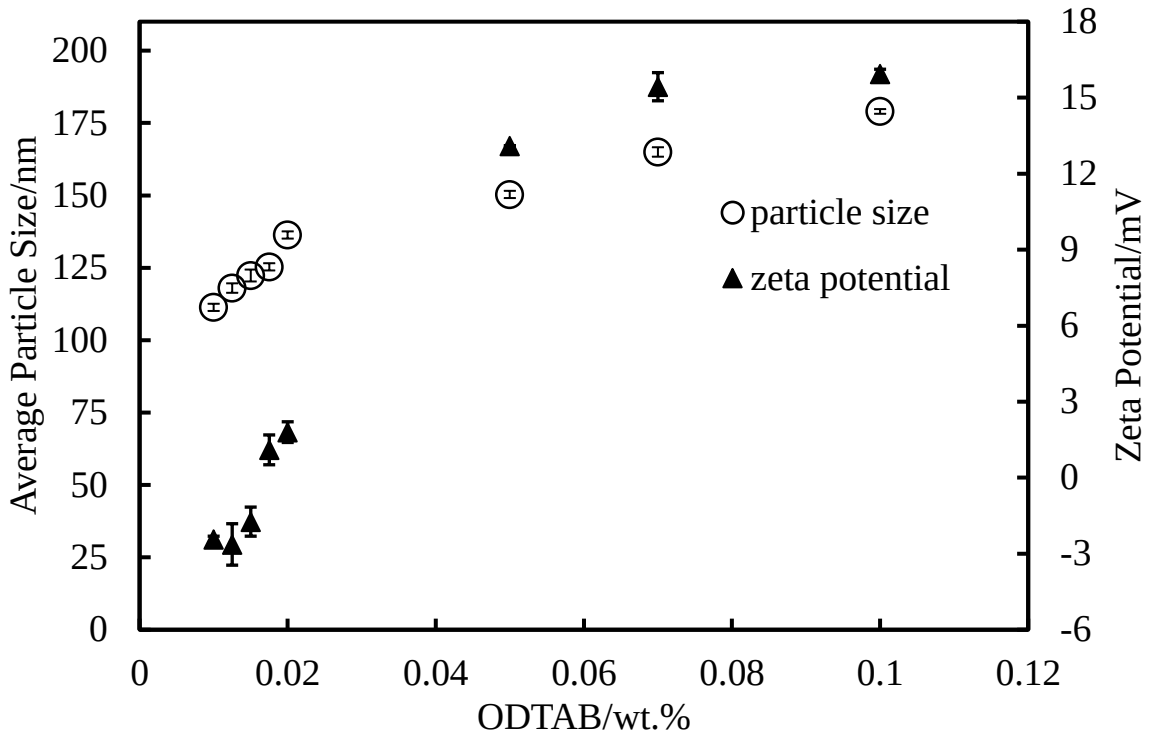

Figure 3.57: The effect of coating 0.03 wt. % of berberine loaded Shellac NPs with different concentrations of ODTAB on the size and zeta potential at pH 5, (n=3).

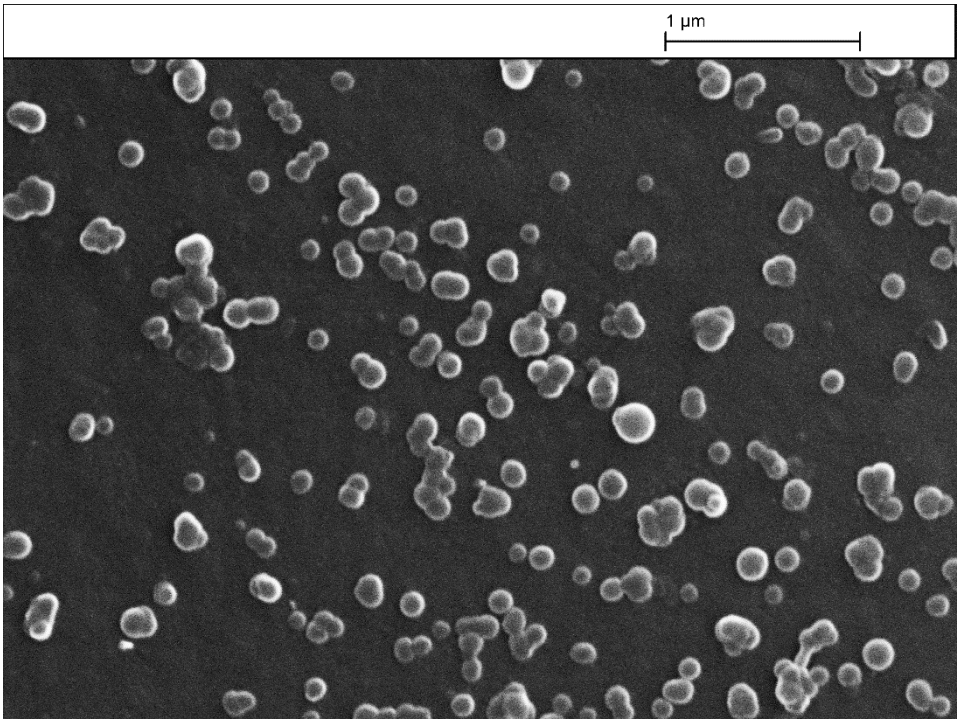

Figure 3.58: Scanning electron microscopy picture of 0.05 wt. % of berberine NPs after coating with 0.05 wt. % of ODTAB.

3.7.2 Functionalization of Chlorhexidine NPs

To enhance the delivery of the drugs to the cells, chlorhexidine loaded shellac NPs was coated with ODTAB; the cationic electrolyte, to change the charge of the NPs surface to be positive, this way enabled the NPs to be attracted efficiently to the cell membrane. After coating, the size of CHX loaded shellac NPs increased from 78 nm to be 105 nm as the amount of ODTAB increased while the surface charge converted from negative to positive by coating with 0.05 wt.% of ODTAB to be +12 mV (Figure 3.59, A&B). Figure 3.60 shows that the size of CHX-NPs was increased directly when the amount of ODTAB increased, while the surface charged converted from negative to positive. Also, choosing 0.05 wt. % of ODTAB to be used in the further experiment as best results in terms of the surface charge and the particle size. Correspondingly, Figure 3.61 shows the SEM image of CHX NPs coated with 0.05 wt. % ODTAB have a spherical shape.

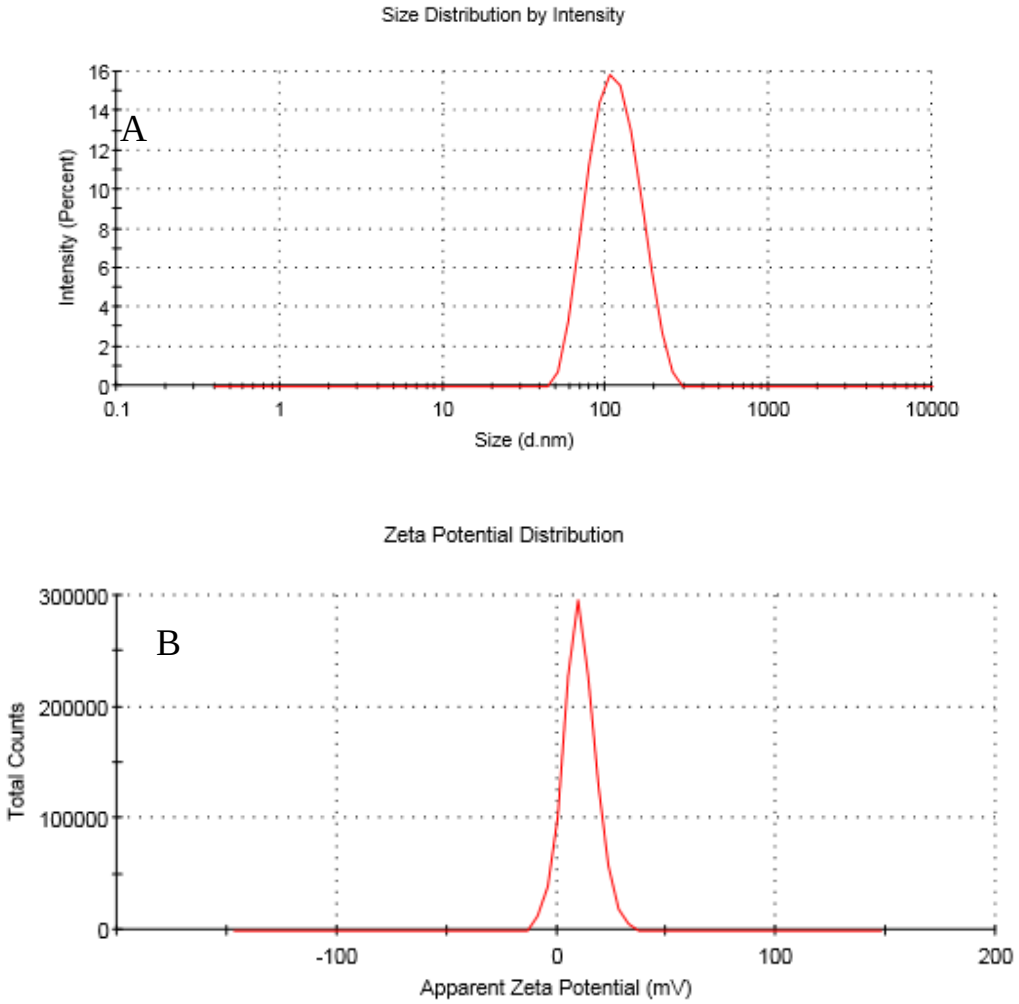

Figure 3.59: (A) The average particle size of 0.03 wt. % CHX loaded Shellac NPs and (B) zeta potential after coating with 0.05 wt. % of ODTAB at pH 5.

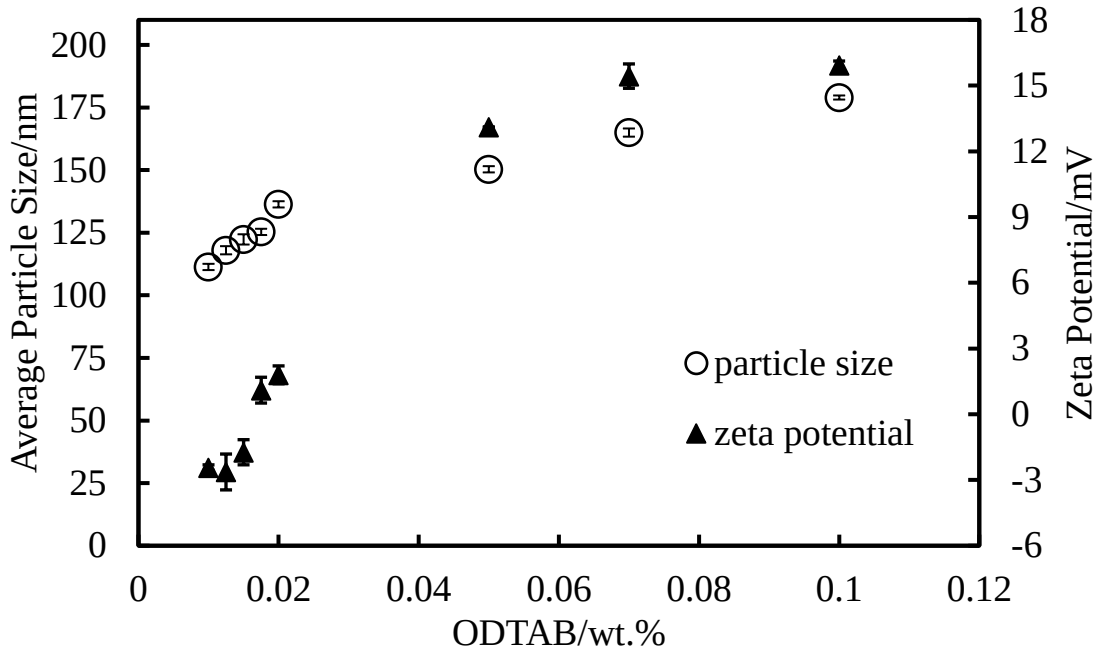

Figure 3.60: The effect of coating 0.03 wt. % of CHX loaded Shellac NPs with different concentrations of ODTAB on the size and zeta potential at pH 5, (n=3).

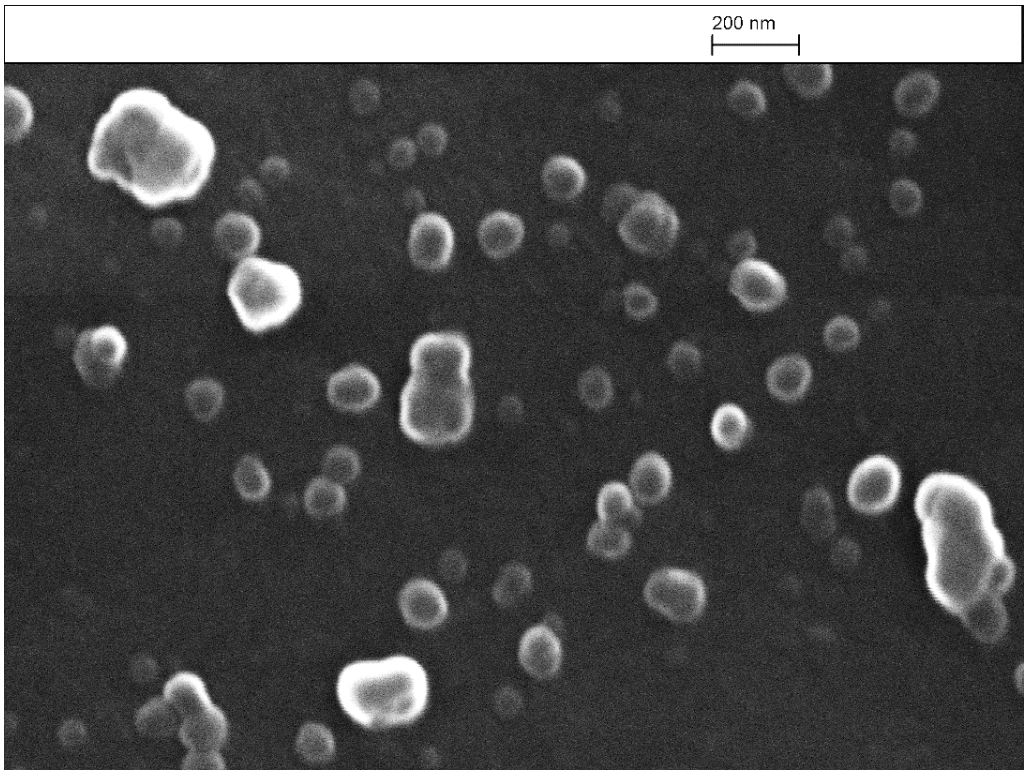

Figure 3.61: Scanning electron microscopy picture of 0.03 wt. % of chlorhexidine NPs after coating with 0.05 wt. % of ODTAB.

3.7.3 Functionalization of Curcumin NPs

Modification of curcumin loaded shellac nanoparticle surface charge can be achieved by coating nanoparticle surface with cationic ODTAB electrolyte. This modification mostly alter the nanoparticle zeta potential, thus increasing the adsorption of NPs on the cell membrane and consequently delivering the efficient amount of drugs. Figure 3.63 displays that curcumin NPs surface charge can be changed by adding 0.03 wt.% of ODTAB or higher with size range around 95 nm. Also 0.05 wt.% of ODTAB was chosen to coated CUR-NPs in further experiments. The coated nanoparticles were observed by SEM, and the picture (Figure 3.67) shows a spherical CUR NPs.

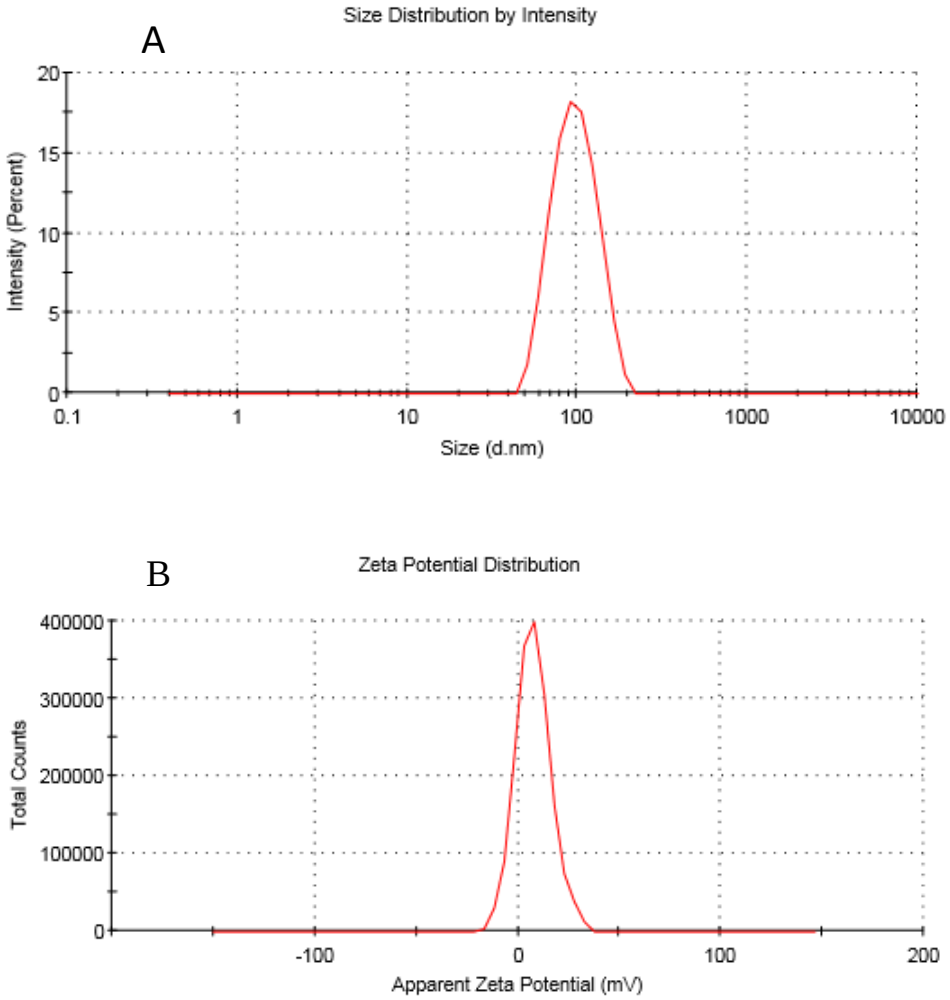

Figure 3.62: (A) the average particle size and (B) zeta potential of 0.03 wt. % CUR loaded Shellac NPs after coating with 0.05 wt. % of ODTAB at pH 5.

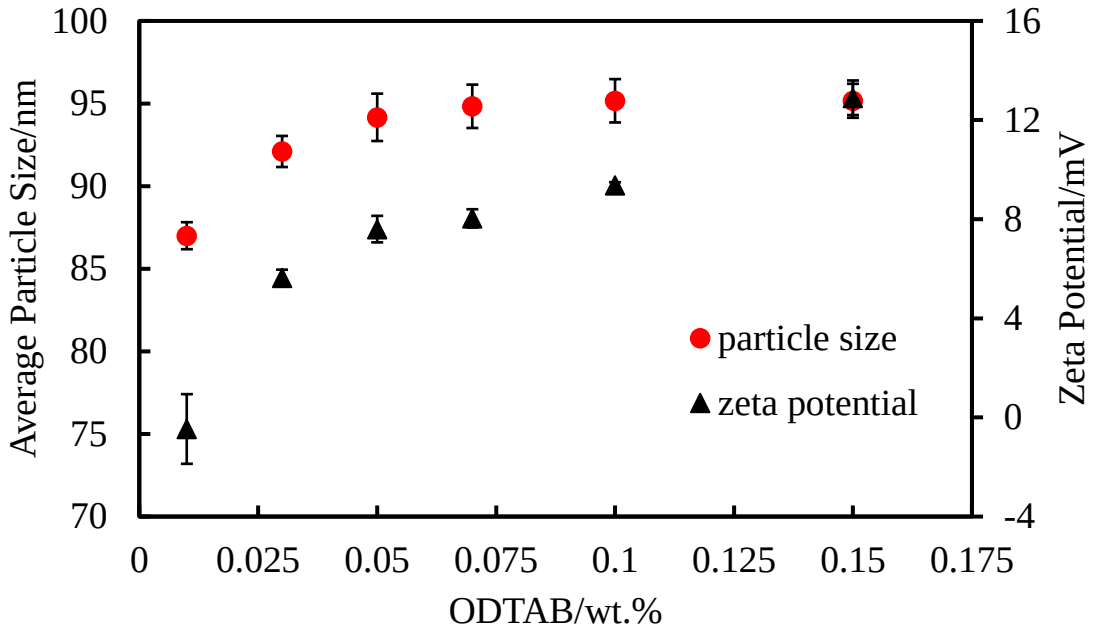

Figure 3.63: The effect of coating 0.03 wt. % of CUR loaded Shellac NPs with different concentrations of ODTAB on the size and zeta potential at pH 5, (n=3).

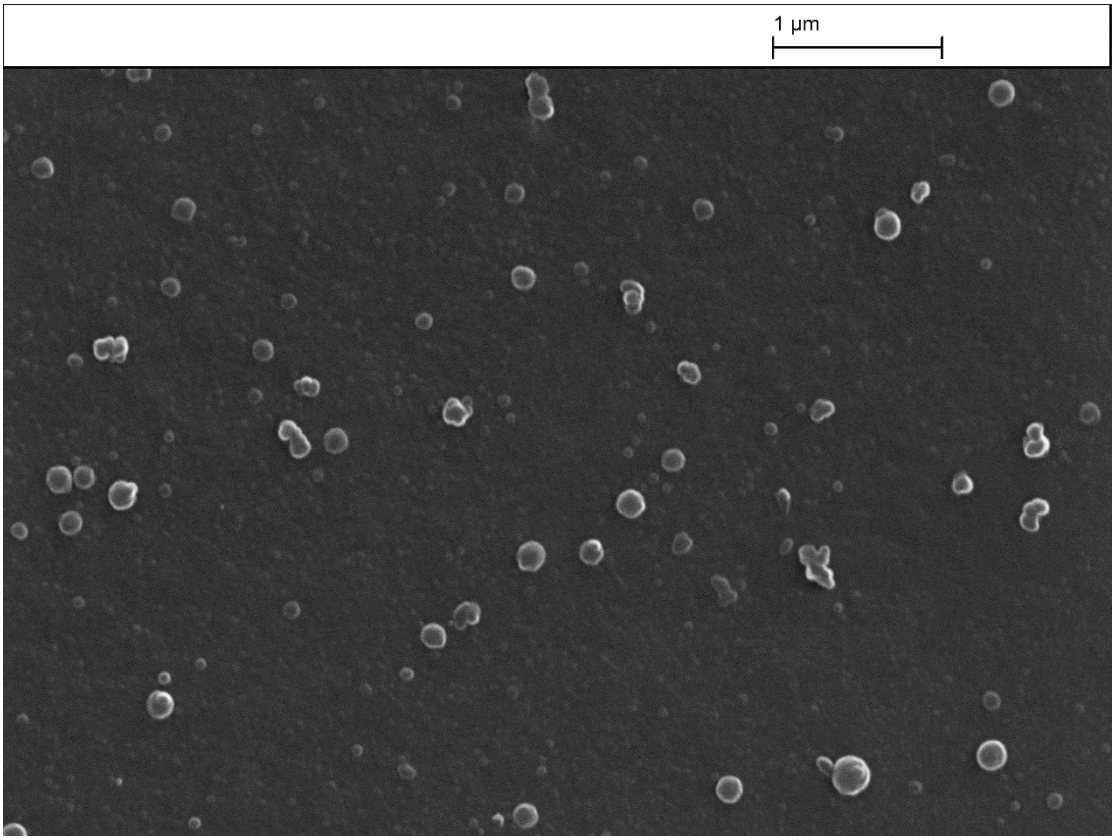

Figure 3.64: Scanning electron microscopy picture of 0.01 wt. % of CUR loaded shellac NPs after coating with 0.05 wt. % of ODTAB.

3.7.4 Functionalization of Vancomycin NPs

Due to the bad attraction of VCM NPs with microorganism's cell membrane, the cationic ODTAB electrolyte has been used to coat the NPs to develop positive nanocarriers. Figure 3.66 shows that VCM loaded shellac NPs surface charge can be altered by adding different amounts of ODTAB after preparing the NPs (at pH 6). As can be seen from figure 3.66 the zeta potential of VCM-NPs decreased when the ODTAB amount increased. 0.07 wt. % ODTAB could be considered as a good amount to coat 0.05 wt. % VCM NPs with surface charge of 10 mV and 98 nm diameter size. Morphological characterisation of the 0.05 wt. % VCM NPs coating with 0.07 wt.% ODTAB using scanning electron microscopy revealed that the NPs have a spherical shape, (Figure 3.67).

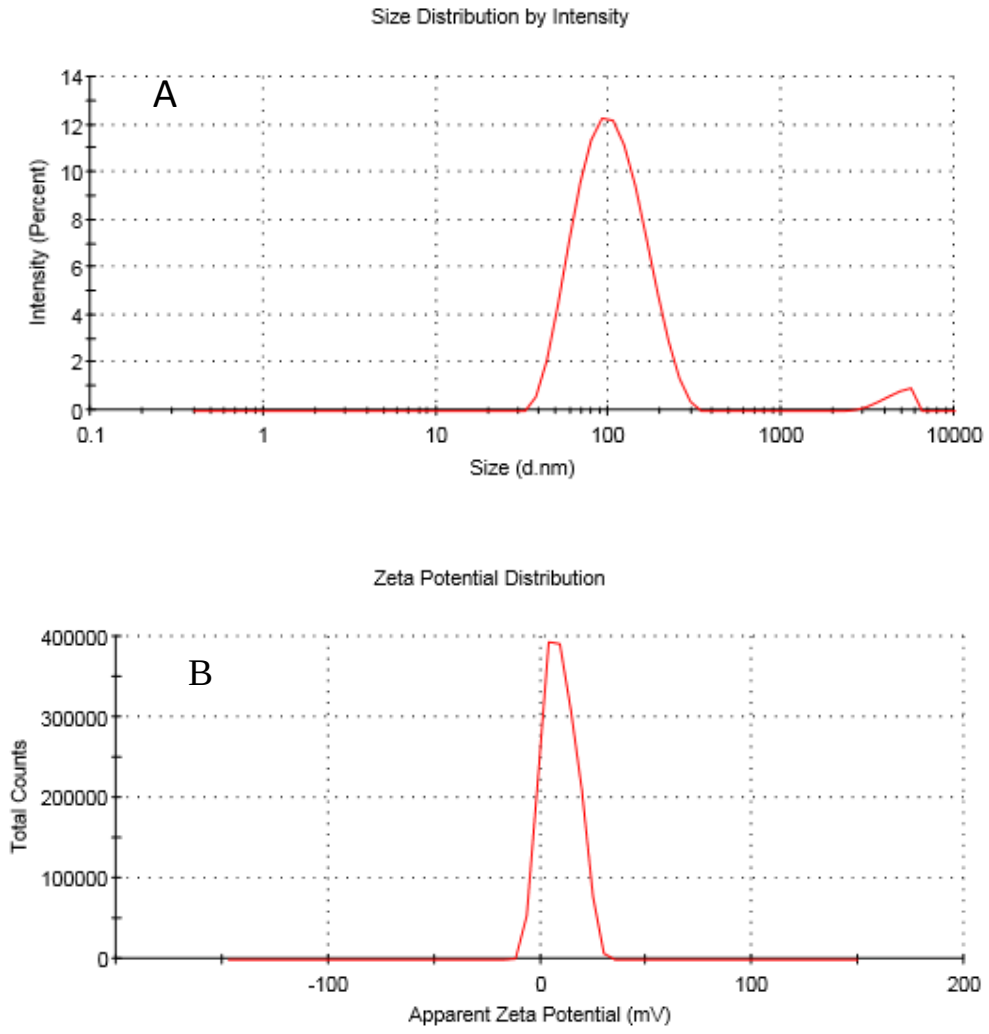

Figure 3.65: (A) the average particle size and (B) zeta potential of 0.05 wt. % VCM loaded Shellac NPs after coating with 0.07 wt. % of ODTAB at pH 5.5.

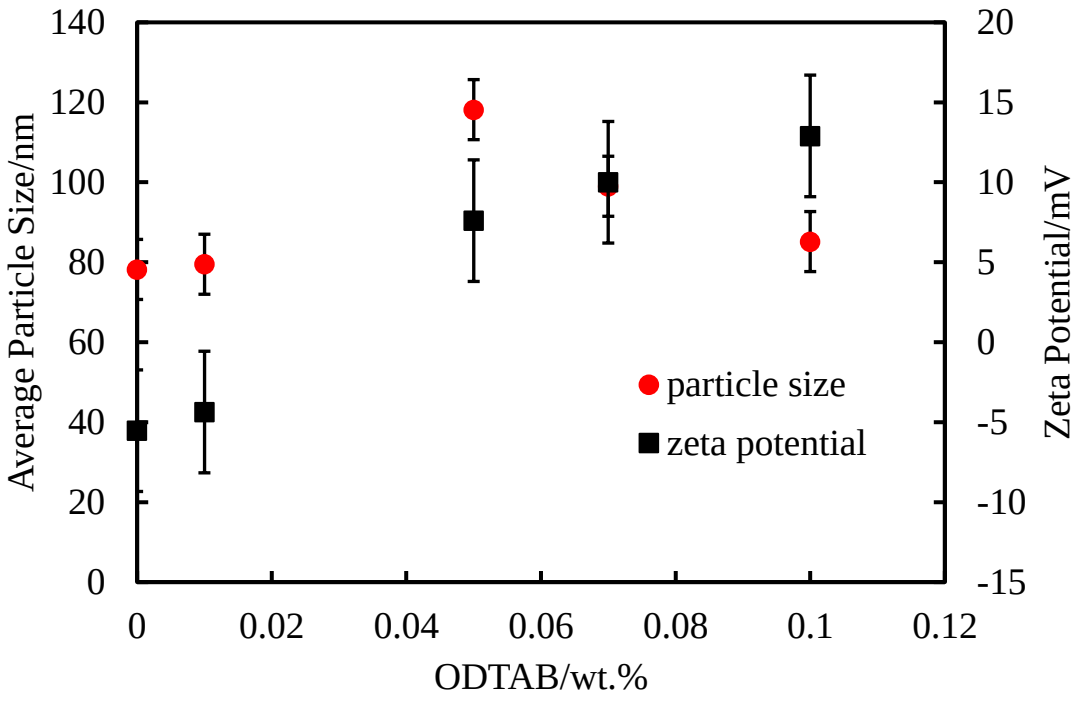

Figure 3.66: The effect of coating 0.05 wt. % of VCM loaded Shellac NPs with different concentrations of ODTAB on the size and zeta potential at pH 5, (n=3).

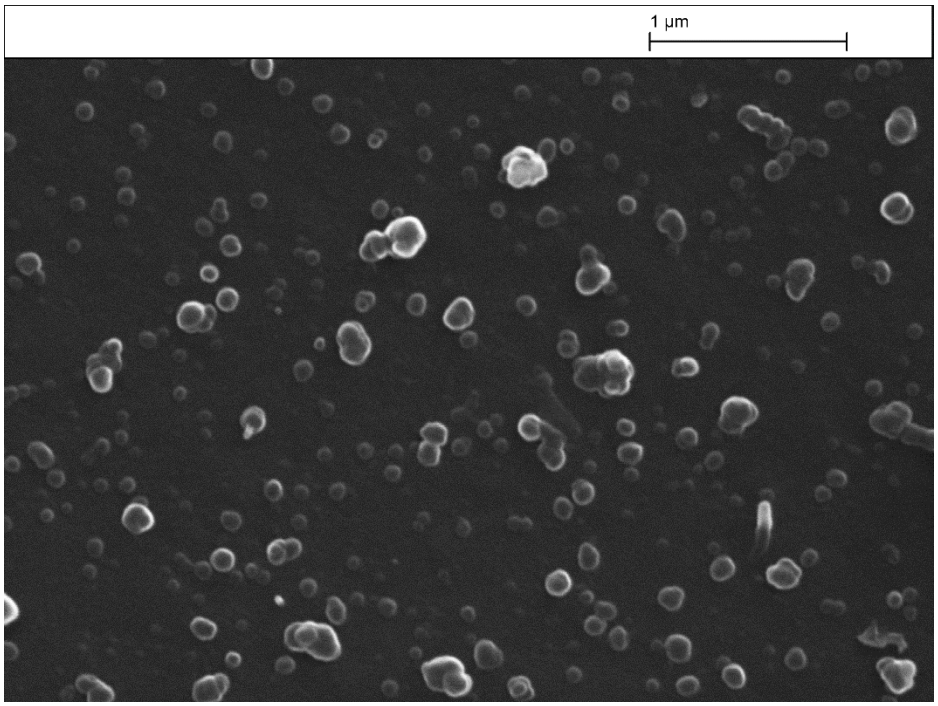

Figure 3.67: Scanning electron microscopy image of 0.05 wt. % of VCM NPs after coating with 0.07 wt. % of ODTAB.

3.8 Conclusion

Most nanoparticle preparation methods, such as emulsification, diffusion and nanoprecipitation require organic solvents such as alcohol, chloroform, acetone, dichloromethane and these must be removed or reduced at the last step of preparation to achieve a therapeutically usable system. The use of organic solvents offers a serious drawback, owing to their toxicity and the need for several purification steps, including complex or long-lasting processes, such as solvent-diffusion or evaporation steps. In this project shellac NPs was prepared in a very simple process using Poloxamer 407 as stabiliser agent and combined by lowering the pH from 8 to 5. The stable NPs were formed depending on steric repulsion effect mechanism produced by Poloxamer 407 micelles by surrounding the shellac particles, the NPs have an average particle size of 66±5 nm with a zeta potential of -18±8 mV. Shellac was chosen to be used as it contains carboxylic groups which can interact with cationic antibiotics agents. Its hydrophobicity characteristics[389], however, means it can be loaded with hydrophobic antimicrobials agents to increase their solubility, so different types of antimicrobials agents were used to be loaded within shellac NPs such as BRB, CHX, CUR, and VCM. These encapsulated NPs were characterised using FTIR, UV-vis, TEM, and SEM techniques to verify the interaction between shellac NPs and the drugs. The TEM and SEM images showed that these NPs have a spherical shape. The encapsulation efficiency and drugs loading contents were measured using UV-vis spectrophotometric method. The releasing profile of each antimicrobials agents changes according to the strength of the interaction between the antimicrobials agents and shellac NPs, as it can be seen that BRB and VCM released faster than CHX and CUR, that is owing to the fact that CHX contains more cationic groups than BRB which interact strongly with shellac molecules which lower the release, while CUR is a hydrophobic agent and it tightly adsorbed on the hydrophobic part of shellac molecules and showed very slow release, whereas VCM is a large molecule so it released fast. At the same time, the pH of the medium plays an important role in releasing amount, which this amount release increases at pH 5,5 due to the protonation of shellac NPs. So according to the nature of the antimicrobials agents and the pH, the release profile can be controlled.

The size of the NPs was increased after loading them with these drugs while the zeta potential decreased due to the interaction between the NPs and the drugs but still negatively charged. To functionalize these NPs by changing the surface charge from negative to positive, insoluble cationic electrolyte ODTAB was used. This functionalization allows the NPs to be attracted rapidly to the cell membrane and the drugs can be released near the

cell vicinity thus small amount of drugs can kill cells. Table 3.5 shows some *in vitro* characteristics of the loaded drugs within shellac NPs including the particle size, the surface charge, the encapsulation efficiency, the drug content within shellac NPs, and the released amount of the drug at pH 5.5 after 8 hours and compared with other nanocarriers loaded with the same drugs in terms of the drug release. By comparing these characteristics of BRB, CHX, CUR, and VCM encapsulated shellac NPs with the same antimicrobials loaded with other nanocarriers, as mentioned in tables 1.2, 1.3, 1.4, and 1.5, it can be seen none of these nanocarriers have been loaded with more than one antimicrobial. In this project it was found that shellac NPs can be loaded with different types of antimicrobial including cationic antimicrobial agents like BRB, CHX, or hydrophobic antimicrobial like CUR, even can be loaded with antimicrobial has bulky molecules like VCM, and this diversity in loading with different type of drugs attributed to the nature of shellac which contains of carboxylic groups as well as hydrophobic parts and this makes it as a universal nanocarrier. By comparing the results of this project with other literatures, it can be noticed that most the nanocarriers' characteristics have some deficiency in their results. Herein, the aimed was to construct stable nanocarrier able to be loaded with different drugs and well characteristics, as well as its surface can be functionalized to produce positive surface charge to promote the adhesion with any type of microorganisms. Also, the drug release of most nanocarriers mentioned in literatures have been studied at one pH media, while in this project the drug released was studied at two different pH media 7.4 and 5.5. Beside shellac NPs showed stability at a range of pH which means the drug release can be studied at range from 4-7. Moreover, the results in table 3.5 show that depending on the requirement of the drug release, i.e. slow or fast, the type of the drug can be loaded within shellac NPs. In other words if it is needed a slow release so an antimicrobial with large amount of positive charge atoms like CHX can be used or hydrophobic drug like CUR may load in case the requirement is a very slow release. While for fast release an antimicrobial with less positive charge atom can be loaded within shellac NPs to insure a weak electrostatic interaction between the drug and shellac NPs and thus fast release, like BRB.

Table 3.5: I*n vitro* characteristics of BRB, CHX, CUR, and VCM loaded shellac NPs.

Antimicrobail agent	Size/ nm & Zeta potential/ mV	E.E%	Drug loaded%	Drug Release % at pH 5.5 after 8 hours	Antimicrobial release% in literatures	Ref.
BRB	77±34 -18.6 ±7	60	28	100	30 after 8 h	393
CHX	79±30 -11±8	92	16	38	88 after 1.5 h	394
CUR	87±26 -5±0.6	100	33.8	2.25	80 after 300 h	212
VCM	80±24 -7±5	87.5	13.6	23	Zero release for 9 h then sustain release for 3 days	236

Chapter 4 : Cytotoxicity Assay of Berberine and Chlorhexidine Loaded Shellac NPs

In the preceding chapter, a new protocol of loading shellac NPs with four different antimicrobial agents, berberine, chlorhexidine, curcumin and vancomycin was developed, their properties in terms of optimizing their colloid stability, encapsulation efficiency and drug release were characterised. In this chapter, the antimicrobial activity of two agents; BRB and CHX are presented. Berberine chloride as a natural chemical which has been used as an antimicrobial agent for many years ago, and chlorhexidine di-gluconate as antiseptic and disinfectant agent which is used for wound cleaning, dental plaque prevention and treating yeast mouth infections treatment. This study included the cytotoxic effect of berberine and chlorhexidine as free agents, and encapsulated within shellac NPs and as functionalised shellac NPs with cationic electrolyte ODTAB. These were studied against different microorganisms such as microalgae, yeast and *E.coli*. The objective of this work was to develop natural nanocarrier-formulated antimicrobials to sustain the release of drugs as well as increase the effectiveness of their antimicrobial activity by encapsulating them at very low overall concentrations into shellac nanoparticles to be used for wound treatment.

4.1 Cytotoxic Assay of Shellac NPs

The cytotoxic assay of shellac NPs on algae, yeast and *E.coli* was carried out following incubation of different concentrations of shellac NPs suspensions at a range of time. Figure 4.1 to Figure 4.3 show the cytotoxic effects of shellac NPs; without drugs on *C. reinhardtii*, *S. cerevisiae*, and *E. coli*, respectively. As can be seen from Figure 4.1 there is a small effect of shellac nanoparticles on algal cells due to the antibacterial adherence property of Poloxamer 407 (P407); which is used as a stabiliser for the shellac NPs. Many researchers have previously reported that Poloxamer 407 might create a hydrated layer on the bacteria surface, [395-397] so the combination between Poloxamer 407 and the antibiotic may play a synergistic antimicrobial role within this nanocarrier design. The shellac NPs however showed pronounced effect when incubated with yeast and *E.coli* cells for 6 hours, and this related to the effect of Poloxamer 407 as it plays a role in breaking out or disrupting the membrane of microorganisms' cells[10] as clear in Figure 4.2 and Figure 4.3.

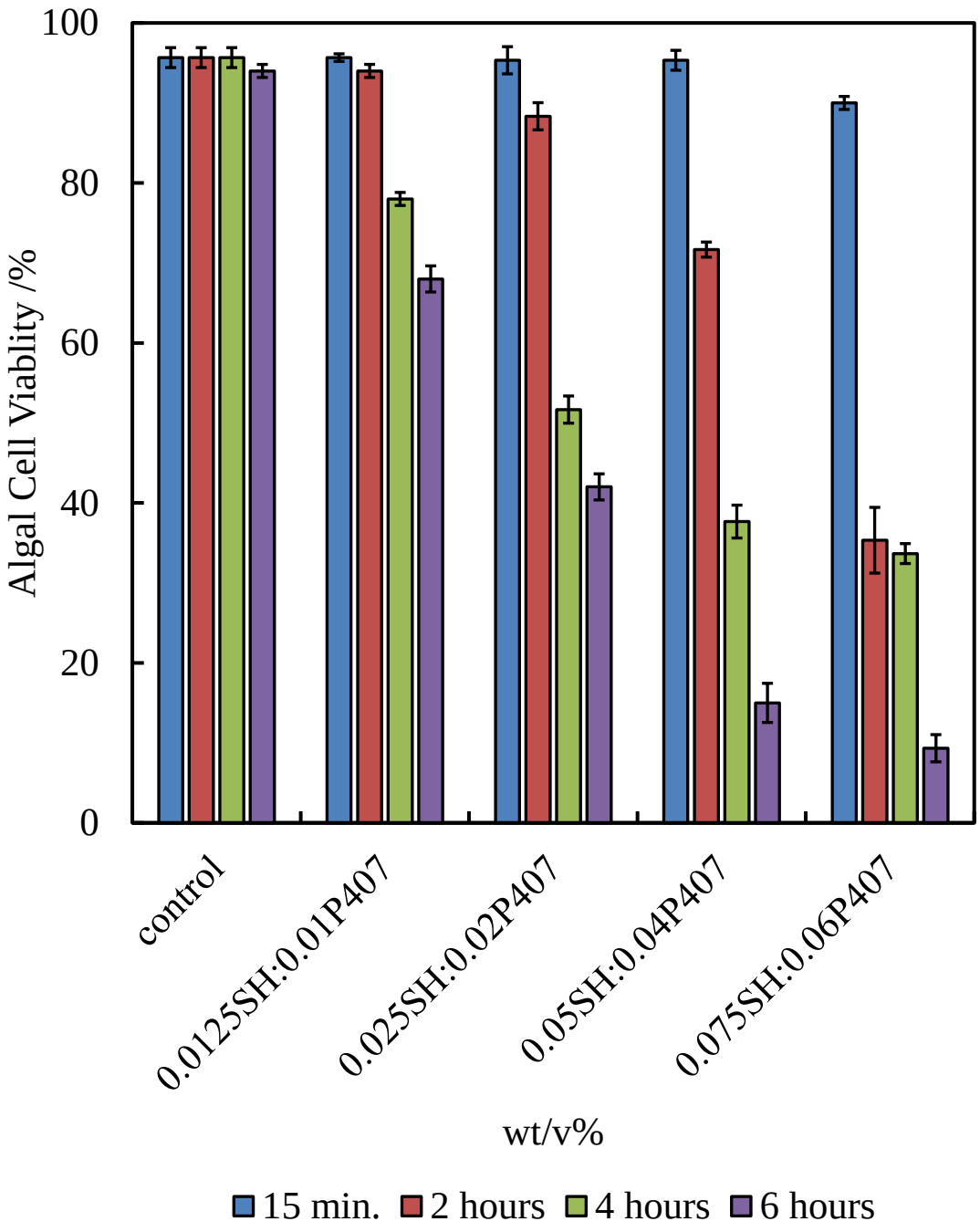

Figure 4.1: The viability of *C. reinhardtii* cells incubated with different concentrations of shellac nanoparticles at different incubation time at room temperature tested by using FDA cell viability assay at pH 5.5, (n=3).

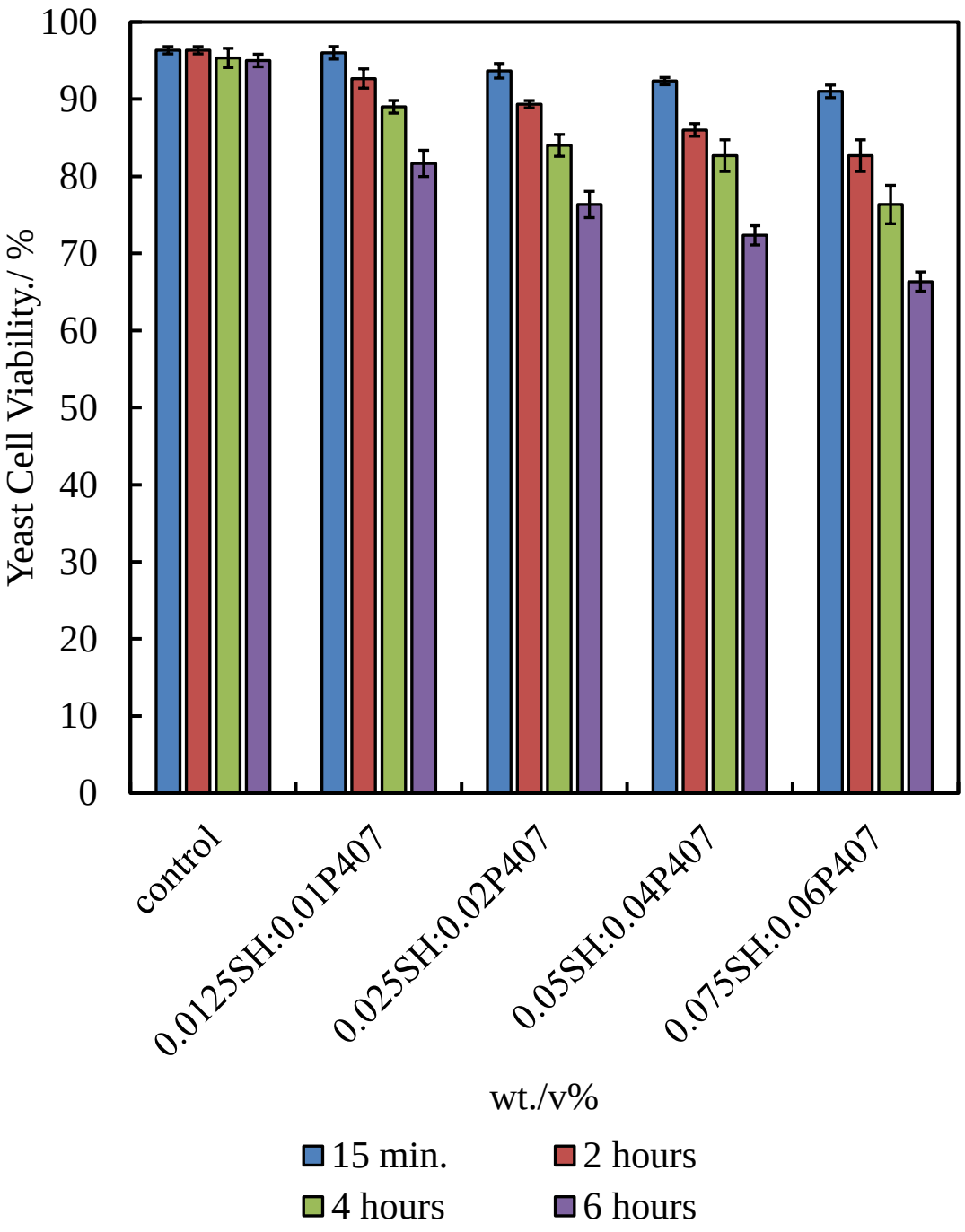

Figure 4.2: The viability of yeast cells upon incubation with different concentrations of shellac nanoparticles at different incubation time at room temperature tested by using FDA cell viability assay at pH 5.5, (n=3).

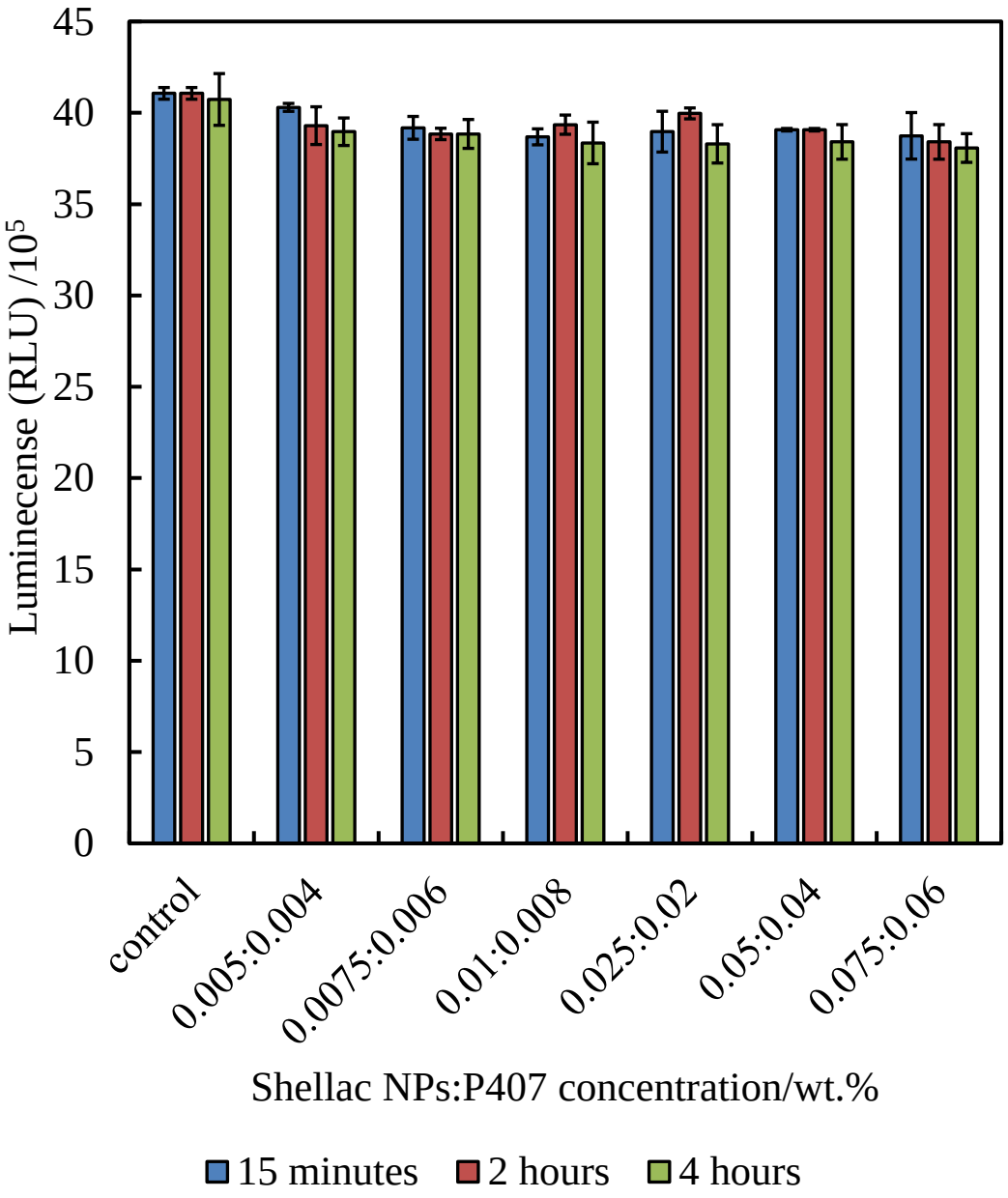

Figure 4.3: The relative luminescence intensities representing the viability of *E.coli* cells incubated with different concentrations of shellac nanoparticles at different incubation time at room temperature tested by using bactiter luciferase assay at pH 5.5, (n=3).

4.2 Antimicrobial Activity of Berberine Loaded Shellac NPs

The antimicrobial activity of free berberine and berberine loaded shellac NPs on some microorganisms such as *C. reinhardtii* (microalgae), *S. cerevisiae* (yeast) and *E. coli* was investigated and compared. This approach may determine whether the loading of berberine within shellac nanoparticles could enhance the antimicrobial activity of berberine. The following three sections 4.2.1, 4.2.2 and 4.2.3 describe the investigation of the antimicrobial efficacy of berberine loaded shellac NPs with microalgae, yeast and *E.coli* in comparison with free berberine.

4.2.1 Antimicrobial Activity of Berberine Loaded Shellac NPs on Algal Cells

The purpose of encapsulating berberine within shellac NPs was to increase the antimicrobial action of berberine by increasing the surface area of the nanocarrier, hence using less amount of antimicrobial to reduce the side effect of the drug as well as to increase its solubility that leads to enhance stability and the bioavailability in medical formulations increasing its efficacy.[398-402] Figure 4.4 displays the cell viability of the *C. reinhardtii* as a function of free berberine concentration after washing the cells from the tested solution using FDA assay. As it can be seen that when the cells incubated for 15 minutes with 0.01 wt.% and 0.05 wt.% free BRB, the viability of the cells reduced instantly from 91% at control to be 18% and 11% respectively. After 2 hours of incubation time, the algal cells viability rapidly declined from 90% to be 3% at 0.01wt.% of free BRB, while at 0.05wt.% all cells were killed. The cell viability kept reducing as the incubation time increased, and after 6 hours most cells died at BRB concentrations of 0.007wt.% and higher. These findings[403] supports the literature that berberine is an effective antimicrobial agent at reasonable concentrations over an adequately long period. Correspondingly the cytotoxicity of berberine loaded shellac NPs on the algal cell was studied, in section3.3.3 it was shown that berberine could be efficiently encapsulated within shellac NPs up to 60% with the release reaching up to 100% of the total amount of berberine at pH 5.5 after 8 hours. Figure 4.5 shows the effect of different concentrations of berberine loaded shellac NPs on the algal cell viability at room temperature up to 6 hours. After 15 minutes incubation, the cells appeared to be not significantly affected by the encapsulated antimicrobial as the viability reduced slightly to be 77% at 0.01wt.% BRB-NPs in comparison with the control 92% which represent the algal cells alone in a solution of pH

5.5. After 6 hours of incubation, the viability of the cell decreased slightly, at 0.007 and 0.01 wt.% of BRB loaded shellac NPs the viability decreased to be 6% and 1.5% respectively. By comparing these results with the results obtained from the antialgal action of free berberine on algal cells, we can notice that free berberine has stronger antimicrobial effect than encapsulated BRB with shellac NPs and this is attributable to the surface charge of the nanoparticles which is negative even after being loaded with BRB. This leads to a lower attraction between these nanoparticles and the cell membrane as well as the drug being sustained within shellac particles as they are attracted electrostatically.

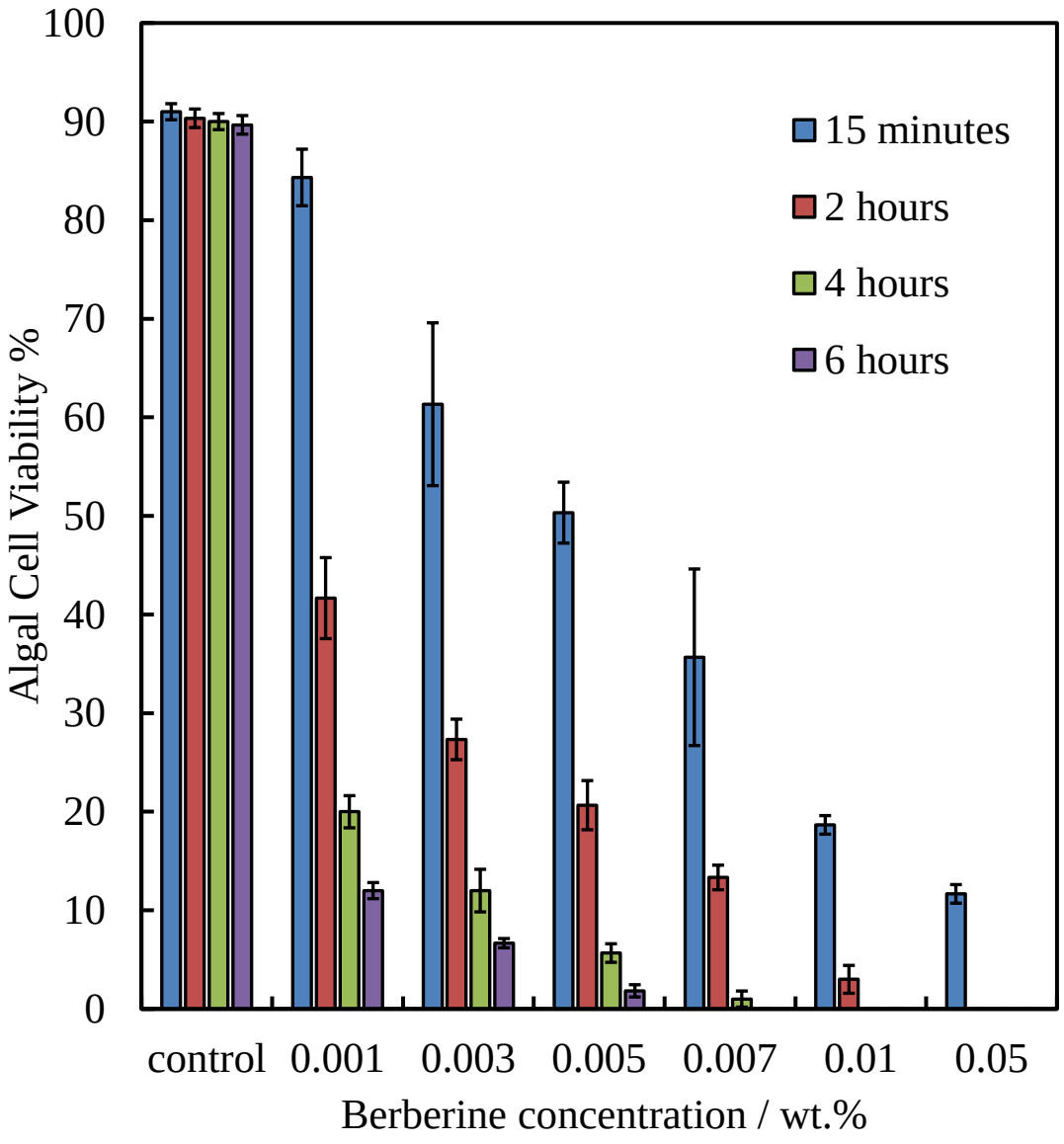

Figure 4.4: The viability of algal cells upon incubation at pH 5.5 with aqueous solutions of varying concentrations of free berberine chloride at room temperature up to 6 hours incubation time at pH 5.5 using FDA assay, (n=3).

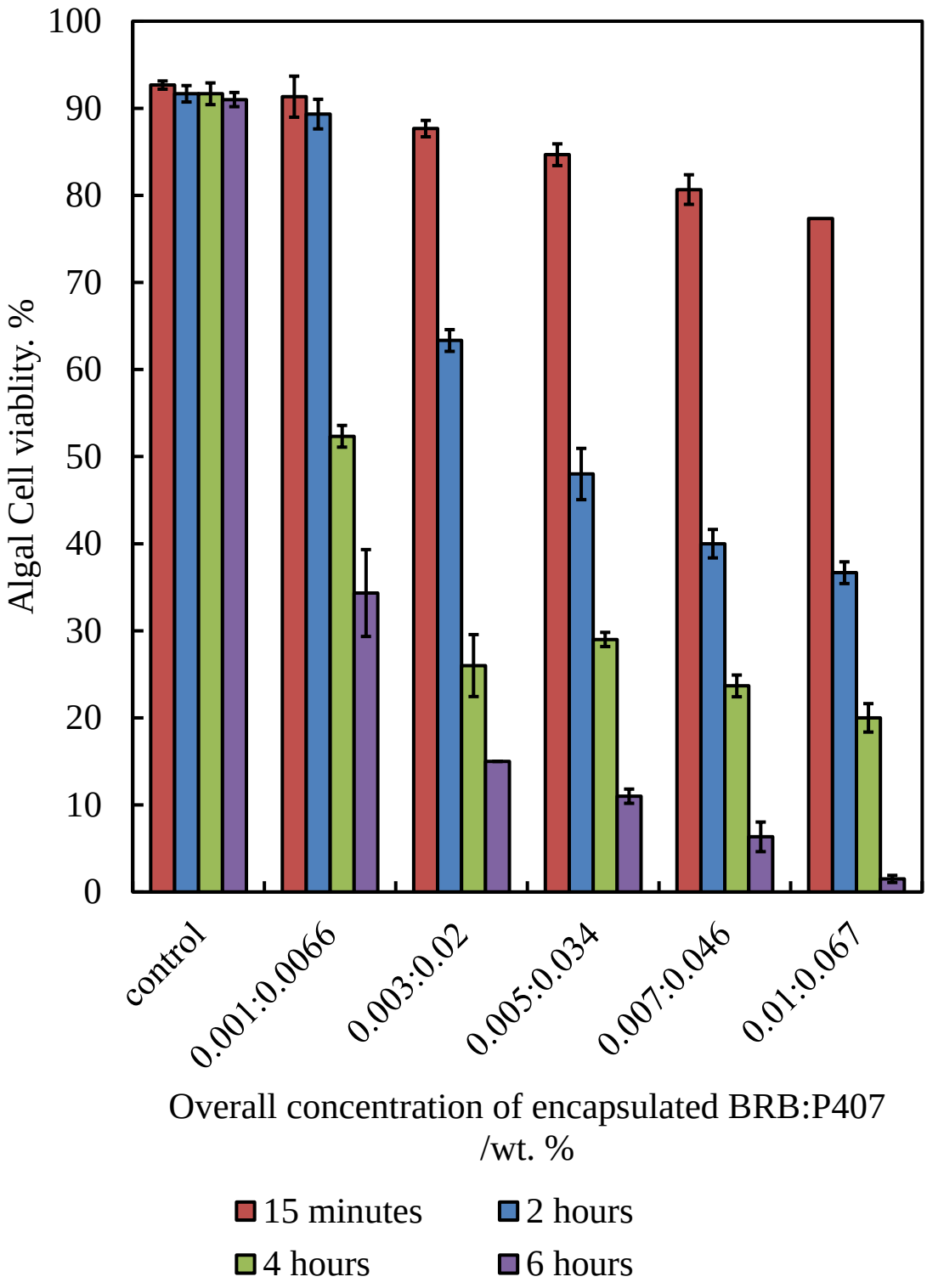

Figure 4.5: The viability of algal cells upon incubation at pH 5.5 with varying concentrations of berberine loaded shellac NPs at room temperature for 15 min, 2 h, 4 h, and 6 hours incubation time at pH 5.5 using FDA assay, (n=3).

The SEM images revealed a good evidence for the effect of berberine as free agent and encapsulated within shellac NPs on the cells after 4 hours of incubation. Figure 4.6 C&D show that the morphology of the algal cells has changed to irregular shapes after incubating with 0.01 wt.% free berberine and they lose their flagella compared with the control cells (Figure 4.6 A&B). While, when the *C. reinhardtii* cells incubated with berberine loaded shellac NPs for the same period and concentration (Figure 4.6 E&F), the cells were not affected for the reasons mentioned previously, that the shellac NPs after loading with BRB still maintain their negative charge which caused a repulsion between them and the negatively charged surface of the cell membrane.

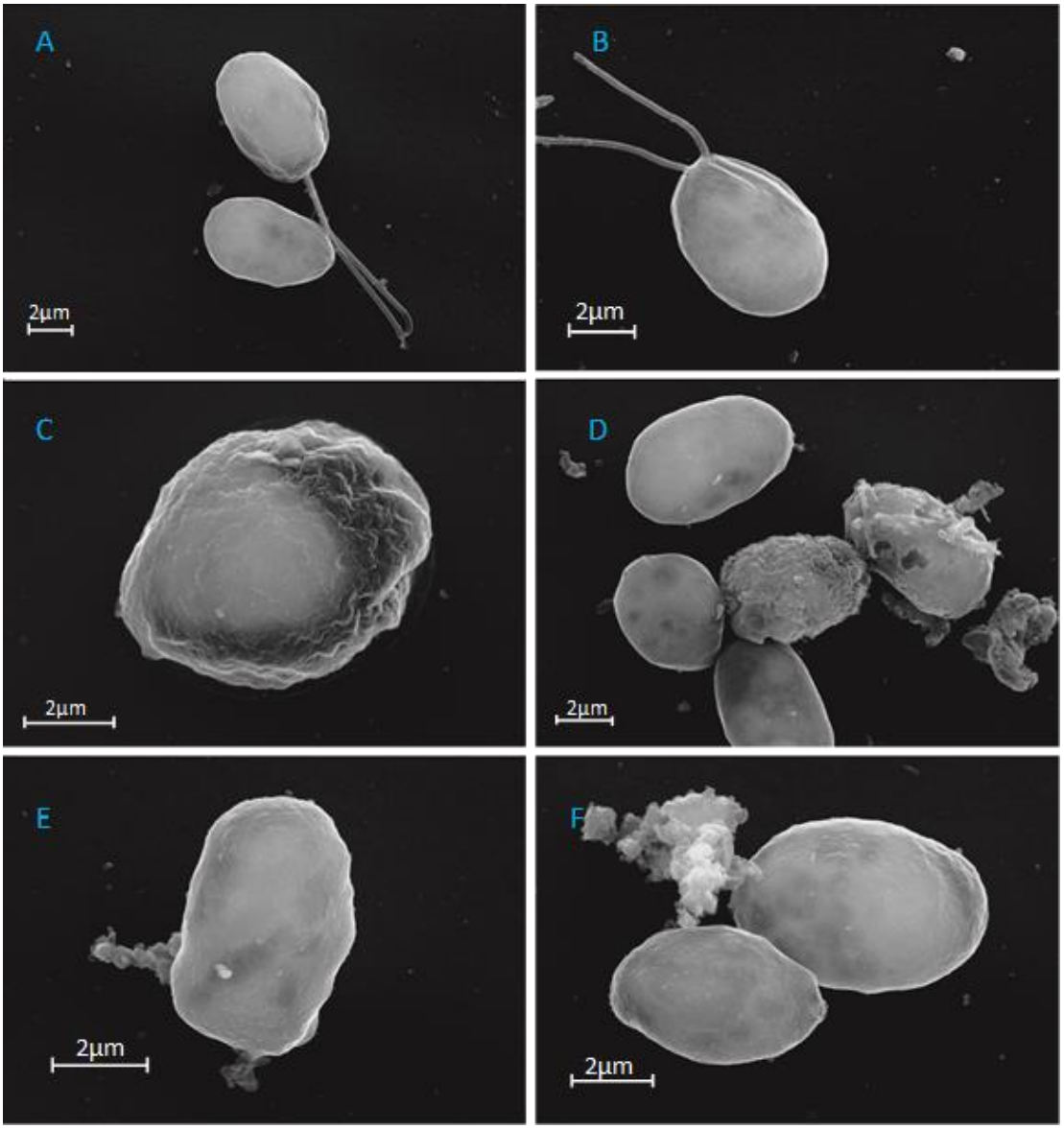

Figure 4.6: SEM images of *C. reinhardtii* microalgae cells whereby (A&B) Control sample of the microalgae cells. (C, and D) *C. reinhardtii* cells incubated with 0.01 wt. % free BRB after 4 hours incubation, (E&F) *C. reinhardtii* cells incubated with 0.01 wt. % BRB loaded shellac NPs up to 4 hours.

4.2.2 Antimicrobial Activity of Berberine Loaded Shellac NPs on Yeast Cells

Yeast cells have been chosen as a model to study the antifungal action of berberine. These cells were incubated with free berberine and berberine loaded shellac NPs for 6 hours at room temperature at pH 5.5, as good conditions to release encapsulated berberine. Free berberine did not show any antifungal activity toward yeast cells in comparison with control sample even after 6 hours of incubation as can be seen in Figure 4.7. Berberine loaded shellac NPs did have a small effect on the yeast cells at different incubation times, and this could be attributed to the effect of Poloxamer 407, not to berberine, Poloxamer 407 play a role in breaking out or disrupting the membrane of microorganisms' cells thus allowing the drug,[404] such as berberine, to improve their action and efficacy against fungus and yeast infections. Figure 4.8 shows the cell viability which decreased gradually from 98% for the control to 36% at 0.01wt.% overall concentration of BRB loaded shellac NPs. This can also be seen in SEM pictures after incubating yeast cells with 0.01 wt.% free and encapsulated berberine for 4 hours (Figure 4.9). Some particles can be seen on the yeast cells which did not penetrate through the membrane (E&F). Berberine showed no effect on yeast cells, and this is likely to be due to the fact that they have a very thick and rigid shell of chitin and glucan around their cell membrane.[405] Moreover the negatively charged shellac NPs loaded with BRB repel with the negatively charged cell wall.

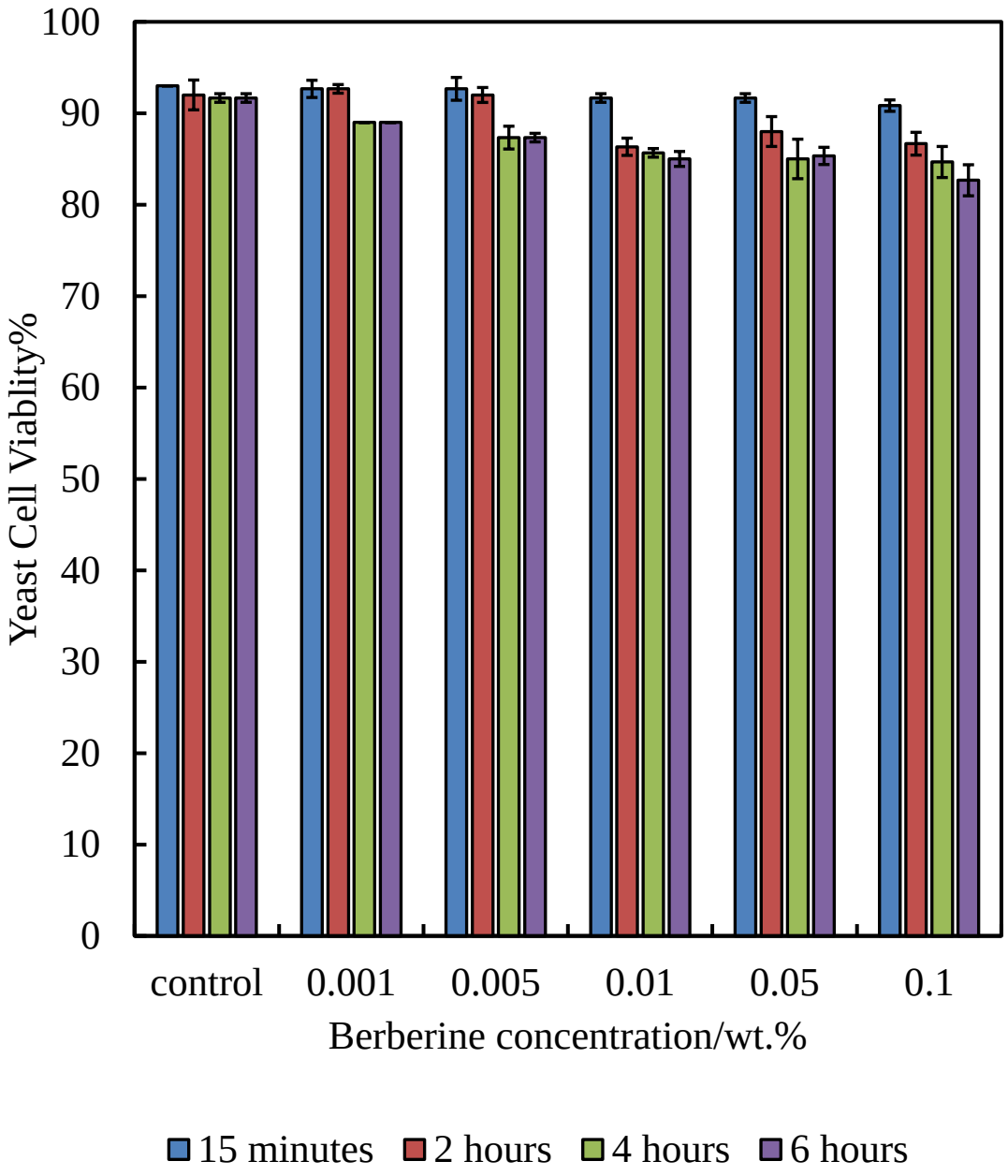

Figure 4.7: The viability of yeast cells incubated with different concentrations of free berberine at different incubation time for 15 min, 2 h, 4 h, and 6 hours at room temperature and pH 5.5, (n=3).

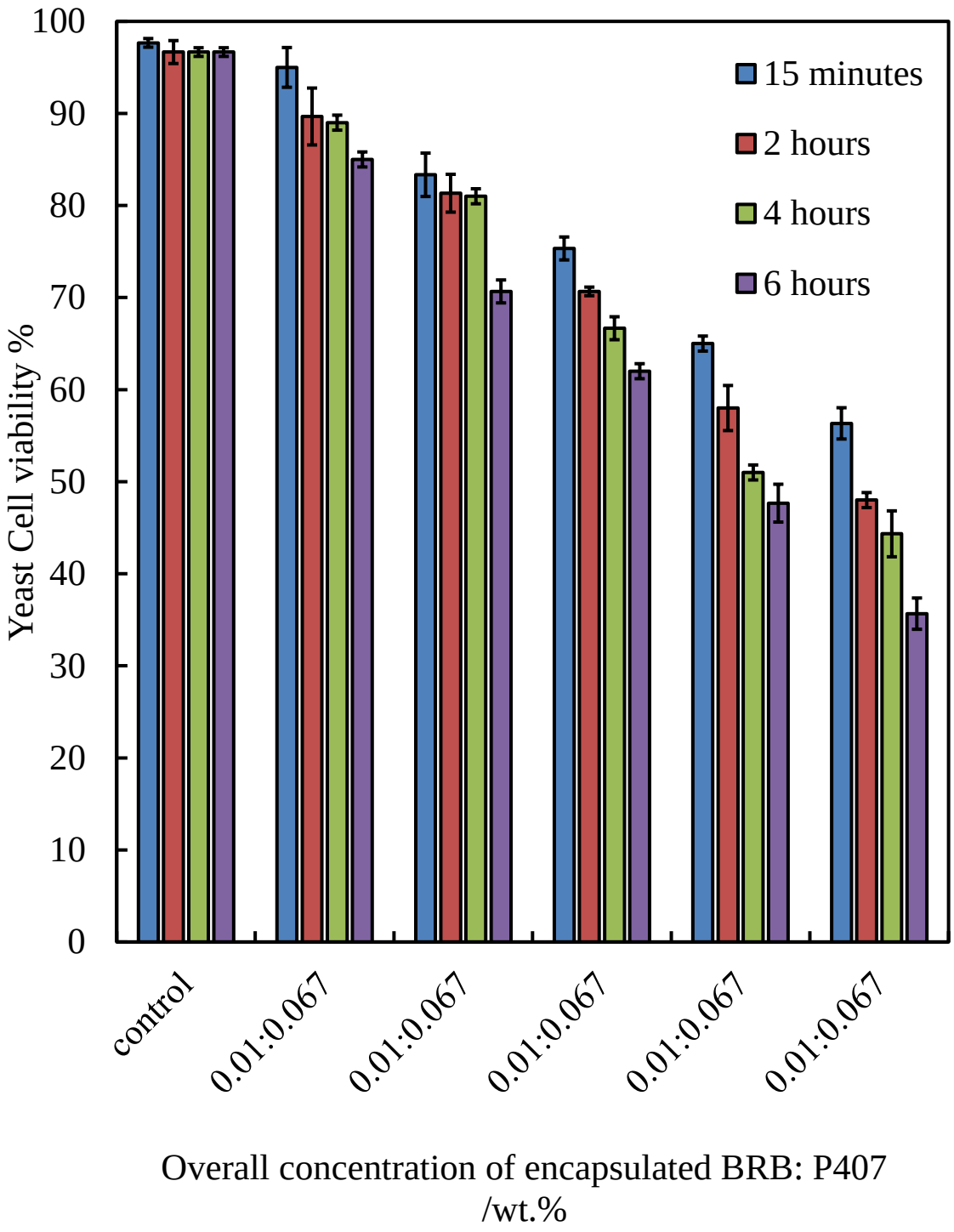

Figure 4.8: The viability of yeast cells incubated with different concentrations of berberine loaded shellac NPs at different incubation time for 15 min, 2 h, 4 h, and 6 hours at room temperature and pH 5.5, (n=3).

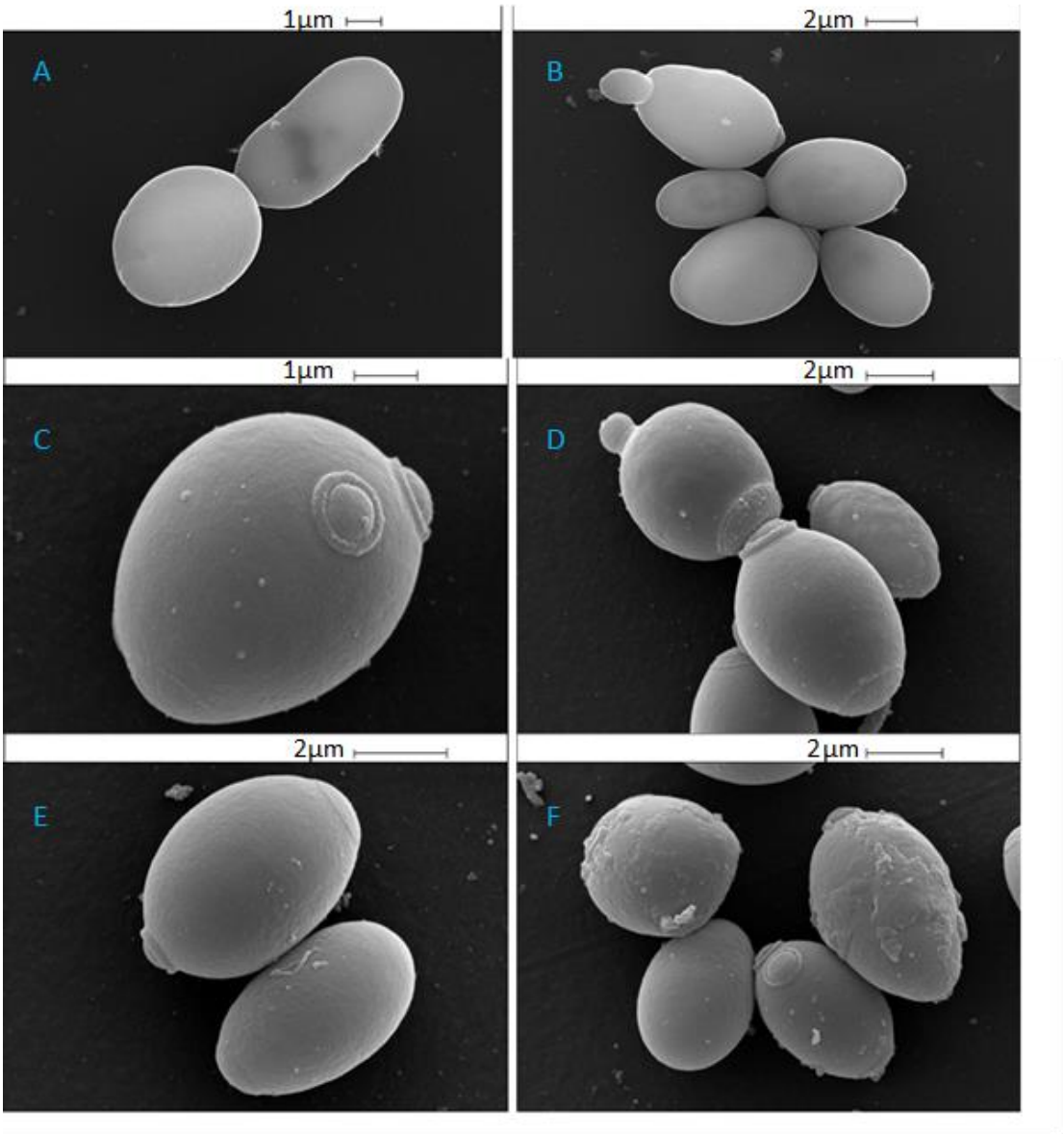

Figure 4.9: SEM images of yeast cells. (A&B) Control sample of yeast cell and (C&D) yeast cells that incubated with 0.01 wt.% free BRB after four hours of incubation, (E&F) yeast cell incubated for four hours with 0.01 wt.% of BRB loaded shellac NPs.

4.2.3 Antimicrobial Activity of Berberine Loaded Shellac NPs on *E.Coli*

The antibacterial activity of free berberine and berberine loaded shellac NPs on *E.coli* was examined at different incubation times. Figure 4.10 and Figure 4.11 show the effects of incubating of different concentrations of free berberine and berberine loaded shellac NPs up to 0.05 wt.% and 0.01 wt.%, respectively with *E.coli*. The viability of the cells was represented by measuring relative luminescence after mixing 100 µL from both the cells; after removing the tested solution and the bactiter luciferase reagent in 96 microwell plate. Free berberine shows an antibacterial effect on the cells after 15 minutes incubation time, at 0.01wt. % of free BRB and higher concentrations, the viability of the cells decreased from $41x10^5$ RLU at control to $16x10^5$ and less. While after 2 hours most of the cells were killed at 0.025 and 0.05 wt. % free BRB. Upon increasing the incubation time up to 4 hours, the viability of the cells in terms of luminescence reduced as compared with the control sample with the decrease being $6x10^5$ and $4x10^5$ at 0.025 and 0.05 wt. % free BRB, respectively, and this is shown in Figure 4.10. The results for the antimicrobial activity of the same overall concentrations of berberine loaded shellac NPs on *E.coli* are presented in Figure 4.11. Berberine loaded shellac NPs seemed to have a much lower antibacterial action than free berberine. After 4 hours incubation time, there was a very low cytotoxic action. If we compare between the cytotoxicity of free berberine and berberine loaded shellac NPs after 2 hours incubation and at 0.005wt. %, the cell viabilities decreased to $15x10^5$ and $22x10^5$, respectively. This low cytotoxicity of berberine loaded shellac NPs can be attributed to the repulsion between the negatively charged NPs and cell membrane, as well as the cationic drug being sustained within the negatively charged shellac NPs which lead to the slow release of berberine. Figure 4.12 shows the SEM images of *E.coli* cells incubated with 0.01 wt.% of free BRB (C&D) and BRB loaded shellac NPs (E&F) in comparison with control (A&B). As can be seen the encapsulated BRB did not have a significant effect on bacteria cells after 4 hours of incubation, as the free BRB did, for the same reasons mentioned before relating to the charge. To overcome this problem, a cationic electrolyte was used to convert the NPs surface charge from negative to positive, as will be explained in detail in the next sections.

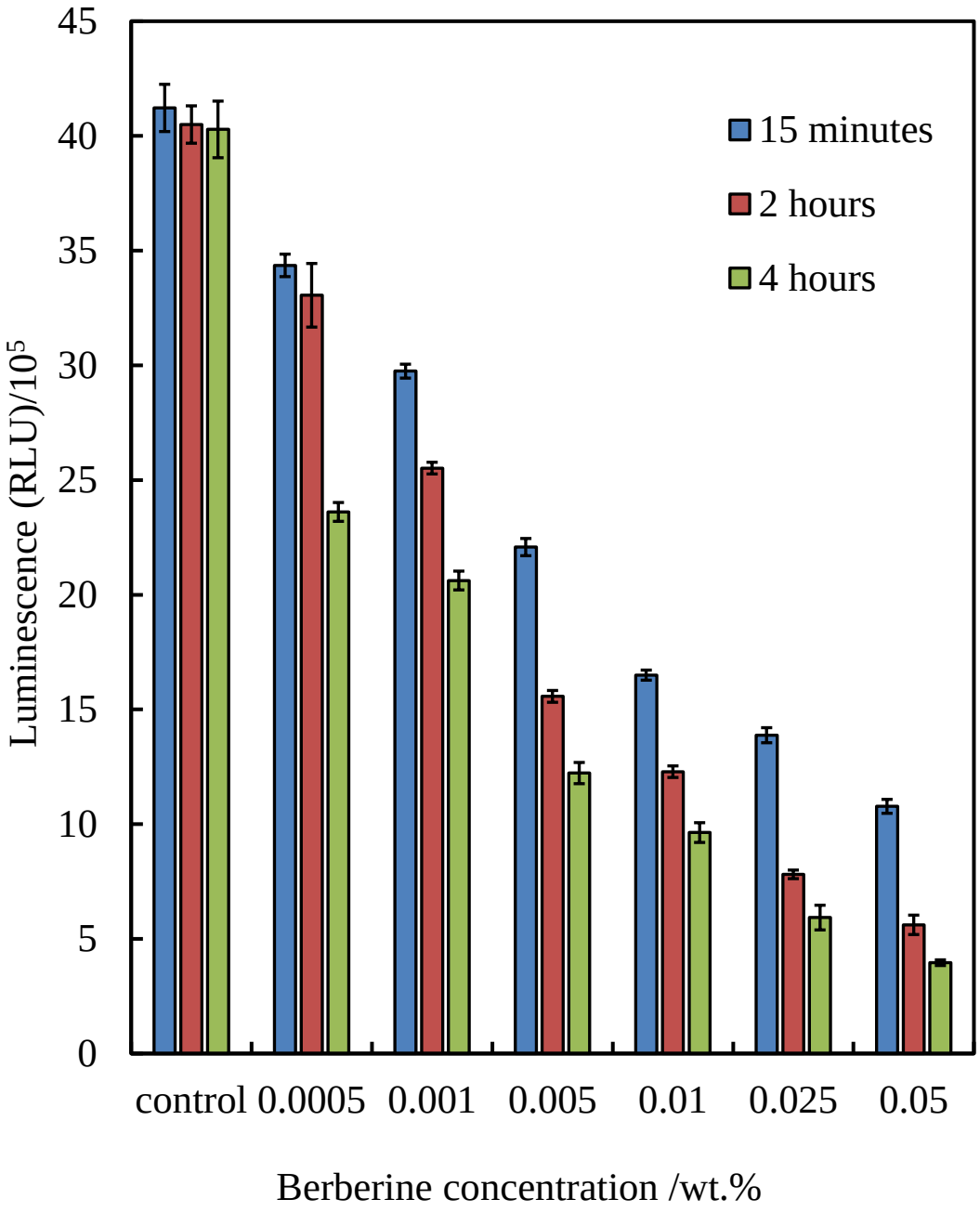

Figure 4.10: The relative luminescence intensities which representing the *E.coli* cells viability incubated with different concentrations of free berberine chloride at different incubation time for 15 min, 2 h, and 4 hours at room temperature at pH 5.5 using bactiter luciferase reagent, (n=3).

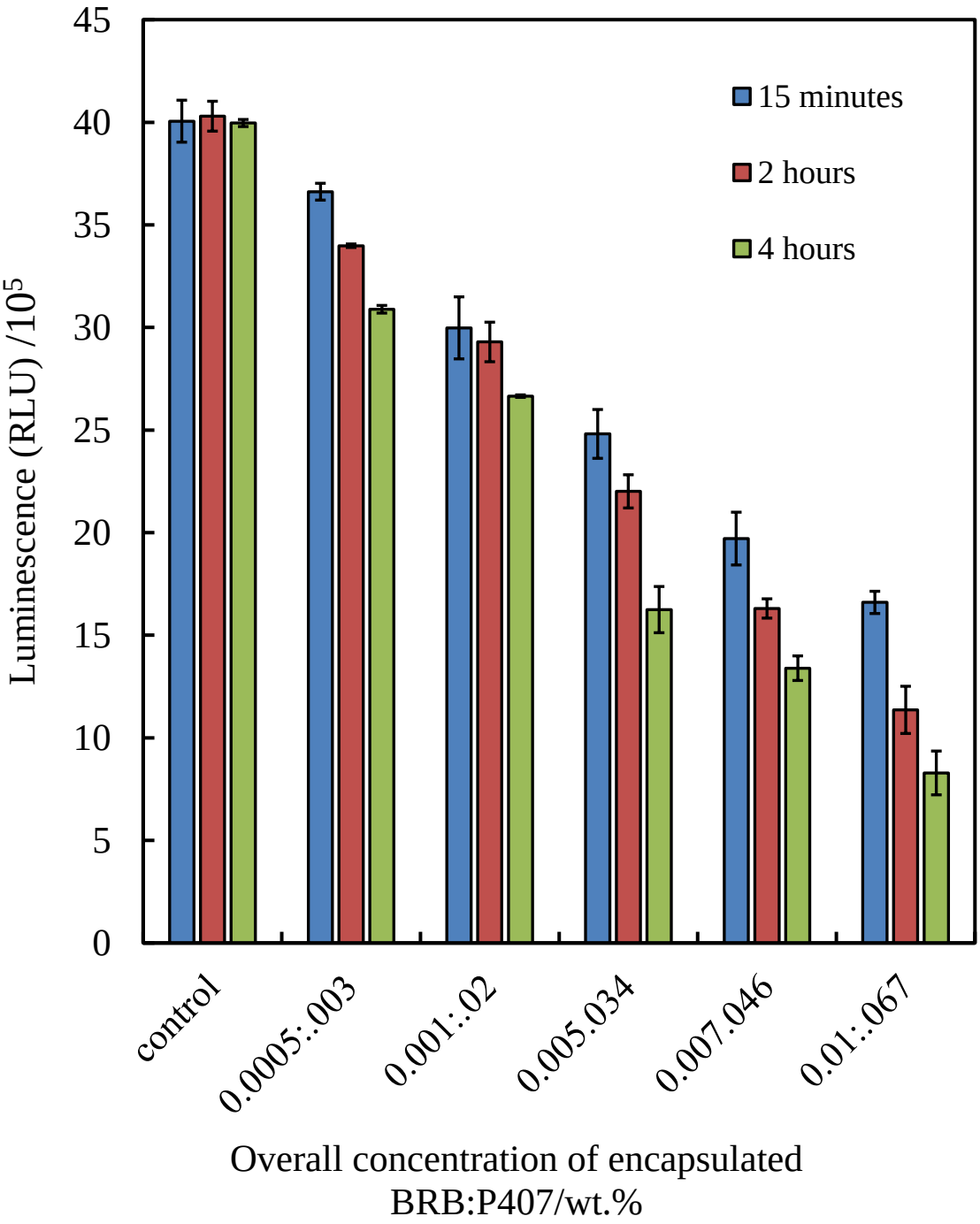

Figure 4.11: The relative luminescence intensities representing the *E.coli* cells viability incubated with different of overall concentrations of berberine encapsulated shellac NPs at different incubation time for 15 min, 2 h, and 4 hours at room temperature at pH 5.5 using bactiter luciferase reagent, (n=3).

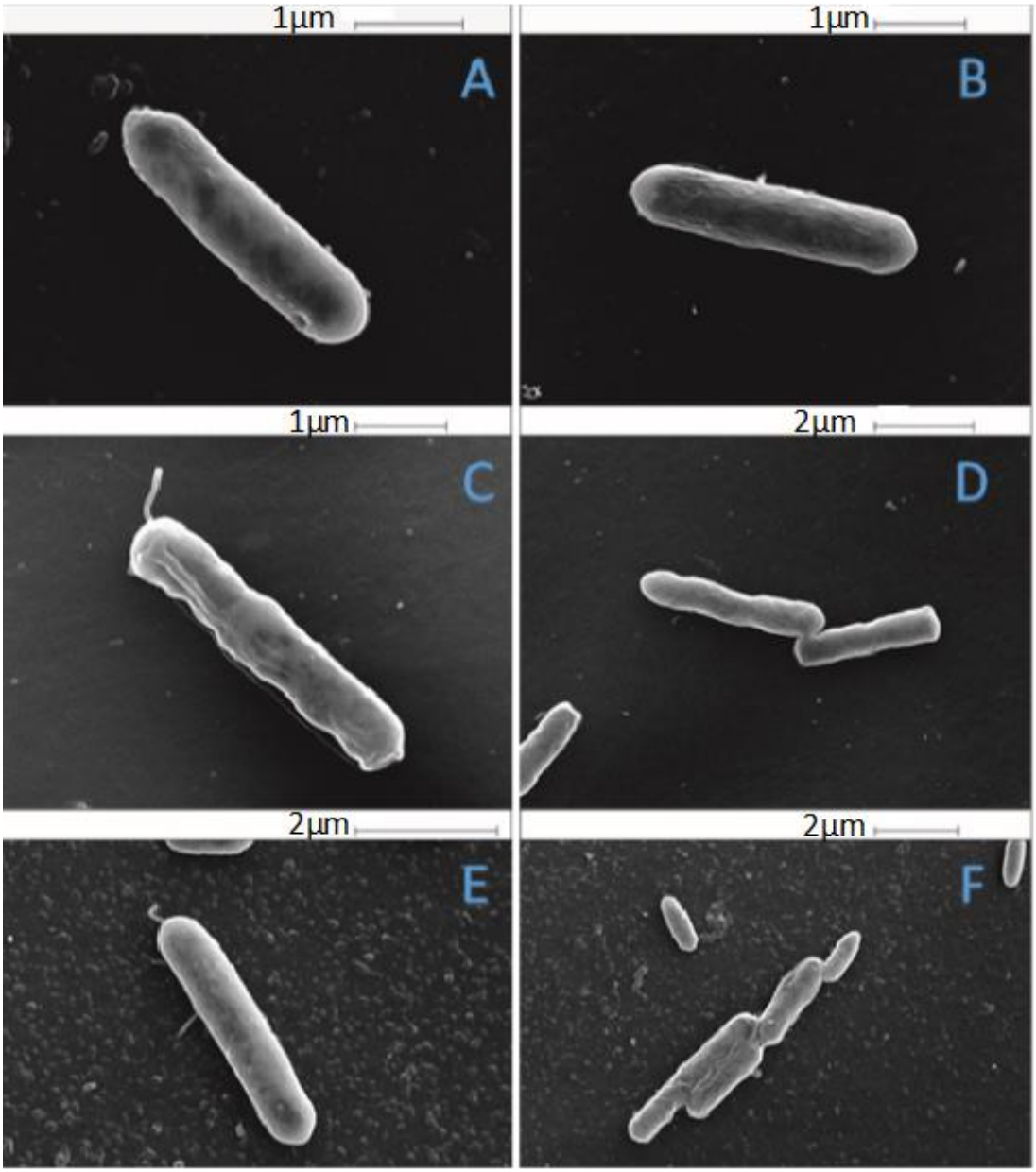

Figure 4.12: SEM images of *E.coli* cells. (A&B) Control sample of *E.coli* and (C&D) incubation of *E.coli* cells with solution of 0.01wt. % free BRB after 4 hours incubation, (E&F) sample of *E.coli* incubated with 0.01 wt.% BRB loaded shellac NPs for 4 hours incubation. All samples incubated at pH 5.5 and room temperature.

4.3 Cytotoxic Effect of ODTAB Coated Shellac NPs

The previous experiments on the antimicrobial activities of encapsulated BRB within shellac NPs showed lesser antimicrobial activity on a range of microorganisms in comparison with free BRB. The main reason for this was that shellac NPs maintain their negative surface charge even after being encapsulated with the cationic drug so that the negatively charged cell membrane repel the negatively charged NPs and thus does not allow them to release the encapsulated antimicrobial drugs near the cell membrane vicinity. To overcome this problem, the shellac NPs encapsulating BRB were coated with a cationic electrolyte to increase their adhesion to the cell membrane and increase the antimicrobial action. Therefore, to reverse the surface charge of shellac NPs from negative to positive, a cationic electrolyte octadecyltrimethyl ammonium bromide (ODTAB) was used to functionalize the NPs surface after preparing them as mentioned in section 2.2.2. ODTAB was chosen instead of using other cationic polyelectrolyte to maintain the stability of the NPs which arises from the steric repulsion of Poloxamer 407 molecules that adsorbed hydrophobically around the hydrophobic part of shellac molecules. To distinguish between the cytotoxicity of the drug encapsulated within functionalised nanocarriers and the other components; the cytotoxicity of the functionalised shellac NPs and pure ODTAB were studied for each component in the following sections.

4.3.1 Cytotoxic Effect of Pure ODTAB on Algae, Yeast, and *E.coli* Cells

The cytotoxicity of pure ODTAB was tested on microalgae, yeast, and *E.coli* to differentiate between its own cytotoxicity and the cytotoxicity of the NPs after coating with it before and after being encapsulating with antimicrobial. This was achieved by incubating different concentrations of ODTAB with microorganisms at different incubation times. Figure 4.13, figure 4.14, and figure 4.15 show the cytotoxic effect of different concentrations of ODTAB on *microalgae*, yeast and *E.coli*, respectively. As it can be observed from these figures that ODTAB showed an extremely strong antimicrobial action on algae, yeast and less on *E.coli* in a wide range of concentrations from 0.0001 wt.% to 0.033 wt.%.

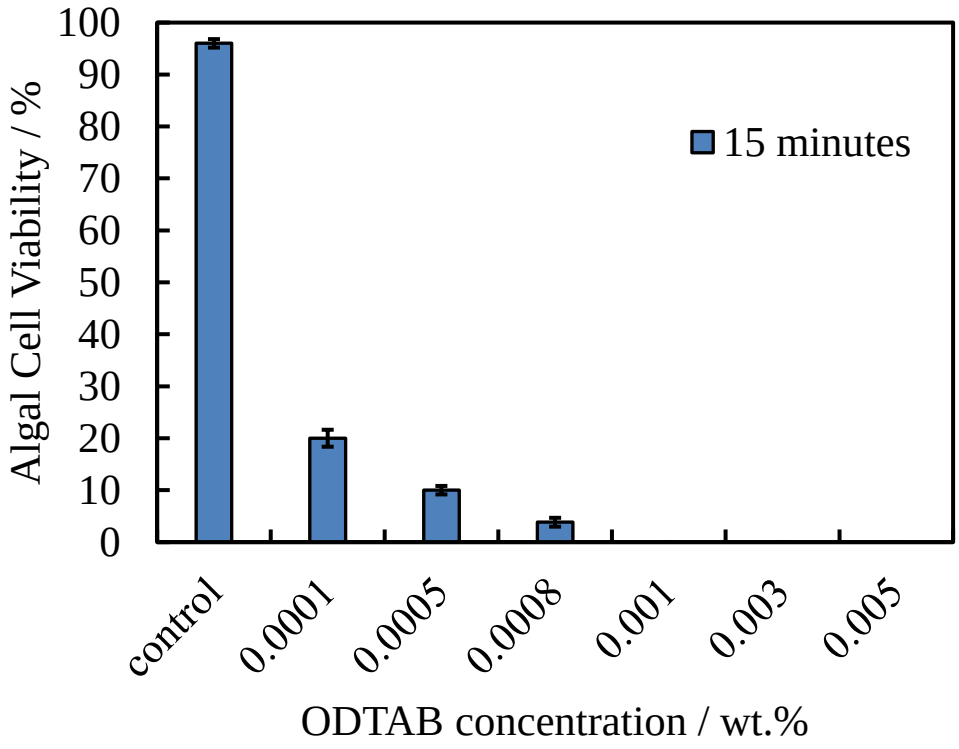

Figure 4.13: The cytotoxic effect of solutions of different ODTAB concentration on microalgae cells *(C. reinhardtii*) for 15 minutes incubation time at room temperature using FDA assay, (n=3).

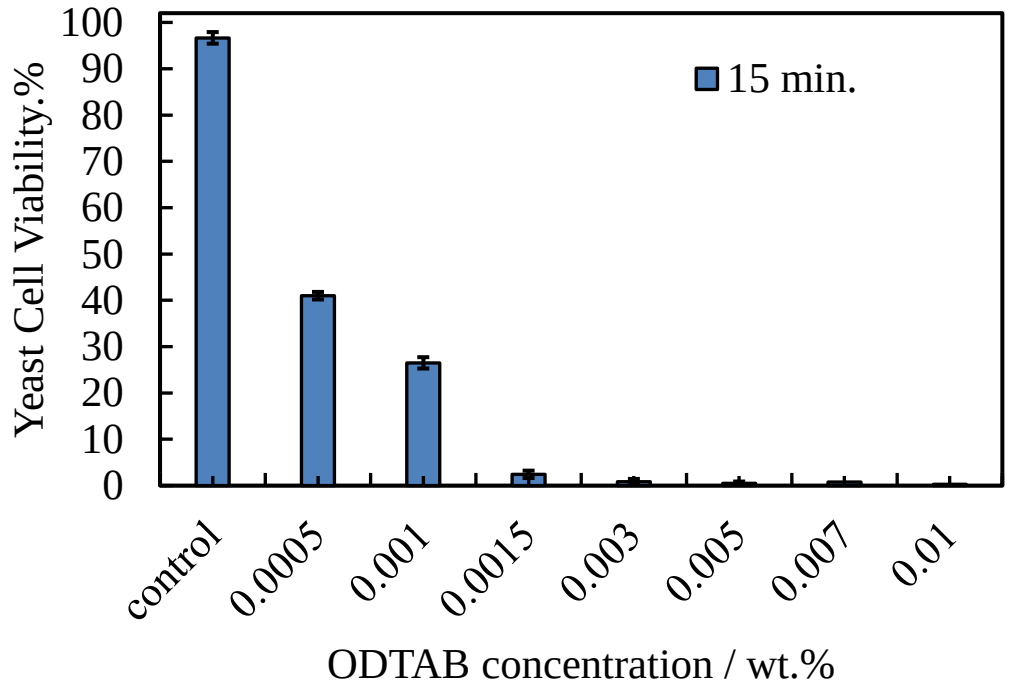

Figure 4.14: The cytotoxic effect of solutions of different concentrations of pure ODTAB on yeast cells for 15 minutes incubation time at room temperature using FDA assay, (n=3).

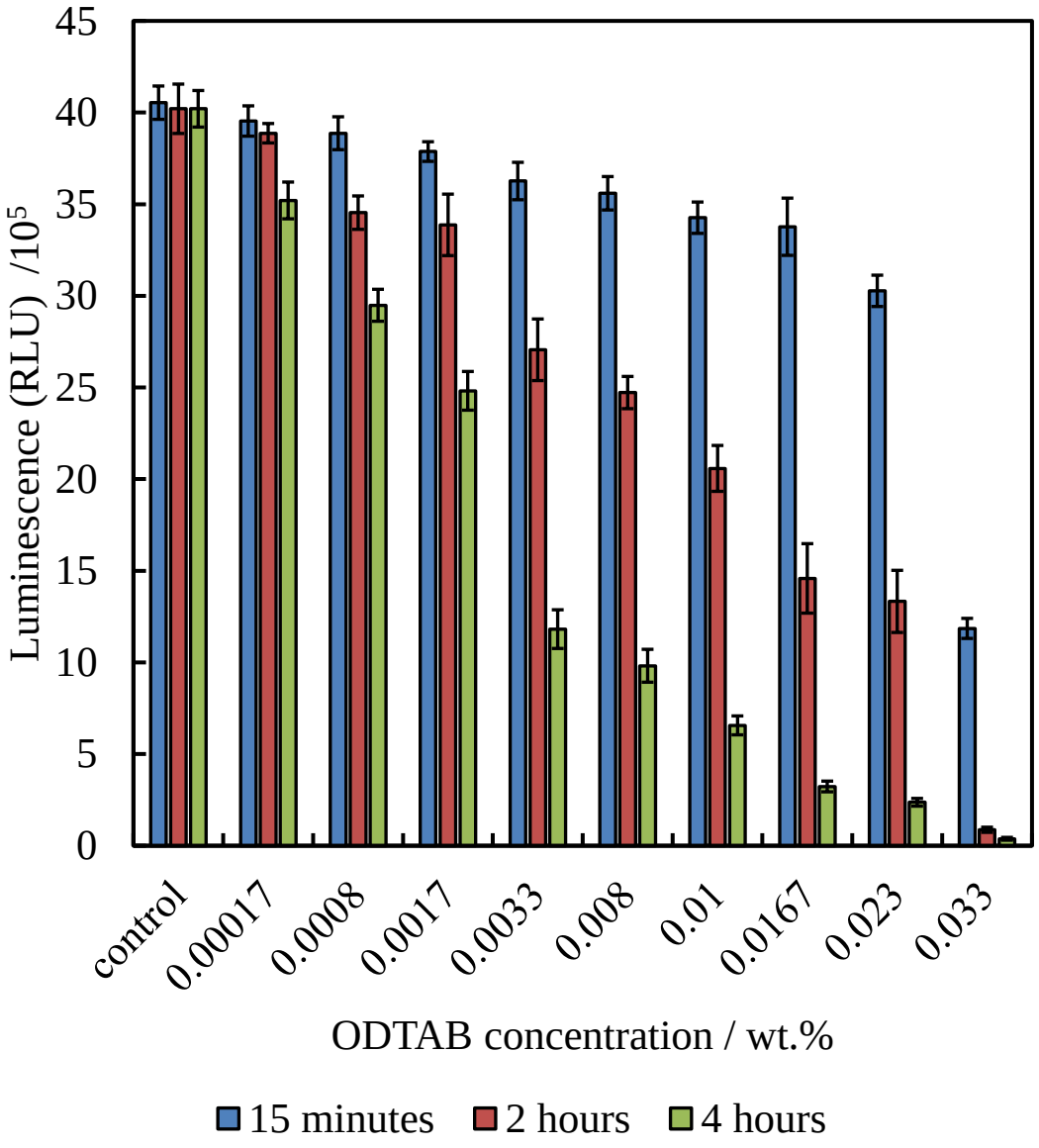

Figure 4.15: The relative luminescence unit which represents the *E.coli* viability when incubating with solutions of a different concentration of ODTAB for 15 min, 2 h, and 4 hours incubation time at room temperature using bactiter luciferase assay, (n=3).

4.3.2 Cytotoxic Effect of Shellac NPs Coated with ODTAB on Algae, Yeast, and *E.coli* Cells

To distinguish between the cytotoxic effect of shellac NPs coated with ODTAB (without the antimicrobial) and that of the drugs encapsulated shellac NPs coated with ODTAB on microorganisms, different concentrations of shellac NPs coated with ODTAB were incubated with microalgae, yeast, and *E.coli* at pH 5.5 and room temperature. Figure 4.16 shows the algal cell viability when incubated with different concentrations of ODTAB

coated shellac NPs, as can be seen after 2 hour incubation there was a noticeable cytotoxic effect from 0.001 wt.% to 0.01 wt.% where most of the cells were strongly affected or killed. At this range even after 15 minutes, shellac NPs coated with ODTAB seemed to be damaging the thin cell membrane of microalgae due to the strong adhesion of the cationic charged NPs which make the algae cells aggregated and clustered, as can be seen from SEM images (figure 4.19, A&B).

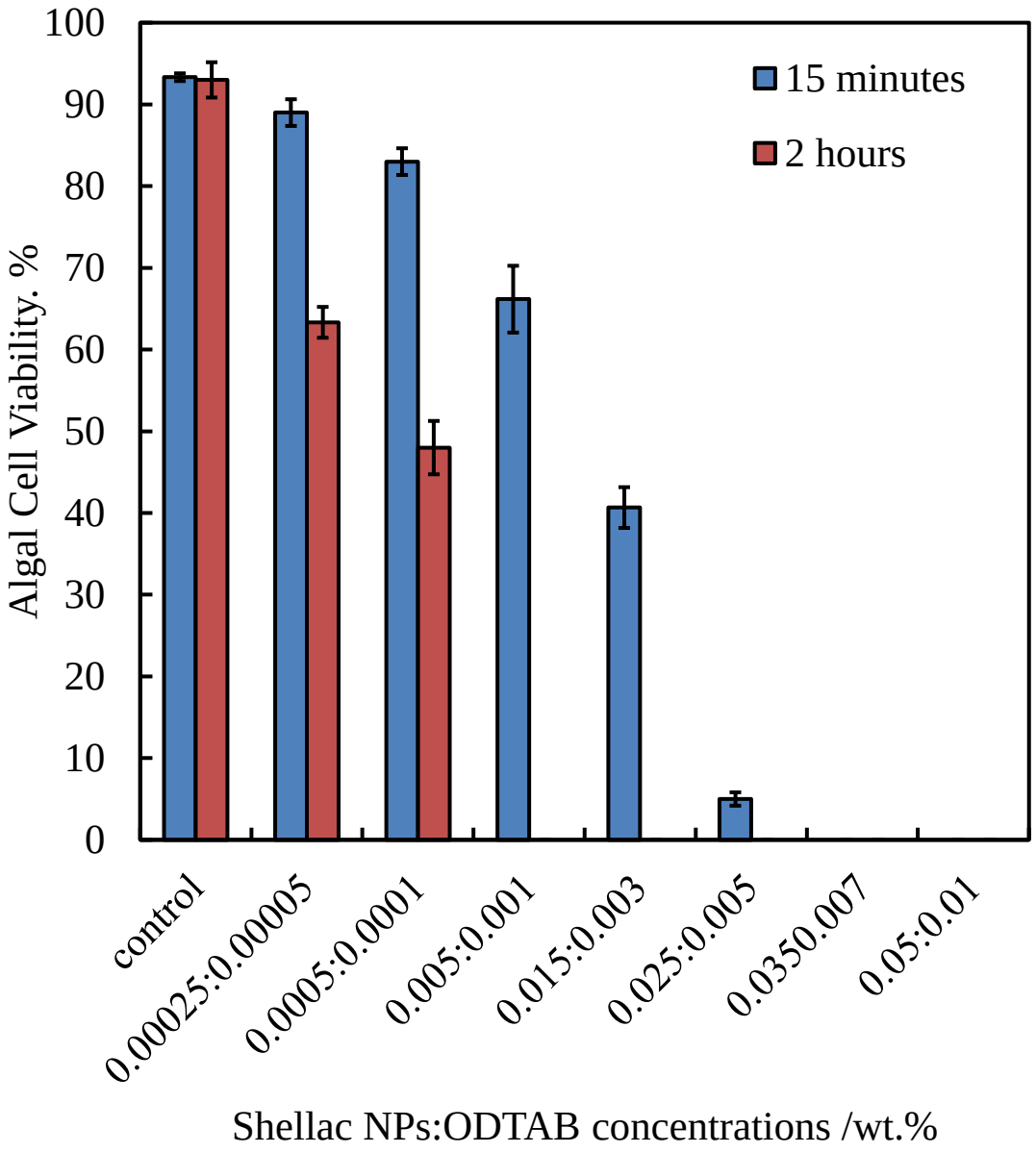

Figure 4.16: The viability of algal cells upon incubation for 15 min, and 2 hours at pH 5.5 with different amounts of Shellac NPs coated with ODTAB at room temperature, (n=3).

Figure 4.17 shows the cytotoxic impact of the shellac NPs coated with the cationic electrolyte ODTAB on yeast cells upon 6 hour incubation at pH 5.5. With yeast cells, the coated NPs showed a cytotoxic effect but not as much as that with algae, a slight decrease was seen at low concentrations from 0.0005 to 0.003 wt.% after 4 hours. This was because yeast cells have thick cell membrane which prevents the ODTAB coated shellac NPs from penetrating it.[405]

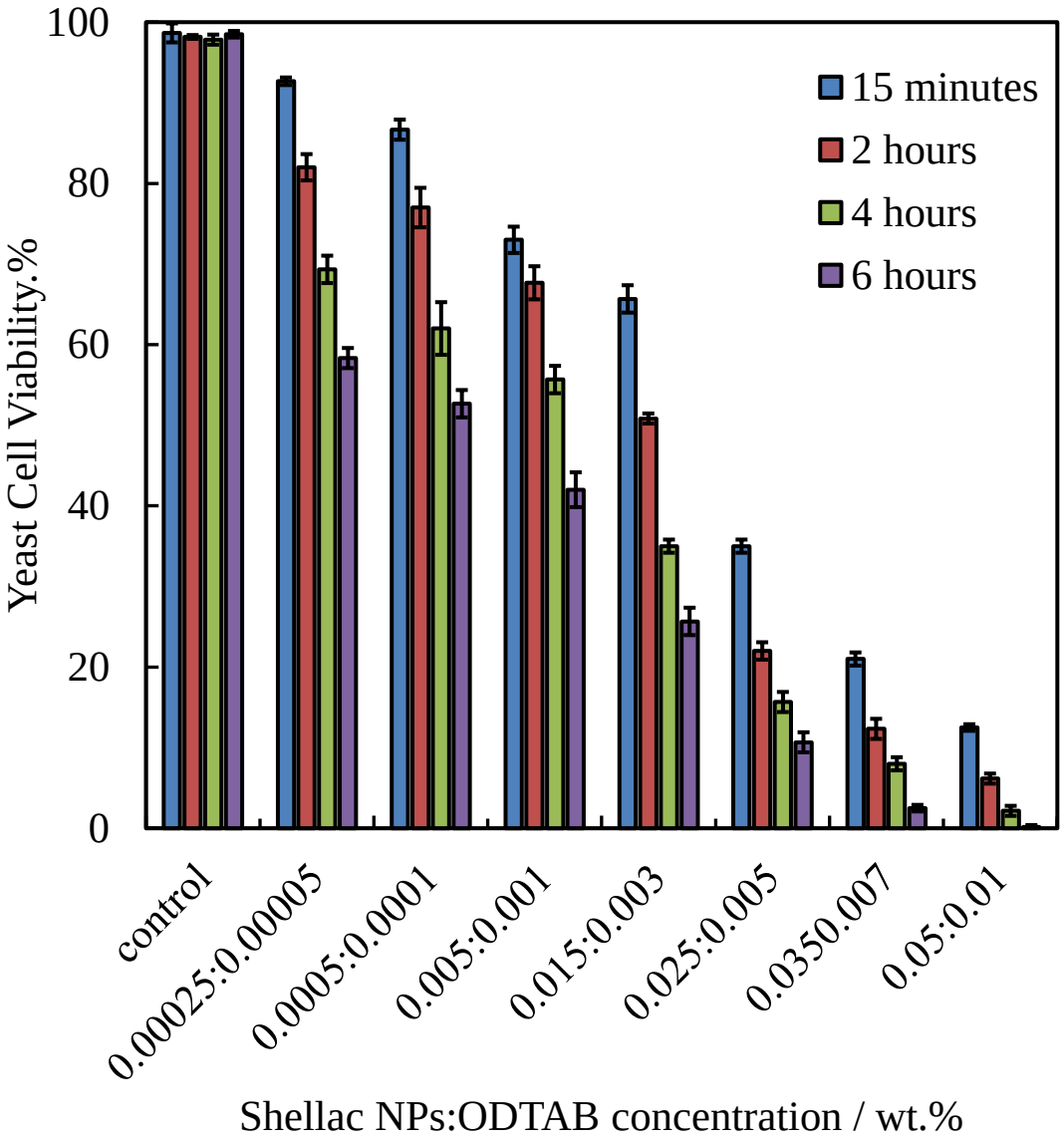

Figure 4.17: The viability of yeast cells incubated with different concentrations of shellac NPs coated with ODTAB at different incubation time for 15 min, 2 h, 4 h, and 6 hours at pH 5.5 using FDA assay, (n=3).

The cytotoxic effect of ODTAB coated shellac NPs was also experienced on *E.coli*. Figure 4.18 shows that ODTAB in the concentration range of 0.0000176 to 0.013 wt.% had limited toxicity up to 2 hours incubation time, whereas at 0.017 wt.% of ODTAB there was a drop in the *E.coli* cells viability. After 4 hours the cell viability decreased noticeably at 0.013 and 0.017 wt.% ODTAB from $40x10^5$ RLU for the control to $24x10^5$ RLU and $20x10^5$ RLU, respectively. The cytotoxic effect of ODTAB reduced when it was bonded to shellac molecules and showed less effect on microorganisms in comparison to pure ODTAB, figure 4.15. This strong adhesion gives the power to the nanocarrier system to release the antimicrobial through the cell membrane directly.

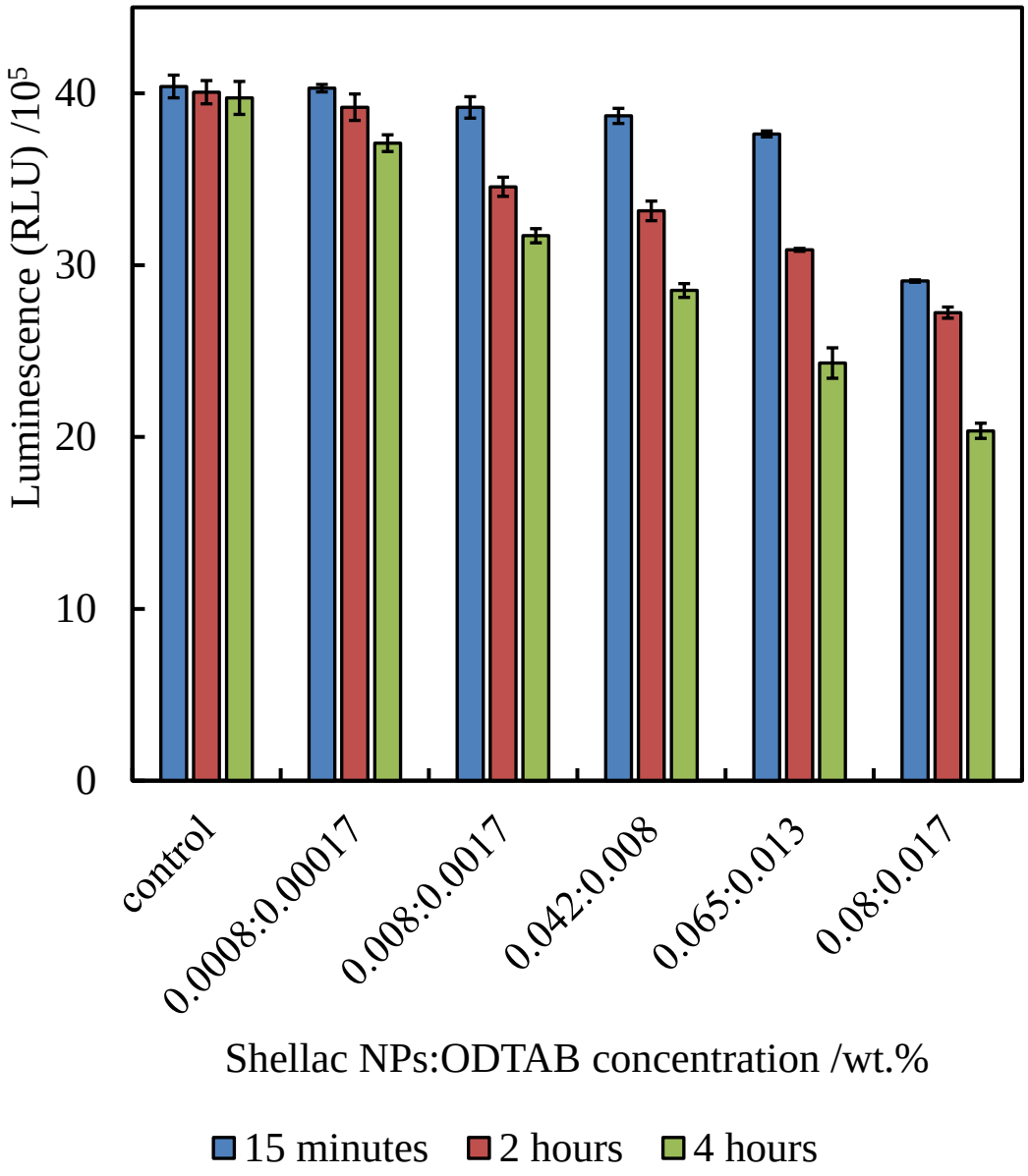

Figure 4.18: The relative luminescence unit of *E.coli* cells incubated with different concentrations of shellac NPs coated with ODTAB at different incubation times, (n=3).

Figure 4.19 shows the SEM images of microalgae (A&B), yeast (C&D), and *E.coli* (E&F) after 4 hours incubation with 0.025 wt.% ODTAB coated 0.125 wt.% shellac NPs. As can be seen the positive charged NPs attracted strongly to the negative charged surface cell membrane, this can enhance the antimicrobial activity of functionalized shellac NPs encapsulated drugs by releasing drugs near vicinity of the cell membrane.

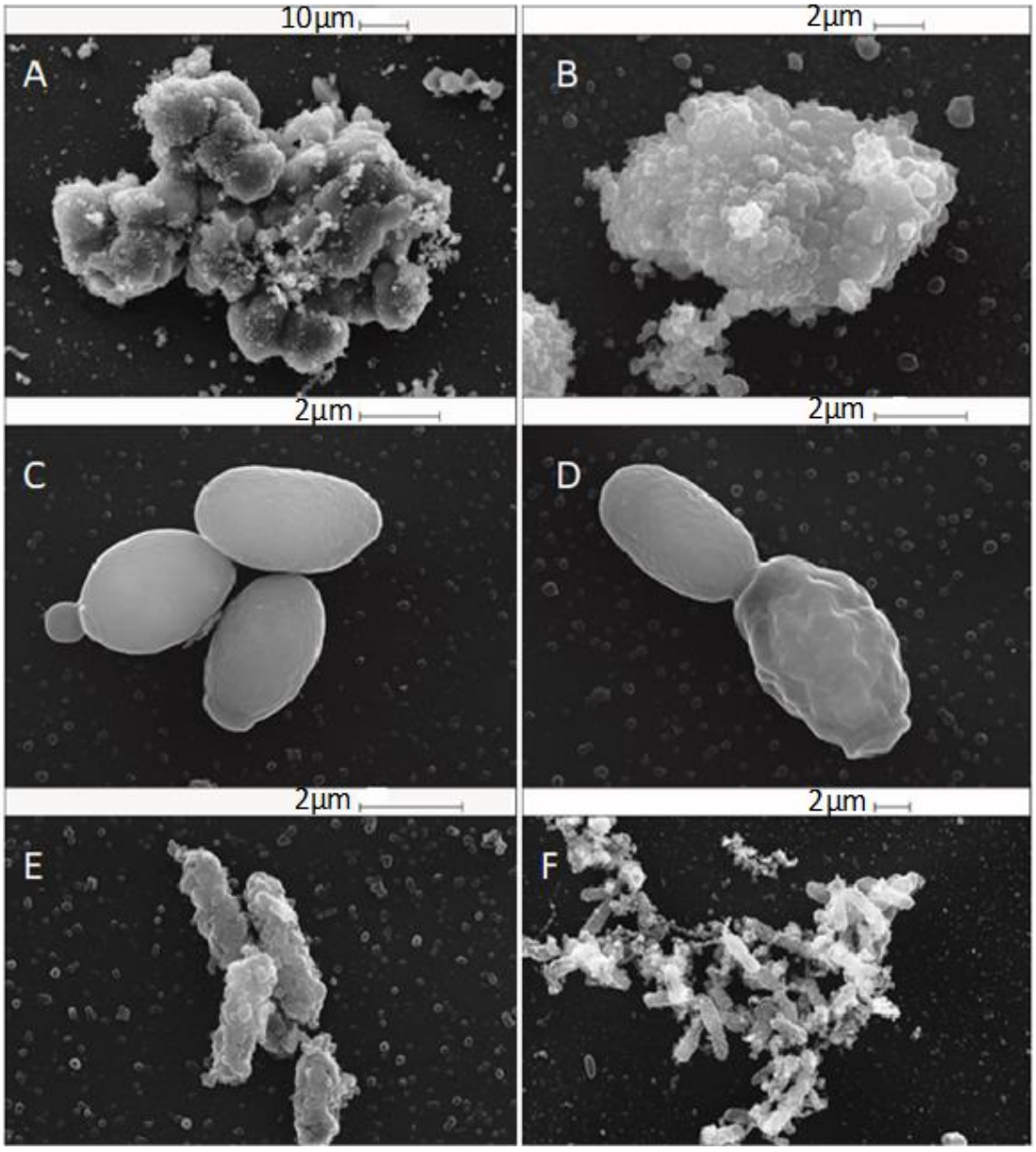

Figure 4.19: SEM images of microorganisms cells with 0.025 wt.% ODTAB coated 0.125 wt.% shellac NPs after 4 hour incubation at pH 5.5. (A&B) algal cells, (C&D) yeast cells, and (E&F) *E.coli* cell.

4.4 Cytotoxic Effect of BRB Loaded Shellac NPs Coated with ODTAB

After studying the cytotoxicity effect of shellac NPs coated with ODTAB (without antimicrobial), the antimicrobial activity of encapsulated berberine coated with ODTAB was studied by incubating the NPs with algae, yeast, and *E.coli*. Berberine loaded shellac NPs was coated with the cationic electrolyte ODTAB to improve the attraction between the positively charged shellac NPs encapsulated BRB coated with ODTAB and the negatively charged cell membrane of microorganisms.

4.4.1 Cytotoxic Effect of BRB Loaded Shellac NPs Coated with ODTAB on Microalgae Cells

Figure 4.20 shows the antimicrobial activity of different concentrations of berberine loaded shellac NPs coated with ODTAB on algal cells at different incubation times at room temperature. The figure illustrates that after changing the charge of the NPs to be positive using ODTAB, berberine NPs became more effective. After only 15 minutes incubation, all cells died at concentrations from 0.003 wt.% to 0.01 wt.%, and the cell viability sharply reduced to 50% at 0.00005 wt.% of encapsulated BRB. After 2 hours, the cell viability decreased significantly to about 75% at 0.001 wt.% of BRB loaded shellac NPs. Figure 4.21 represents a comparison among the antimicrobial activities of 0.0001 wt.% encapsulated BRB, 0.0001 wt.% free BRB, 0.0005 wt.% shellac NPs coated with 0.0001 wt.% ODTAB, 0.0001 wt.% encapsulated berberine coated with 0.0001 wt.% ODTAB, and 0.0001 wt.% pure ODTAB. As can be seen there was an increase in the antimicrobial activity for the encapsulated berberine after being coated with ODTAB in comparison with the free berberine. The reason behind the increase in the antimicrobial activity of BRB after being coating with ODTAB is the positive charge of the complex which means the NPs are rapidly attracted to the cell walls after mixing which allows the drug to penetrate through the cells directly without losing any drugs. Figure 4.22 shows the SEM images of *C. reinhardtii* microalgae cells after incubating for 2 hours with 0.005 wt.% of BRB loaded shellac NPs coated with 0.005 wt.% ODTAB, the images (B, C and D) show how the positively charged surface NPs attracted to the cell membrane, thus increasing the releasing of berberine near the cell membrane vicinity.

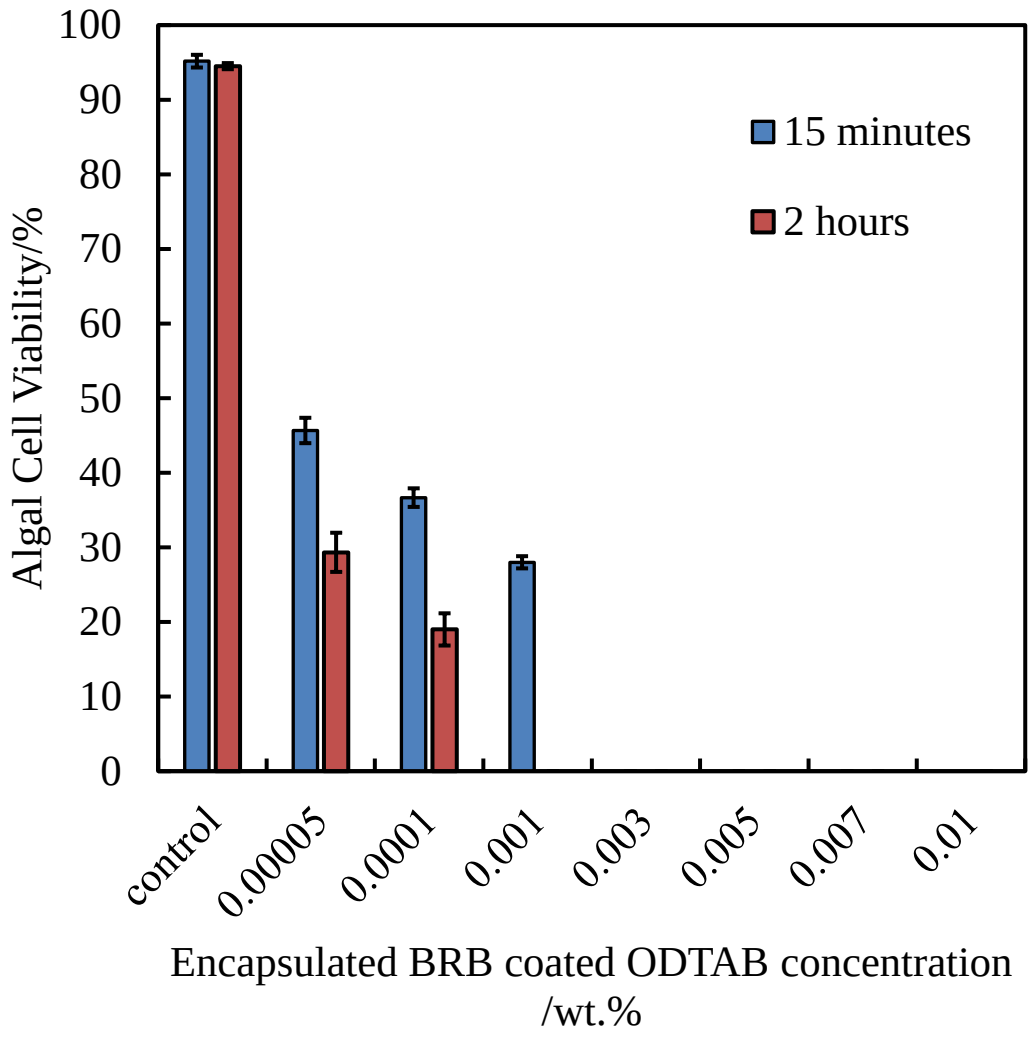

Figure 4.20: The viability of algal cells upon incubation at pH 5.5 with different amounts of berberine loaded shellac NPs coated with ODTAB at room temperature for 15 min and 2 hours of incubation time. The solutions were prepared from 0.05 wt.% BRB NPs stock solution coated with 0.05 wt.% ODTAB, (n=3).

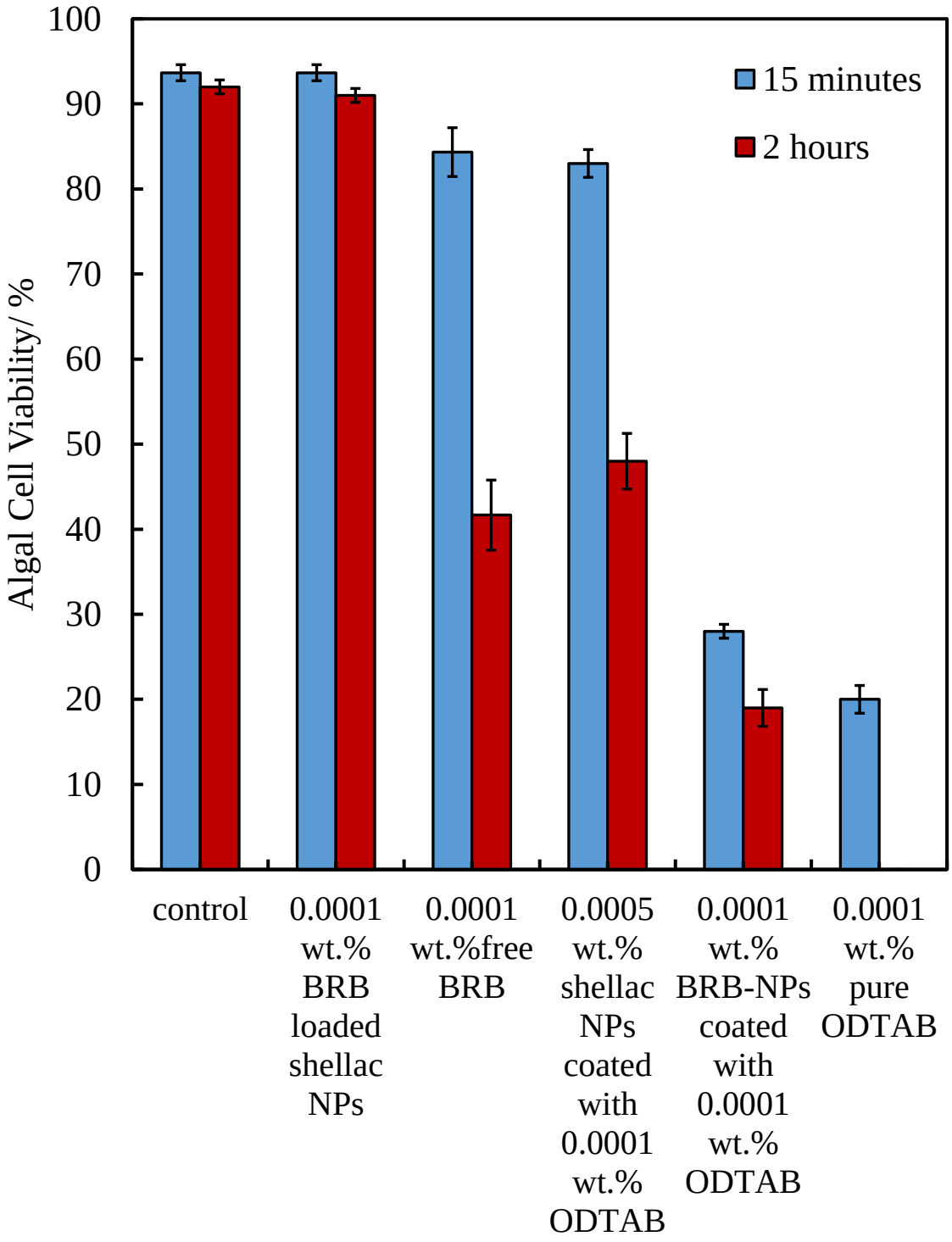

Figure 4.21: The *C.reinhardtii* microalgae cells viability upon incubation with 0.0001 wt.% encapsulated BRB, 0.0001 wt.% free BRB, 0.0005 wt.% shellac NPs coated with 0.0001 wt.% ODTAB, 0.0001 wt.% berberine-NPs coated with 0.0001 wt.% ODTAB, and 0.0001 wt.% pure ODTAB at pH 5.5 and at room temperature, (n=3).

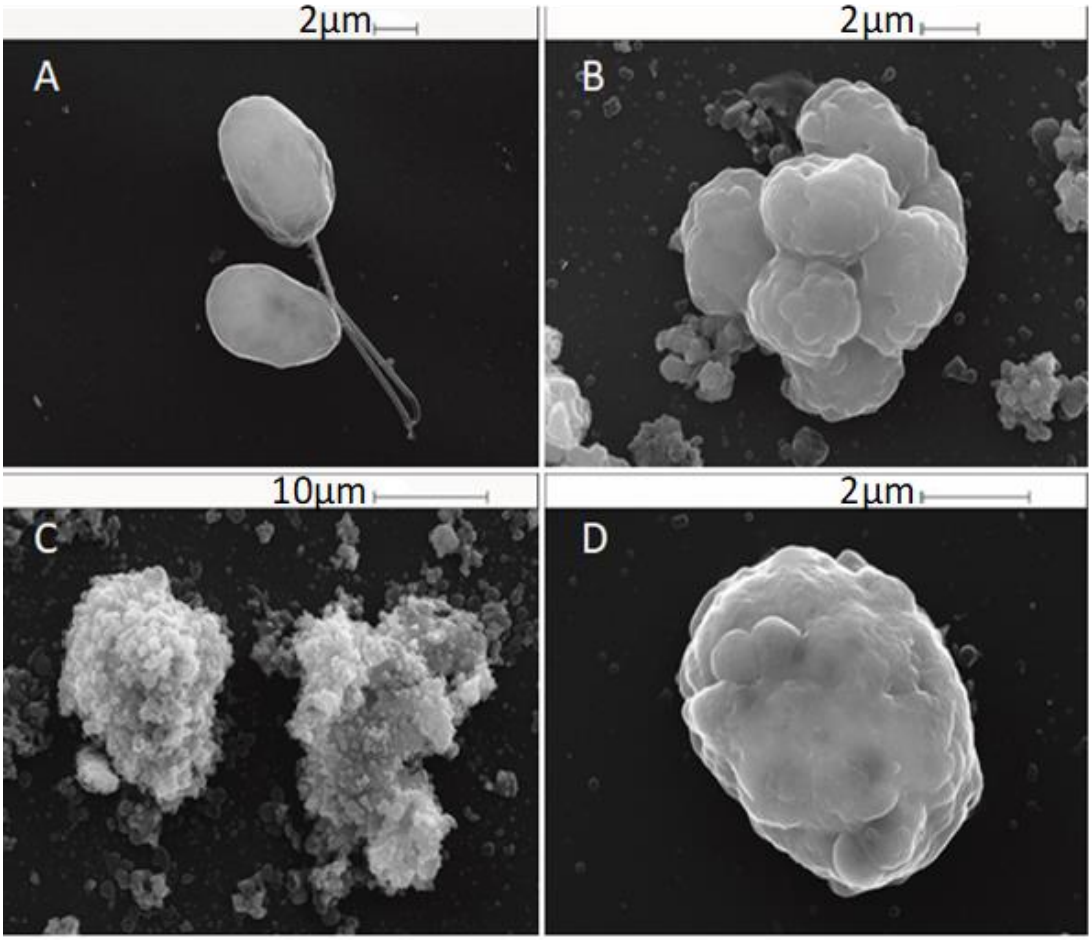

Figure 4.22: SEM images of microalgae cells. (A) A control sample of the microalgae cells. (B, C, and D) microalgae cells incubated with 0.005 wt.% berberine loaded shellac NPs coated with 0.005 wt. % ODTAB after 2 hours incubation at room temperature.

4.4.2 Cytotoxic Effect of Encapsulated BRB Coated with ODTAB on Yeast

In earlier studies it was found that free BRB and encapsulated BRB within shellac NPs has no cytotoxic effect on yeast due to the fact that yeast cell membrane is thick and hard to penetrate. Herein, the antifungal activity of BRB loaded shellac NPs after being coated with ODTAB to overcome the problem of the surface charge was studied on baker's yeast cells. Figure 4.23 shows the yeast cell viability upon incubation with different concentrations of encapsulated BRB coated with ODTAB. After 15 minutes exposure time, the cell viability severely decreased from 99% at control to 25%, 17% and 11% at (0.005, 0.007, and 0.01) wt.% of BRB loaded shellac NPs coated with (0.005, 0.007, and 0.01) wt.% ODTAB respectively. After 4 hours most cells died at 0.007 and 0.01 wt.% BRB loaded shellac NPs coated with ODTAB. Although, figure 4.24 illustrates a comparison

among the antimicrobial activities of 0.001 wt.% BRB-NPs, 0.001 wt.% free BRB, 0.005 wt.% shellac NPs coated with 0.001 wt.% ODTAB, 0.001 wt.% encapsulated berberine coated with 0.001 wt.% ODTAB, and 0.001 wt.% pure ODTAB. As can be seen after coating the encapsulated berberine with ODTAB to change the surface charge of the NPs to be positive, the antimicrobial activity increased. Free BRB and BRB loaded shellac NPs did not show any antifungal effect on yeast while as NPs berberine attracted strongly to the cell membrane and made a noticeable damage to yeast cells, as clear in figure 4.25 which displays the SEM images of the yeast cells that were incubated with 0.01 wt.% of berberine loaded shellac NPs coated with 0.01 wt.% ODTAB for 2 hours. The coated NPs also shows antimicrobial effect due to the positive surface charge, and this antimicrobial effect increased when the NPs loaded with BRB.

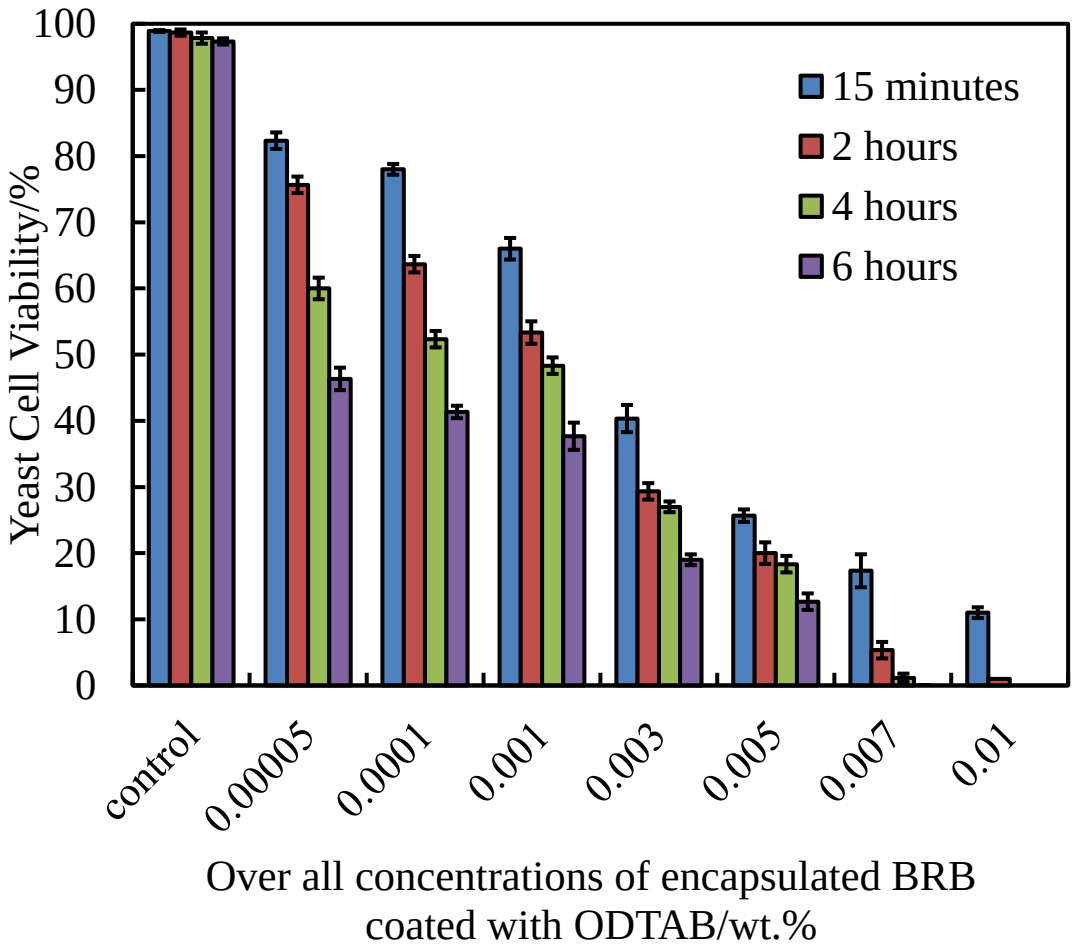

Figure 4.23: The viability of yeast cells upon incubation at pH 5.5 with different amounts of berberine loaded shellac NPs coated with ODTAB at room temperature at different incubation time. The solutions were prepared from 0.05 wt.% BRB NPs stock solution coated with 0.05 wt.% ODTAB, (n=3).

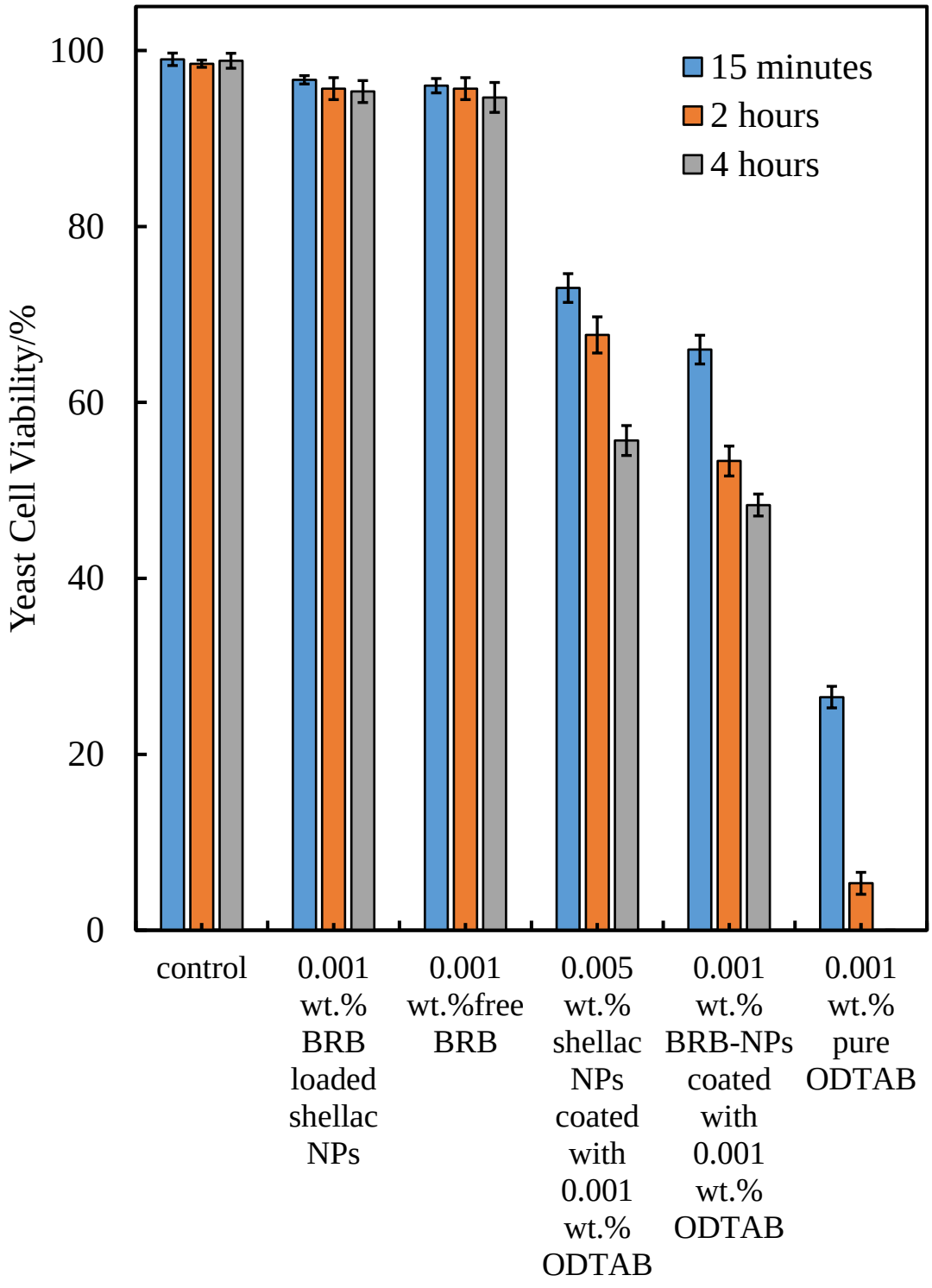

Figure 4.24: The yeast cells viability upon incubation with 0.001 wt.% BRB-NPs, 0.001 wt.% free BRB, 0.005 wt.% shellac NPs coated with 0.001 wt.% ODTAB, 0.001 wt.% berberine-NPs coated with 0.001 wt.% ODTAB, and 0.001 wt.% pure ODTAB at pH 5.5 and room temperature, (n=3).

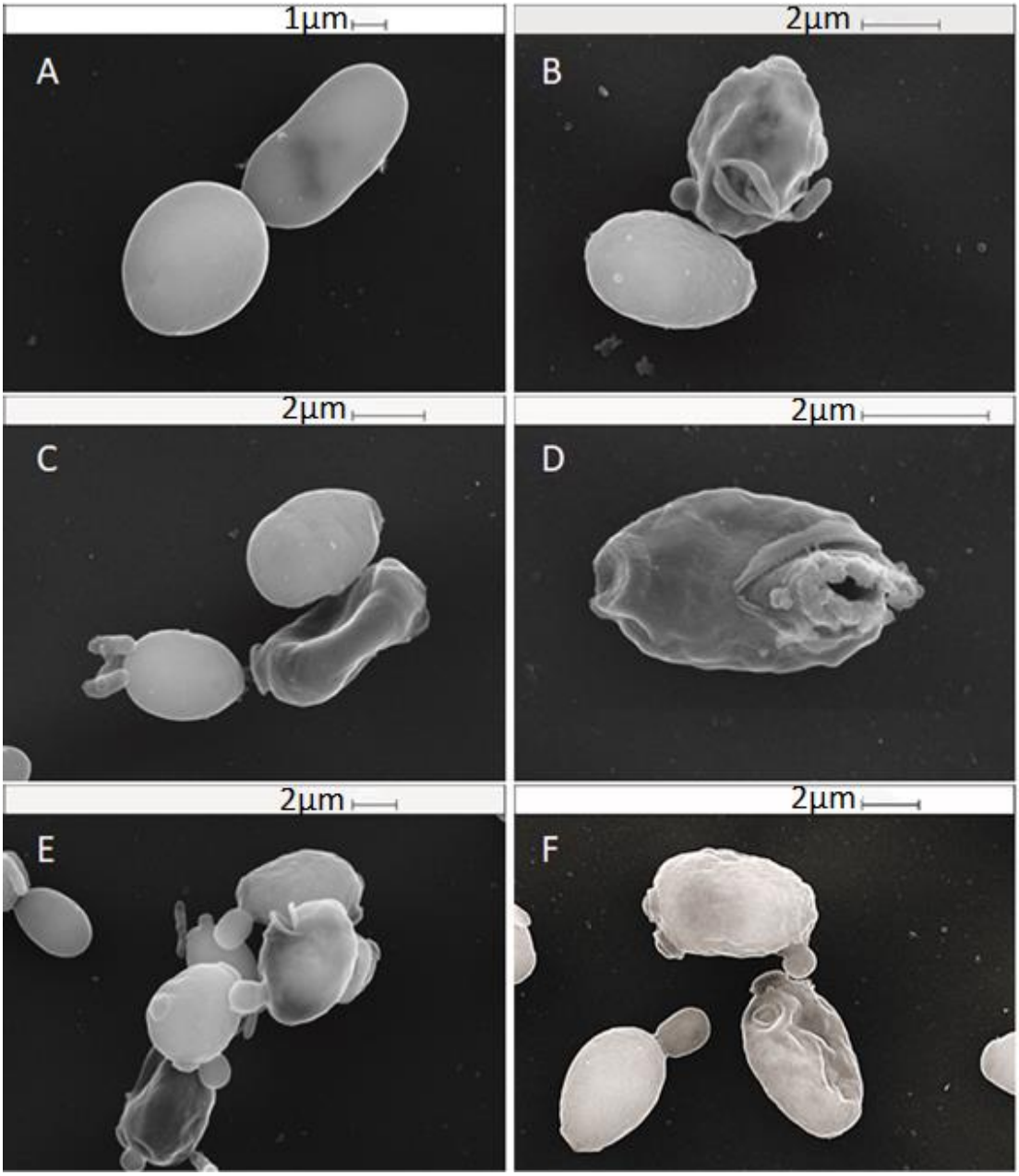

Figure 4.25: SEM images of yeast cells. (A) A control sample of the yeast cells. (B, C, D, E, and F) yeast cells incubated with 0.01 wt.% berberine loaded shellac NPs coated 0.01 wt. % ODTAB after 2 hours incubation time at room temperature.

4.4.3 The Cytotoxic Effect of Encapsulated BRB Coated ODTAB on *E.coli* Cells

The antibacterial activity of berberine loaded shellac NPs coated with ODTAB on *E.coli* cells was examined by incubating various concentration of berberine loaded shellac NPs coated with ODTAB with a fixed amount of culture media free *E.coli* cells for 2 hours at pH 5.5. Figure 4.26 shows that there was a clear antibacterial activity for berberine at concentrations of 0.001 wt. % to 0.01 wt. % after 15 minutes of incubation, and the cell viability declined from $40x10^5$ RLU at control to (15, 13, and 11) $x10^5$ RLU at (0.005, 0.007, and 0.01) wt.% overall concentration of encapsulated BRB coated with (0.008, 0.01, 0.017) wt. % ODTAB, respectively. After 1 hour the cell viability decreased strongly from $39x10^5$ RLU to (4.3, 3.6, and 3.2) $x10^5$ RLU at (0.005, 0.007, and 0.01) wt. % overall concentration of encapsulated BRB coated with (0.008, 0.01, 0.017) wt. % ODTAB, respectively. Also, the cell viability decreased extremely after 2 hours, and most cells died at 0.005 wt. % encapsulated BRB coated ODTAB and at higher concentrations. Figure 4.27 shows a comparison among free, uncoated and coated berberine loaded shellac NPs upon incubation with *E.coli* cells in regards to the antibacterial activity of ODTAB coated shellac NPs and pure ODTAB. The uncoated encapsulated BRB showed less toxicity than the free BRB after 2 hours of incubation time, whereas, shellac NPs coated with ODTAB also showed an effect on the cell viability due to the possession of a positive charge. In comparison, a considerable increase in the antibacterial activity was observed after incubating *E. coli* cells with ODTAB coated 0.005 wt.% berberine loaded shellac NPs at the same incubation time, this was for the same reason discussed for the yeast and algae cells. SEM images in figure 4.28 shows how the coated shellac NPs loaded with BRB attracted to *E.coli* cell after 2 hours incubation, this shows that BRB loaded shellac NPs coated ODTAB can attach to the cell's membrane faster than uncoated one.

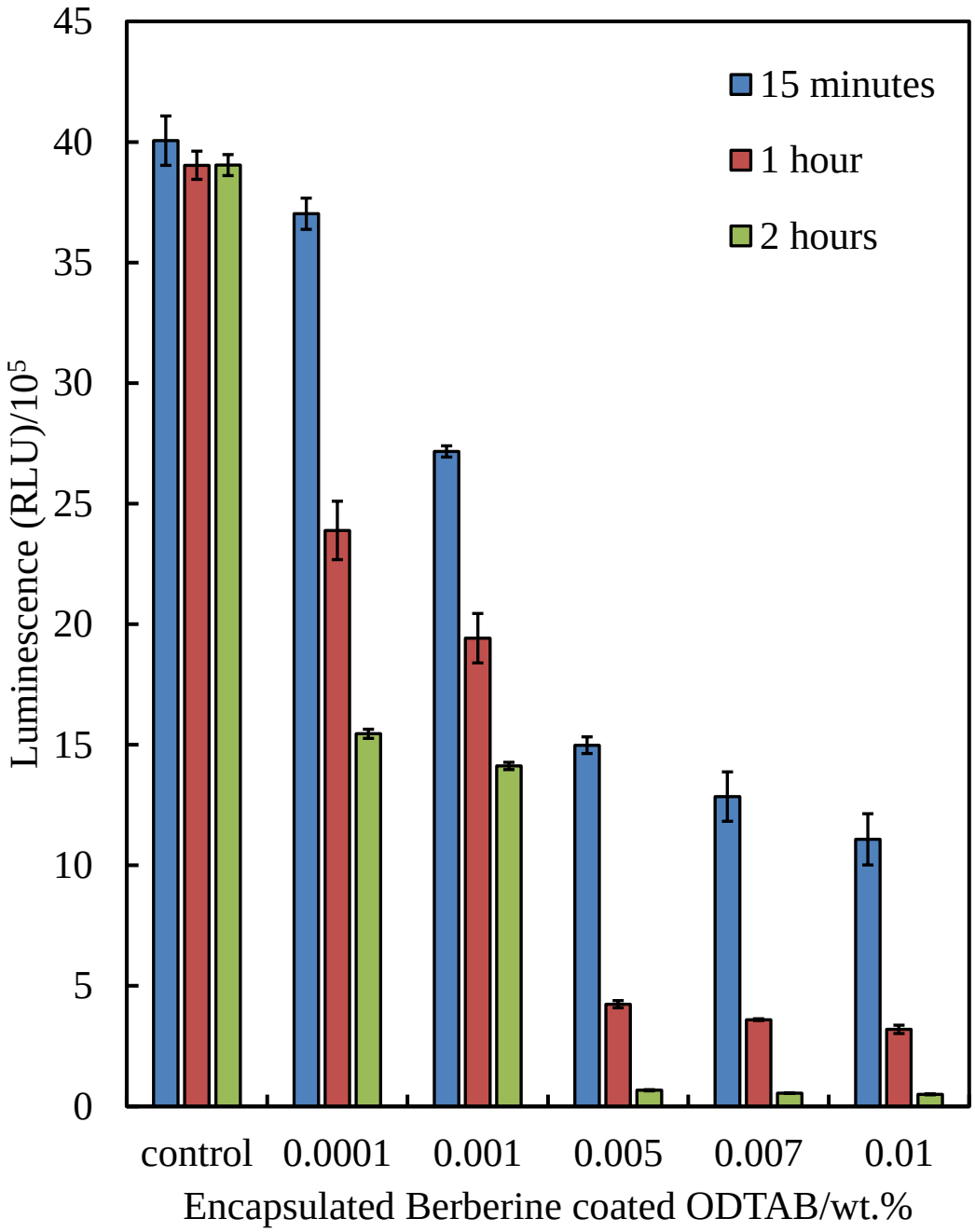

Figure 4.26: The antimicrobial activity of different concentrations of berberine loaded shellac NPs coated with ODTAB against *E.coli* cells at 15 min, 1 h, and 2 h. These solutions were prepared from 0.03 wt.% BRB loaded shellac NPs coated with 0.05 wt.% ODTAB as stock solution, (n=3).

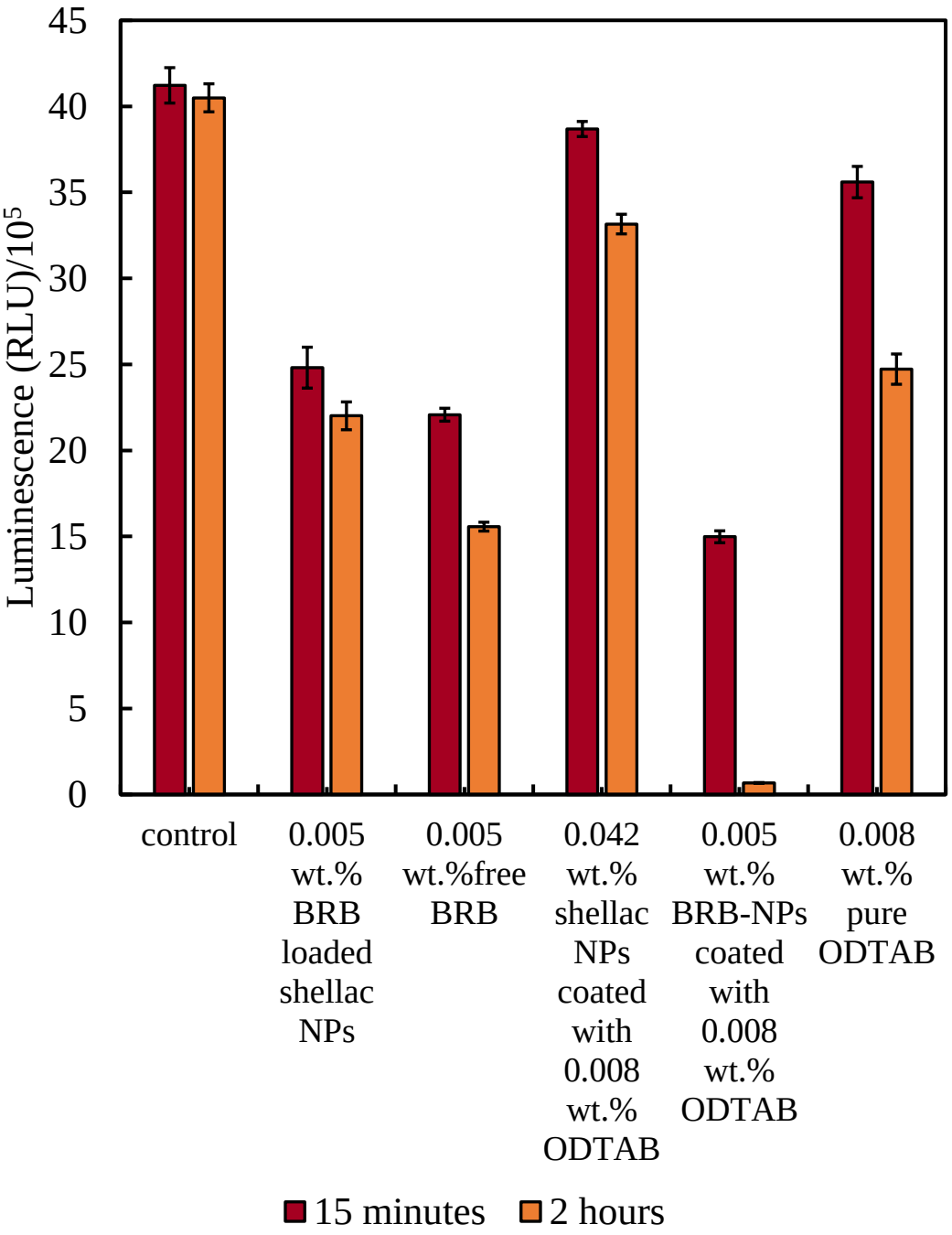

Figure 4.27: The relative luminescence unit representing the *E.coli* viability upon incubation with 0.005 wt.% berberine loaded shellac NPs coated with 0.008 wt.% ODTAB in regards to the antimicrobial activity of free and shellac NPs encapsulated berberine and the cytotoxic effect of pure ODTAB, and ODTAB coated shellac NPs. The incubation was also achieved through incubating each concentration with a fixed amount of *E.coli* cells at pH 5.5 and room temperature, (n=3).

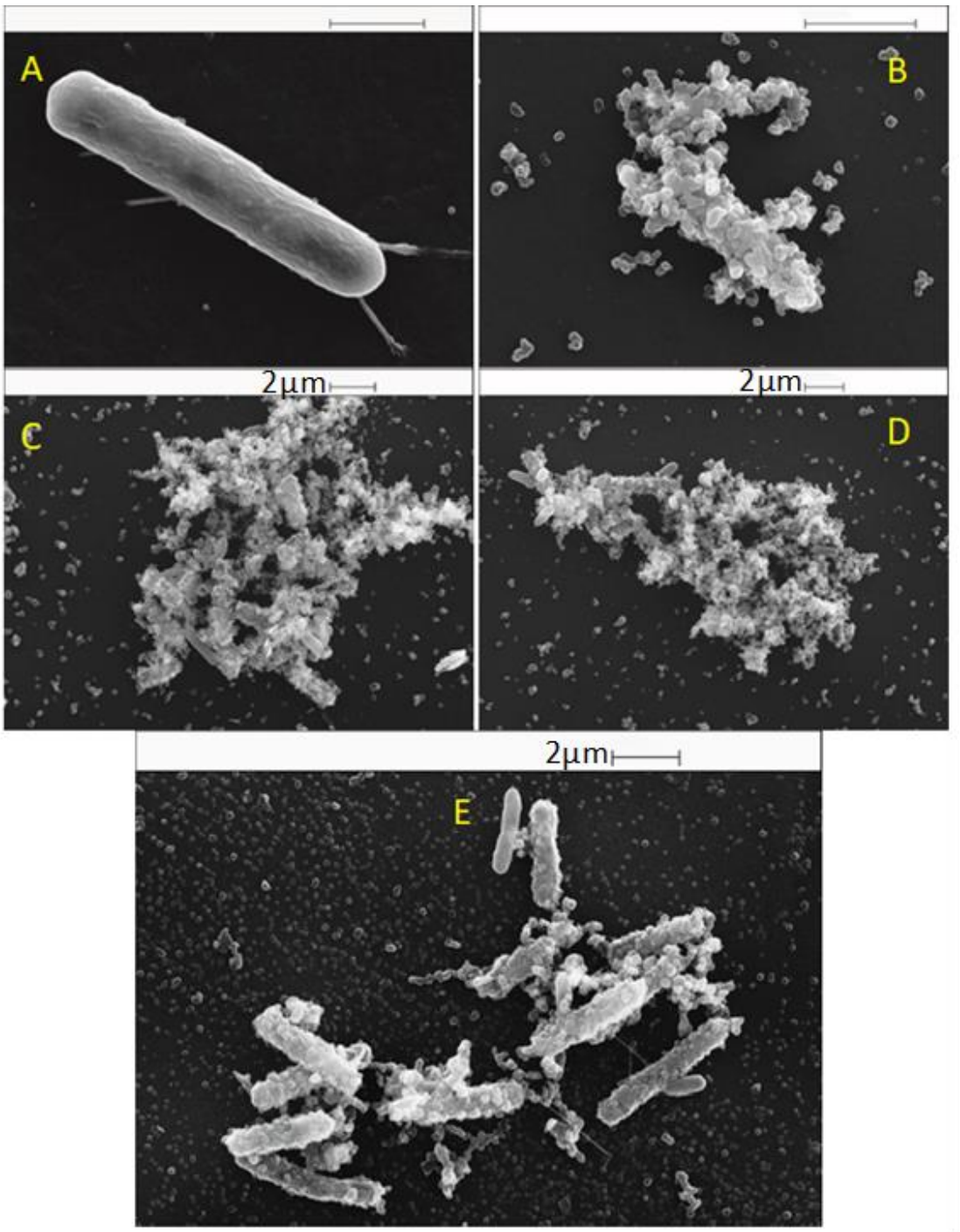

Figure 4.28: SEM images of *E.coli* cells. (A) Control sample of *E.coli* cells. (B, C, and D) *E.coli* cells incubated with 0.01 wt.% berberine loaded shellac NPs coated with 0.017 wt. % ODTAB, (E) *E.coli* cells incubated with 0.005 wt.% berberine loaded shellac NPs coated with 0.008 wt. % ODTAB after 2 hours incubation time at room temperature.

4.5 Antimicrobial Activity of Chlorhexidine Loaded Shellac NPs

Chlorhexidine as any antiseptic shows weak allergen, also it may seldom cause immunological contact urticaria as well as life-threatening anaphylaxis when be used at high concentration.[406] In this study, the aim was to use chlorhexidine at low concentrations with high effectiveness by loading it on functionalized surface nanocarrier as well as to sustain its release from the NPs. The antimicrobial actions of free chlorhexidine and chlorhexidine loaded shellac NPs on *C. reinhardtii*, yeast and *E.coli* cells were also examined.

4.5.1 Antialgal Activity of CHX Loaded Shellac NPs on Algal Cells

Figure 4.29 and Figure 4.30 show the antialgal actions of free chlorhexidine and chlorhexidine loaded shellac NPs on microalgae for different incubation times at room temperature. As is obvious from Figure 4.29 free chlorhexidine exhibits high toxicity for algae cells, and the viability of the cells reduced immediately after 15 minutes incubation, this is most clear at 0.01 wt.% of CHX as the viability went down from 94% for the control to 16%. After 2 hours incubation, the viability sharply decreased and all cells died at 0.005 wt.% of CHX and higher. In contrast, the antimicrobial activity of chlorhexidine decreased slightly after encapsulating it within shellac NPs as can be seen in Figure 4.30. This reduce in the antimicrobial activity of CHX is due to the repulsion between the negatively charged shellac NPs loaded with CHX and the negatively charged cell membrane and this will not allow the loaded chlorhexidine to be released near the cell wall, as it showed slow release (about 36% of total amount of CHX released after 9 hours at pH 5.5) and this is attributed to the strong interaction between shellac carboxylic group and chlorhexidine nitrogen atoms (as CHX has 10 nitrogen atoms) , as can be seen in figure 4.47. SEM images prove what has been mentioned above, with free CHX the cells shrank and appeared wrinkled (figure 4.31B&D) in comparison with the control sample as shown in figure 4.31 A&B, while (figure 4.31) E&F show algal cells after incubating with 0.005 wt.% of CHX loaded shellac NPs which showed that encapsulated CHX had less effect than free CHX on algal cells.

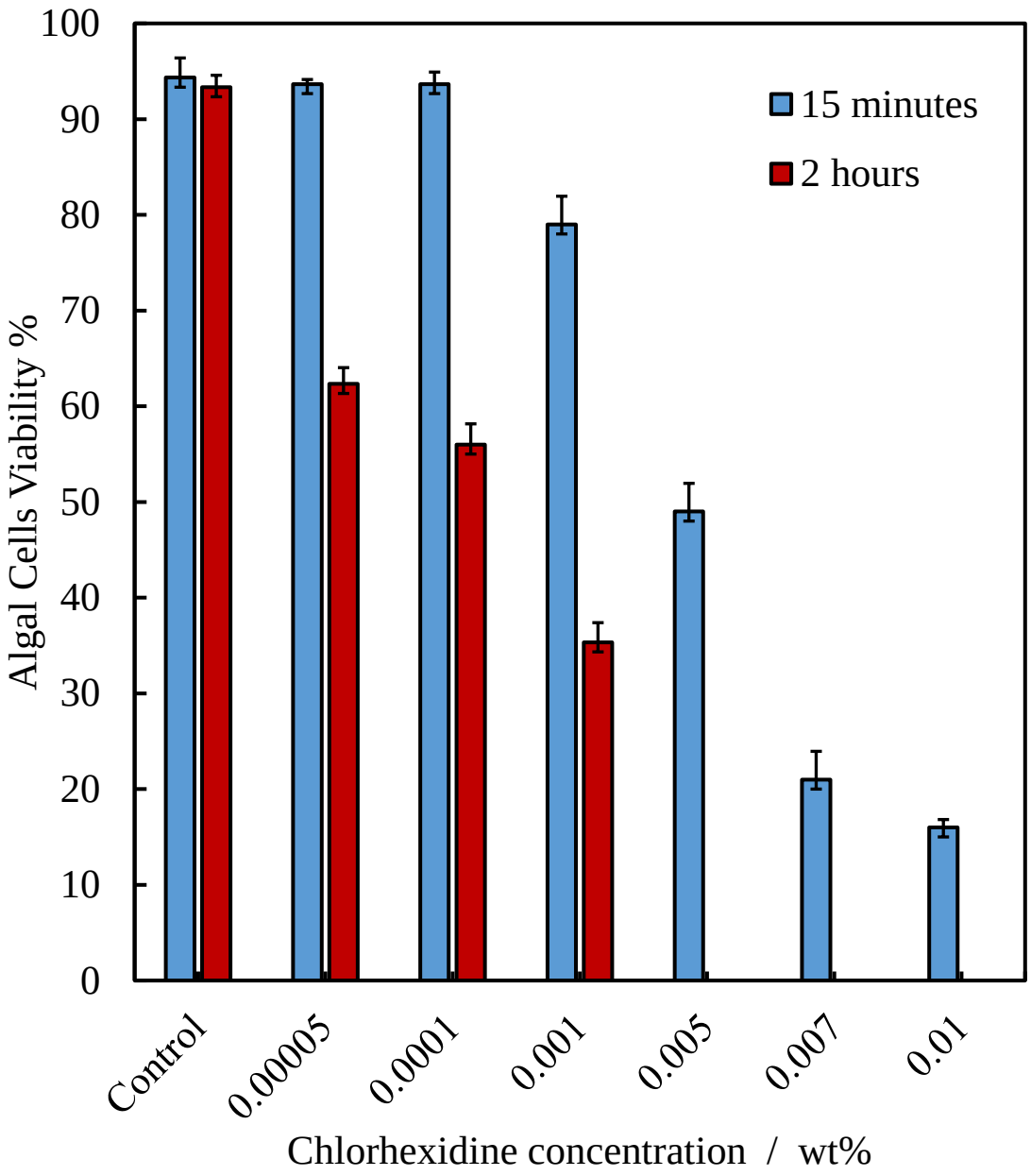

Figure 4.29: The viability of algal cells upon incubation with varying concentrations of free chlorhexidine at room temperature upon 15 min, and 2 hours incubation time at pH 5.5 using FDA assay, (n=3).

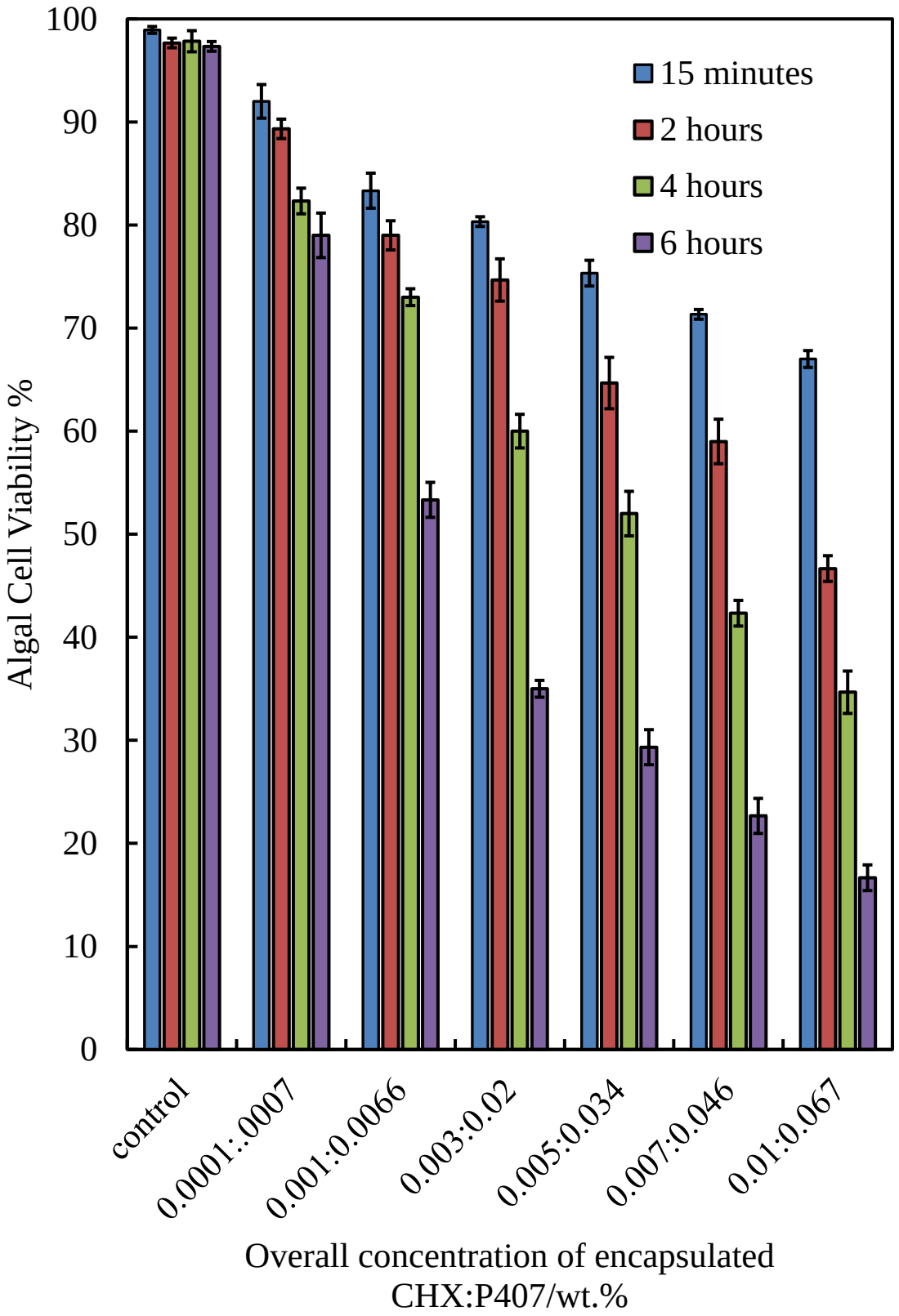

Figure 4.30: The viability of algal cells upon incubation with varying concentrations of chlorhexidine loaded shellac NPs at room temperature upon 15 min, 2 h, 4 h, and 6 hours incubation time at pH 5.5 using FDA assay, (n=3).

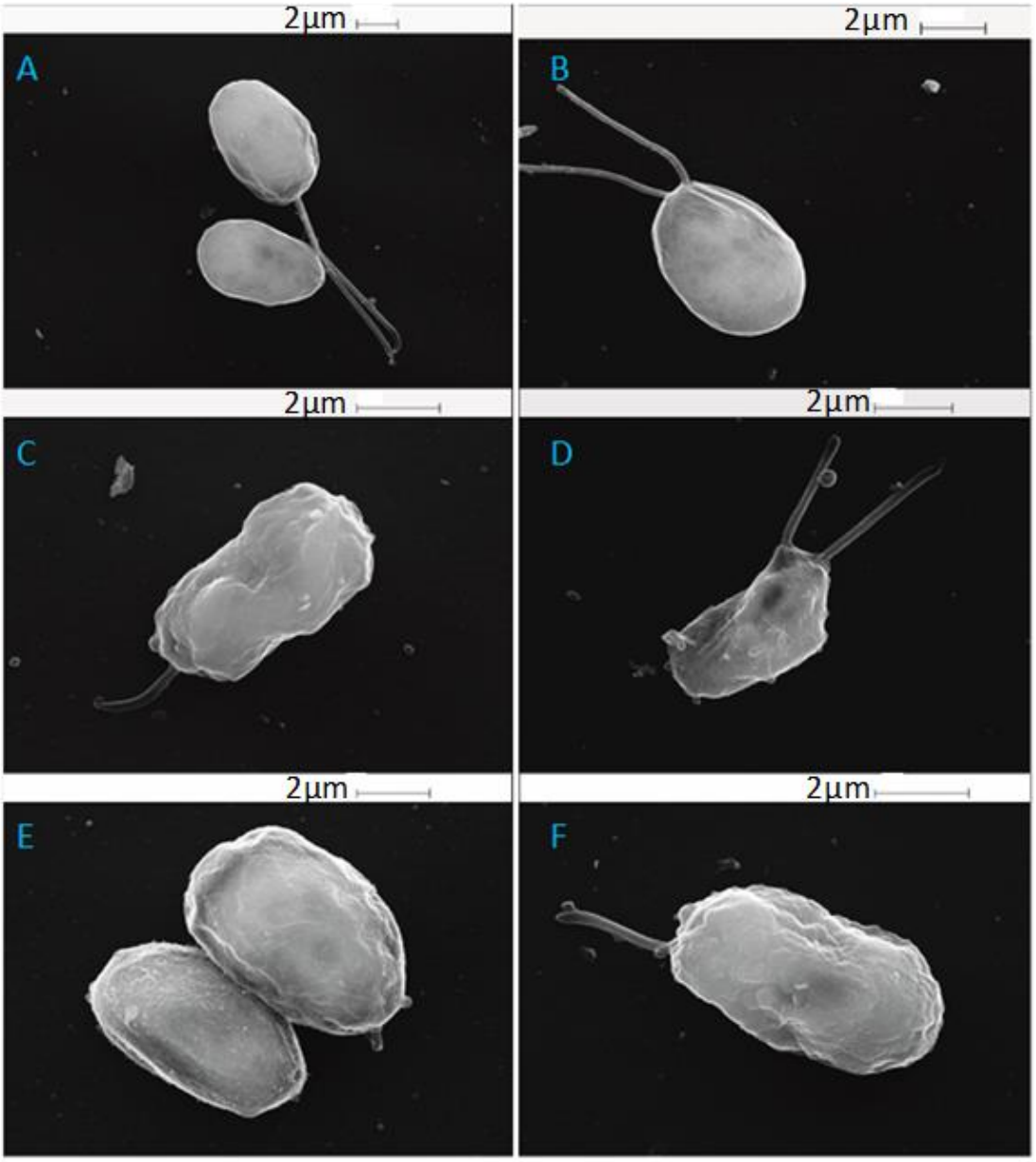

Figure 4.31: SEM images of algae cells. (A&B) Control sample of algae and (C&D) algae cells incubated with a solution of 0.005 wt.% free CHX after 4 hours incubation, (E&F) sample of algae cells incubated with 0.005 wt.% CHX loaded shellac NPs for 4 hours incubation, all cell incubated at pH 5.5 at room temperature.

4.5.2 Antimicrobial Activity of CHX Loaded Shellac NPs on Yeast Cells

The antifungal activity of free chlorhexidine and chlorhexidine loaded shellac NPs was investigated on yeast cells. Figure 4.32 displays the viability of yeast cells after incubating with different concentrations of an aqueous solution of free chlorhexidine. As can be seen from the figure that after 15 minutes of exposure, the cell viability decreased to the half at 0.003 wt. % and to quarter at 0.005 wt. % in comparison with the control which was 98%. Moreover, most cells have been killed after 2 hours incubation at a concentration of free CHX higher than 0.005 wt.%. Furthermore after 4 hours of incubation and at 0.001, 0.003 wt.% free CHX the cell viability declined to 22% and 8%, respectively. By encapsulating chlorhexidine within shellac NPs, the antimicrobial activity became less or none existent at low concentrations of encapsulated CHX. As can be seen in figure 4.33, the cell viability steadily decreased after 6 hours of exposure from 98% for control to be (75, 70, and 65)% at (0.005, 0.007, and 0.01) wt.% overall concentrations of encapsulated CHX. These results indicated that the antifungal action of CHX was reduced about 75 % after encapsulating it within shellac NPs. This could be attributed to the fact that besides yeast cells having a rigid and thick wall consisting of chitin and glucan around their cell membrane, also the negative charge surface of the NPs means there is a repulsion between the cell membrane and NPs. Moreover, chlorhexidine release is slow (about 36% of total amount of CHX released after 9 hours at pH 5.5) because of the strong interaction between the shellac carboxylic group and chlorhexidine nitrogen atoms (CHX molecule has 10 nitrogen atoms), figure 4.47. The explanation of the results was supported by SEM images. As can be seen from figure 4.34 free CHX (C&D) has much greater effect on cell membrane rather than the encapsulated CHX (E&F) in comparison with the yeast control (A&B).

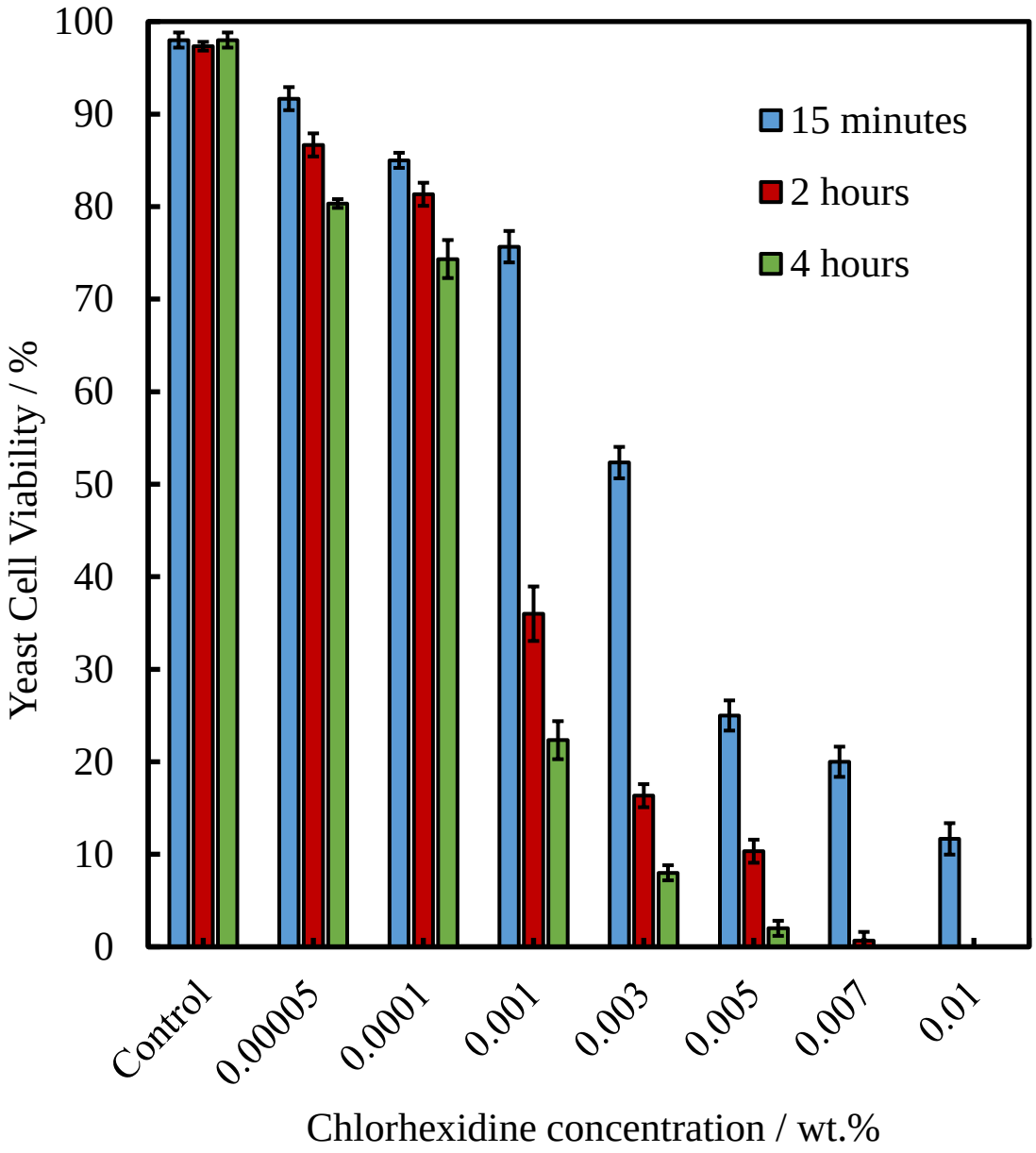

Figure 4.32: The viability of yeast cells upon incubation at pH 5.5 with varying concentrations of free chlorhexidine at room temperature upon 15 min, 2 h, and 4 hours incubation time using FDA assay, (n=3).

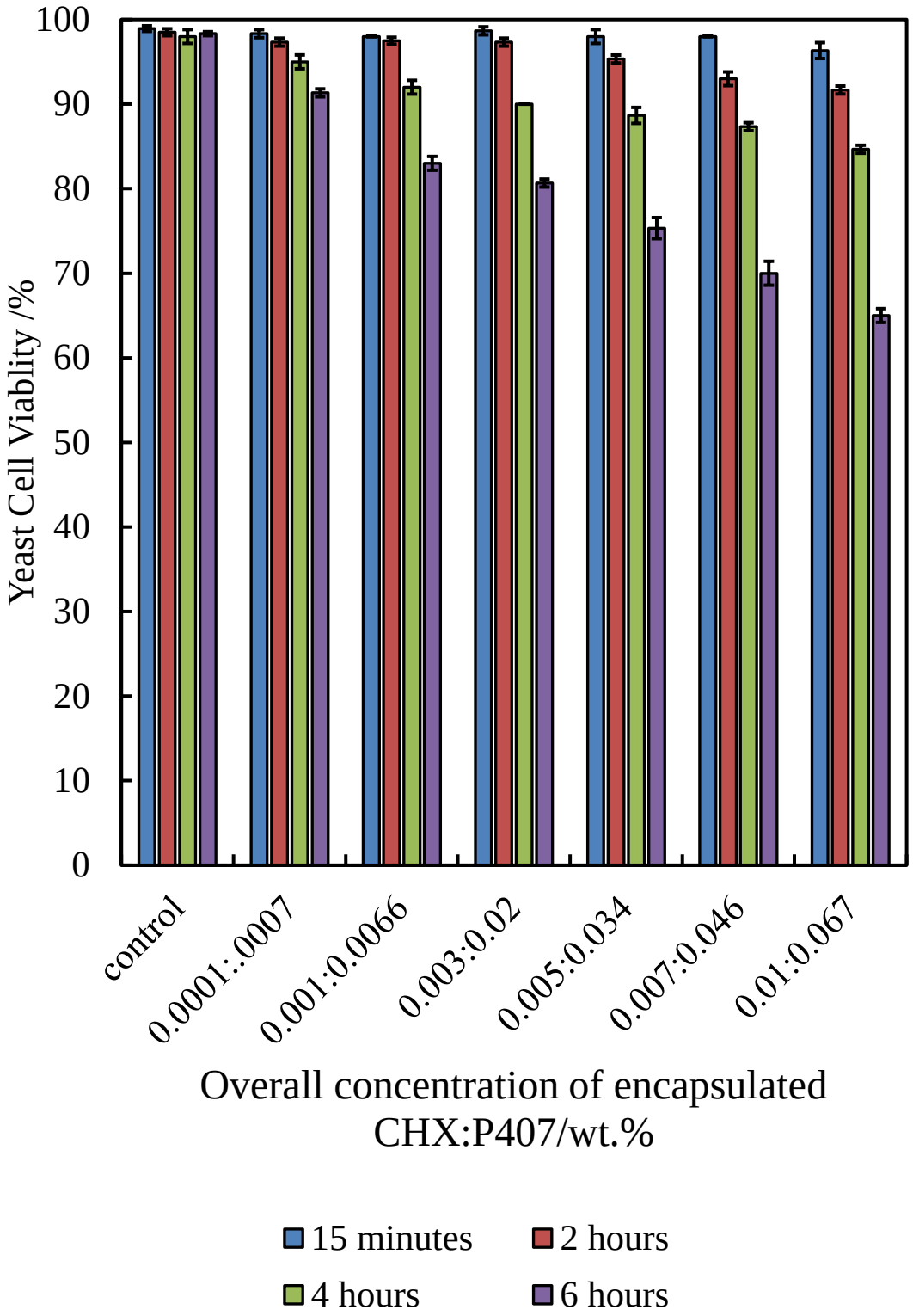

Figure 4.33: The viability of yeast cells upon incubation at pH 5.5 with varied overall concentrations of chlorhexidine loaded shellac NPs at room temperature upon 15 min, 2 h, 4 h, and 6 hours incubation time using FDA assay,(n=3).

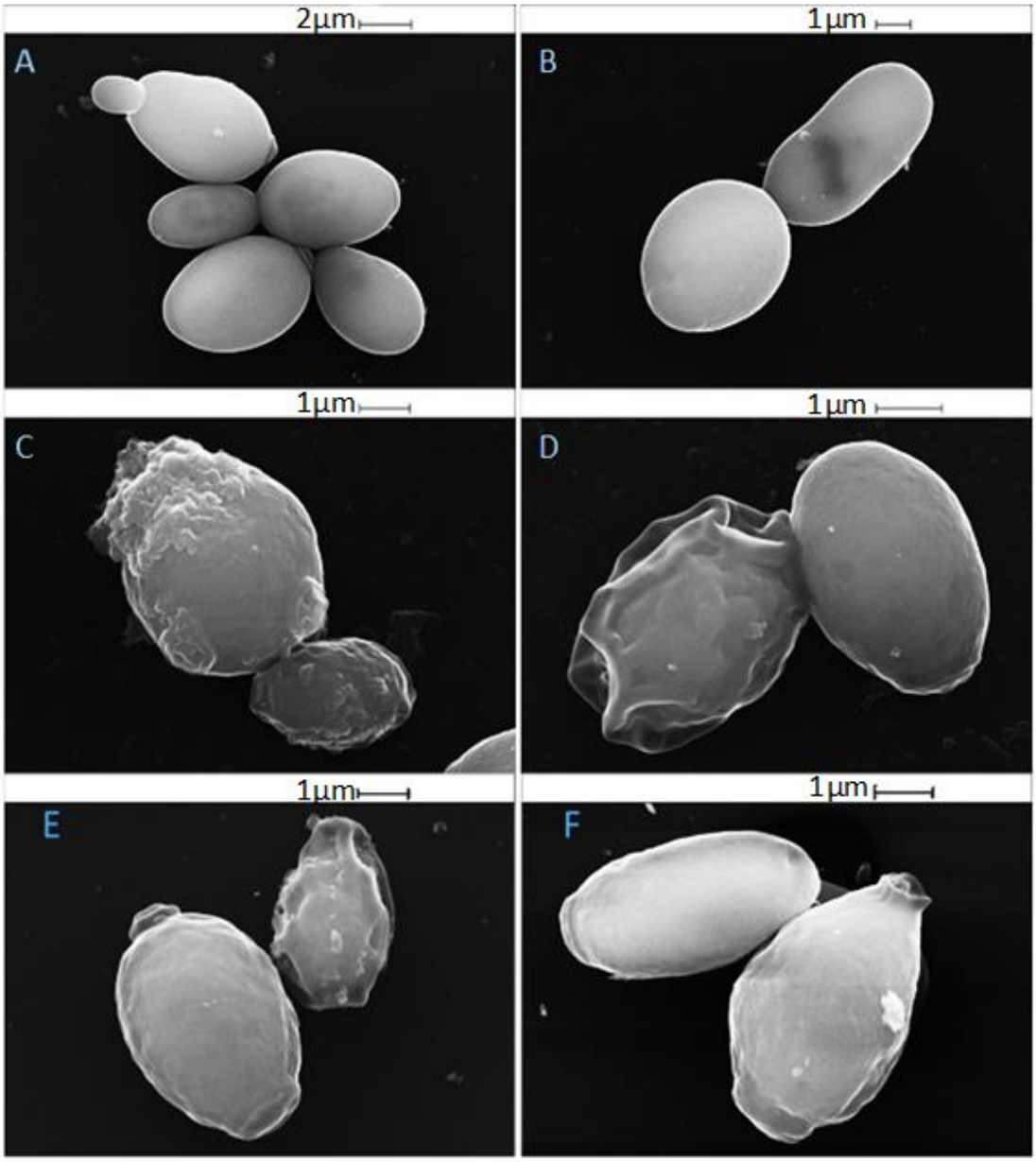

Figure 4.34: SEM images of yeast cells. (A&B) Control sample of yeast cell and (C&D) yeast cells that incubated with 0.005 wt.% free CHX after four hours of incubation, (E&F) yeast cell incubated for four hours with 0.005 wt.% of CHX loaded shellac NPs.

4.5.3 Antimicrobial Activity of CHX Loaded Shellac NPs on *E.coli*

To study the antibacterial activity of free chlorhexidine and chlorhexidine loaded shellac NPs various concentrations of them were incubated with *E.coli* cells. The cell viability was measured in terms of luminescence by treating the washed cells with bactiter luciferase reagent. As can be seen from figure 4.35 free chlorhexidine shows a high antibacterial effect even at low concentrations after only 15 minutes of incubation. The viability of the cells represented by the relative luminescence unit was sharply decreased to $9x10^5$, $7x10^5$, $4x10^5$, and $3x10^5$ RLU at CHX concentrations of (0.005, 0.01, 0.025, and 0.05) wt.%, respectively, in comparison with the viability of the control which was $4.1x10^6$ RLU. Moreover, the viability of the bacteria kept declining after 2 and 4 hours of incubation and reached to near zero at CHX concentration higher than 0.01wt. %. While the cytotoxicity of chlorhexidine decreased after encapsulating it within shellac NPs, figure 4.36 shows that the viability of the bacteria slightly declined after 6 hours of incubation. At 0.01 wt.% of overall concentration of CHX loaded shellac NPs the viability of the cells decreased from $40x10^5$ for control to $2.7x10^6$, $1.85x10^6$, $1.6.5x10^6$, and $1.25x10^6$ RLU after 15 minutes, 2, 4, 6 hours, respectively. The reason behind the decreasing of the effect of CHX antibacterial after loading it within shellac NPs is the same as described previously with the negatively surface charge of the NPs being repelled by the negatively charged cell membrane, as well as the slow release of CHX due to the strong interaction between shellac carboxylic groups and chlorhexidine nitrogen atoms. SEM images reflect these findings as shown in figure 4.37. In (B) the free CHX has caused some damage to *E.coli* in comparison to the control (A), but with the encapsulated CHX the NPs seem to be repelled by the cell wall (C&D). To overcome the problem, the surface charge of shellac NPs was functionalised to change the charge from negative to positive by coating it with cationic electrolyte, as will be explained in the next sections.

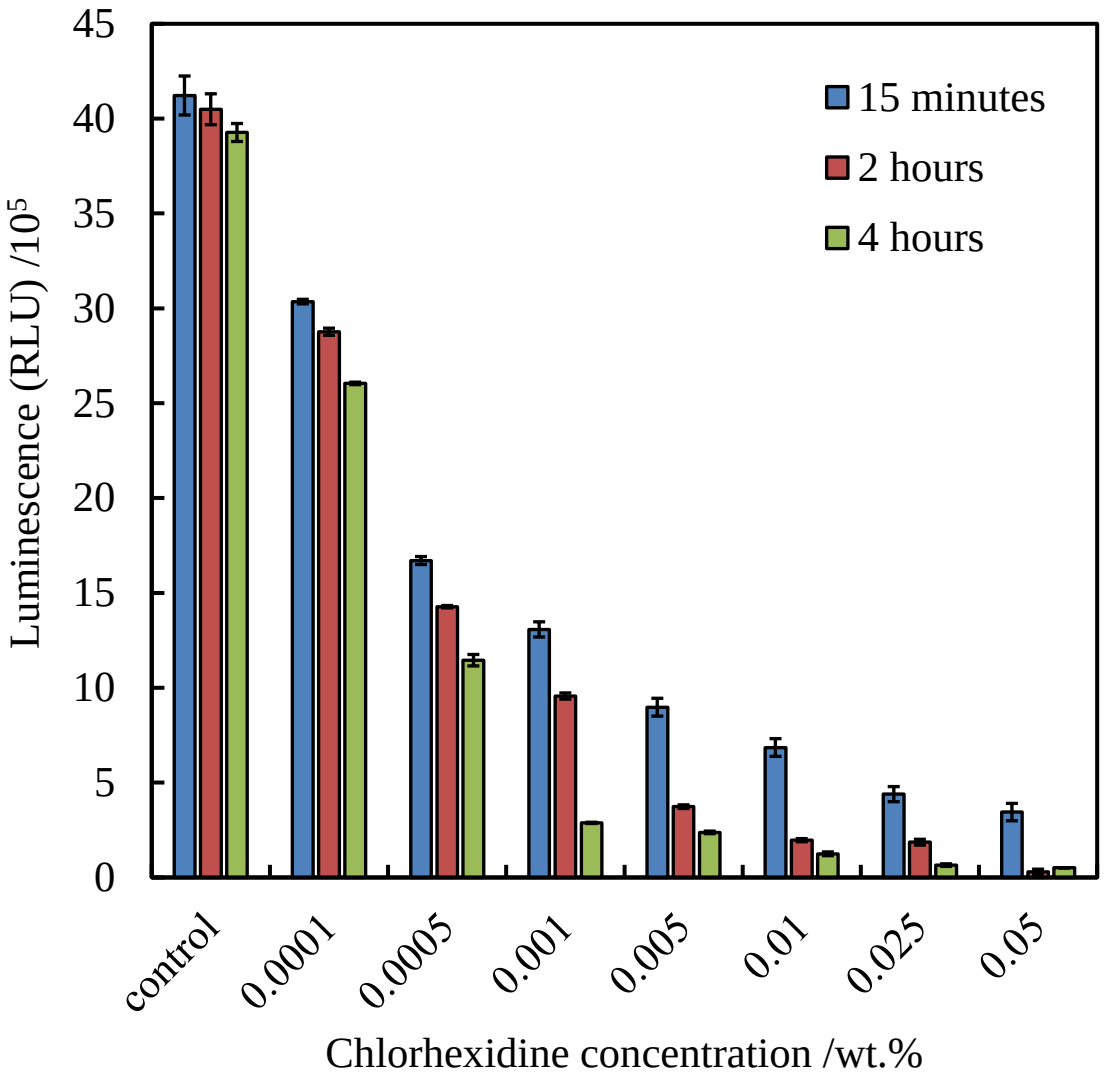

Figure 4.35: The relative luminescence unit which represents the viability of *E.coli* cells incubated at pH 5.5 with different concentrations of an aqueous solution of free chlorhexidine at different incubation time for 15 min, 2 h, and 4 h, at room temperature using bactiter luciferase reagent, (n=3).

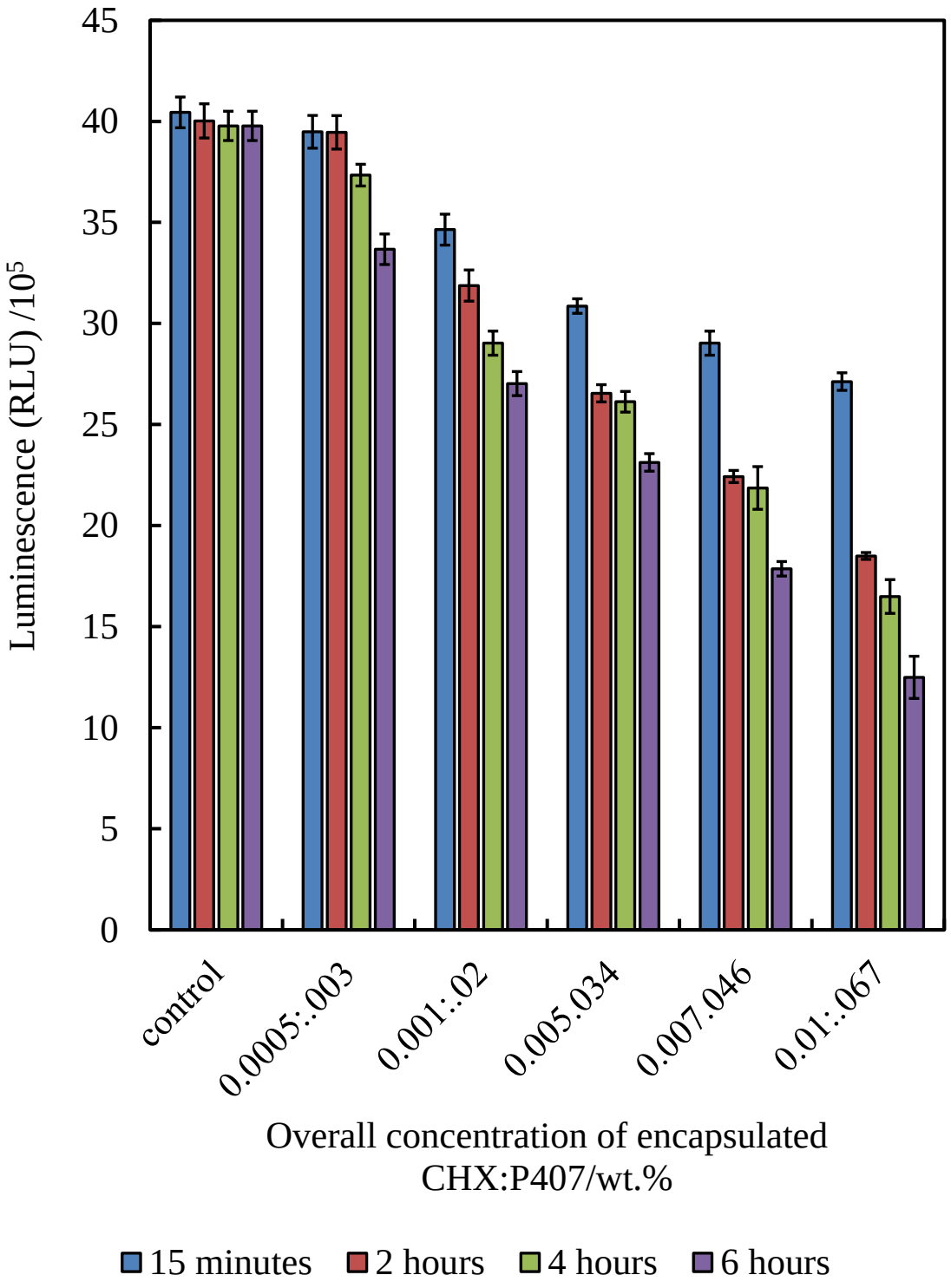

Figure 4.36: The relative luminescence unit representing *E.coli* cells viability incubated at pH 5.5 with different overall concentrations of chlorhexidine loaded shellac NPs at different incubation time 15 min, 2 h, 4 h, and 6 h, at room temperature using bactiter luciferase reagent, (n=3).

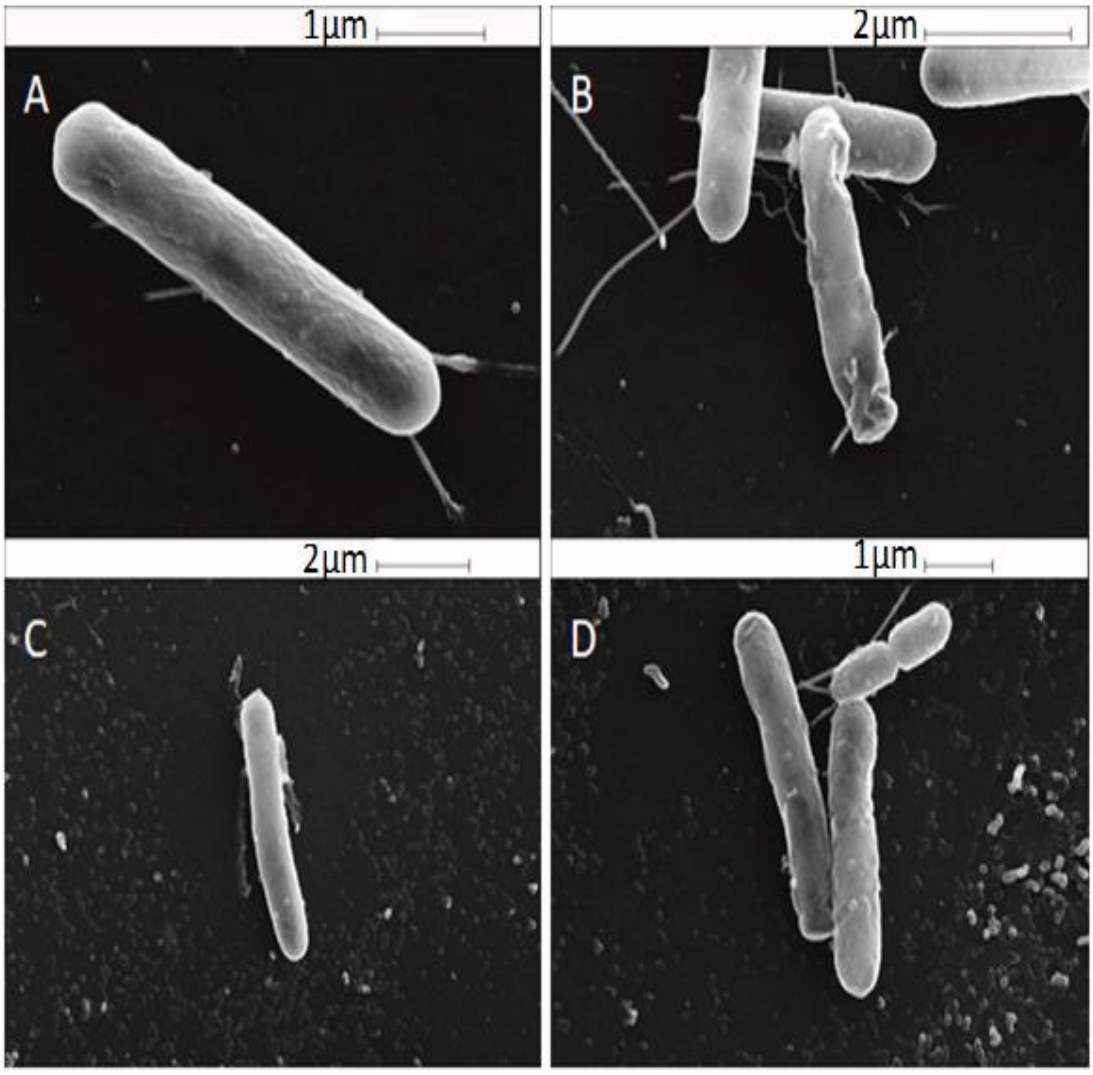

Figure 4.37: SEM images of *E.coli*. (A) Control sample of *E.coli* and (B) *E.coli* that incubated with 0.005 wt.% free CHX after four hours of incubation, (C&D) *E.coli* incubated for four hours with 0.005 wt.% of CHX loaded shellac NPs.

4.6 The Cytotoxic Effect of CHX Loaded Shellac NPs Coated with ODTAB on Microorganisms

To overcome the problem of the negative charge of the nanoparticles as well as the drug sustained within the NPs, the surface of shellac NPs loaded with CHX was functionalised and coated with cationic electrolyte ODTAB; mentioned previously (sec 4.3), ODTAB was chosen due to its zeta potential +12 mV. The antialgal, antifungal and antibacterial activity of CHX loaded shellac NPs after coating with ODTAB was studied by incubating different amount of CHX-NPs coated ODTAB with microalgae, yeast, and *E.coli* cells.

4.6.1 The Cytotoxic Effect of CHX Loaded Shellac NPs Coated with ODTAB on Microalgae

The antialgal activity of CHX loaded shellac NPs coated with ODTAB was investigated on C. reinhardtii microalgae cells at different concentrations and incubation times. Figure 4.38 shows the algal cell viability upon incubation for 15 minutes with various concentrations of encapsulated CHX coated ODTAB; it can be seen that all cells were killed after 15 minutes incubation time at 0.0001 wt. % CHX loaded shellac NPs coated with 0.0001 wt.% ODTAB and higher amounts. A comparison among the antialgal activities of 0.0001 wt.% encapsulated CHX, 0.0001 wt.% free CHX, 0.0005 wt.% shellac NPs coated with 0.0001 wt.% ODTAB, 0.0001 wt.% chlorhexidine-NPs coated with 0.0001 wt.% ODTAB, and 0.0001 wt.% pure ODTAB is given in Figure 4.39. This shows that there was a decrease in the antimicrobial activity of chlorhexidine when loaded within shellac NPs in comparison with the free chlorhexidine, while there was a pronounced change in the cytotoxicity of CHX after coating it with ODTAB. The positively charged NPs are attracted fast to the cell membrane, and subsequently, CHX is released in the vicinity. Figure 4.40 shows SEM pictures of the microalgal cell after incubated with 0.005 wt.% CHX loaded shellac NPs coated with 0.005 wt.% ODTAB for 2 hours. Pictures show how the cells clustered, and the NPs accumulated around the cells in abundance due to the positively charged surface of the NPs loaded with CHX coated with ODTAB.

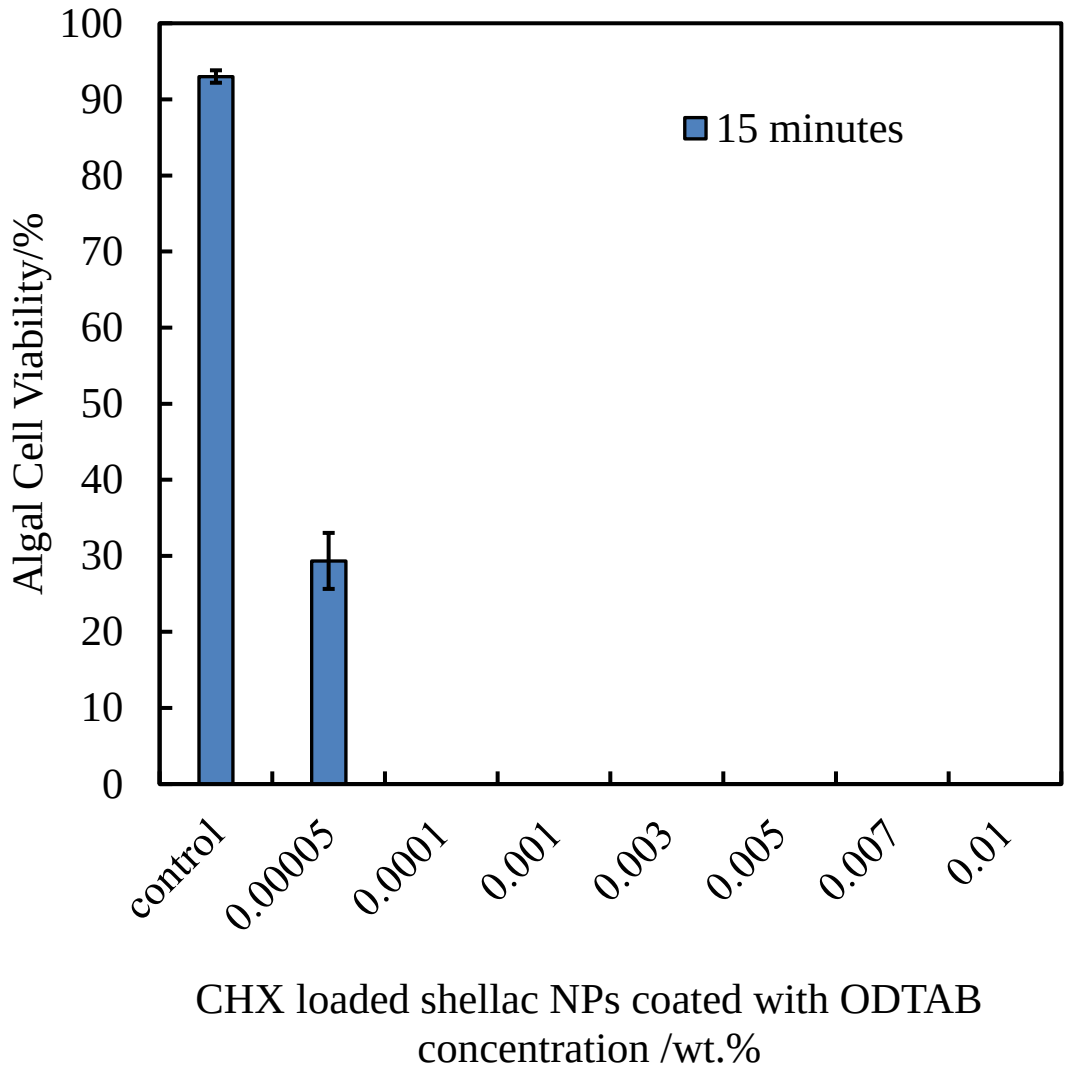

Figure 4.38: The viability of algal cells upon incubation at pH 5.5 with different amounts of chlorhexidine loaded shellac NPs coated with ODTAB measured by using FDA assay after washing the cells from the treatment at room temperature at 15 min of incubation time. The solutions were prepared from 0.05 wt.% CHX NPs stock solution coated with 0.05 wt.% ODTAB, (n=3).

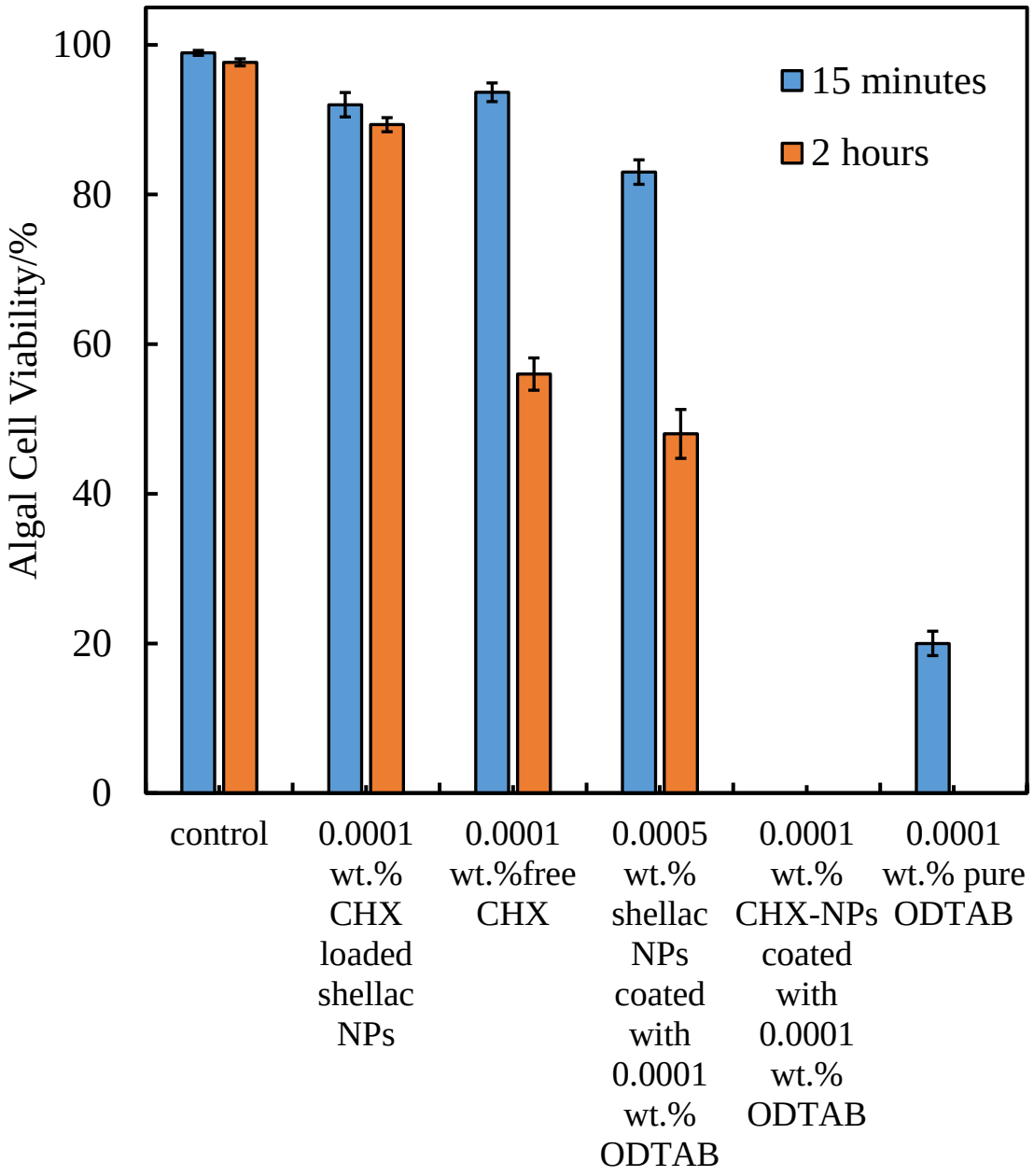

Figure 4.39: The algal cells viability upon incubation with 0.0001 wt.% CHX-NPs, 0.0001 wt.% free CHX, 0.0005 wt.% shellac NPs coated with 0.0001 wt.% ODTAB, 0.0001 wt.% CHX-NPs coated with 0.0001 wt.% ODTAB, and 0.0001 wt.% pure ODTAB at pH 5.5 and room temperature, (n=3).

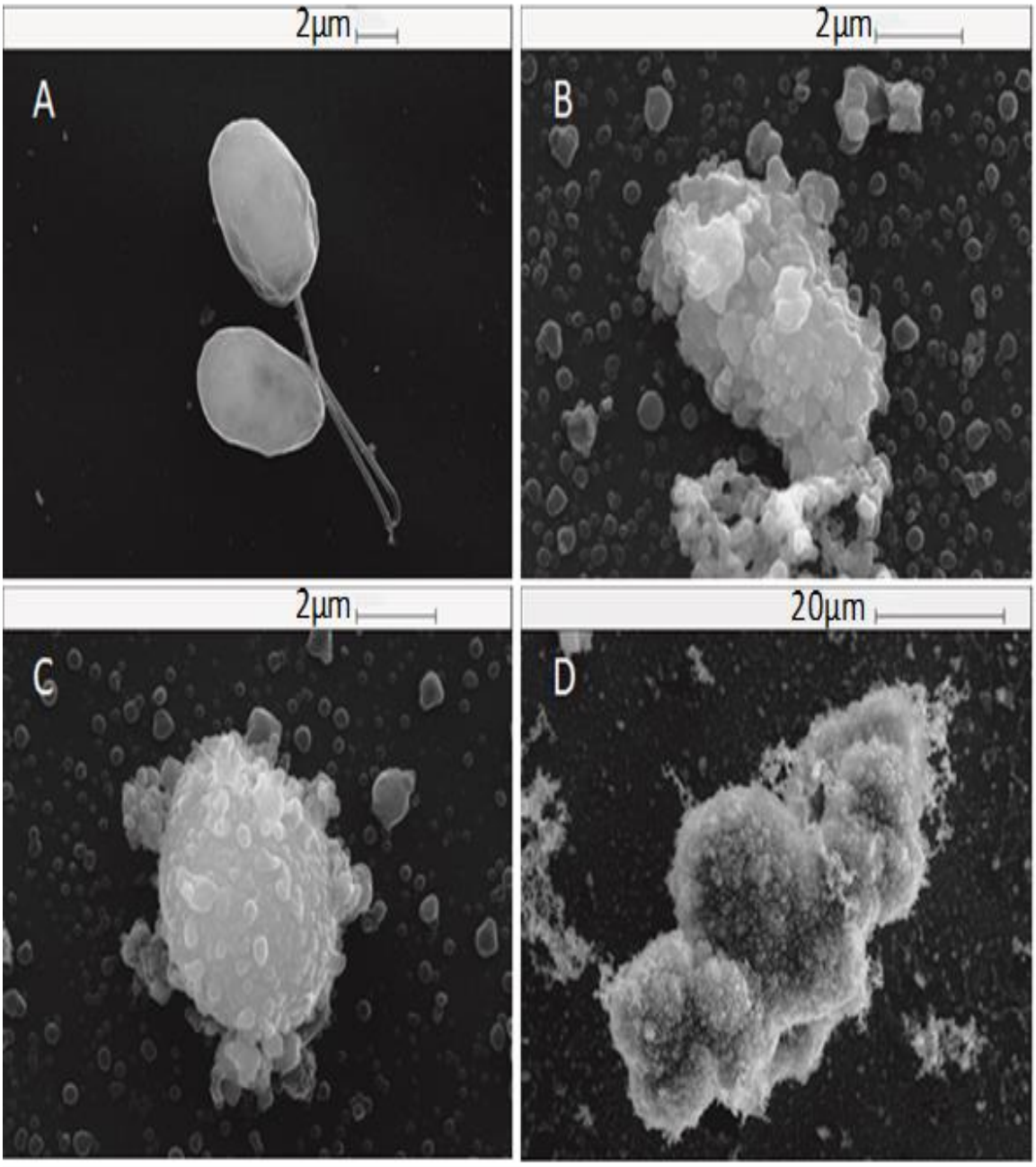

Figure 4.40: SEM images of *C. reinhardtii* cells. (A) A control sample of the *C. reinhardtii* microalgae cells. (B, C, and D) *C. reinhardtii* microalgae cells incubated with 0.005 wt.% CHX loaded shellac NPs coated with 0.005 wt. % ODTAB after 2 hours incubation time at room temperature.

4.6.2 Cytotoxic Effect of CHX Loaded Shellac NPs Coated ODTAB on Yeast Cells

Figure 4.41 shows the cytotoxic effect of chlorhexidine loaded shellac NPs coated with ODTAB on yeast cells up to 4 hours incubation time. In this study, there was an obvious toxic effect on the cell viability after 15 minutes incubation, at (0.003, 0.005, 0.007, and 0.01) wt.% of chlorhexidine loaded shellac NPs coated with ODTAB, the viability sharply reduced from 98.5% for control to 12%, 7%, 2.4%, and 0.8%, respectively. Also after 4 hours of incubation, the cell viability strongly decrease at 0.005 wt.% and higher concentrations. Figure 4.42 demonstrates a comparison of 0.0001 wt.% free chlorhexidine and 0.0001 wt.% chlorhexidine NPs coated with 0.0001 wt.% ODTAB on yeast cells in regards to the antimicrobial activity of 0.0001 wt.% encapsulated CHX, 0.0001 wt.% ODTAB coated 0.0005 wt.% shellac NPs and 0.0001 wt.% pure ODTAB. The results show that after coating CHX-NPs with cationic electrolyte ODTAB, the cytotoxic effect of CHX increased due to the strong attraction between CHX-NPs coated ODTAB and cell membrane hence more CHX can be released inside the cells. SEM images show that the cells were severely damaged after 2 hours incubation with 0.005 wt. % CHX-NPs coated with 0.005 wt.% ODTAB as shown in Figure 4.43.

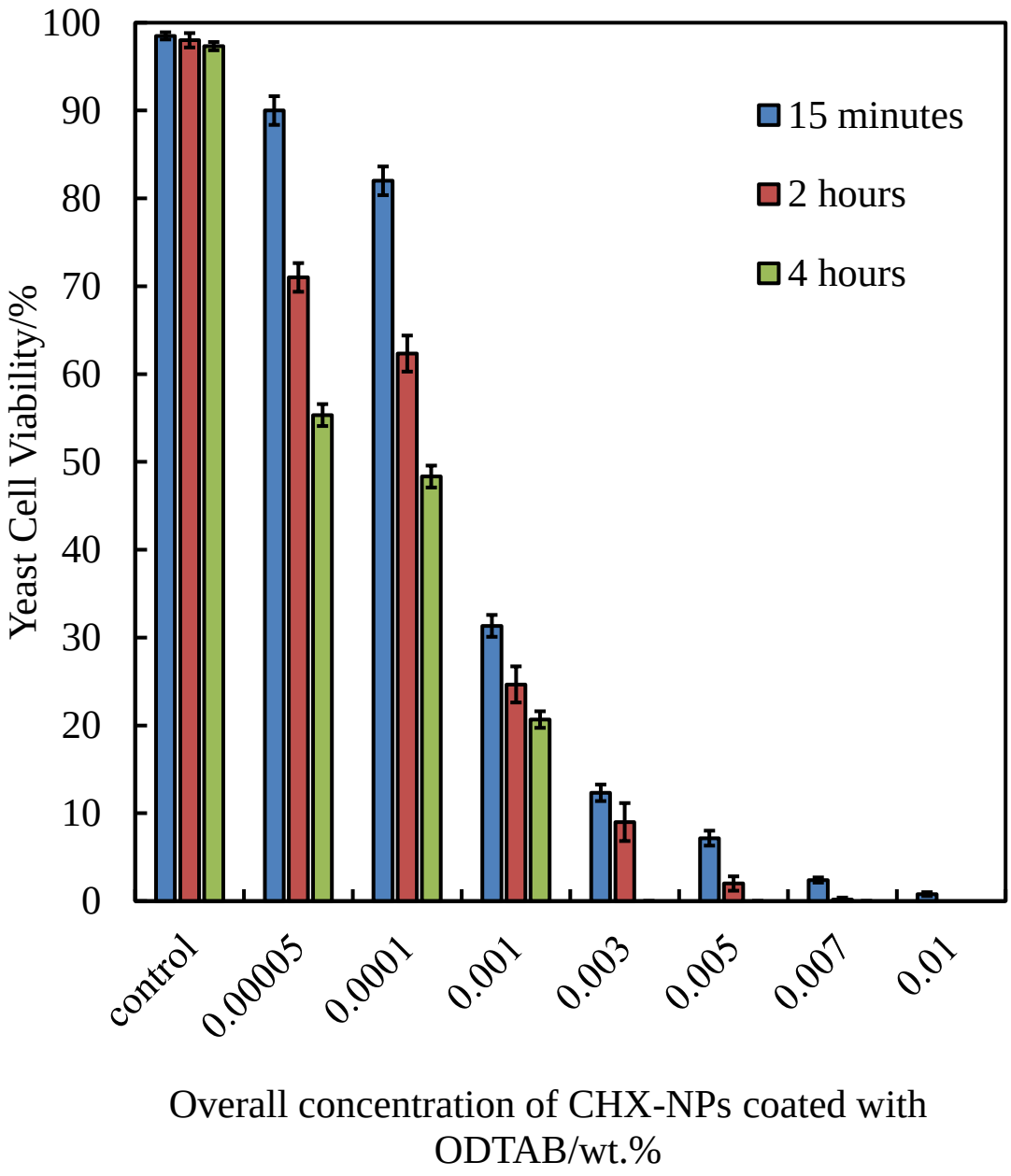

Figure 4.41: The cytotoxic effect of different concentrations of chlorhexidine loaded shellac NPs coated with ODTAB upon incubation with yeast cells at room temperature up to 15 min, 2 h, and 4 hours using FDA assay. The suspensions were prepared from 0.05 wt.% stock solution of CHX-NPs coated with 0.05 wt.% ODTAB, (n=3).

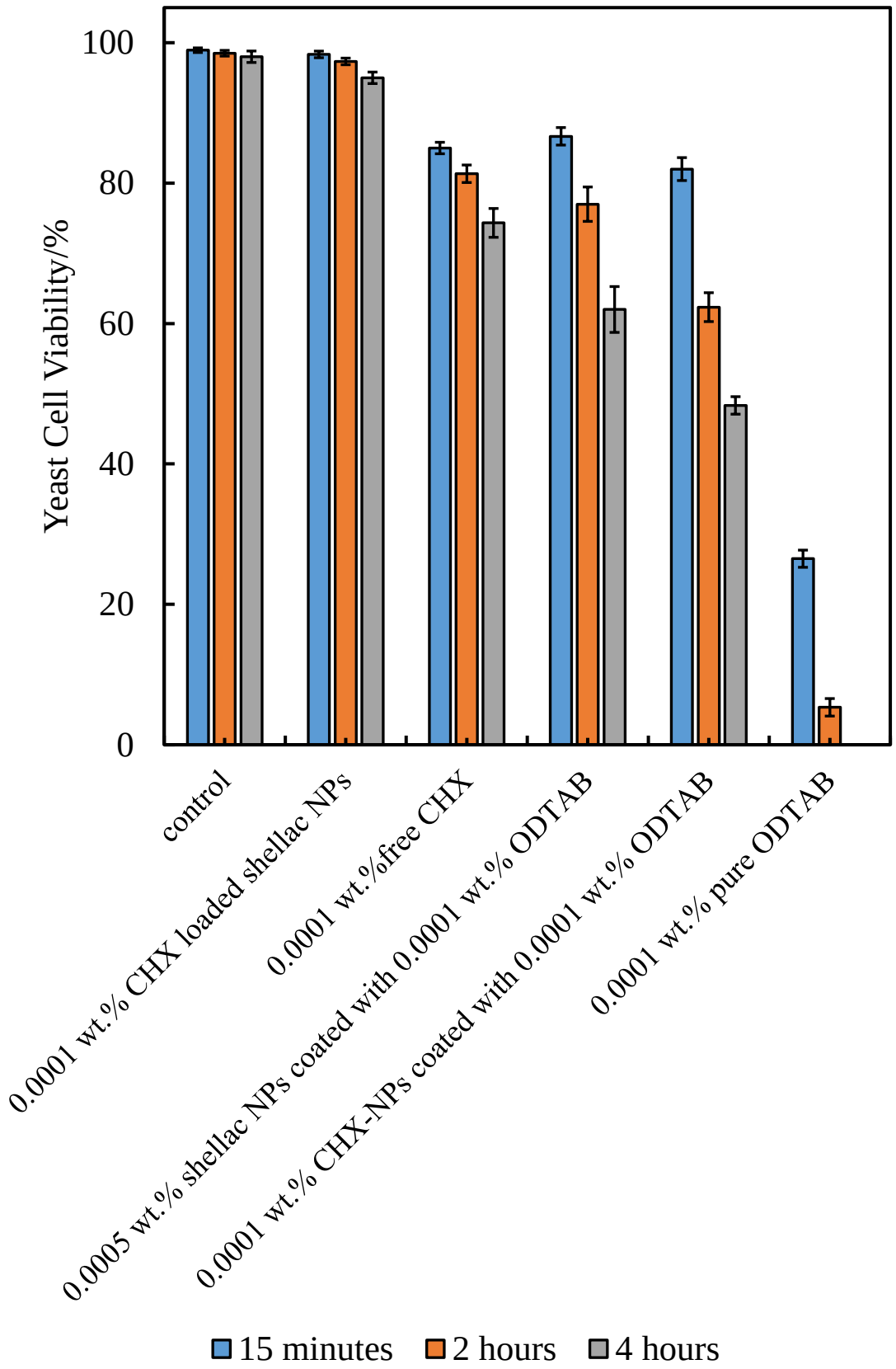

Figure 4.42: The yeast cells viability upon incubation with 0.0001 wt.% CHX-NPs, 0.0001 wt.% free CHX, 0.0005 wt.% shellac NPs coated with 0.0001 wt.% ODTAB, 0.0001 wt.% CHX-NPs coated with 0.0001 wt.% ODTAB, and 0.0001 wt.% pure ODTAB at pH5.5 and at room temperature, (n=3).

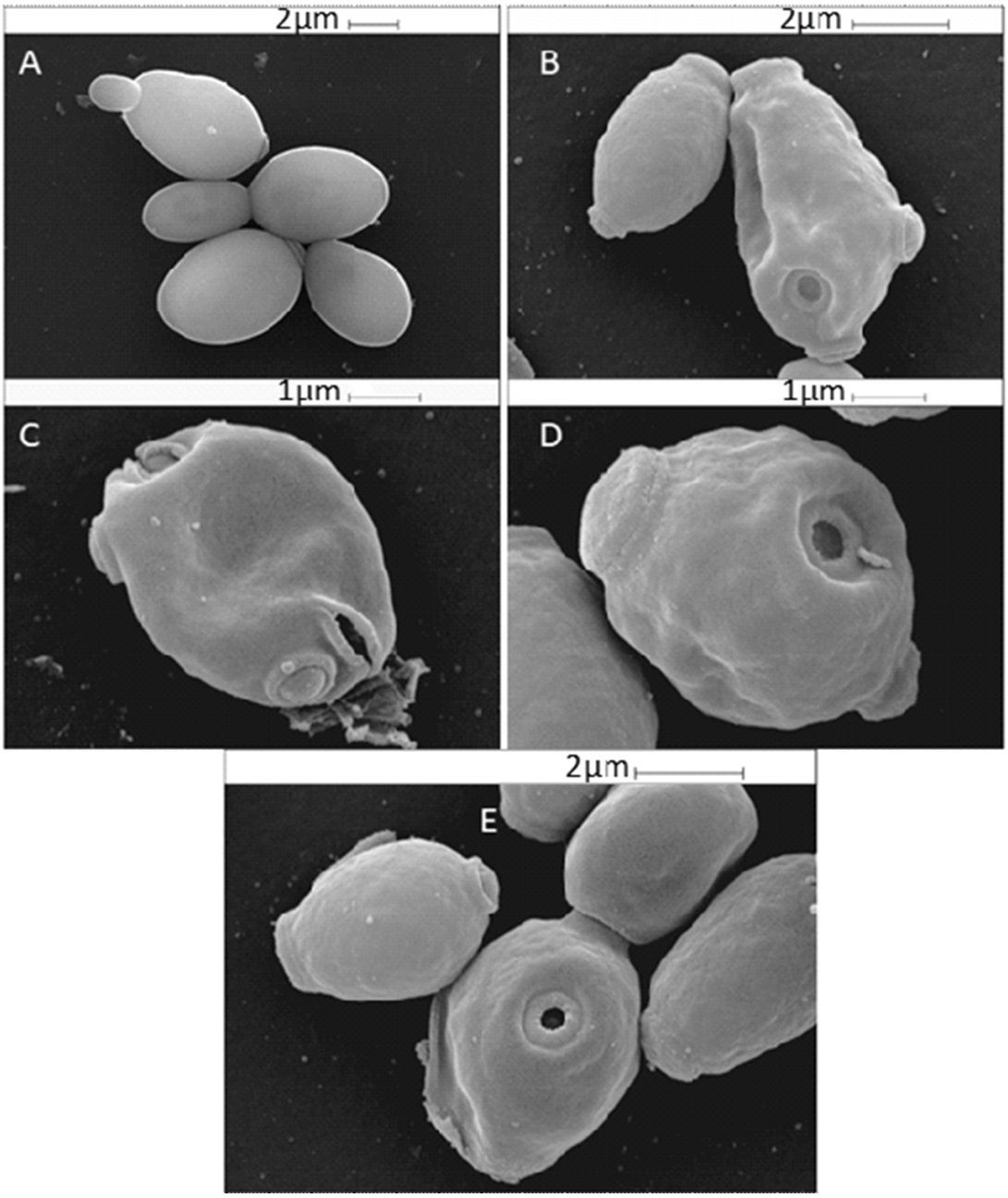

Figure 4.43: SEM images of yeast cells. (A) A control sample of the yeast cells. (B, C, D and E) yeast cells incubated with 0.005 wt.% CHX loaded shellac NPs coated with 0.005 wt. % ODTAB after 2 hours incubation time at room temperature.

4.6.3 The Cytotoxic Effect of CHX Loaded Shellac NPs Coated ODTAB on *E.coli* Cells

The antibacterial activity of CHX loaded shellac NPs after coating with the cationic electrolyte ODTAB to convert the surface charge from negative to positive to enhance the electrostatic adhesion between the NPs and cell wall was studied at pH 5.5 on *E.coli* cells. Figure 4.44 shows that after 15 minutes of incubation, encapsulated CHX coated with ODTAB affected little at concentrations (0.0001, 0.0005, 0.001) wt.%, while at higher concentrations, the cell viability decreased noticeably. After 2 hours, most cells died at 0.001wt.% encapsulated CHX coated with ODTAB and higher. Moreover, the cell viability declined strongly after 4 hours of incubation from 3.9 $x10^6$ RLU at control to $5x10^5$ RLU at 0.005 wt.% CHX-NPs coated with 0.008 wt.% ODTAB, and all cells died at higher concentrations. Figure 4.45 shows a comparison among free, uncoated and coated chlorhexidine loaded shellac NPs upon incubation with *E.coli* cells in regards to the antimicrobial activity of ODTAB coated shellac NPs and pure ODTAB. The uncoated CHX-NPs showed less cytotoxicity than the free CHX after 4 hours of incubation, whilst as expected, shellac NPs coated with ODTAB had an effect on the cell viability due to the positive surface charge. A considerable increase in the antimicrobial activity was observed after incubating *E. coli* cells with ODTAB coated 0.005 wt.% chlorhexidine loaded shellac NPs at the same incubation time, for the reasons previously described. Figure 4.46 shows a scanning electron microscopy images of E.coli cell incubated with 0.005 wt.% CHX loaded shellac NPs coated with ODTAB after 2 hours incubation time, these pictures prove that CHX loaded shellac NPs coated with ODTAB can adhesive to the cell's membrane faster than uncoated one.

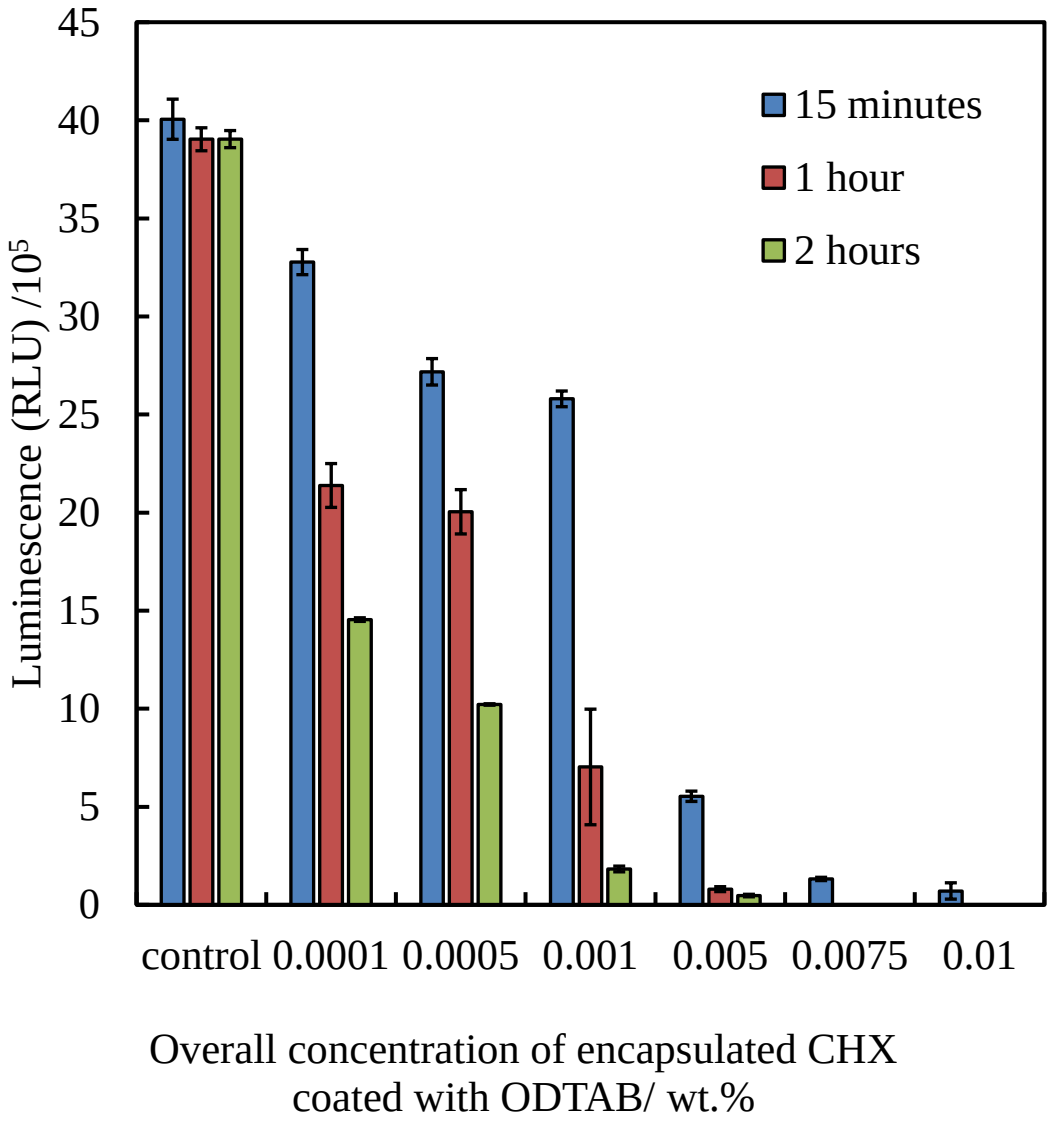

Figure 4.44: The antibacterial activity of different concentrations of chlorhexidine loaded shellac NPs coated with ODTAB at 15 min, 1 h, and 2 h. against *E.coli* cells. The cell viability represented by relative luminescence unit. These solutions were prepared from stock solution of 0.03 wt.% CHX loaded shellac NPs coated with 0.05 wt.% ODTAB, (n=3).

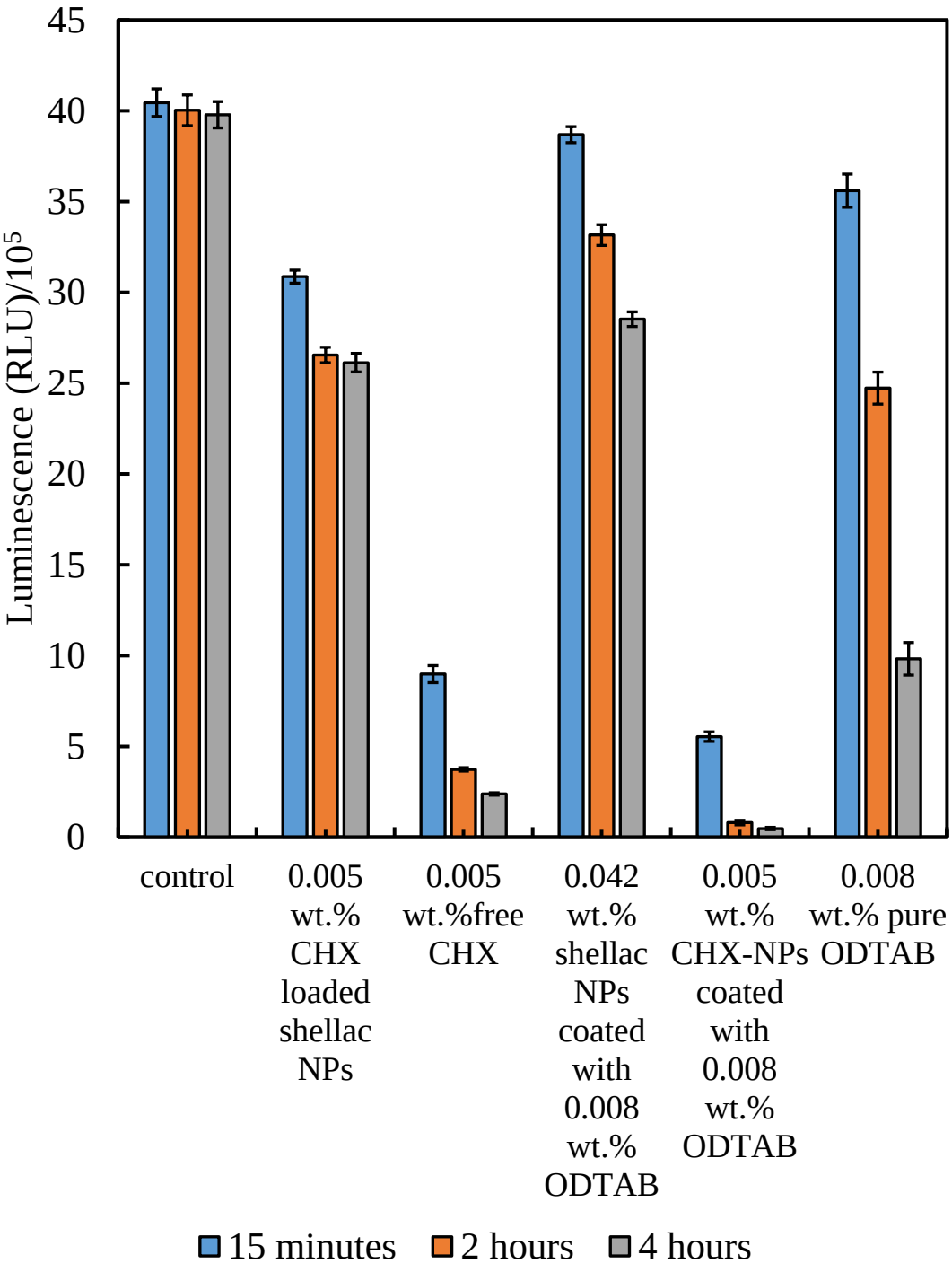

Figure 4.45: The antimicrobial activity of 0.005 wt.% chlorhexidine loaded shellac NPs coated with 0.008 wt.% ODTAB towards *E.coli* cells as a function of both the antimicrobial activity of free and shellac NPs encapsulated chlorhexidine and the cytotoxic effect of pure ODTAB, and ODTAB coated shellac NPs. The incubation was also achieved through incubating each concentration with a fixed amount of *E.coli* cells at pH 5.5 at room temperature using bactiter luciferase assay, (n=3).

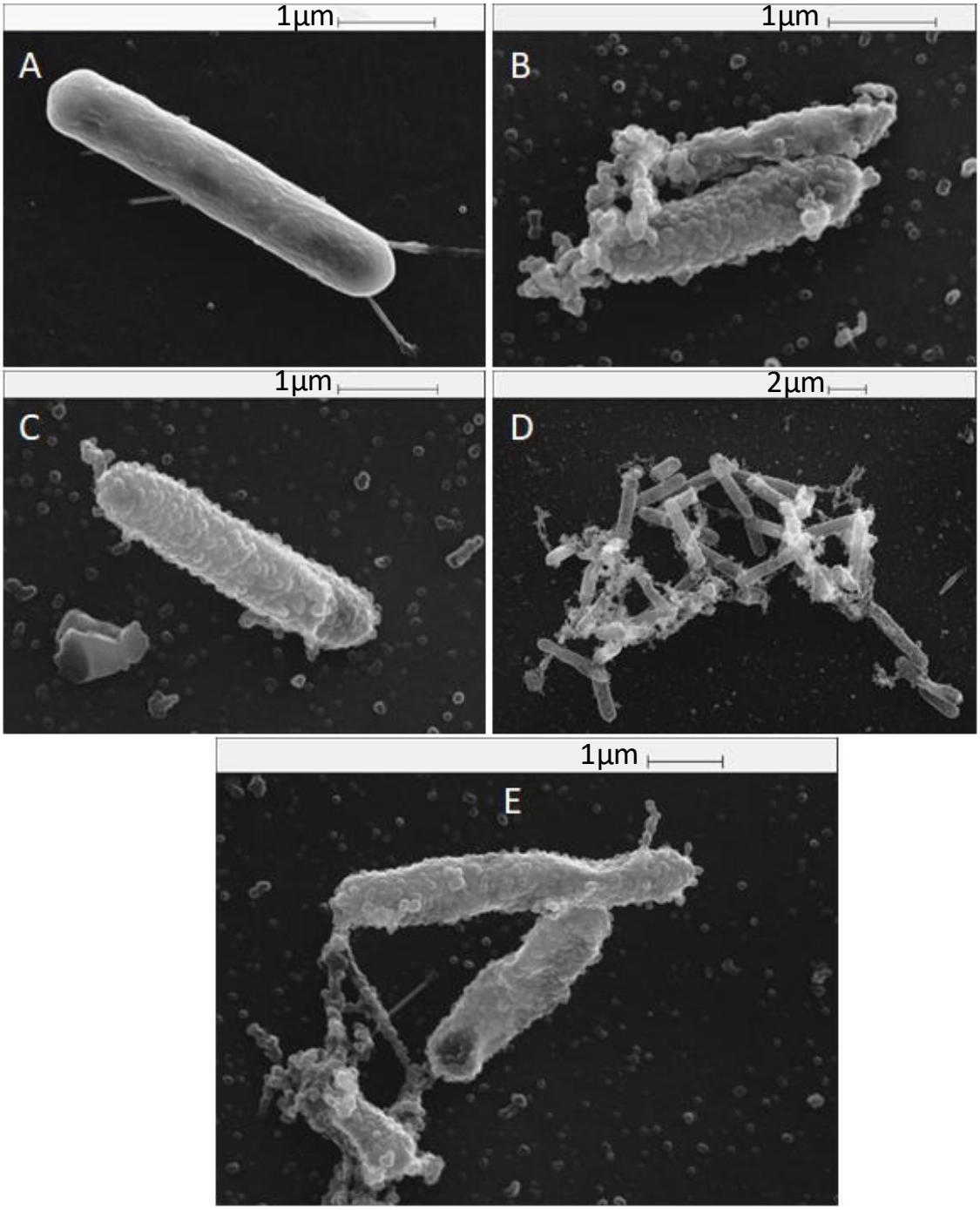

Figure 4.46: SEM images of *E.coli* cells. (A) Control sample of *E.coli* cells. (B, C, D and E) *E.coli* cells incubated with 0.005 wt.% chlorhexidine loaded shellac NPs coated with ODTAB at pH 5.5 at room temperature.

4.7 Conclusion

In this chapter the cytotoxic effect of shellac NPs and encapsulated BRB and CHX within shellac NPs on some microorganisms including algae, yeast, and *E.coli* cells was discussed. The results showed that shellac NPs did not express any effect on these microorganisms except very little effect on algae due to the existence of Poloxamer 407 which has been used to stabilise the shellac nanoparticles by producing steric repulsion among the particles. Free berberine showed a cytotoxic effect on algae and *E.coli*, but not on yeast. After encapsulating it within shellac NPs its effect reduced due to the interaction between the cationic BRB and anionic shellac NPs which sustain the drug release. Besides the negatively charged NPs are repelled by the negatively charged cell membrane and this cause drug being released away from the cell membrane vicinity. To overcome the charge problem, the nanocarriers loaded with BRB were coated with cationic electrolyte ODTAB to change the charge from negative to positive; this electrolyte has been chosen instead of other polyelectrolytes to maintain the stability of shellac NPs. The cytotoxic effect of encapsulated BRB coated with ODTAB increased sharply due to the rapid attraction between the coated encapsulated BRB and the cell membrane. Thus the least amount of released drug will kill the cells. Encapsulated BRB coated with ODTAB showed severe cytotoxic effect on algae cells, and less on *E.coli* and yeast cells, attributed to the thickness of the cell membrane. The coated encapsulated BRB expressed cytotoxicity about 20 times more than the free BRB on algae and yeast and about 5 times more on *E.coli*. Very little literature showed the cytotoxic effect of encapsulated BRB on algae, yeast and *E.coli*,[379] the designed nanocarrier loaded with BRB and coated with ODTAB showed much more cytotoxic effect than the others after a short time of incubation.

Free chlorhexidine showed a significant cytotoxic effect on algae, yeast, and *E.coli*, but when it was encapsulated within shellac NPs this action reduced, owing to the same reasons mentioned before, i.e. the high interaction between shellac molecules and CHX as well as the repulsion between the negatively charged NPs surface and the cell membrane. Therefore, the NPs were also coated with the cationic electrolyte ODTAB to overcome the charge problem. After coating the encapsulated CHX with ODTAB the cytotoxic effect increased severely due to the rapid attraction between the coated encapsulated CHX and the cell membrane; as SEM images showed. This lead the drug to be released near the cell membrane vicinity and kill the cells even at very small amounts of the drug. The coated encapsulated CHX displayed significant cytotoxicity on algal cells more than yeast and *E.coli* that related to the thickness of the cell membrane. Table 4.1 shows the cytotoxic

effect of BRB and CHX as free drugs, loaded within shellac NPs and ODTAB coated these drugs loaded with shellac NPs, as well as the cytotoxic effect of free shellac NPs coated and uncoated with ODTAB. By comparing the cytotoxicity of berberine loaded with different nanocarriers mentioned in section 1.7.2 and the cytotoxicity of berberine loaded with shellac and coated with ODTAB, it can be seen BRB cytotoxicity increased 10 times more than its cytotoxicity when was loaded with other nanocarriers. A recent study showed that the minimum inhibition concentrations (MIC) of BRB NPs were 0.064 and 0.032 $mg.mL^{-1}$ on yeast and *E.coli*, respectively.[407] While the current study showed the MIC of encapsulated BRB coated with ODTAB was 0.005 and 0.01 $mg.mL^{-1}$ on yeast and *E.coli*, respectively. Also for CHX the results show that when it loaded with shellac NPs and coated with ODTAB its cytotoxicity amplified more than 10 times than its cytotoxicity when loaded with other nanocarriers as mentioned in section 1.7.4. One of the studies showed the cytotoxicity of encapsulated CHX on different type of bacteria was 0.02-1.25 $mg.mL^{-1}$, whereas in this project it was 0.01 $mg.mL^{-1}$ on *E.coli* cells.[408] This was attributed to the positive surface charge of shellac NPs which increase the attraction with the cell membrane and thus at very small amount of drug can kill the cell fast, while most nanocarriers used before they have negative surface charge as can be seen in tables 1.2 and 1.3.

Table 4.1: The cytotoxicity effect of each component on algae, yeast, and *E.coli* which represented by (++++: very strong, +++: strong, ++: medium, and +: weak).

Component	The effect of the component on microorganisms		
	Algae	Yeast	*E.coli*
Shellac NPs	+++	++	+
Shellac NPs coated with ODTAB	+++	++	++
Free BRB	+++	+	+++
Encapsulated BRB	+++	++	++
Encapsulated BRB coated with ODTAB	++++	+++	++++
Free CHX	++++	++++	++++
Encapsulated CHX	+++	++	++
Encapsulated CHX coated with ODTAB	++++	++++	++++

The designed nanocarrier loaded with BRB and CHX and coated with ODTAB showed significant cytotoxicity on microorganisms faster than those of encapsulated CHX in the literatures.[169, 409-411] Figure 4.47 shows the negatively NPs charged repel to the cell membrane and released drug far away from the cell membrane vicinity (a), while after being coated with ODTAB, they attracted and released drugs near or inside the cell membrane, (b).

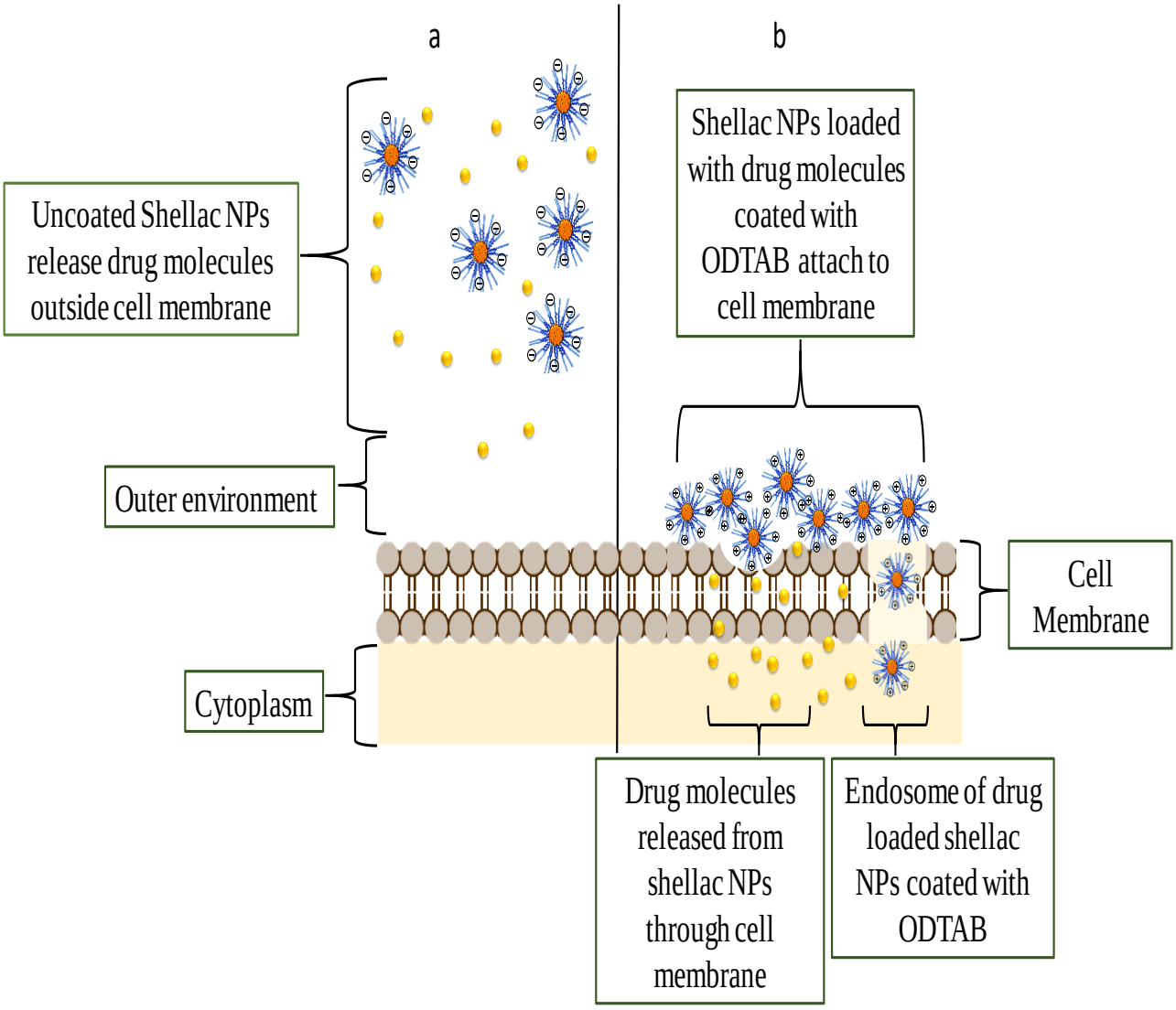

Figure 4.47: Schematic diagram illustrate the release of drug from shellac NPs; a) through direct diffusion in the outer cell membrane of cell when the shellac NPs holding negative surface charge, b) by the internalization of drug loaded shellac NPs through the cell membrane forming endosome of drug loaded shellac NPs by endocytosis whereby drug molecules can be further released inside the cell's cytoplasm, and this mechanism occurs when the shellac NPs coated with cationic electrolyte ODTAB.

Chapter 5 : Cytotoxicity Assay of CUR and VCM Loaded Shellac NPs

In the preceding chapter, the cytotoxicity of two antimicrobial (BRB and CHX) loaded within shellac NPs before and after functionalizing the surface of the NPs with cationic electrolyte ODTAB were studied. In this chapter, the antimicrobial activity of CUR and vancomycin hydrochloride is investigated. CUR is a natural product with broad spectrum antimicrobial activity including antiviral, antibacterial, antimalarial and antifungal activities.[412] CUR is not easy to solubilise and was therefore encapsulated within shellac NPs. Furthermore this approach would allow the release of the CUR near the cell membrane vicinity. Vancomycin, is an antibiotic produced from *Streptomyces orientalis* strains and this was also loaded within shellac NPs, this approach should also allow sustained release of the antibiotic and the cell membrane thus enhancing its effectiveness. The study included testing of the antimicrobial action of CUR and VCM loaded shellac NPs before and after functionalizing the surface of the NPs with cationic electrolyte ODTAB to study the effect of the surface charge of the NPs.

5.1 Cytotoxic Activity of CUR Loaded Shellac NPs on Microorganisms

The antialgal, antifungal and antibacterial assay of aqueous solutions of CUR loaded shellac NPs were demonstrated compared to free CUR in the next three sections. As mentioned in section 3.5.3 CUR has an encapsulation efficiency of 99% of its total concentration with very slow release at pH 5.5.

5.1.1 Antialgal Activity of CUR Loaded Shellac NPs on Algal Cells

The antialgal activity of free CUR and CUR loaded shellac NPs was tested on microalgae (*C. reinhardtii*) cells at different concentrations for 6 hours incubations at room temperature and a pH of 5.5 using an FDA assay. Figure 5.1 shows the effect of various concentrations of free CUR on the algal cell viability; the viability decreased sharply from 95% for the control to 17% at 0.005 wt.% free CUR and less at higher concentrations once they were incubated for 15 minutes. After 2 hours incubation, at 0.001 wt.% of free CUR and higher concentrations, most cells were killed. Moreover, even at very low

concentrations of 0.0003 wt.% CUR, the cell viability declined severely from 95% to 5% after 4 hours of incubation.

Figure 5.2 shows the results of the cell viability after incubation with different concentrations of CUR loaded shellac NPs for up to 6 hours. Comparing the two figures (Figure 5.1 and Figure 5.2) it can be seen that the antimicrobial activity of CUR declined when it was encapsulated within the shellac NPs, and at high concentrations (0.002 and 0.0025) wt.% the cell viability decreased from 91% for the control to 44% and 41% respectively after 2 hours of incubation. The free CUR was much more effective. After 6 hours of exposure, the cell viability continued to decrease slightly. The reason for this finding is the high hydrophobic-hydrophobic interaction between the shellac molecules and CUR which makes its release very slow along with the repulsion between the NPs and cell membrane due to the negatively charged surface of both of them. SEM images can confirm the above results, Figure 5.3 shows pictures of algae cells after incubation with free CUR and CUR loaded shellac NPs, (C&D) images display how the cell membrane was damaged after treatment with 0.005 wt.% of free CUR in comparison with the control (A&B) and the CUR NPs (E&F).

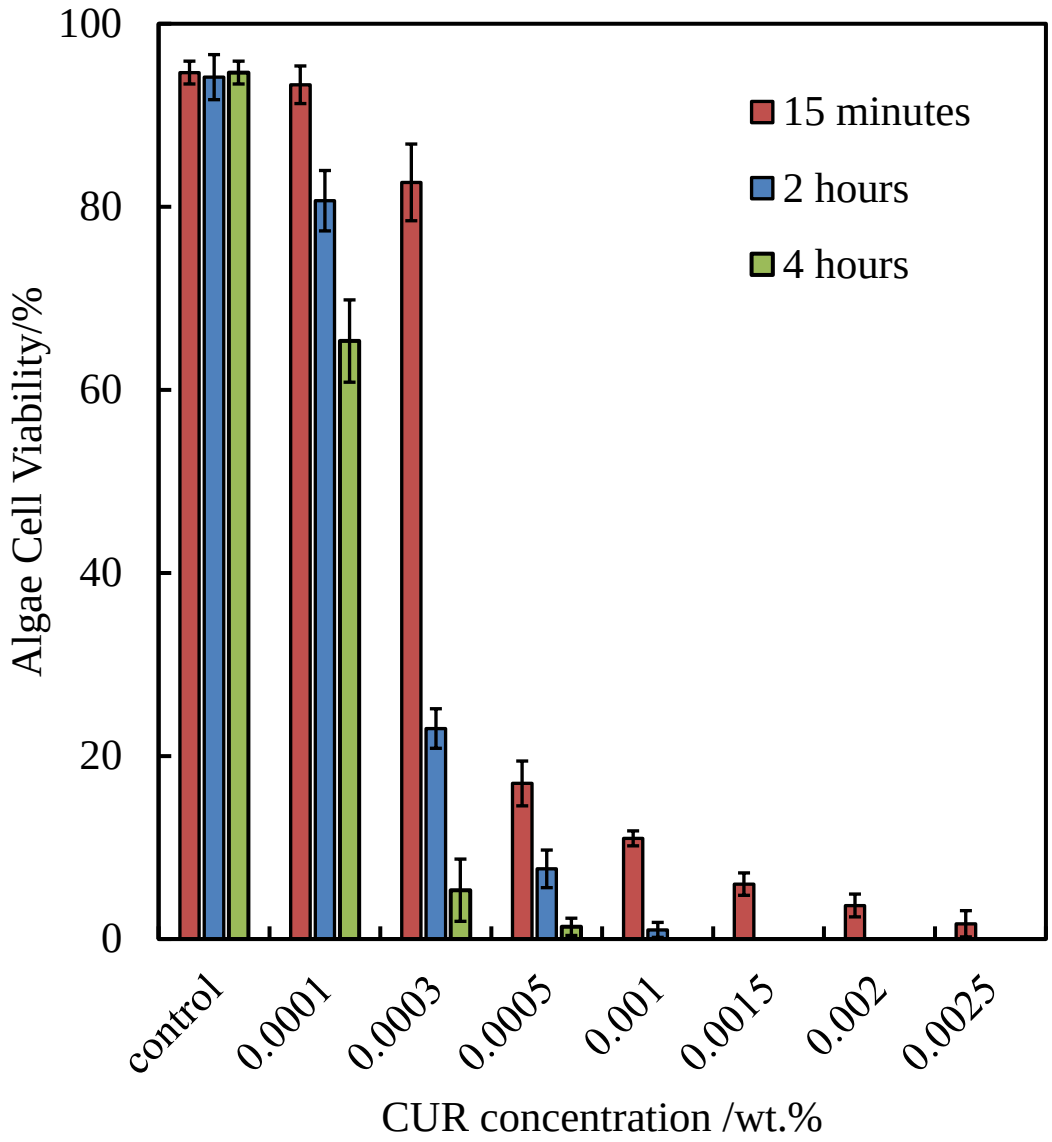

Figure 5.1: The viability of algal cells upon incubation with different concentrations of free CUR at room temperature upon 15 min., 2 h, and 4 h incubation time at pH 5.5 using the FDA assay, (n=3).

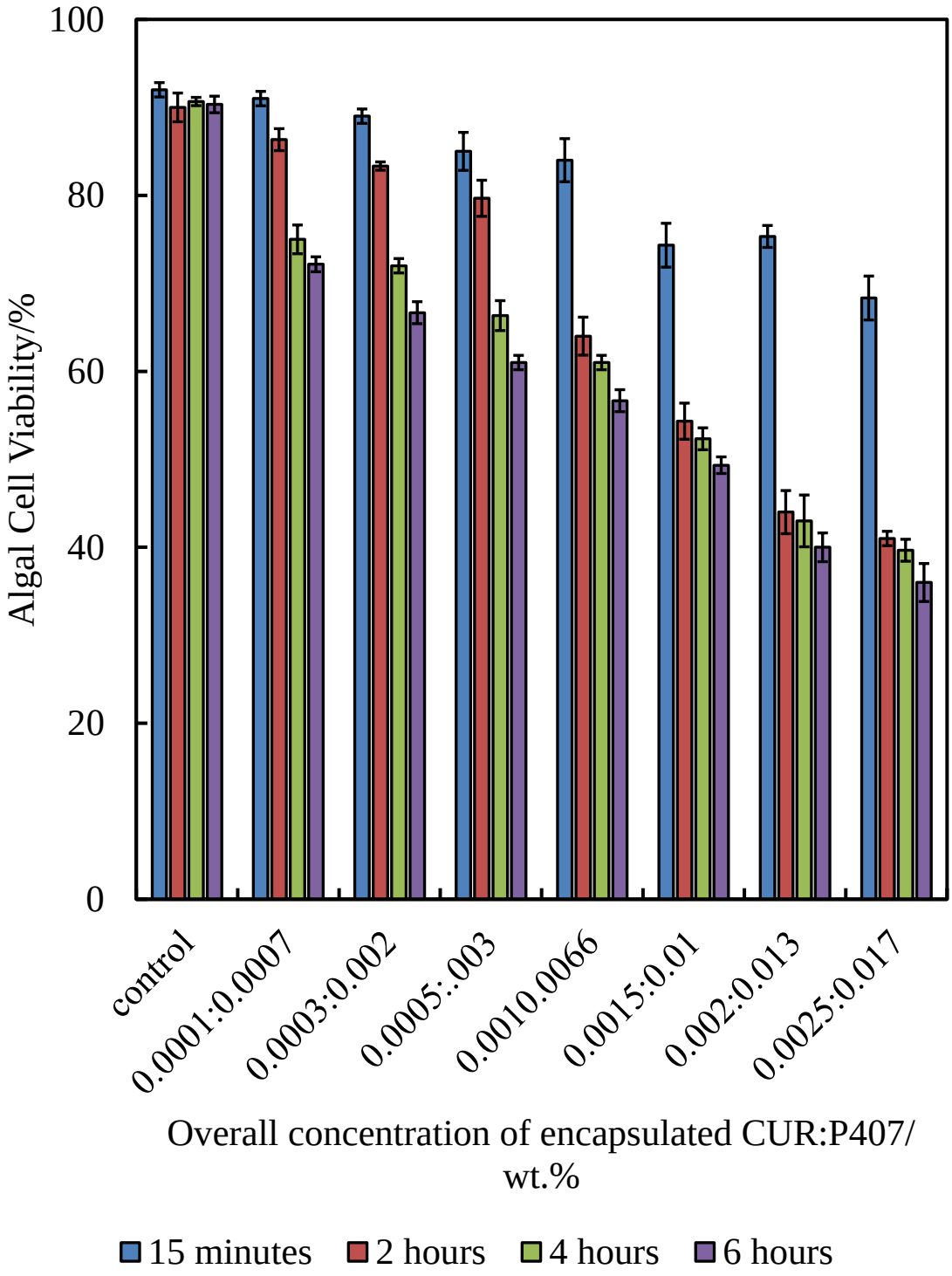

Figure 5.2: The viability of algal cells upon incubation with different concentrations of CUR NPs at room temperature upon 15 min., 2 h, 4 h, and 6 hours incubation time at pH 5.5 using FDA assay, (n=3).

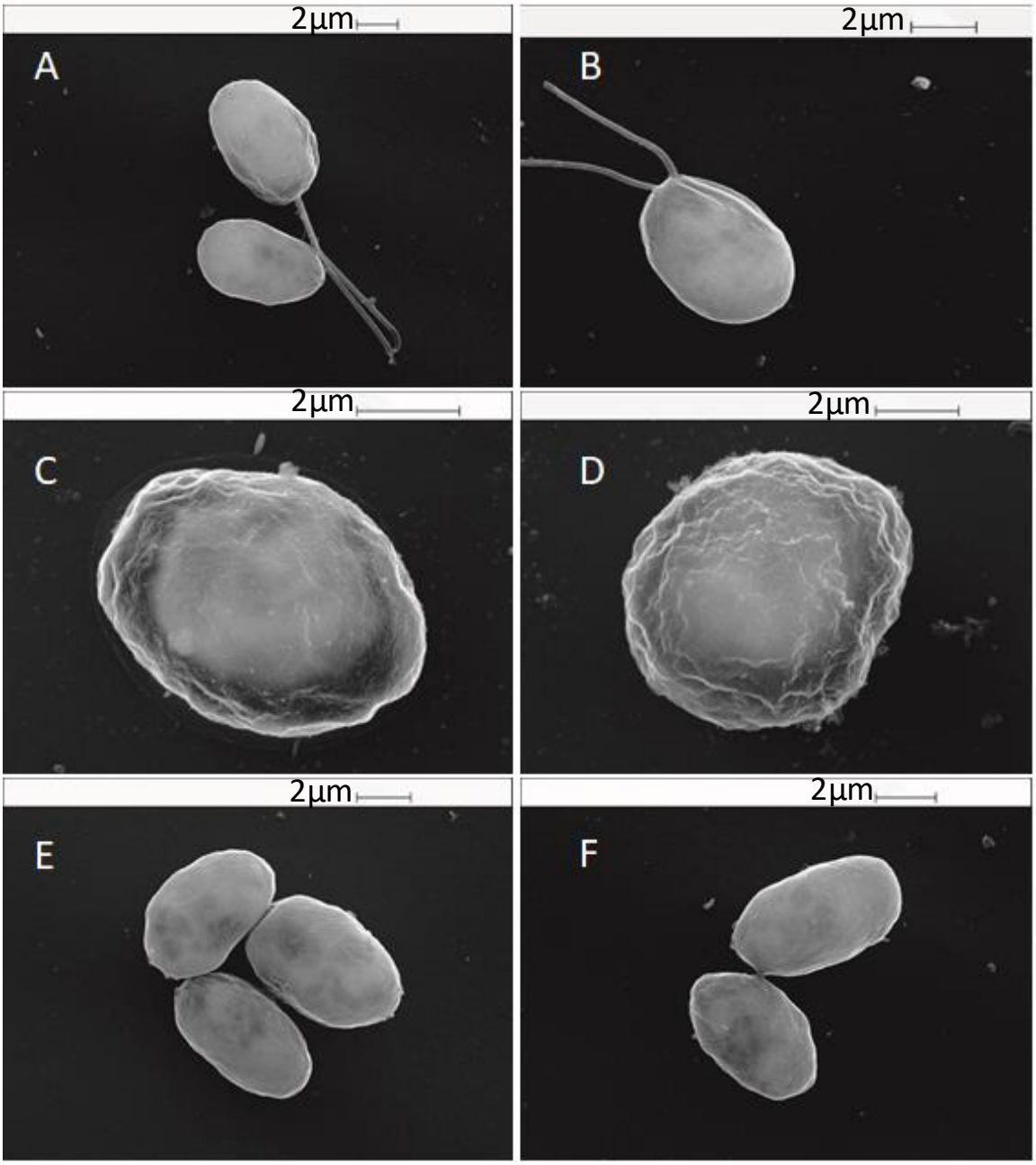

Figure 5.3: SEM images of algal cells. (A&B) A control sample of the algal cell and (C&D) algal cells that incubated with 0.005 wt.% free CUR after four hours of incubation, (E&F) algal cell incubated for four hours with 0.005 wt.% of CUR loaded shellac NPs.

5.1.2 The Antifungal Activity of CUR Loaded Shellac NPs on Yeast Cells

The antifungal effect of free CUR and CUR loaded shellac NPs was then studied at different concentrations and for a range of incubation times at pH 5.5 as shown in Figure 5.4 and Figure 5.5. As can be seen from Figure 5.4 the free CUR shows strong antifungal activity when incubated with baker's yeast cells. After 15 minutes the cell viability sharply reduced by half at 0.0005 wt.% in comparison with control viability which was 97%, and declined to 36%, 23%, 18%, and 16% at 0.001, 0.0015, 0.002, and 0.0025 wt.% free CUR, respectively. After 2 hours of incubation, the viability dropped from 97% for control to 16%, 10% and 5.5% at 0.0015 wt.%, 0.002 wt.%, and 0.0025 wt.% of free CUR, and after 4 hours all cells died at 0.002 wt.% and 0.0025 wt.%. The antifungal activity of CUR loaded shellac NPs was then studied as shown in Figure 5.5. The cell viability decreased but only slightly even after 6 hours of exposure (the viability only decreased to 62%, 58%, and 56% at 0.0015 wt.%, 0.002 wt.%, and 0.0025 wt.% of CUR NPs). This effect occurred for the same reasons described previously (the high hydrophobic-hydrophobic interaction between shellac molecules and CUR and the repulsion between the NPs and cell membrane). SEM images of the yeast cells can be seen in Figure 5.6. The cell treated with 0.005 wt.% of free CUR after 4 hours, the free CUR penetrated through the cell membrane and making holes, as can be seen in images(C&D) . While encapsulated CUR did not affect the yeast cells after 4 hours of incubation as can be seen in (E&F).

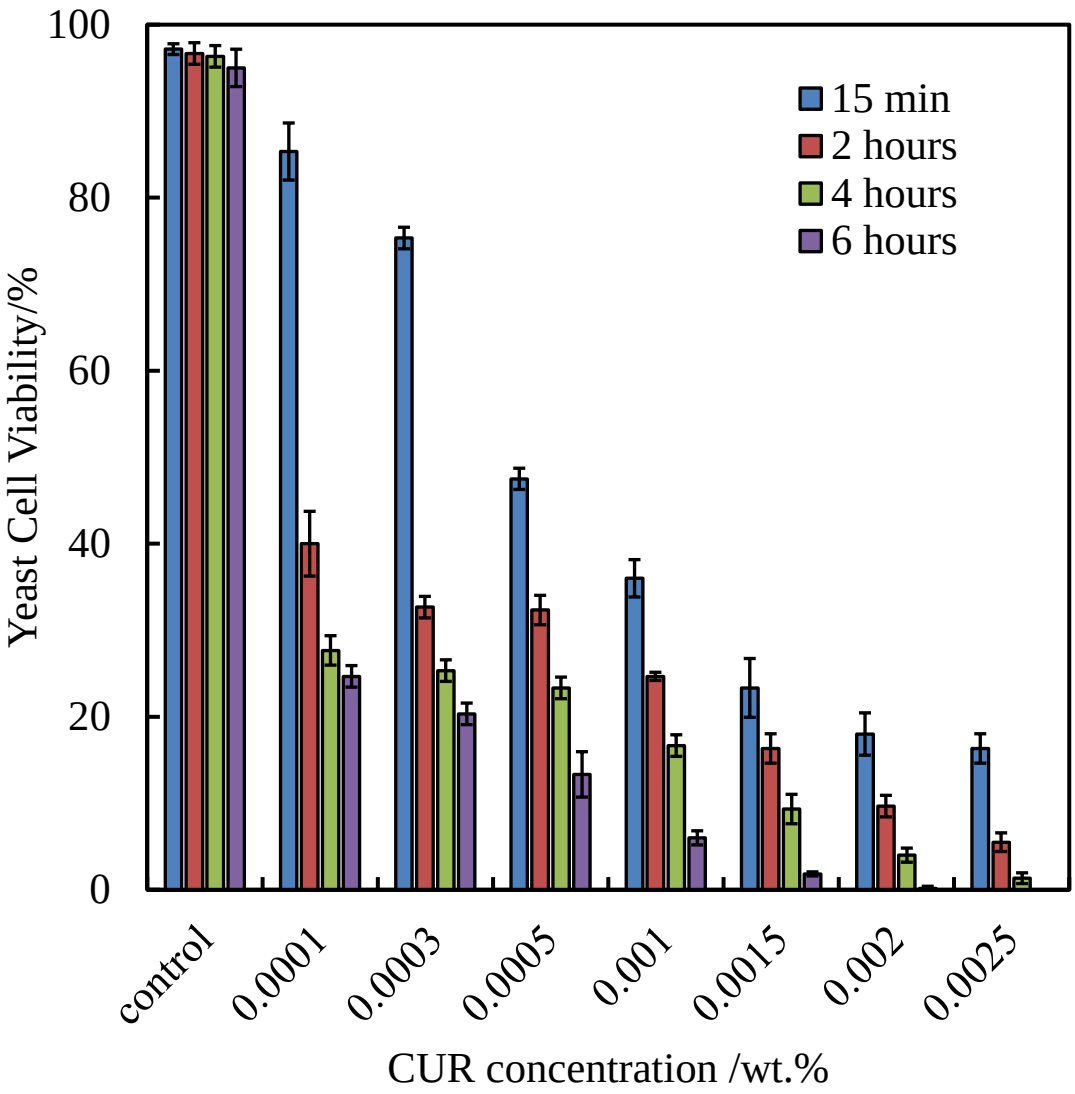

Figure 5.4: The viability of yeast cells upon incubation with varying concentrations of free CUR at room temperature upon 15 min., 2h, 4 h, and 6 hours incubation time at pH 5.5 using FDA assay, (n=3).

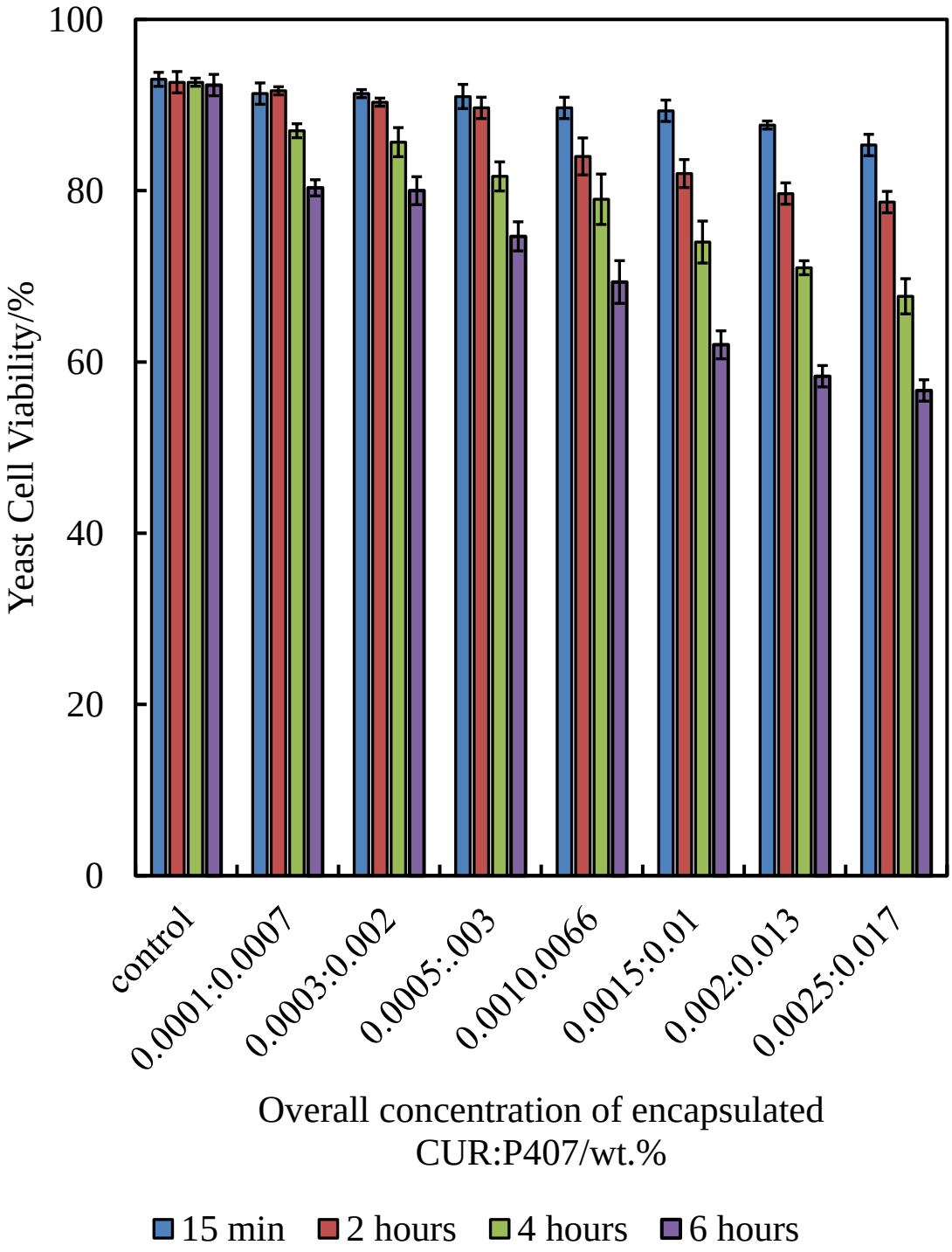

Figure 5.5: The viability of yeast cells upon incubation with varied concentrations of CUR loaded shellac NPs at room temperature upon 15 min., 2h, 4 h, and 6 hours incubation time at pH 5.5 using FDA assay, (n=3).

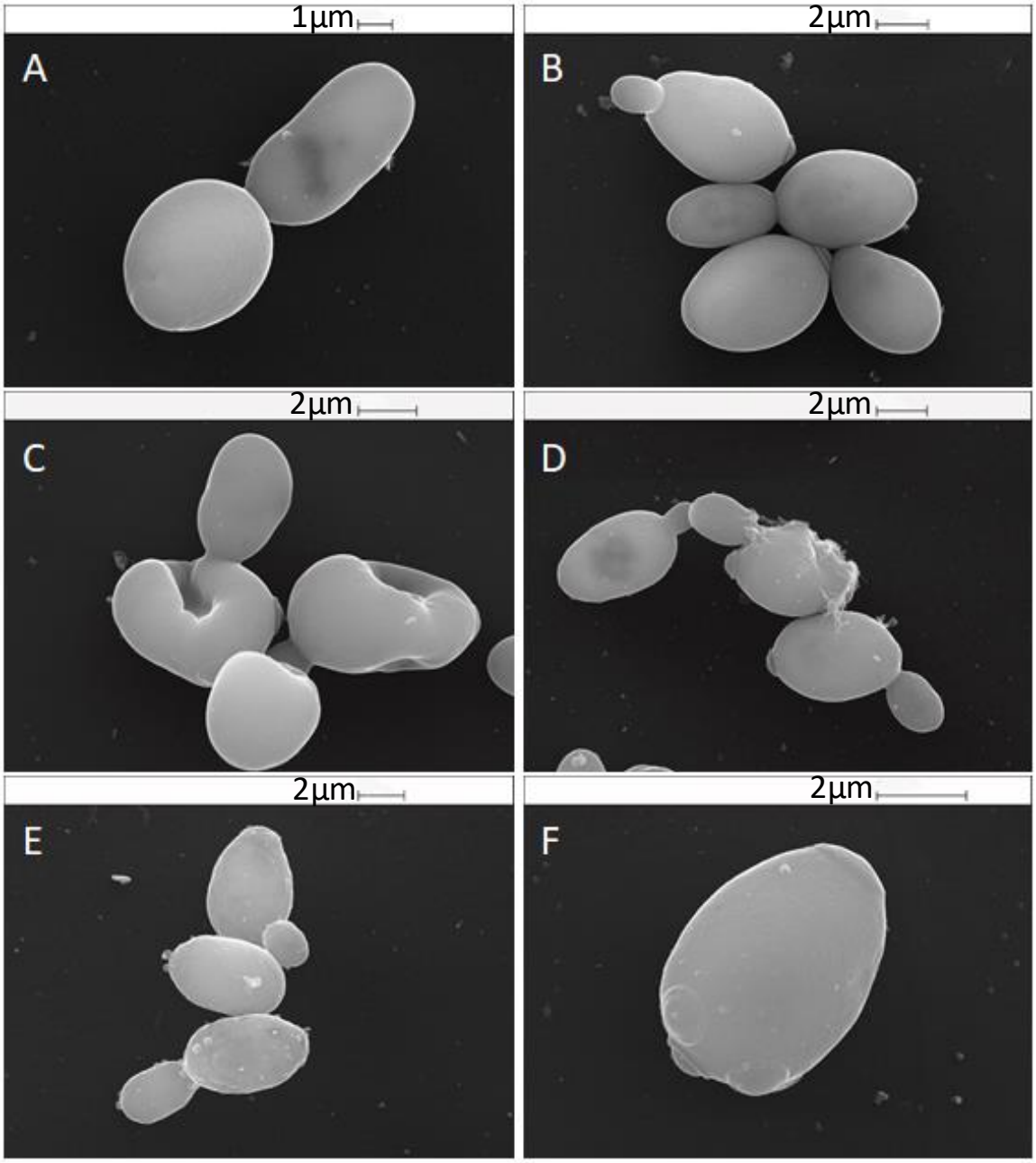

Figure 5.6: SEM images of yeast cells. (A&B) Control sample of yeast cell and (C&D) yeast cells that incubated with 0.005 wt.% free CUR after four hours of incubation, (E&F) yeast cell incubated for four hours with 0.005 wt.% of CUR loaded shellac NPs.

5.1.3 Antibacterial Activity of CUR Loaded Shellac NPs on *E.coli*

CUR has been reported to have antibacterial activity against many kinds of bacteria.[179, 413, 414] In this study CUR was encapsulated within shellac NPs then their effect on *E.coli* was compared with free CUR using bactiter luminescence assay. Figure 5.7 shows the effect of different concentrations of free CUR for 4 hours incubation on *E.coli* viability. CUR has a clear effect on this bacteria even at low concentrations, after 15 minutes of incubation the cell viability represented by luminescence decreased sharply from $41x10^5$ RLU as control to $9.5x10^5$ RLU, $7.5x10^5$ RLU, $6x10^5$ RLU, and $5.7x10^5$ RLU at (0.001, 0.0025, 0.005, 0.01) wt.% of free CUR. After 2 hours, the cell viability kept decreasing to be $3.5x10^5$ RLU, and $2.5x10^5$ RLU at 0.005 wt.% and 0.01 wt.% of CUR respectively. And after 4 hours of incubation, the *E.coli* viability has declined at all concentrations of CUR from 0.0001 wt.% to 0.01 wt.%. Figure 5.8 shows the effect of encapsulated CUR when incubated with *E.coli* for a period up to 4 hours. The antibacterial activity of CUR dropped after encapsulation for the same reasons as explained previously. SEM pictures reveal how free CUR effects the *E.coli* cells (C&D) in comparison with the control cells (A&B) while the encapsulated CUR was not showing any significant effect on the cells (E&F).

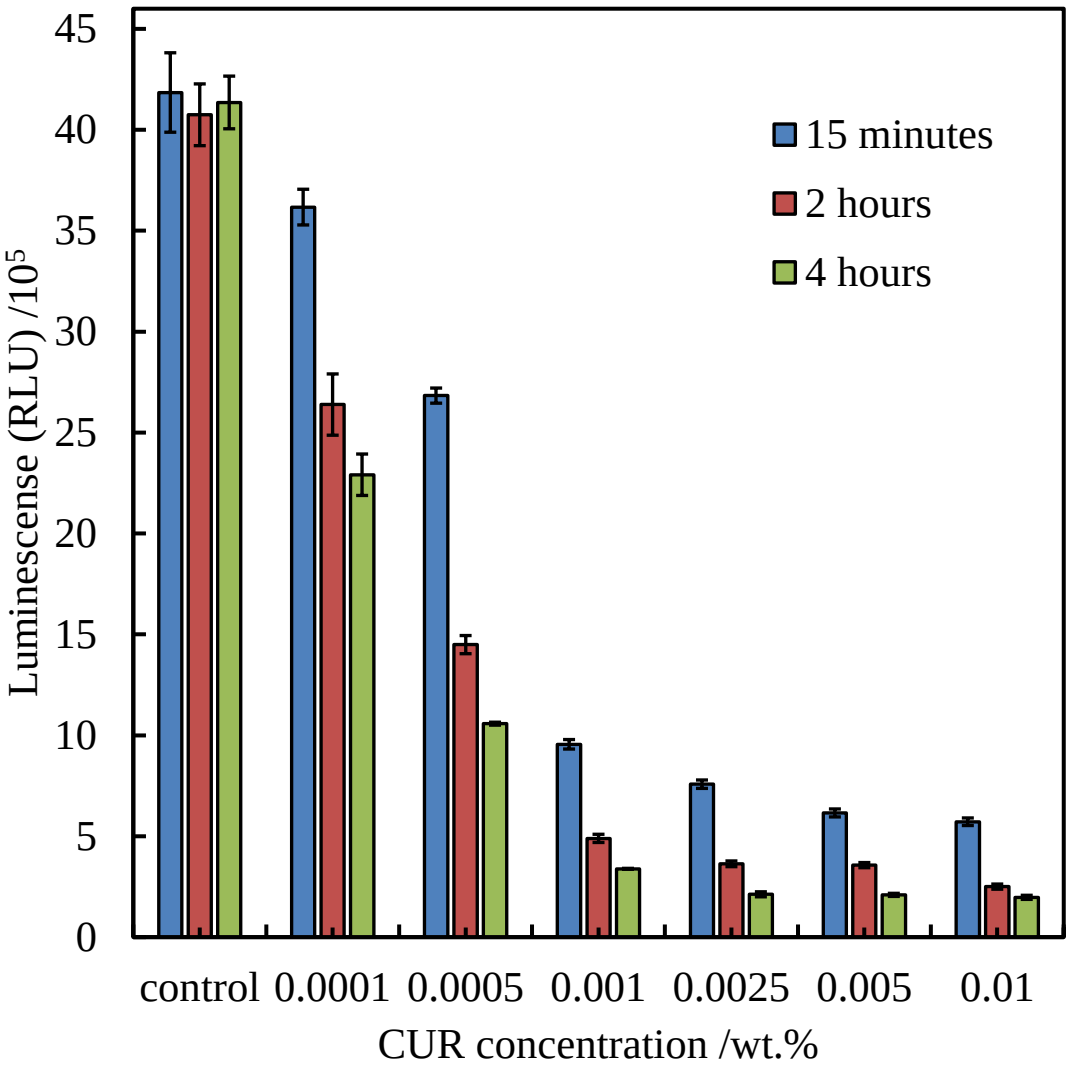

Figure 5.7: The relative luminescence unit representing the viability of *E.coli* cells incubated at pH 5.5 with different concentrations of free CUR at different incubation time of 15 min, 2 h, and 4 h at room temperature using bactiter luciferase reagent, (n=3).

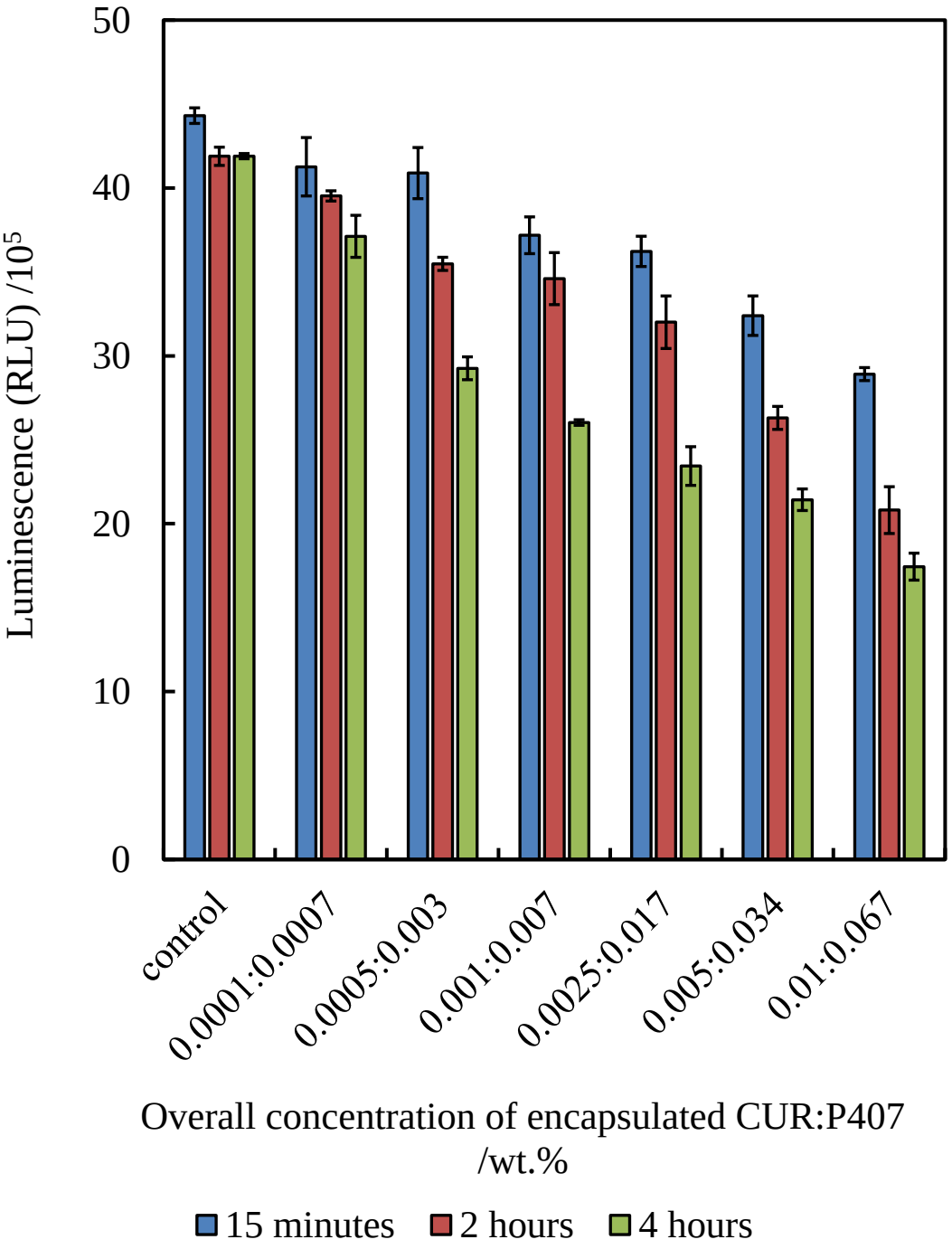

Figure 5.8: The relative luminescence unit which represents the viability of *E.coli* cells incubated at pH 5.5 with different concentrations of encapsulated CUR at different incubation time, 15 min, 2 h, and 4 h, at room temperature using bactiter luciferase reagent, (n=3).

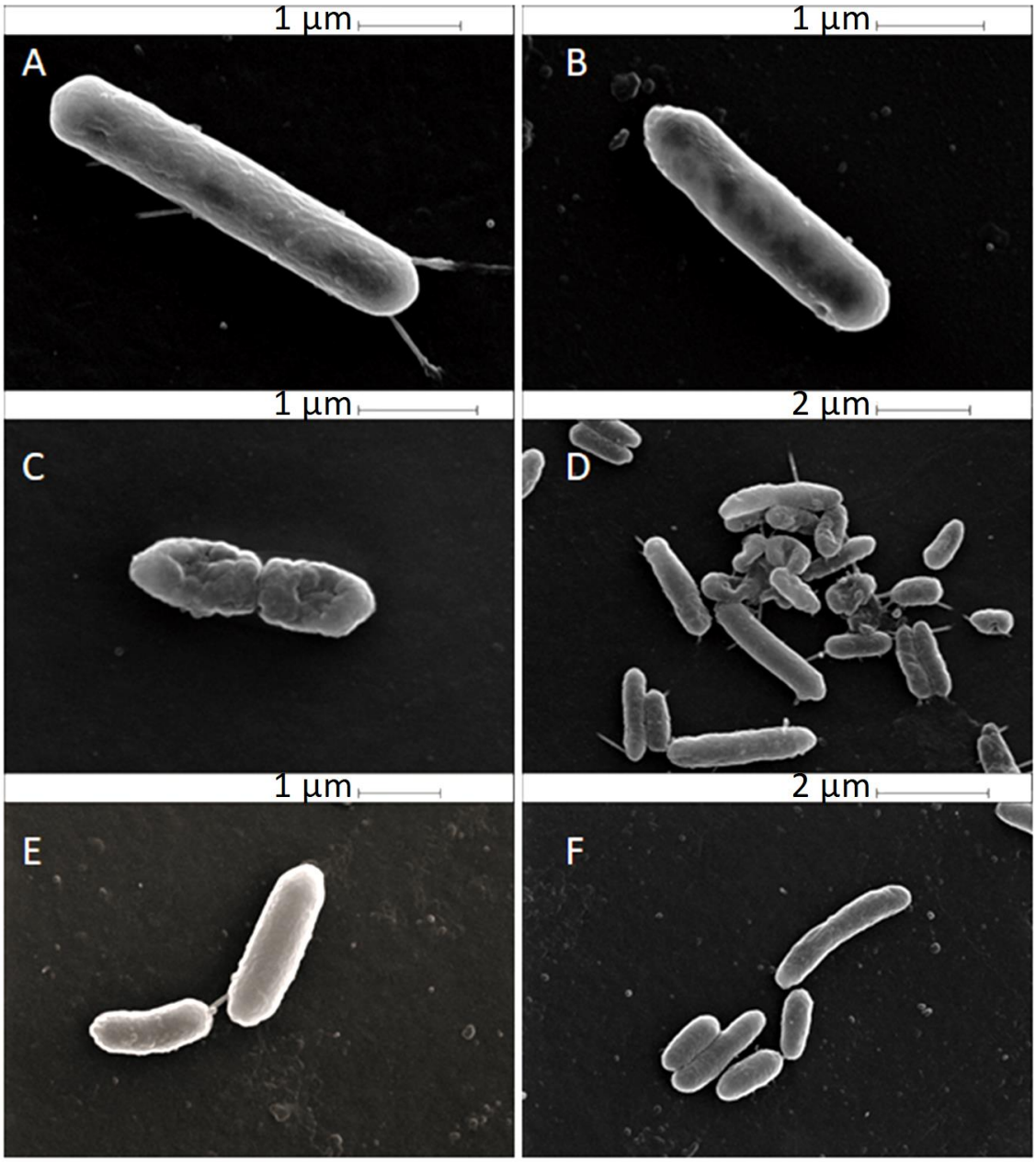

Figure 5.9: SEM images of *E.coli* cells. (A&B) Control samples of *E.coli* cell and (C&D) *E.coli* cells that incubated with 0.005 wt.% free CUR, (E&F) *E.coli* cell incubated with 0.005 wt.% CUR loaded shellac NPs. All cells were incubated for 4 hours at pH 5.5 at room temperature.

5.2 Cytotoxic Effect of Encapsulated CUR Coated with ODTAB on Microorganisms

In Chapter 4 the shellac NPs surface was coated with cationic electrolyte ODTAB to reverse the charge of the NPs to be positive, and this was shown to be effective. The next sections describe the cytotoxic effect of encapsulated CUR after being coated with ODTAB on algae, yeast and *E.coli*. The cytotoxic effect of pure ODTAB and ODTAB coated shellac NPs (without antimicrobial) are given in section 4.3.

5.2.1 Cytotoxic Effect of Encapsulated CUR Coated ODTAB on Algal Cells

Figure 5.10 shows the antimicrobial activity of different concentrations CUR loaded shellac NPs coated with ODTAB on algal cells at different incubation time at room temperature. The figure shows that CUR-NPs coated with ODTAB have an extremely antimicrobial effect on algae after 15 minutes of incubation with the cell viability decreasing from 94% to 34%, 5%, and 1.5% at 0.0003, 0.0005, and 0.001 wt.% CUR-NPs coated with 0.0005, 0.0008 and 0.0017 wt.% ODTAB respectively. After 2 hours of incubation, all the cells died at 0.0005 wt.% of CUR-NPs coated with 0.0008 wt.% ODTAB and higher concentrations.

Figure 5.11 compares the antimicrobial activities of the 0.0005 wt.% CUR-NPs, 0.0005 wt.% free CUR, 0.0042 wt.% shellac NPs coated with 0.0008 wt.% ODTAB, 0.0005 wt.% CUR-NPs coated with 0.0008 wt.% ODTAB, and 0.0008 wt.% pure ODTAB. This clearly shows that coating the CUR NPs with the ODTAB is effective. The antimicrobial activity of CUR coating with ODTAB was increased due to the positive charge of the complex; this proves the fact that CUR as nano acts as antimicrobial better than free which is more soluble within shellac NPs even at few released CUR amount. Figure 5.12 shows the SEM pictures of the microalgal cell after incubation with (0.005 and 0.001) wt.% CUR loaded shellac NPs coated with (0.0017 and 0.008) wt.% ODTAB for 2 hours. These show how the NPs encapsulated CUR coated with ODTAB accumulate around the cell in abundance due to the positive charge of the NPs surface.

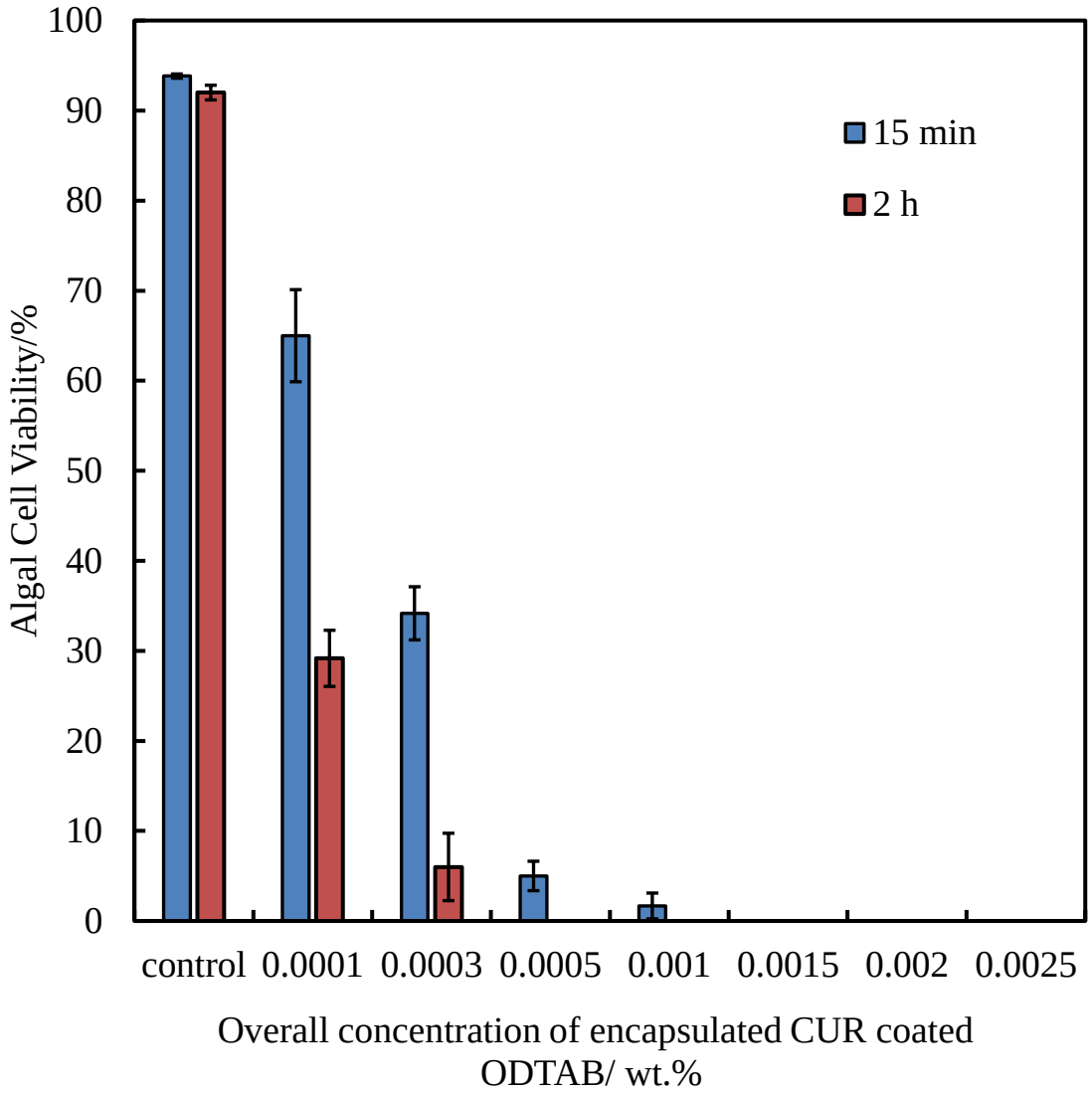

Figure 5.10: The viability of algal cells upon incubation at pH 5.5 with different concentrations of CUR loaded shellac NPs coated with ODTAB at room temperature at different incubation time. The solutions were prepared from 0.03 wt.% CUR NPs stock solution coated with 0.05 wt.% ODTAB using FDA assay, (n=3).

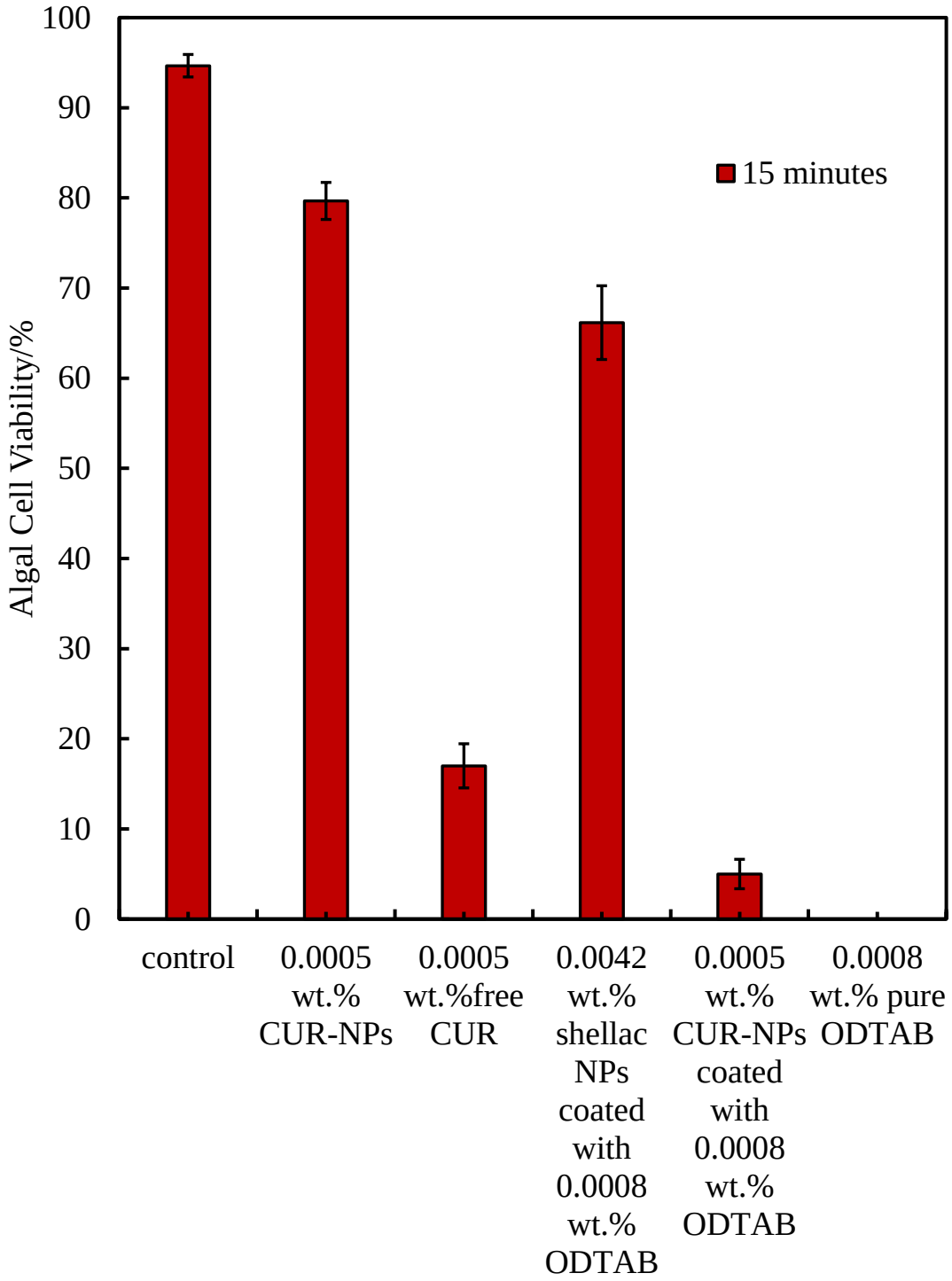

Figure 5.11: The algal cells viability upon incubation with 0.0005 wt.% CUR-NPs, 0.0005 wt.% free CUR, 0.0042 wt.% shellac NPs coated with 0.0008 wt.% ODTAB, 0.0005 wt.% CUR-NPs coated with 0.0008 wt.% ODTAB, and 0.0008 wt.% pure ODTAB at pH 5.5 and at room temperature for 15 minutes incubation using FDA assay, (n=3).

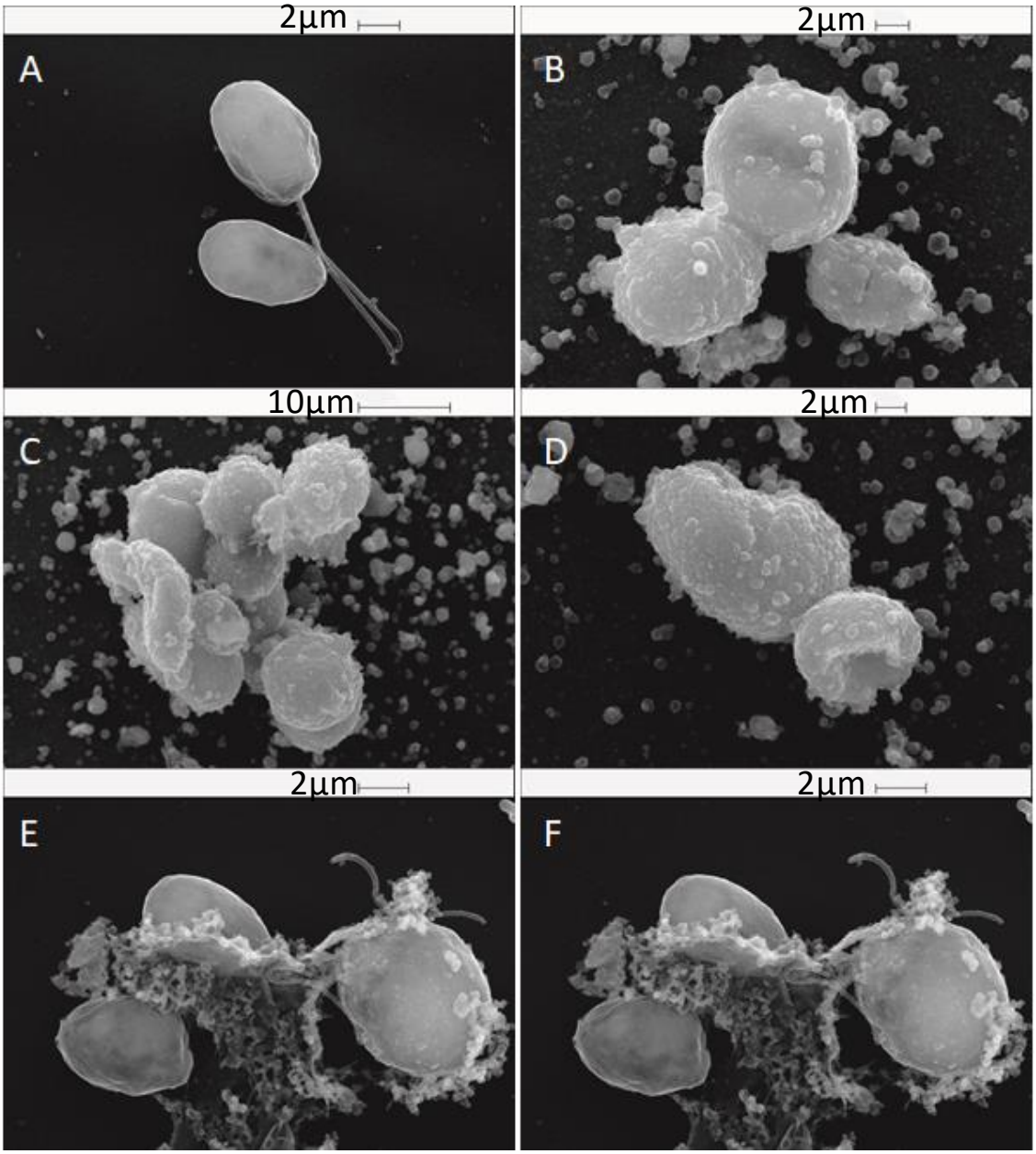

Figure 5.12: SEM images of *C. reinhardtii* cells. (A) A control sample of the *C. reinhardtii* microalgae cells. (B, C, and D) *C. reinhardtii* microalgae cells incubated with 0.005 wt.% CUR loaded shellac NPs coated with 0.008 wt.% ODTAB, (E&F) *C. reinhardtii* microalgae cells incubated with 0.001 wt.% CUR loaded shellac NPs coated with 0.0017 wt.% ODTAB after 2 hours incubation time at room temperature.

5.2.2 Cytotoxic Effect of Encapsulated CUR Coated ODTAB on Yeast Cells

The antifungal activity of CUR loaded shellac NPs coated with ODTAB was examined on baker's yeast cells at different incubation time at pH 5.5. As can be seen in Figure 5.13 that yeast cell viability upon incubation with different concentrations of CUR loaded shellac NPs coated with ODTAB has sharply decreased. After 15 minutes exposure time, the cell viability severely decreased from 98% to 12% and 2.5% at 0.0005 and 0.001 wt.% of CUR loaded shellac NPs coated with 0.0008 and 0.0017 wt.% ODTAB, respectively, and at higher concentrations of CUR, all cells died. After 2 hours the cell viability reduced hugely from 98% for the control to 6%, 4%, and 2 % at 0.0001, 0.0003, 0.0005 wt.% CUR loaded shellac NPs coated with 0.00017, 0.0005, and 0.0008 wt.% ODTAB, respectively. In Figure 5.14 are compared the antifungal activities of 0.0005 wt.% CUR-NPs, 0.0005 wt. % free CUR, 0.0042 wt.% shellac NPs coated with 0.0008 wt.% ODTAB, 0.0005 wt.% CUR-NPs coated with 0.0008 wt.% ODTAB, and 0.0008 wt.% pure ODTAB. As observed previously, the antimicrobial activity of CUR-NPs increased after coating with ODTAB. Figure 5.15 shows the SEM images of the yeast cells incubated with 0.005 wt.% of CUR loaded shellac NPs coated with 0.008 wt.% for 1 hour, the NPs are attracted to the cells and surround the membrane due to a positive charge.

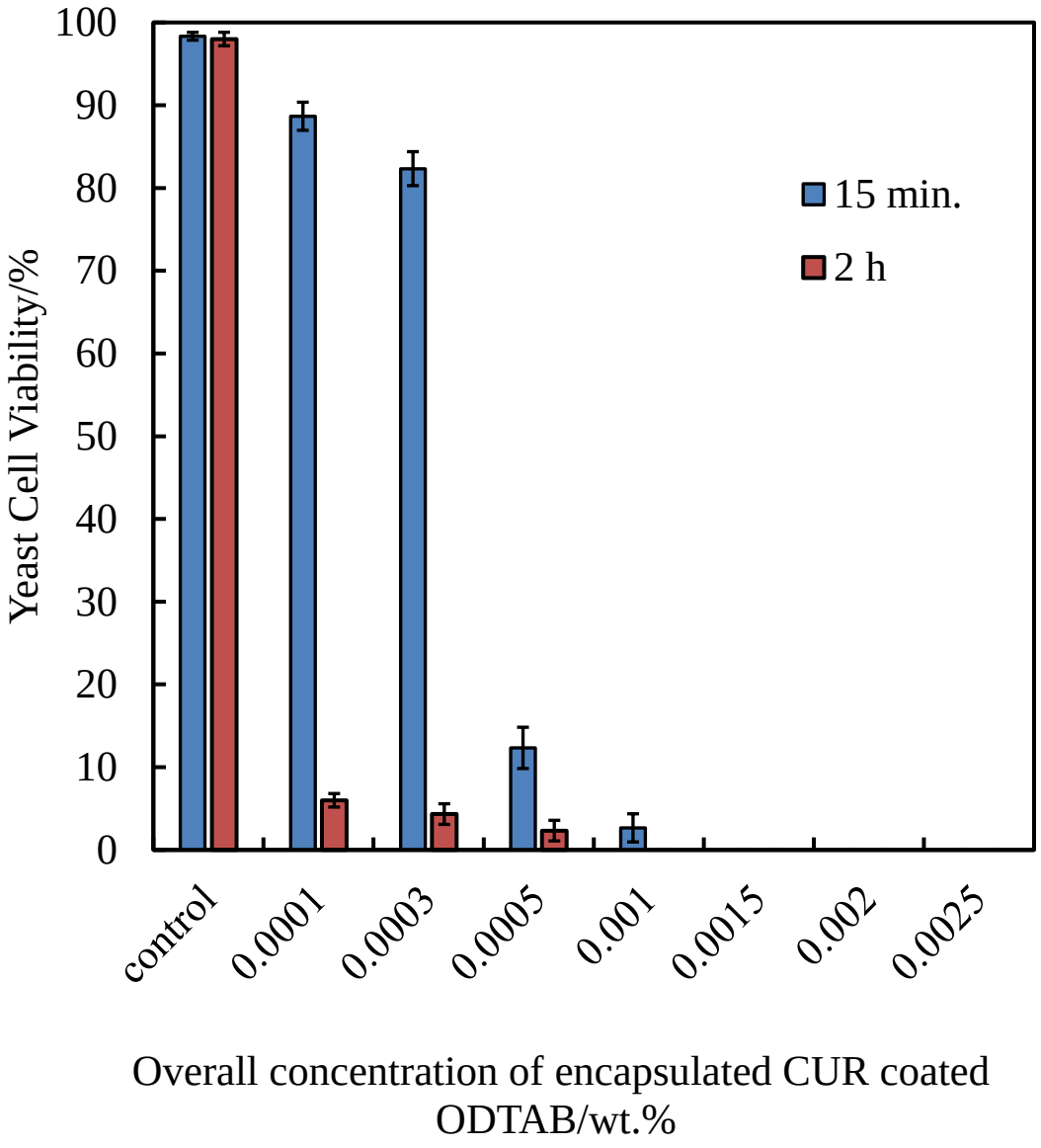

Figure 5.13: The cytotoxic effect of different concentrations of CUR loaded shellac NPs coated with ODTAB upon incubation with yeast cells at room temperature at 15 min, and 2 hours using FDA assay. All nanoparticles suspensions were prepared from stock solution of 0.03 wt.% CUR-NPs coated with 0.05 wt.% ODTAB and mixed with cells at pH 5.5 using FDA assay, (n=3).

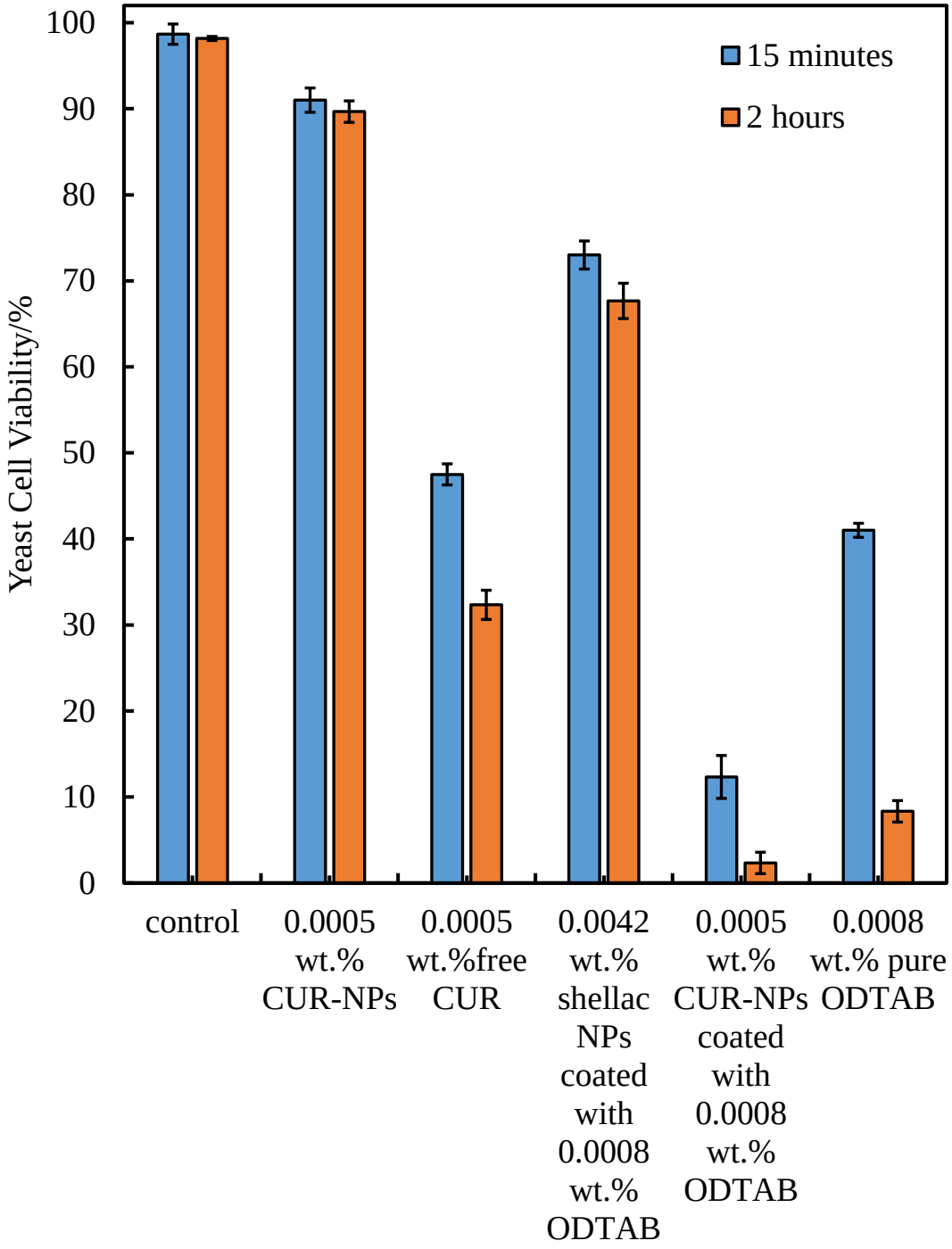

Figure 5.14: Yeast cell viability upon incubation with 0.0005 wt.% CUR-NPs, 0.0005 wt.% free CUR, 0.0042 wt.% shellac NPs coated with 0.0008 wt.% ODTAB, 0.0005 wt.% CUR-NPs coated with 0.0008 wt.% ODTAB, and 0.0008 wt.% pure ODTAB at pH 5.5 and at room temperature using FDA assay, (n=3).

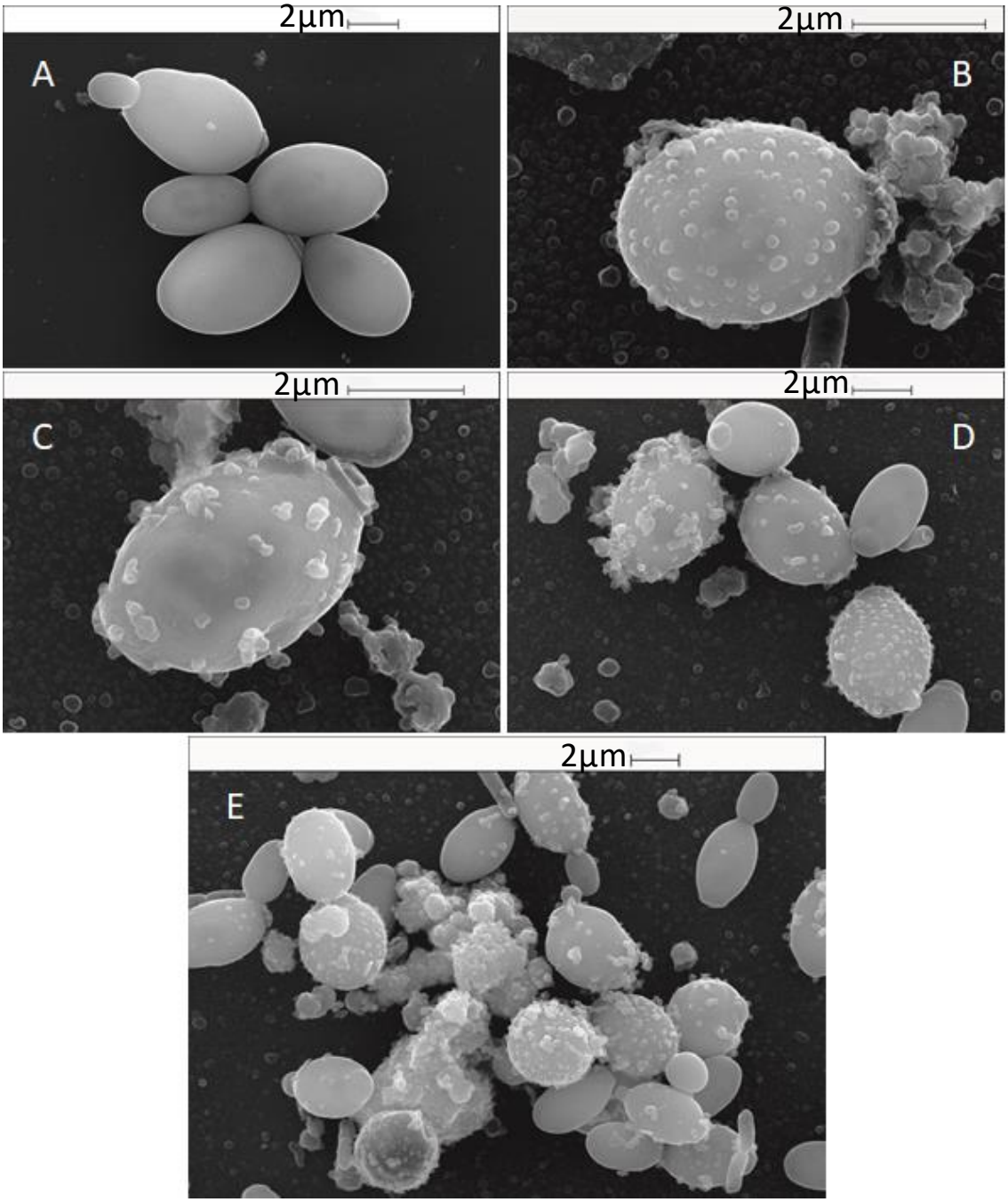

Figure 5.15: SEM images of yeast cells. (A) A control sample of the yeast cells. (B, C, D and E) yeast cells incubated with 0.005 wt.% CUR loaded shellac NPs coated with 0.008 wt. % ODTAB after 1 hour incubation at room temperature.

5.2.3 Cytotoxic Effect of Encapsulated CUR Coated with ODTAB on *E.coli* Cells

The antibacterial activity of the CUR-NPs after coating with ODTAB was then tested on *E.coli* cells at different incubation time and pH 5.5 as can be seen in Figure 5.16. The cell viability decreased gradually after 15 minutes incubation, while after 2 hours the antibacterial activity of CUR-NPs coated with ODTAB increased noticeably and the cell viability reduced from 39 $x10^5$ RLU as control to (6, 4, and 2) $x10^5$ RLU at 0.0025, 0.005, and 0.01wt.% CUR-NPs coated with 0.004, 0.008, and 0.017 wt.% ODTAB. After 4 hours the cell viability declined considerably from 40 $x10^5$ RLU for the control to be 2 $x10^5$ RLU at 0.01 wt.%, CUR-NPs coated with 0.017 wt.% ODTAB. Figure 5.17 shows a comparison among all components that were used to formulate the CUR-NPs coated with ODTAB, as it can be seen that free CUR showed more antibacterial action than CUR-NPs and CUR-NPs coated with ODTAB and this belongs to the slow released of CUR from the shellac NPs due to the strong interaction between them. The surface morphology of *E.coli* cells incubated with 0.001 and 0.005 wt.% CUR-NPs coated with 0.0017 and 0.008 wt.% ODTAB was examined using scanning electron microscopy as shown in Figure 5.18. It can be seen that the CUR loaded shellac NPs coated with ODTAB were strongly attracted to the cell membrane but did not affect as the free CUR did due to the slow release of CUR which makes it sustain longer within shellac NPs.

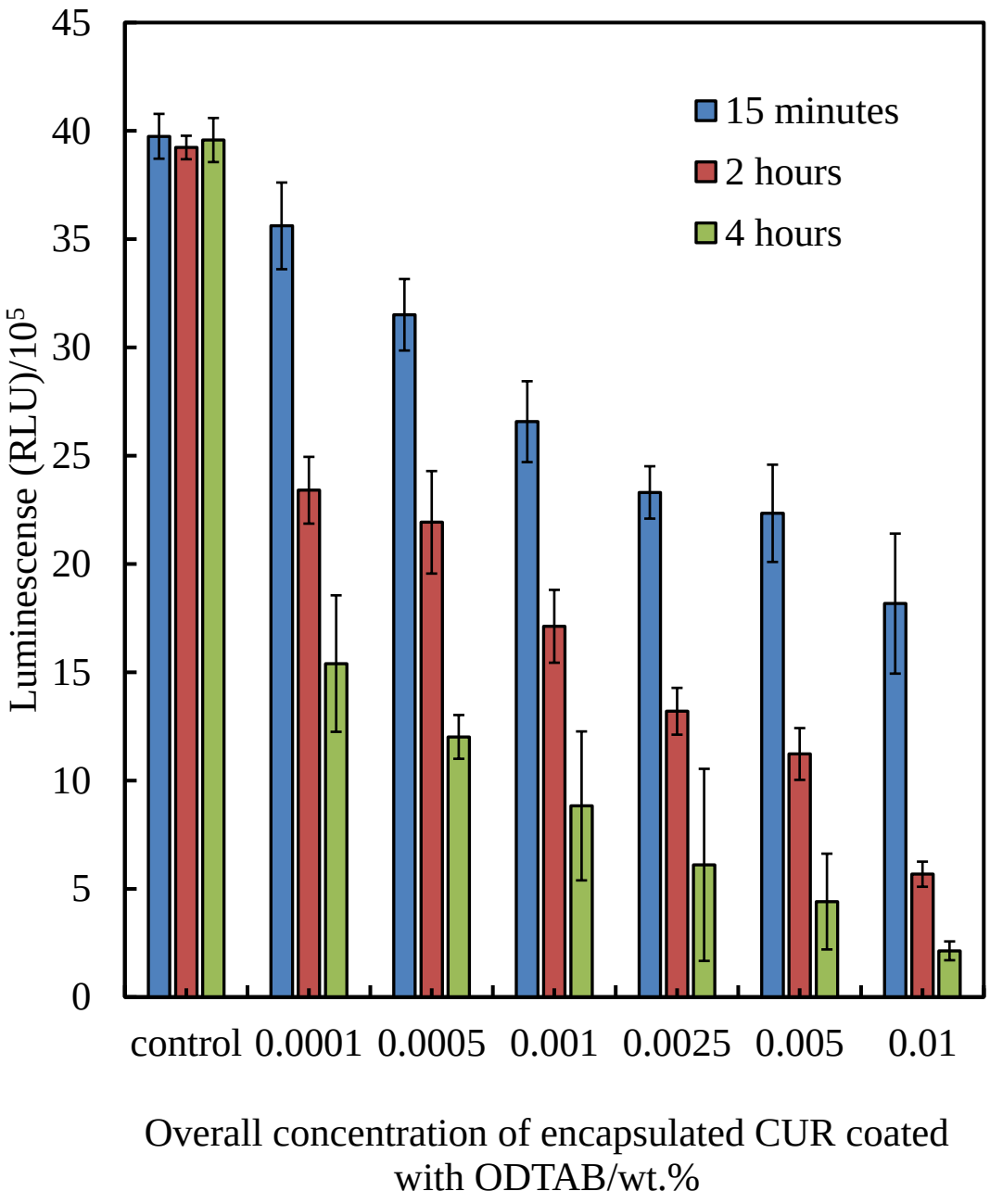

Figure 5.16: The antimicrobial activity of different concentrations of CUR loaded shellac NPs coated with ODTAB against *E.coli* cells at 15 min, 2 h, and 4 h. These solutions were prepared from a stock solution of 0.03 wt.% CUR loaded shellac NPs coated with 0.05 wt.% ODTAB, (n=3).

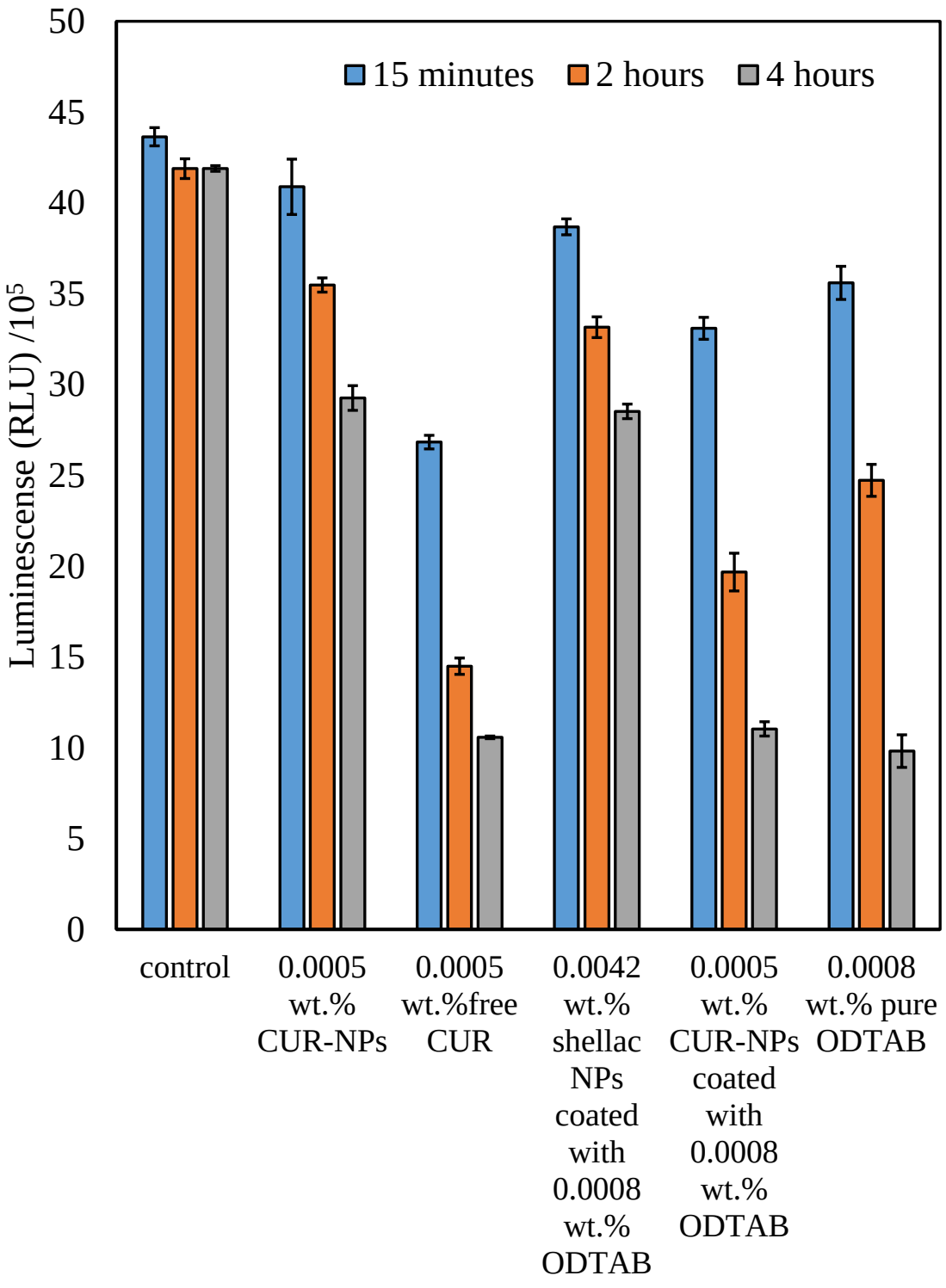

Figure 5.17: The antimicrobial activity of 0.0005 wt.% CUR loaded shellac NPs coated with 0.0008 wt.% ODTAB towards *E.coli* cells as a function of both the antimicrobial activity of free and shellac NPs encapsulated CUR in regards to the cytotoxic effect of pure ODTAB and ODTAB coated shellac NPs. The incubation was also achieved through incubating each concentration with a fixed amount of *E.coli* cells at pH 5.5 at room temperature using bactiter luciferase assay, (n=3).

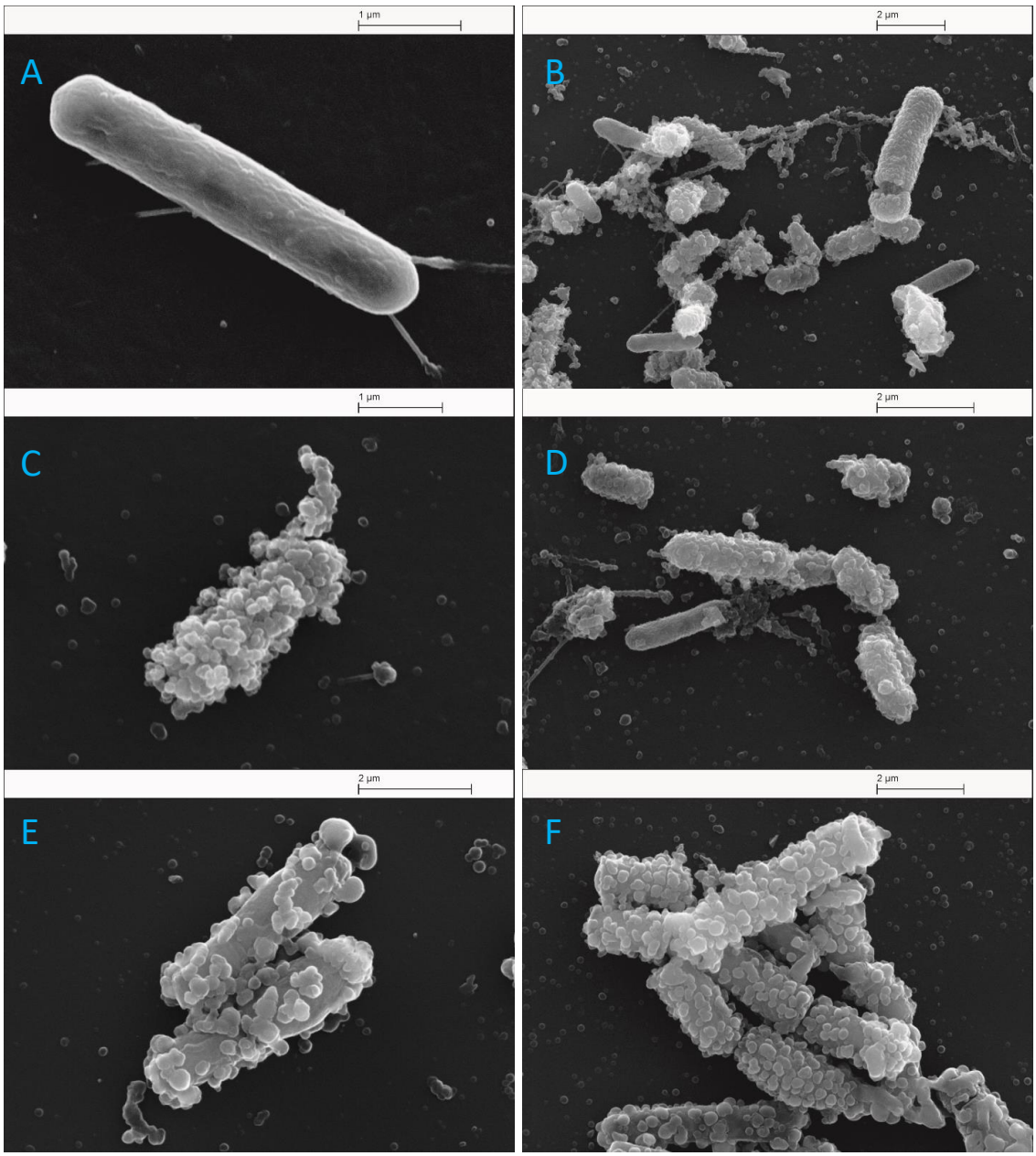

Figure 5.18: SEM images of *E.coli* cells. (A) Control sample of *E.coli* cells. (B, C, and D) *E.coli* cells incubated with 0.001 wt.% CUR loaded shellac NPs coated with 0.0017 wt. % ODTAB, (E&F) *E.coli* cells incubated with 0.005 wt.% CUR loaded shellac NPs coated with 0.008 wt. % ODTAB. All cell were incubated at pH 5.5 for 2 hours at room temperature.

5.3 The Cytotoxic Effect of VCM Loaded Shellac NPs on Microorganisms

The same experiments were carried out on VCM which was encapsulated within shellac NPs at pH 6 with 87.5% of encapsulation efficiency and average particle size of 80±24 nm.

5.3.1 The Cytotoxic Effect of Encapsulated VCM on Microalgae Cells

The antialgal activities of free vancomycin and VCM loaded shellac NPs were studied on microalgae at different incubation times and at room temperature to examine their effects on C. reinhardtii cells as presented in Figure 5.19 and Figure 5.20. Figure 5.19 shows that when various concentrations of VCM up to 0.1 wt.% were incubated with algae, the viability steadily declined from 0.001 wt.% to 0.1 wt.% for free VCM, after 6 hours of incubation it decreased by about 50% at the highest concentration of VCM. As would be expected the encapsulated VCM showed lower activity after loading it within shellac NPs as is clear in Figure 5.20. After 4 hours incubation of the cells with different concentrations of VCM loaded shellac NPs, the cell viability did decrease slightly by about 10% at 0.05 wt.% of VCM. After 6 hours, the cell viability dropped by 15-20 %. The low cytotoxic activity of VCM is contributed to the fact that VCM is gram-positive antibacterial more than gram-negative antibacterial,[415, 416] and the reason why the antimicrobial activity decreased after loading VCM within shellac NPs is because of the repulsion between negative shellac NPs and the negative cell membrane which does not allow VCM to be released near the cell membrane. The SEM pictures for C. reinhardtii cells in Figure 5.21 display that the free VCM caused damage to the membrane of the cells whereby cells have shrunk and appear wrinkled (B&C) in comparison with control sample as shown in (A&B), while the effect of VCM loaded shellac NPs on the cell membrane of algae seems less as in pictures (E&F).

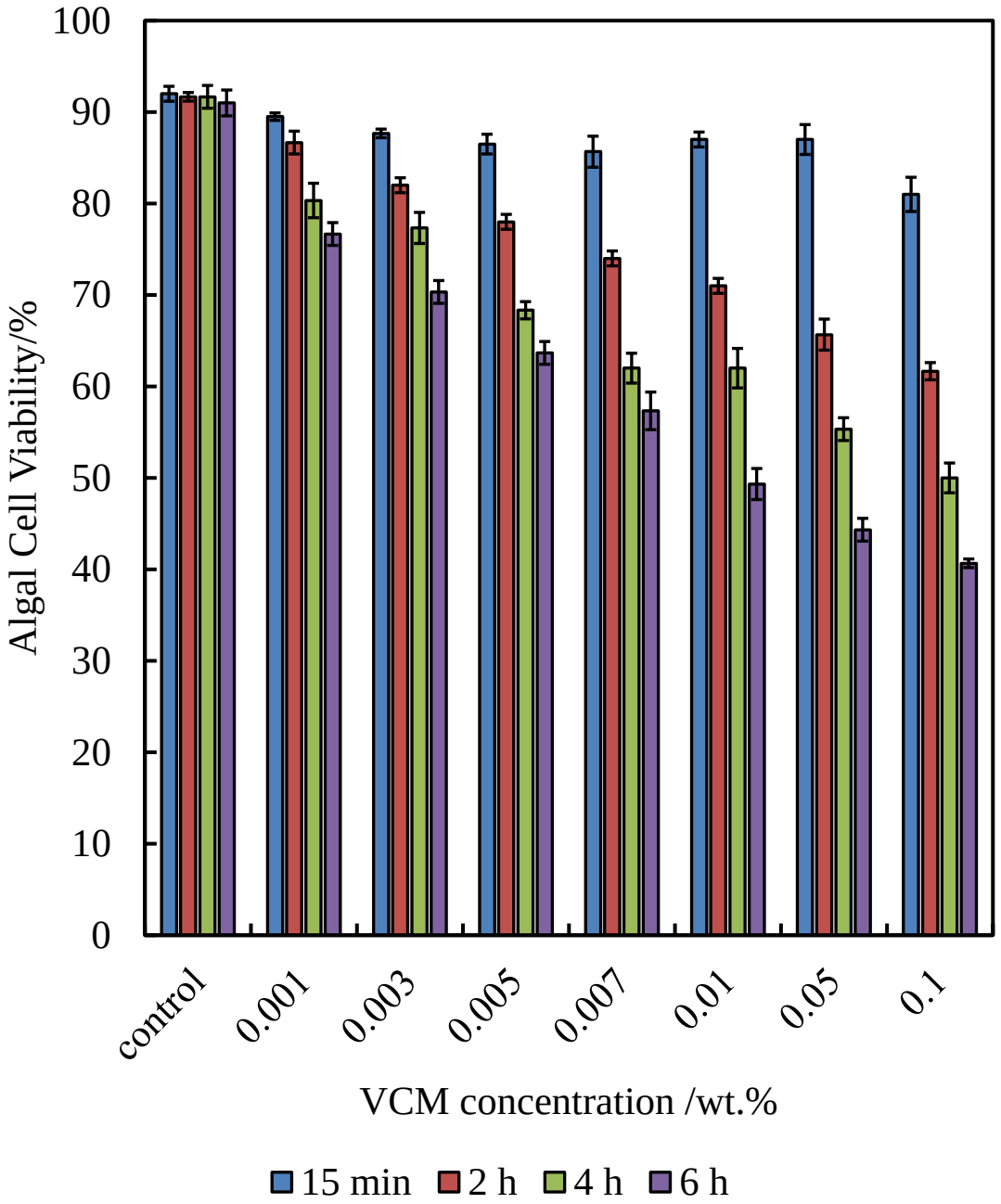

Figure 5.19: The viability of *C. reinhardtii* cells incubated with solutions of varied concentrations of free vancomycin at incubation times of 15 min, 2 h, 4 h, and 6h, using FDA assay. The cell viability measured by means of cell counter instrument, (n=3).

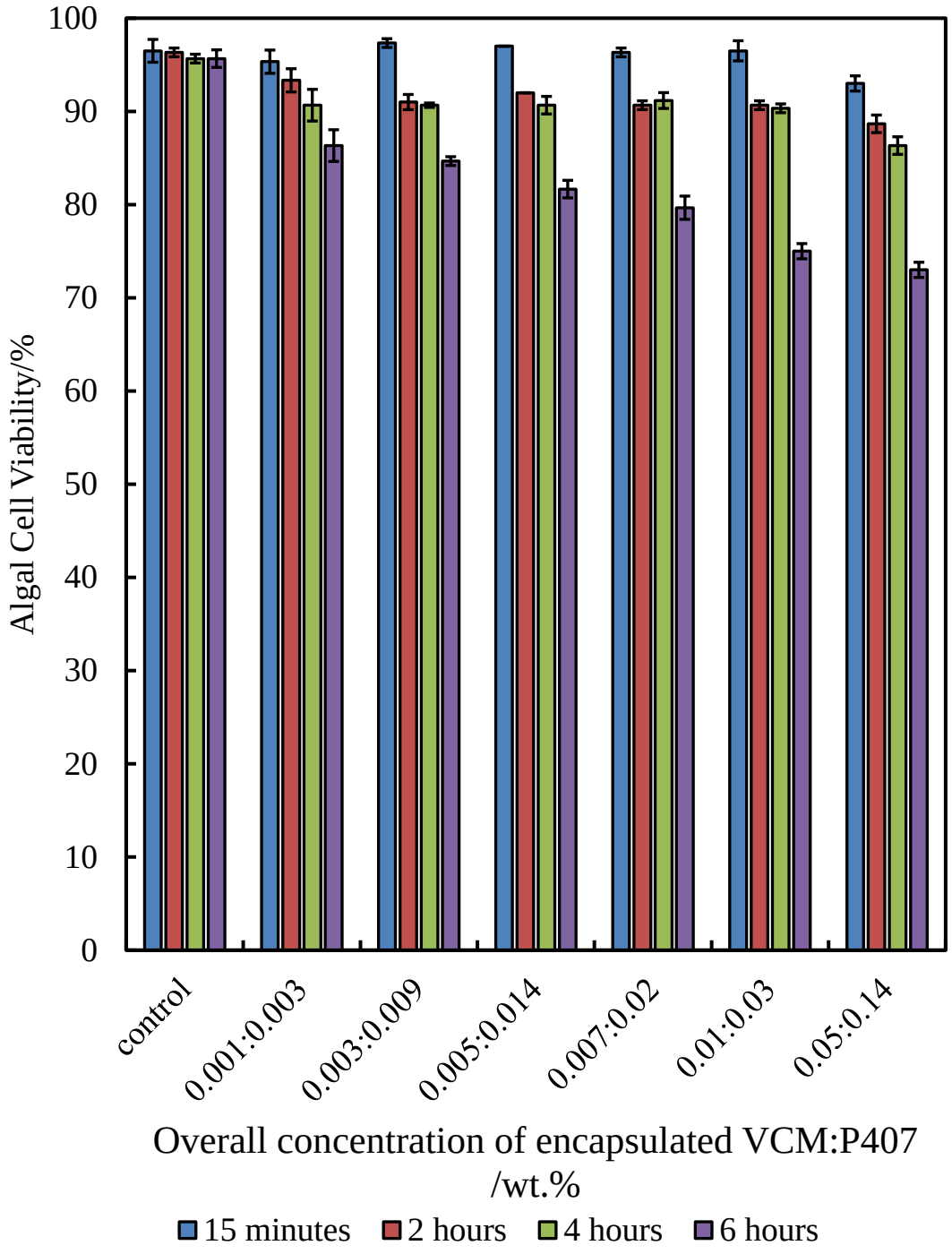

Figure 5.20: The viability of *C. reinhardtii* cells incubated with solutions of varied concentrations of vancomycin loaded shellac NPs at different incubation times, 15 min, 2 h, 4 h, and 6 h, using FDA assay, cell viability measured by means of cell counter instrument, (n=3).

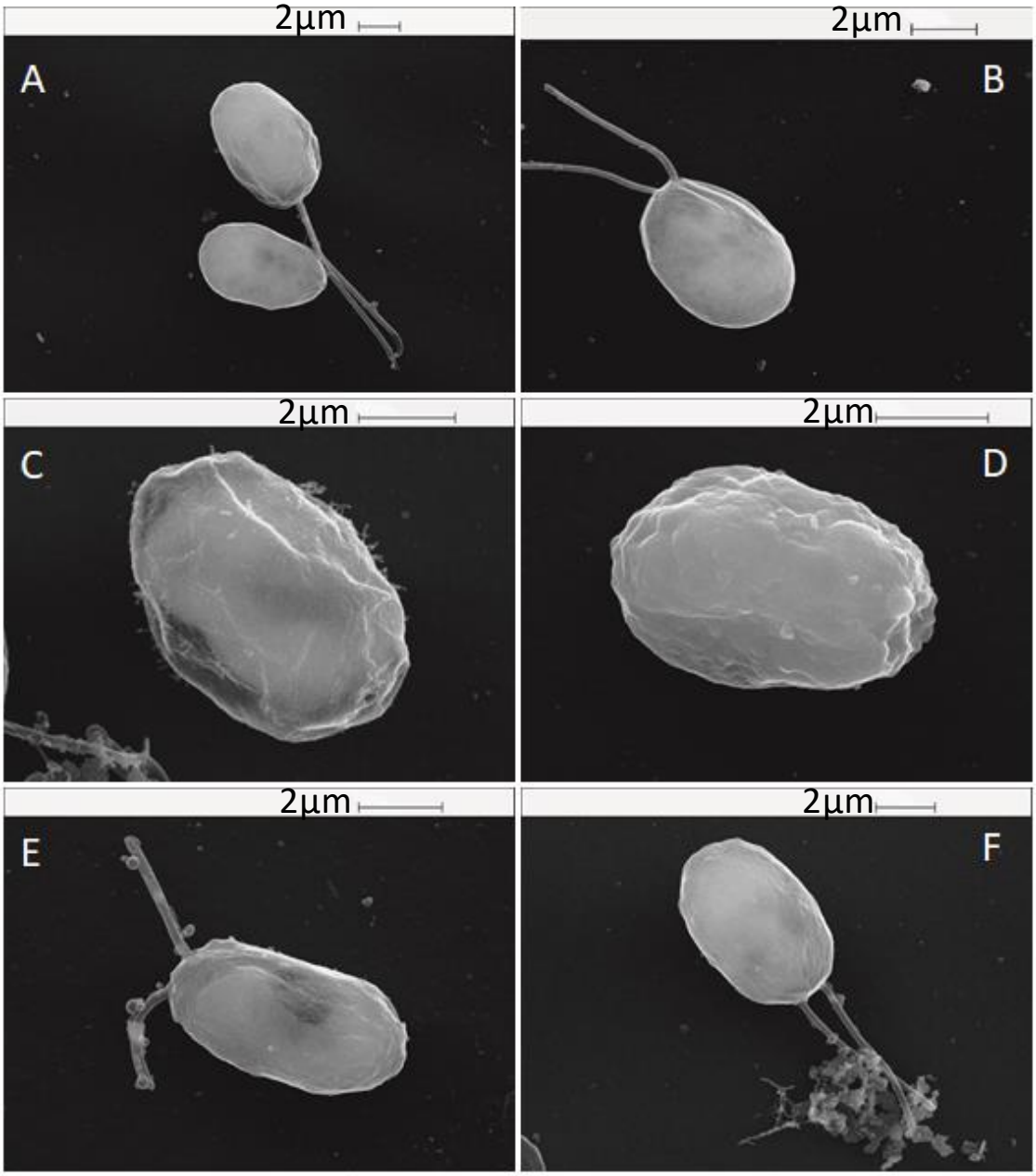

Figure 5.21: SEM images of algal cells. (A&B) A control sample of algal cells and (C&D) algal cells that incubated with 0.01 wt.% free VCM, (E&F) algal cells incubated with 0.01 wt.% of VCM loaded shellac NPs. All cells were incubated at pH 5.5 for 4 hours at room temperature.

5.3.2 The Cytotoxicity Effect of Encapsulated VCM on Yeast Cells

The antifungal activity of free VCM and VCM loaded shellac NPs were studied on baker's yeast cells at different concentrations at pH 5.5 using the FDA assay. Figure 5.22 and Figure 5.23 show the effect of free VCM and VCM loaded NPs on S. cerevisiae yeast cells at a range of incubation time. Figure 5.22 shows that free VCN had little effect on yeast cell. VCM does not enter the outer membrane of gram-negative organisms, due to its complex structure and large size,[417, 418] although some effect was seen at high concentrations of free VCM, at 0.1, 0.15, and 0.25 wt.% of VCM the cell viability decreased from 97% at control to be 70%, 62%, and 58% respectively after 4 hours of incubation. After 6 hours of exposure to VCM, the cell viability declined slightly from 98% at control to be 62%, 54% and 45% at (0.1, 0.15, and 0.25) wt. %, respectively. Loading the VCM within shellac NPs is seen to reduce the antifungal effect as shown previously in (Figure 5.23). So, VCM loaded shellac NPs showed very low antifungal activity toward yeast cells due to the repulsion between the NPs and cell wall. Figure 5.24 shows the SEM images of yeast after incubated for 4 hours with 0.01 wt.% of free VCM and VCM loaded shellac NPs, as it is clear the free VCM did not effect on yeast cells (C&D) as well as the VCM loaded shellac NPs did (E&F) in comparison with control cells (A&B).

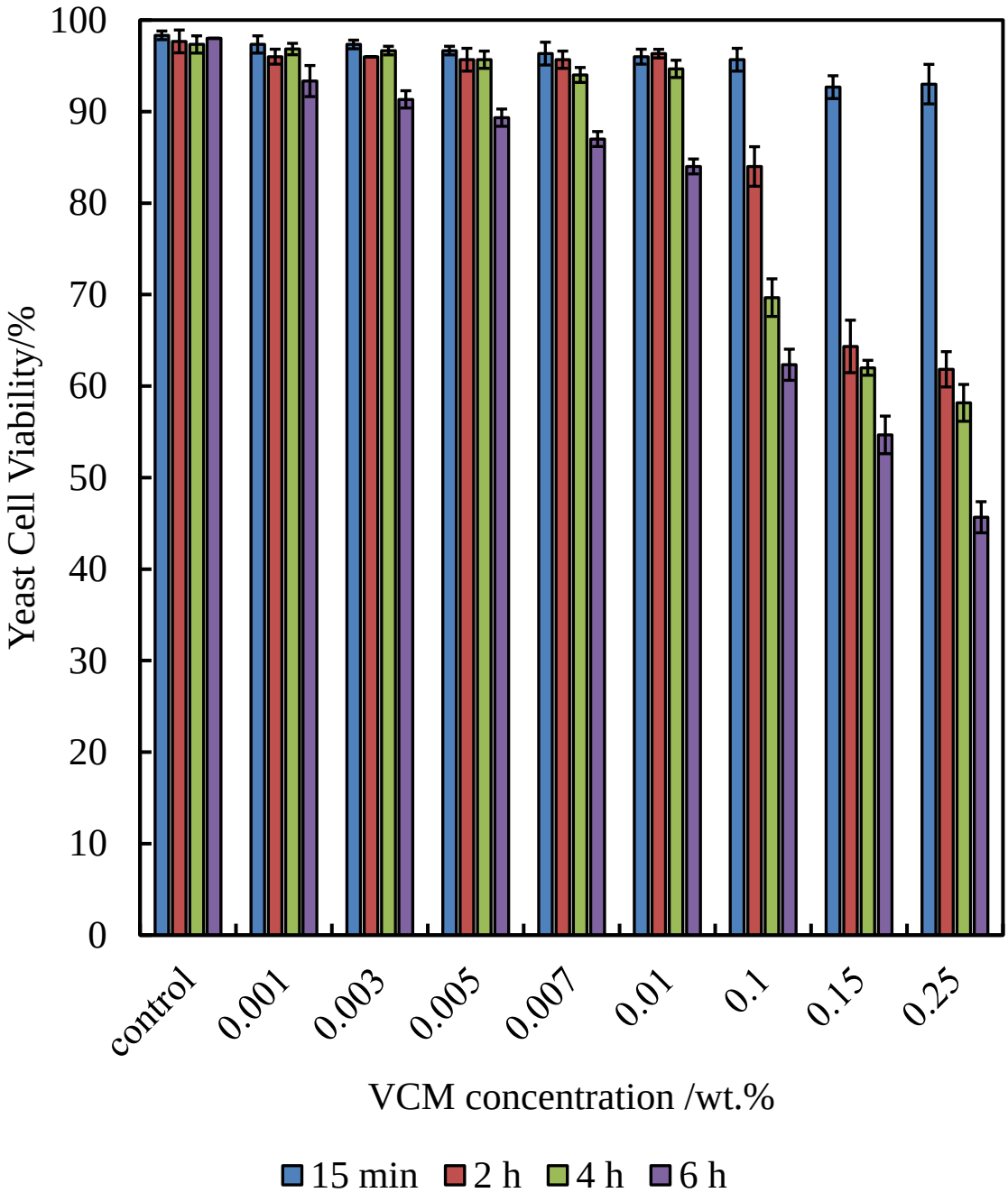

Figure 5.22: The viability of yeast cells incubated with series of solutions of free vancomycin at pH 5.5 using FDA assay at room temperature, at 15 min., 2 h, 4 h, and 6 hours of incubation, (n=3).

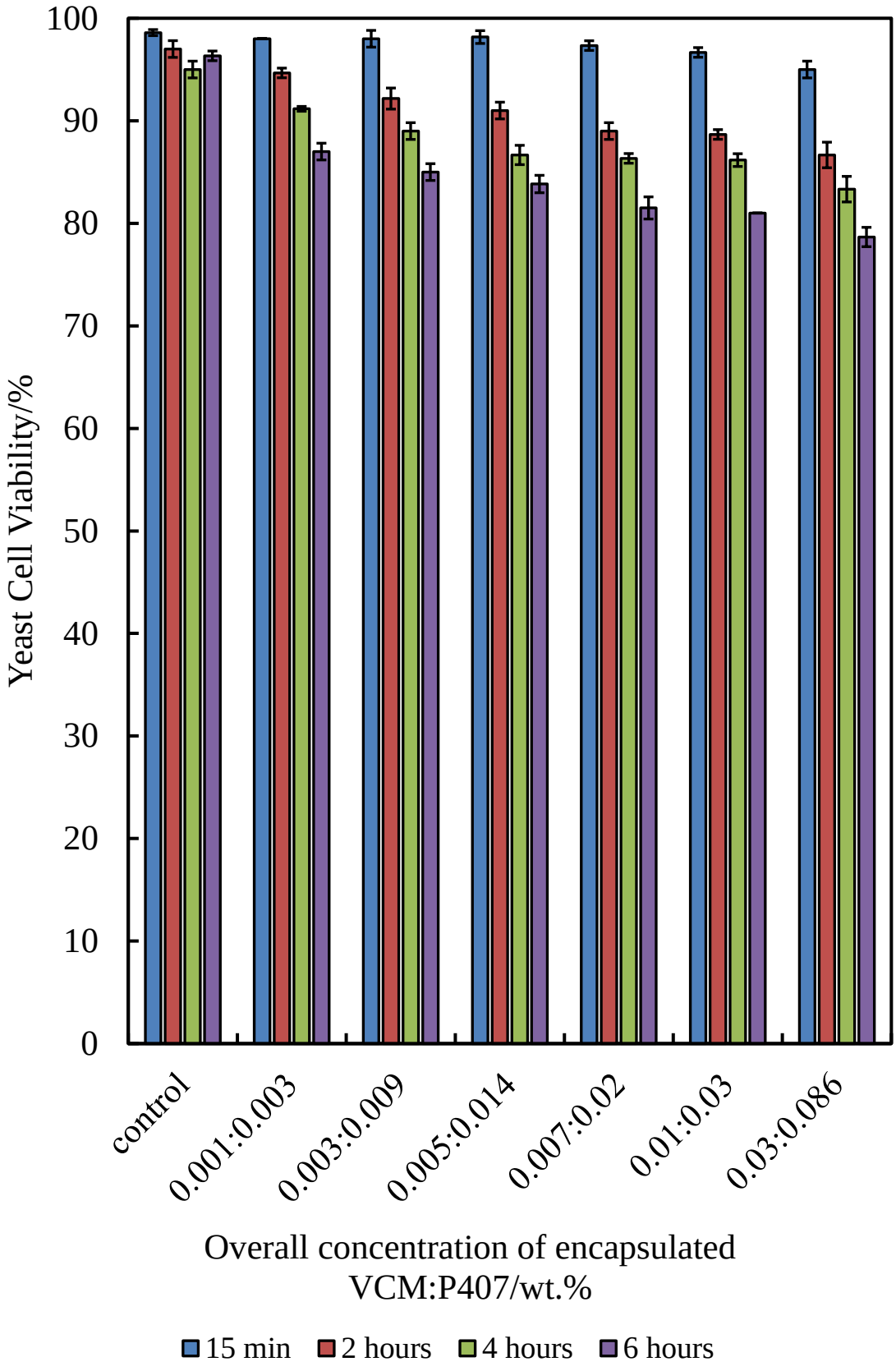

Figure 5.23: The viability of yeast cells incubated with various concentrations of vancomycin loaded shellac NPs at pH 5.5 using FDA assay at room temperature, at 15 min., 2 h, 4 h, and 6 hours of incubation, (n=3).

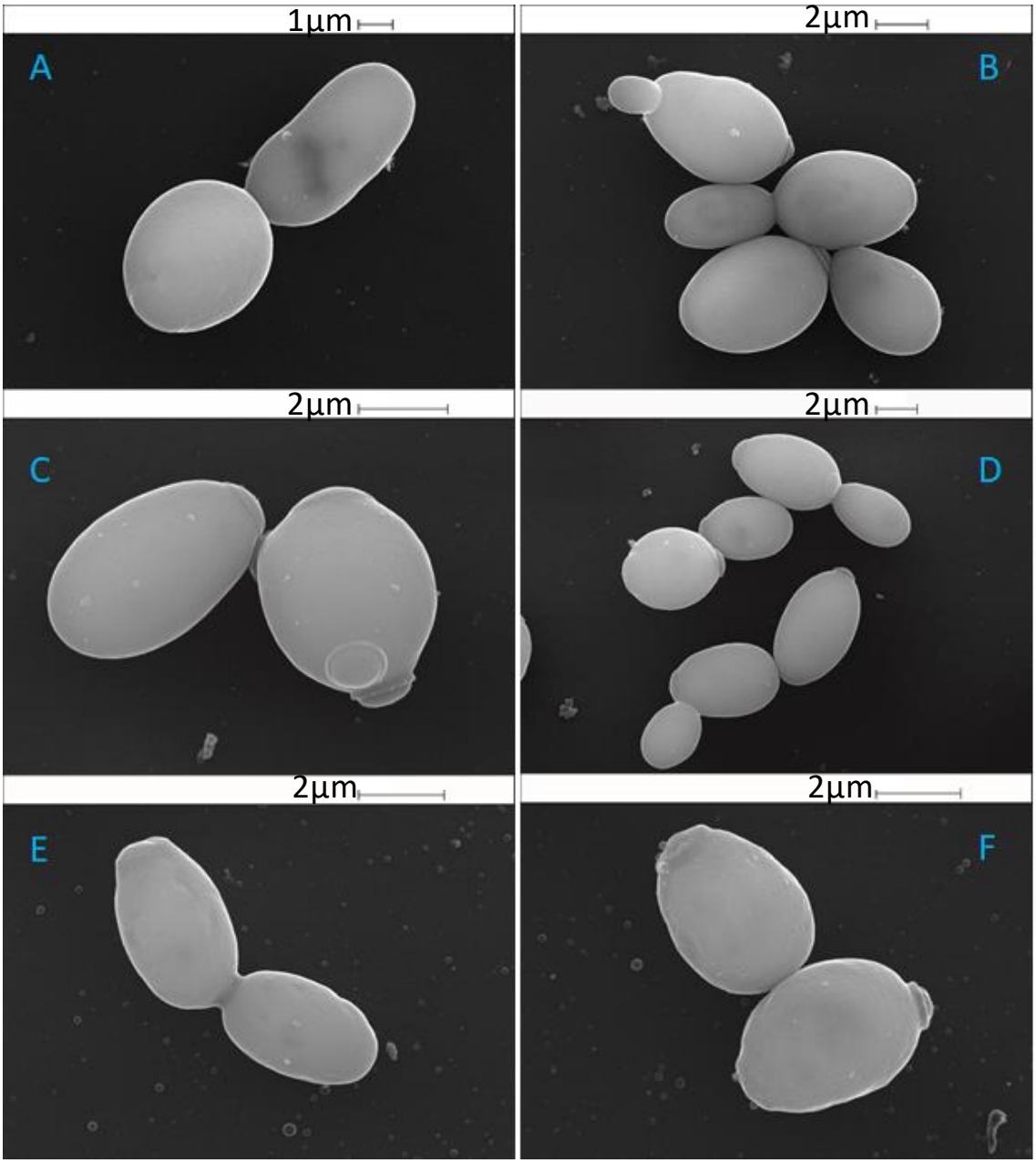

Figure 5.24: SEM images of yeast cells. (A&B) Control sample of yeast cell, (C&D) yeast cells that incubated with 0.01 wt.% free VCM after four hours of incubation, and (E&F) yeast cell incubated for four hours with 0.01 wt.% of VCM loaded shellac NPs.

5.3.3 The Cytotoxicity Effect of Encapsulated VCM on *E.coli* Cells

The antibacterial activity of free VCM and VCM loaded shellac NPs were studied after incubating culture media free *E.coli* cells with different concentrations of VCM at pH 5.5 and measuring the cell viability by means of luminometer using bactiter luciferase assay. Figure 5.25 shows the effect of free VCM at different exposure time. After 15 minutes incubation, the cell viability only decreased slightly from $41x10^5$ RLU at control to (27, 22, 20, and 19) $x10^5$ RLU at (0.01, 0.05, 0.1, and 0.15) wt.% of free VCM respectively. Even at longer times the effect was not great with VCM showing less antibacterial activity than the other three antibacterials studied (BRB, CHX, and CUR), this is because it is gram-positive antibacterial and due to its large size it hardly penetrates the cell wall.[417, 418] As would be expected the antimicrobial effect of the VCM NPs was even less as shown in Figure 5.26. After 4 hours of exposure, the cell viability declined by about 20% at (0.0005, 0.001, and 0.005) wt.% of total VCM. While it reduced by about 50% at 0.025 wt.% of VCM after 6 hours. Figure 5.27 shows the SEM images of *E.coli* cells incubated with 0.01 wt.% of free VCM (C&D) and VCM loaded shellac NPs (E&F) in comparison with control (A&B).

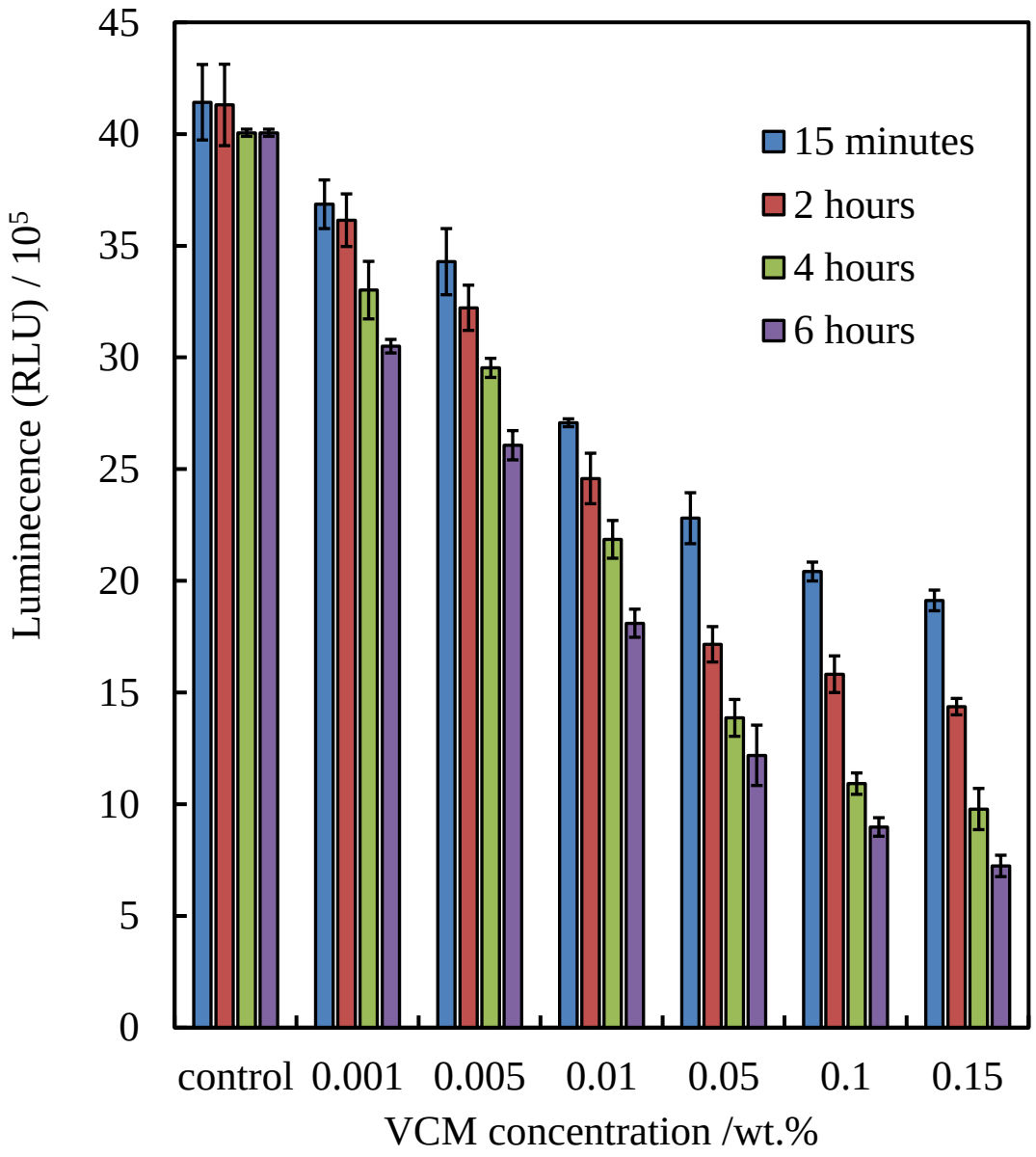

Figure 5.25: The relative luminescence unit of *E.coli* cells incubated at pH 5.5 with different concentrations of free VCM at different incubation time, 15 min., 2 h, 4 h, and 6 hours at room temperature using bactiter luciferase reagent, (n=3).

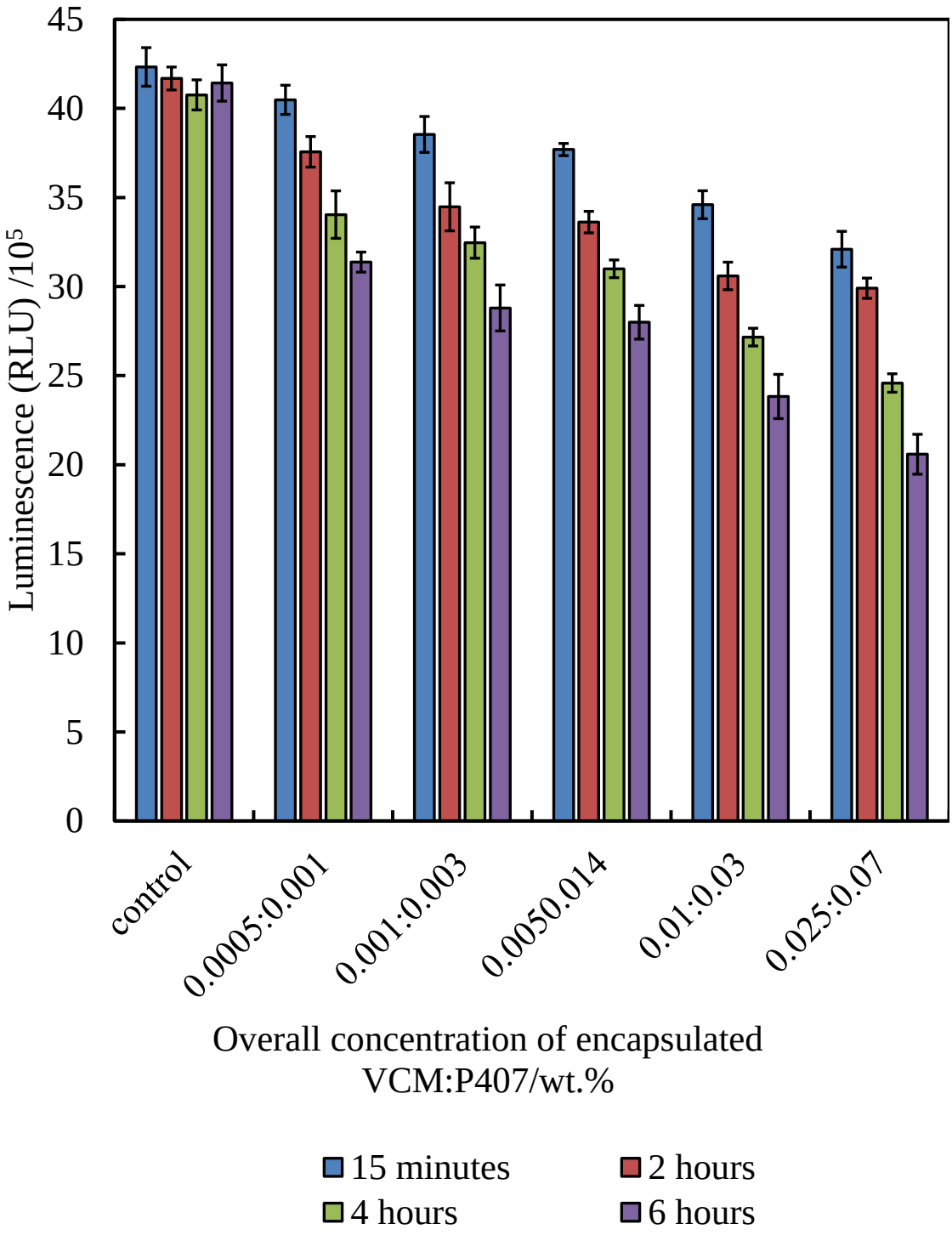

Figure 5.26: The relative luminescence unit of *E.coli* cells incubated at pH 5.5 with different concentrations of VCM-NPs at different incubation, 15 min., 2 h, 4 h, and 6 hours, at room temperature using bactiter luciferase reagent, (n=3).

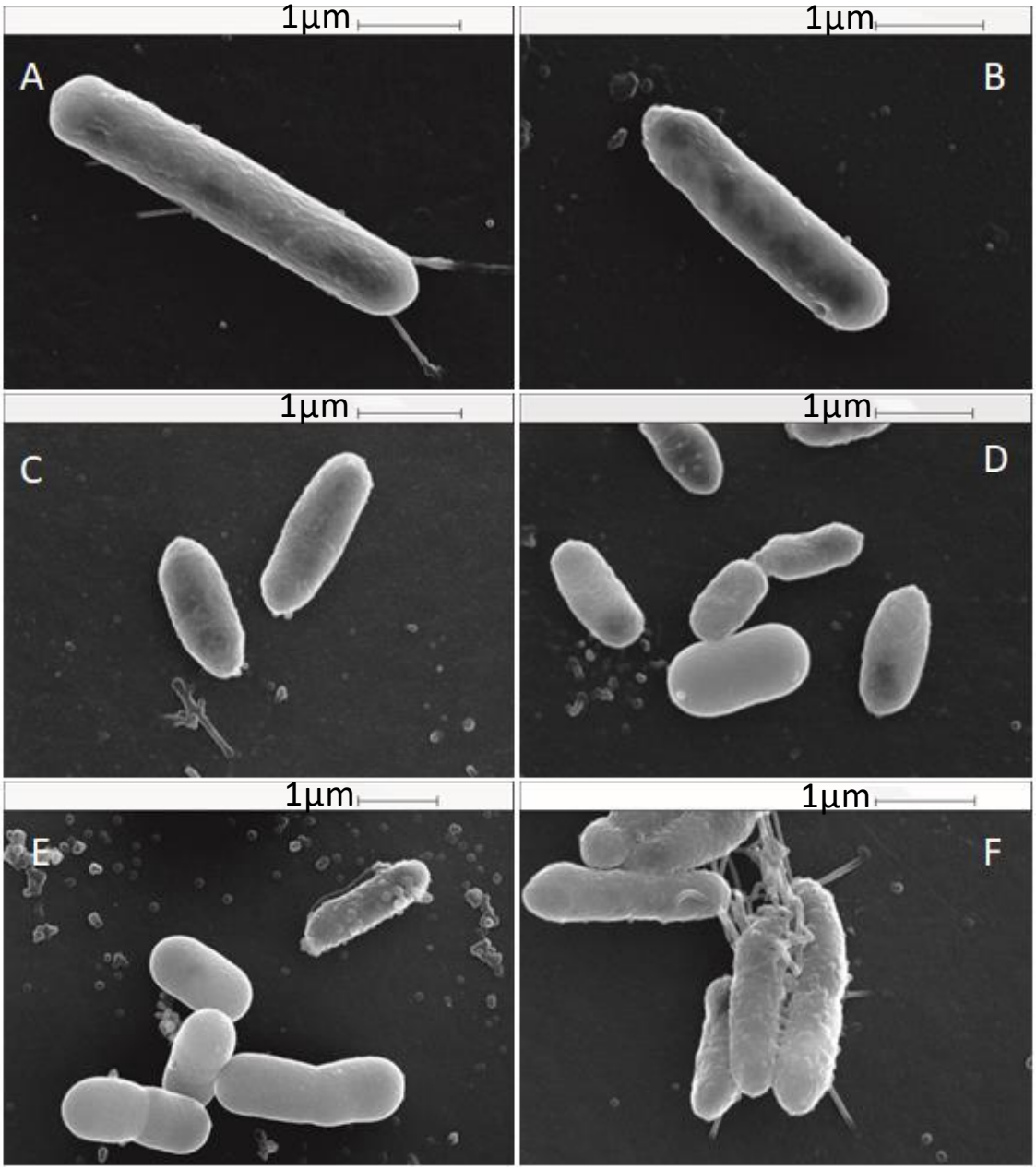

Figure 5.27: SEM images of *E.coli* cells. (A&B) Control sample of *E.coli* cells and (C&D) *E.coli* cells that incubated with 0.01 wt.% free VCM, (E&F) *E.coli* cell incubated with 0.01 wt.% of VCM loaded shellac NPs. All cells were incubated at pH 5.5 for 4 hours at room temperature.

5.4 Cytotoxic Effect of Encapsulated VCM Coated with ODTAB on Microorganisms

The antialgal, antifungal and antibacterial activity of vancomycin loaded shellac NPs coated with ODTAB were then studied by incubating it with algae, yeast, and *E.coli* cells.

5.4.1 Cytotoxic Effect of Encapsulated VCM Coated with ODTAB on Microalgae

The antialgal activity of encapsulated VCM coated with ODTAB was studied by incubating culture media free C. reinhardtii microalgae with different concentrations of VCM-NPs coated with ODTAB. Figure 5.28 shows that after 15 minutes of incubation, the cell viability of microalgae decreased sharply from 92% for control to (25, 18.5, 14, and 8.5)% at (0.003, 0.005, 0.007, and 0.01) wt.% VCM-NPs coated with ODTAB. After 2 hours the cell viability of C. reinhardtii microalgae continued decreasing to be (9.5, 7, and 2.5) % at (0.005, 0.007, and 0.01) wt.%, VCM-NPs coated with ODTAB. This shows that after coating the VCM-NPs with ODTAB, the antimicrobial action of VCM increased. Figure 5.29 compares the antimicrobial activities of 0.001 wt.% VCM-NPs, 0.001 wt.% free VCM, 0.005 wt.% shellac NPs coated with 0.001 wt.% ODTAB, 0.001 wt.% VCM-NPs coated with 0.0014 wt.% ODTAB, and 0.0015 wt.% pure ODTAB. There is a clear change in the cytotoxic action of VCM after coating it with ODTAB. Scanning electron microscopy pictures of microalgal cell after incubated with 0.01 wt.% VCM loaded shellac NPs coated with 0.014 wt.% ODTAB for 2 hours can be seen in Figure 5.30. Pictures show how the NPs accumulate around the cell wall in abundance; this attraction gives the option to either the NPs release drug inside the cell or the whole NPs penetrate inside the cells with drug leading to kill them as explained in figure 4.47,b.

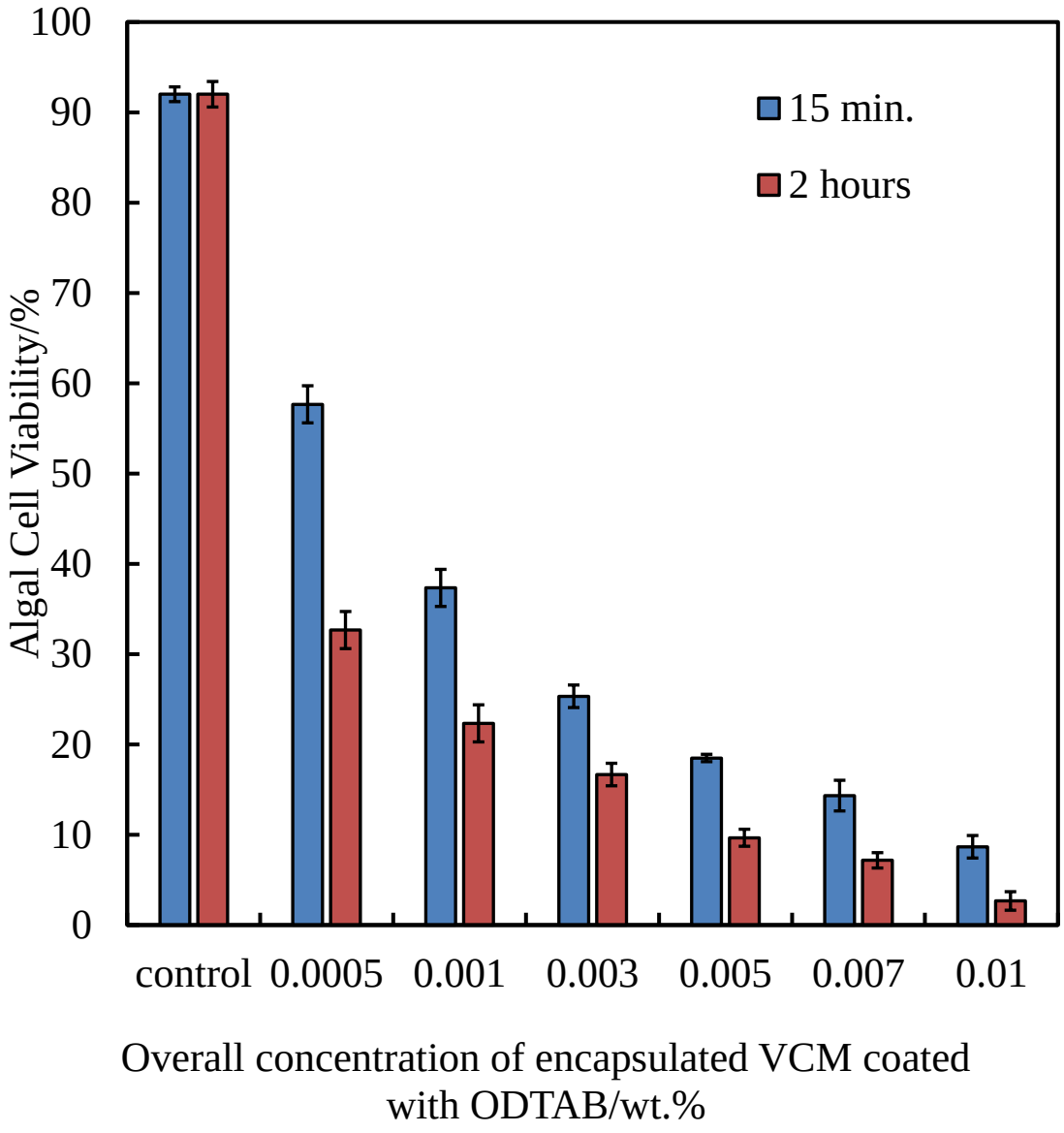

Figure 5.28: The viability of algal cells upon incubation at pH 5.5 with different concentrations of VCM loaded shellac NPs coated with ODTAB at room temperature at different incubation time, at 15 min., and 2 hours. The solutions were prepared from 0.05 wt.% VCM- NPs stock solution coated with 0.07wt.% ODTAB, (n=3).

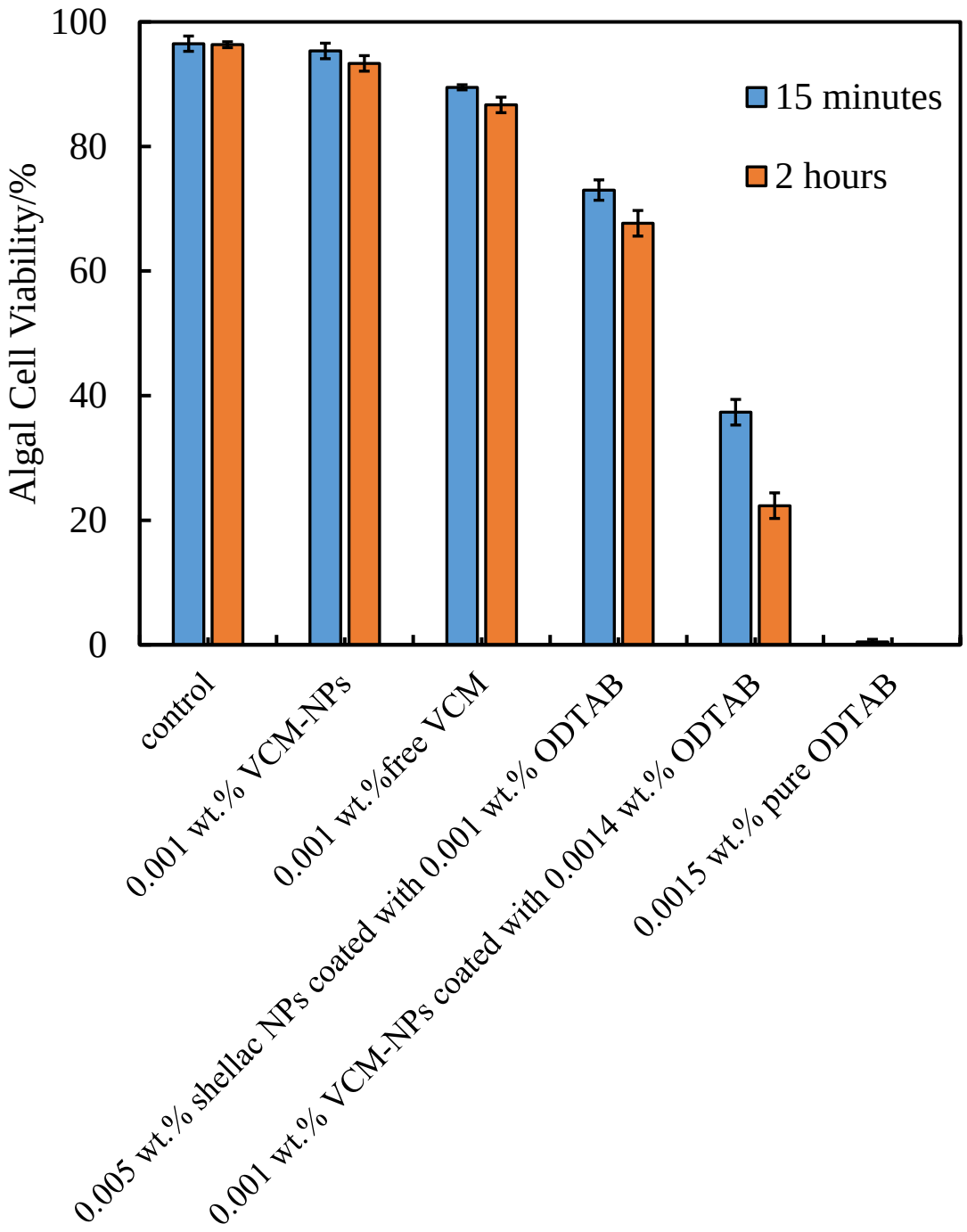

Figure 5.29:The algal cells viability upon incubation with 0.001 wt% VCM-NPs, 0.001 wt% free VCM, 0.005 wt.% shellac NPs coated with 0.001 wt.% ODTAB, 0.001 wt% VCM-NPs coated with 0.0014 wt.% ODTAB, and 0.0015 wt% pure ODTAB at pH 5.5 and at room temperature, (n=3).

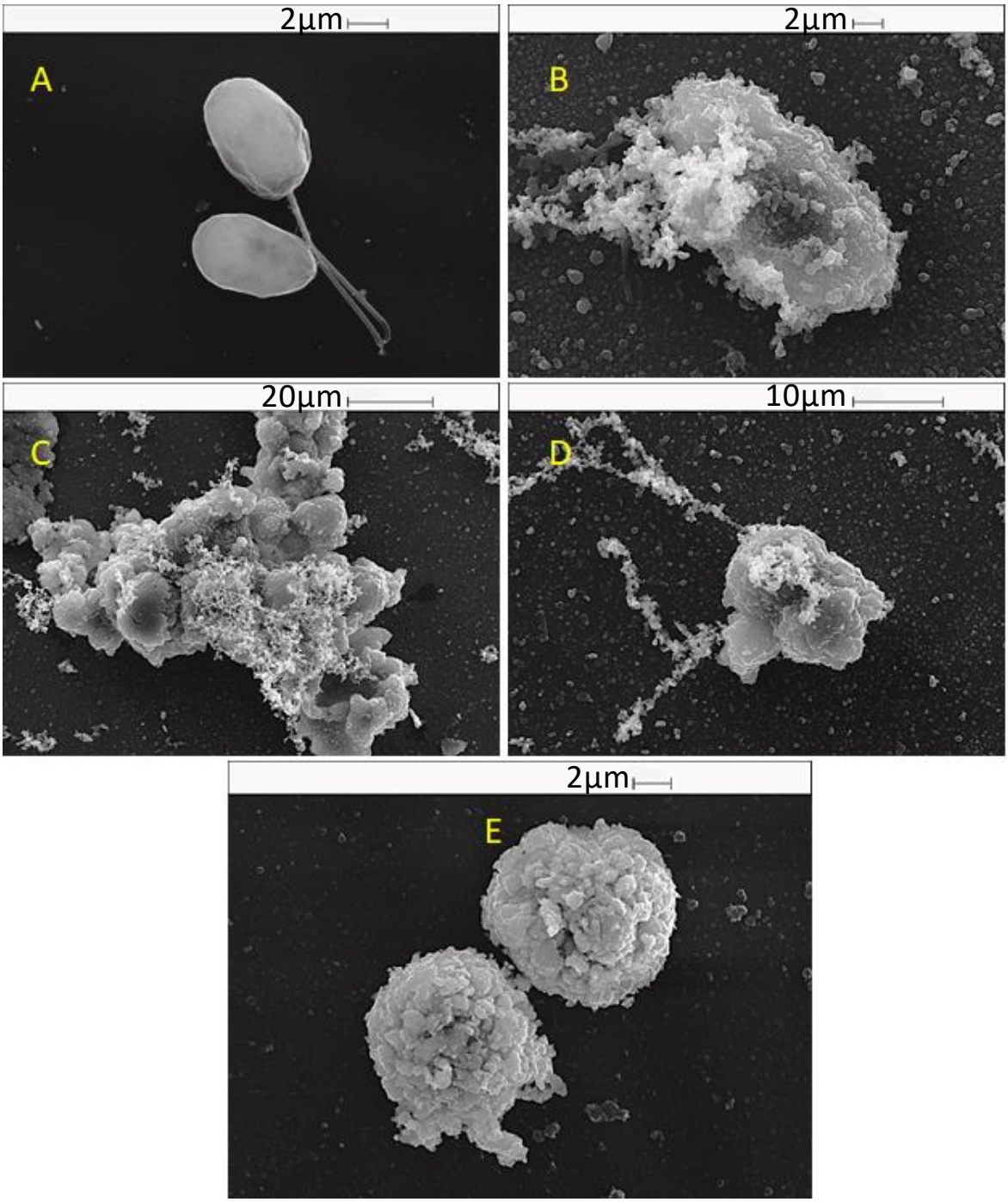

Figure 5.30: SEM images of *C. reinhardtii* cells. (A) A control sample of the *C. reinhardtii* microalgae cells. (B, C, D, and E) *C. reinhardtii* microalgae cells incubated with 0.01 wt.% VCM loaded shellac NPs coated with 0.014 wt.% ODTAB after 2 hours incubation time at room temperature.

5.4.2 Cytotoxic Effect of Encapsulated VCM Coated with ODTAB on Yeast Cells

The antifungal effect of VCM loaded shellac NPs coated with ODTAB was examined by incubating culture media free yeast cells with different concentrations of VCM loaded shellac NPs coated with ODTAB at different incubation time. Figure 5.31 displays the yeast cell viability upon incubation with different concentrations of VCM loaded shellac NPs coated with ODTAB for 15 minutes. The cell viability severely decreases from 94%; which is represent the control to 38%, 32%, 3.3, and 2.8% at (0.0005, 0.001, 0.003 and 0.005) wt.% of VCM loaded shellac NPs coated with (0.0007, 0.0014, 0.0042, and 0.007) wt.% ODTAB, respectively. Figure 5.32 compares the antimicrobial actions of 0.005 wt.% VCM-NPs, 0.005 wt.% free VCM, 0.025 wt.% shellac NPs coated with 0.007 wt.% ODTAB, 0.005 wt.% VCM-NPs coated with 0.007 wt.% ODTAB, and 0.007 wt.% pure ODTAB. Using ODTAB to change the surface charge of the NPs significantly increased the antimicrobial activity. Figure 5.33 is the SEM images of yeast cells incubated with 0.01 wt.% of vancomycin loaded shellac NPs coated with 0.014 wt.%. ODTAB. The coated NPs also shows antimicrobial effect due to the positive surface charge which allows VCM either enter the cells directly as free or within shellac NPs.

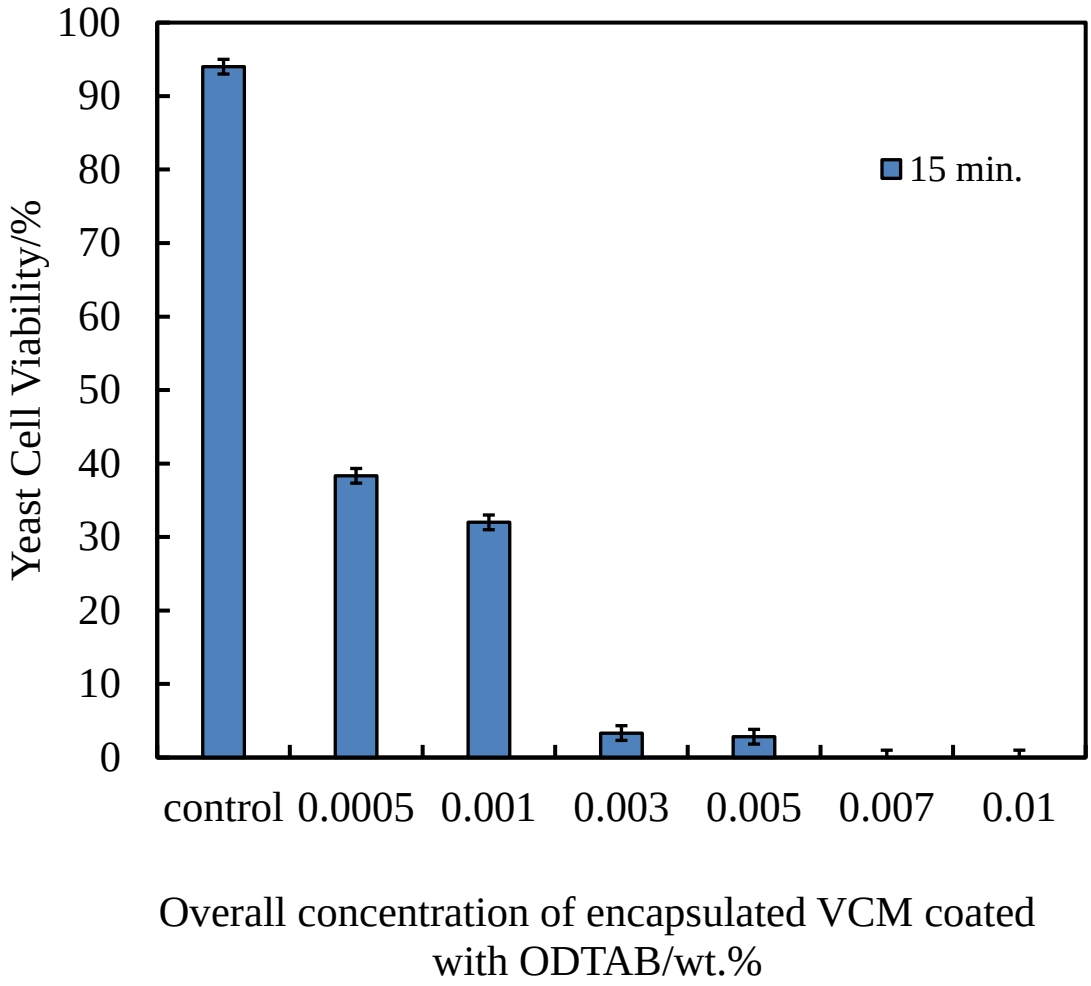

Figure 5.31: Yeast cell viability upon incubation with different concentrations of vancomycin loaded shellac NPs coated with ODTAB at room temperature up to 15 minutes using FDA assay and measured by means of the cellometer instrument at pH 5.5. These suspensions were prepared from 0.05 wt.% VCM-NPs coated with 0.07 wt.% as a stock solution, (n=3).

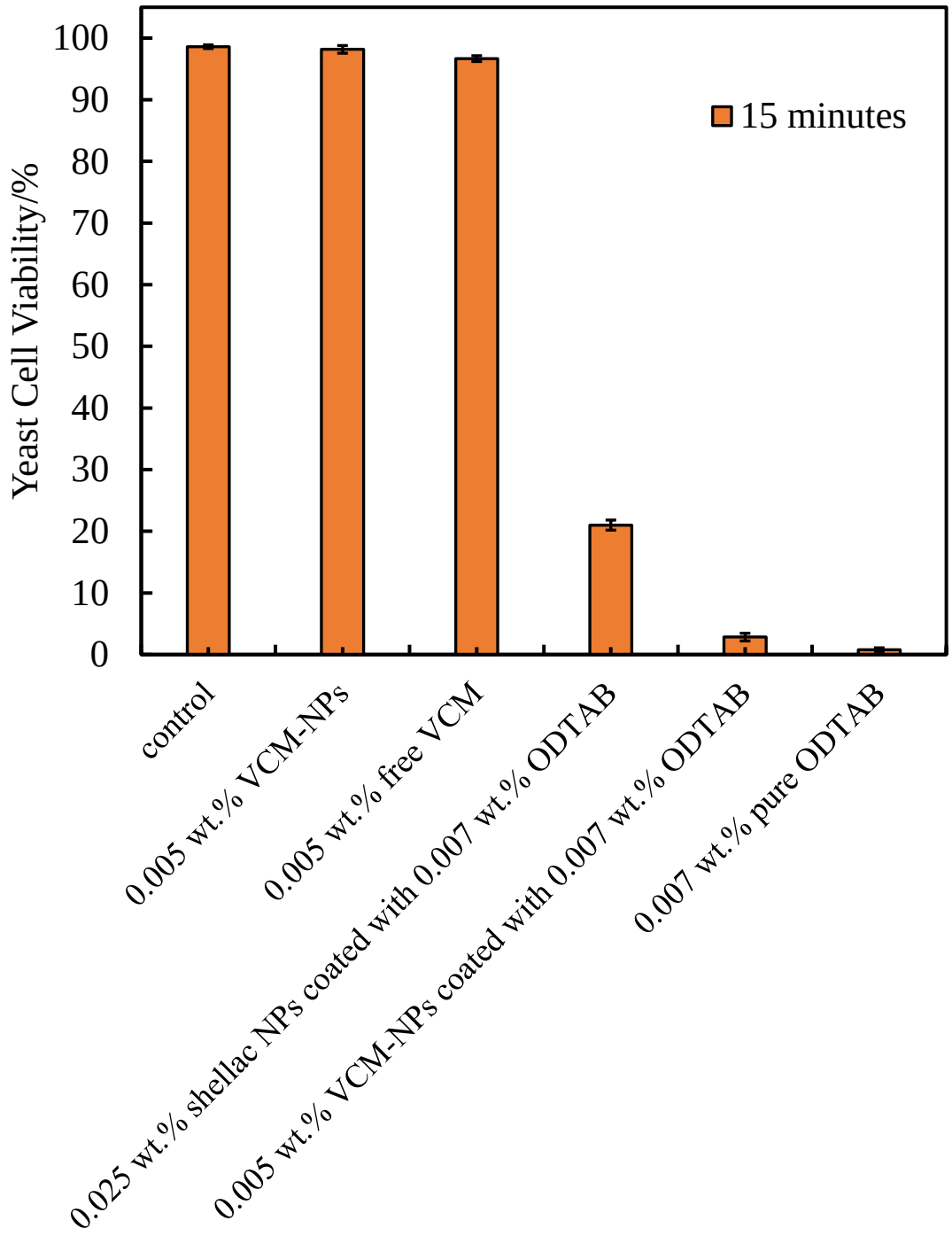

Figure 5.32: Yeast cells viability upon incubation with 0.005 wt.% VCM-NPs, 0.005 wt.% free VCM, 0.025 wt.% shellac NPs coated with 0.007 wt.% ODTAB, 0.005 wt.% VCM-NPs coated with 0.007 wt.% ODTAB, and 0.007 wt.% pure ODTAB at pH5.5 at room temperature, (n=3).

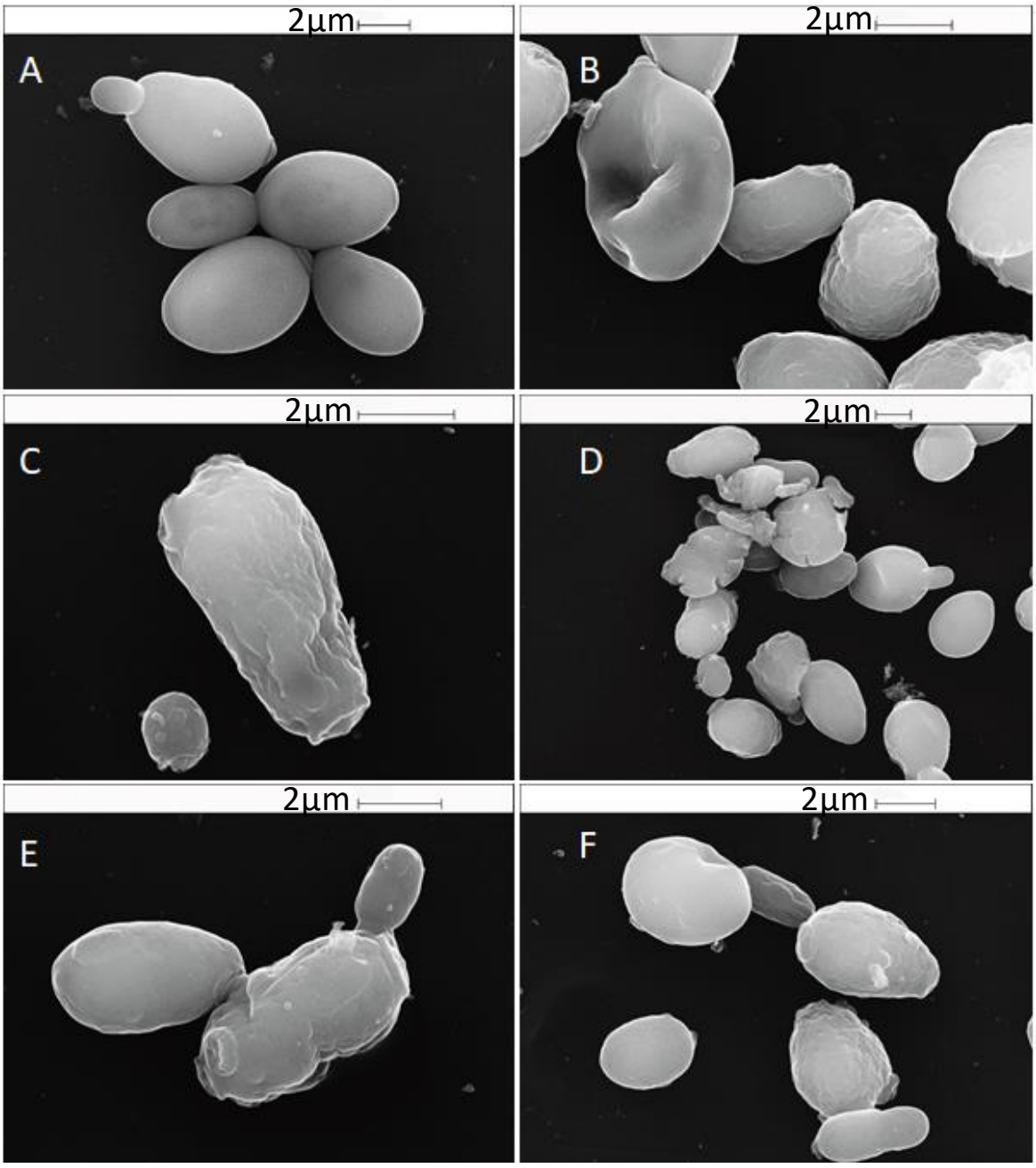

Figure 5.33: SEM images of yeast cells. (A) Control sample of yeast cells, (B, C, D, E, and F) yeast cells incubated with 0.01 wt.% VCM loaded shellac NPs coated with 0.014 wt.% ODTAB incubated for 2 hours.

5.4.3 The Cytotoxic Effect of Encapsulated VCM Coated with ODTAB on *E.coli* Cells

Figure 5.34 shows the antibacterial activity of different concentrations of VCM-NPs after coating with cationic electrolyte ODTAB to change the surface charge from negative to positive at pH 5.5. After 15 minutes of incubation the VCM-NPs coated with ODTAB showed little effect on the bacteria at concentrations of 0.0001, 0.0005, and 0.001 wt.%, coated with 0.00017, 0.0008, and 0.0017wt.% ODTAB, but at higher concentration of 0.01 wt.% VCM-NPs coated with ODTAB the cell viability decreased sharply from 40 $x10^5$ RLU at control to $0.8x10^5$ RLU. After 1 hour, most cells died at 0.01wt.% VCM-NPs coated with ODTAB, while the cell viability represented by luminescence declined from 39 $x10^5$ RLU as control to be 29, 22, and $17x10^5$ RLU at (0.0001, 0.0005, and 0.001) wt.% VCM loaded shellac NPs coated with 0.00017, 0.0008, and 0.0017 wt.% ODTAB, respectively. After 2 hours incubation the cell viability dropped from 39 $x10^5$ RLU to (20, 18, and 7) $x10^5$ RLU at (0.001, 0.0005, and 0.001) wt.% VCM-NPs coated with ODTAB, respectively. Figure 5.35 shows the comparison between free, uncoated and coated vancomycin loaded shellac NPs. The uncoated VCM-NPs showed less toxicity than the free VCM and both had an unnoticeable effect on *E.coli* after 1 hour of incubation time, whereas, shellac NPs coated with ODTAB had an effect on the cell viability after 1 hour incubation due to the positive surface charge. Scanning electron microscopy images of *E.coli* cells incubated with 0.01 wt.% VCM loaded shellac NPs coated with 0.014 wt. % ODTAB after 2 hours incubation can be seen in Figure 5.36. These pictures prove that VCM loaded shellac NPs coated with ODTAB can attach to the cell's membrane faster than uncoated one.

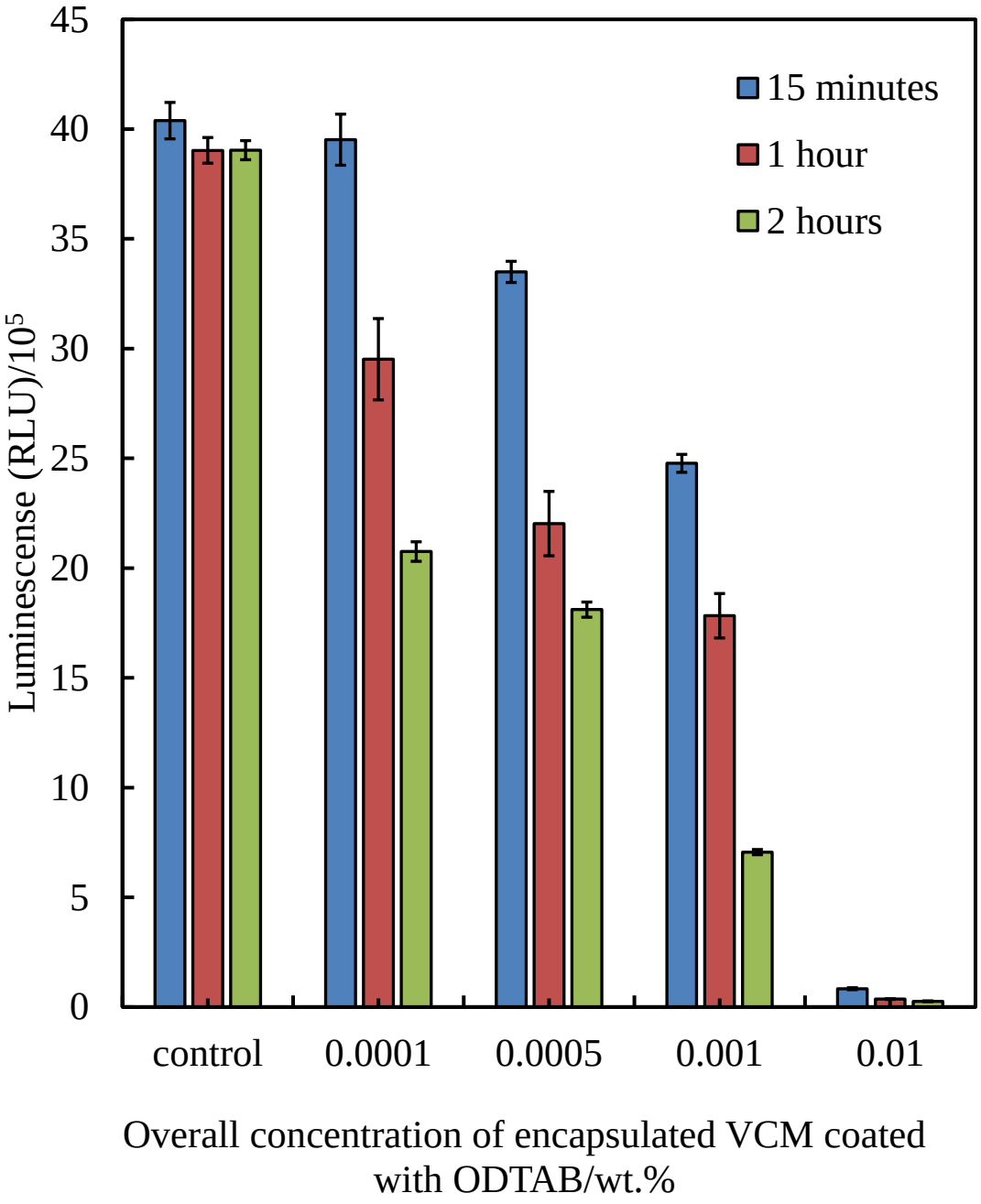

Figure 5.34: The antimicrobial activity of different concentrations of vancomycin loaded shellac NPs coated with ODTAB against *E.coli* cells at 15 min, 1 h, and 2 h incubation time. These solutions were prepared from stock solution of 0.05 wt.% VCM loaded shellac NPs coated with 0.07 wt.% ODTAB, (n=3).

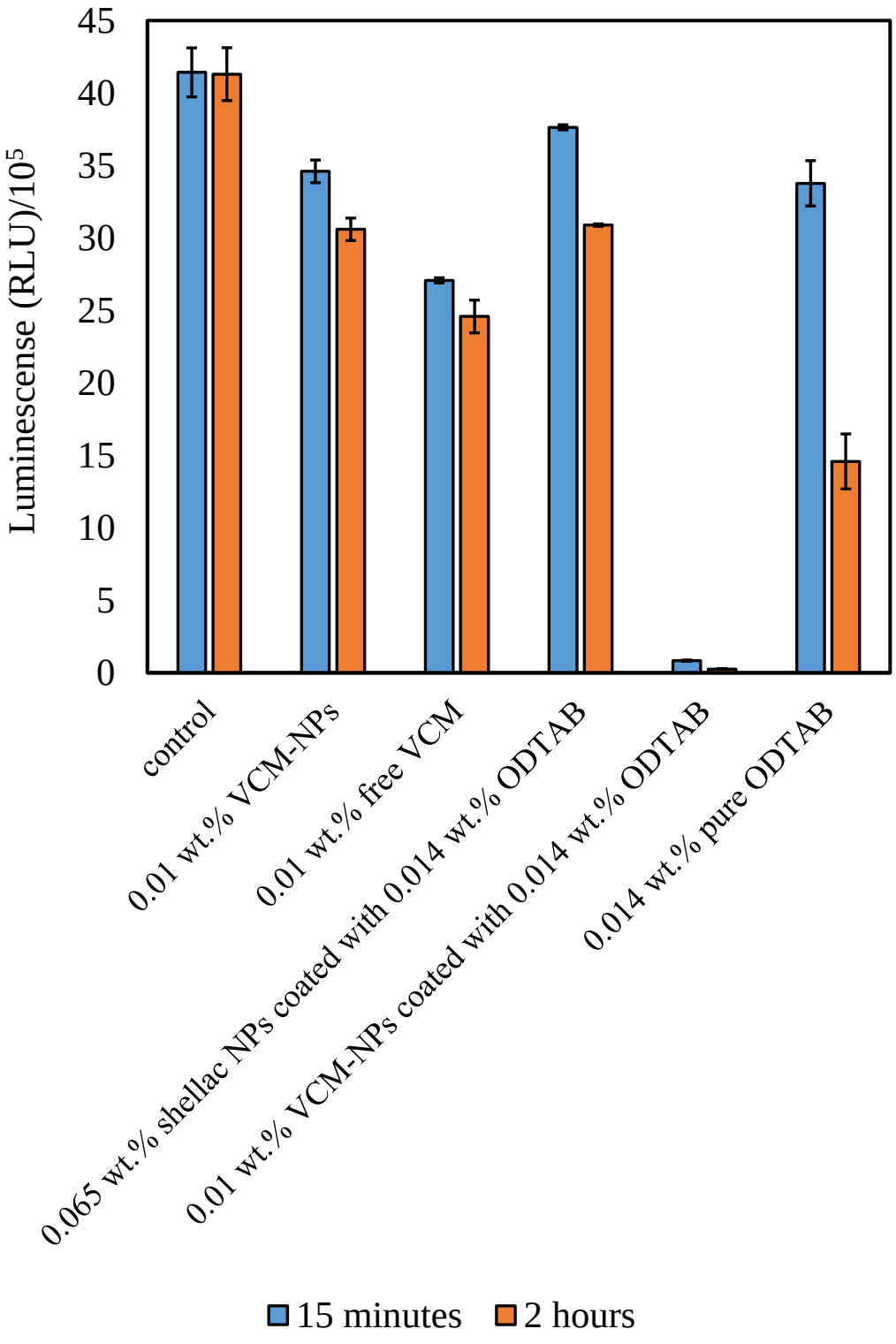

Figure 5.35: The antimicrobial activity of 0.01 wt.% vancomycin loaded shellac NPs coated with 0.014 wt.% ODTAB towards *E.coli* cells as a function of both the antimicrobial activity of 0.01 wt.% free VCM and shellac NPs encapsulated 0.01 wt.%VCM and the cytotoxic effect of pure ODTAB, and ODTAB coated shellac NPs. The incubation was also accomplished through incubating each concentration with a fixed amount of *E.coli* cells at pH 5.5 at room temperature using bactiter luciferase assay, (n=3).

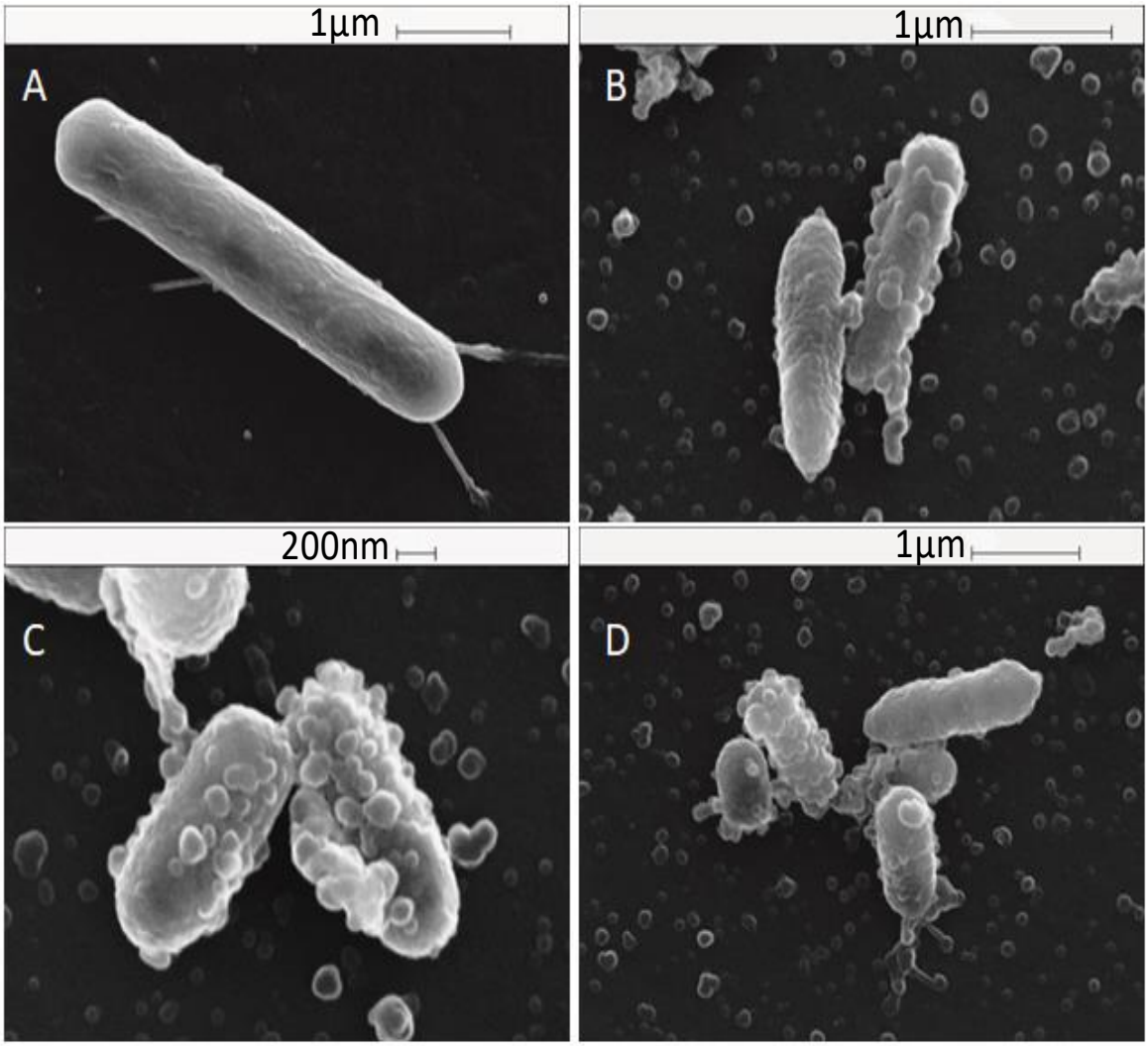

Figure 5.36: SEM images of *E.coli* cells. (A) Control sample of *E.coli* cells. (B, C, and D) *E.coli* cells incubated with 0.01 wt.% VCM loaded shellac NPs coated with 0.014 wt. % ODTAB for 2 hours incubation time at pH 5.5.

5.5 Conclusion

In this chapter the cytotoxic effect of encapsulated CUR and VCM within shellac NPs was studied on some microorganisms including algae, yeast, and *E.coli* cells. The results showed that free curcumin showed significant cytotoxic effect on these cells at low concentrations, but after loading it within shellac NPs this cytotoxicity was reduced, owing to the high affinity between shellac and CUR particles which led to slow release as well as the negative NPs surface charge which repels with the cell membrane. However, by coating the encapsulated CUR with the cationic electrolyte ODTAB to change the surface charge of the NPs loaded with CUR from negative to positive, the cytotoxic action on these microorganisms increased, owings to the rapid attraction between the NPs coated ODTAB and the cell membrane; as clear in SEM images, which allow small amount of CUR to be released inside or on the membrane and kill the cells. The minimum concentration of encapsulated CUR coated with ODTAB which kills 90% of the cells after 15 minutes for algae, yeast, and *E.coli* was 0.0005, 0.0005, and > 0.01 wt.%, respectively, compared to 0.001, 0.0025, and 0.01 wt.% for free curcumin. As can be seen from the results that encapsulated CUR coated with ODTAB showed significant cytotoxicity than free CUR on algae and yeast, while on *E.coli* the effect was less and that may attribute to the very slow CUR amount release. At 0.0005 wt.% of encapsulated CUR coated with ODTAB and after 15 minutes of incubation the higher cytotoxic effect follows the order: algae > yeast > *E.coli*. These results are in agreement with earlier research where nanocurcumin showed cytotoxic action on microorganisms more than the free curcumin.[388, 419, 420]

On the other hand, free VCM did not represent noticeable cytotoxic effect when incubated with the same microorganisms, even at high concentrations, as well as when it encapsulated within shellac NPs. The reasons behind this are VCM is bulky molecule and it expresses antibiotic against gram-positive bacteria more than gram-negative bacteria, and when it loaded within shellac NPs a repulsion between these NPs and the cell membrane happened due to the negative charge for both. But when it coated with ODTAB to change the surface charge to be positive, this cytotoxic action was increased significantly. The cytotoxic effect of encapsulated VCM coated with ODTAB follow the order: yeast > algae > *E.coli*. The literatures show that VCM, when loaded on a carrier for delivering, can express cytotoxic effect on *E.coli*.[237, 421] In a recent study Katiraee *et.al,*[422] presented that 0.04 wt.% of nanocurcumin can show antifungal action against different types of fungi, while in current study only 0.0005 wt.% of ODTAB coated shellac NPs loaded with CUR can significantly kill the fungi after 2 hours. In another study,[388] and by

using a wet-milling technique to prepare nanocurcumin, it was found that minimum inhibitory concentration (MIC) of nanocurcumin on *E.coli* was 0.25 $mg.mL^{-1}$, while the present study showed that 0.01 $mg.mL^{-1}$ of encapsulated CUR coated with ODTAB can effect significantly on *E.coli*. Whereas no literatures were found to showed that nanocurcumin cytotoxicity was studied against algae. On the other hand, a study showed that the MIC of nanovancomycin on *E.coli* was >1.28 $mg.mL^{-1}$, while this study showed that minimum inhibition concentration of encapsulated VCM coated with ODTAB was 0.01 $mg.mL^{-1}$.[421] Most published literatures of nanovancomycin were studied its cytotoxicity against gram-positive bacteria, and no researches for nanovancomycin against algae or yeast. Table 5.1 shows the cytotoxic effect of CUR and VCM as free drugs, loaded within shellac NPs and ODTAB coated these drugs loaded with shellac NPs, as well as the cytotoxic effect of free shellac NPs coated and uncoated with ODTAB. As can be seen that the cytotoxicity of these drugs increased when loaded within shellac NPs and coated with ODTAB due to the positive charge of the nanocarrier surface which promote the adhesion of these nanocarriers with the cell membrane, and that action was illustrated in figure 4.47.

Table 5.1: The cytotoxicity effect of each component on algae, yeast, and *E.coli* which represented by (++++: very strong, +++: strong, ++: medium, and +: weak).

Component	The effect of the component on microorganisms		
	Algae	Yeast	*E.coli*
Shellac NPs	+++	++	+
Shellac NPs coated ODTAB	+++	++	++
Free CUR	++++	++++	++++
Encapsulated CUR	++	+	++
Encapsulated CUR coated with ODTAB	++++	++++	+++
Free VCM	++	+	++
Encapsulated VCM	+	+	+
Encapsulated VCM coated with ODTAB	++++	++++	+++

Chapter 6 : Cytotoxicity Assay of Shellac NPs Loaded Antibacterial Using Microfluidic Device

The two previous chapters 4 and 5 demonstrated the effect of the encapsulated nanocarriers on microorganisms. The experiments that were carried out were batch experiments that were very time-consuming. In this chapter, the development of a microfluidic device is described to enable more automated and rapid screening of the effect of the nanocarriers on the microorganisms. As described previously in the introduction microfluidic systems can offers a number of advantages including flexibility in design, short times for reaction, small supplies for reagents, solvents, and samples (particularly for valuable samples and for high-throughput screening), low power consumption, portability and low cost.[423, 424] The system designed is shown in section 2.13 and relied on magnetised microbeads to form a plug with the help of an external magnet, this plug held the micro-organisms within the device. The nanocarriers could then be passed over the microchamber.

6.1 Synthesizing of Magnetized Micro Beads

The anisotropic spherical magnetic micro particles were synthesised according to the method of Dyab *et al.*[380] with some amendments as showing in figure 6.1. The oleic acid coated magnetic nanoparticles OCMNs were dispersed in styrene to produce hydrophobic magnetite nanoparticles as oleic acid has a great affinity to the surface of superfine magnetite,[425] figure 6.2. Agarose gel was added to stop the coagulation of the oil drops of the magnetic emulsion when introducing to an external magnetic field since they form chains in aqueous solution under an external magnetic field.[380] The magnetic micro beads produced were designed to have different sizes ranging from 10-30 µm, this allowed fluids to flow through the pores between micro beads and prevent back pressures when liquids were pumped from the inlet channels. The magnetic beads were introduced into the microfluidic chamber using a syringe pump and were retained near the outlet channel by using neodymium magnet placed underneath the microfluidic device on the glass side which allows the neodymium magnet to be stronger than if it was put underneath the PDMS side as PDMS has electrical insulation property.[426] The movement of the prepared magnetic beads was examined using neodymium magnet, as can be seen in Figure 6.2 they responded well to the magnet. The response of the magnetic beads was examined, and they showed strong response upon approaching the neodymium magnet, this gives the

micro beads ability to be controlled and moved at any direction, and they can be used as gate keeper as can be seen in Figure 6.3, Figure 6.4, and Figure 6.5. Consequently, these beads were utilised to trap cells into the micro chambers of the chip and at the same time allow the fluid to pass out.

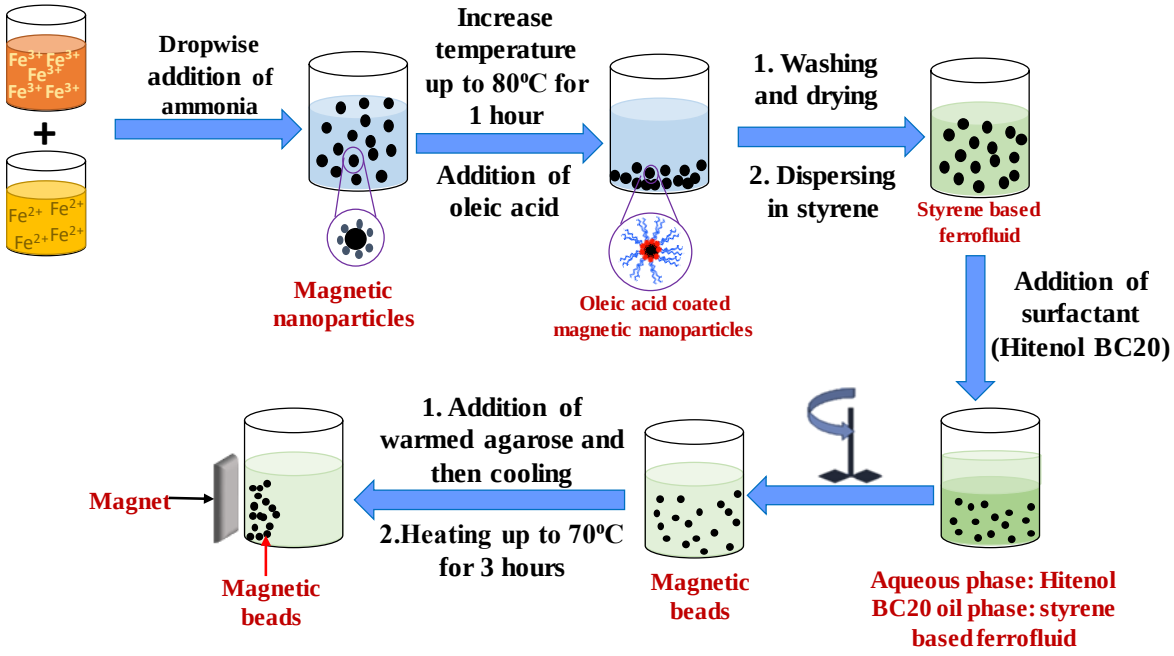

Figure 6.1: Schematic diagram for the manual synthesis of magnetized micro beads using the precursor's ferric and ferrous ions in the basic medium of ammonia to form magnetic nanoparticles which in turn functionalized with oleic acid and dispersed in styrene to form styrene based Ferrofluid. The latter then homogenized with equal amount of 2% Hitenol BC20 to form oil in water emulsion using pipette. After that, the emulsion was added to warmed agarose and cooled down to room temperature, which then heated up to 70ºC for three hours to polymerise the beads.

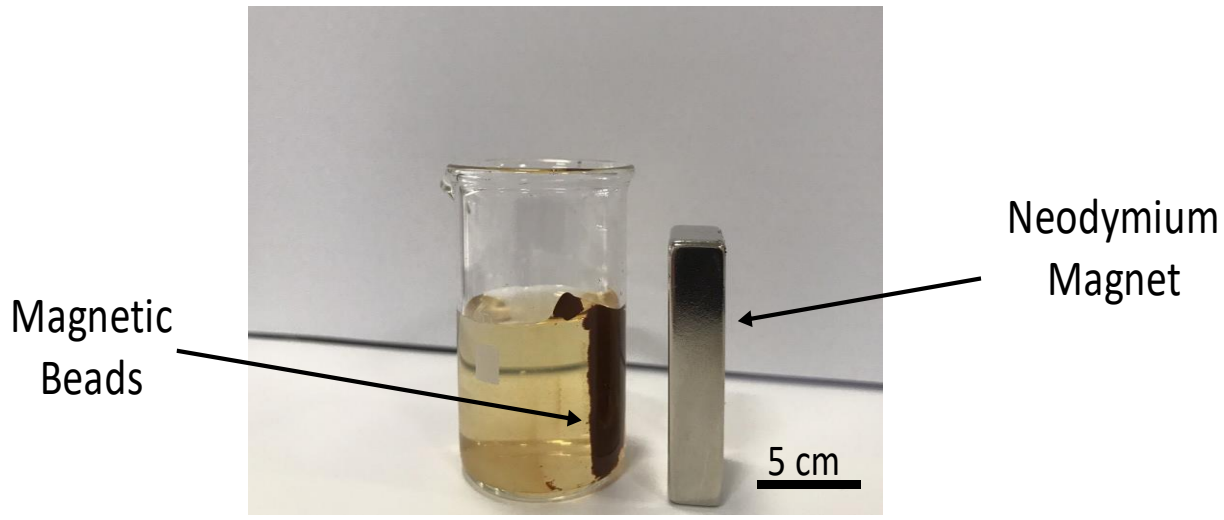

Figure 6.2: Photograph of magnetic particles dispersed in Milli Q water and attracted by neodymium magnet.

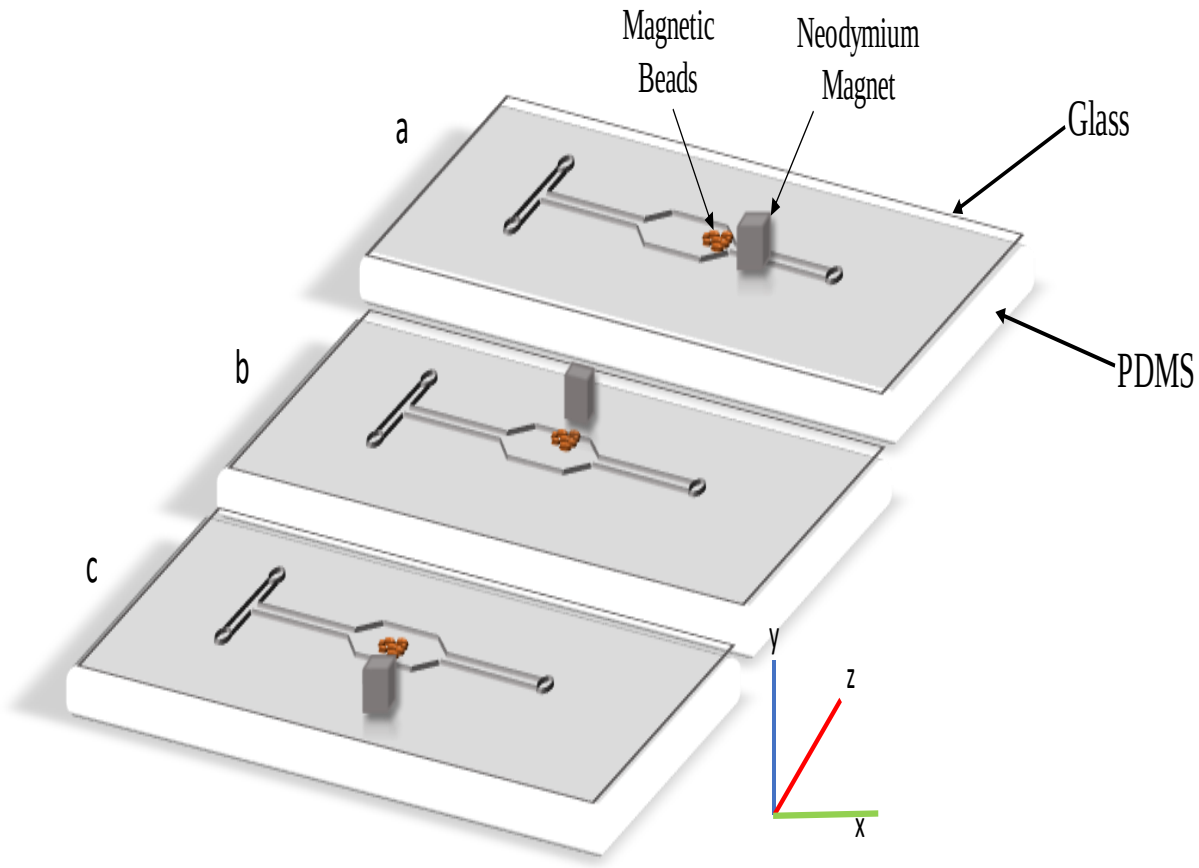

Figure 6.3: Schematic diagrams of the PDMS-glass microfluidic chip using magnetic micro beads as gate keeper inside the micro chamber show the attraction of magnetic beads toward neodymium magnet upon approaching the magnet at any direction around the chamber, a)when approach the magnet from the right side of the chamber, b) when approaching the magnet from the upside the chamber, c) when approaching the magnet from the downside the chamber.

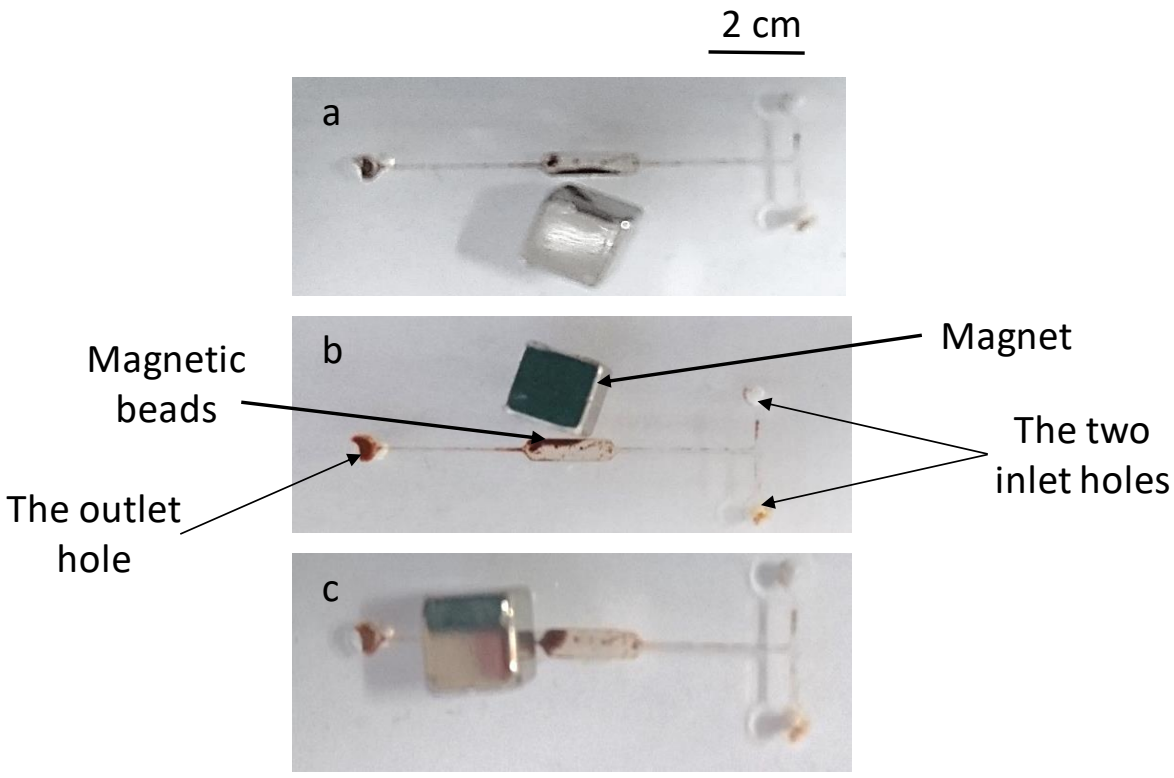

Figure 6.4: Photographs of PDMS/glass microfluidic device show how the magnetic beads can be used as gate keepers inside micro chamber of the microchip. (a) Magnetic beads upon approaching the magnet from the downside of the chip. (b) Magnetic beads upon approaching the magnet from the upside of the chip. (c) Magnetic beads upon approaching the magnet from the left hand of the chip.

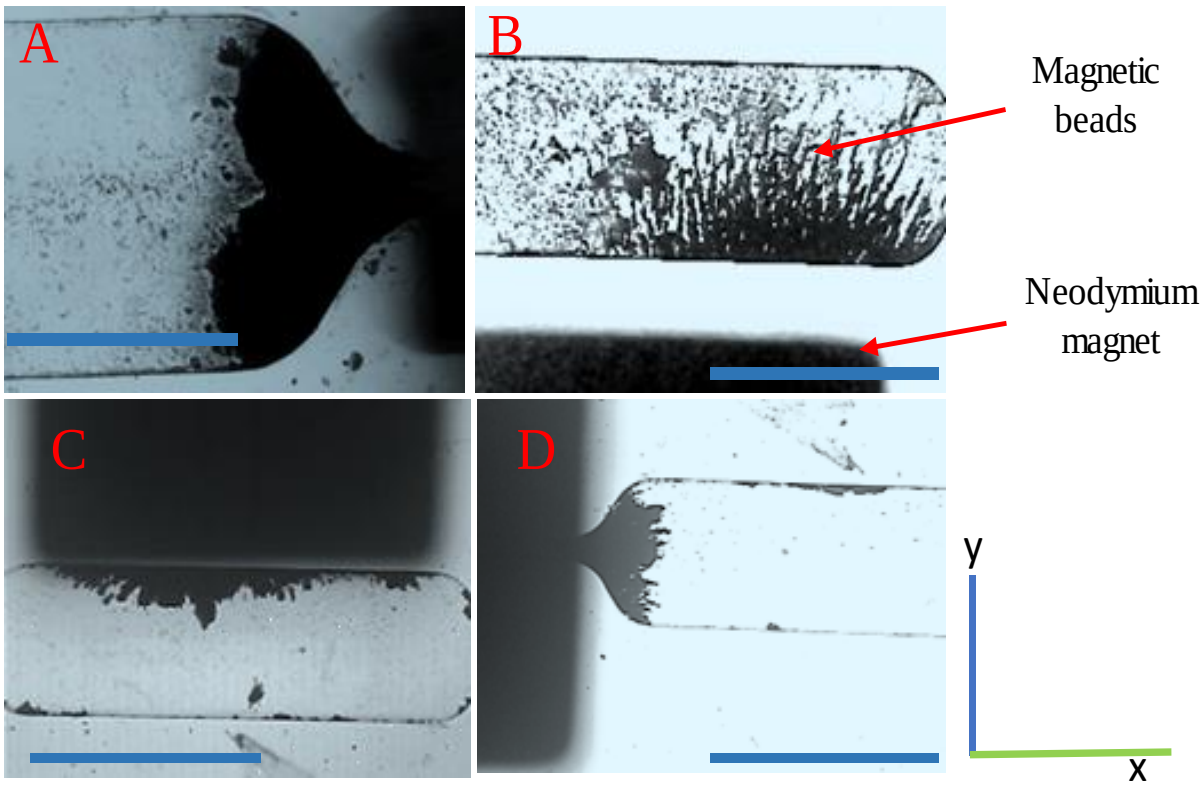

Figure 6.5: Bright field microscopic images of the PDMS-glass microfluidic chamber which show the attraction of magnetic beads toward neodymium magnet upon approaching the magnet from the micro beads. (A) Magnetic beads upon approaching the magnet from the right side of the chip. (B) Magnetic beads upon approaching the magnet from the downside of the chip. (C) Magnetic beads upon approaching the magnet from the upside of the chip. (D) Magnetic beads upon approaching the magnet from the left-hand side of the chip. All scale bars are 500 µm in size.

6.2 Microfluidic Device Cell Based Assay

The closed PDMS-glass microfluidic chip was fabricated by bonding PDMS with microscope glass using an oxygen plasma cleaner machine to activate their surfaces after washing them with detergents and absolute ethanol. Many difficulties were found during bonding the PDMS with microscopic glass such as; the microchamber from PDMS side sometimes bonds with glass layer if they pressed incorrectly; poor bonding between the PDMS and the glass layers leads to fluids leakage from channels or chamber, and hard pressing may break the glass. So to bond these two layers a professional press may be require. The PDMS microfluidic chip with microstructures; two inlet and one outlet channels with holes punched using a 1.25 mm diameter biopsy punch and micro chamber which manufactured by using the mould, as clear in Figure 6.6 (A&B). The polytetrafluoroethylene (PTFE) tubes were placed into the holes, and they fitted perfectly

without the need to add adhesive. Figure 6.6, C, shows how tubes were inserted and fitted directly into microfluidic chip holes from PDMS side without any fluids leakage at 2.5 – 5 µL.min^{-1} flow rate.

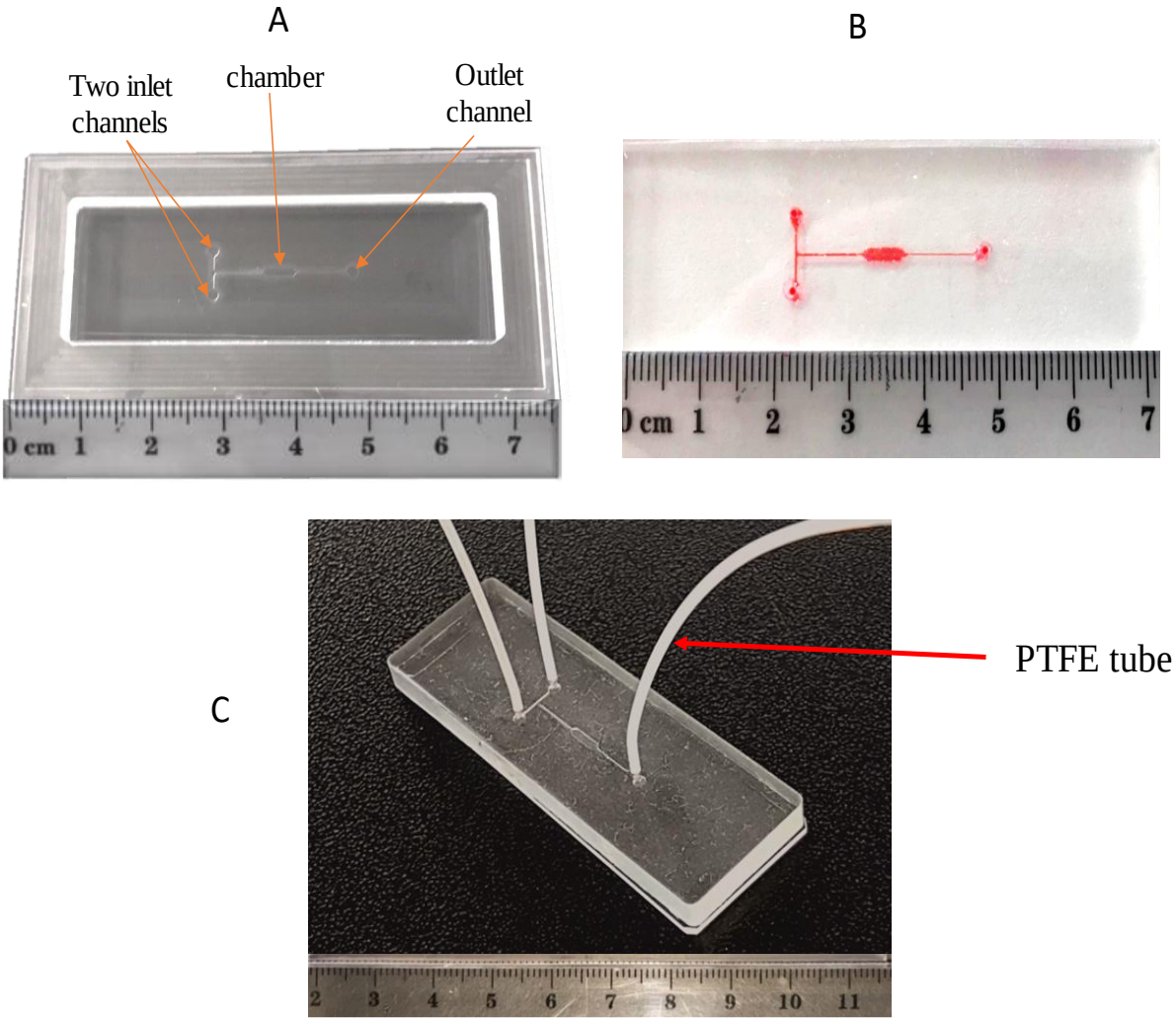

Figure 6.6: (A) PMMA microfluidic mould which can be used for constructing microstructured PDMS chip. (B) The PDMS/glass microfluidic cell based assay for trapping cells using magnetic micro beads as gate keepers into the micro chamber of the microchip. (C) Microfluidics chip cell trapping with PTFE tubes inserted in holes without using any adhesive.

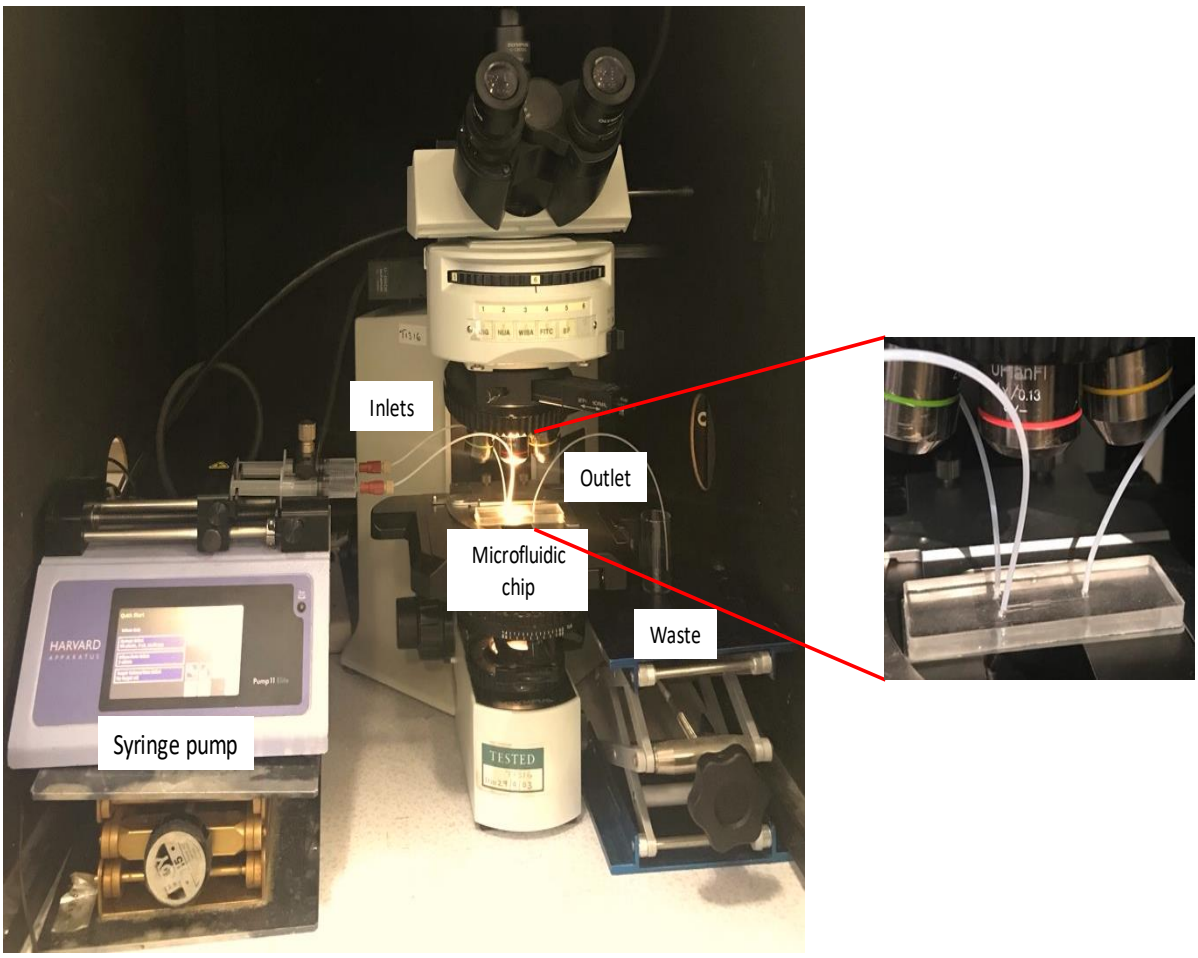

Figure 6.7: The experimental setup of the PDMS/glass microfluidic for cell trapping into the micro chambers using magnetic beads as gate keeper.

Basically, this microfluidic system was designed to be used as a lab on a chip for detecting the cytotoxicity of nanoparticles as pure or loaded with an antimicrobial agent by measuring the intensity of cell viability using a microscope instrument after incubation inside the micro chamber as shown in Figure 6.7. In the first step the cells were trapped by the magnetic beads were pumped using syringe pump then retained inside the chamber using neodymium magnet to hold them at the beginning of the outlet channel as they work as gate keeper, then algae or yeast cells were pumped using syringe pump with flow rate of 2.5-5 $\mu L.min^{-1}$. The cells were left in the device for up to 4 hours to test their toxicity on algae cells. To detect the cell viability FDA reagent assay was pumped slowly through the microchamber and left to react with the cells for 10 minutes, then the cells were washed using PBS or Milli Q water. The intensity of the cell viability was measured using a microscope under the fluorescent field. It can be seen in Figure 6.8 (A&B) that magnetic beads did not show any toxic effect on algal cells. After that, the cells were flushed out of the chamber by moving the magnetic beads aside away from the outlet channel with the

help of neodymium magnet put underneath the chip from the glass side, and the chamber was cleaned using ethanol and Milli Q water, and this enables it to be used again. As a result, the chip can be used to grow algae by flushing culture media and using PDMS layer allow the gases to exchange with the environment as it is known that PDMS has gas permeability property.[427]

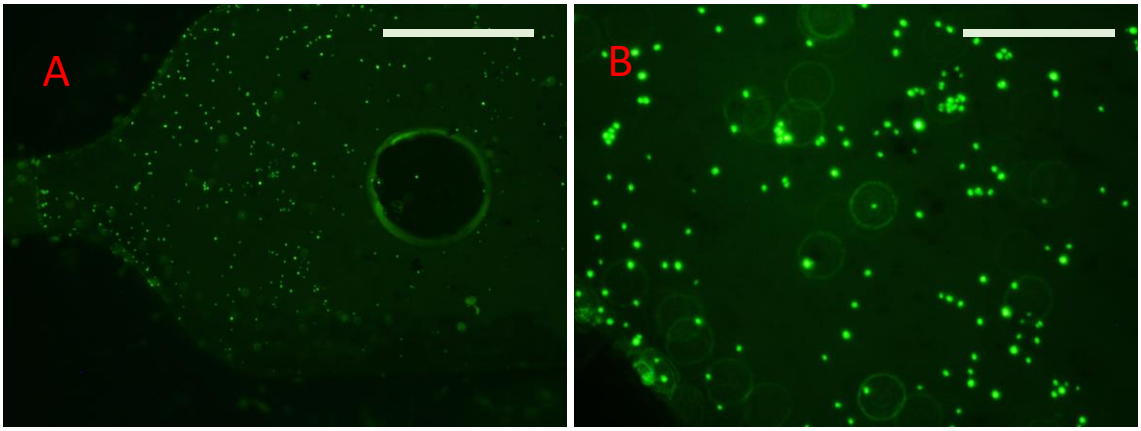

Figure 6.8: Microscopic images of algal cells; A&B: Fluorescent images of algal cells trapped with magnetic beads for 4 hours inside the microfluidic chamber stained with FDA reagent. All scale bars are 500 µm in size and A at 4x, B at 10x.

6.3 Studying the cytotoxicity of Encapsulated CHX coated with ODTAB using Microfluidic Device

To study the cytotoxicity effect of shellac NPs alone and encapsulated CHX coated with ODTAB, first, the cytotoxic effect of shellac NPs on algal cells was studied. The algal cells were trapped inside the chamber as explained before using magnetic beads, then 1 ml of 0.025 wt.% of shellac NPs was pumped at a flow rate of 2.5 µl.min^{-1} and incubated for 4 hours then flushed out the chamber using Milli Q water. To measure the intensity of the cell viability, FDA reagent pumped from two channels and left with the cell for 10 min. then washed using PBS buffer solution, the intensity of the cell viability was measured using microscope instrument. The same process was repeated, but the algal cells were incubated with 0.0001 wt.% of CHX loaded shellac NPs coated with ODTAB for 30 min, (Figure 6.9, A) shows the cell viability of algal cells after incubated with 0.025 wt.% shellac NPs, the picture shows that shellac NPs has no cytotoxic effect on algal cells after 4 hours of incubation and this result is in agreement with *in vitro* study. Figure 6.9, C&D,

show the algal cell viability after incubation with 0.0001 wt.% CHX-NPs coated with ODTAB. As can be seen, the intensity of the cell viability decreased significantly.

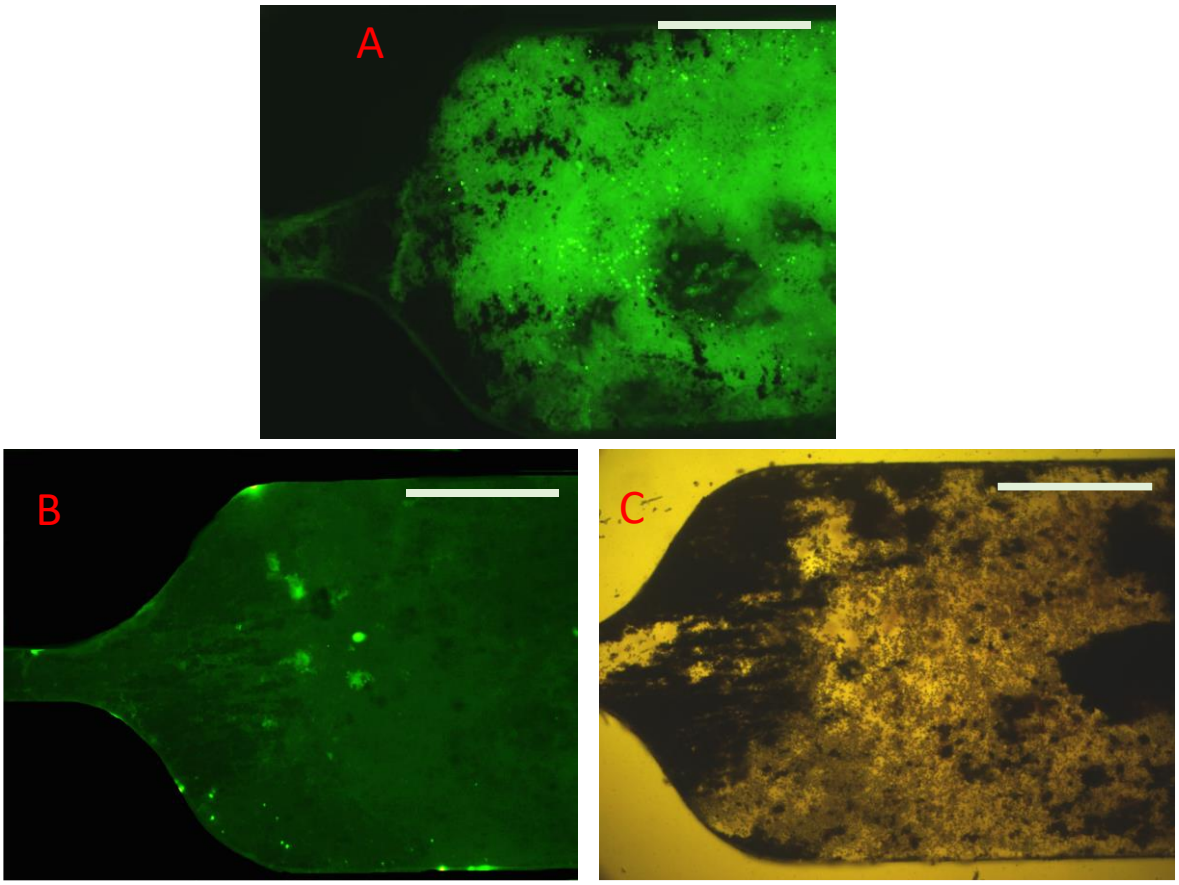

Figure 6.9 Microscopic images of algal cells; A; Fluorescent image of algal cells trapped with shellac NPs using magnetic beads for 4 hours inside the microfluidic chamber stained with FDA reagent, C; Florescent and bright images of algal cells trapped with 0.0001 wt.% CHX loaded shellac NPs coated with ODTAB for 30 minutes stained with FDA reagent. All scale bars are 500 µm in size.

The PDMS-glass microfluidic chip has considerable advantages which can be summarized as low cost of fabrication, simple in design, reusable and time consume, in spite of these advantages there are some disadvantages has been noticed while working with it such as some cells and fluids can be leaked outside the chamber or channels as shown in Figure 6.10. The reason behind this is due to the poor bonding between PDMS and glass, also blocking may occur within magnetic beads and cells which prevent fluids to flush out and creating back pressure which then led to leaks. To avoid these disadvantages a glass/glass microfluidic chip were constructed with the same design as PDMS-glass chip and was used for the same purpose to monitor the cytotoxicity of the nanoparticles loaded antimicrobial agents, Figure 6.11. Also, a block occurred sometimes when trapping algae cells with magnetic beads and this may contribute to the reason that algae cells have flagella and

these may overlap with each other and block the outlet channel. Due to the narrow time working on the microfluidic, using another kind of microorganisms like yeast cells at very low concentrations may work as it was used before in some research using microfluidic chips.[428]

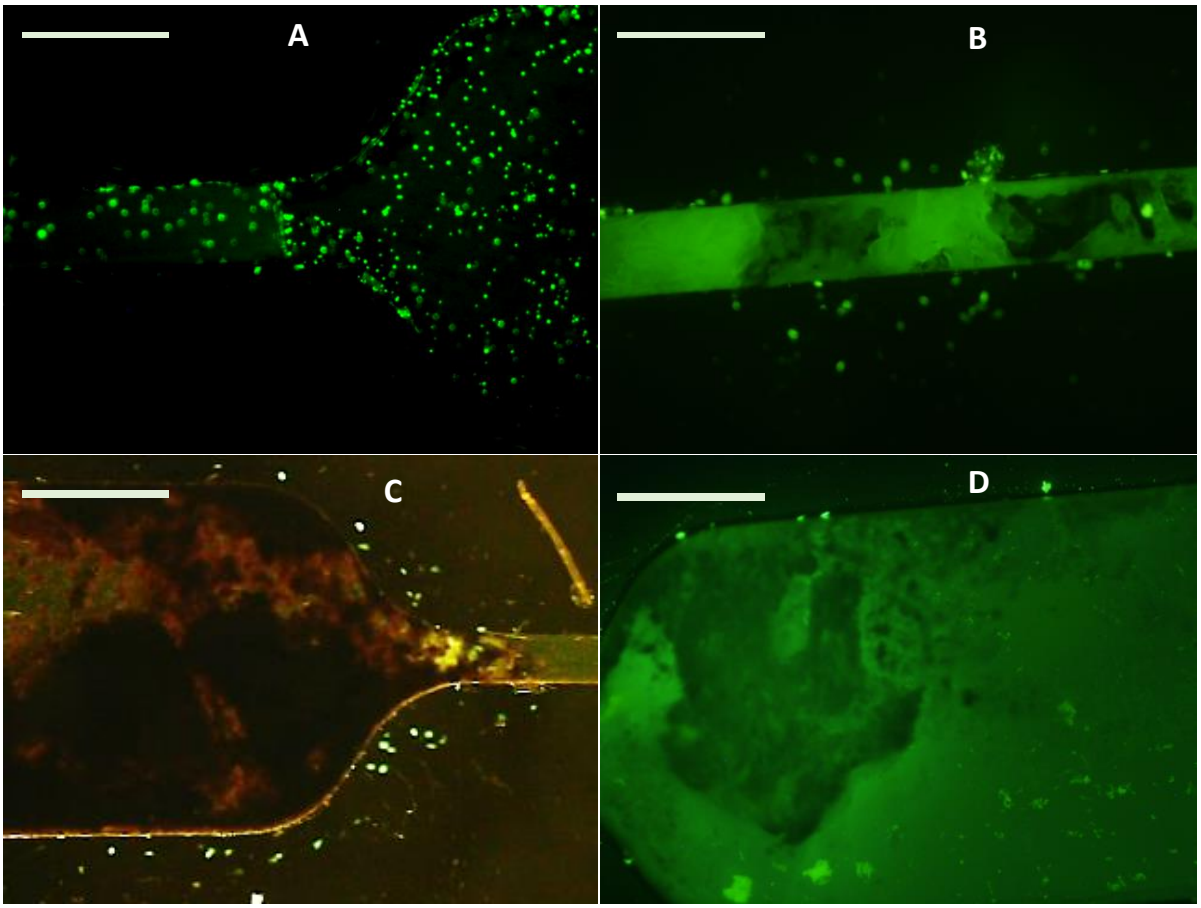

Figure 6.10: (A, B, C, and D) are fluorescent microscopic images of algal cells stained with FDA reagent shows the leaking of some cells through chamber or channels. All scale bars are 500µm in size.

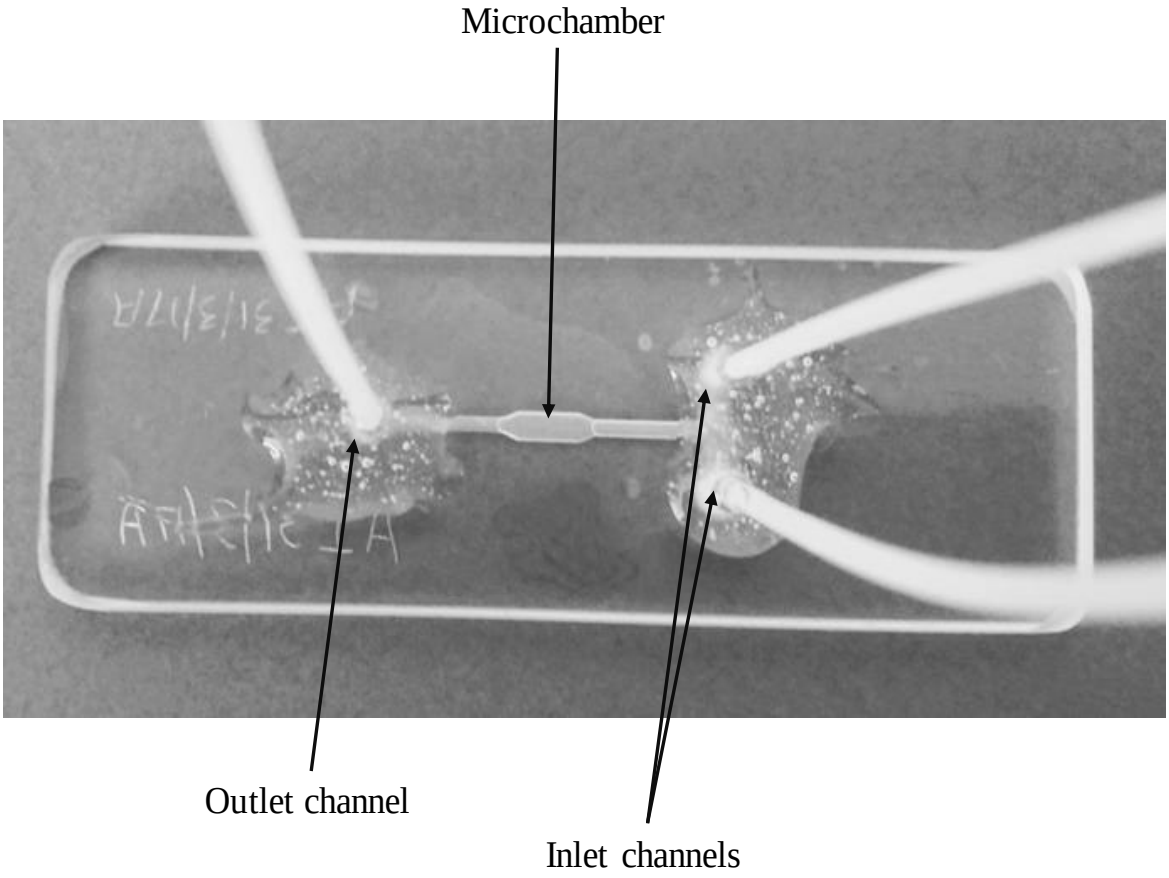

Figure 6.11: The glass/glass microfluidic chips for cell trapping assay.

6.4 Conclusion

This chapter presents the application of microfluidic device cell based assay. PDMS/glass microfluidic chip was fabricated using a master mould, the PDMS and glass layer were bonded using plasma machine. The chip included two inlet channels, micro chamber and one outlet channel. The top layer was PDMS and the bottom layer was microscope glass. Magnetic beads were used as gate keeper to retain the cells inside the micro chamber and allow the fluids to pass through the outlet channel, a magnet was used to move the magnetic beads at any direction inside the chamber. Algal cells were incubated with encapsulated chlorhexidine coated with ODTAB for 30 min, the intensity of the viable cells was decreased when they exposed to the nanoparticles loaded CHX coated with ODTAB comparing to algal cell intensity alone, while shellac NPs unloaded antimicrobial did not show any cytotoxicity on this microorganism.

Chapter 7 : The Summary

Nanoparticles are very promising tool for development of drug-delivery vehicles for the pharmaceutical industries due to their unique combination of properties. Their large surface area due to their nanoscale size, and the possibility for surface functionalisation allow novel targeted drug delivery approaches to be developed to target different diseased tissues. In this thesis a new type of nanocarriers was developed based on shellac and explored their ability to be loaded or encapsulated with various antimicrobials and antibiotics with controlled release and their effect on a range of microorganisms. The aim of the work in this thesis was to construct a universal nanocarrier can be loaded with different kind of antimicrobial by using different component as well as systematically characterised and can be used for wound treatment. Shellac, a natural biodegradable and biocompatible polymer was chosen to be used as nanocarrier owing to its composition which contains carboxylic groups that allow it to be loaded with cationic antimicrobial, and hydrophobic part which allow hydrophobic antimicrobial to be loaded within it. Also, depending on the interaction strength between the shellac NPs and the antimicrobial the drug release can be defined, i.e. for slow release an antimicrobial with many cationic groups or hydrophobic antimicrobial can be used like CHX or CUR where they showed slow release owing to the strong interaction with shellac NPs. While for fast drug release an antimicrobial with few or one cationic group can be loaded like BRB which showed fast release due to the weak interaction with shellac NPs. Moreover, shellac nature allow it to be functionalised to change the surface charge to be positive at the same time retain balanced stability. Changing the surface charge of shellac NPs into positive is one of the most requirements that's enable it to be used against any type of microorganisms as well as amplify the cytotoxicity of the loaded antimicrobial. Poloxamer 407 was used as stabilizer agent for shellac NPs by conducting a steric repulsion among shellac particles as can be seen in figure 3.2 B. Besides its role in maintain the stability of shellac NPs, Poloxamer 407 has been widely used in pharmaceutical product and as drug delivery vehicle owing to its low toxicity. [429, 430] Shellac as nanocarrier was rarely used, only 2 literatures showed that it was loaded with bovine serum albumin, and silibinin using chitosan and xanthan gum as stabilizers, respectively. Shellac NPs were loaded for the first time with BRB, CHX, CUR, and VCM, and their cytotoxicity addressed against different kind of microorganisms like *C. reinhardtii, Saccharomyces Cerevisiae,* and *E.coli*.

Chapter 2, described the methods and materials for preparation of the nanocarriers as well as the procedures of loading the antimicrobial agents and surface modification. Also,

the particle characterisation methods were presented and using cell viability assays for assessment of antimicrobial action. As well as, the construction and design of a microfluidic chip was discussed with using magnetic beads operated chamber gates for entrapment of cells for testing antimicrobial action.

In chapter 3, the choice of materials was explained and the ideas behind the nanocarrier design. Shellac was selected as a suitable material as it is easy to process and formulate as nanoparticle suspension and it has high hydrophobicity which allows encapsulation of diverse antimicrobial agents. In this study shellac NPs were used as nanocarrier for delivering four different antimicrobial agents, namely, berberine chloride, chlorhexidine di-gluconate, curcumin, and vancomycin hydrochloride. These antimicrobial agents were encapsulated within shellac NPs. Shellac nanocarriers can be loaded with different types of antimicrobials as it contains carboxylic groups which allow it to interact with cationic antimicrobials like chlorhexidine, berberine and vancomycin. Shellac also offers sufficient hydrophobicity which enables it to be directly loaded with hydrophobic antimicrobials such as curcumin and thus increase their solubility and bioavailability. The shellac nanoparticles were prepared by pH-induced precipitation and sterically stabilised by the surface active polymer Poloxamer 407 as stabilizer agent. The Poloxamer 407 enabled steric repulsion between the shellac particles accompanied by reducing the pH from 8 to 5 using diluted HCl. Poloxamer 407 was preferred over three other different types of surfactants to obtain stable shellac NPs such as; sodium dodecyl sulfate (SDS), Cetyltrimethylammonium bromide (CTAB), and Tween 20. These nanoparticles were successfully prepared at 0.25:0.2 wt.% mixture of shellac:P407, with an average particle size of 66±5 nm and zeta potential -18±8 mV. These NPs showed a stability exceeding 3 months at 20±4 °C and at different range of pH (4-7). To enhance the interaction of the drug loaded nanoparticles with the microbial cells membrane they were further functionalized to change the surface charge from negative to positive using the insoluble cationic surfactant octadecyltrimethyl ammonium bromide (ODTAB). Conditions were found enabling charge-reverse the drug-loaded shellac NP with ODTAB without changing the size and stability but having positive zeta potential, which promotes electrostatic attraction to the microbial cell walls. Berberine chloride was encapsulated within shellac NPs at pH 5 with average particle size of 77±34 nm and ζ-potential -14.8 mV before coating with ODTAB. The encapsulation efficiency was 60% at pH 5 with a drug loading of 28% at $10.4x10^{-6}$ $mol.mL^{-1}$. 100% of the BRB was released at pH 5.5 and 75% at pH 7.4 after 8 hours. Chlorhexidine di-gluconate was encapsulated within shellac NPs at

various concentrations up to 0.07 wt.% with an average particle size 79±30 nm and ζ-potential -11±8 mV before coating with ODTAB. Around 92 % of the total concentration of CHX was encapsulated within shellac NPs with a drug loading of 16 % at $5.57x10^{-7}$ $mol.mL^{-1}$. In this case only 36% was released at pH 5.5 and 12% at 7.4 after 8 hours. The electrostatic interaction between shellac NPs and BRB and CHX was verified using UV-Visible and FTIR techniques. CUR was encapsulated within shellac NPs with an average particle size distribution of 87±26 nm and zeta potential of -5±0.6 mV (before ODTAB coating). 100% of the total curcumin concentration was encapsulated within shellac NPs with a drug loading content of up to 33.8% at 13.6 $x10^{-6}$ $mol.mL^{-1}$. It was found that the CUR release was very slow at both pHs 5.5 and 7.4, and it was 3.5% after 2 days at pH 5.5 and half the amount at pH 7.4. VCM was loaded within shellac NPs at pH 6 with an average particle size of 80±24 nm and ζ-potential -7 mV. 87.5% encapsulation efficiency was achieved at pH 6 with VCM loading content of 13.6% at 48.3 $x10^{-7}$ $mol.mL^{-1}$. For VCM, 54% of the drug was released at pH 5.5 and 37% at pH 7.4 after 30 hours. Although good for sustained release of VCM, this effect impaired its antimicrobial effects which were obtained only from using high dosages. The adsorption interaction between shellac NPs and CUR as well as the electrostatic interaction between shellac NPs and VCM were confirmed using UV-Visible and FTIR techniques. Table 3.5 shows some *in vitro* characteristics of the loaded drugs within shellac NPs including the particle size, the surface charge, the encapsulation efficiency, the drug content within shellac NPs, and the released amount of the drug at pH 5.5 after 8 hours and compared with other nanocarriers loaded with the same drugs in terms of the drug release. By comparing these characteristics of BRB, CHX, CUR, and VCM encapsulated shellac NPs with the same antimicrobials loaded with other nanocarriers, as mentioned in tables 1.2, 1.3, 1.4, and 1.5, it can be seen none of these nanocarriers have been loaded with more than one antimicrobial. In this project it was found that shellac NPs can be loaded with different types of antimicrobial including cationic antimicrobial agents like BRB, CHX, or hydrophobic antimicrobial like CUR, even can be loaded with antimicrobial has bulky molecules like VCM, and this diversity in loading with different type of drugs attributed to the nature of shellac which contains of carboxylic groups as well as hydrophobic parts and this makes it as a universal nanocarrier. By comparing the results of this project with other literatures, it can be noticed that most the nanocarriers' characteristics have some deficiency in their results. Herein, the aimed was to construct stable nanocarrier able to be loaded with different drugs and well characteristics, as well as its surface can be functionalized to produce positive surface charge to promote the adhesion with any type of microorganisms. Also, the drug release

of most nanocarriers mentioned in literatures have been studied at one pH media, while in this project the drug released was studied at two different pH media 7.4 and 5.5. Beside shellac NPs showed stability at a range of pH which means the drug release can be studied at range from 4-7. Moreover, the results in table 3.5 show that depending on the requirement of the drug release, i.e. slow or fast, the type of the drug can be loaded within shellac NPs. In other words if it is needed a slow release so an antimicrobial with large amount of positive charge atoms like CHX can be used or hydrophobic drug like CUR may load in case the requirement is a very slow release. While for fast release an antimicrobial with less positive charge atom can be loaded within shellac NPs to insure a weak electrostatic interaction between the drug and shellac NPs and thus fast release, like BRB.

In Chapter 4, the cytotoxic effect of berberine and chlorhexidine loaded shellac NPs was then studied on microalgae, yeast and *E.coli* cells. These three kind of cells were chosen as different kind of microorganisms. Algae is kind of plankton, yeast is eukaryotic, and *E.coli* is prokaryotic. The results showed that unloaded shellac NPs did not express any antimicrobial action on yeast and *E.coli* except minor effect on algae due to the presence of Poloxamer 407 which was used as stabilizer. It was found that solutions of free BRB showed moderate cytotoxic effect on microalgae and *E.coli*, but not on yeast. After encapsulating BRB within shellac NPs this effect reduced further due to the interaction between the cationic BRB and anionic shellac NPs which delays the BRB release. This was partially caused by the negatively charged shellac NPs (uncoated with ODTAB) which are repelled away from the negative charged cell membranes. Free chlorhexidine showed significant cytotoxic effect on algae, yeast, and *E.coli*, but when it was encapsulated within shellac NPs this action was reduced due to similar reasons. After coating the drug-loaded NPs with ODTAB, the encapsulated BRB and CHX, their cytotoxic effect increased sharply due to rapid attraction between the cationic ODTAB-coated shellac NPs with encapsulated BRB and CHX and the negatively charged microbial cell membranes, which lead the drug to be released directly onto the cell walls. This strongly increased the antimicrobial action of both BRB and CHX which exceeded those of solutions with equivalent total concentrations of BRB and CHX, as can be seen in table 4.1. In section 1.7.2, some literatures presented the cytotoxicity of berberine loaded with different nanocarriers on different type of cells. One of the most recent studies showed that the minimum inhibition concentrations (MIC) of BRB NPs were 0.064 and 0.032 $mg.mL^{-1}$ on yeast and *E.coli*, respectively.[407] While the current study showed the MIC of encapsulated BRB coated with ODTAB was 0.005 and 0.01 $mg.mL^{-1}$ on yeast and *E.coli*, respectively.

Also literatures showed the cytotoxicity of encapsulated CHX on different type of bacteria was 0.02-1.25 mg.mL^{-1}, whereas in this project it was 0.01 mg.mL^{-1} on *E.coli* cells.[408] [237, 421] Also, the cytotoxicity of BRB was studied after encapsulating it with carbopol and coated with PDAC on algae and *E.coli.* The study showed the MIC was 0.0015 and 0.0025 g.mL^{-1} on algae and *E.coli*, respectively.[379] While the results of the current project showed that the MIC was 0.0005 and 0.0001 g.mL^{-1} on algae and *E.coli*, respectively. The high cytotoxicity of the drug loaded shellac NPs and coated with ODTAB attributed to the positive surface charge of shellac NPs which increase the attraction with the cell membrane and thus kill the cell fast at very small amount of drug.

In Chapter 5, the antimicrobial activity of curcumin (CUR) and vancomycin hydrochloride (VCM) was investigated. Curcumin is a natural product with broad spectrum antimicrobial activity including antiviral, antibacterial, antimalarial and antifungal activities.[412, 419] However, it is not easy to solubilise in water and was therefore encapsulated within shellac nanocarriers, which allow to release CUR directly on the microbial cell membranes. Vancomycin, is an antibiotic produced from *Streptomyces orientalis* strains[218] and this was also loaded within shellac nanocarriers, this approach should also allow sustained release of the antibiotic and the cell membrane thus enhancing its effectiveness. The study included testing of the antimicrobial action of CUR and VCM loaded shellac NPs before and after functionalizing the surface of the NPs with cationic surfactant ODTAB to study the effect of the surface charge of the NPs. The results showed that free CUR showed significant cytotoxic effect on these cells at low concentrations, but after loading it within shellac NPs its cytotoxicity was reduced, probably due to the high affinity between shellac and CUR particles which led to slower release. However, shellac NP with encapsulated CUR coated with ODTAB showed very strong cytotoxic action on these microorganisms. It also was found that VCM did not have noticeable cytotoxic effect even at high concentration for both free VCM and when it encapsulated within shellac NPs. The ODTAB-coated VCM loaded shellac nanocarriers, however, showed significant cytotoxic action across all tested microorganism, as can be seen in table 5.1. In a recent study Katiraee *et.al,*[422] presented that 0.04 wt.% of nanocurcumin can show antifungal action against different types of fungi, while in current study only 0.0005 wt.% of CUR loaded shellac NPs coated with ODTAB can significantly kill the fungi after 2 hours. In another study,[388] and by using a wet-milling technique to prepare nanocurcumin, it was found that the minimum inhibitory concentration (MIC) of nanocurcumin on *E.coli* was 0.25 mg.mL^{-1}, while the present study showed that 0.01 mg.mL^{-1} of encapsulated CUR

coated with ODTAB can effect significantly on *E.coli*. Whereas no literatures were found to show the nanocurcumin cytotoxicity against algae. On the other hand, a study showed that the MIC of nanovancomycin on *E.coli* was >1.28 $mg.mL^{-1}$, while this study showed that the minimum inhibition concentration of encapsulated VCM coated with ODTAB was 0.01 $mg.mL^{-1}$.[421] Most published literatures of nanovancomycin were about studying its cytotoxicity on gram-positive bacteria, and no researches were found for nanovancomycin against algae or yeast. The high cytotoxicity of the drug loaded shellac NPs and coated with ODTAB attributed to the positive surface charge of shellac NPs which increase the attraction with the cell membrane and thus kill the cell fast at very small amount of drug.

In Chapter 6, the development of a microfluidic device cell- based assay was studied. The closed PDMS-glass microfluidic chip was fabricated by bonding PDMS with microscope glass using an oxygen plasma cleaner machine to activate their surfaces. The initial microfluidic device was composed of two layers, the top was PDMS which incorporated the channels, and the bottom layer was a microscope slide. The device consisted of two inlet channels, a micro-chamber and one outlet channel. The cells were trapped inside the micro-chamber and allowed to be exposed to the studied solution of antimicrobial nanoparticle suspensions to test their antimicrobial action on the cells by measuring the intensity of their fluorescence through a viability assay. The novelty here is the use of magnetic beads operated gates of the cell testing chambers which were used to trap the cells on the chip and allow fluids to pass through the outlet channel. These magnetic beads were successfully positioned and moved around the micro-chamber using a permanent magnet. Algae cells were trapped inside the micro-chamber using magnetic beads, as these beads showed no toxicity upon incubation with algae. A suspension of 0.0001 wt.% ODTAB coated shellac NPs encapsulated with CHX was incubated with algae cell inside the micro-chamber for 30 min and it showed significant cytotoxicity. The developed chip has the advantage of being able to hold the tested microorganisms in a flow-through micro-chamber which allows different NPs formulations to be flown and tested *in-situ*. Although the working chip functionality for loading and holding the tested cell in the chamber and the operating of the magnetic gates was demonstrated, the work on testing the constructed chip is still in progress and will be completed beyond the duration of this PhD project.

Chapter 8 : References

1. D. Peer, Karp, Jeffrey M.Hong, SeungpyoFarokhzad, Omid C.Margalit, RimonaLanger, Robert, *Nature Nanotechnology*, 2007, **2**, 751-760.
2. R. Feynman, *Science*, 1991, **254**.
3. P. Gajjar, Pettee, Brian Britt, David W.Huang, Wenjie,Johnson, William P. Anderson, Anne J., *Journal of Biological Engineering*, 2009, **3**, 9-9.
4. N. Sanvicens and M. P. Marco, *Trends in Biotechnology*, 2008, **26**, 425-433.
5. H. Hillaireau, Couvreur, Patrick, *Cellular and Molecular Life Sciences*, 2009, **66**, 2873-2896.
6. G. P. A. M. Gupta, S. P. Vyas, *Current Molecular Medicine*, 2013, **13**, 179-204.
7. A. C. S. Samia, Dayal, Smita,Burda, Clemens, *Photochemistry and Photobiology*, 2006, **82**, 617-625.
8. W. H. De Jong and P. J. A. Borm, *International Journal of Nanomedicine*, 2008, **3**, 133-149.
9. A. Lamprecht, U. Schäfer and C.-M. Lehr, *Pharmaceutical Research*, 2001, **18**, 788-793.
10. M. Rawat, D. Singh, S. Saraf and S. Saraf, *Biological and Pharmaceutical Bulletin*, 2006, **29**, 1790-1798.
11. B. E. Rabinow, *Nature Reviews Drug Discovery*, 2004, **3**, 785-796.
12. C. R. Martin and P. Kohli, *Nature Reviews Drug Discovery*, 2003, **2**, 29-37.
13. D. Luo, E. Han, N. Belcheva and W. M. Saltzman, *Journal of Controlled Release*, 2004, **95**, 333-341.
14. A. D. Bangham, M. M. Standish and J. C. Watkins, *Journal of Molecular Biology*, 1965, **13**, 238-IN227.
15. M. M. Frank, *The Journal of Laboratory and Clinical Medicine*, 1993, **122**, 487-488.
16. W. Mehnert and K. Mäder, *Advanced Drug Delivery Reviews*, 2001, **47**, 165-196.
17. K. Akiyoshi, S. Kobayashi, S. Shichibe, D. Mix, M. Baudys, S. Wan Kim and J. Sunamoto, *Journal of Controlled Release*, 1998, **54**, 313-320.
18. H. Weng, J. Zhou, L. Tang and Z. Hu, *Journal of Biomaterials Science, Polymer Edition*, 2004, **15**, 1167-1180.
19. A. M. Hillery, I. Toth and A. T. Florence, *Pharmacy and Pharmacology Communications*, 1996, **2**, 281-283.
20. N. Nishiyama and K. Kataoka, in *Polymer Drugs in the Clinical Stage*, Springer, 2004, pp. 155-177.
21. R. Savić, L. Luo, A. Eisenberg and D. Maysinger, *Science*, 2003, **300**, 615-618.
22. D. A. Tomalia, H. Baker, J. Dewald, M. Hall, G. Kallos, S. Martin, J. Roeck, J. Ryder and P. Smith, *Polymer Journal*, 1985, **17**, 117-132.
23. D. F. Emerich and C. G. Thanos, *Expert Opinion on Biological Therapy*, 2003, **3**, 655-663.
24. G. T. Hermanson, *Bioconjugate techniques*, Academic press, 2013.
25. K. R. K. Vyas S. P., *Targeted and Control Drug Delivery*, CBS Publishers and Distributors, New Delhi, 1st ed edn., 2002.

26. L. Brannon-Peppas, *International Journal of Pharmaceutics*, 1995, **116**, 1-9.
27. K. S. Soppimath, T. M. Aminabhavi, A. R. Kulkarni and W. E. Rudzinski, *Journal of Controlled Release*, 2001, **70**, 1-20.
28. K. J., *Nanoparticles. In Colloidal drug delivery systems*, J, K., Ed. Marcel Dekker, New York,, 1994.
29. Y. P. Li, Y. Y. Pei, Z. H. Zhou, X. Y. Zhang, Z. H. Gu, J. Ding, J. J. Zhou and X. J. Gao, *Journal of Controlled Release*, 2001, **71**, 287-296.
30. T. Niwa, H. Takeuchi, T. Hino, N. Kunou and Y. Kawashima, *Journal of Controlled Release*, 1993, **25**, 89-98.
31. G. Puglisi, M. Fresta, G. Giammona and C. A. Ventura, *International Journal of Pharmaceutics*, 1995, **125**, 283-287.
32. P. Calvo, C. Remuñán-López, J. L. Vila-Jato and M. J. Alonso, *Journal of Applied Polymer Science*, 1997, **63**, 125-132.
33. A. R. Reverchon E, *The Journal of Supercritical Fluids*, 2006, **37**, 1-22.
34. M. B. Rolland JP, Euliss LE, Exner AE, Denison and D. J. GM, *Journal of the American Chemical Society*, 2005, **127**, 10096-10100.
35. J. Xu, D. H. C. Wong, J. D. Byrne, K. Chen, C. Bowerman and J. M. DeSimone, *Angewandte Chemie International Edition*, 2013, **52**, 6580-6589.
36. K. Ranjit and A. Ahmed, *International Research Journal of Pharmacy*, 2013, **4**.
37. J. Möschwitzer, *Nanotechnology: Particle Size Reduction Technologies in the Pharmaceutical Development Process*, 2010.
38. F. Martinez-Gutierrez, P. L. Olive, A. Banuelos, E. Orrantia, N. Nino, E. M. Sanchez, F. Ruiz, H. Bach and Y. Av-Gay, *Nanomedicine: Nanotechnology, Biology and Medicine*, 2010, **6**, 681-688.
39. V. Mohanraj and Y. Chen, *Tropical Journal of Pharmaceutical Research*, 2006, **5**, 561-573.
40. J. L. West and N. J. Halas, *Current Opinion in Biotechnology*, 2000, **11**, 215-217.
41. M. C. Roco, *Current Opinion in Biotechnology*, 2003, **14**, 337-346.
42. S. K. Sahoo and V. Labhasetwar, *Drug Discovery Today*, 2003, **8**, 1112-1120.
43. J. M. Wilkinson, *Medical Device Technology*, 2003, **14**, 29-31.
44. H. Yamamoto, Y. Kuno, S. Sugimoto, H. Takeuchi and Y. Kawashima, *Journal of Controlled Release*, 2005, **102**, 373-381.
45. J. E. Kipp, *International Journal of Pharmaceutics*, 2004, **284**, 109-122.
46. L. Ould-Ouali, M. Noppe, X. Langlois, B. Willems, P. Te Riele, P. Timmerman, M. E. Brewster, A. Ariën and V. Préat, *Journal of Controlled Release*, 2005, **102**, 657-668.
47. P. Arbós, M. A. Campanero, M. A. Arangoa and J. M. Irache, *Journal of Controlled Release*, 2004, **96**, 55-65.
48. L. Brannon-Peppas and J. O. Blanchette, *Advanced Drug Delivery Reviews*, 2004, **56**, 1649-1659.
49. J. Kreuter, *Advanced Drug Delivery Reviews*, 2001, **47**, 65-81.
50. H. Cohen, R. Levy, J. Gao, I. Fishbein, V. Kousaev, S. Sosnowski, S. Slomkowski and G. Golomb, *Gene Therapy*, 2000, **7**, 1896-1905.

51. R. Löbenberg and J. Kreuter, *AIDS Research and Human Retroviruses*, 1996, **12**, 1709-1715.
52. P. H. Hoet, I. Brüske-Hohlfeld and O. V. Salata, *Journal of Nanobiotechnology*, 2004, **2**, 1-15.
53. I. J. Ogaji, E. I. Nep and J. D. Audu-Peter, *Pharmaceutica Analytica Acta*, 2012, **3**, 146.
54. S. K. Sharma, S. K. Shukla and D. N. Vaid, *Defence Science Journal*, 1983, **33**, 261-271.
55. W. H. Gardner and W. F. Whitmore, *Industrial and Engineering Chemistry*, 1929, **21**, 226-229.
56. O. P. Chauhan, P. S. Raju, A. Singh and A. S. Bawa, *Food Chemistry*, 2011, **126**, 961-966.
57. S. Limmatvapirat, C. Limmatvapirat, S. Puttipipatkhachorn, J. Nuntanid and M. Luangtana-anan, *European Journal of Pharmaceutics and Biopharmaceutics*, 2007, **67**, 690-698.
58. M. P. L. M. Bellan , D. M. Cropek , R. Langer *Advanced Materials*, 2012, **24**, 5187.
59. S. R. Palit, *Journal of Indian Chemical Society*, 1940, **17**, 308.
60. S. R. Palit, *Indian Lac Research Institute, Bulletin*, 1942, **46**.
61. P. Kraisit, S. Limmatvapirat, J. Nunthanid, P. Sriamornsak and M. Luangtana-anan, *Pharmaceutical Development and Technology*, 2013, **18**, 686-693.
62. R. C. Rowe, P. J. Sheskey and P. J. Weller, *Handbook of pharmaceutical excipients*, London ; Chicago : Washington, DC : Pharmaceutical Press ; American Pharmaceutical Association, England, 4th edn., 2003.
63. A. Tschirch, Farner, A. ,Studien über den Stocklack., *Archiv der Pharmazie*, 1899, **237**, 35-48
64. R. Prasad and S. C. Sengupta, *Journal of the Oil and Colour Chemists'Association*, 1978, **61**, 49-51.
65. H. S. Cockeram, Levine, S.A., *Journal of the Society of Cosmetic Chemists*, 1961, **12**, 316-323.
66. K. Buch, Penning, M., Wächterbach, E., Maskos, M., Langguth, P., *Drug Development and Industrial Pharmacy*, 2009, **35**, 694-703.
67. M. S. Wadia, R. G. Khurana, V. V. Mhaskar and S. Dev, *Tetrahedron*, 1969, **25**, 3841-3853.
68. L. Wang, Y. Ishida, H. Ohtani, S. Tsuge and T. Nakayama, *Analytical Chemistry*, 1999, **71**, 1316-1322.
69. S. Limmatvapirat, C. Limmatvapirat, M. Luangtana-anan, J. Nunthanid, T. Oguchi, Y. Tozuka, K. Yamamoto and S. Puttipipatkhachorn, *International Journal of Pharmaceutics*, 2004, **278**, 41-49.
70. H. H. Mathur, Bhattacharya, S.C., *Journal of the Chemical Society*, 1963, 114-118.
71. M. K. Mishra, *Journal of Macromolecular Science: Part A - Chemistry*, 1983, **20**, 619-625.
72. J. Möller-Kemsa, *Fat Science Technology*, 1992, **94**, 277-279.

73. P. K. Bose, Y. Sankaranarayanan and S. C. Sen Gupta, *Chemistry of lac*, Indian Lac Research Institute, Ranchi, 1963.
74. C. E. Barnes, *Industrial and Engineering Chemistry*, 1938, **30**, 449-451.
75. Y. Farag and C. S. Leopold, *Dissolution Technologies*, 2009, **16**, 33-39.
76. R. C. Rowe, P. J. Sheskey, S. n. C. Owen and A. American Pharmacists, *Handbook of pharmaceutical excipients*, APhA/Pharmaceutical Press, London; Chicago, 2009.
77. D. Nath Goswami, N. Prasad, B. Baboo, K. Kishore Kumar and M. Fahim Ansari, *Pigment & Resin Technology*, 2009, **38**, 211-217.
78. F. Specht, M. Saugestad, T. Waaler and B. Müller, *Pharmaceutical Technology*, 1999, **23**, 146-154.
79. M. Luangtana-Anan, S. Limmatvapirat, J. Nunthanid and C. Wanawongthai, *Journal of Agricultural and Food Chemistry*, 2007, **55**, 687-692.
80. https://www.indiamart.com/tolaram/new-items.html#stick-lac, 02/10/2017).
81. M. F. Ansari and D. N. Goswami, *Pigment & Resin Technology*, 2006, **35**, 183-187.
82. G. Chiavari, Fabbri, D., Mazzeo, R., Bocchini, P., Galletti, G.C., *Chromatographia*, 1995, **41**, 273-281.
83. A. Nevin, D. Comelli, G. Valentini and R. Cubeddu, *Analytical Chemistry*, 2009, **81**, 1784-1791.
84. A. Azouka, Huggett, R., Harrison, A., *Journal of Oral Rehabilitation*, 1993, **20**, 393-400.
85. A. Harrison, Huggett, R., Azouka, A., *Journal of Oral Rehabilitation*, 1995, **22**, 509-513.
86. B. T. Hoang-Dao, Hoang-Tu, H., Tran-Hung, L., Camps, J., Koubi, G., About, I., *Dental Materials*, 2008, **24**, 1001-1007.
87. B. T. Hoang-Dao, Hoang-Tu, H., Tran-Thi, N.N., Koubi, G., Camps, J., About, I., *Journal of Oral Rehabilitation*, 2009, **36**, 124-131.
88. E. W. Cornell, V. Fadeyev, C. Haber, J. Jin, R. Nordmeyer and M. Golden, *Nuclear Instruments and Methods in Physics Research Section A: Accelerators, Spectrometers, Detectors and Associated Equipment*, 2007, **579**, 901-904.
89. S. Y. Lee, K. L. Dangaran and J. M. Krochta, *Journal of Food Science*, 2002, **67**, 1121-1125.
90. J. Nickel and U. Riedel, *Biorelated Polymers: Structural materials from renewable resources (biocomposites).* 2001.
91. S. Leick, M. Kott, P. Degen, S. Henning, T. Pasler, D. Suter and H. Rehage, *Physical Chemistry Chemical Physics*, 2011, **13**, 2765-2773.
92. S. A. Hamad, S. D. Stoyanov and V. N. Paunov, *Soft Matter*, 2012, **8**, 5069.
93. R. D. Hagenmaier and P. E. Shaw, *Journal of Agricultural and Food Chemistry*, 1991, **39**, 825-829.
94. J. Lu, H. Wang, J. Huang, G. Li, Q. Wang, W. Xu, Y. Chen, K. Zhang and J. Wang, *Fitoterapia*, 2014, **97**, 64-70.
95. D. S. Sheorey, Shastri, A.S., Dorle, A.K., *International Journal of Pharmaceutics*, 1991, **68**, 19-23.

96. A. L. Campbell, S. D. Stoyanov and V. N. Paunov, *Chemphyschem*, 2009, **10**, 2599-2602.
97. A. Nadian and L. Lindblom, *International Journal of Pharmaceutics*, 2002, **242**, 63-68.
98. V. D. Labhasetwar, P. K. Puranik and A. K. Dorle, *Journal of Microencapsulation*, 1989, **6**, 115-118.
99. V. D. Labhasetwar, P. K. Puranik and A. K. Dorle, *Journal of Microencapsulation*, 1990, **7**, 553-554.
100. D. S. Sheorey, Kshirsagar, M.D., Dorle, A.K., *Journal of Microencapsulation*, 1991, **8**, 375-380.
101. J. Xue and Z. Zhang, *Journal of Microencapsulation*, 2008, **25**, 523-530.
102. A. Patel, P. Heussen, J. Hazekamp and K. P. Velikov, *Soft Matter*, 2011, **7**, 8549.
103. L. Cui, Z.-P. Liu, D.-G. Yu, S.-P. Zhang, S. W. A. Bligh and N. Zhao, *Colloid and Polymer Science*, 2014, **292**, 2089-2096.
104. K. Krause and R. Müller, *International Journal of Pharmaceutics*, 2001, **223**, 89-92.
105. I. Bala, S. Hariharan and M. N. V. R. Kumar, 2004, **21**, 387-422.
106. M. J. Rosen, *Surfactants and interfacial phenomena*, John Wiley&Sons, Inc., Hoboken, N.J. :, 4th ed. edn., 2012.
107. A. V. Kabanov, E. V. Batrakova and V. Y. Alakhov, *Journal of Controlled Release*, 2002, **82**, 189-212.
108. G. Dumortier, J. L. Grossiord, F. Agnely and J. C. Chaumeil, *Pharmaceutical Research*, 2006, **23**, 2709-2728.
109. J. C. Gilbert, J. Hadgraft, A. Bye and L. G. Brookes, *International Journal of Pharmaceutics*, 1986, **32**, 223-228.
110. S. Miyazaki, S. Takeuchi, C. Yokouchi and M. Takada, *Chemical and Pharmaceutical Bulletin*, 1984, **32**, 4205-4208.
111. E. B. Jørgensen, S. Hvidt, W. Brown and K. Schillén, *Macromolecules*, 1997, **30**, 2355-2364.
112. P. Alexandridis and T. Alan Hatton, *Colloids and Surfaces A: Physicochemical and Engineering Aspects*, 1995, **96**, 1-46.
113. S. Miyazaki, T. Tobiyama, M. Takada and D. Attwood, *Journal of Pharmacy and Pharmacology*, 1995, **47**, 455-457.
114. Y.-Y. Wang, C.-T. Hong, W.-T. Chiu and J.-Y. Fang, *International Journal of Pharmaceutics*, 2001, **224**, 89-104.
115. J.-Y. Fang, Y.-L. Leu, Y.-Y. Wang and Y.-H. Tsai, *European Journal of Pharmaceutical Sciences*, 2002, **15**, 417-423.
116. S.-C. Shin, C.-W. Cho and I.-J. Oh, *International Journal of Pharmaceutics*, 2001, **222**, 199-203.
117. J. Liaw and Y.-C. Lin, *Journal of Controlled Release*, 2000, **68**, 273-282.
118. J. J. Escobar-Chávez, D. Quintanar-Guerrero and A. Ganem-Quintanar, *Drug Development and Industrial Pharmacy*, 2005, **31**, 447-454.
119. C.-e. CHONCHEEWA and T. PHAECHAMUD, *Journal of Metals, Materials and Minerals*, 2012, **22**, 67-74.

120. J. "Antimicrobial." Merriam-Webster.com. Merriam-Webster, *Journal*, 2018.
121. antimicrobial, *Journal*, 3 January 2018.
122. G. McDonnell and A. D. Russell, *Clinical Microbiology Reviews*, 1999, **12**, 147-179.
123. M. N. Swartz, *Antimicrobial Agents and Chemotherapy*, 2000, **44**, 2009-2016.
124. A. Manten, *Veterinary Quarterly*, 1981, **3**, 179-182.
125. M. Tillhon, L. M. Guamán Ortiz, P. Lombardi and A. I. Scovassi, *Biochemical Pharmacology*, 2012, **84**, 1260-1267.
126. K. C. Singhal, *Indian Journal of Experimental Biology*, 1976, **14**, 345-347.
127. T. Satou, N. Akao, R. Matsuhashi, K. Koike, K. Fujita and T. Nikaido, *Biological and Pharmaceutical Bulletin*, 2002, **25**, 1651-1654.
128. M. Jang, S.-W. Jeong, S. K. Cho, K.-S. Ahn, B.-K. Kim and J.-C. Kim, *Food Science and Biotechnology*, 2013, **22**, 213-220.
129. J. E. Sykes and J. S. Weese, in *Canine and Feline Infectious Diseases*, W.B. Saunders, Saint Louis, 2014, DOI: https://doi.org/10.1016/B978-1-4377-0795-3.00011-9, pp. 105-118.
130. B. D. Eden, in *Prevention in Clinical Oral Health Care*, ed. C. C. Mobley, Mosby, Saint Louis, 2008, DOI: https://doi.org/10.1016/B978-0-323-03695-5.50020-3, pp. 213-229.
131. V. John, J. A. Weddell, D. E. Shin and J. E. Jones, in *McDonald and Avery's Dentistry for the Child and Adolescent (Tenth Edition)*, Mosby, St. Louis, 2016, DOI: https://doi.org/10.1016/B978-0-323-28745-6.00014-4, pp. 243-273.
132. D. J. Speare and G. J. Arsenault, *Canadian Journal of Fisheries and Aquatic Sciences*, 1997, **54**, 2653-2658.
133. B. Aggarwal, A. Kumar, M. S. Aggarwal and S. Shishodia, *Curcumin Derived from Turmeric (Curcuma longa): a Spice for All Seasons*, 2004.
134. M. C. Heng, M. K. Song, J. Harker and M. K. Heng, *British Journal of Dermatology*, 2000, **143**, 937-949.
135. E. Tourkina, P. Gooz, J. C. Oates, A. Ludwicka-Bradley, R. M. Silver and S. Hoffman, *American Journal of Respiratory Cell and Molecular Biology*, 2004, **31**, 28-35.
136. D. Madhavi and D. Kagan, *Integrative Medicine: A Clinician's Journal*, 2014, **13**, 24-30.
137. G. Nordberg and L. Gerhardsson, *Handbook on Toxicity of Inorganic Compounds*, 1988, 619-624.
138. X. Chen and H. J. Schluesener, *Toxicology Letters*, 2008, **176**, 1-12.
139. E. Elkrewi, C. P. Randall, N. Ooi, J. L. Cottell and A. J. O'Neill, *Journal of Antimicrobial Chemotherapy*, 2017, **72**, 3043-3046.
140. H. T. Tan, R. A. Rahman, S. H. Gan, A. S. Halim, S. A. Hassan, S. A. Sulaiman and K.-K. BS, *BMC Complementary and Alternative Medicine*, 2009, **9**, 34.
141. P. C. Molan, *American Journal of Clinical Dermatology*, 2001, **2**, 13-19.
142. M. Imanshahidi and H. Hosseinzadeh, *Phytotherapy Research*, 2008, **22**, 999-1012.
143. M. Ikram, *Planta Medica*, 1975, **28**, 353-358.
144. C. V. Diogo, N. G. Machado, I. A. Barbosa, T. L. Serafim, A. Burgeiro and P. J. Oliveira, *Current Drug Targets*, 2011, **12**, 850-859.

145. L. Yan, K. Yan, W. Kun, L. Xu, Q. Ma, Y. Tang, W. Jiao, G. Gu, Y. Fan and Z. Xu, *Tumour Biology*, 2013, **34**, 215-221.
146. C.-M. Wu, T.-M. Li, T.-W. Tan, Y.-C. Fong and C.-H. Tang, *Evidence-based Complementary and Alternative Medicine : eCAM*, 2013, **2013**, 423164.
147. K. Wang, C. Zhang, J. Bao, X. Jia, Y. Liang, X. Wang, M. Chen, H. Su, P. Li, J.-B. Wan and C. He, *Scientific Reports*, 2016, **6**, 26064.
148. J. B. Patil, J. Kim and G. K. Jayaprakasha, *European Journal of Pharmacology*, 2010, **645**, 70-78.
149. K. Fukuda, Y. Hibiya, M. Mutoh, M. Koshiji, S. Akao and H. Fujiwara, *Journal of Ethnopharmacology*, 1999, **66**, 227-233.
150. https://en.wikipedia.org/wiki/Berberis#cite_note-1, 24/10/2017).
151. J. Suksiriworapong, T. Rungvimolsin, A. Atitaya, V. B. Junyaprasert and D. Chantasart, *American Association of Pharmaceutical Scientists*, 2014, **15**, 52-64.
152. W. Tan, Y. Li, M. Chen and Y. Wang, *International Journal of Nanomedicine*, 2011, **6**, 1773.
153. T. L, L. G, C. J, S. W and R. K, *Journal of Practical Medical Techniques*, 2007, **14**, 1385–1386.
154. M. Xue, M.-x. Yang, W. Zhang, X.-m. Li, D.-h. Gao, Z.-m. Ou, Z.-p. Li, S.-h. Liu, X.-j. Li and S.-y. Yang, *International Journal of Nanomedicine*, 2013, **8**, 4677-4687.
155. S. Wang, T. Chen, R. Chen, Y. Hu, M. Chen and Y. Wang, *International Journal of Pharmaceutics*, 2012, **430**, 238-246.
156. L. Wang, H. Li, S. Wang, R. Liu, Z. Wu, C. Wang, Y. Wang and M. Chen, *American Association of Pharmaceutical Scientists*, 2014, **15**, 834-844.
157. M. Khemani, M. Sharon and M. Sharon, *ISRN Nanotechnology*, 2012, **2012**, 1-9.
158. R. Kapoor, S. Singh, M. Tripathi, P. Bhatnagar, P. Kakkar and K. C. Gupta, *PloS One*, 2014, **9**, e89124.
159. F. Yu, M. Ao, X. Zheng, N. Li, J. Xia, Y. Li, D. Li, Z. Hou, Z. Qi and X. D. Chen, *Drug delivery*, 2017, **24**, 825-833.
160. G. Calogiuri, E. Leo, A. Trautmann, E. Nettis, A. Ferrannini and A. Vacca, *Journal Allergy & Therapy*, 2013, **4**, 141.
161. G. Radhika, C. Vidya, R. G. Sushama and M. Mithilesh, *The Global Journal of Medicine and Public Health*, 2012, **1**, 43-44.
162. S. Jenkins, M. Addy and R. Newcombe, *Journal of Clinical Periodontology*, 1993, **20**, 20-25.
163. N. P. Lang, J. C. Hase, M. Grassi, C. H. Hammerle, C. Weigel, E. Kelty and F. Frutig, *Oral Diseases*, 1998, **4**, 105-113.
164. M. E. Vianna, B. P. Gomes, V. B. Berber, A. A. Zaia, C. C. Ferraz and F. J. de Souza-Filho, *Oral Surgery, Oral Medicine, Oral Pathology, Oral Radiology and Endodontics*, 2004, **97**, 79-84.
165. P. Bonesvoll and P. Gjermo, *Archives of Oral Biology*, 1978, **23**, 289-294.
166. H. Löe and C. Rindom Schiøtt, *Journal of Periodontal Research*, 1970, **5**, 79-83.
167. L. Flotra, P. Gjermo, G. Rolla and J. Waerhaug, *Scandinavian Journal of Dental Research*, 1971, **79**, 119-125.

168. S. Balagopal and R. Arjunkumar, *Chlorhexidine: The gold standard antiplaque agent*, 2013.
169. H. Lboutounne, J.-F. Chaulet, C. Ploton, F. Falson and F. Pirot, *Journal of Controlled Release*, 2002, **82**, 319-334.
170. I. C. Yue, J. Poff, M. a. E. Cortés, R. D. Sinisterra, C. B. Faris, P. Hildgen, R. Langer and V. P. Shastri, *Biomaterials*, 2004, **25**, 3743-3750.
171. C. J. Seneviratne, K. C. Leung, C. H. Wong, S. F. Lee, X. Li, P. C. Leung, C. B. Lau, E. Wat and L. Jin, *PloS One*, 2014, **9**, e103234.
172. N. J. Wood, H. F. Jenkinson, S. A. Davis, S. Mann, D. J. O'Sullivan and M. E. Barbour, *Journal of Materials Science: Materials in Medicine*, 2015, **26**, 201.
173. B. M. Priyadarshini, S. T. Selvan, T. B. Lu, H. Xie, J. Neo and A. S. Fawzy, *Journal of Dental Research*, 2016, **95**, 1065-1072.
174. A. Kovtun, D. Kozlova, K. Ganesan, C. Biewald, N. Seipold, P. Gaengler, W. H. Arnold and M. Epple, *RSC Advances*, 2012, **2**, 870-875.
175. H. Phuengkham and N. Nasongkla, *Journal of Materials Science: Materials in Medicine*, 2015, **26**, 78.
176. M. E. Barbour, S. E. Maddocks, N. J. Wood and A. M. Collins, *International Journal of Nanomedicine*, 2013, **8**, 3507-3519.
177. A. Goel, A. B. Kunnumakkara and B. B. Aggarwal, *Biochemical Pharmacology*, 2008, **75**, 787-809.
178. B. B. Aggarwal and B. Sung, *Trends in Pharmacological Sciences*, 2009, **30**, 85-94.
179. P. Anand, A. B. Kunnumakkara, R. A. Newman and B. B. Aggarwal, *Molecular Pharmaceutics*, 2007, **4**, 807-818.
180. O. P. Sharma, *Biochemical Pharmacology*, 1976, **25**, 1811-1812.
181. A. J. Ruby, G. Kuttan, K. Dinesh Babu, K. N. Rajasekharan and R. Kuttan, *Cancer Letters*, 1995, **94**, 79-83.
182. Y. Sugiyama, S. Kawakishi and T. Osawa, *Biochemical Pharmacology*, 1996, **52**, 519-525.
183. R. C. Srimal and B. N. Dhawan, *Journal of Pharmacy and Pharmacology*, 1973, **25**, 447-452.
184. W. C. Jordan and C. R. Drew, *Journal of the National Medical Association*, 1996, **88**, 333.
185. G. B. Mahady, S. L. Pendland, G. Yun and Z. Z. Lu, *Anticancer Research*, 2002, **22**, 4179-4181.
186. M. K. Kim, G. J. Choi and H. S. Lee, *Journal of Agricultural and Food Chemistry*, 2003, **51**, 1578-1581.
187. R. C. Reddy, P. G. Vatsala, V. G. Keshamouni, G. Padmanaban and P. N. Rangarajan, *Biochemical and Biophysical Research Communications*, 2005, **326**, 472-474.
188. R. Kuttan, P. Bhanumathy, K. Nirmala and M. C. George, *Cancer Letters*, 1985, **29**, 197-202.
189. S. M. Khopde, K. I. Priyadarsini, P. Venkatesan and M. N. A. Rao, *Biophysical Chemistry*, 1999, **80**, 85-91.
190. B. B. Aggarwal, A. Kumar and A. C. Bharti, *Anticancer Research*, 2003, **23**, 363-398.

191. F. Yang, G. P. Lim, A. N. Begum, O. J. Ubeda, M. R. Simmons, S. S. Ambegaokar, P. P. Chen, R. Kayed, C. G. Glabe, S. A. Frautschy and G. M. Cole, *Journal of Biological Chemistry*, 2005, **280**, 5892-5901.
192. A. Ukil, S. Maity, S. Karmakar, N. Datta, J. R. Vedasiromoni and P. K. Das, *British Journal of Pharmacology*, 2003, **139**, 209-218.
193. M. E. Egan, M. Pearson, S. A. Weiner, V. Rajendran, D. Rubin, J. Glockner-Pagel, S. Canny, K. Du, G. L. Lukacs and M. J. Caplan, *Science*, 2004, **304**, 600-602.
194. O. Naksuriya, S. Okonogi, R. M. Schiffelers and W. E. Hennink, *Biomaterials*, 2014, **35**, 3365-3383.
195. V. Ravindranath and N. Chandrasekhara, *Toxicology*, 1981, **22**, 337-344.
196. A. Kunwar, A. Barik, R. Pandey and K. I. Priyadarsini, *Biochimica et Biophysica Acta*, 2006, **1760**, 1513-1520.
197. S. Bisht, G. Feldmann, S. Soni, R. Ravi, C. Karikar, A. Maitra and A. Maitra, *Journal of Nanobiotechnology*, 2007, **5**, 3-3.
198. K. Sou, S. Inenaga, S. Takeoka and E. Tsuchida, *International Journal of Pharmaceutics*, 2008, **352**, 287-293.
199. V. Kumar, S. A. Lewis, S. Mutalik, D. B. Shenoy, Venkatesh and N. Udupa, *Indian Journal of Physiology and Pharmacology*, 2002, **46**, 209-217.
200. S. Salmaso, S. Bersani, A. Semenzato and P. Caliceti, *Journal of Drug Targeting*, 2007, **15**, 379-390.
201. P. K. Vemula, J. Li and G. John, *Journal of the American Chemical Society*, 2006, **128**, 8932-8938.
202. Z. Ma, A. Shayeganpour, D. R. Brocks, A. Lavasanifar and J. Samuel, *Biomedical Chromatography*, 2007, **21**, 546-552.
203. A. Sahu, U. Bora, N. Kasoju and P. Goswami, *Acta Biomaterialia*, 2008, **4**, 1752-1761.
204. R. K. Das, N. Kasoju and U. Bora, *Nanomedicine: Nanotechnology, Biology and Medicine*, 2010, **6**, 153-160.
205. A. Karewicz, D. Bielska, A. Loboda, B. Gzyl-Malcher, J. Bednar, A. Jozkowicz, J. Dulak and M. Nowakowska, *Colloids and Surfaces B: Biointerfaces*, 2013, **109**, 307-316.
206. M. Sun, X. Su, B. Ding, X. He, X. Liu, A. Yu, H. Lou and G. Zhai, *Nanomedicine (Lond)*, 2012, **7**, 1085-1100.
207. F. Danhier, E. Ansorena, J. M. Silva, R. Coco, A. Le Breton and V. Préat, *Journal of Controlled Release*, 2012, **161**, 505-522.
208. S. Fredenberg, M. Wahlgren, M. Reslow and A. Axelsson, *International Journal of Pharmaceutics*, 2011, **415**, 34-52.
209. R. A. Jain, *Biomaterials*, 2000, **21**, 2475-2490.
210. J. M. Anderson and M. S. Shive, *Advanced Drug Delivery Reviews*, 1997, **28**, 5-24.
211. J. Shaikh, D. D. Ankola, V. Beniwal, D. Singh and M. N. V. R. Kumar, *European Journal of Pharmaceutical Sciences*, 2009, **37**, 223-230.
212. L. Song, Y. Shen, J. Hou, L. Lei, S. Guo and C. Qian, *Colloids and Surfaces A: Physicochemical and Engineering Aspects*, 2011, **390**, 25-32.

213. H. Tang, C. J. Murphy, B. Zhang, Y. Shen, M. Sui, E. A. Van Kirk, X. Feng and W. J. Murdoch, *Nanomedicine (Lond)*, 2010, **5**, 855-865.
214. L. Mayol, C. Serri, C. Menale, S. Crispi, M. T. Piccolo, L. Mita, S. Giarra, M. Forte, A. Saija, M. Biondi and D. G. Mita, *European Journal of Pharmaceutics and Biopharmaceutics*, 2015, **93**, 37-45.
215. X. Yang, Z. Li, N. Wang, L. Li, L. Song, T. He, L. Sun, Z. Wang, Q. Wu, N. Luo, C. Yi and C. Gong, *Scientific Reports*, 2015, **5**, 10322.
216. W. Tiyaboonchai, W. Tungpradit and P. Plianbangchang, *International Journal of Pharmaceutics*, 2007, **337**, 299-306.
217. J. E. Geraci, F. R. Heilman, D. R. Nichols, E. W. Wellman and G. T. Ross, *Antibiotics annual*, 1956, 90-106.
218. R. S. Griffith and F. B. Peck, Jr., *Antibiot Annu*, 1955, **3**, 619-622.
219. H. R. Perkins, *Biochemical Journal*, 1969, **111**, 195-205.
220. R. Hancock and P. C. Fitz-James, *Journal of Bacteriology*, 1964, **87**, 1044-1050.
221. W. Dehority, *The Pediatric Infectious Disease Journal*, 2010, **29**, 462-464.
222. A. L. Robles-Piedras and E. H. Gonzalez-Lopez, *Proceedings of the Western Pharmacology Society*, 2009, **52**, 21-23.
223. A. Gupta, M. Biyani and A. Khaira, *Netherlands Journal of Medicine*, 2011, **69**, 379-383.
224. O. Plan, G. Cambonie, E. Barbotte, P. Meyer, C. Devine, C. Milesi, O. Pidoux, M. Badr and J. C. Picaud, *Archives of Disease in Childhood: Fetal and Neonatal Edition*, 2008, **93**, F418-421.
225. A. Vandendriessche, K. Allegaert, V. Cossey, G. Naulaers, V. Saegeman and A. Smits, *Current Therapeutic Research, Clinical and Experimental*, 2014, **76**, 51-57.
226. M. O. Nunn, C. E. Corallo, C. Aubron, S. Poole, M. J. Dooley and A. C. Cheng, *Annals of Pharmacotherapy*, 2011, **45**, 757-763.
227. L. Pritchard, C. Baker, J. Leggett, P. Sehdev, A. Brown and K. B. Bayley, *The American Journal of Medicine*, 2010, **123**, 1143-1149.
228. C. Caroom, J. M. Tullar, E. G. J. Benton, J. R. Jones and C. D. Chaput, *Spine*, 2013, **38**, 1183-1187.
229. H. Yan, J. He, S. Chen, S. Yu and C. Fan, *Journal of Shoulder and Elbow Surgery*, 2014, **23**, 686-692.
230. L. Xiong, Q. Pan, G. Jin, Y. Xu and C. Hirche, *Orthopaedics & Traumatology: Surgery & Research*, 2014, **100**, 785-789.
231. H.-Y. Chiang, L. A. Herwaldt, A. E. Blevins, E. Cho and M. L. Schweizer, *The Spine Journal*, 2014, **14**, 397-407.
232. N. Abed and P. Couvreur, *International Journal of Antimicrobial Agents*, 2014, **43**, 485-496.
233. J. Xu, B. Xu, D. Shou, X. Xia and Y. Hu, *Polymers*, 2015, **7**, 1488.
234. P. Zakeri-Milani, B. D. Loveymi, M. Jelvehgari and H. Valizadeh, *Colloids and Surfaces B: Biointerfaces*, 2013, **103**, 174-181.

235. R. S. Kalhapure, C. Mocktar, D. R. Sikwal, S. J. Sonawane, M. K. Kathiravan, A. Skelton and T. Govender, *Colloids and Surfaces B: Biointerfaces*, 2014, **117**, 303-311.
236. B. González, M. Colilla and M. Vallet-Regí, *Chemistry of Materials*, 2008, **20**, 4826-4834.
237. A. Esmaeili and S. Ghobadianpour, *International Journal of Pharmaceutics*, 2016, **501**, 326-330.
238. B. D. Loveymi, M. Jelvehgari, P. Zakeri-Milani and H. Valizadeh, *Advanced Pharmaceutical Bulletin*, 2012, **2**, 43-56.
239. S. Lankalapalli, V. S. V. K. Tenneti and S. K. Nimmali, *Indian Journal of Pharmaceutical Education and Research*, 2015, **49**, 208-215.
240. P. Zakeri-Milani, B. D. Loveymi, M. Jelvehgari and H. Valizadeh, *Colloids and Surfaces B: Biointerfaces*, 2013, **103**, 174-181.
241. D. R. Sikwal, R. S. Kalhapure, S. Rambharose, S. Vepuri, M. Soliman, C. Mocktar and T. Govender, *Materials Science and Engineering: C*, 2016, **63**, 489-498.
242. H. M. Redhead, S. S. Davis and L. Illum, *Journal of Controlled Release*, 2001, **70**, 353-363.
243. L. Betancor and H. R. Luckarift, *Trends in Biotechnology*, 2008, **26**, 566-572.
244. B. J. Berne, *Dynamic light scattering with applications to chemistry, biology and physics*, Wiley., London :, 1976.
245. D. N. de Assis, V. C. Mosqueira, J. M. Vilela, M. S. Andrade and V. N. Cardoso, *International Journal of Pharmaceutics*, 2008, **349**, 152-160.
246. R. Pecora, *Dynamic Light Scattering: Applications of Photon Correlation Spectroscopy*, Springer US, 2013.
247. J. Molpeceres, M. R. Aberturas and M. Guzman, *Journal of Microencapsulation*, 2000, **17**, 599-614.
248. P. D. Brown, *Microscopy and Microanalysis*, 1999, **5**, 452-453.
249. K. Jores, W. Mehnert, M. Drechsler, H. Bunjes, C. Johann and K. Mäder, *Journal of Controlled Release*, 2004, **95**, 217-227.
250. E. Buhr, N. Senftleben, T. Klein, D. Bergmann, D. Gnieser, C. G. Frase and H. Bosse, *Measurement Science and Technology*, 2009, **20**, 084025.
251. https://www.azonano.com/article.aspx?ArticleID=4118, 26/09/2017).
252. D. J. Shaw, *Introduction to colloid and surface chemistry*, Butterworth-Heinemann, Oxford :, 4th ed. edn., 1992.
253. J. W. Swan and E. M. Furst, *Journal of Colloid and Interface Science*, 2012, **388**, 92-94.
254. R. J. Hunter, *Colloid Science A2* Academic Press, 1981.
255. P. D. Scholes, A. G. A. Coombes, L. Illum, S. S. Davis, J. F. Watts, C. Ustariz, M. Vert and M. C. Davies, *Journal of Controlled Release*, 1999, **59**, 261-278.
256. K. Westesen, H. Bunjes and M. Koch, *Journal of Controlled Release*, 1997, **48**, 223-236.
257. J. Kreuter, *International Journal of Pharmaceutics*, 1983, **14**, 43-58.

258. K. S. Kumar, D. Bhowmik, S. Srivastava, S. Paswan and A. S. Dutta, *The pharma innovation*, 2012, **1**.
259. C. D. Subas and P. Gurudutta, *Current Pharmaceutical Biotechnology*, 2013, **14**, 1264-1274.
260. R. Khanbabaie and M. Jahanshahi, *Current Neuropharmacology*, 2012, **10**, 370-392.
261. J.-C. Leroux, E. Allémann, F. De Jaeghere, E. Doelker and R. Gurny, *Journal of Controlled Release*, 1996, **39**, 339-350.
262. M. D. Blanco and M. J. Alonso, *European Journal of Pharmaceutics and Biopharmaceutics*, 1997, **43**, 287-294.
263. S. Nicoli, P. Santi, P. Couvreur, G. Couarraze, P. Colombo and E. Fattal, *International Journal of Pharmaceutics*, 2001, **214**, 31-35.
264. C. Xiao, X. Qi, Y. Maitani and T. Nagai, *Journal of Pharmaceutical Sciences*, 2004, **93**, 1718-1724.
265. C.-W. Chi, A. H. R. Ahmed, Z. Dereli-Korkut and S. Wang, *Bioanalysis*, 2016, **8**, 921-937.
266. L. M. Mayr and P. Fuerst, *Journal of Biomolecular Screening*, 2008, **13**, 443-448.
267. P. Szymański, M. Markowicz and E. Mikiciuk-Olasik, *International Journal of Molecular Sciences*, 2012, **13**, 427-452.
268. M. J. Plewa, Y. Kargalioglu, D. Vankerk, R. A. Minear and E. D. Wagner, *Water Science and Technology*, 2000, **42**, 109-116.
269. M. J. Plewa, J. E. Simmons, S. D. Richardson and E. D. Wagner, *Environmental and Molecular Mutagenesis*, 2010, **51**, 871-878.
270. Y. Fujikawa, T. Nakanishi, H. Kawakami, K. Yamasaki, M. H. Sato, H. Tsuji, M. Matsuoka and N. Kato, *Rice (N Y)*, 2014, **7**, 11.
271. K. Mae, T. Maki, I. Hasegawa, U. Eto, Y. Mizutani and N. Honda, *Chemical Engineering Journal*, 2004, **101**, 31-38.
272. Y. Okubo, M. Toma, H. Ueda, T. Maki and K. Mae, *Chemical Engineering Journal*, 2004, **101**, 39-48.
273. M. Ståhl, B. L. Åslund and Å. C. Rasmuson, *AIChE Journal*, 2001, **47**, 1544-1560.
274. H.-C. Schwarzer, F. Schwertfirm, M. Manhart, H.-J. Schmid and W. Peukert, *Chemical Engineering Science*, 2006, **61**, 167-181.
275. E. M. Miller and A. R. Wheeler, *Analytical Chemistry*, 2008, **80**, 1614-1619.
276. Y. Ukita, T. Asano, K. Fujiwara, K. Matsui, M. Takeo, S. Negoro, T. Kanie, M. Katayama and Y. Utsumi, *Sensors and Actuators A: Physical*, 2008, **145-146**, 449-455.
277. S. J. Haswell, R. J. Middleton, B. O'Sullivan, V. Skelton, P. Watts and P. Styring, *Chemical Communications*, 2001, DOI: 10.1039/B008496O, 391-398.
278. V. Hessel, C. Hofmann, P. Löb, J. Löhndorf, H. Löwe and A. Ziogas, *Organic Process Research & Development*, 2005, **9**, 479-489.
279. T. Iwasaki and J.-i. Yoshida, *Macromolecules*, 2005, **38**, 1159-1163.
280. A. Nagaki, K. Kawamura, S. Suga, T. Ando, M. Sawamoto and J.-i. Yoshida, *Journal of the American Chemical Society*, 2004, **126**, 14702-14703.

281. O. Bilsel, C. Kayatekin, L. A. Wallace and C. R. Matthews, *Review of Scientific Instruments*, 2005, **76**, 014302.
282. X. Chen, D. Cui, C. Liu, H. Li and J. Chen, *Analytica Chimica Acta*, 2007, **584**, 237-243.
283. C. Zhang, D. Xing and Y. Li, *Biotechnology Advances*, 2007, **25**, 483-514.
284. K. Sato, A. Hibara, M. Tokeshi, H. Hisamoto and T. Kitamori, *Advanced Drug Delivery Reviews*, 2003, **55**, 379-391.
285. T. Park, S. Lee, G. H. Seong, J. Choo, E. K. Lee, Y. S. Kim, W. H. Ji, S. Y. Hwang, D. G. Gweon and S. Lee, *Lab Chip*, 2005, **5**, 437-442.
286. S. J. Maerkl, *Integrative Biology*, 2009, **1**, 19-29.
287. M. Lidija, H. Marc, D. H. Xuyen and T. Maryam, *Recent Patents on Engineering*, 2007, **1**, 71-88.
288. C. J. Ingham and J. E. T. van Hylckama Vlieg, *Lab on a Chip*, 2008, **8**, 1604-1616.
289. S. Z. Razzacki, P. K. Thwar, M. Yang, V. M. Ugaz and M. A. Burns, *Adv Drug Deliv Rev*, 2004, **56**, 185-198.
290. M. Micheletti and G. J. Lye, *Current Opinion in Biotechnology*, 2006, **17**, 611-618.
291. D. Schapper, M. N. Alam, N. Szita, A. Eliasson Lantz and K. V. Gernaey, *Analytical and Bioanalytical Chemistry*, 2009, **395**, 679-695.
292. T. H. Schulte, R. L. Bardell and B. H. Weigl, *Clinica Chimica Acta*, 2002, **321**, 1-10.
293. B. E. Rapp, F. J. Gruhl and K. Lange, *Analytical and Bioanalytical Chemistry*, 2010, **398**, 2403-2412.
294. A. M. Streets and Y. Huang, *Biomicrofluidics*, 2013, **7**, 011302.
295. A. J. deMello, *Nature*, 2006, **442**, 394-402.
296. L. Capretto, W. Cheng, M. Hill and X. Zhang, *Topics in Current Chemistry*, 2011, **304**, 27-68.
297. K. Liu, H. Wang, K. J. Chen, F. Guo, W. Y. Lin, Y. C. Chen, D. L. Phung, H. R. Tseng and C. K. Shen, *Nanotechnology*, 2010, **21**, 445603.
298. M. Rhee, P. M. Valencia, M. I. Rodriguez, R. Langer, O. C. Farokhzad and R. Karnik, *Advanced Materials*, 2011, **23**, H79-H83.
299. P. M. Valencia, P. A. Basto, L. Zhang, M. Rhee, R. Langer, O. C. Farokhzad and R. Karnik, *ACS Nano*, 2010, **4**, 1671-1679.
300. B. Yu, R. J. Lee and L. J. Lee, *Methods in Enzymology*, 2009, **465**, 129-141.
301. C. Besson, E. E. Finney and R. G. Finke, *Journal of the American Chemical Society*, 2005, **127**, 8179-8184.
302. Y. Song, J. Hormes and C. S. Kumar, *Small*, 2008, **4**, 698-711.
303. F. X. Gu, R. Karnik, A. Z. Wang, F. Alexis, E. Levy-Nissenbaum, S. Hong, R. S. Langer and O. C. Farokhzad, *Nano Today*, 2007, **2**, 14-21.
304. E. r. group, http://unam.bilkent.edu.tr/~celbuken/, 02/11/2017).
305. S. Li, Z. Xu, A. Mazzeo, D. J. Burns, G. Fu, M. Dirckx, V. Shilpiekandula, X. Chen, N. C. Nayak, E. Wong, S. F. Yoon, Z. P. Fang, K. Youcef-Toumi, D. Hardt, S. B. Tor, C. Y. Yue and J.-H. Chun, *SPIE Photonics Europe*, 2008, **6993**, 12.
306. C. Gartner, H. Becker, B. Anton and O. Roetting, *Micromachining and Microfabrication*, 2003, **5345**, 4.

307. J. Wang, M. Pumera, M. P. Chatrathi, A. Escarpa, R. Konrad, A. Griebel, W. Dorner and H. Lowe, *Electrophoresis*, 2002, **23**, 596-601.
308. G. Jenkins, *Methods in Molecular Biology*, 2013, **949**, 153-168.
309. M. Zagnoni, M. E. Sandison, P. Marius, A. G. Lee and H. Morgan, *Lab on a Chip*, 2007, **7**, 1176-1183.
310. W. X. Zhou and M. B. Chan-Park, *Lab on a Chip*, 2005, **5**, 512-518.
311. B. Andrea, L. Xianming and V. E. Amanda, *Smart Materials and Structures*, 2007, **16**, 367.
312. H. Mohamed, A. P. Russo, D. H. Szarowski, E. McDonnell, L. A. Lepak, M. G. Spencer, D. L. Martin, M. Caggana and J. N. Turner, *Journal of Chromatography A*, 2006, **1111**, 214-219.
313. J. Luo, T. Dziubla and R. Eitel, *Sensors and Actuators B: Chemical*, 2017, **240**, 392-397.
314. H. Becker and L. E. Locascio, *Talanta. Proceedings of the Dutch Archaeological and Historical Society*, 2002, **56**, 267-287.
315. S. L. R. Barker, M. J. Tarlov, H. Canavan, J. J. Hickman and L. E. Locascio, *Analytical Chemistry*, 2000, **72**, 4899-4903.
316. L. E. Locascio, C. E. Perso and C. S. Lee, *Journal of Chromatography A*, 1999, **857**, 275-284.
317. W. I. Wu, K. N. Sask, J. L. Brash and P. R. Selvaganapathy, *Lab Chip*, 2012, **12**, 960-970.
318. A. Mata, A. J. Fleischman and S. Roy, *Biomedical Microdevices*, 2005, **7**, 281-293.
319. Y. X. and and G. M. Whitesides, *Annual Review of Materials Science*, 1998, **28**, 153-184.
320. J. C. McDonald, D. C. Duffy, J. R. Anderson, D. T. Chiu, H. Wu, O. J. Schueller and G. M. Whitesides, *Electrophoresis*, 2000, **21**, 27-40.
321. H. Wu, T. W. Odom, D. T. Chiu and G. M. Whitesides, *Journal of the American Chemical Society*, 2003, **125**, 554-559.
322. F. K. Balagadde, L. You, C. L. Hansen, F. H. Arnold and S. R. Quake, *Science*, 2005, **309**, 137-140.
323. A. Khademhosseini, R. Langer, J. Borenstein and J. P. Vacanti, *Proceedings of the National Academy of Sciences of the United States of America*, 2006, **103**, 2480-2487.
324. X. Mu, W. Zheng, J. Sun, W. Zhang and X. Jiang, *Small*, 2013, **9**, 9-21.
325. J. El-Ali, P. K. Sorger and K. F. Jensen, *Nature*, 2006, **442**, 403-411.
326. B. Huang, H. Wu, D. Bhaya, A. Grossman, S. Granier, B. K. Kobilka and R. N. Zare, *Science*, 2007, **315**, 81-84.
327. D. Ryan, K. Ren and H. Wu, *Biomicrofluidics*, 2011, **5**, 021501.
328. D. C. Duffy, J. C. McDonald, O. J. A. Schueller and G. M. Whitesides, *Analytical Chemistry*, 1998, **70**, 4974-4984.
329. F. M. Wisser, B. Schumm, G. Mondin, J. Grothe and S. Kaskel, *Journal of Materials Chemistry C*, 2015, **3**, 2717-2731.

330. R. Seemann, M. Brinkmann, T. Pfohl and S. Herminghaus, *Reports on Progress in Physics*, 2012, **75**, 016601.
331. K. F. Lei, in *Microfluidics in Detection Science: Lab-on-a-chip Technologies*, The Royal Society of Chemistry, 2015, DOI: 10.1039/9781849737609-00001, pp. 1-28.
332. B.-H. Jo, L. M. Van Lerberghe, K. M. Motsegood and D. J. Beebe, *Journal of Microelectromechanical Systems*, 2000, **9**, 76-81.
333. M. J. Madou, *Fundamentals of microfabrication: the science of miniaturization*, CRC press, 2002.
334. N. Maluf and K. Williams, *Introduction to microelectromechanical systems engineering*, Artech House, 2004.
335. J. C. McDonald, M. L. Chabinyc, S. J. Metallo, J. R. Anderson, A. D. Stroock and G. M. Whitesides, *Analytical Chemistry*, 2002, **74**, 1537-1545.
336. M. K. Chaudhury and G. M. Whitesides, *Langmuir*, 1991, **7**, 1013-1025.
337. M. J. Owen and P. J. Smith, *Journal of Adhesion Science and Technology*, 1994, **8**, 1063-1075.
338. J. C. McDonald and G. M. Whitesides, *Accounts of Chemical Research*, 2002, **35**, 491-499.
339. M. Morra, E. Occhiello, R. Marola, F. Garbassi, P. Humphrey and D. Johnson, *Journal of Colloid and Interface Science*, 1990, **137**, 11-24.
340. N. R. Council, *Toxicity Testing in the 21st Century: A Vision and a Strategy*, The National Academies Press, Washington, DC, 2007.
341. M. H. Wu, S. B. Huang and G. B. Lee, *Lab Chip*, 2010, **10**, 939-956.
342. J. Hong, J. B. Edel and A. J. deMello, *Drug Discovery Today*, 2009, **14**, 134-146.
343. G. A. Cooksey, J. T. Elliott and A. L. Plant, *Analytical Chemistry*, 2011, **83**, 3890-3896.
344. M. W. Toepke and D. J. Beebe, *Lab Chip*, 2006, **6**, 1484-1486.
345. K. J. Regehr, M. Domenech, J. T. Koepsel, K. C. Carver, S. J. Ellison-Zelski, W. L. Murphy, L. A. Schuler, E. T. Alarid and D. J. Beebe, *Lab Chip*, 2009, **9**, 2132-2139.
346. J. N. Lee, X. Jiang, D. Ryan and G. M. Whitesides, *Langmuir*, 2004, **20**, 11684-11691.
347. Y.-C. Tan, J. S. Fisher, A. I. Lee, V. Cristini and A. P. Lee, *Lab on a Chip*, 2004, **4**, 292-298.
348. J. D. Tice, H. Song, A. D. Lyon and R. F. Ismagilov, *Langmuir*, 2003, **19**, 9127-9133.
349. M. Chabert and J.-L. Viovy, *Proceedings of the National Academy of Sciences*, 2008, **105**, 3191-3196.
350. M. He, J. S. Edgar, G. D. M. Jeffries, R. M. Lorenz, J. P. Shelby and D. T. Chiu, *Analytical Chemistry*, 2005, **77**, 1539-1544.
351. A. Huebner, M. Srisa-Art, D. Holt, C. Abell, F. Hollfelder, A. J. deMello and J. B. Edel, *Chemical Communications*, 2007, DOI: 10.1039/B618570C, 1218-1220.
352. S. Koster, F. E. Angile, H. Duan, J. J. Agresti, A. Wintner, C. Schmitz, A. C. Rowat, C. A. Merten, D. Pisignano, A. D. Griffiths and D. A. Weitz, *Lab on a Chip*, 2008, **8**, 1110-1115.
353. G. E. Croston, *Trends in Biotechnology*, 2002, **20**, 110-115.

354. A. Tourovskaia, X. Figueroa-Masot and A. Folch, *Lab on a Chip*, 2005, **5**, 14-19.
355. D. T. Chiu, N. L. Jeon, S. Huang, R. S. Kane, C. J. Wargo, I. S. Choi, D. E. Ingber and G. M. Whitesides, *Proceedings of the National Academy of Sciences*, 2000, **97**, 2408-2413.
356. Y. Mi, Y. Chan, D. Trau, P. Huang and E. Chen, *Polymer*, 2006, **47**, 5124-5130.
357. S. W. Rhee, A. M. Taylor, C. H. Tu, D. H. Cribbs, C. W. Cotman and N. L. Jeon, *Lab on a Chip*, 2005, **5**, 102-107.
358. W. Tan and T. A. Desai, *Tissue Engineering*, 2003, **9**, 255-267.
359. D. M. Thompson, K. R. King, K. J. Wieder, M. Toner, M. L. Yarmush and A. Jayaraman, *Analytical Chemistry*, 2004, **76**, 4098-4103.
360. K. R. King, S. Wang, D. Irimia, A. Jayaraman, M. Toner and M. L. Yarmush, *Lab on a Chip*, 2007, **7**, 77-85.
361. N. Li Jeon, H. Baskaran, S. K. W. Dertinger, G. M. Whitesides, L. Van De Water and M. Toner, *Nature Biotechnology*, 2002, **20**, 826.
362. P. J. Hung, P. J. Lee, P. Sabounchi, R. Lin and L. P. Lee, *Biotechnology and Bioengineering*, 2005, **89**, 1-8.
363. A. Khademhosseini, J. Yeh, G. Eng, J. Karp, H. Kaji, J. Borenstein, O. C. Farokhzad and R. Langer, *Lab on a Chip*, 2005, **5**, 1380-1386.
364. W.-G. Koh and M. V. Pishko, *Analytical and Bioanalytical Chemistry*, 2006, **385**, 1389-1397.
365. B. Ma, G. Zhang, J. Qin and B. Lin, *Lab on a Chip*, 2009, **9**, 232-238.
366. K. Ziolkowska, E. Jedrych, R. Kwapiszewski, J. Lopacinska, M. Skolimowski and M. Chudy, *Sensors and Actuators B: Chemical*, 2010, **145**, 533-542.
367. A. T. O'Neill, N. Monteiro-Riviere and G. M. Walker, *Conference Proceedings of the Annual International Conference of the IEEE Engineering in Medicine and Biology Society*, 2006, **1**, 2836-2839.
368. D. S. Gorman and R. Levine, *Plant Physiology*, 1966, **41**, 1643-1647.
369. D. S. Gorman and R. P. Levine, *Proceedings of the National Academy of Sciences of the United States of America*, 1965, **54**, 1665-1669.
370. S. Hutner, L. Provasoli, A. Schatz and C. Haskins, *Proceedings Of the American Philosophical Society*, 1950, **94**, 152-170.
371. *Cold Spring Harbor Protocols*, 2006, **2006**, pdb.rec8194.
372. *Cold Spring Harbor Protocols*, 2009, **2009**, pdb.rec11945.
373. B. Söderström, *Soil Biology and Biochemistry*, 1977, **9**, 59-63.
374. G. Adam and H. Duncan, *Soil Biology and Biochemistry*, 2001, **33**, 943-951.
375. M. Koresawa and T. Okabe, *Assay and drug development technologies*, 2004, **2**, 153-160.
376. D. B. Sofia Papadimitriou, *Journal of Controlled Release*, 2009, **138**, 177–184.
377. A. Ahmed, J. Hearn, W. Abdelmagid and H. Zhang, *Journal of Materials Chemistry*, 2012, **22**, 25027-25035.
378. Z. C. Xiaodan Zhou, *Archives of Pharmacal Research*, 2015, **38**, 2193–2200.
379. M. J. Al-Awady, A. Fauchet, G. M. Greenway and V. N. Paunov, *Journal of Materials Chemistry B*, 2017, **5**, 7885-7897.

380. A. K. F. Dyab, M. Ozmen, M. Ersoz and V. N. Paunov, *Journal of Materials Chemistry*, 2009, **19**, 3475-3481.
381. R. Watkins, L. Wu, C. Zhang, R. M. Davis and B. Xu, *International Journal of Nanomedicine*, 2015, **10**, 6055-6074.
382. D. Attwood, *Surfactant systems : their chemistry, pharmacy and biology*, Chapman and Hall, London :, 1983.
383. H. R. Patel, R. P. Patel and M. Patel, *International Journal of PharmTech Research*, 2009, **1**, 299-303.
384. J. Suksiriworapong, T. Rungvimolsin, A. A-gomol, V. B. Junyaprasert and D. Chantasart, *American Association of Pharmaceutical Scientists*, 2014, **15**, 52-64.
385. V. Kunasekaran and K. Krishnamoorthy, *International Journal of Pharmacy and Pharmaceutical Sciences*, 2015, **7**, 73-80.
386. P. Larkin, *Infrared and Raman spectroscopy: principles and spectral interpretation*, Elsevier, 2011.
387. X. Cai, B. Han, Y. Liu, F. Tian, F. Liang and X. Wang, *ACS Applied Materials & Interfaces*, 2017, **9**, 12949-12958.
388. R. K. Basniwal, H. S. Buttar, V. Jain and N. Jain, *Journal of Agricultural and Food Chemistry*, 2011, **59**, 2056-2061.
389. D. Chen, C.-X. Zhao, C. Lagoin, M. Hai, L. Arriaga, S. Koehler, A. Abbaspourrad and D. A. Weitz, *Royal Society Open Science*, 2017, **4**, 170919.
390. Y.-J. Wang, M.-H. Pan, A.-L. Cheng, L.-I. Lin, Y.-S. Ho, C.-Y. Hsieh and J.-K. Lin, *Journal of Pharmaceutical and Biomedical Analysis*, 1997, **15**, 1867-1876.
391. J. Shubham, M. Sai Rama Krishna and C. Kaushik, *Biomedical Materials*, 2016, **11**, 055007.
392. P. R. K. Mohan, G. Sreelakshmi, C. V. Muraleedharan and R. Joseph, *Vibrational Spectroscopy*, 2012, **62**, 77-84.
393. G. Sailor, A. Seth, G. Parmar, S. Chauhan and A. Javia, *Journal of Applied Pharmaceutical Science*, 2015, **5**, 023-028.
394. S. Şenel, G. İkinci, S. Kaş, A. Yousefi-Rad, M. F. Sargon and A. A. Hıncal, *International Journal of Pharmaceutics*, 2000, **193**, 197-203.
395. M.-L. Veyries, F. Faurisson, M.-L. Joly-Guillou and B. Rouveix, *Antimicrobial Agents and Chemotherapy*, 2000, **44**, 1093-1096.
396. H. Yamada, N. Koike, T. Ehara and T. Matsumoto, *Journal of Infection and Chemotherapy*, 2011, **17**, 195-199.
397. M. Portoles, M. F. Refojo and F. L. Leong, *Journal of Biomedical Materials Research*, 1994, **28**, 303-309.
398. M. Mehra, J. Sheorain and S. Kumari, *AIP Conference Proceedings*, 2016, **1724**, 020060.
399. J. Yin, H. Xing and J. Ye, *Metabolism: Clinical and Experimental*, 2008, **57**, 712-717.
400. J. A. Marin-Neto, B. C. Maciel, A. L. Secches and L. Gallo Junior, *Clinical Cardiology*, 1988, **11**, 253-260.
401. F. Y. Fung and Y. C. Linn, *Evidence-Based Complementary and Alternative Medicine*, 2015, **2015**, 425037.

402. J. Bateman, R. D. Chapman and D. Simpson, *Scottish Medical Journal*, 1998, **43**, 7-15.
403. M. Cernakova and D. Kostalova, *Folia Microbiologica*, 2002, **47**, 375-378.
404. *US Pat.,* US20150250727 A1, 2015.
405. S. M. Bowman and S. J. Free, *Bioessays*, 2006, **28**, 799-808.
406. J.-M. Lachapelle, *European Journal of Dermatology*, 2014, **24**, 3-9.
407. M. U. K. Sahibzada, A. Sadiq, H. S. Faidah, M. Khurram, M. U. Amin, A. Haseeb and M. Kakar, *Drug Design, Development and Therapy*, 2018, **12**, 303-312.
408. C. J. Seneviratne, K. C.-F. Leung, C.-H. Wong, S.-F. Lee, X. Li, P. C. Leung, C. B. San Lau, E. Wat and L. Jin, *PloS One*, 2014, **9**, e103234.
409. X. Li, C.-H. Wong, T.-W. Ng, C.-F. Zhang, K. C.-F. Leung and L. Jin, *International Journal of Nanomedicine*, 2016, **11**, 2471.
410. U. S. Barreras, F. T. Méndez, R. E. M. Martínez, C. S. Valencia, P. R. M. Rodríguez and J. P. L. Rodríguez, *Materials Science and Engineering: C*, 2016, **58**, 1182-1187.
411. N. Lavoine, I. Desloges, C. Sillard and J. Bras, *Cellulose*, 2014, **21**, 4429-4442.
412. S. Zorofchian Moghadamtousi, H. Abdul Kadir, P. Hassandarvish, H. Tajik, S. Abubakar and K. Zandi, *BioMed Research International*, 2014, **2014**, 12.
413. P. La Colla, E. Tramontano, C. Musiu, M. Marongiu, E. Novellino, G. Greco, S. Massa, R. Di Santo, R. Costi and A. Marino, *Antiviral Research*, 1998, **37**, 57-57.
414. L. Ammayappan and J. J. Moses, *Fibers and Polymers*, 2009, **10**, 161-166.
415. J. Singh, B. Burr, D. Stringham and A. Arrieta, *Paediatric Drugs*, 2001, **3**, 733-761.
416. C. Watanakunakorn, *Reviews of Infectious Diseases*, 1981, **3 suppl**, S210-215.
417. A. Zhou, T. M. Kang, J. Yuan, C. Beppler, C. Nguyen, Z. Mao, M. Q. Nguyen, P. Yeh and J. H. Miller, *Antimicrobial Agents and Chemotherapy*, 2015, **59**, 276-281.
418. T. S. Lundstrom and J. D. Sobel, *Infectious Disease Clinics of North America*, 2000, **14**, 463-474.
419. S.-Y. Teow, K. Liew, S. A. Ali, A. S.-B. Khoo and S.-C. Peh, *Journal of Tropical Medicine*, 2016, **2016**, 2853045.
420. R. Mirnejad, M. A. Mofazzal Jahromi, S. Al-Musawi, M. Pirestani, M. Fasihi Ramandi, K. Ahmadi, H. Rajayi, Z. Mohammad Hassan and M. Kamali, *Iranian Journal of Biotechnology*, 2014, **12**, 1-8.
421. H. Gu, P. L. Ho, E. Tong, L. Wang and B. Xu, *Nano Letters*, 2003, **3**, 1261-1263.
422. F. Katiraee, J. Ashrafai Helan, S. J. Emami, G. Hamidian and E. Babaei, *Current Medical Mycology*, 2016, **2**, 7-12.
423. J. García-Alonso, G. M. Greenway, J. D. Hardege and S. J. Haswell, *Biosensors and Bioelectronics*, 2009, **24**, 1508-1511.
424. Q. Chen, G. Li, Q.-H. Jin, J.-L. Zhao, Q.-S. Ren and Y.-S. Xu, *Journal of Microelectromechanical Systems*, 2007, **16**, 1193-1200.
425. V. V. Korolev, A. G. Ramazanova and A. V. Blinov, *Russian Chemical Bulletin*, 2002, **51**, 2044-2049.
426. L. Zhu, D. Xie, J. Ma, J. Shao and X. Shen, *Smart Materials and Structures*, 2013, **22**, 045015.

427. T. Merkel, V. Bondar, K. Nagai, B. Freeman and I. Pinnau, *Journal of Polymer Science Part B: Polymer Physics*, 2000, **38**, 415-434.
428. J. Garcia-Alonso, R. F. Fakhrullin, V. N. Paunov, Z. Shen, J. D. Hardege, N. Pamme, S. J. Haswell and G. M. Greenway, *Analytical and Bioanalytical Chemistry*, 2011, **400**, 1009-1013.
429. L. Zhang, D. L. Parsons, C. Navarre and U. B. Kompella, *Journal of Controlled Release*, 2002, **85**, 73-81.
430. G. G. Pereira, F. A. Dimer, S. S. Guterres, C. P. Kechinski, J. E. Granada and N. S. M. Cardozo, *Quimica Nova*, 2013, **36**, 1121-1125.